



**LUCIE SOLANGE
NOGUEIRA**

**CATALISADORES SUPRAMOLECULARES
BASEADOS EM RECETORES MACROCÍCLICOS E
COMPLEXOS DE METAIS DE TRANSIÇÃO**

Tese apresentada à Universidade de Aveiro para cumprimento dos requisitos necessários à obtenção do grau de Doutor em Química Sustentável, realizada sob a orientação científica da Doutora Isabel Maria de Sousa Gonçalves, Professora Associada do Departamento de Química da Universidade de Aveiro, e sob co-orientação científica da Doutora Anabela Tavares Aguiar Valente, Investigadora Principal do CICECO-Instituto de Materiais de Aveiro, Departamento de Química da Universidade de Aveiro

Apoio financeiro da POCI no âmbito do III Quadro Comunitário de Apoio.

Apoio financeiro da FCT (PD/BD/109666/2015), e do POPH/FSE no âmbito do III Quadro Comunitário de Apoio.



Dedico este trabalho à minha mãe e ao meu irmão por me terem apoiado sempre ao longo da minha vida.

“Imagination is more important than knowledge. For knowledge is limited to all we now know and understand, while imagination embraces the entire world, and all there ever will be to know and understand.” Albert Einstein

o júri

presidente

Doutor João Carlos de Oliveira Matias

Professor Catedrático do Departamento de Economia, Gestão, Engenharia Industrial e Turismo da Universidade de Aveiro

Doutora Beatriz Royo Cantabrana

Investigadora Principal do Instituto de Tecnologia Química e Biológica da Universidade Nova de Lisboa

Doutor José Eduardo dos Santos Félix Castanheiro

Professor Auxiliar do Departamento de Química da Universidade de Évora

Doutora Maria de La Saete da Silva Balula

Investigadora Principal da Faculdade de Ciências da Universidade do Porto

Doutor Paulo Jorge Ribeiro Claro

Professor Associado com agregação do Departamento de Química da Universidade de Aveiro

Doutora Isabel Maria de Sousa Gonçalves

Professora Associada do Departamento de Química da Universidade de Aveiro (Orientadora)

agradecimentos

Agradeço profundamente à minha orientadora Professora Isabel Gonçalves e à minha co-orientadora Doutora Anabela Valente por me ter recebido tão bem quando cheguei repentinamente no grupo uma vez que não me conhecia, pela disponibilidade/apoio, pelo voto de confiança depositado em mim e por tudo aquilo que me ensinaram sobre Síntese, Caracterização e Catálise durante estes quatro anos.

Ao Doutor Martyn Pillinger agradeço toda a ajuda na discussão dos resultados, elaboração dos artigos, e sempre que eu precisava de algo.

Ao Doutor Luís Silva (REQUIMTE, Faculdade de Ciências, Universidade do Porto) e Doutor Filipe Paz (CICECO, Universidade de Aveiro) pelos estudos de DRX de monocristal e pela discussão dos mesmos.

Ao Professor André Lopes (CIQA - Centro de Investigação em Química do Algarve, Faculdade de Ciências e Tecnologia do Algarve) pelo síntese e caracterização dos cucurbiturilos.

À Celeste Azevedo, Manuela Marques, Rosário Soares, Hilário Tavares, Paula Santos e Tiago Silva pelo apoio dado e execução de diversas técnicas de caracterização (termogravimetria, espectroscopia de FT-Raman e FT-IR, análise elementar, difração de raio-X de pós, RMN e SEM).

À Doutora Ana Gomes e Doutora Tatiana Amarante pela ajuda na Síntese e Caracterização dos compostos. À Doutora Margarida Antunes, Doutora Patrícia Neves e Doutora Sofia Bruno por todo o trabalho incansável realizado na Catálise e pela discussão do estudo realizado. Obrigada mais uma vez às minhas colegas de grupo por terem-me recebido de braços abertos. Não podia ter pedido melhores companheiras e que me ajudaram a tornar o local de trabalho num lugar muito agradável!

Um obrigado também especial a outras pessoas que fui conhecendo pela sua amizade e simpatia, Ana Luísa Costa, Clara Magalhães, Bárbara Ferreira e Daniela Rodrigues.

Ao Professor João Rocha, ao Departamento de Química/CICECO e à Universidade de Aveiro pelas condições cedidas que permitiram a realização deste trabalho. Agradeço à Fundação para a Ciência e Tecnologia, pela bolsa de doutoramento (PD/BD/109666/2015), co-financiada pelo MCTES e pelo Fundo Social Europeu através do programa POPH do QREN. e pelos subsídios concedidos à realização do meu plano de trabalho. Este trabalho foi desenvolvido no âmbito do projeto (Laboratório Associado) CICECO-Instituto de Materiais de Aveiro-POCI-01-0145-FEDER-007679 [FCT (Fundação para a Ciência e Tecnologia) ref. UID/CTM/50011/2013], financiado por fundos nacionais através da FCT/MEC e, quando aplicável, co-financiado pelo FEDER (Fundo Europeu de Desenvolvimento Regional) no âmbito do Contrato de Parceria PT2020.

Finalmente, agradeço à minha mãe, ao meu irmão e ao resto da minha família por terem sido o meu maior apoio mesmo sem entenderem o mundo da Ciência e ajudado a tomar as melhores decisões, e aos meus amigos por terem tornado os meus dias muito mais leves durante esta jornada.

palavras-chave

Complexos de molibdênio, óxidos de molibdênio, ligandos bidentados de azoto, materiais híbridos, cucurbiturilos, catálise, epoxidação de olefinas

resumo

A presente tese descreve o *design*, síntese, caracterização e aplicação em catálise de novos materiais híbridos orgânicos-inorgânicos de molibdênio. Foram investigados seis diferentes ligandos quelantes N,N', que incluem brometo de 2-(1-propiltrimetilamônio-3-pirazolil)piridina, 2-(1-pentil-3-pirazolil)piridina, aminas pirindanilo quirais, triazóis, 2,2'-bipiridina e 2-(2-piridil)-benzimidazole. A seleção desses ligandos baseou-se na diversidade estrutural, que inclui moléculas neutras e iônicas, simétricas e assimétricas, algumas com grupos substituintes e outras menos impedidas estereoquimicamente, e possível quiralidade. A diversidade desses ligandos quelantes N,N' promoveu a formação de novos materiais com propriedades catalíticas diferentes. Neste trabalho, os complexos de molibdênio(VI) foram preparados pela oxidação dos respectivos precursores, através da descarboxilação oxidativa de complexos tri- e tetracarbonilos com excesso de hidroperóxido de *tert*-butilo (TBHP) em decano, ou da hidrólise e condensação de complexos $[\text{MoO}_2\text{Cl}_2\text{L}]$ em água. Os (pré)catalisadores preparados foram explorados em reações de epoxidação de (bio)olefinas e catálise ácida, nomeadamente na alcoólise do óxido de estireno. As vias para a conversão dos precursores em compostos de oxomolibdênio, durante os processos de síntese (*ex situ*) ou catalítico (*in situ*, envolvendo isolamento/caracterização de espécies metálicas após os ensaios catalíticos), ajudaram a estabelecer relações entre o tipo de espécies metálicas formadas e o desempenho catalítico. Geralmente, os (pré)catalisadores preparados foram transformados em sais de octamolibdato, $(\text{L})_x[\text{Mo}_8\text{O}_{26}]$ (L = ligando orgânico presente no precursor) na presença de TBHP durante as reações catalíticas, ou em espécies de oxoperoxo na presença de H_2O_2 . Estas descobertas ajudaram a explicar os diferentes desempenhos catalíticos obtidos. Com vista ao desenvolvimento de novos materiais híbridos baseados em complexos metálicos com novos suportes, procedeu-se à incorporação de um complexo aqua-molibdênio pré-preparado ($[\text{MoO}_2\text{Cl}_2(\text{H}_2\text{O})_2]$) em CB[6], originando o composto $2[\text{MoO}_2\text{Cl}_2(\text{H}_2\text{O})_2]\cdot\text{CB}[6]\cdot 2(\text{HCl})\cdot 14\text{H}_2\text{O}$. O complexo $2[\text{MoO}_2\text{Cl}_2(\text{H}_2\text{O})_2]\cdot\text{CB}[6]$ apresentou bom desempenho catalítico para as reações *one-pot* de conversão de olefinas em produtos alcóxi, através de catálise oxidativa e ácida. Foi demonstrada a sua recuperação e reutilização através de procedimentos relativamente simples. Este trabalho é o primeiro estudo de estratégias *one-pot* para a conversão de alcenos com H_2O_2 em meio álcool para dar produtos alcóxi-cetona, na presença de catalisadores à base de molibdênio.

keywords

Molybdenum complexes, molybdenum oxides, nitrogen bidentate ligands, hybrid materials, cucurbiturils, catalysis, olefins epoxidation

abstract

The present thesis describes the design, synthesis, characterization and application in catalysis of new molybdenum organic-inorganic hybrid materials. Six distinct N,N'-chelate ligands were investigated, which include 2-(1-propyltrimethylammonium-3-pyrazolyl)pyridine bromide, 2-(1-pentyl-3-pyrazolyl)pyridine, chiral pyridanyl amines, triazoles, 2,2'-bipyridine and 2-(2-pyridyl)-benzimidazole. The selection of these ligands was based on structural diversity, which includes neutral and ionic molecules, symmetrical and unsymmetrical, some with substituent groups and other less sterically hindered, and possible chirality. The diversity of these N,N'-chelating ligands promoted the formation of new materials, possessing different catalytic performances. Herein, molybdenum(VI) complexes were prepared by oxidation of the respective precursors, via oxidative decarbonylation of tri- and tetracarbonyl complexes with excess TBHP (*tert*-butyl hydroperoxide) in decane, or via hydrolysis and condensation of complexes $[\text{MoO}_2\text{Cl}_2\text{L}]$ in water. The prepared (pre)catalysts were explored for epoxidation reactions of (bio)olefins and acid catalysis namely the alcoholysis of styrene oxide. The routes for the conversion of the precursors to oxomolybdenum compounds, during either the synthesis (*ex situ*) or catalytic (*in situ*) processes (involving isolation/characterisation of metal species after the catalytic runs), helped establish relationships between the type of metal species formed and the catalytic performances. Generally, the prepared (pre)catalysts were transformed into β -octamolybdate salts, $(\text{L})_x[\text{Mo}_8\text{O}_{26}]$ (L = organic ligand present in the precursor) in the presence of TBHP during the catalytic reactions, or into oxoperoxo species with H_2O_2 . These findings helped to explain the different catalytic performances. Envisaging the development of new hybrid materials based on metallic complexes with new supports, a pre-made aqua molybdenum complex $([\text{MoO}_2\text{Cl}_2(\text{H}_2\text{O})_2])$ was incorporated in CB[6], giving the compound $2[\text{MoO}_2(\text{Cl}_2)(\text{H}_2\text{O})_2]\cdot\text{CB}[6]\cdot 2(\text{HCl})\cdot 14\text{H}_2\text{O}$. The $2[\text{MoO}_2(\text{Cl}_2)(\text{H}_2\text{O})_2]\cdot\text{CB}[6]$ complex was efficient for the one-pot conversion of olefins to alkoxy products, which involves oxidation and acid chemistry. The results also demonstrated their recovery and reuse via relatively simple procedures. This study was the first report of the one-pot oxidation of alkenes with H_2O_2 in alcohol medium to give alkoxy ketone products, in the presence of molybdenum-based catalysts.

Published articles in scientific journals

- Neves, P.; Nogueira, L. S.; Gomes, A. C.; Oliveira, T. S. M.; Lopes, A. D.; Valente, A. A.; Gonçalves, I. S.; Pillinger, M.; Chemistry and catalytic performance of pyridyl-benzimidazole oxidomolybdenum(VI) compounds in (bio)olefin epoxidation, *European Journal of Inorganic Chemistry* **2017**, *19*, 2617-2627.
- Nogueira, L. S.; Neves, P.; Gomes, Ana C.; Valente, A. A.; Pillinger, M.; Gonçalves, I. S.; Performance of a tetracarbonylmolybdenum(0) pyrazolylpyridine (pre)catalyst in olefin epoxidation and epoxide alcoholysis, *Journal of Organometallic Chemistry* **2017**, *846*, 185-192.
- Neves, P.; Nogueira, L. S.; Valente, A. A.; Pillinger, M.; Gonçalves I. S.; Sampaio-Dias, I. E.; Sousa, C. A. D.; Rizzo-Aguiar, F.; Rodríguez-Borges, J. E.; Performance of chiral tetracarbonylmolybdenum pyrindanyl amine complexes in catalytic olefin epoxidation, *Journal of Organometallic Chemistry* **2018**, *858*, 29-36.
- Bruno, S. M.; Nogueira, L. S.; Gomes, A. C.; Valente, A. A.; Goncalves, I. S.; Pillinger, M; High-yield synthesis and catalytic response of chainlike hybrid materials of the [(MoO₃)(m)(2,2'-bipyridine)(n)] family, *New Journal of Chemistry* **2018**, *42*, 16483-16492.
- Nogueira, L. S.; Neves, P.; Gomes, A. C.; Lavrador, P.; Cunha-Silva, L.; Valente, A. A.; Gonçalves, I. S.; Pillinger, M.; Molybdenum(0) tricarbonyl and tetracarbonyl complexes with a cationic pyrazolylpyridine ligand: synthesis, crystal structures and catalytic performance in olefin epoxidation, *RSC Advances* **2018**, *8*, 16294-16302.
- Nogueira, L. S.; Neves, P.; Gomes, A. C.; Amarante, T. A.; Paz, F. A. A.; Valente, A. A.; Goncalves, I. S.; Pillinger, M; A comparative study of molybdenum carbonyl and oxomolybdenum derivatives bearing 1,2,3-triazole or 1,2,4-triazole in catalytic olefin epoxidation, *Molecules* **2019**, *24*, 105-122.
- Nogueira, L. S.; Antunes, M. M.; Gomes, A. C.; Cunha-Silva, L.; Pillinger, M., Lopes, A. D.; Valente, A. A.; Gonçalves, I. S.; A hydrogen-bonded assembly of cucurbit[6]uril and [MoO₂Cl₂(H₂O)₂] with catalytic efficacy for the one-pot conversion of olefins to alkoxy products, *submitted*.

List of abbreviations

1C8 = 1-octene

2C8 = *trans*-2-octene

AcOEt = ethyl acetate

ArH = arene (six membered ring with 3 double bonds, C=H)

BA = benzaldehyde

BDMLPX = di(1,2-dimethylimidazolium) β -xylenedichloride

bim = benzimidazole

bipy = bipyridine

[bmim]BF₄ = 1-butyl-3-methylimidazolium tetrafluoroborate

[bmim]Cl = 1-butyl-3-methylimidazolium chloride

[bmim]₄[β -Mo₈O₂₆] = tetra(1-butyl-3-methylimidazolium) octamolybdate

[bmim]PF₆ = 1-butyl-3-methylimidazolium hexafluorophosphate

[bmim]NTf₂ = 1-butyl-3-methylimidazolium bis(trifluoromethylsulfonyl)imide)

BuOH = 1-butanol

Bz = benzyl

[C₈mim]PF₆ = 1-octyl-3-methylimidazolium hexafluorophosphate

Conv. = conversion

Cp = cyclopentadienyl

Cp' = η^5 -C₅R₅ (R = H, alkyl, *ansa*-bridge)

CPA = campholenic aldehyde

CPHA = *N*-cinnamoyl *N*-phenyl hydroxamic acid ligand

CP MAS = cross-polarization with rotation according to the magic angle (NMR spectroscopy)

Cp^{ox} = chiral oxazoline pendant group

CT = contact test

Cy = *cis*-cyclooctene

Cy6 = cyclohexene

Cy12 = cyclododecene

CyO = cyclooctene oxide

d = doublet

d^l = orbital designation and angular momentum number /

DBU = 1,8-diazabicyclo[5.4.0]undec-7-ene

dd = doublet of doublets
ddd = doublet of doublet of doublets
Dhmim = 1,2-dimethyl-3-hexylimidazolium
di-*t*Bu-bipy = 4,4'-di-*tert*-butyl-2,2'-bipyridine
DL-Lim = DL-limonene
DMF = N,N-Dimethylformamide
DMSO-*d*₆ = dimethyl sulfoxide-*d*₆
dt = doublet of triplet
ee = enantiomeric excess
eppa = ethyl[3-(2-pyridyl)-1-pyrazolyl]acetate
EDS = energy-dispersive X-ray spectroscopy
EPE = 2-ethoxy-2-phenylethanol
ESI-MS = electrospray ionization mass spectrometry
EtOH = ethanol
FT-IR = Fourier-transform infrared spectroscopy
FT-Raman = Fourier-transform Raman spectroscopy
GC = gas chromatography
Hbpd_c = protonated 2,2'-bipyridyl-3,3'-dicarboxylate
H₂biim = 2,2'-biimidazole
HCl = hydrochloric acid
Hmim = 1-hexyl-3-methylimidazolium
H₂O₂ = hydrogen peroxide
Hpy = 1-hexylpyridinium
HT = hydrothermal
ICP-OES = inductively coupled plasma optical emission spectrometry
im = imidazole
IMes = 1,3-bis(2,4,6-trimethylphenyl)imidazol-2-ylidene.
IPC = *iso*-pinocamphone
L = organic ligand or liquid phase
L* = 1,4-(2,6-dimethyl)phenyl-2,3-dimethyldiazabutadiene
L** = 1,4-(2,6-diisopropyl)-phenyldiazabutadiene
L*** = 1,4-(4-chloro)phenyl-2,3-naphthalenediazabutadiene
Lim = (*R*)-(+)-limonene

LimDiOx = 1,2:8,9-diepoxy-*p*-menthane
LimOx = 1,2-epoxy-*p*-menth-8-ene
LinOle = methyl linoleate
m = medium intensity (vibrational bands in FT-IR and FT-Raman spectroscopy) or multiplet (multiplicity of signal in NMR spectroscopy)
Me₂pz = 3,5-dimethylpyrazolyl
Me₃-tame = 1,1,1-tris(methylaminomethyl)ethane
Methanol = MeOH
MS = mass spectrometry
MW = microwave
NaBH(OAc)₃ = sodium triacetoxyborohydride
NHC = N-heterocyclic carbene
NMR = nuclear magnetic resonance spectroscopy
NP = nanoparticle
O = octahedral
OD = oxidative decarbonylation
Ole = oleate
OleO = methyl 9,10-epoxyoctadecanoate
PCV = *trans*-pinocarveol
PEA = methylbenzylamine
Pin = α-pinene
PinO = α-pinene oxide
pip = piperidine
pbim = 2-(2-pyridyl)benzimidazole
Ph = phenyl
PhCF₃ = benzotrifluoride
POM = polyoxometalate
ppm = parts per million
ppp = 2-(1-pentyl-3-pyrazolyl)pyridine
P(2-py)₃ = tris(2-pyridyl)phosphine
PrOH = 1-propanol
[ptapzpy]Br = 2-(1-propyltrimethylammonium-3-pyrazolyl)pyridine bromide
PTFE = polytetrafluoroethylene
P₄VP = poly(4-vinylpyridine)

pyim = N-(*n*-propyl)-2-pyridylmethanimine
PyNHC = 3-methyl-1-picolylimidazol-2-ylidene
pypz = 2-[3(5)-pyrazolyl]pyridine
pz = pyrazolyl
pzpyEA = ethyl[3-(2-pyridyl)-1-pyrazolyl]acetate
q = quartet (multiplicity of signal in NMR spectroscopy)
QO = 8-quinolinol
R = 2,2'-bipy/Mo ratio
RISS = reaction-induced self-separating
r.t. = room temperature
S = solid phase
s = strong intensity (vibrational bands in FT-IR and FT-Raman spectroscopy) or singlet (multiplicity of signal in NMR spectroscopy)
SEM = scanning electron microscope
sh = shoulder intensity (vibrational bands in FT-IR and FT-Raman spectroscopy)
solv = cosolvent
StyOx = styrene oxide
T = tetrahedral
TBHP = *tert*-butyl hydroperoxide
TBHP_A = TBHP in aqueous solution
TBHP_D = TBHP in decane solution
fbms = *trans*-β-methylstyrene
td = triplet of duplet (multiplicity of signal in NMR spectroscopy)
TFT = α,α,α-trifluorotoluene
TGA = thermogravimetric analysis
THF = tetrahydrofuran
TOF = turnover frequency
TON = turnover number
Tpm = tris(1-pyrazolyl)methane
Tpms = (tris(pyrazolyl) methanesulfonic acid
trethbz = (*S*)-4-(1-phenylpropyl)-1,2,4-triazole
trz = triazole
UV-Vis = ultraviolet-visible

w = weak intensity (vibrational bands in FT-IR and FT-Raman spectroscopy)

ws = without solvent

List of symbols

c = concentration of the compound

$\alpha_D^{20^\circ C}$ = specific rotation measured at 20 °C using a light with 589 nanometers (the sodium D line) of wavelength

γ_{as} = asymmetric deformation vibrations associated do out-of-plane modes (FT-IR and FT-Raman spectroscopy)

γ_s = symmetric deformation vibrations associated do out-of-plane modes (FT-IR and FT-Raman spectroscopy)

η = hapticity of a ligand or coordination of a ligand to a metal center via an uninterrupted and contiguous series of atoms.

δ = chemical shift (NMR spectroscopy)

θ = angle of diffraction (powder x-ray diffraction)

ν = stretching vibrations (FT-IR and FT-Raman spectroscopy)

GENERAL INDEX

Published articles in scientific journals	i
List of abbreviations	ii
List of symbols	vii
CHAPTER 1	
Introduction	1
1.1. Oxomolybdenum(VI) chemistry	3
1.1.1. General considerations	3
1.1.2. Structural diversity of compounds with <i>cis</i> -MoO ₂ ²⁺ core	4
1.1.3. Metallic precursors for the synthesis of oxomolybdenum(VI) hybrid materials	5
1.1.4. Preparation methods for oxomolybdenum(VI) compounds	14
1.1.5. An overview about the application of the oxomolybdenum(VI) compounds as (pre)catalysts for organic reactions: epoxidation of olefins and acid catalysis	17
1.1.6. Carbonyl molybdenum complexes as synthesis precursors and (pre)catalysts	25
1.1.7. Dioxomolybdenum(VI) complexes as synthesis precursors and (pre)catalysts	31
1.2. Cucurbit[<i>n</i>]urils as supramolecular hosts	37
1.2.1. Historical context	38
1.2.2. Synthesis	39
1.2.3. Structural and physicochemical properties	39
1.2.4. Host-guest chemistry of CB[<i>n</i>]s through noncovalent interactions	40
1.3. Catalytic systems based on molybdenum compounds with CB[<i>n</i>]s	52
1.4. Aim of this work	55
1.5. References	57

CHAPTER 2

Molybdenum(0) tricarbonyl and tetracarbonyl complexes with a cationic pyrazolylpyridine ligand: synthesis, crystal structures and catalytic performance in olefin epoxidation 73

2.1. Introduction 75

2.2. Results and discussion 77

2.2.1. Synthesis and characterisation of [ptapzpy]Br, (pre)catalysts [Mo(CO)₃(ptapzpy)Br] (**1**) and *cis*-[Mo(CO)₄(ptapzpy)]Br (**2**) 77

2.2.2. Single-crystal X-ray structure analyses of [ptapzpy]Br, **1** and **2** 80

2.2.3. Oxidative decarbonylation of **1** 83

2.2.4. Reactions between Mo complexes and cucurbit[7]uril 85

2.3. Catalytic studies 86

2.3.1. Catalytic epoxidation of *cis*-cyclooctene with TBHP 86

2.3.2. Catalytic epoxidation of others (bio)olefins (styrene and DL-limonene) 88

2.3.3. Characterization of solids after catalytic epoxidation of Cy with TBHP 88

2.3.4. Ionic liquid-supported metal species for olefin epoxidation 89

2.3.5. Characterization of solids after catalytic epoxidation in the presence of ionic liquid 90

2.3.6. Catalytic epoxidation with H₂O₂ 94

2.3.7. Characterization of solids after catalytic epoxidation with H₂O₂ 95

2.4. Conclusions 96

2.5. References 97

CHAPTER 3

Performance of a tetracarbonylmolybdenum(0) pyrazolylpyridine (pre)catalyst in olefin epoxidation and epoxide alcoholysis 101

3.1. Introduction 103

3.2. Results and discussion 104

3.2.1. Synthesis and characterisation of ppp and pre-catalysts [Mo(CO)₄(ppp)] (**1**) 104

3.2.2. Oxidative decarbonylation 107

3.3. Catalytic studies 110

3.3.1. Catalytic epoxidation with TBHP 110

3.3.2. Characterization of solids after catalytic epoxidation with TBHP	111
3.3.3. Catalytic epoxidation with H ₂ O ₂	112
3.3.4. Characterization of solids after catalytic epoxidation with H ₂ O ₂	113
3.3.5. [MoO(O ₂) ₂ (ppp)] as active specie for the catalytic epoxidation	114
3.3.6. Ionic liquid-supported metal species for olefin epoxidation	115
3.3.7. Characterization of solids after catalytic epoxidation in ionic liquids	115
3.3.8. Acid catalysis	115
3.3.9. Characterization of solids after acid catalysis	116
3.4. Conclusions	117
3.5. References	118

CHAPTER 4

Performance of chiral tetracarbonylmolybdenum pyridanyl amine complexes in catalytic olefin epoxidation	121
--	-----

4.1. Introduction	123
4.2. Results and discussion	124
4.2.1. Synthesis and characterisation of [(<i>R,R</i>)-pyC ₅ H ₅ N(CH ₃)CH(CH ₃)Ph] and [(<i>S,S</i>)-pyC ₅ H ₅ N(CH ₃)CH(CH ₃)Ph], (pre)catalysts <i>cis</i> -[Mo(CO) ₄ (L ₄)] (1) and <i>cis</i> -[Mo(CO) ₄ (L ₅)] (2)	124
4.3. Catalytic studies	127
4.3.1. Catalytic epoxidation of <i>cis</i> -cyclooctene with TBHP	127
4.3.2. Epoxidation of prochiral olefins	128
4.3.3. Types of active species	134
4.4. Conclusions	135
4.5. References	136

CHAPTER 5

A comparative study of molybdenum carbonyl and oxomolybdenum derivatives bearing 1,2,3-triazole or 1,2,4-triazole in catalytic olefin epoxidation	139
--	-----

5.1. Introduction	141
5.2. Results and discussion	142

5.2.1. Synthesis and characterization of complexes $\text{Mo}(\text{CO})_3(1,2,3\text{-trz})_3$ (1) and $[\text{Mo}(\text{CO})_3(1,2,4\text{-trz})_3]$ (2)	142
5.2.2. Oxidative decarbonylation compounds from $[\text{Mo}(\text{CO})_3(1,2,3\text{-trz})_3]$ (1^{OD}) and $[\text{Mo}(\text{CO})_3(1,2,4\text{-trz})_3]$ (2^{OD})	145
5.2.3. Dinuclear complex $(\text{NH}_4)_{1.8}(\text{H}_3\text{O})_{0.2}[\text{Mo}_2\text{O}_2(\mu_2\text{-O})(\text{O}_2)_4(1,2,4\text{-trz})]\cdot\text{H}_2\text{O}$ (5)	149
5.2.4. Single-crystal X-ray structure analyses of 5	149
5.3. Catalytic studies	150
5.3.1. Catalytic epoxidation of <i>cis</i> -cyclooctene with TBHP	150
5.3.2. Characterization of solids after catalytic epoxidation of Cy with TBHP	152
5.3.3. Catalytic epoxidation with H_2O_2	153
5.4. Conclusions	155
5.5. References	155

CHAPTER 6

High-yield synthesis and catalytic response of chainlike hybrid materials of the $[(\text{MoO}_3)_m(2,2'\text{-bipyridine})_n]$ family	159
6.1. Introduction	161
6.2. Results and discussion	162
6.2.1. Synthesis and characterization of complexes $[\text{MoO}_3(2,2'\text{-bipy})]_n$, $[\text{Mo}_2\text{O}_6(2,2'\text{-bipy})]_n$ and $[\text{Mo}_3\text{O}_9(2,2'\text{-bipy})_2]_n$	162
6.3. Catalytic studies	171
6.3.1. Catalytic epoxidation of <i>cis</i> -cyclooctene with TBHP	171
6.3.2. Catalytic epoxidation of <i>cis</i> -cyclooctene with H_2O_2	175
6.3.3. Characterization of solids after catalytic epoxidation	175
6.3.4. Catalytic epoxidation of other cyclic and linear non-functionalized olefins	179
6.3.5. Catalytic epoxidation of the biomass-derived olefins	180
6.3.6. Acid catalysis	181
6.4. Conclusions	184
6.5. References	185

CHAPTER 7

Chemistry and catalytic performance of pyridyl-benzimidazole oxidomolybdenum(VI) compounds in (bio)olefin epoxidation 189

7.1. Introduction	191
7.2. Results and discussion	192
7.2.1. Synthesis and characterisation of (pre)catalysts [MoO ₂ Cl ₂ (pbim)] (1) and [MoO(O ₂) ₂ (pbim)] (2)	192
7.2.1. Hydrolytic stability of 1	198
7.3. Catalytic studies	200
7.3.1. Catalytic epoxidation with TBHP	200
7.3.2. Influence of cosolvent on the catalytic epoxidation with TBHP	202
7.3.3. Characterization of solids after catalytic epoxidation with TBHP	205
7.3.4. Reuse of recovered solids	206
7.3.5. Characterization of reused solids	206
7.3.6. Identification of the catalytic active specie in catalytic epoxidation with TBHP	207
7.3.7. <i>cis</i> -Cyclooctene epoxidation with H ₂ O ₂ (including cosolvent influence and characterization of recovered solids)	210
7.3.8. Bio-olefins epoxidation with H ₂ O ₂ (including characterization of recovered solids)	212
7.4. Conclusions	214
7.5. References	215

CHAPTER 8

Molybdenum-Cucurbit[*n*]uril multifunctional catalysts for one-pot liquid phase acid and oxidation catalysis 219

8.1. Introduction	221
8.2. Results and discussion	222
8.2.1. Synthesis and single-crystal X-ray structure analyses of supramolecular adduct 2[MoO ₂ Cl ₂ (H ₂ O) ₂](C ₃₆ H ₃₆ N ₂₄ O ₁₂)· <i>x</i> H ₂ O· <i>y</i> HCl· <i>z</i> (CH ₃ COCH ₃) (1)	222
8.2.2. Complementary characterization of 1	226
8.3. Catalytic studies	230
8.3.1. Olefin epoxidation	230
8.3.2. One-pot conversion of olefins to alkoxy products	232

8.3.3. Catalyst reuse	236
8.4. Conclusions	240
8.5. References	242
CHAPTER 9	
Final considerations	245
9.1. Conclusions and future considerations	247
9.2. References	250
CHAPTER 10	
Experimental techniques and characterization methods	253
10.1. List of chemical compounds	255
10.2. Experimental techniques	257
10.3. Characterization and analytical techniques	257
10.3.1. Elemental analysis	258
10.3.2. Inductively coupled plasma optical emission spectrometry (ICP-OES)	258
10.3.3. Thermogravimetric analysis (TGA)	258
10.3.4. Vibrational spectroscopy (FT-IR and FT-Raman)	258
10.3.5. Nuclear magnetic resonance spectroscopy (NMR)	259
10.3.6. X-ray powder diffraction (PXRD)	259
10.3.8. Mass spectrometry (MS)	260
10.3.9. Polarimetry	260
10.3.10. Scanning electron microscopy (SEM) / Energy-dispersive X-ray spectroscopy (EDS)	260
10.4. Synthesis	260
10.4.1. Chapter 2	260
10.4.2. Chapter 3	265
10.4.3. Chapter 4	267
10.4.4. Chapter 5	270
10.4.5. Chapter 6	273
10.4.6. Chapter 7	276
10.4.7. Chapter 8	277
10.5. Single-crystal X-ray diffraction studies	278
10.5.1. Chapter 2	278

10.5.2. Chapter 5	283
10.5.3. Chapter 8	285
10.6. Catalytic tests	286
10.6.1. Gas chromatography	286
10.6.2. Formulae - catalytic studies	287
10.6.3. Chapter 2	288
10.6.4. Chapter 3	288
10.6.5. Chapter 4	290
10.6.6. Chapter 5	291
10.6.7. Chapter 6	291
10.6.8. Chapter 7	293
10.6.9. Chapter 8	294
10.7. References	297

CHAPTER 1

Introduction



Seek

Capture

Act upon

Chapter 1

Index

1.1. Oxomolybdenum(VI) chemistry	3
1.1.1. General considerations	3
1.1.2. Structural diversity of compounds with <i>cis</i> -MoO ₂ ²⁺ core	4
1.1.3. Metallic precursors for the synthesis of oxomolybdenum(VI) hybrid materials	5
1.1.4. Preparation methods for oxomolybdenum(VI) compounds	14
1.1.5. An overview about the application of the oxomolybdenum(VI) compounds as (pre)catalysts for organic reactions: epoxidation of olefins and acid catalysis	17
1.1.6. Carbonyl molybdenum complexes as synthesis precursors and (pre)catalysts	25
1.1.7. Dioxomolybdenum(VI) complexes as synthesis precursors and (pre)catalysts	31
1.2. Cucurbit[<i>n</i>]urils as supramolecular hosts	37
1.2.1. Historical context	38
1.2.2. Synthesis	39
1.2.3. Structural and physicochemical properties	39
1.2.4. Host-guest chemistry of CB[<i>n</i>]s through noncovalent interactions	40
1.3. Catalytic systems based on molybdenum compounds with CB[<i>n</i>]s	52
1.4. Aim of this work	55
1.5. References	57

Chapter 1

1.1. Oxomolybdenum(VI) chemistry

1.1.1. General considerations

Inorganic oxides are a vast family of materials with very special interest for the scientific community since their physical properties are reflected in diverse applications, such as sorption, catalysis, biomineralization, microelectronics, gas storage, conductivity, magnetism, photochromism, optics and ceramics.¹⁻⁵ Since the middle of the XIXth century complexes of transition metals with high valence, such as molybdenum(VI), tungsten(VI), vanadium(V) and titanium(IV) are known and have been used in industrial and biological systems.⁶

In particular, molybdenum(VI) oxides are one of the most important families of compounds from Mo(VI) chemistry and represent an area of great interest due to their importance in several applications.^{7,8} The structural inorganic chemistry of molybdenum is generally in parallel with the chemistry of tungsten. On the other hand, there are differences in their physicochemical properties (such as Pauling electronegativity, ionic radius, reduction potential, Lewis acid strength of the cations, and M=O bond strengths), which can result in isotypical complexes or materials that exhibit contrasting behaviours for certain applications. For example, Mo(VI) and W(VI) oxides can exhibit unique catalytic properties, taking into account the contrasting behaviours often encountered for molecular Mo(VI)/W(VI) catalysts.⁹⁻¹³ In catalytic olefin epoxidation, W-based catalysts usually show a lower activity than Mo-based catalysts in the presence of *tert*-butyl hydroperoxide (TBHP) as the oxidant. However, the situation is often reversed when H₂O₂ is the oxidant, with the W-based catalysts being superior.¹⁰⁻¹² These differences may be due to various factors, such as different inhibiting effects of water (much stronger for Mo than for W), greater oxophilicity, and Lewis acidity of the M(VI) center.¹²

As a subclass of oxides, the molybdenum oxide substructures are represented by mononuclear, binuclear, polynuclear and one-, two- or three dimensional secondary metal-organic complex cations.³ The structures of these inorganic oxide compounds comprise one-dimensional (1D) chains, two-dimensional (2D) sheets, and three-dimensional (3D) networks, as well as discrete clusters.

Chapter 1

1.1.2. Structural diversity of compounds with *cis*-MoO₂²⁺ core

Molybdenum(VI) oxide compounds are defined as a complex containing Mo(VI) as metal center attached to a surrounding array of oxido (O²⁻) ligands (Figure 1.1). The nature of the complex is defined by the type of atoms or ligands bonded to the metal center. Complexes with inorganic nature have no carbon present or bonded to the metal center, *e.g.*, MoO₃, polyoxometalates and MoO₂X₂ (X = halide), while organometallic complexes possess a carbon directly bonded to the metal, *e.g.*, CpMoO₂X (Cp = cyclopentadienyl), and organic-inorganic complexes have an organic component bonded through a coordinative covalent bond to the metal center, *e.g.*, [MoO₂X₂(L)]. The complexes may comprise one bidentate ligand with nitrogen^{14–16}, oxygen¹⁰ or sulfur¹⁷ donor atoms, or two monodentate ligands (*e.g.* DMF¹⁸, THF¹⁹, RCN²⁰, R₂SO^{21,22}, H₂O^{23–26}, OPR₃¹⁷). Complexes formed with neutral bidentate ligands containing oxygen donor atoms have not attracted much attention, possibly due to the instability of the complexes. As alternative, complexes bearing N-donor ligands, particularly bidentates, have been shown to be stable during chemical reactions.

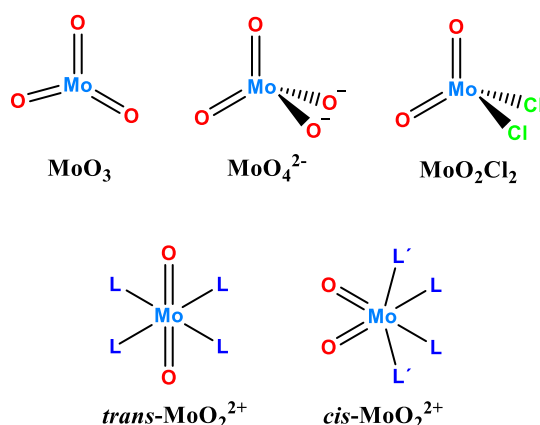


Figure 1.1. Structural representations of the different oxide cores present in molybdenum oxide compounds.

The organonitrogen class of ligands has received great interest in coordination chemistry. The most explored organonitrogen ligands in coordination chemistry are bipyridine, such as 2,2'-bipyridine^{27–29} and 4,4'-bipyridine³⁰, pyrazine³¹, 2,4,6-tripyridyltriazine³², 1,2,3-triazole³³, 1,2,4-triazole^{34,35}, 1,10-phenanthroline³⁶, diazabutadiene³⁷, 2,2'-dipyridylamine³⁸, 4,4'-dipyridylamine³⁹, pyridylimine⁴⁰, 2-[3(5)-pyrazolyl]pyridine and ethyl[3-(2-pyridyl)-1-pyrazolyl]acetate^{41,42}. These organic molecules are highly interesting since they can be used as versatile metal chelating ligands also amenable to chemical modification. Organonitrogen ligands coordinate to

Chapter 1

molybdenum in order to form organic-molybdenum compounds, which the organic unity can be manipulated through the inclusion of different groups on, for example, the pyridyl moieties.

In organodiamine ligands, such as bipyridine, 1,10-phenanthroline and 2-[3(5)-pyrazolyl]pyridine derivatives, the two rings are connected by a covalent C–C bond and coordinates to the metal through the two nitrogen atoms, forming a chelate ring where the two lone pairs of nitrogen atoms can form σ -bonds with the metal center⁴³. During this process, the cyclic residue can take part in back-bonding where the π -electron density is delocalized over the chelate ring through the metal-diimine bonding.

In the literature, the most common precursors used to prepare molybdenum(VI) oxide compounds, containing the MoO_2^{2+} core, and which will be discussed in this chapter, include molybdenum(VI) trioxide (MoO_3), sodium molybdate ($[\text{Na}_2\text{MoO}_4] \cdot 2\text{H}_2\text{O}$), molybdenum carbonyl ($\text{Mo}(\text{CO})_6$), dichlorodioxomolybdenum(VI) (MoO_2Cl_2) and, less common for specific chemical reaction, the cyclopentadienylmolybdenum(II) tricarbonyl ($\text{CpMo}(\text{CO})_3\text{R}'$).

Dioxomolybdenum(VI) chemistry is dominated by the *cis*- MoO_2^{2+} core, which has received the greatest attention due to its prevalence in chemical reactions, ease of synthesis, and chemical properties, being extensively explored for homogeneous⁴⁴ and heterogeneous catalysis⁴⁵, as materials precursors⁴⁶ and enzymes⁴⁷.

The *cis*- MoO_2^{2+} core can be easily identified by vibrational spectroscopy (FT-IR or FT-Raman) with the presence of two intense spectra bands between 850-950 cm^{-1} , corresponding to the symmetric and asymmetric Mo=O stretching modes. The geometrical range of the compounds containing the *cis*- MoO_2^{2+} core coordinated to organic ligands can go from monomeric to polymeric structures, while the link between adjacent molybdenum centers is mostly established through an oxygen atom.

1.1.3 Metallic precursors for the synthesis of oxomolybdenum(VI) hybrid materials

Hexacarbonylmolybdenum ($\text{Mo}(\text{CO})_6$)

Transition metal carbonyls are one of the most important classes of transition metal organometallic compounds. The classic σ bonding ligands form complexes with transition metals. In transition metal carbonyls, the σ bonding is reinforced by additional π bonding that stabilizes the complexes and also stabilizes very low oxidation states of the metal. Many carbonyl compounds exist with the metal in a zero oxidation state, for example, hexacarbonylmolybdenum, $\text{Mo}(\text{CO})_6$. $\text{Mo}(\text{CO})_6$ adopts an octahedral

Chapter 1

geometry consisting of six rod-like CO ligands coordinated to the central Mo atom. In this complex, the binding Mo-carbonyl corresponds to an interaction between (a) the occupied molecular orbital 5σ of CO to the empty d orbital of the metal with σ symmetry, and (b) the retro-donation of the occupied π -orbital of the metal to the π^* molecular orbital of CO. Thus, the carbon monoxide is acting as a Lewis base and donating a pair of electrons to the Mo atom that acts as a Lewis acid. The first type of interaction (a) leads to high electron density on the Mo atom from the six ligands donating simultaneously electrons to a metal center with low oxidation state. However, in the second type of interaction (b), the electron density is removed from the Mo atom center back onto the carbonyl ligands to some extent. So, the carbon monoxide is said to be a σ donor and a π acceptor, and the Mo atom is a σ acceptor and a π donor. Thus, there is a flow of electrons from the carbon monoxide to the metal through the σ system and a flow involving the π system in the reverse direction (Figure 1.2).⁴⁸

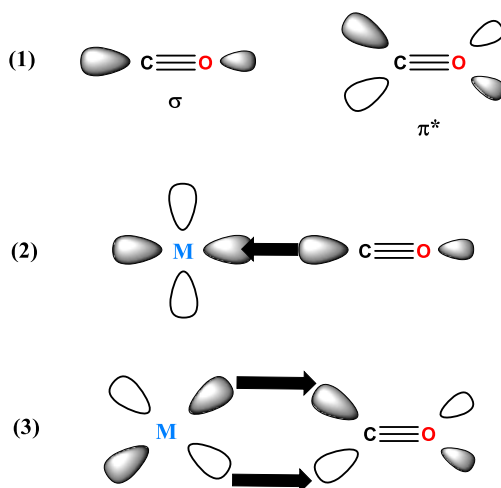


Figure 1.2. The highest-energy occupied molecular orbital (σ) and the lowest-energy unoccupied molecular orbital (π^*) for carbon monoxide (1); σ donation from the carbonyl ligand to the metal (2); and π back bonding from the metal to the carbonyl ligand (3).

The most important reactions of $\text{Mo}(\text{CO})_6$ are substitution reactions. The substitution may be activated by either heat or light. For example, for the octahedral complex $\text{Mo}(\text{CO})_6$, the reaction with another ligand may lead to a trisubstituted carbonyl (Figure 1.3). Subsequent substitutions by the incoming ligand always happen in the position *cis* relatively to the initial ligand, due to the better σ donor but poorer π acceptor property of the incoming ligand compared to the carbonyl ligand, resulting in an increase in the back bonding between the Mo atom and the carbonyl ligand *trans* to

Chapter 1

the incoming ligand. The substitution reactions rarely proceed further than $\text{Mo}(\text{CO})_3\text{L}_3$ because the electron density on the metal would be too great.

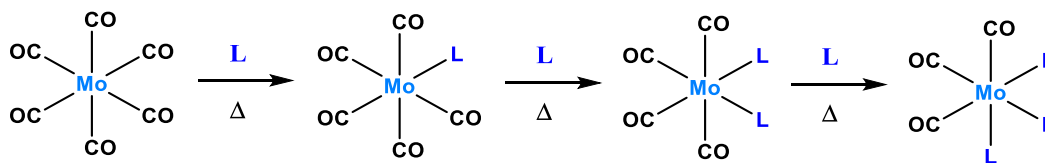


Figure 1.3. Reaction between $\text{Mo}(\text{CO})_6$ and a ligand until the formation of the trisubstituted carbonyl.

$\text{Mo}(\text{CO})_6$ is a common reagent in organometallic synthesis because one or more CO ligands can be displaced by other donor ligands, forming usually $[\text{Mo}(\text{CO})_{6-n}(\text{L})_n]$ ($n = 1-4$) complex. The synthesis method of molybdenum carbonyl complexes generally involves reaction between $\text{Mo}(\text{CO})_6$ and the organic ligand L as starting materials, with thermal activation or microwaves heating.^{49,50} Reaction by thermal activation in an inert atmosphere forms compounds with higher purity, but with low yields and long reaction times. Microwaves-assisted synthesis (in the absence of inert atmosphere) leads to high yields at short reaction times⁴², although the compounds are formed with lower purity.

The oxidative decarbonylation (OD) of molybdenum carbonyl complexes is a rewarding approach for the preparation of compounds containing Mo centers in high oxidation states. The OD synthetic chemistry is not limited to the formation of mononuclear and dinuclear complexes. Some of the more complex species formed include tetranuclear $[\text{Mo}_4\text{O}_{12}(\text{pypz})_4]$ from *cis*- $[\text{Mo}(\text{CO})_4(\text{pypz})]$ ($\text{pypz} = 2$ -[3(5)-pyrazolyl]pyridine)⁴², octanuclear $[\text{Mo}_8\text{O}_{24}(\text{di-}t\text{Bu-bipy})_4]$ containing a central cubane-type $\text{Mo}_4(\mu_3\text{-O})_4$ core from *cis*- $[\text{Mo}(\text{CO})_4(\text{di-}t\text{Bu-bipy})]$ ($\text{di-}t\text{Bu-bipy} = 4,4'$ -di-*tert*-butyl-2,2'-bipyridine)⁵¹, and the one-dimensional (1D) molybdenum oxide/bipyridine polymer $[\text{MoO}_3(2,2'\text{-bipy})]_n$ from *cis*- $[\text{Mo}(\text{CO})_4(2,2'\text{-bipy})]$ ($2,2'\text{-bipy} = 2,2'$ -bipyridine)⁵¹ as shown in Figure 1.4. The latter reaction is remarkable since it can be performed at ambient temperature with excess TBHP as the oxidant, and within a few hours, it leads to quantitative yield of the 1D polymer, which had only previously been obtained by the hydrothermal treatment of a mixture of MoO_3 , 2,2'-bipy and H_2O at 160 °C for at least 5 days.^{27,52}

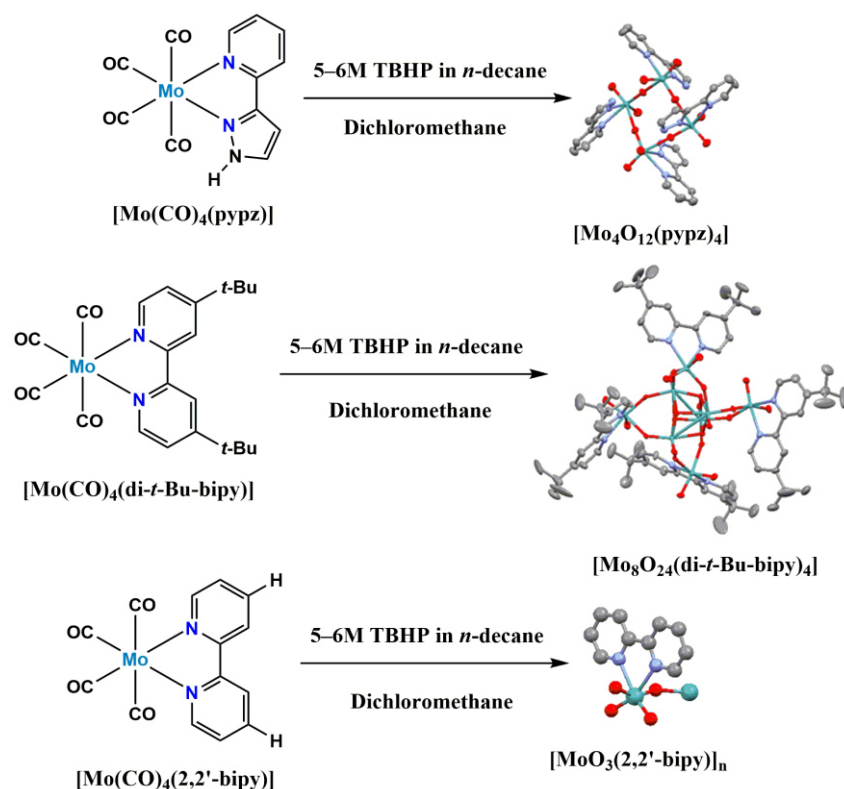


Figure 1.4. Oxidative decarbonylation of Mo carbonyl complexes $[\text{Mo}(\text{CO})_4(\text{pypz})]^{42}$, $[\text{Mo}(\text{CO})_4(\text{di-}t\text{-Bu-bipy})]^{53}$ and $[\text{Mo}(\text{CO})_4(2,2'\text{-bipy})]^{53}$ into the oxides compounds $[\text{Mo}_4\text{O}_{12}(\text{pypz})_4]$, $[\text{Mo}_8\text{O}_{24}(\text{di-}t\text{-Bu-bipy})_4]$ and $[\text{MoO}_3(2,2'\text{-bipy})]_n$ with Mo centers in high oxidation states (Mo - turquoise, O - red, C - dark grey, N - blue).

Cyclopentadienyl molybdenum carbonyls of the type $\text{CpMo}(\text{CO})_3\text{R}'$

As already referred previously, the oxidative decarbonylation of molybdenum carbonyl complexes is a very successful method to prepare Mo(VI) oxide compounds. During the last decade there has been increasing interest in the use of cyclopentadienyl molybdenum carbonyls of the type $[\text{Cp}'\text{Mo}(\text{CO})_3\text{X}]$ (Cp' = cyclopentadienyl ligand, X = halide, alkyl, alkyl ester, *ansa*-bridged alkyl or cycloalkyl group) as precatalysts for olefin epoxidation.^{54,55} Great variability by ligand modification (both on the Cp-ring and directly at the metal center) is possible, opening the way to immobilization^{56,57} and chirality introduction.^{58,59} Cyclopentadienyl complexes have deserved a large amount of attention and have been widely used in synthetic chemistry, among other reasons, because of their coordination versatility, which allows for haptotropic migrations from the η^5 coordination mode, to the η^3 , and finally to the η^1 one.^{60,61} As each of these shifts takes place, the donor capability of the ligand decreases by two units. Thus, a perfect η^5 coordination is found in most Cp complexes.⁶²

Chapter 1

For example, the oxidation of $\text{Cp}'\text{Mo}(\text{CO})_3\text{X}$ with TBHP gives molybdenum(VI) complexes of the type $[\text{Cp}'\text{MoO}_2\text{X}]$, $[\text{Cp}'\text{MoO}(\text{O}_2)\text{X}]$, $[(\text{Cp}'\text{MoO}_2)_2(\mu\text{-O})]$ and $[(\text{Cp}'\text{MoO}(\text{O}_2))_2(\mu\text{-O})]$ (Figure 1.5).^{63–71} A complete oxidative decarbonylation occurs *in situ* by reaction with the oxidant (usually TBHP or hydrogen peroxide), resulting in the formation of oxomolybdenum(VI) compounds ranging from mononuclear species such as CpMoO_2Cl from $\text{CpMo}(\text{CO})_3\text{Cl}$.⁶⁴

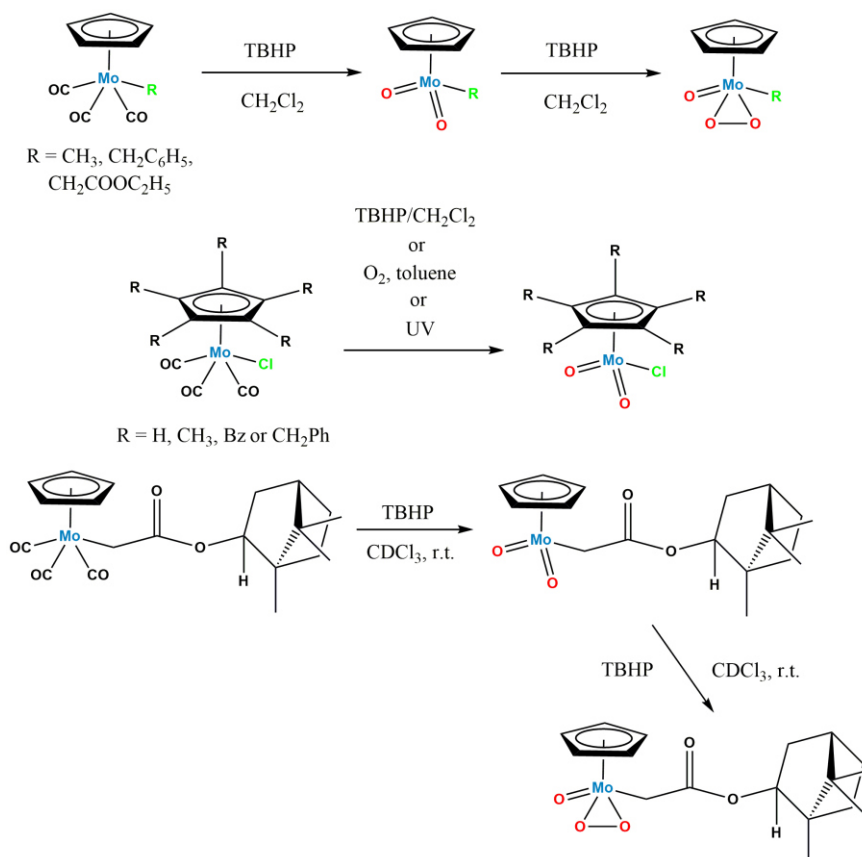


Figure 1.5. Oxidative decarbonylation of tricarbonyl complexes into dioxo and oxo-peroxo species.^{63,64,66–69,71}

Oxidomolybdenum structures containing halides of the type MoO_2X_2

The complexes with chemical formula $[\text{MoO}_2\text{X}_n]$ ($\text{X} = \text{F}, \text{Cl}, \text{Br}, \text{alkyl}, \text{OR}, \text{OSiR}_3, \text{SCN}$)^{72–75} are well known due to their performances as molybdoenzyme models, oxo-transfer reagents, and catalysts for the epoxidation of olefins.^{16,76} The first oxo-metal molecular fragment was described by J. J. Berzelius in 1826, identified as dichlorodioxomolybdenum(VI), MoO_2Cl_2 .^{16,76} Today, the MoO_2Cl_2 compound is easily commercially available. The MoO_2Cl_2 structure consists of a distorted tetrahedral arrangement of the chloride and oxygen ligands around the molybdenum atom.⁷⁷ The

Chapter 1

structure and chemical environment of $[\text{MoO}_2\text{Cl}_2]$ make this precursor able to coordinate with several types of Lewis base organic ligands around Mo, forming a hexacoordinated complexes of general formula $[\text{MoO}_2\text{Cl}_2(\text{L})_n]$, where L is a mono- ($n = 2$) or bidentate ($n = 1$) ligand.⁷⁸ One interesting example of transformations of a dichlorodioxomolybdenum(VI) into oxide complexes was reported by Amarante *et al.*⁷⁹, using $[\text{MoO}_2\text{Cl}_2(\text{pypz})]$ as precursor (Figure 1.6). The reaction of this complex with water in an open reflux system (16 h), using microwaves heating (120 °C, 2 h), or in a Teflon-lined stainless steel digestion bomb (100 °C, 19 h) gave the molybdenum oxide/pyrazolylpyridine polymeric hybrid material $[\text{Mo}_3\text{O}_9(\text{pypz})]_n$ (yields of 72–79 %). This oxide compound can also be obtained by the hydrothermal reaction of MoO_3 , pypz, and H_2O at 160 °C for 3 days. However, secondary products were isolated from the reaction solutions: the salt $(\text{pypz})_2(\text{MoCl}_4)$ and the tetranuclear compound $[\text{Mo}_4\text{O}_{12}(\text{pypz})_4]$. Also, the reaction of $[\text{Mo}_3\text{O}_9(\text{pypz})]_n$ with excess TBHP led to the isolation of the oxodiperoxo complex $[\text{MoO}(\text{O}_2)_2(\text{pzpy})]$.

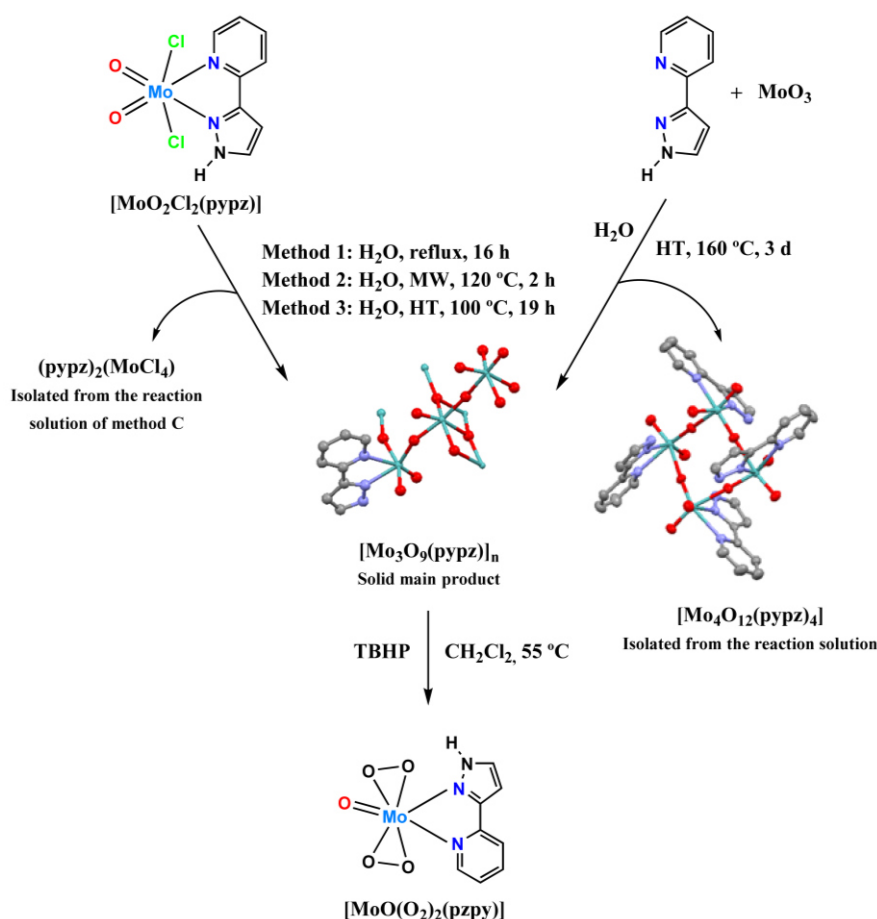


Figure 1.6. Synthesis of oxide compounds $\text{Mo}_3\text{O}_9(\text{pypz})_n$ and $[\text{Mo}_4\text{O}_{12}(\text{pypz})_4]$ starting from the dioxomolybdenum(VI) complex $[\text{MoO}_2\text{Cl}_2(\text{pypz})]$ (Mo - turquoise, O - red, C - dark grey, N - blue).⁷⁹

Chapter 1

Molybdates oxoanions of the type $[MoO_4]^{2-}$ and $[Mo_8O_{26}]^{4-}$

Because of the variety of shapes and sizes, highly negative charges, oxo-enriched surfaces, and solubility in organic solvents, the utilization of polyoxometalates (POMs) in the construction of organic-inorganic hybrid materials has allowed access to 1D-chains, 2D-layers and 3D-extended frameworks with new physical properties. Polyoxometalates can be defined as molecular metal oxides formed through condensation reactions of early transition metal–oxygen anions, typically with metals such as W, Mo, V, etc., in their highest oxidation state.^{80,81} POMs have great versatility and possible applications range across fields from medicine to catalysis^{82,83}. POMs chemistry is a modern science with a long and successful history, for which the number of publications has massively increased over the last 25 years. Not surprisingly, anionic POMs exhibiting strong acceptor features have been widely applied in preparing charge transfer salts with organic cation donors.^{84–86}

In solution, sodium molybdate forms molybdate oxoanions, $[MoO_4]^{2-}$, which are frequently used as commercially available starting materials for the synthesis of dioxomolybdenum(VI) hybrid materials containing organic ligands with N,N'-donor atoms.⁴⁶ The crystalline structure of $[MoO_4]^{2-}$ is tetrahedral and the anion can usually be transformed by condensation at lower pH values into wide range of other polyanion structures.^{87,88} The second smaller oxoanionic structure contains tetrahedral $Mo_2O_7^{2-}$ core centres, in which the two tetrahedra are sharing a corner through a single bridge established by an oxygen atom. More extensive molybdate oxoanions can be formed in which the environment becomes more complex. If the structures of molybdenum anions is larger than $Mo_8O_{26}^{4-}$, these structures contain octahedral and tetrahedral molybdenum environments and can also be isolated in α and β isomeric forms.^{89,90} The structures containing the larger molybdenum anions can coordinate generally, but not exclusively, 6 oxygen atoms with edges or vertices of the $[MoO_6]^{6-}$ octahedra being shared.

Amongst the manifold of polyoxomolybdate structures, the octamolybdate $[Mo_8O_{26}]^{4-}$ is known for its stability, and therefore observed quite often. $[Mo_8O_{26}]^{4-}$ based salts are types of cheap and easily prepared POM materials compared to the well-established Keggin type POM catalyst $[PMo_{12}O_{40}]^{3-}$ based salt.^{91–93} The published synthetic procedure for some hybrid polyoxometalate compounds starts with the synthesis of tetrabutylammonium (TBA) octamolybdate $(TBA)_4[\alpha-Mo_8O_{26}]$ from $Na_2MoO_4 \cdot 2H_2O$.^{89,94} $[Mo_8O_{26}]^{4-}$ has been described to occur with as much as eight isomeric forms that have been isolated, *i.e.*, α -, β -, γ -, δ -, ϵ -, ζ -, η - and θ -isomers, with the most common being the α - and β -forms.^{94,95} The structural diversity of POMs is

Chapter 1

often based on characteristic large building units, e.g. the $[\text{Mo}_8\text{O}_{26}]^{4-}$ octamolybdate anion, that are interconnected by different linkers to allow for a wide range of novel structural motifs, ranging from closed cages to basket-, bowl-, barrel-, and belt-shaped building units.^{96–98} Moreover, there has been growing interest in introducing ligands that allow for conformational flexibility.^{99–101} The combination of POMs as building blocks with such flexible linkers, has already given rise to a novel class of open framework structures.^{102,103} For example, the $[\alpha\text{-Mo}_8\text{O}_{26}]^{4-}$ building unit exhibits a center of inversion, resulting in only four crystallographically independent Mo sites. In sum, the molybdate cage is constituted by six (MoO_6) -octahedra and two (MoO_4) -tetrahedra.¹⁰⁴ The octahedra are corner- as well as edge-sharing, whereas the tetrahedra are only connected via joint corners, and exclusively to (MoO_6) -octahedra. The $[\alpha\text{-Mo}_8\text{O}_{26}]^{4-}$ unity is shaped like a distorted cube-octahedron, in which the six-valent molybdenum atoms of the molybdate cage are bound to 10 terminal, 10 doubly bridging and six triply bridging oxygen atoms.¹⁰⁵ Infrared and Raman vibrational spectroscopy is usually used to clarify the structure of the $[\text{Mo}_8\text{O}_{26}]^{4-}$ anions; the FT-IR and FT-Raman spectra of the compounds should exhibit several characteristic Mo–O stretching bands in the region of 700–1000 and 900–1000 cm^{-1} , respectively.^{106,107}

Molybdenum trioxide

Molybdenum trioxide is possibly the most used precursor for the preparation of molybdenum(VI) oxides, since it is easily available for a relatively low cost from commercial sources. In the gas phase, the structure of MoO_3 presents three oxygen atoms double bonded to the central molybdenum atom. In the solid state, MoO_3 is formed by layers of linked distorted MoO_6 octahedra in an orthorhombic crystal. The MoO_6 octahedra share edges and form chains that are cross-linked by oxygen atoms to form the layers where the octahedra are bonded through a molybdenum-oxygen bond to a non-bridging oxygen, resulting in a three-dimensional network.

In view of these transformations, Zubieta and co-workers^{27,108} have investigated the syntheses and structural characterization of a series of inorganic/organic hybrid materials incorporating 2,2'-bipyridine components as ligands, represented by three members of the new family of materials $[(\text{MoO}_3)_n(2,2'\text{-bipy})_m]$: $[\text{MoO}_3(2,2'\text{-bipy})]_n$, $[\text{Mo}_2\text{O}_6(2,2'\text{-bipy})]_n$, and $[\text{Mo}_3\text{O}_9(2,2'\text{-bipy})_2]_n$ (Figure 1.7). The reaction of MoO_3 , 2,2'-bipyridine, and H_2O in the mole ratio 1:0.68:680 at 160 °C for 120 h in a 23 mL Teflon-lined Parr acid digestion bomb produced colourless rods of $[\text{MoO}_3(2,2'\text{-bipy})]_n$ mixed with colourless octahedra of $[\text{Mo}_3\text{O}_9(2,2'\text{-bipy})_2]_n$. The structure of $[\text{MoO}_3(2,2'\text{-bipy})]_n$ consists of one-dimensional chains of corner-sharing distorted $\{\text{MoO}_4\text{N}_2\}$ octahedra.

Chapter 1

$[\text{Mo}_2\text{O}_6(2,2'\text{-bipy})]_n$ was prepared from a mixture of $\text{Na}_2\text{MoO}_4 \cdot 2\text{H}_2\text{O}$, MoO_3 , 2,2'-bipyridine, $\text{MnCl}_2 \cdot 4\text{H}_2\text{O}$, and H_2O in the mole ratio 1:1:2:1.9:263 and was isolated as colourless plates. In contrast to the structure of $[\text{MoO}_3(2,2'\text{-bipy})]_n$, compound $[\text{Mo}_2\text{O}_6(2,2'\text{-bipy})]_n$ consists of a chain of alternating corner-sharing $\{\text{MoO}_4\text{N}_2\}$ octahedra and $\{\text{MoO}_4\}$ tetrahedra. The structure of $[\text{Mo}_3\text{O}_9(2,2'\text{-bipy})_2]_n$ consists of a chain of corner-sharing $\{\text{MoO}_4\text{N}_2\}$ octahedra and $\{\text{MoO}_4\}$ tetrahedra that alternate such that each $\{\text{MoO}_4\text{N}_2\}$ octahedron corner-shares with another such octahedron and a $\{\text{MoO}_4\}$ tetrahedron; consequently, each $\{\text{MoO}_4\}$ unit corner-shares with two $\{\text{MoO}_4\text{N}_2\}$ octahedra.

Posteriorly, the author has described the chemistry of 1,2,3-triazole/molybdate system. Hydrothermal reactions of MoO_3 in the presence of 1,2,3-triazole (1,2,3-trz) gave the compound $[\text{MoO}_3(1,2,3\text{-trz})_{0.5}]$.

Amarante *et al.*¹⁰⁹ have shown that the reaction between MoO_3 , 2,2'-bipyridine-5,5-dicarboxylic acid (H_2bpdC), water, and dimethylformamide in the mole ratio 1:1:1730:130 at 150 °C for 3 days in a rotating Teflon-lined digestion bomb leads to the isolation of the molybdenum oxide/bipyridinedicarboxylate hybrid material $(\text{DMA})[\text{MoO}_3(\text{HbpdC})] \cdot n\text{H}_2\text{O}$ (DMA = dimethylammonium).

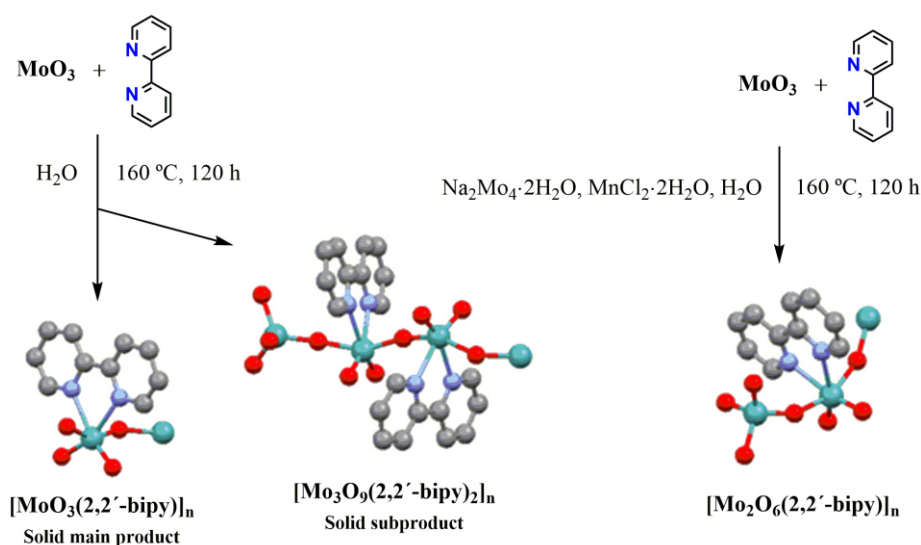


Figure 1.7. Schematic representation of the synthesis of the materials $[\text{MoO}_3(2,2'\text{-bipy})]_n$, $[\text{Mo}_2\text{O}_6(2,2'\text{-bipy})]_n$, and $[\text{Mo}_3\text{O}_9(2,2'\text{-bipy})_2]_n$ using MoO_3 as precursor.^{27,108}

Chapter 1

1.1.4. Preparation methods for oxomolybdenum(VI) compounds

Discrete complexes

Discrete complexes include mono- and dinuclear structures of oxomolybdenum(VI) hybrid materials. Their preparations are usually carried out by dissolution at ambient temperature of the precursors, or reflux of Mo(VI) precursors, in aprotic solvents, and stirring for several hours.

Frequently, for the formation of mononuclear compounds, $[\text{MoO}_2\text{Cl}_2]$ is used as precursor, and the synthesis is based on two steps (Figure 1.8). First, an *in situ* step reaction occurs via ligand addition in a selected solvent (*e.g.*, THF, DMSO, DMF, CH_3CN), forming the $\text{MoO}_2\text{Cl}_2(\text{solvent})_2$ complex. This intermediate complex reacts easily with a Lewis base ligand in order to give more stable complexes via solvent substitution.⁴⁵ In the second step, the solvent ligand leaves the coordination sphere, followed by the Lewis base ligand addition to the Mo atom. For $[\text{MoO}_2\text{Cl}_2\text{L}]$ complexes, where L = bidentate chelating N,N'-donor ligands, their formation are usually nearly quantitative at ambient temperature within a few minutes of reaction.¹¹⁰ These types of precursors display the advantages of the two different ligands X and L that can be easily varied in order to improve the coordination sphere of the Mo(VI) center.

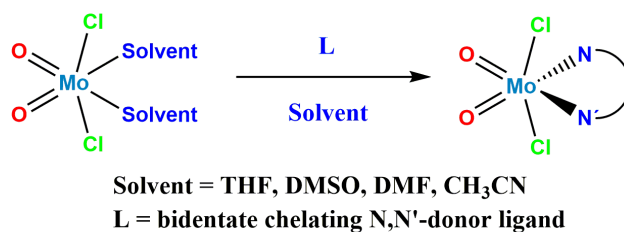


Figure 1.8. Formation of a $[\text{MoO}_2\text{Cl}_2(\text{N},\text{N}'\text{-L})]$ complex by the solvent substitution reaction with a Lewis base ligand addition.

The first dinuclear structure was synthesized by Arzoumanian *et al.*¹¹¹, consisting of a thiocyanatomolybdenum(VI) dioxo- μ -oxo complex with di-*t*Bu-bipy as N,N-chelating ligand: $[\text{Mo}_2\text{O}_5(\text{NCS})_2(\text{di-}t\text{Bu-bipy})_2]$. Gonçalves and co-workers¹⁵ were the first to obtain crystals of a dinuclear structure with two chloro ligands; crystals of $[\text{Mo}_2\text{O}_4\text{Cl}_2(\text{pypz})]$ were isolated via slow diffusion of diethyl ether in an acetonitrile solution containing $[\text{MoO}_2\text{Cl}_2(\text{pypz})]$.

Chapter 1

Organic-inorganic hybrid materials

Oxomolybdenum(VI) hybrid materials with N,N'-donor ligands are typically prepared by hydrothermal synthesis. The hydrothermal method is usually carried out at high temperature in the range of 120-260 °C and under autogenous pressure, with aqueous solutions containing the organic ligand and the Mo precursor, which is commonly MoO₃, Na₂MoO₄, or less commonly (NH₄)₆Mo₇O₂₄. The main advantage of the hydrothermal synthesis is the formation of crystalline compounds, since under autogenous pressure the water viscosity is reduced and the diffusion processes are favoured promoting crystal growth.¹¹² The technique of hydrothermal synthesis, in combination with the structure directing properties of the organic ligands, proved to be one step closer for the isolation of metastable inorganic-organic hybrids that retain the structural elements of the synthetic precursors. However, the disadvantages of this method are i) lower yields, ii) mixtures of phases in some cases, requiring mechanical separation, and iii) formation of other products when small changes in one or more of the reaction parameters occurs, *e.g.* stoichiometry, time, temperature and pH.³

Gonçalves and co-workers have been exploring alternative approaches that use stable and easily storable mononuclear molybdenum complexes as single-source molecular precursors. The group found that the oxidative decarbonylation of the tetracarbonyl complexes [Mo(CO)₄(L)] (L = 2,2'-bipy, pypz) by reaction with TBHP at room temperature gives microcrystalline [MoO₃(2,2'-bipy)] and [Mo₄O₁₂(pypz)₄] in excellent yields.^{42,51}

The hydrolysis and condensation of complexes of the type [MoO₂Cl₂L] is another potentially interesting route to molybdenum oxide/organic hybrids. This approach borrows concepts from sol-gel chemistry, *i.e.*, hydrolysis of a metal chloride bond in a molecular precursor to give reactive M-OH species that condense through oxolation and/or ololation reactions to give metal-oxo clusters, oligomers, and polymers assembled via M-O-M and/or M-OH-M bridges.¹¹³ Gonçalves and co-workers¹¹⁴ found that the reaction of [MoO₂Cl₂(2,2'-bipy)] with water at 100-120 °C gives the molybdenum oxide/bipyridine material {[MoO₃(2,2'-bipy)][MoO₃(H₂O)]}_n with a crystal structure containing 1D inorganic and inorganic/organic hybrid polymers linked by O-H...O hydrogen bonds. In this study, the reaction of [MoO₂Cl₂(2,2'-bipy)] with water was carried out either hydrothermally in a sealed Teflon-lined stainless steel digestion bomb (autogenous pressure, 100 °C, 19 h), in an open reflux system under air (12 h, oil bath heating), or in a sealed glass vessel with microwave-assisted heating (120 °C, 4 h). The yields of {[MoO₃(2,2'-bipy)][MoO₃(H₂O)]}_n were 72 % for the hydrothermal method and 91-92 % for the microwave-assisted and reflux methods.

Chapter 1

A similar treatment of $[\text{MoO}_2\text{Cl}_2(\text{di-}t\text{Bu-bipy})]$ gives octanuclear $[\text{Mo}_8\text{O}_{22}(\text{OH})_4(\text{di-}t\text{Bu-bipy})_4]$ with a structure that comprises a purely inorganic core, $\text{Mo}_4(\mu_3\text{-OH})_2\text{O}_8(\mu_2\text{-O})_2$, attached to two peripheral oxo-bridged binuclear units, $\text{Mo}_2\text{O}_4(\mu_2\text{-O})_2(\text{OH})(\text{di-}t\text{Bu-bipy})$.¹¹⁵

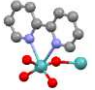

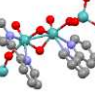
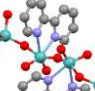
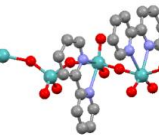
A literature search on polymeric structures containing the *cis*- MoO_2^{2+} core and N,N-chelating ligands revealed a massive range of publications. Polymeric structures based on chains of oxomolybdenum(VI) polyhedra are generally characteristic of dimolybdate $\{[\text{Mo}_2\text{O}_7]^{2-}\}$, e.g. $\text{Na}_2[\text{Mo}_2\text{O}_7]$,¹¹⁶ trimolybdate $\{[\text{Mo}_3\text{O}_{10}]^{2-}\}$, e.g. $[\text{H}_3\text{NCH}_2\text{CH}_2\text{NH}_3][\text{Mo}_3\text{O}_{10}]$,¹¹⁷ and tetramolybdate systems. The structures of these polymers has in common the occurrence of edge-sharing between adjacent polyhedra as part of their structural pattern.¹¹⁸ However, there were some differences in their polyhedral connectivities promoted by the effects of the cations.

Polymeric oxomolybdenum(VI) compounds containing N,N-chelating ligands coordinated directly to the Mo atom share the same type of 1D backbone between them, but possess structural differences between adjacent polyhedra, establishing generally corner-sharing linkages. Zubieta *et al.*¹¹⁸ have attributed this phenomenon to the presence of the ligand which passivates the molybdenum oxide coordination sphere by blocking more Mo–oxo bond formation, and consequently limiting the polymeric growth to corner-sharing linkages.

The polymers are frequently constructed from alternating sequences of one, two or three $\{\text{MoO}_4\text{N}_2\}$ corner-sharing octahedra (O) with one $\{\text{MoO}_4\}$ tetrahedron (T). For example, for the family of polymers containing the 2,2'-bipy ligand (Table 1.1): $[\text{Mo}_2\text{O}_6(\text{bipy})]_n$ presents a –O–T–O–T–O– distribution with alternating sequences of one $\{\text{MoO}_4\text{N}_2\}$ corner-sharing octahedron; $[\text{Mo}_3\text{O}_9(2,2'\text{-bipy})_2]_n$ has a –T–O–O–T–O–O–T– distribution of two alternated $\{\text{MoO}_4\text{N}_2\}$ corner-sharing octahedra; and $[\text{Mo}_4\text{O}_{12}(\text{bipy})_3]_n$ presents –T–O–O–O–T– distribution of three alternated $\{\text{MoO}_4\text{N}_2\}$ corner-sharing octahedra. As exceptions, $[\text{MoO}_3(2,2'\text{-bipy})]_n$ is constructed from only $\{\text{MoO}_4\text{N}_2\}$ corner-sharing octahedral motifs –O–O–, and $[\text{Mo}_3\text{O}_8(2,2'\text{-bipy})_2]_n$ is composed of binuclear units of edge-sharing $\{\text{MoO}_4\text{N}_2\}$ octahedra linked by $\{\text{MoO}_4\}$ tetrahedra through corner-sharing –T–(O–O)–T–(O–O)–T–.

Chapter 1

Table 1.1. Structural sequence present in the polymeric compounds $[\text{MoO}_3(2,2'\text{-bipy})]_n$, $[\text{Mo}_2\text{O}_6(2,2'\text{-bipy})]_n$, $[\text{Mo}_3\text{O}_8(2,2'\text{-bipy})_2]_n$, $[\text{Mo}_3\text{O}_9(2,2'\text{-bipy})_2]_n$ and $[\text{Mo}_4\text{O}_{12}(2,2'\text{-bipy})_3]_n$ (O = octahedron and T = tetrahedron; Mo - turquoise, O - red, C - dark grey, N - blue).

Compound	Polymeric structure	Structural sequence	Ref.
$[\text{MoO}_3(2,2'\text{-bipy})]_n$		-O-O-	118
$[\text{Mo}_2\text{O}_6(2,2'\text{-bipy})]_n$		-O-T-O-T-O-	118
$[\text{Mo}_3\text{O}_8(2,2'\text{-bipy})_2]_n$		-T-(O-O)-T-(O-O)-T-	29
$[\text{Mo}_3\text{O}_9(2,2'\text{-bipy})_2]_n$		-T-O-O-T-O-O-T-	118
$[\text{Mo}_4\text{O}_{12}(2,2'\text{-bipy})_3]_n$		-T-O-O-O-T-	28

1.1.5. An overview about the application of the oxomolybdenum(VI) compounds as (pre)catalysts for organic reactions: epoxidation of olefins and acid catalysis

Organic reactions catalyzed by molecular transition metal compounds continues to be a topic of considerable academic and industrial interest.^{124,144} Several industrial processes such as ammoxidation of propene to acrylonitrile, olefin epoxidation, and olefin metathesis reactions are carried out over molybdenum catalysts. The molybdenum(VI) oxides, based on *cis*- MoO_2^{2+} core with N-donor ligands have assumed an increasing level of attention in recent years, in particular because of their roles as catalysts for organic reactions such as the oxidation of sulfides¹¹⁹, alcohols^{120,121} and amines¹²², the epoxidation of olefins and the *cis*-dehydroxylation of olefins^{54,123,124} (Figure 1.9). The well-known industrial example is the Arco-Lyondel or Oxirane process for the epoxidation of propene using $\text{Mo}(\text{CO})_6$ as a precursor, which is oxidized *in situ* by the oxidant TBHP in the homogeneous phase to give the active *cis*-dioxo Mo(VI) catalyst.^{125,145}

Epoxides are important organic intermediates, commonly synthesized from olefins, with patented technologies including the use of homogeneous Mo(VI) catalysts.¹²⁵⁻¹²⁷ Epoxides can be used as intermediates and precursors in the synthesis

Chapter 1

of paints, epoxy resins, surfactants, polymer and pharmaceuticals.¹²⁴ Epoxides can undergo ring-opening reactions in the presence of acid catalysts to give a plethora of useful intermediates and products for the fine chemicals industry.^{128–130} Commonly used Lewis acid catalysts such as metal halide salts present numerous drawbacks such as corrosion problems, fast deactivation, the production of large volumes of acidic waste, and the need for high catalyst/substrate ratios. Hence, there is much interest in the development of novel reaction processes catalysed by highly active and highly selective Lewis acids, such as Mo(VI) compounds, that significantly reduce acidic wastes and increase the product selectivities. The catalytic performances may be improved through ligand exchange and/or functionalization.^{131–133} Molybdenum-based catalysts are especially attractive due to the ready availability and relatively low cost of this element.

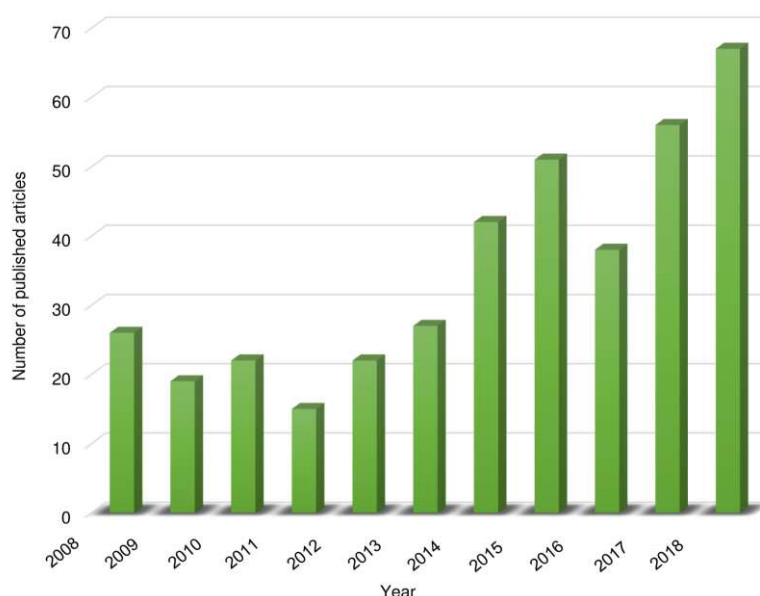


Figure 1.9. Number of published articles during the period of 2008 to 2018 related to molybdenum oxides applied in catalysis. The search output gave 385 results in the database Scopus using the keywords: “molybdenum oxide and catalysis”.

Recently, Amarante *et al.*¹³⁴ have describe a new type of self-separating catalyst based on a molybdenum oxide hybrid material. The material $[\text{MoO}_3(1,2,4\text{-trz})_{0.5}]$ (trz = triazole), which was first reported by Zubieta and co-workers¹³⁵, was synthesized and tested as catalyst for olefin epoxidation with H_2O_2 as oxidant (Table 1.2, entry 1). These results were outstanding, since depending on the structure and composition of these hybrids, as well as the catalytic reaction conditions, the materials typically act either as sources of soluble active species or (more rarely) as

Chapter 1

heterogeneous catalysts. For example, when the materials $[\text{Mo}_2\text{O}_6(\text{ppp})]$ ($\text{ppp} = 2\text{-}(1\text{-pentyl-3-pyrazolyl})\text{pyridine}$)¹⁶, $[\text{Mo}_3\text{O}_9(\text{pypz})]$ ⁷⁹ and $[\text{MO}_3(2,2'\text{-bipy})]_n$ ($M = \text{Mo}, \text{W}$)¹³⁶ are used in catalytic olefin epoxidation with either TBHP or hydrogen peroxide as oxidant, they are irreversibly converted into soluble oxodiperoxo complexes of the type $[\text{MO}(\text{O}_2)_2(\text{L})]$, which are responsible for the homogeneous catalytic reaction of the olefin. The efficient recovery and reuse of these complexes is not trivial, typically requiring precipitation with organic solvents. Thus, in the research carried out by Amarante using $[\text{MoO}_3(1,2,4\text{-trz})_{0.5}]$, a solid–liquid–solid phase transfer takes place, with spontaneous reassembly and self-precipitation of the original molybdenum oxide-triazole solid upon completion of the reaction.

Antunes *et al.*¹³⁷ have tested the hybrid material $[\text{MoO}_3(1,2,4\text{-trz})_{0.5}]$ as an acid catalyst for the methanolysis of styrene oxide (StyOx) at 35 °C (Table 1.2, entry 1). The conversion for this reaction was 60 % at 6 h and 100 % at 24 h. An initial induction period of 30 min was observed which may be partly due to poor solubility and slow dissolution of the metal species. This hypothesis was supported by measuring the mass of undissolved solid for this system after stirring for 1 h at 35 °C, obtaining >97 wt % of the recovered solid.

The use of molybdenum carbonyl complexes as precursors to molybdenum(VI) catalysts for the epoxidation of olefins has been intensively researched since 2003, when Abrantes *et al.*⁶⁴ reported that highly active $[(\eta^5\text{-C}_5\text{R}_5)\text{MoO}_2\text{Cl}]$ catalysts ($R = \text{H}, \text{CH}_3, \text{Bz}$) ($\text{Bz} = \text{benzyl}$) could be generated *in situ* by reaction of the tricarbonyl complexes $[(\eta^5\text{-C}_5\text{R}_5)\text{Mo}(\text{CO})_3\text{Cl}]$ with TBHP as oxidant. The authors have shown that $[\text{CpMoO}_2\text{Cl}]$ complexes can be easily obtained from carbonyl precursors by oxidation with TBHP in yields up to 75 %. The use of $[\text{CpMo}(\text{CO})_3\text{Cl}]$ ($\text{Cp} = \eta^5\text{-C}_5\text{H}_5$) for catalytic oxidation with TBHP, has led to similar results as those obtained using complex $[\text{CpMoO}_2\text{Cl}]$. The carbonyl precursor was oxidized into the oxide and used as a catalyst for olefin epoxidation with the same oxidant. During this oxidation process the ligands Cp and Cl remained attached to the metal.

Based on catalytic activities obtained for the epoxidation of *cis*-cyclooctene (Cy, used as a benchmark substrate), other $[\text{CpMo}(\text{CO})_3\text{R}']$ complexes stand out as precatalysts: the *ansa*-complex $[\text{Mo}(\eta^5\text{-C}_5\text{H}_4(\text{CH}(\text{CH}_2)_3)\text{-}\eta^1\text{-CH})(\text{CO})_3]$ ¹⁴⁶ (with a room temperature ionic liquid as a solvent) (Table 1.2, entry 2), and the fluorinated complex $[\text{CpMo}(\text{CO})_3\text{CF}_3]$ ¹⁴⁷ (with hexafluoroisopropanol as a solvent) (Table 1.2, entry 3). These tricarbonyl complexes undergo oxidative decarbonylation *in situ* by reaction with TBHP, forming catalytically active Mo-oxo ($[\text{Cp}'\text{MoO}_2\text{X}]$) and Mo-oxo-peroxo, ($[\text{Cp}'\text{MoO}(\eta^2\text{-O}_2)\text{X}]$) species. More complex species may also be formed as in the analogous oxidation of $[(\text{CpBz}_5)\text{Mo}(\text{CO})_3\text{Me}]$ that gives $[\{\text{Mo}(\text{CpBz}_5)(\text{O}_2)\}_2(\mu\text{-O})]$.⁶⁵

Chapter 1

However, the carbonyl complexes are more stable than the dioxo complexes, and therefore can be used directly as easily storable forms of catalyst precursors.⁶⁴ In fact, the carbonyl compounds lead to similar turnover frequencies (TOF) as the oxides for olefin epoxidation with TBHP.⁶⁴ Computational studies support a mechanism in which active intermediates of the type $[\text{Cp}'\text{MoO}(\text{OH})(\text{OO}^t\text{Bu})\text{X}]$ and $[\text{Cp}'\text{Mo}(\eta^2\text{-O}_2)(\text{OH})(\text{OO}^t\text{Bu})\text{X}]$ are formed by reaction of the respective Mo-oxo and Mo-oxo-peroxo complexes with excess of TBHP.^{68,148}

Kühn and co-workers¹⁴⁹ reported high reaction rates using carbonyl complexes of the type $[\text{CpM}(\text{CO})_3\text{R}]$ (M= Mo, W; R = alkyl), with TOFs up to ca. 6000 h^{-1} and TON greater than 50, and good epoxide selectivity (Table 1.2, entry 5). The carbonyl compounds were *in situ* oxidized by TBHP and transformed to catalytically active species, consisting of $[\text{CpMoO}(\text{O}_2)\text{R}]$ type complexes, without loss of the Cp- and R-ligands. Molybdenum complexes were far more active than tungsten compounds, and increasing alkylation of the Cp ligand lowers the catalytic activity. The catalysts lost activity after several runs, possibly due to accumulation of the by-product *t*-BuOH, which may compete with TBHP in the coordination to the metal center.

Posteriorly, several studies were carried out in order to verify the ligand effects on the Lewis acidity of the metal center for $[\text{CpMo}(\text{CO})_3\text{R}]$ precatalysts.⁶⁹ The R ligands were alkyl moieties of the type $-\text{CHR}^2-\text{COOR}^1$ (R^1 = ethyl, menthyl, and bornyl, R^2 = H; R^1 = ethyl, R^2 = methyl and phenyl). Compared to the inductive effect of the chloro (electron-withdrawing) and the methyl (electron-donating) group in complexes $[\text{CpMo}(\text{CO})_3\text{Cl}]$ and $[\text{CpMo}(\text{CO})_3(\text{CH}_3)]$, respectively, the alkyl ester group renders the metal center more electron deficient than the methyl substituent but less than the chloro substituent. The alkyl ester complexes were designed to be less active than the chloro and methyl analogues.

In a study reported by Bruno *et al.*¹⁵⁰, the cyclopentadienyl molybdenum carbonyl complexes $[(\eta^5\text{-C}_5\text{H}_5)\text{Mo}(\text{CO})_3(\text{CH}_2\text{R})]$ (R = H, COOH) promoted acid-catalysed reactions in liquid phase, under moderate conditions (Table 1.2, entry 4). The catalytic alcoholysis of styrene oxide with ethanol at $35 \text{ }^\circ\text{C}$ gave 2-ethoxy-2-phenylethanol in 100 % yield within 3-6 h for the tricarbonyl complexes. Steady catalytic performances were observed in consecutive runs with the same catalytic solution, suggesting fairly good catalytic stability. In the second acid-catalysed reaction studied, the isomerization of α -pinene oxide at $55 \text{ }^\circ\text{C}$ gave campholenic aldehyde and *trans*-carveol in a total yield of up to 86 % at 100 % conversion. Chemoselectivity was shown to be solvent dependent.

Posteriorly, Gomes *et al.*¹⁵¹ studied the catalytic performance of the complex $[\text{MoO}_2\text{Cl}_2(\text{di-}t\text{Bu-bipy})]$ in the ethanolysis of styrene oxide under mild conditions (Table

Chapter 1

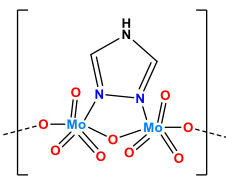
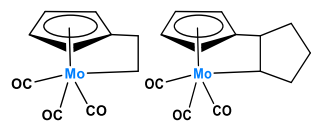
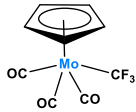
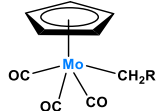
1.2, entry 6). Good results were obtained for the acid-catalysed reaction with good selectivity towards the target product 2-ethoxy-2-phenylethanol. In the presence of styrene oxide, the complex undergoes a transformation to the octanuclear complex $[\text{Mo}_8\text{O}_{24}(\text{di-}t\text{Bu-bipy})_4]$. In separate assays, $[\text{Mo}_8\text{O}_{24}(\text{di-}t\text{Bu-bipy})_4]$ catalysed the ethanolysis of styrene oxide with high activity and selectivity, and could be recovered unchanged at the end of the reaction.

The type of ligand can also influence the catalytic activity of the molybdenum complexes. For example, a family of ligands that have led to effective molecular catalysts of the type $[\text{MoO}_2\text{X}_2(\text{L})]$ ($\text{X} = \text{Cl}, \text{Br}$) for olefin epoxidation are poly(azol-1-yl)alkanes such as bis(pyrazolyl)methanes, tris(pyrazolyl)methanes and tris(benzimidazolyl)methane (Table 1.2, entry 9).^{75,157,158} Santos *et al.* have reported¹⁵⁷ the synthesis and characterization of molybdenum(VI) dioxo complexes bearing poly(pyrazolyl)borate and poly(pyrazolyl)methane ligands, as well as $[\text{MoO}_2\text{Cl}_2\{(3,5\text{-Me}_2\text{pz})_2\}]$ ($3,5\text{-Me}_2\text{pz} = 3,5\text{-dimethylpyrazolyl}$). The presence of these relatively weakly coordinating ligands in the complexes positively influenced the catalytic epoxidation activity.

The β -octamolybdate salts bearing quaternary ammonium cations have been reported as highly active catalysts for oxidation reactions.^{106,152–155} While comparing to the well-established Keggin type POM catalysts $[\text{PM}_{12}\text{O}_{40}]^{3-}$ ($\text{M} = \text{W}$ or Mo), β -octamolybdate is advantageous since it is cheaper, more stable and easier to prepare. The simple organic octamolybdate salts bearing a quaternary ammonium cation have also been reported as highly active catalysts for oxidation reactions.^{154,155} Zhou *et al.*¹⁰⁶ have reported good catalyst recycling for olefin epoxidations using 30 % aqueous hydrogen peroxide as oxidant and alkylimidazolium or alkylpyridinium octamolybdates as catalysts. $[\text{Mo}_8\text{O}_{26}]^{4-}$ based organic polyoxomolybdate salts of general formula $[\text{Hmim}]_4\text{Mo}_8\text{O}_{26}$ ($\text{Hmim} = 1\text{-hexyl-3-methylimidazolium}$), $[\text{Dhmim}]_4\text{Mo}_8\text{O}_{26}$ ($\text{Dhmim} = 1,2\text{-dimethyl-3-hexylimidazolium}$) and $[\text{Hpy}]_4\text{Mo}_8\text{O}_{26}\cdot\text{H}_2\text{O}$ ($\text{Hpy} = 1\text{-hexylpyridinium}$) exhibited excellent catalytic performance and were also self-separating, which is a great advantage for catalyst recycling (Table 1.2, entry 7). The catalysts were reused for at least 10 runs without significant loss of activity.

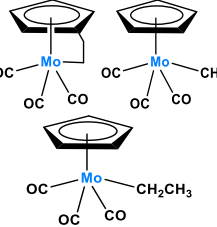
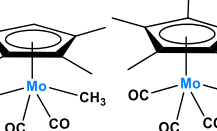
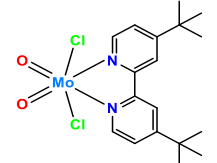
Chapter 1

Table 1.2. Catalytic results for some oxide molybdenum compounds and Mo-carbonyl precursors of oxides molybdenum found in the literature data.

Compound	Catalytic reaction	Conversion (%)	Yield (%)	Ref.
(1) [MoO₃(1,2,4-trz)_{0.5}] 	Epoxidation of <i>cis</i> -cyclooctene ^a	98 (24 h)	98 (24 h, epoxide)	159
	Epoxidation of cyclohexene ^a	90 (24 h)	22 (24 h, epoxide)	159
	Epoxidation of DL-limonene ^a	55 (24 h)	4 (24 h, epoxide)	159
	Epoxidation of <i>trans</i> -2-octene ^a	42 (24 h)	4 (24 h, epoxide)	159
	Epoxidation of methyl oleate ^a	39 (24 h)	20 (24 h, epoxide)	159
	Oxidation of methylphenylsulfide ^a	99 (6 h)	60 (24, sulfone)	159
	Oxidation of benzothiophene ^a	72 (24 h)	72 (24 h, sulfone)	159
	Methanolysis of styrene oxide ^b	100 (24 h)	100 (24 h, β-alkoxy alcohol)	137
(2) [Mo(Cp⁺(CH(CH₂)_n)-η¹-CH)(CO)₃] 	Epoxidation of <i>cis</i> -cyclooctene ^d	100/100 (4 h)	100/100 (6 h, epoxide)	146
	Epoxidation of 1-octene ^d	52/60 (24 h)	52/60 (24 h, epoxide)	146
	Epoxidation of <i>cis</i> -stilbene ^e	68/50 (24 h)	68/50 (24 h, epoxide)	146
(3) [CpMo(CO)₃CF₃] 	Epoxidation of <i>cis</i> -cyclooctene ^f	100 (4 h)	100 (4 h, epoxide)	147
(4) [CpMo(CO)₃(CH₂R)]  R = H, COOH	Ethanolysis of styrene oxide ⁱ	100/100 (120/90 min)	100/100 (120/90 min, β-alkoxy alcohol)	150
	α-Pinene oxide ring-opening ^j	50/100 (24 h)	18/51 (24 h, campholenic aldehyde)	150

Chapter 1

Table 1.2. continuation

(5) [Cp*Mo(CO)₃R]	Epoxidation of <i>cis</i> -cyclooctene ^c	100/100/100/100/100 (24 h)	100/100/100/100/100 (24 h, epoxide)	149
Epoxidation of 1-octene ^g	~60/~60/-/-/ (24 h)	~45/~45/-/-/ (24 h, epoxide)	149	
Epoxidation of styrene ^h	~50/~50/-/-/ (24h)	~50/~50/-/-/ (24 h, epoxide)	149	
				
				
(6) [MoO₂Cl₂(di-<i>t</i>Bu-bipy)]	Acetalisation of benzaldehyde ^k	86 (10 min)	86 (10 min, benzaldehyde diethyl acetal)	151
	Alcoholysis of styrene oxide ^k	98 (24h)	98 (24h, β-alkoxy alcohol)	151
(7) [Hmim]₄Mo₈O₂₆ (Hmim = 1-hexyl-3-methylimidazolium),	Epoxidation of <i>cis</i> -cyclooctene ^l	100/100/93 (1.5 h)	100/100/93 (1.5 h, epoxide)	106
[Dhmim]₄Mo₈O₂₆ (Dhmim = 1,2-dimethyl-3-hexylimidazolium),	Epoxidation of cyclohexene ^l	96/-/ (4 h)	44/-/ (4 h)	106
[Hpy]₄Mo₈O₂₆ (Hpy = 1-hexylpyridinium)	Epoxidation of styrene ^l	100/-/ (4 h)	91/-/ (4 h)	106
	Epoxidation of 1-hexene ^l	99/-/ (4 h)	96/-/ (4 h)	106
	Epoxidation of 1-dodecene ^l	91/-/ (4 h)	87/-/ (4 h)	106
(8) (H₃biim)₄[β-Mo₈O₂₆]	Epoxidation of <i>cis</i> -cyclooctene ^m	97 (24 h)	97 (24 h, epoxide)	156
(H ₂ biim = 2,2'-biimidazole)	Epoxidation of methyl oleate ⁿ	64 (24 h)	60 (24 h, epoxide)	156

Chapter 1

Table 1.2. continuation

(9) $[\text{Mo}_2\text{O}_4(\mu_2\text{-O})\{\text{HC}(3,5\text{-Me}_2\text{pz})_3\}_2](\text{BF}_4)_2$, $[\{\text{HC}(3,5\text{-Me}_2\text{pz})_3\}\text{MoO}_3]$	Epoxidation of <i>cis</i> -cyclooctene ^o	100/76 (24 h)	100/76 (24 h)	158

^a Mo:substrate:H₂O₂ molar ratio = 1:100:152, n_{initial} (substrate) = 1.8 mmol, 1 mL CH₃CN, 70 °C. ^b n (molybdenum complex) = 113 mmol, n (substrate) = 0.4 mmol and V (methanol) = 1 mL, 35 °C. ^c Mo:substrate:TBHP molar ratio = 0.01:1:2, n_{initial} (substrate) = 7.3 mmol, 55 °C. ^d Mo:substrate:TBHP molar ratio = 0.01:1:2, n_{initial} (substrate) = 7.3 mmol, 0.5 mL solvent or ionic liquid, room temperature. ^e Mo:substrate:TBHP molar ratio = 1:100:2.1, n_{initial} (substrate) = 16 μmol, 0.5 mL ionic liquid, room temperature. ^f Mo:substrate:TBHP molar ratio = 0.1:1:2, in benzene, 25 °C. ^g Mo:substrate:TBHP molar ratio = 0.01:1:2, n_{initial} (substrate) = 24 μmol, 55 °C. ^h Mo:substrate:TBHP molar ratio = 0.01:1:2, n_{initial} (substrate) = 71 μmol, 55 °C. ⁱ n (molybdenum complex) = 80 mmol, n_{initial} (substrate) = 0.82 mmol, and n (ethanol) = 2.0 mL, 35 °C. ^j n (molybdenum complex) = 17 mmol, n_{initial} (substrate) = 170 mmol, and V (DCE) = 0.5 mL, 55 °C. ^k n (molybdenum complex) = 20 μmol, n (substrate) = 0.4 mmol and V (ethanol) = 1 mL, 55 °C. ^l Mo:substrate:H₂O₂ molar ratio = 0.02:1:1.5, n_{initial} (substrate) = 2 mmol, 1 mL CH₃CN, 60 °C. ^m Mo:substrate:TBHP molar ratio = 1:100:152, n_{initial} (substrate) = 1.8 mmol, 2 mL TFT, 70 °C. ⁿ Mo:substrate:TBHP molar ratio = 1:103:160, n_{initial} (substrate) = 1.8 mmol, 0.3 mL [bmim]NTf₂, 70 °C. ^o Mo:substrate:TBHP molar ratio = 1:100:170, n_{initial} (substrate) = 1.6 mmol, 55 °C.

Chapter 1

The octamolybdate salt $(\text{H}_3\text{biim})_4[\beta\text{-Mo}_8\text{O}_{26}]$ was an effective (pre)catalyst for the epoxidation of olefins using either TBHP or hydrogen peroxide as oxidant (Table 1.2, entry 8).¹⁵⁶ With the ionic liquid (IL) 1-butyl-3-methylimidazolium bis(trifluoromethanesulfonyl)imide as co-solvent and TBHP as oxidant, the catalyst was reused several times without loss of activity for the epoxidation of the bio-olefin methyl oleate (Ole). This compound was the first polyoxomolybdate used for the Ole/TBHP reaction in IL medium.

1.1.6. Carbonyl molybdenum complexes as synthesis precursor and (pre)catalysts

In the field of organometallic chemistry, the most recognized molybdenum complexes possess oxo and carbonyl ligands. It is known that the performance for these complexes is, at least in part, due to differences in the Lewis acidity of the metal center as a result of the different donor properties of their ligands.^{72,160} For example, the presence of nitrogen-donor ligands in the first sphere of the Mo compounds may influence the performances. For example, the catalytic activity of a given complex is influenced by the donor/acceptor ability of the ligand, and steric and strain factors. These features strongly influence the stability of the complex with respect to the metal-ligand interaction.^{110,161} The stabilities are mainly due to the strongly exothermic binding of the bidentate nitrogen-donor ligands.¹⁶¹ Also, the introduction of the organic ligand serves to “passivate” the molybdenum oxide coordination sphere by blocking further Mo-oxo bond formation and somewhat limiting the polymerization process to corner-sharing linkages.

Tetracarbonyl complexes of the type $\text{cis-}[\text{Mo}(\text{CO})_4(\text{L})_n]$, L = mono- or bidentate organic ligand, with octahedral coordination, have shown to be excellent precursors because they can be stored for a long time, principally when compared with the more sensitive oxo complexes (Figure 1.10).⁵¹ The ligand present in the carbonyl-Mo complexes can be neutral, as in $\text{cis-}[\text{Mo}(\text{CO})_4(\text{pypz})]$, or charged. These types of tetracarbonyl complexes are potentially interesting pre-catalysts for various reactions.^{42,50,51,121} During this last decade, investigations were carried out with molybdenum tetracarbonyl complexes of the type $\text{cis-}[\text{Mo}(\text{CO})_4(\text{L})_n]$ as catalyst precursors for olefin epoxidation using TBHP as oxidant.^{42,50,51} In these studies, it was found that the resultant systems were capable of high epoxide selectivities, moderate to high activities, and good stability, functioning as either homogeneous or heterogeneous catalysts partly depending on the type of ligand.

Chapter 1

Mo(CO)₄(L)₂ and Mo(CO)₃(L)₃ containing pyrazolyl ligands

It is often desirable to prepare disubstituted Lewis base derivatives of molybdenum hexacarbonyls. In the decade of 90, Darensbourg *et al.*¹⁶² reported for the first time the synthesis of the complex *cis*-[Mo(CO)₄(pip)₂] (pip = piperidine) obtained in 91 % yield from the reflux of a mixture of Mo(CO)₆ and piperidine in heptane for 4 h (Figure 1.10). Years later, this complex was prepared through the successful application of an inexpensive microwave-assisted reflux technique.¹⁶³ The short reaction time and poor oxygen or water sensitivity allowed the facile preparation of *cis*-[Mo(CO)₄(pip)₂] in good yield. The mixture of Mo(CO)₆ and an excess of piperidine in diglyme and THF was heated to 40 minutes in a microwave-assisted reflux, obtaining 78 % yield. The *cis*-[Mo(CO)₄(pip)₂] complex can also be used as reagent for the preparation of other *cis*-[Mo(CO)₄(L)₂] derivatives in good yields, through a ligand substitution reaction, constituting a particularly convenient and inexpensive route.

Since poly(pyrazolyl)alkanes ligands were discovered by Trofimenko, their coordination chemistry has been extensively developed with particular interest arising from the ability of this class of ligands to modify or control the steric and electronic environment of the metal center by variation of the pyrazolyl group. Following previous works presented by this author^{164,165}, classical tris(pyrazolyl)alkanes stand out from the the coordination chemistry of poly(pyrazolyl)alkanes.

Tris(pyrazolyl)alkanes of the type RC(pz^x)₃ (R = alkane; pz^x = generic pyrazolyl) constitute a family of stable and flexible polydentate ligands which are isoelectronic and isosteric. Pyrazole-derived ligands are derived from two or more N-deprotonated pyrazole rings bound to a main group atom through one of the ring nitrogen atoms.¹⁶⁶ These donors can be readily prepared, and various substituents may replace each hydrogen atom, resulting in varied electronic and steric effects. These molecules contain azole rings which are generally very stable towards chemical attack, by for example oxidizing and reducing agents.¹⁶⁷

The RC(pz^x)₃ ligands are suitable to form organoamine metallic complexes, which generally form square-planar complexes, and to extend their coordination environment to square-pyramidal or octahedral via axial interactions. RC(pz^x)₃ produces a relatively strong ligand field, consistent with the rather short M–N bond lengths in the complexes.

Some publications refers that tris(1-pyrazolyl)methane (Tpm), HC(pz)₃, acts as a neutral tridentate ligand and displays a wealth of coordination chemistry (Figure 1.10).^{166,167} In his landmark paper¹⁶⁸, Trofimenko reported the formation [M(CO)₃(HC(pz)₃)] (M = Cr, Mo or W) from the reaction between HC(pz)₃ and group 6

Chapter 1

transition metal hexacarbonyls. The resultant compounds were considered poorly soluble.

The reaction of tris(3,5-dimethyl-1-pyrazolyl)methane, HC(3,5-Me₂pz)₃, with Mo(CO)₆ to give [Mo(CO)₃(HC(3,5-Me₂pz)₃)] was also reported. In recent years, the discovery of improved synthetic procedures has led to the preparation of a molybdenum tricarbonyl complex anchored by Tpm ligands (Figure 1.10).¹⁶⁹ One disadvantage in the coordination chemistry of poly(pyrazolyl)alkanes is the difficulty in preparing a large quantity of these ligands.¹⁶⁷

Tris(pyrazolyl)methylsilane can also be used as tripod ligand in Mo tricarbonyl complexes [Mo(CO)₃{MeSi(3,5-Me₂pz)₃}]¹⁷⁰, being prepared by reaction of the corresponding tris(acetonitrile) adducts [Mo(CO)₃(CH₃CN)₃] with MeSi(Me₂pz)₃ or thermally by direct substitution on the hexacarbonyl Mo(CO)₆. For both methods, the complex was obtained in 71 % yield (Figure 1.10).

Posteriorly, Sánchez-Méndez *et al.*¹⁷¹ reported the synthesis of [Mo(CO)₃{1,3,5-Me₃SiOCH₂C(pz)₃}] (Figure 1.10). The formation of this molybdenum compound required the use of a polar solvent such as THF or acetonitrile, whereas no reaction occurred in toluene. The authors presented the Mo tricarbonyl complexes as a moderately sensitive solid to air. The structures of these complexes are defined by the three pyrazolyl rings in a three-bladed propeller conformation.

Reaction of the lithium salt Li(Tpms) (Tpms = (tris(pyrazolyl)methanesulfonic acid) with [Mo(CO)₆] in CH₃CN under reflux afforded Li[Mo(Tpms)(CO)₃], isolated in high yield (Figure 1.10).¹⁷² This compound revealed to be air-sensitive, particularly in solution, and is readily soluble in water and in other polar solvents such as MeOH, CH₃CN, THF and CH₂Cl₂. In this compound, the Tpms ligand replaces three stronger π-acceptor carbonyl groups in [Mo(CO)₆], thereby increasing the metal-electron density.

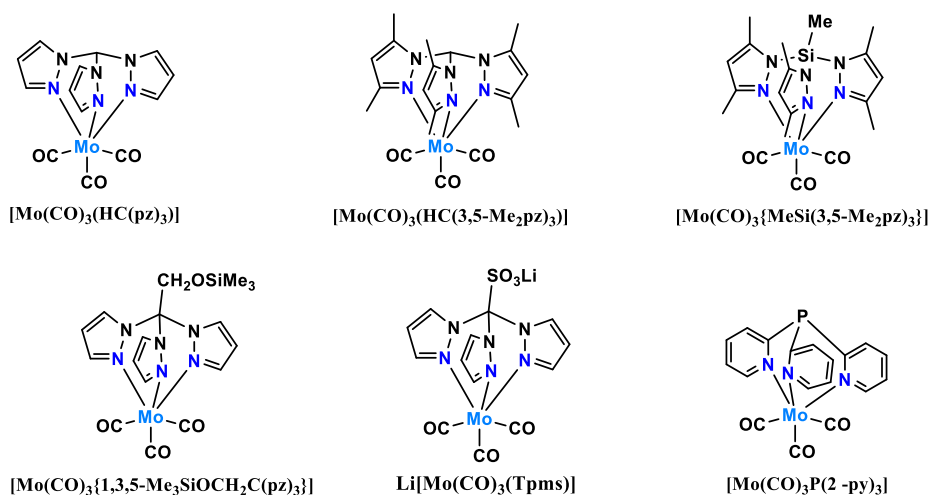
Treatment of P(2-py)₃ (P(2-py)₃ = tris(2-pyridyl)phosphine) with Mo(CO)₆ in CH₃CN affords compounds of the type, P(2-py)₃Mo(CO)₃ (Figure 1.10).¹⁷³ Complex P(2-py)₃Mo(CO)₃·CH₂Cl₂ was structurally characterized by X-ray crystallography, showing an almost perfect octahedral arrangement around the Mo center, and the P(2-py)₃ ligand occupying the facial position of the octahedron through the coordination of three pyridyl nitrogen atoms. Four coordination modes were found for complexes containing P(2-py)₃, affording numerous novel and useful complexes.

[Mo(CO)₃(L)] complexes bearing coordinated tridentate nitrogen donor ligands proved to be useful starting materials for the preparation of other complexes in higher oxidation states, including molybdenum(VI) complexes. For example, oxidation of [Mo(CO)₃(HC(3,5-Me₂pz)₃)] with nitric acid yields [(HC(3,5-Me₂pz)₃)MoO₃]¹⁶⁵, and the

Chapter 1

reaction of $\text{Li}[\text{Mo}(\text{CO})_3(\text{Tpms})]$ (Tpms = tris(1-pyrazolyl)methanesulfonate) with AgBF_4 in air gives dinuclear $[\{\text{MoO}_2(\text{Tpms})\}_2(\mu_2\text{-O})]$.¹⁷²

Tricarbonyl complexes of the type $[\text{Mo}(\text{CO})_3(\text{L})_3]$



Tetracarbonyl complexes of the type $\text{cis-}[\text{Mo}(\text{CO})_4(\text{L})_n]$, $n = 1$ or 2

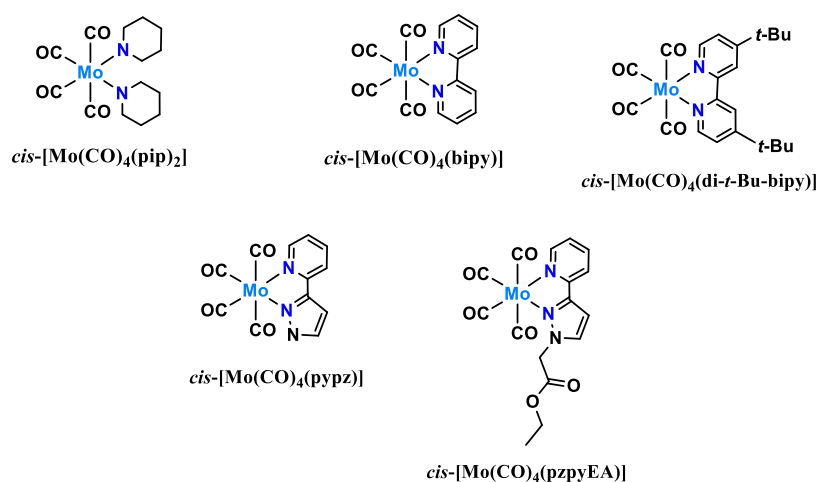


Figure 1.10. Examples of published tri- and tetracarbonyl complexes of the type and $[\text{Mo}(\text{CO})_3(\text{L})_3]$ ^{166,167,170–174} and $\text{cis-}[\text{Mo}(\text{CO})_4(\text{L})_n]$ ($\text{L} = \text{N-donor ligand}$, $n = 1$ or 2).^{42,51,163}

Gomes *et al.*¹⁷⁴ reported the use of the complexes $[\text{Mo}(\text{CO})_3\text{L}]$ with $\text{L} = \text{Tpm}$ and its 3,5-dimethyl derivative as catalyst precursors in the epoxidation of different types of olefins with TBHP using different cosolvents. The molybdenum tricarbonyl complexes $[\text{Mo}(\text{CO})_3(\text{HC}(3,5\text{-Me}_2\text{pz})_3)]$ and $[\text{Mo}(\text{CO})_3(\text{HC}(\text{pz})_3)]$ were obtained in good yields by the microwave-assisted reaction of $\text{Mo}(\text{CO})_6$ with the respective organic ligand. Complete oxidative decarbonylation of both complexes was achieved by reaction with

Chapter 1

excess TBHP in 1,2-dichloroethane at 55 °C. For $[\text{Mo}(\text{CO})_3(\text{HC}(3,5\text{-Me}_2\text{pz})_3)]$, the $(\mu_2\text{-oxo})\text{bis}[\text{dioxomolybdenum}(\text{VI})]$ hexamolybdate of composition $[\{\text{MoO}_2(\text{HC}(3,5\text{-Me}_2\text{pz})_3)\}_2(\mu_2\text{-O})][\text{Mo}_6\text{O}_{19}]$ was obtained in good yield, and its structure was determined by single crystal X-ray diffraction. The compounds were examined for the first time as homogeneous (pre)catalysts for the epoxidation of olefins with TBHP, using different types of cosolvents at 55 °C. During the catalytic reactions, $[\text{Mo}(\text{CO})_3(\text{HC}(3,5\text{-Me}_2\text{pz})_3)]$ and $[\text{Mo}(\text{CO})_3(\text{HC}(\text{pz})_3)]$ transform *in situ* into their $(\mu_2\text{-oxo})\text{bis}[\text{dioxomolybdenum}(\text{VI})]$ hexamolybdate compounds, and the latter two were fairly stable catalysts.

Mo(CO)₄(L) containing N,N'-bidentate ligands

During this last decade, Gonçalves and co-workers have turned their attention to tetracarbonyl complexes of the type *cis*- $[\text{Mo}(\text{CO})_4\text{L}]$, where L is a bidentate diamine ligand, which are readily available from $\text{Mo}(\text{CO})_6$ by thermal¹⁷⁵, photochemical¹⁷⁶ or microwave-assisted^{50,177} synthesis methods.

These compounds are usually prepared directly from $\text{Mo}(\text{CO})_6$ by thermal or photochemical activation or by treating *cis*- $[\text{Mo}(\text{CO})_4(\text{pip})_2]$ (pip = piperidine) with a refluxing solution of the ligand L in an organic solvent. Conventional thermal heating of reaction mixtures containing $\text{Mo}(\text{CO})_6$ is disadvantageous due to the sublimation and deposition of the metal hexacarbonyl on the reflux condenser, returning mechanically to the reaction solution inside the schlenk.¹⁷⁸ Sublimation of $\text{Mo}(\text{CO})_6$ is not a problem when the reactions are carried out using microwave-assisted heating, either in an open reflux system^{163,179} or in sealed Teflon vessels.^{177,180} Ardon *et al.*¹⁶³ showed that *cis*- $[\text{Mo}(\text{CO})_4(\text{pip})_2]$ could be prepared in 80-90 % yield over 30-40 min by microwave-assisted reflux (in comparison to 4 h required for conventional reflux). It was subsequently reported that the microwave-assisted synthesis of various compounds of the type $[\text{M}(\text{CO})_4(\text{L})]$, using either an open reflux system or a sealed Teflon-lined autoclave, results in a reduction of reaction times and in an increase of yields over previously published syntheses.^{179,180}

When used directly as catalyst precursors for oxidation reactions, the molybdenum carbonyl complexes undergo oxidative decarbonylation by reaction with the oxidant, usually TBHP or H_2O_2 , to form Mo(VI) species, such as, the polymeric $[\text{MoO}_3(2,2'\text{-bipy})]_n$ from *cis*- $[\text{Mo}(\text{CO})_4(2,2'\text{-bipy})]$, the tetrameric $[\text{Mo}_4\text{O}_{12}(\text{pypz})_4]$ from *cis*- $[\text{Mo}(\text{CO})_4(\text{pypz})]$, the octameric $[\text{Mo}_8\text{O}_{24}(\text{di-}t\text{Bu-bipy})_4]$ from *cis*- $[\text{Mo}(\text{CO})_4(\text{di-}t\text{Bu-bipy})]$, and $[\text{Mo}_8\text{O}_{24}(\text{pzpyEA})_4]$ from *cis*- $[\text{Mo}(\text{CO})_4(\text{pzpyEA})]$ (pzpyEA = ethyl[3-(2-pyridyl)-1-pyrazolyl]acetate) (Figure 1.10). Due to the structure-directing influence of

Chapter 1

the organoamine ligand, oxidative decarbonylation of these complexes leads to diverse molybdenum(VI) species with different catalytic performances.

The compounds $[\text{MoO}_3(2,2'\text{-bipy})]_n$ and $[\text{Mo}_8\text{O}_{24}(\text{di-}t\text{Bu-bipy})_4]$ exhibit good stability, high selectivity and moderate activity for the epoxidation of Cy (used as a model substrate) (Table 1.3).⁵¹ Under the same reaction conditions (1,2-dichloroethane as cosolvent), the octanuclear complex is completely soluble in the reaction medium and is an active homogeneous catalyst, while $[\text{MoO}_3(2,2'\text{-bipy})]_n$ is mostly insoluble and the reaction seemed to have heterogeneous and homogeneous contributions. So, changing the nature of the bidentate ligand in the tetracarbonyl precursors may influence not only the species formed by oxidative decarbonylation but also their catalytic performance. The stability of these catalysts was confirmed by carrying out six consecutive reaction runs at 75 °C under microwave-assisted heating.

The molybdenum oxide/pyrazoly|pyridine compounds $[\text{Mo}_4\text{O}_{12}(\text{pypz})_4]$ and $[\text{Mo}_8\text{O}_{24}(\text{pzpyEA})_4]$ revealed to be active and stable heterogeneous catalysts for the epoxidation of Cy by TBHP, giving 1,2-epoxycyclooctane as the only product (Table 1.3).⁴² *cis*- $[\text{Mo}(\text{CO})_4(\text{pzpyEA})]$ showed the highest activity with 90 % epoxide yield after 6 h reaction at 55 °C. Further experiments confirmed that *cis*- $[\text{Mo}(\text{CO})_4(\text{pzpyEA})]$ was also selective for epoxidation of R-(+)-limonene by TBHP (in *n*-decane), and for the oxidation of methyl phenyl sulfide to the corresponding sulfoxide by aqueous TBHP or H_2O_2 at 35 °C.

Table 1.3. Catalytic results for some published carbonyl complexes and *cis*- $[\text{Mo}(\text{CO})_4(\text{pzpyEA})]$, and the molybdenum oxide compounds.

Compound	Substrate	Conv. (%)	Yield (%)	Ref.
<i>cis</i> - $[\text{Mo}(\text{CO})_4(2,2'\text{-bipy})]$	<i>cis</i> -Cyclooctene ^a	71	71	51
<i>cis</i> - $[\text{Mo}(\text{CO})_4(\text{di-}t\text{Bu-bipy})]$	<i>cis</i> -Cyclooctene ^a	84	84	51
$[\text{MoO}_3(2,2'\text{-bipy})]_n$	<i>cis</i> -Cyclooctene ^a	95	95	51
$[\text{Mo}_8\text{O}_{24}(\text{di-}t\text{Bu-bipy})_4]$	<i>cis</i> -Cyclooctene ^a	97	97	51
<i>cis</i> - $[\text{Mo}(\text{CO})_4(\text{pypz})]$	<i>cis</i> -Cyclooctene ^b	77	78	42
<i>cis</i> - $[\text{Mo}(\text{CO})_4(\text{pzpyEA})]$	<i>cis</i> -Cyclooctene ^b	92	92	42
	R-(+)-limonene ^b	88	100	42
$[\text{Mo}_4\text{O}_{12}(\text{pypz})_4]$	<i>cis</i> -Cyclooctene ^b	92	92	42
$[\text{Mo}_8\text{O}_{24}(\text{pzpyEA})_4]$	<i>cis</i> -Cyclooctene ^b	100	100	42

^a Mo:substrate: H_2O_2 molar ratio = 0.1:100:153, n_{initial} (substrate) = 1.8 mmol, 1.2 mL DCE, 75 °C. ^b Mo:substrate: H_2O_2 molar ratio = 1:100:152, 55 °C.

Chapter 1

1.1.7. Dioxomolybdenum(VI) complexes as synthesis precursors and (pre)catalysts

Monomeric hybrid compounds with the *cis*-MoO₂²⁺ core are discrete complexes with general formula [MoO₂X₂(L)_n], where X = halide, R, OR, OSiR₃, L = Lewis base or donor solvent and n = 1 or 2).^{15,77,79,110,181–185} The MoO₂X₂ fragment can be stabilised by adduct formation with relatively strong basic donor ligands (denoted D-ligands, D = N, O or S). [MoO₂X₂(L)_n] complexes have shown their importance through their performances as catalysts for the epoxidation of olefins and oxo-transfer reactions.^{24,186,187}

MoO₂X₂(L) containing N,N'-bidentate ligands

The stability of these compounds toward moisture varies from quite stable in the case of the 2,2'-bipyridine adducts to extremely sensitive in the case of the thio and seleno-ether complexes. Their reactivity in oxygen transfer reactions is strongly modulated by the nature of the L ligands. The complexes of the type [MoO₂X₂(L)] (L = N,N'-bidentate ligand) possess a distorted octahedral geometry¹⁸⁸, with the two oxido ligands in *cis* positions to each other. The arrangement of the anionic X are *trans*, and neutral L ligands are frequently *trans* to oxo and *cis* to each other.¹⁸⁹ Exceptions may arise if the neutral donors are in the form of a bidentate ligand such as tetramethylethylenediamine (tmen): MoO₂Cl₂(tmen) has one N-donor *trans* to oxygen and another *trans* to chlorine.¹⁹⁰ The dioxomolybdenum(VI) complexes of the type [MoO₂Cl₂(L)] with neutral N,N'-bidentate L ligands have been widely investigated due to their excellent catalytic behaviour in olefin epoxidation using TBHP as oxidant.^{46,56,184}

The most common monomeric compounds with the *cis*-MoO₂²⁺ are the [MoO₂Cl₂L]-type complexes. In the last decades, the research groups of Gonçalves, Kühn, Romão and co-workers have described several complexes, with N,N'-chelated molecules, such as N,N'-dibenzylidene-1,2-ethylenediamine¹⁹¹, ethyl(3-(2-pyridyl)pyrazol-1-yl)acetate⁷², 2-(3-pyrazole)pyridine¹⁵, 2,2'-bipyridine^{192,193}, and 2,2'-bipyrimidine (bpym)^{20,193}.

Many studies refer to the effect of N-ligands and Cl-ligands on the solubility, stability and other properties of these complexes.⁷⁹ From the several types of ligands investigated, bidentate N-ligands, such as 2,2'-bipy, pypz and derivatives, appear to be more advantageous since they are fairly resistant to degradation.^{15,16,110,161} Trofimenko gave an important contribution in this research field with the introduction of 'second generation' ligands in which the pyrazolyl rings contain bulky substituents, especially at

Chapter 1

the C-3 position.^{169,194} Their coordinative stability and their excellent solubility in organic solvents make these complexes interesting candidates as catalysts.

Generally, the monomeric complexes reported by the authors mentioned above where prepared by treatment of MoO_2Cl_2 with a donor solvent (CH_3CN or THF), forming the solvent adduct $[\text{MoO}_2\text{Cl}_2(\text{solvent})_2]$, and by an *in situ* substitution reaction of the solvent by the N,N'-donor ligand. The interest of Gonçalves and Kühn for the catalytic performance of these oxido complexes, influenced by the type of ligand¹⁹³, and the catalyst stability^{110,161}, led them to conclude that bipyridines and pyrazolylpyridines are excellent ligands for molybdenum catalysed epoxidation reactions of olefins, in particular using TBHP as oxidant. The two ligands revealed resistance to oxidative degradation and ligand exchange during the catalytic reactions.

Bruno *et al.*⁷² have reported the influence of the X halide ligand in $[\text{MoO}_2\text{Cl}_2(\text{L})]$ -type complexes with $\text{L} = 2\text{-(1-butyl-3-pyrazolyl)pyridine}$ or ethyl[3-(2-pyridyl)-1-pyrazolyl]acetate in their catalytic performance by changing the nature of X from Cl to OSiPh_3 (Figure 1.11). They verified that the TOFs for Cy epoxidation at 55 °C were around $340 \text{ mol mol}_{\text{Mo}}^{-1} \text{ h}^{-1}$ for the chloro complexes and $160 \text{ mol mol}_{\text{Mo}}^{-1} \text{ h}^{-1}$ for the triphenylsiloxy complexes.

A study reported by Kühn *et al.*¹⁹³ showed that the $[\text{MoO}_2\text{X}_2(\text{L})]$ -type complexes (X = halide) with the polypyridyl ligands bipy and 2,2'-bipyrimidine are rather slow catalysts of generally low catalytic activity but good epoxide selectivity in the epoxidation of Cy in liquid-phase with TBHP (Figure 1.11). Posteriorly, Gonçalves and co-workers have shown that other ligands such as substituted 1,4-diazabutadienes, *e.g.* bidentate ligand *N,N-p*-tolyl-2,3-dimethyl-1,4-diazabutadiene (*p*-tolyl(CH_3 DAB)), and pyrazolylpyridines are more promising ligands^{37,183}, giving high initial TOF ($360 \text{ mol mol}_{\text{Mo}}^{-1} \text{ h}^{-1}$) in the case of the complex $[\text{MoO}_2\text{Cl}_2(\text{pzpyEA})]$ (Figure 1.11). It is thought that the variable catalytic activities observed for $[\text{MoO}_2\text{X}_2(\text{L})]$ -type complexes are due, at least in part, to differences in the Lewis acidity of the metal center because of the different donor properties of the ligands.¹⁶⁰

The success of molybdenum(VI) complexes in reactions to produce racemic epoxides led to the belief that some derivatives of these complexes could be applied as chiral catalysts.^{74,195} Research focused on the synthesis of chiral monometallic complexes with the $[\text{MoO}_2]^{2+}$ core bearing bidentate, tridentate or tetradentate N, O, S-ligands derived from pyridyl alcohols^{196–200}, oxazolines and bis(oxazolines)^{198,201,202}, sugar derived Schiff bases²⁰³, oximes, *cis*-diols and 8-phenylthiomenthols⁴⁵, tetradentate salen ligands^{200,204}, and diazabutenes²⁰⁵. The enantiomeric excesses obtained for the epoxidation of unfunctionalised olefins using chiral complexes as catalysts are typically in the range of 20–40 %. Oxazolines and bis(oxazolines) are

Chapter 1

chiral ligands that have been frequently used in metal-catalysed asymmetric organic transformations.^{206–209} In the field of oxomolybdenum(VI) chemistry, complexes of the type $[\text{MoO}_2\text{Cl}_2(\text{N},\text{N})]$ bearing C_2 -symmetric bis(oxazolines) (N,N) were prepared and evaluated as catalysts for the asymmetric epoxidation of *trans*- β -methylstyrene with TBHP.¹⁹⁸ The complexes showed good catalytic activities (up to 86 % conversion at 4 h reaction) but led to very low enantiomeric excess (4–6 %). Posteriorly, Bruno *et al.*²¹⁰ reported the synthesis of dioxomolybdenum(VI) complexes with the general formula $[\text{MoO}_2\text{X}_2(\text{N},\text{N})]$ (X = Cl, OSiPh₃) containing a chiral bidentate oxazoline ligand (N,N = 2,2'-bis[(4S)-4-benzyl-2-oxazoline]) (Figure 1.11). The complex $[\text{MoO}_2\text{Cl}_2(\text{N},\text{N})]$ exhibited initial catalytic activity of 147 mol mol⁻¹Mo h⁻¹ for the epoxidation of Cy using TBHP as the oxidant, giving 1,2-epoxycyclooctane quantitatively within 24 h at 55 °C. With *trans*- β -methylstyrene as the substrate, the bis(chloro) complex gave the respective epoxide as the only product at 64 % of conversion after 24 h. However, this complex was less active than the triphenylsiloxy complex in this catalytic reaction.

Even for the most stable complexes the Mo–Cl bond is susceptible to cleavage in the presence of water, leading to diverse Mo(VI) species with different features and performances. Thus, in the presence of residual or small amounts of water, $[\text{MoO}_2\text{Cl}_2(\text{L})]$ complexes have been shown to dimerize, leading to the isolation of dioxo(μ -oxo)molybdenum(VI) complexes with the general formula $[\text{Mo}_2\text{O}_4(\mu_2\text{-O})\text{Cl}_2(\text{L})_n]$, e.g. the oxo-bridged dinuclear complex $[\text{Mo}_2\text{O}_4(\mu_2\text{-O})\text{Cl}_2(\text{L})_4]$ (L = N,N-dialkylamides).^{15,211} For example, the complex $[\text{Mo}_2\text{O}_4(\mu_2\text{-O})\text{Cl}_2(\text{pzpyEA})_2]$ was obtained upon the treatment of $[\text{MoO}_2\text{Cl}_2(\text{pzpyEA})]$ with ethanol.²¹² The molecular structure of this oxo-bridged dinuclear complex consists of two highly distorted $\{\text{MoClN}_2\text{O}_3\}$ octahedra sharing a corner oxygen atom. Besides to the favourable catalytic results obtained with $[\text{Mo}_2\text{O}_4(\mu_2\text{-O})\text{Cl}_2(\text{pzpyEA})_2]$ for the epoxidation of Cy with TBHP, the catalytic reaction was homogeneous in nature, and the dissolved complex was partly converted to the oxodiperoxo complex $[\text{MoO}(\text{O}_2)_2(\text{pzpyEA})]$.

Several higher nuclearity oxomolybdenum(VI) compounds have been isolated after the reaction of dichlorodioxomolybdenum(VI) complexes with excess water, namely the hexamolybdate isopolyanion in $[(\text{H}_3\text{O})(18\text{-crown-6})]_2[\text{Mo}_6\text{O}_{19}]$ (L = H₂O in the precursor complex), the mononuclear complex $[\text{MoO}(\text{O}_2)_2(\text{ppp})]$, the dinuclear complex $[\text{Mo}_2\text{O}_6(\text{ppp})]$, the octanuclear complex $[\text{Mo}_8\text{O}_{22}(\text{OH})_4(\text{di-}t\text{Bu-bipy})_4]$, and the polymeric materials $\{[\text{MoO}_3(2,2'\text{-bipy})][\text{MoO}_3(\text{H}_2\text{O})]\}_n$ and $[\text{Mo}_2\text{O}_6(\text{HpzpyA})]_n$ (HpzpyA = [3-(pyridinium-2-yl)-1H-pyrazol-1-yl]acetate).^{16,79,114} Thus, the hydrolysis and condensation of dichlorodioxomolybdenum(VI) complexes is an interesting pathway to Mo(VI) oxide-based organic–inorganic hybrid materials, with potential application in catalysis.^{79,109}

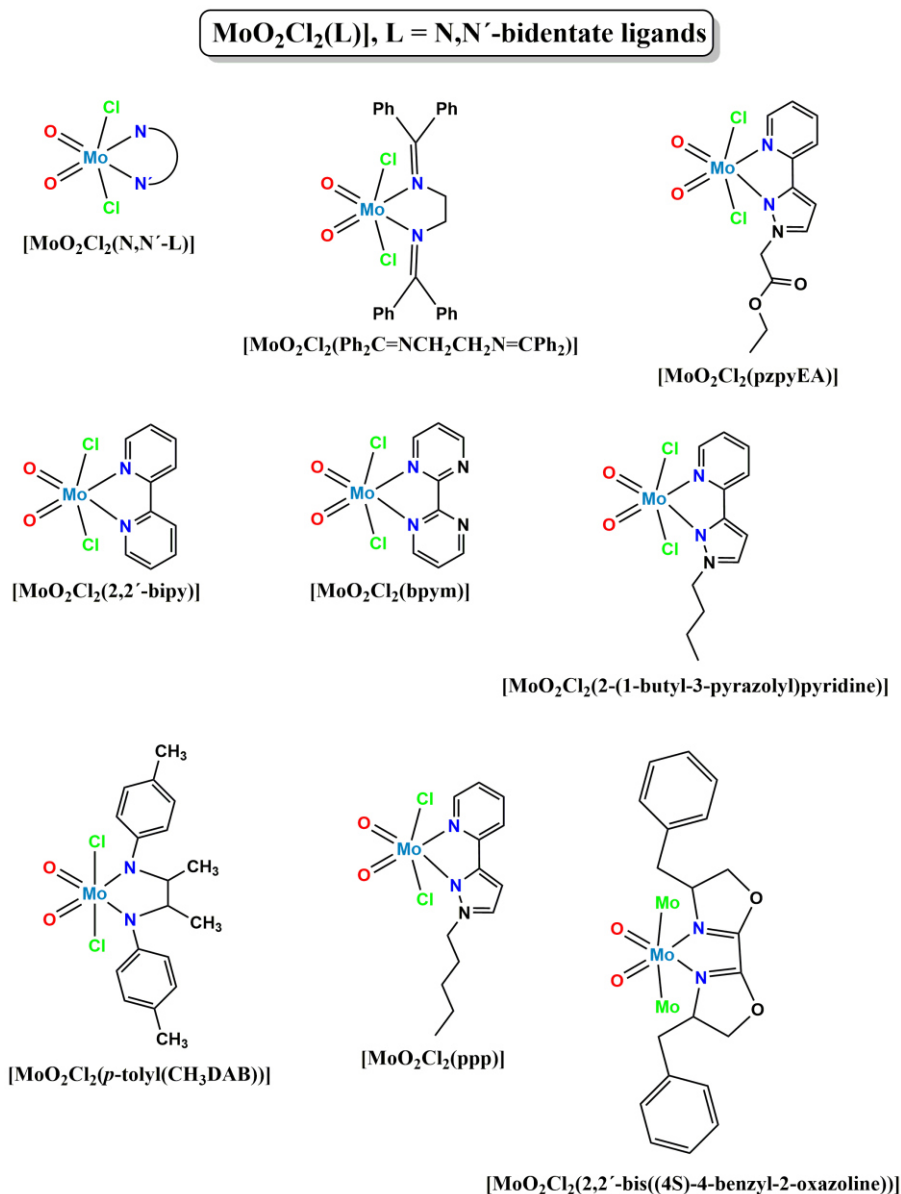
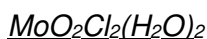


Figure 1.11. Examples of [MoO₂Cl₂(L)] with N,N'-donor bidentate ligands.

Amarante *et al.*¹⁶ reported that the treatment of the dichloro complex [MoO₂Cl₂(ppp)] (Figure 1.11) with water under hydrothermal conditions led to the isolation of the organic–inorganic hybrid material [Mo₂O₆(ppp)]. Both compounds were tested as (pre)catalysts and showed high activity and selectivity for the epoxidation of Cy with TBHP at 55 °C as oxidant. [Mo₂O₆(ppp)] was also tested for the catalytic epoxidation of bio-derived olefins namely DL-limonene (Lim) and methyl oleate (Ole). In the presence of Lim, the reaction gave mainly 1,2-epoxy-*p*-menth-8-ene and 1,2;8,9-diepoxy-*p*-menthane in a combined yield of 93 % at 97 % conversion at 6 h. The substrate Ole was mainly converted to 9,10-epoxystearate in 78 % yield at 82 % conversion (6 h). Also, it was verified that the catalytic reactions are homogeneous in

Chapter 1

nature, and $[\text{Mo}_2\text{O}_6(\text{ppp})]$ converts to the oxodiperoxo complex $[\text{MoO}(\text{O}_2)_2(\text{ppp})]$ which was isolated from the catalytic reaction.



As already mentioned above, researchers have a particular interest on dioxomolybdenum(VI) halides because of their utility in the preparation of other relevant compounds derived from halogen substitution and their capability to work as catalysts.

There is evidence for the presence of the species $[\text{MoO}_2\text{X}_2(\text{H}_2\text{O})_2]$ ($\text{X} = \text{Cl}$ or Br) in solutions of molybdates in concentrated hydrochloric or hydrobromic acid as well as in diethyl ether or acetone extracts.^{215–219} Molybdenum in the +6 oxidation state can be efficiently extracted from aqueous HCl or HBr into an ether or ketone phase and this procedure provides a useful method of separation. Coddington *et al.*²²⁰ have investigated this method of separation via solvent extraction and found that the extracted complex is of the type *cis*- $[\text{MoO}_2\text{X}_2(\text{H}_2\text{O})_2]$ ($\text{X} = \text{Cl}$ or Br).

The crystalline structure of $[\text{MoO}_2\text{Cl}_2(\text{H}_2\text{O})_2]$ was determined by Taylor *et al.*²²² and revealed $[\text{MoO}_2\text{Cl}_2(\text{H}_2\text{O})_2]$ units with *cis*, *trans*, *cis* arrangement of ligands oxo, Cl and H_2O respectively, which are linked by forming hydrogen bonds with the H_2O molecules of crystallization (Figure 1.12). The complex was prepared by the dissolution of tetraethylammonium chloride in concentrated hydrochloric acid, followed by the slow addition of this mixture to a solution of $\text{Na}_2\text{MoO}_4 \cdot 2\text{H}_2\text{O}$ in a concentrated HCl solution. The X-ray structure determination shows that the solid which forms from a solution of $[\text{MoO}_2\text{Cl}_2(\text{H}_2\text{O})_2]$ in hydrochloric acid, containing tetraethylammonium chloride, consists of Et_4N^+ and Cl^- ions cocrystallized with $\text{MoO}_2\text{Cl}_2(\text{H}_2\text{O})_2$ molecules. Additional water molecules exist in the solid structure as water of crystallization: its position shows it to be involved in hydrogen bonding between the aqua ligands of different molecules of the molybdenum complex occurs throughout the structure.

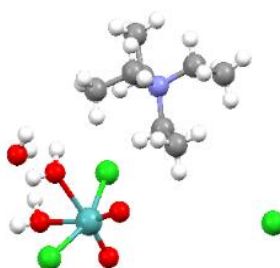


Figure 1.12. Octahedral $[\text{MoO}_2\text{Cl}_2(\text{H}_2\text{O})_2] \cdot \text{H}_2\text{O} \cdot \text{Et}_2\text{NCl}$ complex (Mo - turquoise, O - red, H - white, C - dark grey, N - blue, Cl - light green).²²²

Chapter 1

Yuan and co-worker have reported the preparation of $[\text{MoO}_2\text{Br}_2(\text{H}_2\text{O})_2]$ supported on a zinc modified mesoporous silica and the catalytic cycles for the partial oxidation of methane initiated by the decomposition of $[\text{MoO}_2\text{Br}_2(\text{H}_2\text{O})_2]$.²⁵ $[\text{MoO}_2\text{Br}_2]$ reacted readily with O_2 to release Br_2 , which oxidized C-H bonds to form H-Br and a C-Br bond with higher selectivity than O_2 . Then MoO_3 scavenged the bromine atoms from H-Br and the C-Br functionality to yield the oxidized products and regenerate MoO_2Br_2 . The ultimate oxidant was oxygen, and bromine acted as the oxidation mediator.

Luan *et al.*²⁶ have studied the potential of the complex $[\text{MoO}_2\text{Cl}_2(\text{H}_2\text{O})_2] \cdot (\text{H}_2\text{dipy-pra})\text{Cl}_2$ (dipy-pra = 1,3-bis(4-pyridyl)propane) as an olefin epoxidation catalyst with hydrogen peroxide as the oxidant, revealing to be an efficient catalyst (Table 1.4). A good yield (99 %) of cyclooctene oxide and cyclohexene oxide was achieved using 1 mol-% catalyst and NaHCO_3 as cocatalyst (25 mol-%) after 1 h at room temperature (25 °C). Inspired by these results, Sánchez Costa *et al.*²²³ synthesized the complex $[\text{MoO}_2\text{Cl}_2(\text{H}_2\text{O})_2] \cdot \text{Hdpa} \cdot \text{Cl} \cdot \text{H}_2\text{O}$ (Hdpa = 2,2'-dipyridylammonium) which was effective catalysis properties for the epoxidation of Cy with H_2O_2 , under different reaction conditions. This molybdenum(VI)/aminopyridinium compound was considered a promising catalyst, since 1 mol-% of the Mo compound led to 80 % conversion of the substrate to the epoxide, at 24 h, without any co-catalyst added (Table 1.4).

Table 1.4. Catalytic results for the complex $[\text{MoO}_2\text{Cl}_2(\text{H}_2\text{O})_2]$.

Compound	Substrate	Conv. (%)	Yield (%)	Ref.
$[\text{MoO}_2\text{Cl}_2(\text{H}_2\text{O})_2] \cdot (\text{H}_2\text{dipy-pra})\text{Cl}_2$	<i>cis</i> -Cyclooctene ^a	99	99	26
	Cyclohexene ^a	99	99	26
	Styrene ^a	99	86	26
	1-Hexene ^a	99	92	26
	Prop-2-en-1-ol ^a	99	95	26
$[\text{MoO}_2\text{Cl}_2(\text{H}_2\text{O})_2] \cdot \text{Hdpa} \cdot \text{Cl} \cdot \text{H}_2\text{O}$	<i>cis</i> -Cyclooctene ^b	80	80	223

^a Mo:substrate: H_2O_2 molar ratio = 0.1:10:40, n_{initial} (substrate) = 10 mmol, 10 mL CH_3CN , 25 °C.

^b Mo:substrate: H_2O_2 molar ratio = 0.1:100:150, n_{initial} (substrate) = 10 mmol, 10 mL CH_3CN , 50 °C.

Currently, researchers have been encouraged and motivated with the necessity to prepare new hybrid materials based on metallic complexes, which allow a superior performances in several applications, in particular catalysis. This led to the development of new supports and consequently new methods of preparation. In the last decades, cyclodextrins, calixarenes and cucurbiturils have been used as organic capsules for the encapsulation of complexes described above.^{224–236} However, the emerging research on cucurbit[*n*]uril has not yet reached the extent of the research on

Chapter 1

cyclodextrins and calixarenes. Cyclodextrins and their derivatives are known to bind oxomolybdenum compounds such as MoO_3 ²³⁶, $\beta\text{-(Bu}_4\text{N)}_4\text{Mo}_8\text{O}_{26}$ ²³¹, $[(\eta^5\text{-C}_5\text{H}_4\text{-CO-R})\text{Mo}(\text{CO})_2(\eta^3\text{-C}_3\text{H}_5)]$ ($\text{R} = \text{OH, Phe-OMe}$)²²⁸, $\text{CpMo}(\text{CO})_3(\text{CH}_2\text{-}p\text{-C}_6\text{H}_4\text{-CO}_2\text{CH}_3)$ ($\text{Cp} = \eta^5\text{-C}_5\text{H}_5$)²²⁶, $[\text{CpMoL}_2(\text{CO})_2](\text{BF}_4)$ ($\text{L} = \text{MeCN, L}_2 = 2,2'\text{-biimidazole}$)^{232,235}, $\text{CpMo}(\text{CO})_3\text{Cl}$ ²³⁴, $\text{CpMo}(\text{CO})_3\text{CH}_2\text{CONH}_2$ ²³³, $\text{MoO}_2\text{Cl}_2(\text{FcNN})$ ($\text{N,N}'\text{-bis(ferrocenylmethylene)ethylenediamine}$)²³⁰, Cp_2MoCl_2 ²²⁹, $[\text{Cp}'\text{Mo}(\eta^4\text{-C}_6\text{H}_8)(\text{CO})_2][\text{BF}_4]$ and the neutral derivatives $\text{Cp}'\text{Mo}(\eta^3\text{-C}_6\text{H}_7)(\text{CO})_2$ [$\text{Cp}' = \text{Cp} (\eta^5\text{-C}_5\text{H}_5), \text{Ind} (\eta^5\text{-C}_9\text{H}_7)$]²⁸, and $\text{MoCp}'(\eta^3\text{-C}_3\text{H}_5)(\text{CO})_2$ ($\text{Cp}' = \text{Cp, C}_5\text{H}_4\text{SiMe}_3, \text{C}_9\text{H}_7$)²²⁴. Several oxomolybdenum compounds have been coordinated to calixarenes and hybrid compounds isolated, which include $[\text{calix[4]arene-(OH)}_4\text{-calix[4]arene-(O)}_4\text{Mo=O-Ph-NO}_2\cdot\text{H}_2\text{O}]$ ²³⁷, $[\text{Mo}_2(\text{O}_2\text{CR})_2(\text{H}_2\text{-}p\text{-tert-butylcalix[4]arene} (\text{R} = \text{CH}_3, \text{CF}_3)$ and $[\text{Mo}_2(\text{O}_2\text{CR})_2(\text{H}_2\text{-calix[4]arene})]$ ($\text{R} = \text{CH}_3, \text{CF}_3$)²³⁸, $[\text{Mo}_2(\text{OAc})_2(\text{H}_2\text{-}p\text{-tert-butylcalix[4]arene})]$ and $[\text{Mo}_2(\text{OAc})_2(\text{H}_2\text{-}p\text{-tert-butylcalix[4]arene})]$ ²³⁹, $\text{Mo}(\text{NAr})(p\text{-tert-butylcalix[4]arene})\text{K}_2(\text{NCCH}_3)_3\text{O}]_2$ ²⁴⁰, $(\text{R}_2\text{-calix[4]arene})\text{MoOCl}_2$ ($\text{R} = \text{CH}_3, \text{CH}_2\text{CH}_3$)²⁴¹ and $\text{R-calix[4]arene-(OH)}_4\text{MoO}$ ²⁴². Some hybrid material based on supramolecular adduct of di- or trinuclear molybdenum oxoclusters with macrocyclic cavitand cucurbiturils have already be explored, such as $[\text{Mo}_3\text{O}_4(\text{H}_2\text{O})_6\text{Cl}_3]_2\text{Cl}_2@\text{CB[6]}$ ²⁴³, $[\text{Mo}_2\text{O}_4\text{Cl}_4(\text{H}_2\text{O})_2]@\text{CB[6]}$ ²⁴⁴, $[\{\text{Mo}_3\text{O}_4(\text{H}_2\text{O})_6\text{Cl}_3\}_2]@\text{CB[5]}$ ²⁴⁵, $[\text{Mo}_3\text{O}_2\text{S}_2\text{Cl}_6(\text{H}_2\text{O})_3]_2@\text{CB[6]}$ ²⁴⁶ and $[\text{Mo}_3(\mu_3\text{-S})(\mu_2\text{-O})_3(\text{H}_2\text{O})_6\text{Cl}_3]_2@\text{CB[6]}$ ²⁴⁶.

1.2. Cucurbit[*n*]urils as supramolecular hosts

Cucurbit[*n*]urils, $\text{CB}[n]$ s: $n = 5\text{-}8, 10, 14$ (Figure 1.13), are a new family of molecular container macrocycles formed via catalytic conversion of cheap starting materials, namely glycoluril and formaldehyde, under acidic conditions.^{247–250} Cucurbit[*n*]urils are built of glycoluril units linked by methylene bridges with highly symmetric structure.²⁵⁰

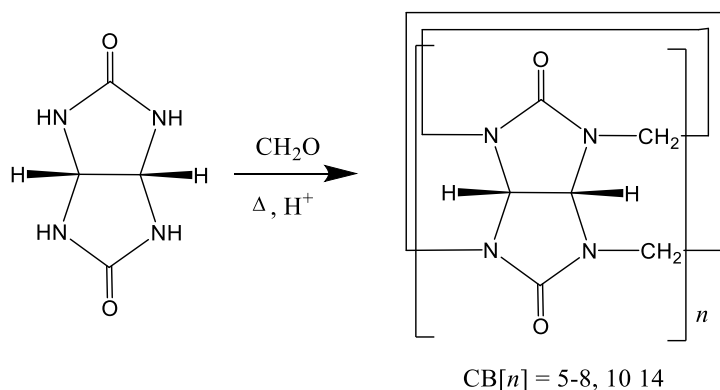


Figure 1.13. Synthesis and molecular structures of $\text{CB}[n]$ homologues.

Chapter 1

1.2.1. Historical context

The first scientists to synthesize a cucurbit[n]uril ($n = 6$) were Behrend *et al.*²⁵¹ in 1905. They reported that the condensation of glycoluril (acetyleneurea) and formaldehyde in concentrated HCl led to an insoluble polymeric substance presently known as Behrend's polymer. This crystalline substance was obtained in fair yield (40–70 %) by recrystallization of the product from concentrated H₂SO₄. However, the structure of this substance remained unclear until 1981 when Mock and co-workers reinvestigated the previous work and were able to determine the structure of this macrocyclic structure comprising six glycoluril units and twelve methylene bridges. In fact, the name "cucurbituril" was attributed due to the similarity of its structure to a pumpkin, which belongs to the botanical family *cucurbitaceae*.²⁵² In the beginning of this century, Kim and Day were able to synthesize different homologues of CB[n]s: CB[5], CB[7], CB[8], and CB[10].^{253,254} Almost every year since 2000, new CB[n]s members have been reported, such as functionalized CB[n]s, inverted-CB[n]s, nor-*sec*-CB[n]s, and other congeners (Figure 1.14).²⁵⁰

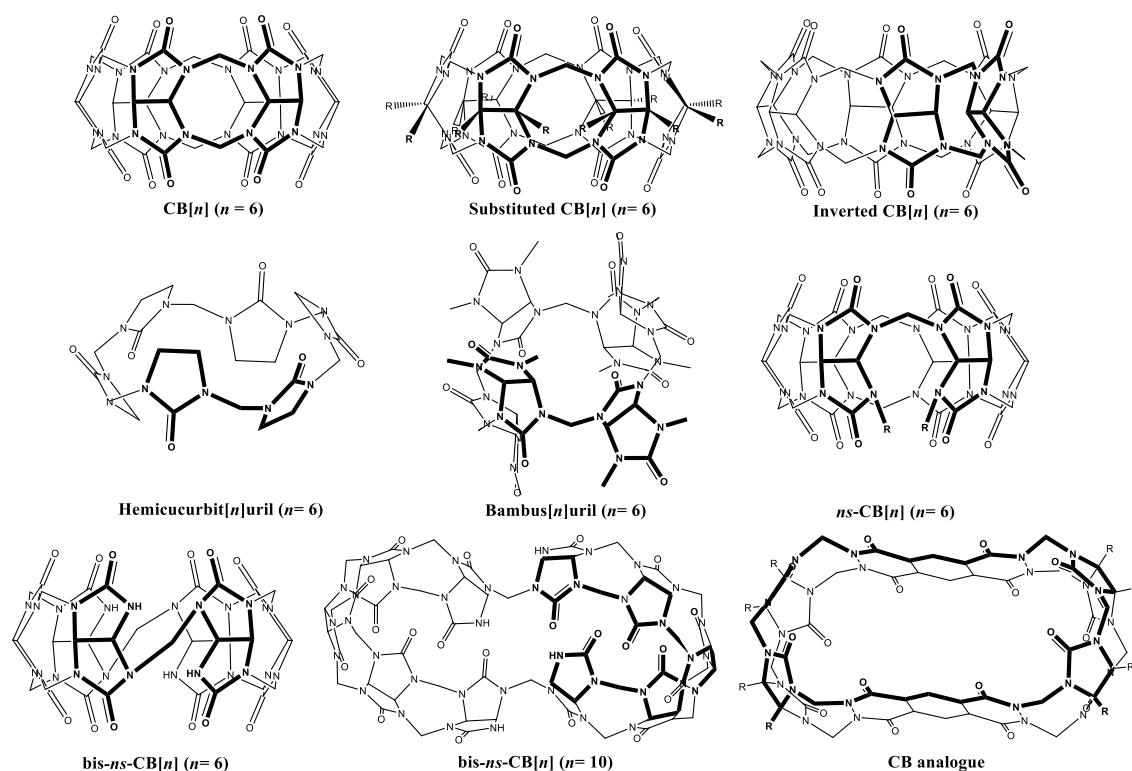


Figure 1.14. Molecular structures of cucurbit[n]urils congeners.

Chapter 1

1.2.2. Synthesis

Several homologues of CB[*n*]s can be synthesized using different reaction conditions.^{253,254} Various procedures have been proposed for their preparation, all based on general protocols developed by Day²⁵⁴, Kim²⁵³ and Isaacs²⁵⁵. The synthetic protocol of CB[*n*] homologues is similar to the conventional CB[6] synthesis.²⁵⁶ Reaction of glycoluril with formaldehyde in acids, such as 9 M H₂SO₄ or concentrated HCl, at 75–90 °C for 24 h gave a mixture of CB[*n*] (*n* = 5-11).²⁵⁷ Apparently, this reaction first generates linear oligomeric products which then cyclise to produce the mixture of CB[*n*]s.²⁵³ The cyclization at lower reaction temperature compared to that employed in conventional CB[6] synthesis^{251,252} (110 °C) allows the formation of significant amounts of CB[*n*] homologues in addition to CB[6].²⁵³ The reaction mixture contains CB[*n*] homologues, mostly from pentamer to octamer, with typical contents being 10-15 % of CB[5], 50-60 % of CB[6], 20-25 % of CB[7], 10-15 % of CB[8] and trace amounts of higher homologues (CB[*n*], *n* = 9-11) are formed.²⁵⁶ On standing, the reaction mixture first gives crystals of CB[8].²⁵⁶ CB[*n*] (*n* = 5, 7 and 8) can be separated in pure form using fractional crystallization and dissolution²⁵³, or chromatography²⁵⁴. CB[6] is then separated usually by fractional dissolution of other CB[*n*] homologues with acetone or methanol and water.²⁵⁶ From the soluble portion, CB[5] and CB[7] are isolated and further separated by fractional crystallization.²⁵⁶ It should be noted that the separation of the homologues is based on their different solubility in solvent and acid, being also affected by traces of NH₄⁺ ion, which may be formed via thermal decomposition of glycoluril.²⁵⁶ It was recently discovered that microwave assisted synthesis provides a fast and efficient way of producing a CB[*n*] mixture, which might be useful for the industrial scale production of CB[*n*]s in the future.

1.2.3. Structural and physicochemical properties

The number of glycoluril units determines the available volume within a CB[*n*]. One important detail is that all CB[*n*]s homologues have the same height (*d* = 9.1 Å), but differ in the inner cavity diameter, as can be seen from Table 1.5 and Figure 1.15. On going from CB[5] to CB[10], the inner cavity diameter increases progressively from 4.4 to 10.7-12.6 Å.^{255,256,259} Note that the inner diameters increase by ≈ 1.5 Å compared to the next lower homologue.²⁵⁷ The oxygen-bounded portal increases its mean diameter from 2.4 to ≈ 9.9-11.0 Å.^{253,255,256,259} The diameter of the CB[*n*] portal is approximately 2 Å narrower than the inner cavity.²⁴⁹ The CB[*n*]s cavity volumes cover a very large range from 82–870 Å³.^{251,255,256,259} The stability of CB[*n*]s homologues is

Chapter 1

affected by the angular tension after cyclization, and can be inferred from the relative strain energy upon cyclization (Table 1.5).²⁵⁶ The most stable homologue is CB[6], closely followed by CB[7] with relative strain energy ≈ 1 kcal/mol. CB[5] and CB[8] have less than 6 kcal/mol relative strain energy, while CB[10] possess a significantly high value (above 20 kcal/mol). CB[n]s have high thermal stability in the solid state.^{256,260} No decomposition is observed up to 420 °C for CB[n] ($n = 5, 6$ and 8) although CB[7] starts decomposing at lower temperature (370 °C).^{254,256}

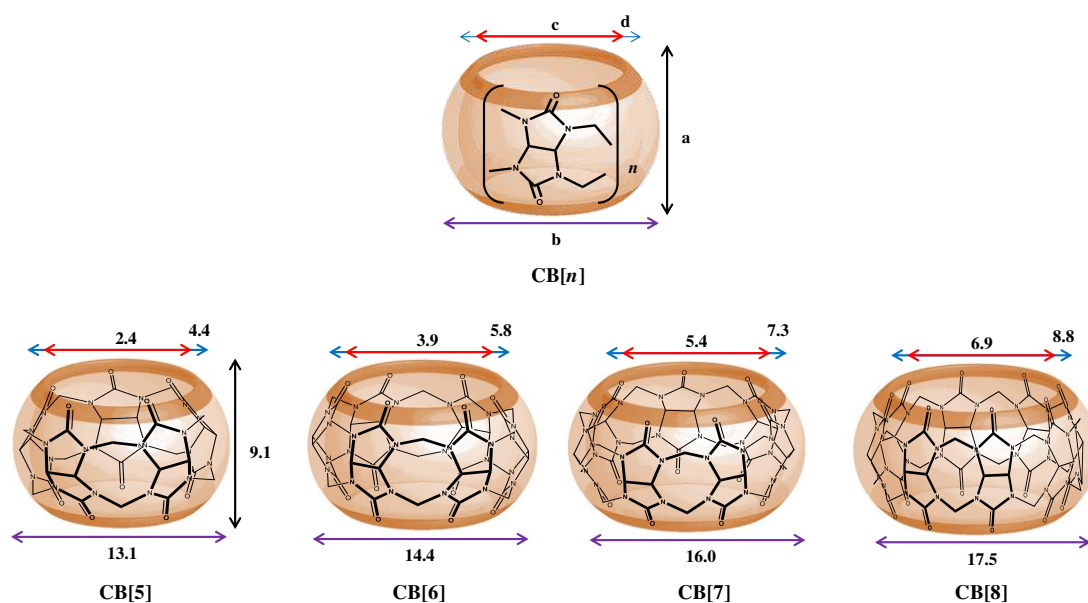


Figure 1.15. Structural representations of cucurbiturils. The cavity height (a), outside diameter (b), portal diameter (c) and inner cavity diameter (d) in Å are shown for CB[5]-CB[8].

1.2.4. Host-guest chemistry of CB[n]s through noncovalent interactions

The glycoluril unit provides a hydrophobic nanocavity in which the portals are composed of polar carbonyl groups (Figure 1.16), allowing the CB[n]s to bind to polar and nonpolar organic molecules and encapsulate small molecules by noncovalent interactions (*e.g.*, hydrogen-bonding, Van der Waals, coulombic and π - π interactions).^{253,257} The carbonyl oxygen atoms possess high electron density and consequently improve the cation-receptor ability.

Chapter 1

Table 1.5. Structural and physicochemical properties of CB[*n*]s (*n* = 5-8, 10).

Parameters	CB[5]	CB[6]	CB[7]	CB[8]	CB[10]	Ref.
Number of monomers	5	6	7	8	10	
Molecular weight	830	997	1163	1329	1661	
Water solubility (mM)	20-30	0.018	20-30	< 0.01	< 0.05	255,256,258
Cavity height, a (Å)	9.1	9.1	9.1	9.1	9.1	253,255,256,259
Outside diameter, b (Å)	13.1	14.4	16.0	17.5	18.7-21.0	253,324,325,258,347
Portal diameter, c (Å)	2.4	3.9	5.4	6.9	9.0-11.0	253,324,325,258,347
Inner cavity diameter, d (Å)	4.4	5.8	7.3	8.8	10.7-12.6	253,324,325,258,347
Cavity volume (Å ³)	82	164	279	479	870	253,324,325,258,347
Strain energy (kcal/mol) ^a	5.06	0.00	1.14	5.86	21.41	198,258
Stability (°C)	> 420	425	370	> 420	—	198,256,258,260

^a The relative strain energies were obtained through *ab initio* calculation.^{198,258}

Chapter 1

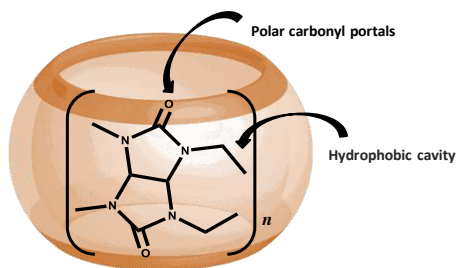


Figure 1.16. Opening of the cavity and hydrophobic nature of the cavity in CB[n]s.

CB[n]s are able to form stable complexes with various guests, like drug molecules²⁶¹, amino acids and peptides^{262,263}, saccharides²⁶⁴, proteins²⁶⁵, dyes²⁶⁶, perfluorinated hydrocarbons²⁵⁰, organometallic complexes^{267–269}, inorganic cations and complexes^{270–272}. Due to their rigid structure, ease of synthesis and variety of size and functionality, CB[n]s can be used for a variety of applications such as catalysis^{273,274}, fluorescence sensing²⁷⁵, molecular sensors²⁷⁶.

The macrocyclic hosts require a complementarity between the guest's size and the binding site volume to allow the formation of the inclusion complex. For example, the larger size of CB[7] cavities than CB[6] allows forming compounds with larger guest molecules (and with different properties) which could not be included in CB[6], broadening the applications profile. When a guest is encapsulated inside the cavity of CB[n], it is important to understand the modifications in the physical (particularly electronic and/or magnetic) microenvironment of the inner cavity.²⁵⁰ Solubility of CB[n]s in common solvents is low (< 0.1 mM), excluding CB[5] and CB[7] which have a moderate solubility in water (20-30 mM) at room temperature.^{255,256,277} Compared to other macrocyclic receptors such as cyclodextrins, CB[7] is slightly more voluminous than β -cyclodextrin (β -CD) in terms of cavity size and its solubility is higher in water (16 mM for β -CD at room temperature).²⁵⁷ In addition, the family of CB[n]s exhibits higher affinity constants for positively charged molecules or of neutral charge, which are several orders of magnitude greater than those for CD hosts. This results from the balance between charge, size and hydrophobicity of the guest molecule when the formation of an inclusion complex with the guest molecule is favourable.

The high potential of CB[n]s is associated with the following properties: (1) commercial availability in different sizes, (2) strong binding interactions, (3) high molecular recognition, (4) synthesis control over size, shape and functional-group, (5) high structural integrity, (6) different solubilities in organic and aqueous solution, (7) association and dissociation with controlled kinetics, and (8) control of the molecular recognition processes by suitable electrochemical, photochemical, and chemical stimuli.

Chapter 1

The interest in the CB[*n*] family has been increasing and it is associated with the great advances in many areas of science (chemistry, biology, materials science, and nanotechnology) that rely on the ability to employ and control noncovalent interactions between molecules.

Supramolecular structures based on molybdenum compounds with CB[*n*]s

As already mentioned in the general introduction to cucurbit[*n*]urils, a wide variety of molecules can form inclusion compounds with CB[*n*]s.^{278–281} They included among the guests appropriate inorganic and organometallic compounds with molybdenum. The ability of CB[*n*]s to include a part of these compounds in their internal hydrophobic cavities or carbonyl portals has been demonstrated by few researchers. The inclusion generally modifies the chemical, electrochemical, and photochemical properties of the compounds. Among molybdenum compounds, the following stand out heterometallic cluster aqua complexes^{245,282–286}, molybdenum sulfide aqua complexes^{21,246,287–289}, molybdenum selenide aqua complexes^{21,290,291}, aquaoxochloromolybdenum complexes^{243–245}, metallocene complexes containing hydrophobic ligands such as cyclopentadienyl ($\eta^5\text{-C}_5\text{H}_5$, Cp)²⁹² (Table 1.6).

Chalcogenide homo- and heterometallic cubane complexes of many transition metals belong to basic structures in the chemistry of cluster complexes and are of great importance in bioinorganic chemistry. In heterometallic complexes containing the cubane cluster fragments $[\text{Mo}_3(\mu_3\text{-Q})_4\text{M}']^{4+}$ (Q = S, Se and M' = Ni, Pd), the nickel and palladium atoms are in the tetrahedral environment and are coordinated by three bridging S or Se atoms.²⁹³

Fedin and co-workers can be considered pioneers in the development of supramolecular assemblies containing this type of complexes and CB[*n*]s. The authors have synthesized a Pd/Mo/Se complex containing a new cluster core $[\text{PdMo}_3\text{Se}_4]^{4+}$ in high yield by the reaction of the triangular selenide-bridge molybdenum complex $[\text{Mo}_3\text{Se}_4(\text{H}_2\text{O})_9]^{4+}$ with Pd ions in a hydrochloric solution.²⁹⁴ The supramolecular approach to crystallization of aqua complexes, *i.e.* the construction of a system of complementary hydrogen bonds, was successfully used for the isolation of the heterometallic complex from dilute solutions in 2 M HCl. The structure of the supramolecular adduct with cucurbituril of composition $[\text{ClPdMo}_3\text{Se}_4(\text{H}_2\text{O})_7\text{Cl}_2]@\text{CB}(6)$ (Table 1.6, guest 2) was determined by X-ray diffraction analysis. Another Pd/Mo/Q complex was prepared for the development of the supramolecular material $[\text{Mo}_3\text{PdP}(\text{OH})_3\text{S}_4\text{Cl}_3(\text{H}_2\text{O})_6]_2@\text{CB}[6]^{295}$ (Table 1.6, guest 19), the structure of which was confirmed by X-ray analysis.

Chapter 1

The first examples of hydrolytically stable, supramolecular architectures based on cucurbituril adducts of single-cube Ni-Mo aqua cluster cations were obtained from the $[\text{Mo}_3\text{NiS}_4(\text{H}_2\text{O})_{10}]^{4+}$ cluster cation and the organic cavitand cucurbituril CB[6] in aqueous solutions of HCl.²⁸³ Crystals of $\{[\text{Mo}_3\text{S}_4\text{Ni}(\text{H}_2\text{O})_7\text{Cl}_3]@\text{CB}[6]\text{Cl}\cdot 13\text{H}_2\text{O}$ (Table 1.6, guest 4) were obtained in low yield (12 %) by the reaction of cucurbituril with $[\text{Mo}_3\text{S}_4\text{Ni}(\text{H}_2\text{O})_{10}]^{4+}$ in a 3 M aqueous solution of HCl. The X-ray structure of the crystals reveals an organic-inorganic hybrid material of cucurbituril molecules and $[\text{Mo}_3\text{S}_4\text{Ni}(\text{H}_2\text{O})_7\text{Cl}_3]^+$ cluster cations in a ratio of 1:1, assembled through strong hydrogen bonds. One Cl^- ligand is attached to the Ni center, while the other two Cl^- ligands are coordinated to Mo. Each Mo center is coordinated by two water molecules, and thus six water molecules form hydrogen bonds with six portal oxygen atoms of CB[6]. The Ni-Mo cluster cation and the cucurbituril molecule are held together by complementary H-bonds to form a structure in which only one of the portals of the cucurbituril molecule is effectively covered with the cluster ions to resemble a “lid” on a “barrel”. Crystals of $[\text{Mo}_3\text{S}_4\text{Ni}(\text{H}_2\text{O})_8\text{Cl}_2]@\text{CB}[6]$ (Table 1.6, guest 4) were obtained in very high yield (88 %) when pyridine was added to the reaction mixture of cucurbituril and 2 equivalents of $[\text{Mo}_3\text{S}_4\text{Ni}(\text{H}_2\text{O})_{10}]^{4+}$ in a 3 M aqueous solution of HCl. The X-ray structure analysis of this compound reveals a PyH^+ cation encapsulated in the cucurbituril cavity. These two supramolecules are hydrolytically stable and are insoluble, even in boiling water or 3 M HCl solution.

The cluster aqua complexes $[\text{Mo}_3(\text{MCl})\text{S}_4(\text{H}_2\text{O})_9]^{3+}$ ($\text{M} = \text{Pd}$ or Ni) in HCl solutions induce isomerization of hydrophosphoryl compounds, such as $(\text{HO})_2\text{P}(\text{O})\text{H}$, $(\text{HO})\text{P}(\text{O})\text{H}_2$, $\text{PhP}(\text{O})(\text{OH})\text{H}$, and $\text{Ph}_2\text{P}(\text{O})\text{H}$ into the hydroxo tautomers $\text{P}(\text{OH})_3$, $\text{HP}(\text{OH})_2$, $\text{PhP}(\text{OH})_2$, and $\text{Ph}_2\text{P}(\text{OH})$, which are stabilized by coordination of the phosphorus atom to the Pd or Ni atoms.²⁹⁶ The complex $[\text{Mo}_3(\text{Pd}(\text{PhP}(\text{OH})_2))\text{S}_4(\text{H}_2\text{O})_2\text{Cl}_7]^{3-}$ was isolated as a supramolecular adduct with CB[8], and the complex $[\text{Mo}_3(\text{Ni}(\text{P}(\text{OH})_3))\text{S}_4(\text{H}_2\text{O})_8\text{Cl}]^{3+}$ was isolated as an adduct with CB[6], since the hydroxy tautomers can be easily oxidized, hindering the isolation of the corresponding complex in the solid phase. The structures of both compounds were established by X-ray diffraction analysis. The structural components of the metallic complex and CB[*n*] are linked to each other by a hydrogen bond network involving water molecules of crystallization.

The ability of other cubes $[\text{Mo}_3\text{Q}_4(\text{H}_2\text{O})_9]^{4+}$ ($\text{Q} = \text{S}, \text{Se}$) to form heterometallic Hg-containing derivatives has also been explored with the preparation of a partially Cl-substituted cucurbituril and the double cube $[\text{Mo}_6\text{HgSe}_8(\text{H}_2\text{O})_{18}]^{8+}$, giving $[\text{Mo}_6\text{HgSe}_8\text{Cl}_4(\text{H}_2\text{O})_{14}]@\text{CB}[6]$ (Table 1.6, guest 5).²⁸² The compound has six carbonyl O atoms above and six below the ring of the cucurbituril molecule, which hydrogen

Chapter 1

bond to H₂O ligands of the double cube. Four chlorides are coordinated to Mo, and four chlorides act as counterions. The cations [Mo₆HgSe₈Cl₄·(H₂O)₁₄]⁴⁺ are sandwiched between two cucurbituril units, and the cation and cucurbituril alternate with each other to give linear chains. This structure has pseudohexagonal packing typical of rod-like structures.

The method developed by Fedin in the previous works was also used by Hernandez-Molina *et al.*²⁸⁵ for the construction of supramolecular architecture based on a heterobimetallic cuboidal cluster containing metallic iron with the new [Mo₃FeS₄]⁴⁺ core and CB[6]: [Mo₃(FeCl)S₄(H₂O)₈Cl]₂@CB[6] (Table 1.6, guest 15). The supramolecular approach based on building large aggregates between six of the water molecules coordinated to the cluster core and six carbonyl groups decorating each portal of the macrocyclic cavitand cucurbit[6]uril permits the formation of complementary hydrogen bonds between them, leading to the formation of well-formed crystals of the supramolecular adduct with cluster/cucurbituril stoichiometries of 1:1. By isolation and X-ray analysis of this cucurbituril adduct in HCl solutions, chloride is coordinated to the heterometal (Fe in the present case) while the affinity of Mo for Cl is lower.

For a given equilibrium concentration of Cl⁻ ions, the solution is assumed to have a set of equilibrium forms of [Mo₃Q₄(H₂O)_{9-x}Cl_x]^{(4-x)+} (Q = S or Se) chloroaqua complexes. Supramolecular architectures based on cucurbituril adducts of hydrogen-bonded molybdenum sulfide aqua complexes were reported by Fedin *et al.*^{287,288} Crystals of [Mo₃S₄(H₂O)₆Cl₃][Mo₃S₄(H₂O)₇Cl₂]₂@CB[6] (Table 1.6, guest 1), [Mo₃S₄(H₂O)₇Cl₂]₂@CB[6] (Table 1.6, guest 8), (H₃O)₈[Mo₃S₄(H₂O)_{2.5}Cl_{6.5}]₂@CB[8] (Table 1.6, guest 9), and finally [Mo₃S₄(H₂O)₇Cl₂]₂@CB[6] and [Mo₃S₄(H₂O)₄Cl₅]₂@CB[8] (Table 1.6, guests 13)²¹, were obtained generally by reaction of CB[*n*] (*n* = 6 or 8) and [Mo₃S₄(H₂O)₉]⁴⁺ in aqueous HCl. These supramolecules are rather stable and insoluble in water or hydrochloric acid. The binding of the guest molecule is controlled by effective blocking of the portals of the molecular container, through hydrogen-bonding to the cucurbituril portal and the H₂O molecules coordinated to molybdenum atoms. Abramov *et al.*²⁴⁶ have also synthesized the supramolecular compound [Mo₃S₄Cl_{6.25}Br_{0.25}(H₂O)₂]₂@CB[6].

The last author and co-workers have also studied the formation of supramolecular assemblies based on molybdenum selenide aqua complexes.^{21,290,291} Crystalline adducts of chloroaqua complexes of the type [Mo₃Se₄Cl_x(H₂O)_{9-x}]^{(4-x)+} with cucurbit[*n*]urils were prepared from solutions of the seleno bridged triangular cluster Mo₃Se₄(aq)⁴⁺ in HCl, with different compositions, depending on the HCl concentration. From 2 M HCl, a monosubstituted cationic cluster crystallizes as

Chapter 1

$[\text{Mo}_3\text{Se}_4\text{Cl}(\text{H}_2\text{O})_8]_2@[\text{CB}[6]]^{290}$ (Table 1.6, guest 6), and also $[\text{Mo}_3\text{Se}_4(\text{H}_2\text{O})_6\text{Cl}_3]@[\text{CB}[6]]$ (Table 1.6, Q, guest 13), depending of other reagents and reaction. An increase in HCl concentration to 6 M gave a penta-substituted anionic species, $[\text{Mo}_3\text{Se}_4\text{Cl}_5(\text{H}_2\text{O})_4]_2@[\text{CB}[6]]^{290}$ (Table 1.6, guest 6). The crystal structures of both were determined by X-ray crystallography, which showed the portal of CB[6] to be covered with cluster cations $[\text{Mo}_3\text{Se}_4\text{Cl}(\text{H}_2\text{O})_8]^{3+}$. The oxo-selenido assembly $[\text{Mo}_3(\mu_3\text{-Se})(\mu\text{-O})_3(\text{H}_2\text{O})_6\text{Cl}_3]_2@[\text{CB}[6]]^{291}$ (Table 1.6, guest 14) was obtained. This structure is built of cluster cations $\{[\text{Mo}_3(\mu_3\text{-Se})(\mu\text{-O})_3(\text{H}_2\text{O})_6\text{Cl}_3]^{3+}$ which form adducts with the cavitand molecule CB[6], together with outer-sphere Cl^- and solvent H_2O molecules. The cluster cation contains the Mo_3 triangle, capped with the $\mu_3\text{-Se}$ atom and bridged by three $\mu\text{-O}$ atoms. This cluster unit is coordinated by three Cl^- and six water molecules. The mutual arrangement of the Cl^- and H_2O ligands corresponds to the maximum symmetry of the cluster complex, so that each Mo atom coordinates one Cl^- (*trans* to $\mu_3\text{-Se}$ atom) and two water molecules (*cis* to $\mu_3\text{-Se}$ atom). The supramolecular compound $[\text{Cl}_3\text{SnMo}_3\text{Se}_4\text{Cl}_3(\text{H}_2\text{O})_6][\text{Cl}_3\text{SnMo}_3\text{Se}_4\text{Cl}_2(\text{H}_2\text{O})_7]@[\text{CB}[6]]^{284}$ (Table 1.6, guest 7) was isolated from a solution of the selenium-containing molybdenum cluster $[\text{Cl}_3\text{SnMo}_3\text{Se}_4(\text{H}_2\text{O})_9]^{3+}$, and organic cavitand CB[6]. X-ray diffraction analysis demonstrated that the macrocyclic cucurbituril molecule is coordinated on both sides by the cluster cations through the formation of complementary hydrogen bonds. In this compound, the bridging $\mu_2\text{-Se}$ atoms of the cluster fragment Mo_3Se_4 are coordinated to the Sn atom of the SnCl_3^- ligand, thus losing the ability to be involved in $\text{Se}\cdots\text{Se}$ interactions.

Samsonenko *et al.* were the first to report the interactions of trinuclear molybdenum oxo clusters with chloride as ligand in $\text{CB}[n]$ s ($n = 5$ and 6): $[\text{Mo}_3\text{O}_4(\text{H}_2\text{O})_6\text{Cl}_3]_2@[\text{CB}[6]]^{245}$ and $[\text{Mo}_3\text{O}_4(\text{H}_2\text{O})_6\text{Cl}_3]_2@[\text{CB}[5]]^{243}$ (Table 1.6, guests 3 and 11). Both compounds were prepared by evaporation of a hydrochloric acid solution containing NaCl, the trinuclear aqua complex $[\text{Mo}_3\text{O}_4(\text{H}_2\text{O})_9]^{4+}$, and the macrocyclic cavitand CB[5] or CB[6]. X-ray diffraction analysis demonstrated that the $\text{CB}[n]$ molecules are closed on both sides by the cluster cations through hydrogen bonding between the CO groups of the $\text{CB}[n]$ portals and the aqua ligands of the oxo cluster.

Abramov *et al.*²⁴⁶ found that the addition of CB[6] to a solution of oxothio cluster complex $\text{Mo}_3\text{O}_2\text{S}_2^{4+}$ in 4 M HCl leads to the crystallization of $[\text{Mo}_3\text{O}_2\text{S}_2\text{Cl}_6(\text{H}_2\text{O})_3]_2@[\text{CB}[6]]$. The authors have observed that the adjacent molecules of CB[6] are tilted in the opposite directions to form cavities suitable for bulky cluster anions $[\text{Mo}_3\text{O}_2\text{S}_2\text{Cl}_6(\text{H}_2\text{O})_3]^{2-}$ and the host structures were distorted under the effect of the steric requirements of the guest.²⁴⁶ They also reported the reaction of $[\text{Mo}_2\text{O}_2(\mu_3\text{-$

Chapter 1

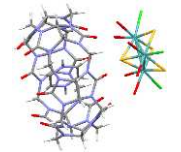
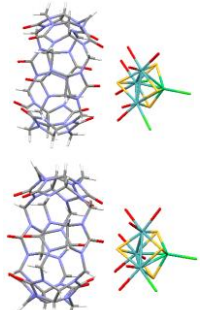
$S)_2(H_2O)_6]^{2+}$ in 2 M HCl, which results in condensation of binuclear clusters with the formation of $\{Mo_3(\mu_3-S)(\mu-O)_3\}^{4+}$ species, culminating in isolation of $[Mo_3(\mu_3-S)(\mu_2-O)_3(H_2O)_6Cl_3]_2@CB[6]$.²⁴⁶ The arrangement in the crystal structure is routinely found in the adducts of 2{cluster}:1CB[6] stoichiometry. In this supramolecular complex, the cluster cations at the opposite portals of CB[6] eclipse each other.

Lin *et al.*²⁴⁴ reported in 2005 the encapsulation of a neutral dinuclear complex in CB[6]. In this study, CB[6] crystallized with bis(μ -oxo- $\kappa^2O:O$)bis[aquaioxodichloromolybdenum(VI)] $\cdot 10.5H_2O$, giving a solid with the formula $[Mo_2O_4Cl_4(H_2O)_2]@CB[6]$ (Table 1.6, guest 10). X-ray crystallography revealed that the molybdenum-bearing component interacts indirectly through hydrogen bond with the polar carbonyl groups of CB[6], through the two coordinated water molecules, forming a three-dimensional network structure. In the dinuclear entity, the Mo atoms are linked by a Mo-Mo bond, and the metal atom in that compound exists in a 5+ oxidation state.

Presently, there is only one publication referring molybdocene included in CB[n], reported by Harding *et al.*²⁹² in 2008 (Table, guest 16). The encapsulation of the 1:1 aquated forms of molybdocene dichloride (Table 1.6, guests 12) by CB[n] ($n = 7$ and 8) was studied by 1H NMR spectroscopy and mass spectrometry. Unfortunately, the inclusion complex was unable to be fully characterised. Upon hydrolysis, the molybdocene forms its hydrated specie present at physiological pH. The structure of the species in aqueous solution was dependent on several parameters, such as concentration, pH and salt. In these complexes, both the cyclopentadienyl ligands and metal center are positioned inside the cucurbituril cavity via hydrophobic interactions. As the portals of CB[8] are significantly wider than those of CB[7], the encapsulated molybdocene is positioned further from the portal rim for CB[8] compared to CB[7]. It was also tested the introduction of Cp_2MoCl_2 in CB[5], but the encapsulation is not possible due to the smaller size of the cavity.²⁹² The aqueous solubility of molybdocene dichloride can be improved by the formation of the inclusion complex CB[7]- $[Cp_2Mo(OH)(OH_2)]^+$. Unexpectedly a significant degradation of the CB[n] framework was observed with the hydrated molybdocene under oxygen atmosphere. The degradation observed in this study is unprecedented and appears to be related to the Mo metal.²⁹²

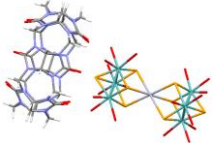
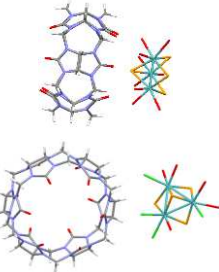
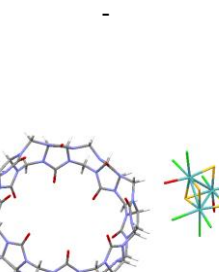
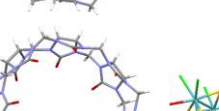
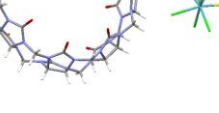
Chapter 1

Table 1.6. Summary of reports of supramolecular assemblies between molybdenum-based guests and CB[*n*]s, and their characterizations. The atoms are identified as: Mo - turquoise, O - red, H - white, C - dark grey, N - blue, Cl - light green, S – yellow, Se – dark yellow, Fe - orange, Hg - light grey, Ni - dark green.

Guest	Host	Characterization	Application	Crystal structure	Ref.
(1) $[\text{Mo}_3\text{S}_4(\text{H}_2\text{O})_6\text{Cl}_3]^+$	CB[6]	Elemental analysis and X-ray crystallography	-		287
(2) $[\text{ClPdMo}_3\text{Se}_4(\text{H}_2\text{O})_7\text{Cl}_2]^+$	CB[6]	X-ray crystallography	-	-	294
(3) $[\text{Mo}_3\text{O}_4(\text{H}_2\text{O})_6\text{Cl}_3]^{2+}$	CB[6]	Elemental analysis and X-ray crystallography	-	-	243
(4) $[\text{Mo}_3\text{S}_4\text{Ni}(\text{H}_2\text{O})_7\text{Cl}_3]^+$ and $[\text{Mo}_3\text{S}_4\text{Ni}(\text{H}_2\text{O})_8\text{Cl}_2]^{3+}$	CB[6]	Elemental analysis and X-ray crystallography	-		283

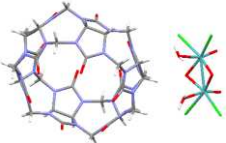
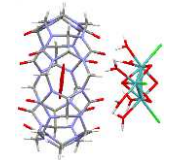
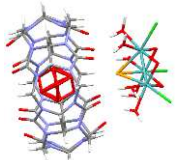
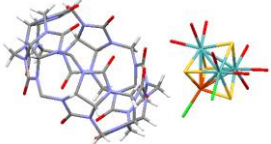
Chapter 1

Table 1.6. continuation

(5) $[\text{Mo}_6\text{HgSe}_8\text{Cl}_4(\text{H}_2\text{O})_{14}]^{4+}$	CB[6]	X-ray crystallography	-		282
(6) $[\text{Mo}_3\text{Se}_4\text{Cl}(\text{H}_2\text{O})_8]^{3+}$ and $[\text{Mo}_3\text{Se}_4\text{Cl}_5(\text{H}_2\text{O})_4]^-$	CB[6]	Elemental analysis and X-ray crystallography	-		290
(7) $\{[\text{Cl}_3\text{SnMo}_3\text{Se}_4\text{Cl}_3(\text{H}_2\text{O})_6][\text{Cl}_3\text{SnMo}_3\text{Se}_4\text{Cl}_2(\text{H}_2\text{O})_7]\}^-$	CB[6]	Elemental analysis, FT-IR spectroscopy and X-ray crystallography	-		284
(8) $[\text{Mo}_3\text{S}_4(\text{H}_2\text{O})_7\text{Cl}_2]^{2-}$	CB[6]	X-ray crystallography	-		288
(9) $[\text{Mo}_3\text{S}_4(\text{H}_2\text{O})_{2.5}\text{Cl}_{6.5}]^{5-}$	CB[8]	X-ray crystallography	-		289

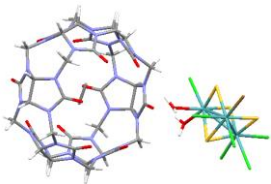
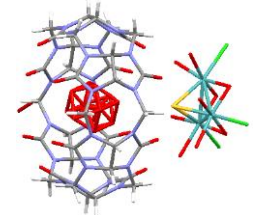
Chapter 1

Table 1.6. *continuation*

(10) $[\text{Mo}_2\text{O}_4\text{Cl}_4(\text{H}_2\text{O})_2]$	CB[6]	X-ray crystallography	-		244
(11) $[\text{Mo}_3\text{O}_4(\text{H}_2\text{O})_6\text{Cl}_3]^+$	CB[5]	Elemental analysis, FT-IR spectroscopy and X-ray crystallography	-		245
(12) $[\text{Mo}_3(\text{Pd}(\text{PhP}(\text{OH})_2))\text{S}_4(\text{H}_2\text{O})_2\text{Cl}_7]^{3-}$ and $[\text{Mo}_3(\text{Ni}(\text{P}(\text{OH})_3))\text{S}_4(\text{H}_2\text{O})_8\text{Cl}]^{3+}$	CB[<i>n</i>] <i>n</i> = 6, 8	Elemental analysis and X-ray crystallography	-	-	245
(13) $[\text{Mo}_3\text{S}_4(\text{H}_2\text{O})_7\text{Cl}_2]^{2+}$, $[\text{Mo}_3\text{Se}_4(\text{H}_2\text{O})_6\text{Cl}_3]^+$ and $[\text{Mo}_3\text{S}_4(\text{H}_2\text{O})_4\text{Cl}_5]^-$	CB[<i>n</i>] <i>n</i> = 6, 7	Elemental analysis and X-ray crystallography	-	-	21
(14) $[\text{Mo}_3(\mu_3\text{-Se})(\mu\text{-O})_3(\text{H}_2\text{O})_6\text{Cl}_3]^+$	CB[6]	Elemental analysis and X-ray crystallography	-		291
(15) $[\text{Mo}_3(\text{FeCl})\text{S}_4(\text{H}_2\text{O})_8\text{Cl}]^{2+}$	CB[6]	X-ray crystallography	-		285

Chapter 1

Table 1.6. *continuation*

(16) $\text{Cp}_2\text{Mo}(\text{OH})(\text{OH}_2)^+$	CB[7]	NMR spectroscopy and mass spectrometry	Antitumour agent	-	292
(17) $[\text{Mo}_3\text{O}_2\text{S}_2\text{Cl}_6(\text{H}_2\text{O})_3]^{2-}$ and $[\text{Mo}_3\text{S}_4\text{Cl}_{6.75}\text{Br}_{0.25}(\text{H}_2\text{O})_2]^{3-}$	CB[6]	X-ray crystallography	-		297
(18) $[\text{Mo}_3(\mu_3\text{-S})(\mu_2\text{-O})_3(\text{H}_2\text{O})_6\text{Cl}_3]^+$	CB[6]	Elemental analysis and X-ray crystallography	-		246
(19) $[\text{Mo}_3\text{PdP}(\text{OH})_3\text{S}_4\text{Cl}_3(\text{H}_2\text{O})_6]^+$	CB[6]	X-ray crystallography	-	-	286

1.3. Catalytic systems based on molybdenum compounds with CB[*n*]s

Until the present, there are no reports concerning supramolecular systems based on molybdenum compounds with CB[*n*]s applied in catalysis for organic reactions. Catalytic applications are still waiting to be extensively explored.

Although CB-mediated catalysis has made important contributions to organic synthesis (Table 1.7), the virtual lack of solubility of CBs in common organic solvents has restricted the reaction scope to transformations involving aqueous solutions *e.g.* acid hydrolysis^{298,299}, oxidation of alcohols³⁰⁰, desilylation³⁰¹, and photodimerisation³⁰². One exception is the use of an oxovanadium(IV)–CB[6] complex as a heterogeneous catalyst for hydrocarbon oxidation.³⁰³

The existence of porosity in CB[*n*]s has been attributed to interstitial voids in amorphous solids³²⁸ or channels in crystalline materials.^{329–332} In addition to water molecules, the voids or channels may be filled with acid molecules, which has led to the suggestion that CB[*n*]s based materials could have potential as acid catalysts.³³³ However, the use of CB[*n*]s assemblies as acid catalysts has hardly been explored.

Bruno *et al.*³²⁷ reported the catalytic activity of CB[7] for the heterogeneous alcoholysis of epoxides (Table 1.8). In this work, metal-free CB[7] solid-state assemblies promote acid-catalysed alcoholysis of aliphatic and aromatic epoxides under mild conditions to give β -alkoxy alcohols. The acid-catalysed alcoholysis of epoxides is an important transformation in the synthesis of β -alkoxy alcohols, which are useful intermediates for the synthesis of α -alkoxy ketones, α -alkoxy acids, enol ethers, and a range of bioactive natural and synthetic products.^{334–338} The catalytic process was heterogeneous, and the catalyst can be reused in consecutive runs via simple separation, washing and drying procedures.

In the ethanolysis of styrene oxide (StyOx), CB[7] was highly active and selective to 2-ethoxy-2-phenylethanol (StyOEt) formed with 100 % selectivity at 100 % conversion within 1 h of reaction at approximately room temperature (35 °C). The alcoholysis reaction rate can be increased with the temperature increase, from 35 to 55 °C, leading to 96 % conversion at 10 min and without significant changes in the product selectivity. At 55 °C, it was possible to reduce the catalyst loading from 10 to 5 g_{cat} L⁻¹ and still obtain complete conversion (at 30 min). The conversion of StyOx was negligible without CB[7]. Other studies reported for metal-free solid acid catalysts tested in the same reaction confirm the efficient catalytic performance of CB[7].^{339–341}

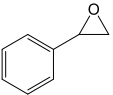
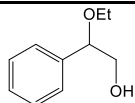
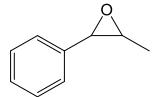
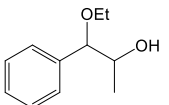
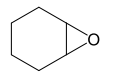
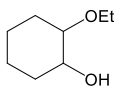
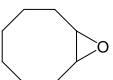
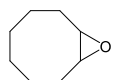
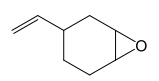
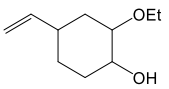
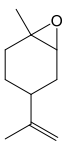
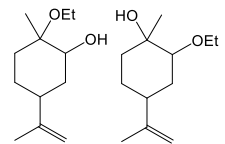
Chapter 1

Table 1.7. Timeline of reports using cucurbit[*n*]urils in chemical reactions.

Year	Reaction	Host	Reaction conditions	Ref.
1983	1,3-Dipolar cycloaddition	CB[6]	Aq. formic acid, 40 °C	304
2001	Photodimerization	CB[8]	$h\nu$ (300 nm)	305
2005, 2006	Photodimerization	CB[8]	$h\nu$ (Hg lamp)	306,307
2005, 2007, 2014	Photodimerization	CB[8]	$h\nu$ (Hg lamp)	308–310
2006	Photodimerization	CB[7]	$h\nu$ (365 nm)	311
2008	Photodimerization	CB[8]	$h\nu$ (Hg lamp)	312,313
2008, 2010, 2011	Photodimerization	CB[8]	$h\nu$ (> 300 nm)	302,314–316
2008, 2014	Photodimerization	CB[8]	$h\nu$ (> 300 nm)	317,318
2009	Hydrolysis	CB[6], CB[7]	-	298
2009, 2011, 2015	Oxidation	CB[8]	σ -iodoxybenzoic acid	300,319,320
2010	Oxidation	CB[6]	Oxovanadium(IV)	303
2010	Desilylation	CB[7]	Ag(I) salts	301
2010	Hydrolysis	CB[7]	-	299
2011	Photolysis	CB[7]	Transition metal ions	321
2013	Oxidation	HemiCB[6]	-	322
2013	Oxidation	HemiCB[6]	σ -iodoxybenzoic acid	323
2013	Retro-Diels-Alder	CB[6], CB[7], CB[8]	Gas phase	324
2014	Photofragmentation	CB[8]	$h\nu$ (Xe lamp)	325
2014	C-C and C-N bond forming	CB[6]	Metal-nanoparticles	326
2016	Alcoholysis	CB[7]	-	327

Chapter 1

Table 1.8. Reaction of different epoxides in the presence of CB[7].³²⁷

Substrate	<i>t</i> (h)	Conv. (%)	Yield (%)	Alkoxy alcohol product
 Styrene oxide	1	100	100	 2-Ethoxy-2-phenylethanol
 (1 <i>R</i> ,2 <i>R</i>)-Phenylpropylene oxide	6	87	100	 1-Ethoxy-1-phenyl-2-propanol
 Cyclohexene oxide	6	96	93	 2-Ethoxycyclohexanol
 Cyclooctene oxide	96	7	4	 2-Ethoxycyclooctanol
 4-Vinylcyclohexene oxide	24	96	62	 2-Ethoxy-4-vinylcyclohexanol
 (<i>R</i>)-(+)-Limonene oxide	24	95	73	 2-Ethoxy-2-methyl-5-(prop-1-en-2-yl)cyclohexanol and 2-ethoxy-1-methyl-4-(prop-1-en-2-yl)cyclohexanol

Chapter 1

The CB[7] was reused for three consecutive batch runs at 35 °C. StyOx conversion reached 100 % at 1 h in three runs, and the reaction was always 100 % selective to StyOEt. Compared with the original catalyst, no changes were observed in the FT-IR spectra and morphology (based on SEM analysis) of the reused catalyst. Thus, the physicochemical integrity of CB[7] was preserved during the catalytic process. The catalytic activity of CB[7] may be justified by the presence of entrapped H₃O⁺ ions, which are associated with the cocrystallised acid molecules that are difficult to remove.³³²

The catalytic performance of CB[7] was further investigated for the ethanolysis of cyclohexene oxide (Cy6Ox) as aliphatic epoxide at 35 °C. The reaction of Cy6Ox was fast, giving 2-ethoxycyclohexanol in 93 % yield at 96 % conversion. CB[7] was also tested for the ethanolysis of substituted aliphatic and aromatic C6-membered ring substrates, namely (1*R*,2*R*)-phenylpropylene oxide (Me-StyOx), 4-vinylcyclohexene oxide (vinyl-Cy6Ox) and the renewable epoxide R-limonene oxide (LimOx). With Me-StyOx as a substrate, 87 % conversion was reached at 6 h and 1-ethoxy-1-phenyl-2-propanol was the only product (100 % selectivity). With vinyl-Cy6Ox as a substrate, 96% conversion was reached at 24 h to give a 62% total yield (65 % total selectivity) of the *cis/trans* alkoxy alcohols. The ethanolysis of LimOx led to 95 % conversion at 24 h, giving 73 % total yield (77 % total selectivity) of alkoxy alcohol isomers, namely 2-ethoxy-2-methyl-5-(prop-1-en-2-yl)cyclohexanol and 2-ethoxy-1-methyl-4-(prop-1-en-2-yl)cyclohexanol.

Thus, the encapsulation of transition metal complexes, such as those of molybdenum, into cucurbiturils is an interesting idea for the preparation of new hybrid catalysts for organic reactions. Host-guest compounds should be explored as catalysts, paying attention to:

- checking the advantage of using host-guest compounds in preventing the decomposition of the catalysts and their reuse, wherein structural characterization of the catalysts recovered after catalytic batch runs could be carried out;
- comparing the catalytic performances of the host-guest compounds and the free (non-encapsulated) complexes.

1.4. Aim of this work

The necessity to form new hybrid materials based on organometallic complexes, which allow the isolation of these compounds from the reaction media, as well as enhanced stability and performance, has led to the development of new

Chapter 1

supports and consequently new methods of preparation. The emerging research on cucurbit[*n*]urils has not yet reached its full extent concerning its knowledge. The motivation to study the creation of supramolecular catalysts based on CB[*n*]s and organomolybdenum complexes stems from the fact that: i) Mo complexes are well-defined catalysts, with single catalytic site; ii) these complexes usually favour high activity and selectivity in important catalytic processes such as oxidation and acid alcoholysis; iii) Mo is economically attractive due to its relatively low cost; iv) the presence of Lewis base organic ligands coordinated to Mo helps to stabilize the compounds; v) CB[*n*]s are able to accommodate Mo compounds; vi) encapsulation of the complexes in CB[*n*]s may avoid deactivation phenomena; vii) they enable working in aqueous medium; and viii) CB[*n*]s are formed from cheap starting materials.

In chapter 2, it is discussed the first attempt to create a host-guest compound between ionic carbonyl complexes of the type $[\text{Mo}(\text{CO})_3\text{Br}(\text{L})]$ and $[\text{Mo}(\text{CO})_4(\text{L})]\text{Br}$ ($\text{L} = 2\text{-}(1\text{-propyltrimethylammonium-3-pyrazolyl})\text{pyridine bromide}$) with CB[7]. The idea consisted of the presence of an alkylammonium group in the organometallic complexes that may render the complexes more suitable for encapsulation in CB[*n*]s, since the binding may be stabilized by favourable hydrogen bonding or electrostatic interactions between the $-\text{NR}_3^+$ group and the carbonyl rimmed portals of the host. However, this attempt was unsuccessful, since no interaction was observed between the complexes and CB[7].

Since the attempt to bind ionic carbonyl complexes to CB[7] failed, a neutral carbonyl complex $[\text{Mo}(\text{CO})_4(\text{ppp})]$ ($\text{ppp} = 2\text{-}(1\text{-pentyl-3-pyrazolyl})\text{pyridine}$) was synthesized as a possible guest molecule to interact with CB[*n*] in chapter 3. However, this complex is insoluble in water, unlike CB[7] which is easily soluble in water, thereby making the formation of an ideal reaction liquid phase difficult. The possibility of using a CB[*n*] with better affinity to organic solvent was also considered, but the complex presented limited stability in several organic solvents, being susceptible to decarbonylation reactions. Also, during the stability studies in the catalytic tests, the complex $[\text{Mo}(\text{CO})_4(\text{ppp})]$ transforms into oxidized compounds: a polymeric hybrid material with the composition $[\text{Mo}_2\text{O}_6(\text{ppp})]$ is formed during olefin epoxidation with TBHP; the octanuclear complex $[\text{Mo}_8\text{O}_{24}(\text{ppp})_4]$ is formed during acid catalysis; $[\text{MoO}(\text{O}_2)_2(\text{ppp})]$ is forming during olefin epoxidation and the β -octamolybdate salt $[\text{bmim}]_4[\beta\text{-Mo}_8\text{O}_{26}]$ is formed in ionic liquid medium.

Apparently, the presence of an ionic or neutral pyrazolylpyridine ligand in organometallic complexes has no positive influence on the preparation of a supramolecular compound, and therefore, chapter 4 describes the synthesis of two tetracarbonylmolybdenum complexes bearing different types of organic ligands:

Chapter 1

specifically two chiral pyridanyl amine complexes. Once again, both complexes revealed to be insoluble in water and unstable when dissolved in organic solvents.

In chapter 5, molybdenum tricarbonyl complexes with isomeric monodentate nitrogen donor ligands (triazoles) were prepared. However, the two complexes were unstable in the presence of TBHP (which is typically used as oxidant in catalytic reactions for the epoxidation of olefins) forming polymeric oxide compounds.

The tendency of the carbonyl complexes to transform into oxidized compounds in the previous chapters led to the preparation of an oxidized compound as possible guest in chapter 6: $[\text{MoO}_3(2,2'\text{-bipy})]_n$. However, solubility tests with several solvents revealed that the compound is apparently insoluble.

Since the presence of carbonyl groups as ligands appears to not favour the formation of a host-guest compound, a different approach was applied in chapter 7, involving the preparation of the dichlorido complex $[\text{MoO}_2\text{Cl}_2(\text{pbim})]$ (pbim = 2-(2-pyridyl)benzimidazole). Its hydrolytic stability was studied, treating the complex with water. However, hydrolysis and condensation reactions gave an insoluble white solid ($[\text{MoO}_3(\text{pbim})]$) suspended in an acidic mother liquor formed by HCl, resulting from the cleavage of the Mo–Cl bonds in $[\text{MoO}_2\text{Cl}_2(\text{pbim})]$.

Finally, due to the unsuccessful influence of organic ligands into an organometallic complex, and the issues related to water solubility and stability, a dioxidomolybdenum(VI) halide complex with no organic ligands was prepared in chapter 8: $[\text{MoO}_2\text{Cl}_2(\text{H}_2\text{O})_2]$. A solution of $[\text{MoO}_2\text{Cl}_2(\text{H}_2\text{O})_2]$ can be prepared from an aqueous solution of molybdenum(VI) in hydrochloric acid, and therefore, be miscible with an acid solution of CB[6]. From this reaction, the new supramolecular hybrid material $[\text{MoO}_2\text{Cl}_2(\text{H}_2\text{O})_2]_2@CB[6]$ was prepared.

1.5. References

- (1) Bruce, D. W.; O'Hare, D. *J. Angew. Chem.* **1994**, *38*, 233–234.
- (2) Cheetham, A. K. *Science (80-.)*. **1994**, *264*, 794–795.
- (3) Hagrman, P. J.; Hagrman, D.; Zubieta, J. *J. Angew. Chem.* **1999**, *38*, 2638–2684.
- (4) Hagrman, D.; Hagrman, P. J.; Zubieta, J. *Comments Inorg. Chem.* **1999**, *796*, 225–261.
- (5) Hagrman, P. J.; Finn, R. C.; Zubieta, J. *Solid State Sci.* **2001**, *3*, 745–774.
- (6) Abrantes, M.; Amarante, T. R.; Antunes, M. M.; Gago, S.; Almeida Paz, F. A.; Margiolaki, I.; Rodrigues, A. E.; Pillinger, M.; Valente, A. A.; Gonçalves, I. S. *Inorg. Chem.* **2010**, *49*, 6865–6873.
- (7) Sheldon, R. A.; Kochi, J. K. *Introduction to Metal-Catalyzed Oxidations*; Academic Press: New York, 1981.

Chapter 1

- (8) Frausto da Silva, J. R. R.; Williams, R. J. P. *The Biological Chemistry of the Elements*; Claredon Press: Oxford, 1991.
- (9) Jørgensen, K. A. *Chem. Rev.* **1989**, *89*, 431–458.
- (10) Jimtaisong, A.; Luck, R. L. *Inorg. Chem.* **2006**, *45*, 10391–10402.
- (11) Tang, J.; Wang, L.; Liu, G.; Liu, Y.; Hou, Y.; Zhang, W.; Jia, M.; Thiel, W. R. *J. Mol. Catal. A Chem.* **2009**, *313*, 31–37.
- (12) Sözen-Aktaş, P.; Manoury, E.; Demirhan, F.; Poli, R. *Eur. J. Inorg. Chem.* **2013**, 2728–2735.
- (13) Amini, M.; Haghdoost, M. M.; Bagherzadeh, M. *Coord. Chem. Rev.* **2014**, *268*, 83–100.
- (14) Günyar, A.; Kühn, F. E. *J. Mol. Catal. A Chem.* **2010**, *319*, 108–113.
- (15) Coelho, A. C.; Nolasco, M.; Balula, S. S.; Antunes, M. M.; Pereira, C. C. L.; Almeida Paz, F. A.; Valente, A. A.; Pillinger, M.; Ribeiro-Claro, P.; Klinowski, J.; Gonçalves, I. S. *Inorg. Chem.* **2011**, *50*, 525–538.
- (16) Amarante, T. R.; Neves, P.; Paz, F. A. A.; Valente, A. A.; Pillinger, M.; Gonçalves, I. S. *Dalton Trans.* **2014**, *43*, 6059–6069.
- (17) Davis, M. F.; Levason, W.; Light, M. E.; Ratnani, R.; Reid, G.; Saraswat, K.; Webster, M. *Eur. J. Inorg. Chem.* **2007**, 1903–1910.
- (18) Monteiro, B.; Gago, S.; Neves, P.; Valente, A. A.; Gonçalves, I. S.; Pereira, C. C. L.; Silva, C. M.; Pillinger, M. *Catal. Lett.* **2009**, *129*, 350–357.
- (19) Nunes, C. D.; Valente, A. A.; Pillinger, M.; Rocha, J.; Gonçalves, I. S. *Chem. Eur. J.* **2003**, *9*, 4380–4390.
- (20) Kühn, F. E.; Herdtweck, E.; Haider, J. J.; Herrmann, W. A.; Gonçalves, I. S.; Lopes, A. D.; Romão, C. C. *J. Organomet. Chem.* **1999**, *583*, 3–10.
- (21) Manwani, N.; Gupta, M. C.; Ratnani, R.; Drake, J. E.; Hursthouse, M. B.; Light, M. E. *Inorg. Chim. Acta* **2004**, *357*, 939–945.
- (22) Bingham, A. L.; Drake, J. E.; Hursthouse, M. B.; Light, M. E.; Kumar, R.; Ratnani, R. *Polyhedron* **2006**, *25*, 3238–3244.
- (23) Arnaiz, F. J.; Aguado, R.; Sanz-Aparicio, J.; Martinez-Ripoll, M. *Polyhedron* **1994**, *13*, 2745–2749.
- (24) Arnáiz, F. J.; Aguado, R.; Pedrosa, M. R.; Mahía, J.; Maestro, M. A. *Polyhedron* **2002**, *21*, 1635–1642.
- (25) Li, F.; Yuan, G. *Angew. Chem., Int. Ed.* **2006**, *45*, 6541–6544.
- (26) Luan, Y.; Wang, G.; Luck, R. L.; Yang, M. *Eur. J. Inorg. Chem.* **2007**, 1215–1218.
- (27) Zapf, P. J.; Haushalter, R. C.; Zubieta, J. *Chem. Mater.* **1997**, *9*, 2019–2024.
- (28) Kim, J.; Lim, W. T.; Koo, B. K. *Inorg. Chim. Acta* **2007**, *360*, 2187–2191.
- (29) Lu, Y.; Wang, E.; Yuan, M.; Li, Y.; Hu, C. *J. Mol. Struct.* **2003**, *649*, 191–195.
- (30) Niu, J.; Wang, Z.; Wang, J. *Inorg. Chem. Commun.* **2004**, *7*, 556–558.
- (31) Xu, Y.; Lu, J.; Goh, N. K. *J. Mater. Chem.* **1999**, *9*, 1599–1602.
- (32) Rarig, R. S. Jr.; Zubieta, J. *Inorg. Chim. Acta* **2001**, *321*, 188–196.
- (33) Chuang, J.; Ouellette, W.; Zubieta, J. *Inorg. Chim. Acta* **2008**, *361*, 2357–2364.

Chapter 1

- (34) Hagrman, P. J.; LaDuca, R. L.; Koo, H. J.; Rarig, R.; Haushalter, R. C.; Whangbo, M. H.; Zubieta, J. *Inorg. Chem.* **2000**, *39*, 4311–4317.
- (35) Lysenko, A. B.; Senchyk, G. A.; Lincke, J.; Lässig, D.; Fokin, A. A.; Butova, E. D.; Schreiner, P. R.; Krautscheid, H.; Domasevitch, K. V. *Dalton Trans.* **2010**, *39*, 4223–4231.
- (36) Zhou, Y.; Zhang, L.; Fun, H.; U, X. Y. *Inorg. Chem. Commun.* **2000**, *3*, 114–116.
- (37) Valente, A. A.; Moreira, J.; Lopes, A. D.; Pillinger, M.; Nunes, C. D.; Romão, C. C.; Kuhn, F. E.; Gonc, I. S. *New J. Chem.* **2004**, *28*, 308–313.
- (38) Xu, Y.; Lu, J. *Inorg. Chim. Acta* **1999**, *295*, 222–228.
- (39) Laduca, R. L.; Rarig, R. S.; Zapf, P. J.; Zubieta, J. *Inorg. Chim. Acta* **1999**, *292*, 131–136.
- (40) Balula, S. S.; Bruno, S. M.; Gomes, A. C.; Valente, A. A.; Pillinger, M.; Gonçalves, I. S.; MacQuarrie, D. J.; Clark, J. H. *Inorg. Chim. Acta* **2012**, *387*, 234–239.
- (41) Amarante, T. R.; Neves, P.; Coelho, A. C.; Gago, S.; Valente, A. A.; Paz, F. A.; Pillinger, M.; Gonçalves, I. S. *Organometallics* **2010**, *29*, 883–892.
- (42) Neves, P.; Amarante, T. R.; Gomes, A. C.; Coelho, A. C.; Gago, S.; Pillinger, M.; Gonçalves, I. S.; Silva, C. M.; Valente, A. A. *Appl. Catal., A* **2011**, *395*, 71–77.
- (43) Kaes, C.; Katz, A.; Hosseini, M. W. *Chem. Rev.* **2000**, *100*, 3553–3590.
- (44) Pedrosa, M. R.; Escribano, J.; Aguado, R.; Sanz, R.; Díez, V.; Arnáiz, F. J. *Inorg. Chim. Acta* **2010**, *363*, 3158–3164.
- (45) Gonçalves, I. S.; Santos, A. M.; Romão, C. C.; Lopes, A. D.; Rodríguez-Borges, J. E.; Pillinger, M.; Ferreira, P.; Rocha, J.; Kühn, F. E. *J. Organomet. Chem.* **2001**, *626*, 1–10.
- (46) Sanz, R.; Pedrosa, M. R. *Curr. Org. Synth.* **2009**, *6*, 239–263.
- (47) Yin, G. *Coord. Chem. Rev.* **2010**, *254*, 1826–1842.
- (48) Rayner-Canham, G.; Overton, T. *Descriptive inorganic chemistry*, Fourth edi.; Freeman: New York, 2006.
- (49) Coelho, A. C.; Almeida Paz, F. A.; Klinowski, J.; Pillinger, M.; Gonçalves, I. S. *Molecules* **2006**, *11*, 528–538.
- (50) Gomes, A. C.; Bruno, S. M.; Gago, S.; Lopes, R. P.; Machado, D. A.; Carminatti, A. P.; Valente, A. A.; Pillinger, M.; Gonçalves, I. S. *J. Organomet. Chem.* **2011**, *696*, 3543–3550.
- (51) Amarante, T. R.; Neves, P.; Coelho, A. C.; Gago, S.; Valente, A. A.; Almeida Paz, F. A.; Pillinger, M.; Gonçalves, I. S. *Organometallics* **2010**, *29*, 883–892.
- (52) Twu, J. E. N.; Yu, Y.; Tang, C. E. I.; Ang, G. W. A. W.; Chen, K. *Appl. Spectrosc.* **1999**, *53*, 1083–1086.
- (53) Amarante, T. R.; Neves, P.; Coelho, A. C.; Gago, S.; Valente, A. A.; Almeida Paz, F. A.; Pillinger, M.; Gonçalves, I. S. *Organometallics* **2010**, *29*, 883–892.
- (54) Grover, N.; Kühn, F. E. *Curr. Org. Synth.* **2012**, *16*, 16–32.
- (55) Szymanska-Buzar, T. *Curr. Org. Chem.* **2012**, *16*, 3–15.
- (56) Jain, K. R.; Herrmann, W. A.; Kühn, F. E. *Coord. Chem. Rev.* **2008**, *252*, 556–568.

Chapter 1

- (57) Vaz, P. D.; Nunes, D.; C. *Curr. Org. Chem.* **2012**, *16*, 89–114.
- (58) Abrantes, M.; Sakthivel, A.; Romão, C. C.; Kühn, F. E. *J. Organomet. Chem.* **2006**, *691*, 3137–3145.
- (59) Abrantes, M.; Paz, F. A. A.; Valente, A. A.; Pereira, C. C. L.; Gago, S.; Rodrigues, A. E.; Klinowski, J.; Pillinger, M.; Gonçalves, I. S. *J. Organomet. Chem.* **2009**, *694*, 1826–1833.
- (60) O'Connor, J. M.; Casey, C. P. *Chem. Rev.* **1987**, *2*, 307–318.
- (61) Calhorda, M. J.; Felix, V.; Veiros, L. F. *Coord. Chem. Rev.* **2002**, *230*, 49–64.
- (62) Prinz, M.; Veiros, L. F.; Calhorda, M. J.; Romão, C. C.; Herdtweck, E.; Kühn, F. E.; Herrmann, W. A. *J. Organomet. Chem.* **2006**, *691*, 4446–4458.
- (63) Kühn, F. E.; Santos, M.; Abrantes, A. M. *Chem. Rev.* **2006**, *106*, 2455–2475.
- (64) Abrantes, M.; Santos, A. M.; Mink, J.; Kühn, F. E.; Romão, C. C. *Organometallics* **2003**, *22*, 2112–2118.
- (65) Martins, A. M.; Romão, C. C.; Abrantes, M.; Azevedo, M. C.; Cui, J.; Dias, A. R.; Duarte, M. T.; Lemos, M. A.; Lourenço, T.; Poli, R. *Organometallics* **2005**, *24*, 2582–2589.
- (66) Freund, C.; Abrantes, M.; Kühn, F. E. *J. Organomet. Chem.* **2006**, *691*, 3718–3729.
- (67) Ahmad, M. A. A.; Veljanovski, D.; Capapé, A.; Zhao, J.; Herdtweck, E.; Calhorda, M. J.; Kühn, F. E. *Organometallics* **2009**, *28*, 639–645.
- (68) Costa, P. J.; Calhorda, M. J.; Kühn, F. E. *Organometallics* **2010**, *29*, 303–311.
- (69) Grover, N.; Pöthig, A.; Kühn, F. E. *Catal. Sci. Technol.* **2014**, *4*, 4219–4231.
- (70) Hauser, S. A.; Reich, R. M.; Mink, J.; Pöthig, A.; Cokoja, M.; Kühn, F. E. *Catal. Sci. Technol.* **2015**, *5*, 2282–2289.
- (71) Grover, N.; Drees, M.; Kühn, F. E. *J. Catal.* **2015**, *329*, 269–285.
- (72) Bruno, S. M.; Pereira, C. C. L.; Balula, M. S.; Nolasco, M.; Valente, A. A.; Hazell, A.; Pillinger, M.; Ribeiro-Claro, P.; Gonçalves, I. S. *J. Mol. Catal. A Chem.* **2007**, *261*, 79–87.
- (73) Sawada, H. *J. Fluor. Chem.* **2003**, *121*, 111–130.
- (74) Santos, A. M.; Herrmann, W. A. *Dalton Trans.* **2005**, 2483–2491.
- (75) Gago, S.; Balula, S. S.; Figueiredo, S.; Lopes, A. D.; Valente, A. A.; Pillinger, M.; Gonçalves, I. S. *Appl. Catal., A* **2010**, *372*, 67–72.
- (76) Colton, R.; Tomkins, I. B. *Aust. J. Chem.* **1965**, *18*, 447–452.
- (77) Thomassen, H.; Hedberg, K. *J. Mol. Struct.* **1992**, *273*, 197–206.
- (78) Larson, M. L.; Moore, F. W. *Inorg. Chem.* **1966**, *5*, 801–805.
- (79) Amarante, T. R.; Neves, P.; Gomes, A. C.; Nolasco, M. M.; Ribeiro-Claro, P.; Coelho, A. C.; Valente, A. A.; Almeida Paz, F. A.; Smeets, S.; McCusker, L. B.; Pillinger, M.; Gonçalves, I. S. *Inorg. Chem.* **2014**, *53*, 2652–2665.
- (80) Pope, M. T.; Müller, A. *Angew. Chem., Int. Ed.* **1991**, *30*, 34–48.
- (81) Long, D. L.; Burkholder, E.; Cronin, L. *Chem. Soc. Rev.* **2007**, *36*, 105–121.
- (82) Hill, C. L. *Chem. Rev.* **1998**, *98*, 1–2.
- (83) Long, D. L.; Tsunashima, R.; Cronin, L. *Angew. Chem., Int. Ed.* **2010**, *49*, 1736–1758.
- (84) Wang, X.; Guo, Y.; Li, Y.; Wang, E.; Hu, C.; Hu, N. *Inorg. Chem.* **2003**, *42*, 4135–4140.

Chapter 1

- (85) Kang, J.; Nelson, J. A.; Lu, M.; Xie, B.; Peng, Z.; Powell, D. R. *Inorg. Chem.* **2004**, *43*, 6408–6413.
- (86) Kim, H. S.; Lee, B. J.; Park, D. H.; Kwon, Y. S. *Synth. Met.* **2005**, *153*, 469–472.
- (87) Housecroft, C. E.; Sharpe, A. G. *Inorganic chemistry*, Second edi.; Pearson Education Limited: Essex, 2005.
- (88) Armour, A. W.; Drew, M. G. B.; Mitchell, P. C. H. *J. Chem. Soc., Dalton Trans.* **1975**, *111*, 1967–1970.
- (89) Klemperer, W. G.; Shum, W. *J. Am. Chem. Soc.* **1976**, *98*, 8291–8293.
- (90) Cotton, F. A.; Wilkinson, G.; Murillo, C. A. . B. M. *Advanced Inorganic Chemistry*, Sixth edit.; Wiley-Interscience, 1999.
- (91) Ikegami, S.; Yagasaki, A. *Materials* **2009**, *2*, 869–875.
- (92) Shi, Y.; Ren, X.; Ren, S.; Fu, F.; Wang, J.; Xue, G. *J. Chem. Crystallogr.* **2010**, *40*, 985–988.
- (93) Gao, H.; Yu, J.; Du, J.; Niu, H.; Wang, J.; Song, X.; Zhang, W.; Jia, M. *J. Clust. Sci.* **2014**, *25*, 1263–1272.
- (94) Allis, D. G.; Burkholder, E.; Zubieta, J. *Polyhedron* **2004**, *23*, 1145–1152.
- (95) Allis, D. G.; Rarig, R. S.; Burkholder, E.; Zubieta, J. *J. Mol. Struct.* **2004**, *688*, 11–31.
- (96) Johnson, G. K.; Schlemper, E. O. *J. Am. Chem. Soc.* **1978**, *100*, 3645–3646.
- (97) Klemperer, W. G.; Marquart, T. A.; Yaghi, O. M. *Angew. Chem. Int. Ed.* **1992**, *31*, 49–51.
- (98) Salta, J.; Chen, Q.; Chang, Y.; Zubieta, J. *Angew. Chem. Int. Ed.* **1995**, *33*, 757–760.
- (99) Yang, J.; Ma, J. F.; Liu, Y. Y.; Li, S. L.; Zheng, G. L. *Eur. J. Inorg. Chem.* **2005**, 2174–2180.
- (100) Zou, R. Q.; Liu, C. Sen; Huang, Z.; Hu, T. L.; Bu, X. H. *Cryst. Growth Des.* **2006**, *6*, 99–108.
- (101) Peng, Y. F.; Ge, H. Y.; Li, B. Z.; Li, B. L.; Zhang, Y. *Cryst. Growth Des.* **2006**, *6*, 994–998.
- (102) Tripathi, A.; Hughbanks, T.; Clearfield, A. *J. Am. Chem. Soc.* **2003**, *125*, 10528–10529.
- (103) Lan, Y. Q.; Li, S. L.; Su, Z. M.; Shao, K. Z.; Ma, J. F.; Wang, X. L.; Wang, E. B. *Chem. Commun.* **2008**, *1*, 58–60.
- (104) Hagrman, D.; Zubieta, C.; Rose, D. J.; Zubieta, J.; Haushalter, R. C. *Angew. Chem. Int. Ed.* **1997**, *36*, 873–876.
- (105) Alam, N.; Feldmann, C. *Solid State Sci.* **2010**, *12*, 471–475.
- (106) Zhou, M. D.; Liu, M. J.; Huang, L. L.; Zhang, J.; Wang, J. Y.; Li, X. B.; Kühn, F. E.; Zang, S. L. *Green Chem.* **2015**, *17*, 1186–1193.
- (107) Himeno, S.; Niiya, H.; Ueda, T. *Bull. Chem. Soc. Jpn.* **1997**, *70*, 631–637.
- (108) Chuang, J.; Ouellette, W.; Zubieta, J. *Inorg. Chim. Acta* **2008**, *361*, 2357–2364.
- (109) Amarante, T. R.; Neves, P.; Valente, A. A.; Almeida Paz, F. A.; Fitch, A. N.; Pillinger, M.; Gonçalves, I. S. *Inorg. Chem.* **2013**, *52*, 4618–4628.
- (110) Günyar, A.; Zhou, M. D.; Drees, M.; Baxter, P. N. W.; Bassioni, G.; Herdtweck, E.; Kühn, F. E. *Dalton Trans.* **2009**, *40*, 8746–8754.

Chapter 1

- (111) Arzoumanian, H.; Agrifoglio, G.; Krentzien, H.; Capparelli, M. *J. Chem. Soc., Chem. Commun.* **1995**, 655–656.
- (112) Laudise, R. A; *Chem. Eng. News* **1987**, *65*, 30–43.
- (113) Sanchez, C.; Shea, K. J.; Kitagawa, S. *Chem. Soc. Rev.* **2011**, *40*, 696–753.
- (114) Abrantes, M.; Amarante, T. R.; Antunes, M. M.; Gago, S.; Almeida Paz, F. A. A.; Margiolaki, I.; Rodrigues, A. E.; Pillinger, M.; Valente, A. A.; Gonçalves, I. S. *Inorg. Chem.* **2010**, *49*, 6865–6873.
- (115) Amarante, T. R.; Neves, P.; Tomé, C.; Abrantes, M.; Valente, A. A.; Paz, F. A. A.; Pillinger, M.; Gonçalves, I. S. *Inorg. Chem.* **2012**, *51*, 3666–3676.
- (116) Scand., A. C. *Acta Chem. Scand.* **1950**, 1066–1074.
- (117) Khan, M. I.; Chen, Q.; Zubieta, J. *Inorg. Chim. Acta* **1993**, *213*, 325–327.
- (118) Zapf, P. J.; Haushalter, R. C.; Zubieta, J. *Chem. Mater.* **1997**, *9*, 2019–2024.
- (119) Thiruvengadam, P.; Chand, D. K. *J. Indian Chem. Soc.*, **2018**, *95*, 781–788.
- (120) Biradar, A. V.; Dongare, M. K.; Umbarkar, S. B. *Tetrahedron Lett.* **2009**, *50*, 2885–2888.
- (121) Wang, Z.; Kee, C. W.; Li, S.; Hor, T. S. A.; Zhao, J. *Appl. Catal., A* **2011**, *393*, 269–274.
- (122) Biradar, A. V.; Dongare, M. K.; Umbarkar, S. B. *Tetrahedron Lett.* **2009**, *49*, 3616–3619.
- (123) Amini, M.; Haghdoost, M. M.; Bagherzadeh, M. *Coord. Chem. Rev.* **2013**, *257*, 1093–1121.
- (124) Hauser, S. A.; Cokoja, M.; Kühn, F. E. *Catal. Sci. Technol.* **2013**, *3*, 552–561.
- (125) J. Kollar. Epoxidation process, 1967.
- (126) Harrod, J. F.; Hilaire, M. S.; Allan, R.; McIntyre, J. S. Epoxidation Process, 1972.
- (127) Oyama, S. T. *Rates, Kinetics, and Mechanisms of Epoxidation: Homogeneous, Heterogeneous, and Biological Routes*; Elsevier Science: Amsterdam, 2008.
- (128) Schneider, C. *Synthesis* **2006**, *23*, 3919–3944.
- (129) Canos, A. C.; Iborra, S.; Veltz, A. *Chem. Rev.* **2007**, *107*, 2411–2502.
- (130) Il'ina, I. V.; Volcho, K. P.; Salakhutdinov, N. F. *Russ. J. Org. Chem.* **2008**, *44*, 1–23.
- (131) Wang, H. S.; Yu, S. J. *Tetrahedron Lett.* **2002**, *43*, 1051–1055.
- (132) Bandini, M.; Eichholzer, A.; Kotrusz, P.; Umani-Ronchi, A. *Adv. Synth. Catal.* **2008**, *350*, 531–536.
- (133) Qiu, R.; Chen, Y.; Yin, S. F.; Xu, X.; Au, C. T. *RSC Adv.* **2012**, *2*, 10774–10793.
- (134) Amarante, T. R.; Neves, P.; Valente, A. A.; Paz, F. A. A.; Pillinger, M.; Gonçalves, I. S. *J. Catal.* **2016**, *340*, 354–367.
- (135) Hargman, P. J.; LaDuca, R. L.; Koo, H. J.; Rarig, R.; Haushalter, R. C.; Whangbo, M. H.; Zubieta, J. *Inorg. Chem.* **2000**, *39*, 4311–4317.
- (136) Amarante, T. R.; Antunes, M. M.; Valente, A. A.; Paz, F. A. A.; Pillinger, M.; Gonçalves, I. S. *Inorg. Chem.* **2015**, *54*, 9690–9703.
- (137) Antunes, M. M.; Amarante, T. R.; Valente, A. A.; Almeida Paz, F. A.; Gonçalves, I. S.; Pillinger, M. *ChemCatChem* **2018**, *10*, 2782–2791.
- (138) Datta, P.; Sarkar, S. K.; Mondal, T. K.; Patra, A. K.; Sinha, C. *J. Org. Chem.* **2009**, *694*, 4124–4133.

Chapter 1

- (139) Cariati, E.; Pizzotti, M.; Roberto, D.; Tessore, F.; Ugo, R. *Coord. Chem. Rev.* **2006**, *250*, 1210–1233.
- (140) Zobi, F. *Inorg. Chem.* **2009**, *48*, 10845–10855.
- (141) Motterlini, R.; Otterbein, L. E. *Nat. Rev. Drug Discov.* **2010**, *9*, 728–743.
- (142) Li, S.; Kee, C. W.; Huang, K.; Hor, T. S. A.; Zhao, J. *Organometallics* **2010**, *29*, 1924–1933.
- (143) Kandepi, V. V. K. M.; Cardoso, J. M. S.; Royo, B. *Catal. Letters* **2010**, *136*, 222–227.
- (144) Srour, H.; Le Maux, P.; Chevance, S.; Simonneaux, G. *Coord. Chem. Rev.* **2013**, *257*, 3030–3050.
- (145) Brégeault, J. M. *J. Chem. Soc. Dalton Trans.* **2003**, *3*, 3289–3302.
- (146) Betz, D.; Raith, A.; Cokoja, M.; Kühn, F. E. *ChemSusChem* **2010**, *3*, 559–562.
- (147) Hauser, S. A.; Cokoja, M.; Drees, M.; Kühn, F. E. *J. Mol. Catal. A Chem.* **2012**, *363–364*, 237–244.
- (148) Calhorda, M. J.; Costa, P. *Curr. Org. Chem.* **2012**, *16*, 65–72.
- (149) Zhao, J.; Santos, A. M.; Herdtweck, E.; Kühn, F. E. *J. Mol. Catal. A Chem.* **2004**, *222*, 265–271.
- (150) Bruno, S. M.; Gomes, A. C.; Abrantes, M.; Valente, A. A.; Pillinger, M.; Gonçalves, I. S. *J. Organomet. Chem.* **2015**, *799–800*, 179–183.
- (151) Gomes, A. C.; Neves, P.; Cunha-Silva, L.; Valente, A. A.; Gonçalves, I. S.; Pillinger, M. *Catal. Sci. Technol.* **2016**, *6*, 5207–5218.
- (152) Drake, J. E.; Hursthouse, M. B.; Light, M. E.; Kumar, R.; Ratnani, R. *J. Chem. Crystallogr.* **2007**, *37*, 421–427.
- (153) Du, J.; Yu, J.; Tang, J.; Wang, J.; Zhang, W.; Thiel, W. R.; Jia, M.; *Eur. J. Inorg. Chem.* **2011**, 2361–2365.
- (154) Carrasco, C. J.; Montilla, F.; Álvarez, E.; Herbert, M.; Galindo, A. *Polyhedron* **2013**, *54*, 123–130.
- (155) Linguito, S. L.; Zhang, X.; Padmanabhan, M.; Biradar, A. V.; Xu, T.; Emge, T. J.; Asefa, T.; Li, J. *New J. Chem.* **2013**, *37*, 2894–2901.
- (156) Neves, P.; Amarante, T. R.; Valente, A. A.; Pillinger, M.; Gonçalves, I. S. *Catal. Lett.* **2016**, *146*, 841–850.
- (157) Santos, A. M.; Kühn, F. E.; Bruus-Jensen, K.; Lucas, I.; Romão, C. C.; Herdtweck, E. *J. Am. Chem. Soc.* **2001**, *8*, 1332–1337.
- (158) Neves, P.; Gago, S.; Balula, S. S.; Lopes, D.; Valente, A. A.; Cunha-silva, L.; Paz, F. A. A.; Pillinger, M.; Silva, C. M.; Gonçalves, I. S. *Inorg. Chem.* **2011**, *50*, 3490–3500.
- (159) Amarante, T. R.; Neves, P.; Valente, A. A.; Paz, F. A. A.; Pillinger, M.; Gonçalves, I. S. *J. Catal.* **2016**, *340*, 354–367.
- (160) Thiel, W. R.; Eppinger, J. *Chem. Eur. J.* **1997**, *3*, 696–705.
- (161) Al-Ajlouni, A. M.; Gunyar, A.; Zhou, M. D.; Baxter, P. N. W.; Kühn, F. E. *Eur. J. Inorg. Chem.* **2009**, 1019–1026.
- (162) Darensbourg, D. J.; Kump, R. L. *Inorg. Chem.* **1978**, *17*, 2680–2682.

Chapter 1

- (163) Ardon, M.; Hayes, P. D.; Hogarth, G. *J. Chem. Educ.* **2002**, *79*, 1249–1251.
- (164) Mani, F.; Morassi, R. *Inorg. Chim. Acta* **1979**, *36*, 63–67.
- (165) Dhawan, I. K.; Bruck, M. A.; Schillings, B.; Grittini, C.; Enemark, J. H. *Inorg. Chem.* **1995**, *34*, 3801–3808.
- (166) Bigmore, H. R.; Lawrence, S. C.; Mountford, P.; Tredget, C. S. *Dalton Trans.* **2005**, *4*, 635–651.
- (167) Pettinari, C.; Pettinari, R. *Coord. Chem. Rev.* **2005**, *249*, 525–543.
- (168) Trofimenko, S. *J. Am. Chem. Soc.* **1970**, *92*, 5118–5126.
- (169) Reger, D. L.; Grattan, T. C.; Brown, K. J.; Little, C. A.; Lamba, J. J. S.; Rheingold, A. L.; Sommer, R. D. *J. Organomet. Chem.* **2000**, *607*, 120–128.
- (170) Pullen, E. E.; Rabinovich, D.; Incarvito, C. D.; Concolino, T. E.; Rheingold, A. L. *Inorg. Chem.* **2000**, *39*, 1561–1567.
- (171) Sánchez-Méndez, A.; Silvestri, G. F.; De Jesús, E.; De La Mata, F. J.; Flores, J. C.; Gómez, R.; Gómez-Sal, P. *Eur. J. Inorg. Chem.* **2004**, 3287–3296.
- (172) Dinoi, C.; Guedes da Silva, M. F. C.; Alegria, E. C. B. A.; Smoleński, P.; Martins, L. M. D. R. S.; Poli, R.; Pombeiro, A. J. L. *Eur. J. Inorg. Chem.* **2010**, 2415–2424.
- (173) Kuo, C. Y.; Fuh, Y. S.; Shiue, J. Y.; Yu, S. J.; Lee, G. H.; Peng, S. M. *J. Organomet. Chem.* **1999**, *588*, 260–267.
- (174) Gomes, A. C.; Neves, P.; Figueiredo, S.; Fernandes, J. A.; Valente, A. A.; Almeida, F. A.; Pillinger, M.; Lopes, A. D.; Gonçalves, I. S.; *J. Mol. Catal. A: Chem.* **2013**, *370*, 64–74.
- (175) Petrovski, Ž.; Braga, S. S.; Rodrigues, S. S.; Pereira, C. C. L.; Gonçalves, I. S.; Pillinger, M.; Freire, C.; Romão, C. C. *New J. Chem.* **2005**, *29*, 347–354.
- (176) Manuta, D. M.; Lees, A. J. *Inorg. Chem.* **1986**, *25*, 1354–1359.
- (177) Coelho, A. C.; Paz, F. A. A.; Klinowski, J.; Pillinger, M.; Gonçalves, I. S. *Molecules* **2006**, *11*, 940–952.
- (178) Nicholls, B.; Whiting, M. C. *J. Chem. Soc.* **1959**, 551–556.
- (179) Ardon, M.; Hogarth, G.; Ocroft, D. T. W. *J. Organomet. Chem.* **2004**, *689*, 2429–2435.
- (180) VanAtta, S. L.; Duclos, B. A.; Green, D. B. *Organometallics* **2000**, *19*, 2397–2399.
- (181) Kühn, F. E.; Santos, A. M.; Gonçalves, I.; Romão, C. C.; Lopes, A. D. *Appl. Organomet. Chem.* **2001**, *15*, 43–50.
- (182) Al-Ajlouni, A.; Valerie, A. A.; Nunes, C. D.; Pillinger, M.; Santos, A. M.; Zhao, J.; Romão, C. C.; Gonçalves, I. S.; Kühn, F. E. *Eur. J. Inorg. Chem.* **2005**, 1716–1723.
- (183) Bruno, S. M.; Fernandes, J. A.; Martins, L. S.; Gonçalves, I. S.; Pillinger, M.; Ribeiro-Claro, P.; Rocha, J.; Valente, A. A. *Catal. Today* **2006**, *114*, 263–271.
- (184) Jeyakumar, K.; Chand, D. K. *J. Chem. Sci.* **2009**, *121*, 111–123.
- (185) Sousa, S. C. A.; Cabrita, I.; Fernandes, A. C. *Chem. Soc. Rev.* **2012**, *41*, 5641–5653.
- (186) Arnáiz, F. J.; Aguado, R.; Pedrosa, M. R.; De Cian, A. *Inorg. Chim. Acta* **2003**, *347*, 33–40.
- (187) Arnaiz, F. J.; Aguado, R. *Polyhedron* **1994**, *13*, 3257–3259.

Chapter 1

- (188) Brewer, D. C.; Templeton, D. L.; Mingos, D. M. P. *J. Am. Chem. Soc.* **1987**, *109*, 5203–5208.
- (189) Barea, G.; Lledos, A.; Maseras, F.; Jean, Y.; Quimica, D. De; Barcelona, U. A. De; li, M.; Cedex, M.; The, L. D. C.; Sud, D. P.; Cedex, O.; September, R. V. *Inorg. Chem.* **1998**, *37*, 3321–3325.
- (190) Dreisch, K.; Andersson C.; StHlhandske, C. *Polyhedron* **2006**, *52*, 2143–2150.
- (191) Petrovski, Ž.; Pillinger, M.; Valente, A. A.; Gonçalves, I. S.; Hazell, A.; Romão, C. C. *J. Mol. Catal. A Chem.* **2005**, *227*, 67–73.
- (192) Bruno, S. M.; Monteiro, B.; Balula, M. S.; Lourenço, C.; Anabela, A.; Pillinger, M.; Ribeiro-claro, P.; Gonçalves, I. S. *Molecules* **2006**, *1*, 298–308.
- (193) Kühn, F. E.; Groarke, M.; Bencze, É.; Herdtweck, E.; Prazeres, A.; Santos, A. M.; Calhorda, M. J.; Romão, C. C.; Gonçalves, I. S.; Lopes, A. D.; Pillinger, M. *Chem. Eur. J.* **2002**, *8*, 2370–2383.
- (194) Trofimenko, S. *Chem. Rev.* **1993**, *93*, 943–980.
- (195) Kühn, F. E.; Zhao, J.; Herrmann, W. A. *Tetrahedron Asymmetry* **2005**, *16*, 3469–3479.
- (196) Bellemin-Laponnaz, S.; Coleman, K.S.; Dierkes, P.; Masson, J.-P. .; Osborn, J. A. *Eur. J. Inorg. Chem.* **2000**, 1645–1649.
- (197) Herrmann, W. A.; Haider, J. J.; Fridgen, J.; Lobmaier, G. M.; Spiegler, M. *J. Organomet. Chem.* **2000**, *1*, 69–79.
- (198) Santos, A.; Lopes, A. *J. Organomet. Chem.* **2001**, *621*, 207–217.
- (199) Valente, A. A.; Gonçalves, I. S.; Lopes, A. D.; Rodríguez-Borges, J. E.; Pillinger, M.; Romão, C. C.; Rocha, J.; García-Mera, X. *New J. Chem.* **2001**, *25*, 959–963.
- (200) Wang, X. Y.; Shi, H. C.; Sun, C.; Zhang, Z. G. *Tetrahedron* **2004**, *60*, 10993–10998.
- (201) Gómez, M.; Jansat, S.; Muller, G.; Noguera, G.; Teruel, H.; Moliner, V.; Cerrada, E.; Hursthouse, M. *Eur. J. Inorg. Chem.* **2001**, 1071–1076.
- (202) Kandasamy, K.; Singh, H. B.; Butcher, R. J.; Jasinski, J. P. *Inorg. Chem.* **2004**, *43*, 5704–5713.
- (203) Zhao, J.; Zhou, X.; Santos, A. M.; Herdtweck, E. *Dalton Trans.* **2003**, 3736–3742.
- (204) Zhou, X.; Zhao, J.; Santos, A. M.; Kühn, F. E. *Z. Naturforsch. B* **2004**, *59*, 1223–1228.
- (205) Gago, S.; Rodríguez-Borges, J. E.; Teixeira, C.; Santos, A. M.; Zhao, J.; Pillinger, M.; Nunes, C. D.; Petrovski, Ž.; Santos, T. M.; Kühn, F. E.; Romão, C. C.; Gonçalves, I. S. *J. Mol. Catal. A Chem.* **2005**, *236*, 1–6.
- (206) Ghosh, A. K.; Mathivanan, P.; Cappiello, J. *Tetrahedron: Asymmetry* **1998**, *9*, 1–45.
- (207) Pfaltz, A. *Acta Chem. Scand.* **1996**, *50*, 189.
- (208) Helmchen, G.; Pfaltz, A. *Acc. Chem. Res.* **2000**, *33*, 336–345.
- (209) Johnson, J. S.; Evans, D. A. *Acc. Chem. Res.* **2000**, *33*, 325–335.
- (210) Bruno, S. M.; Monteiro, B.; Balula, M. S.; Pedro, F. M.; Abrantes, M.; Valente, A. A.; Pillinger, M.; Ribeiro-Claro, P.; Kühn, F. E.; Gonçalves, I. S. *J. Mol. Catal. A Chem.* **2006**, *260*, 11–18.
- (211) Gago, S.; Neves, P.; Monteiro, B.; Pessêgo, M.; Lopes, A. D.; Valente, A. A.; Almeida

Chapter 1

- Paz, F. A.; Pillinger, M.; Moreira, J.; Silva, C. M.; Gonçalves, I. S. *Eur. J. Inorg. Chem.* **2009**, 4528–4537.
- (212) Amarante, T. R.; Gomes, A. C.; Neves, P.; Almeida Paz, F. A.; Valente, A. A.; Pillinger, M.; Gonçalves, I. S. *Inorg. Chem. Commun.* **2013**, *32*, 59–63.
- (213) Kühn, F. E.; Groarke, M. .; Bencze, É.; Herdtweck, E.; Prazeres, A.; Santos, A. M. .; Calhorda, M. J.; Romão, C. C.; Gonçalves, I. S. .; Lopes, A. D. .; Pillinger, M. *Chem. Eur. J.* **2002**, *8*, 2370–2383.
- (214) Fritz E; Herrmann, W. A.; Gonc, I. S.; Lopes, D.; Roma, C. C. *J. Organomet. Chem.* **1999**, *583*, 3–10.
- (215) Nelidow, I.; Diamond, R. M. *J. Phys. Chem.* **1955**, *79*, 707–710.
- (216) Coddington, J. M.; Taylor, M. J. *J. Chem. Soc. Dalton Trans.* **1990**, 41–47.
- (217) Taylor, M. J.; Rickard, C. E. F.; Kloo, L. A. *J. Chem. Soc. Dalton Trans.* **1998**, *461*, 3195–3198.
- (218) Levason, W.; Ratnani, R.; Reid, G.; Webster, M. *Inorg. Chim. Acta* **2006**, *359*, 4627–4630.
- (219) Gomes, A. C.; Pillinger, M.; Nunes, P.; Gonçalves, I. S.; Abrantes, M. *J. Organomet. Chem.* **2014**, *760*, 42–47.
- (220) Coddington, J. M.; Taylor, M. J. *J. Chem. Soc. Dalton Trans.* **1990**, 41–47.
- (221) Minelli, M.; Yamanouchi, K.; Enemark, J. H.; Subramanian, P.; Kaul, B. B.; Spence, J. T. *Inorg. Chem.* **1984**, *23*, 2554–2556.
- (222) Taylor, M. J.; Jirong, W.; Rickard, C. E. F. *Polyhedron* **1993**, *12*, 1433–1435.
- (223) Costa, J. S.; Markus, C. M.; Mutikainen, I.; Gamez, P.; Reedijk, J. *Inorg. Chim. Acta* **2010**, *363*, 2046–2050.
- (224) Braga, S. S.; Gonçalves, I. S.; Lopes, A. D.; Pillinger, M.; Rocha, J.; Romão, C. C.; Teixeira-Dias, J. J. C. *J. Chem. Soc. Dalton Trans.* **2000**, *17*, 2964–2968.
- (225) Lima, S.; Gonçalves, I. S.; Ribeiro-Claro, P.; Pillinger, M.; Lopes, A. D.; Ferreira, P.; Teixeira-Dias, J. J. C.; Rocha, J.; Romão, C. C. *Organometallics* **2001**, *20*, 2191–2197.
- (226) Gomes, A. C.; Bruno, S. M.; Tomé, C.; Valente, A. A.; Pillinger, M.; Abrantes, M.; Gonçalves, I. S. *J. Org. Chem.* **2013**, *730*, 116–122.
- (227) Shao, K.; Yuan, Q. *J. Cryst. Growth* **2013**, *363*, 145–149.
- (228) Braga, S. S.; Mokal, V.; Paz, F. a. A.; Pillinger, M.; Branco, A. F.; Sardão, V. a.; Diogo, C. V.; Oliveira, P. J.; Marques, M. P. M.; Romão, C. C.; Gonçalves, I. S. *Eur. J. Inorg. Chem.* **2014**, 5034–5045.
- (229) Casarin, M.; Falcomer, D.; Glisenti, A.; Vittadini, A. *J. Organomet. Chem.* **2001**, *632*, 11–16.
- (230) Petrovski, Ž.; Braga, S. S.; Santos, A. M.; Rodrigues, S. S.; Gonçalves, I. S.; Pillinger, M.; Kühn, F. E.; Romão, C. C. *Inorg. Chim. Acta* **2005**, *358*, 981–988.
- (231) Chen, L.; Tian, L.; Liu, L.; Tian, X.; Song, W.; Xu, H.; Wang, X. *Sens. Actuators, B* **2005**, *110*, 271–278.
- (232) Pereira, C. C. L.; Braga, S. S.; Almeida Paz, F. A.; Pillinger, M.; Klinowski, J.;

Chapter 1

- Gonçalves, I. S. *Eur. J. Inorg. Chem.* **2006**, 4278–4288.
- (233) Braga, S. S.; Gago, S.; Seixas, J. D.; Valente, A. A.; Pillinger, M.; Santos, T. M.; Gonçalves, I. S.; Romão, C. C. *Inorg. Chim. Acta* **2006**, *359*, 4757–4764.
- (234) Balula, S. S.; Coelho, A. C.; Braga, S. S.; Hazell, A.; Valente, A. A.; Pillinger, M.; Seixas, J. D.; Romão, C. C.; Gonçalves, I. S. *Organometallics* **2007**, *26*, 6857–6863.
- (235) Pereira, C. C. L.; Diogo, C. V.; Burgeiro, A.; Oliveira, P. J.; Marques, M. P. M.; Braga, S. S.; Almeida Paz, F. A.; Pillinger, M.; Gonçalves, I. S. *Organometallics* **2008**, *27*, 4948–4956.
- (236) Shao, Z.-C.; Song, L.-X.; Teng, Y.; Dang, Z.; Xia, J.; *Acta Phys. Chim. Sin* **2013**, *29*, 460–466.
- (237) Corazza, F.; Floriani, C.; Chiesi-Villa, A.; Guastinib, C. *J. Chem. Soc. Dalton Trans.* **1990**, *640*, 2–3.
- (238) Achoj, J. A.; Ren, T.; Yunj, J. W.; Lippard, S. J. *Inorg. Chem.* **1995**, *34*, 5226–5233.
- (239) Acho, J. A.; Lippard, S. J. *Inorg. Chim. Acta* **1995**, *229*, 5–8.
- (240) Gibson, V. C.; Redshaw, C.; Clegg, W.; Elsegood, M. R. J. *Chem. Commun.* **1997**, *832*, 1605–1606.
- (241) Redshaw, C.; Elsegood, M. R. J. *Inorg. Chem.* **2000**, *39*, 5164–5168.
- (242) Liu, L.; Zakharov, L. N.; Golen, J. A.; Rheingold, A. L.; Watson, W. H.; Hanna, T. A. *Inorg. Chem.* **2006**, *45*, 4247–4260.
- (243) Samsonenko, D. G.; Virovets, A. V.; Sharonova, A. A.; Fedin, V. P.; Fenske, D. *Russ. Chem. Bull.* **2001**, *50*, 494–496.
- (244) Lin, R. G.; Long, L. S.; Huang, R. Bin; Zheng, L. S.; Ng, S. W. *Acta Cryst.* **2005**, *61*, 885–889.
- (245) Samsonenko, D. G.; Gerasko, O. A.; Virovets, A. V.; Fedin, V. P. *Russ. Chem. Bull.* **2005**, *54*, 1557–1562.
- (246) Abramov, P. A.; Yu Laricheva, A.; Peresykina, E. V.; Mirzaeva, I. V.; Moroz, N. K.; Sokolov, M. N. *Inorg. Chim. Acta* **2012**, *383*, 7–12.
- (247) Isaacs, L. *Chem. Commun.* **2009**, *6*, 619–629.
- (248) Parvari, G.; Reany, O.; Keinan, E. *Isr. J. Chem.* **2011**, *51*, 646–663.
- (249) Masson, E.; Ling, X.; Joseph, R.; Kyeremeh-Mensah, L.; Lu, X. *RSC Adv.* **2012**, *2*, 1213–1247.
- (250) Assaf, K. I.; Nau, W. M. *Chem. Soc. Rev.* **2015**, *44*, 394–418.
- (251) Behrend, R.; Meyer, E.; Rusche, F. *Justus Liebigs Ann. Chem.* **1905**, *339*, 1–37.
- (252) Freeman, W. A.; Mock, W. L.; Shih, N. Y. *J. Am. Chem. Soc.* **1981**, *103*, 7367–7368.
- (253) Kim, J.; Jung, I.; Kim, S.; Lee, E.; Kang, J.; Sakamoto, S.; Yamaguchi, K.; Kim, K.; Hyojadong, S.; Korea, R. *J. Am. Chem. Soc.* **2000**, *19*, 540–541.
- (254) Day, A.; Arnold, A. P.; Blanch, R. J.; Snushall, B. *J. Org. Chem.* **2001**, *66*, 8094–8100.
- (255) Lagona, J.; Mukhopadhyay, P.; Chakrabarti, S.; Isaacs, L. *Angew. Chem. Int. Ed.* **2005**, *44*, 4844–4870.
- (256) Lee, J. W.; Samal, S.; Selvapalam, N.; Kim, H. J.; Kim, K. *Acc. Chem. Res* **2003**, *36*,

Chapter 1

- 621–630.
- (257) Kim, K.; Selvapalam, N.; Ko, Y. H.; Park, K. M.; Kim, D.; Kim, J. *Chem. Soc. Rev.* **2007**, *36*, 267–279.
- (258) Day, A.I.; Blanch, R.J.; Arnold, A.P.; Lorenzo, S.; Lewis, G.R.; Dance, I. *Angew. Chem. Int. Ed.* **2002**, *14*, 285.
- (259) Bush, M. E.; Bouley, N. D.; Urbach, A. R. *J. Am. Chem. Soc.* **2005**, *127*, 14511–14517.
- (260) Germain, P.; Létoffe, J. M.; Merlin, M. P.; Buschmann, H. J. *Thermochim. Acta* **1998**, *315*, 87–92.
- (261) Chen, Q. L.; Chen, H. B.; Cao, Z. X.; Zhou, Z. H. *Dalton Trans.* **2013**, *42*, 1627–1636.
- (262) Buschmann, H. J.; Jansen, K.; Schollmeyer, E. *Thermochim. Acta* **1998**, *317*, 95–98.
- (263) Buschmann, H. J.; Schollmeyer, E.; Mutihac, L. *Thermochim. Acta* **2003**, *399*, 203–208.
- (264) Assaf, K. I.; Nau, W. M. *Chem. Soc. Rev.* **2014**, *53*, 1003–1007.
- (265) Huang, W. H.; Liu, S.; Zavalij, P. Y.; Isaacs, L. *J. Am. Chem. Soc.* **2006**, *128*, 14744–14745.
- (266) Tarasov, M. A.; Gromov, V. D.; Bogomolov, G. D.; Otto, E. A.; Kuzmin, L. S. *Instruments Exp. Tech.* **2011**, *111*, 7941–7980.
- (267) Ambade, A. V.; Savariar, E. N.; Thayumanavan, S. *Mol. Pharm.* **2005**, *2*, 264–272.
- (268) Sobransingh, D.; Kaifer, A. E. *Org. Lett.* **2006**, *8*, 3247–3250.
- (269) Yi, S.; Captain, B.; Ottaviani, M. F.; Kaifer, A. E. *Langmuir* **2011**, *27*, 5624–5632.
- (270) Corma, A.; García, H.; Montes-Navajas, P.; Primo, A.; Calvino, J. J.; Trasobares, S. *Chem. Eur. J.* **2007**, *13*, 6359–6364.
- (271) Gerasko, O. A.; Mainicheva, E. A.; Naumova, M. I.; Yurjeva, O. P.; Alberola, A.; Vicent, C.; Llusar, R.; Fedin, V. P. *Chem. Eur. J.* **2008**, *3*, 416–424.
- (272) Feng, X.; Lu, X. J.; Xue, S. F.; Zhang, Y. Q.; Tao, Z.; Zhu, Q. J. *Inorg. Chem. Commun.* **2009**, *12*, 849–852.
- (273) Kang, J.; Hilmersson, G.; Santamaría, J.; Rebek, J. *J. Am. Chem. Soc.* **1998**, *120*, 3650–3656.
- (274) Castellano, R. K.; Nuckolls, C.; Rebek, J. *J. Am. Chem. Soc.* **1999**, *121*, 11156–11163.
- (275) Florea, M.; Nau, W. M. *Angew. Chem. Int. Ed.* **2011**, *50*, 9338–9342.
- (276) Kreno, L. E.; Leong, K.; Farha, O. K.; Allendorf, M.; Van Duyne, R. P.; Hupp, J. T. *Chem. Rev.* **2012**, *112*, 1105–1125.
- (277) Liu, S.; Ruspic, C.; Mukhopadhyay, P.; Chakrabarti, S.; Zavalij, P. Y.; Isaacs, L. *J. Am. Chem. Soc.* **2005**, *127*, 15959–15967.
- (278) Macartney, D. H. *Isr. J. Chem.* **2011**, *51*, 600–615.
- (279) Cao, L.; Hettiarachchi, G.; Briken, V.; Isaacs, L. *Angew. Chem. Int. Ed.* **2013**, *52*, 12033–12037.
- (280) Gerasko, O. A.; Fedin, V. P. *Russ. J. Inorg. Chem.* **2011**, *56*, 2025–2046.
- (281) Assaf, K. I.; Nau, W. M. *Supramol. Chem.* **2014**, *26*, 657–669.
- (282) Fedin, V. P.; Sokolov, M.; Lamprecht, G. J.; Hernandez-Molina, R.; Seo, M. S.; Virovets, A. V.; Clegg, W.; Sykes, A. G. *Inorg. Chem.* **2001**, *40*, 6598–6603.

Chapter 1

- (283) Fedin, V. P.; Gramlich, V.; Weber, T. *Inorg. Chem.* **2001**, *40*, 1074–1077.
- (284) Gerasko, O. A.; Virovets, A. V.; Sokolov, M. N.; Dybtsev, D. N.; Gerasimenko, A. V.; Fenske, D.; Fedin, V. P. *Russ. Chem. Bull.* **2002**, *51*, 1800–1805.
- (285) Hernandez-Molina, R.; Kalinina, I. V.; Sokolov, M. N.; Peris, G.; Llusar, R. *Synth. React. Inorganic, Met. Nano-Metal Chem.* **2007**, *37*, 765–770.
- (286) Hernandez-Molina, R.; Sokolov, M. N. *Russ. J. Coord. Chem.* **2012**, *38*, 159–166.
- (287) Fedin, V. P.; Virovets, A. V.; Sokolov, M. N.; Dybtsev, D. N.; Gerasko, O. A.; Clegg, W.; Tyne, N.; Ne, T. *Inorg. Chem.* **2000**, *39*, 2227–2230.
- (288) Chubarova, E. V.; Samsonenko, D. G.; Platas, J. H. .; Sokolov, M. N.; Fedin, V. P. *J. Struct. Chem.* **2004**, *45*, 906–911.
- (289) Chubarova, E. V.; Samsonenko, D. G.; Platas, H. G.; Dolgushin, F. M.; Gerasimenko, A. V.; Sokolov, M. N. .; Starikova, Z. A.; Antipin, M. Y.; Fedin, V. P. *J. Struct. Chem.* **2004**, *45*, 1004–1013.
- (290) Fedin, V. P.; Sokolov, M. N.; Dybtsev, D. N.; Gerasko, O. A.; Virovets, A. V.; Fenske, D. *Inorg. Chim. Acta* **2002**, *331*, 31–38.
- (291) Abramov, P. A.; Sokolov, M. N.; Virovets, A. V.; Peresyphkina, E. V.; Fedin, V. P. *J. Clust. Sci.* **2007**, *18*, 597–605.
- (292) Buck, D. P.; Abeysinghe, P. M.; Cullinane, C.; Day, A. I.; Collins, J. G.; Harding, M. M. *Dalton Trans.* **2008**, 2328–2334.
- (293) Sokolov, M. N.; Chubarova, E. V.; Hernandez-Molina, R.; Clausén, M.; Naumov, D. Y.; Vicent, C.; Llusar, R.; Fedin, V. P. *Eur. J. Inorg. Chem.* **2005**, 2139–2146.
- (294) Sokolov, M. N.; Dybtsev, D. N.; Virovets, A. V.; Hegetschweiler, K.; Fedin, V. P. *Russ. Chem. Bull.* **2000**, *49*, 1877–1881.
- (295) Hernandez-Molina, R.; Sokolov, M. N. *Russ. J. Coord. Chem.* **2012**, *38*, 163–170.
- (296) Sokolov, M. N.; Chubarova, E. V.; Kovalenko, K. A.; Mironov, I. V.; Virovets, A. V.; Peresyphkina, E. V.; Fedin, V. P. *Russ. Chem. Bull.* **2005**, *2*, 615–622.
- (297) Adonin, S. A.; Peresyphkina, E. V.; Sokolov, M. N.; Fedin, V. P. *J. Struct. Chem.* **2010**, *51*, 731–736.
- (298) Dsouza, R. N.; Nau, W. M. *Org. Lett.* **2009**, *11*, 2595–2598.
- (299) Basilio, N.; García-Río, L.; Moreira, J. A.; Pessêgo, M. *J. Org. Chem.* **2010**, *75*, 848–855.
- (300) Wang, Y. H.; Cong, H.; Zhao, F. F.; Xue, S. F.; Tao, Z.; Zhu, Q. J.; Wei, G. *Catal. Commun.* **2011**, *12*, 1127–1130.
- (301) Lu, X.; Masson, E. *Org. Lett.* **2010**, *12*, 2310–2313.
- (302) Pemberton, B. C.; Singh, R. K.; Johnson, A. C.; Jockusch, S.; Da Silva, J. P.; Ugrinov, A.; Turro, N. J.; Srivastava, D. K.; Sivaguru, J. *Chem. Commun.* **2011**, *47*, 6323–6325.
- (303) De Lima, S.; Gómez, J. A.; Barros, V. P.; Vertuan, G. S.; Assis, M.; Graeff, C. F. O.; Demets, G. J. F. *Polyhedron* **2010**, *29*, 3008–3013.
- (304) Mock, W. L.; Irra, T. A.; Wepsiec, J. P.; Manimaran, T. L. *J. Org. Chem.* **1983**, *48*, 3619–3620.

Chapter 1

- (305) Jon, S. Y.; Ko, Y. H.; Park, S. H.; Kim, H.-J.; Kim, K. *Chem. Commun.* **2001**, 1938–1939.
- (306) Pattabiraman, M.; Natarajan, A.; Kaanumalle, L. S.; Ramamurthy, V. *Org. Lett.* **2005**, *7*, 529–532.
- (307) Pattabiraman, M.; Kaanumalle, L. S.; Natarajan, A.; Ramamurthy, V. *Langmuir* **2006**, *22*, 7605–7609.
- (308) Pattabiraman, M.; Natarajan, A.; Kaliappan, R.; Mague, J. T.; Ramamurthy, V. *Chem. Commun.* **2005**, *36*, 4542–4544.
- (309) Maddipatla, M. V. S. N.; Kaanumalle, L. S.; Natarajan, A.; Pattabiraman, M.; Ramamurthy, V. *Langmuir* **2007**, *23*, 7545–7554.
- (310) Yang, H.; Ma, Z.; Wang, Z.; Zhang, X. *Polym. Chem.* **2014**, *5*, 1471–1476.
- (311) Wang, R.; Yuan, L.; Macartney, D. H. *J. Org. Chem.* **2006**, *71*, 1237–1239.
- (312) Wu, X. L.; Luo, L.; Lei, L.; Liao, G. H.; Wu, L. Z.; Tung, C. H. *J. Org. Chem.* **2008**, *73*, 491–494.
- (313) Lei, L.; Luo, L.; Wu, X. L.; Liao, G. H.; Wu, L. Z.; Tung, C. H. *Tetrahedron Lett.* **2008**, *49*, 1502–1505.
- (314) Barooah, N.; Pemberton, B. C.; Sivaguru, J. *Org. Lett.* **2008**, *10*, 3339–3342.
- (315) Barooah, N.; Pemberton, B. C.; Johnson, A. C.; Sivaguru, J. *Photochem. Photobiol. Sci.* **2008**, *7*, 1473–1479.
- (316) Pemberton, B. C.; Barooah, N.; Srivatsava, D. K.; Sivaguru, J. *Chem. Commun.* **2010**, *46*, 225–227.
- (317) Yang, C.; Mori, T.; Origane, Y.; Ko, Y. H.; Selvapalam, N. *J. Am. Chem. Soc.* **2008**, *12*, 8574–8575.
- (318) Biedermann, F.; Ross, I.; Scherman, O. A. *Polym. Chem.* **2014**, *5*, 5375–5382.
- (319) Hang, C.; Fang-fang, Z.; Jian-xin, Z.; Xi, Z.; Zhu, T.; Sai-feng, X.; Qian-jiang, Z. *Catal. Commun.* **2009**, *11*, 167–170.
- (320) Cong, H.; Chen, Q.; Geng, Q.; Tao, Z.; Yamato, T. *Chin. J. Chem.* **2015**, *33*, 545–549.
- (321) Koner, A. L.; Márquez, C.; Dickman, M. H.; Nau, W. M. *Angew. Chem., Int. Ed.* **2011**, *50*, 545–548.
- (322) Cong, H.; Yamato, T.; Tao, Z. *J. Mol. Catal. A Chem.* **2013**, *379*, 287–293.
- (323) Cong, H.; Yamato, T.; Tao, Z. *New J. Chem.* **2013**, *37*, 3778–3783.
- (324) Lee, T. C.; Kalenius, E.; Lazar, A. I.; Assaf, K. I.; Kuhnert, N.; Grün, C. H.; Jänis, J.; Scherman, O. A.; Nau, W. M. *Nat. Chem.* **2013**, *5*, 376–382.
- (325) Smitka, J.; Lemos, A.; Porel, M.; Jockusch, S.; Belderrain, T. R.; Tesařová, E.; Da Silva, J. P. *Photochem. Photobiol. Sci.* **2014**, *13*, 310–315.
- (326) Yun, G.; Hassan, Z.; Lee, J.; Kim, J.; Lee, N. S.; Kim, N. H.; Baek, K.; Hwang, I.; Park, C. G.; Kim, K. *Angew. Chem., Int. Ed.* **2014**, *53*, 6414–6418.
- (327) Bruno, S. M.; Gomes, A. C.; Oliveira, T. S. M.; Antunes, M. M.; Lopes, A. D.; Valente, A. A.; Gonçalves, I. S.; Pillinger, M. *Org. Biomol. Chem.* **2016**, *14*, 3873–3877.
- (328) Tian, J.; Ma, S.; Thallapally, P. K.; Fowler, D.; McGrail, B. P.; Atwood, J. L. *Chem. Commun.* **2011**, *47*, 7626–7628.

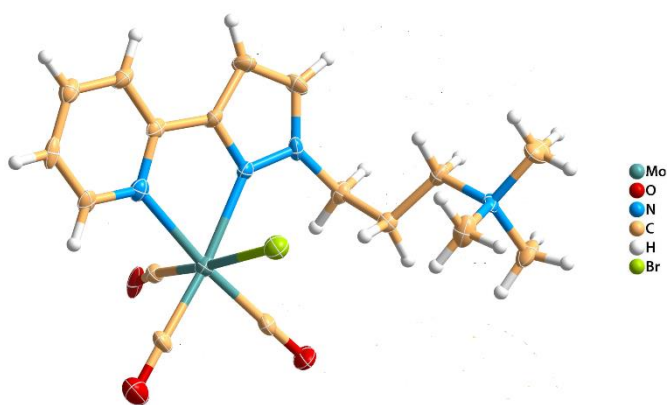
Chapter 1

- (329) Bardelang, D.; Udachin, K. A.; Leek, D. M.; Ripmeester, J. A. *CrystEngComm* **2007**, *9*, 973–975.
- (330) Hwang, I.; Jeon, W. S.; Kim, H. J.; Kim, D.; Kim, H.; Selvapalam, N.; Fujita, N.; Shinkai, S.; Kim, K. *Angew. Chem., Int. Ed.* **2007**, *46*, 210–213.
- (331) Lim, S.; Kim, H.; Selvapalam, N.; Kim, K. J.; Cho, S. J.; Seo, G.; Kim, K. *Angew. Chem., Int. Ed.* **2008**, *47*, 3352–3355.
- (332) Bardelang, D.; Udachin, K. A.; Leek, D. M.; Margeson, J. C.; Chan, G.; Ratcliffe, C. I.; Ripmeester, J. A. *Cryst. Growth Des.* **2011**, *11*, 5598–5614.
- (333) Yoon, M.; Suh, K.; Kim, H.; Kim, Y.; Selvapalam, N.; Kim, K. *Angew. Chem., Int. Ed.* **2011**, *50*, 7870–7873.
- (334) Baylon, C.; Prestat, G.; Heck, M. P.; Mioskowski, C. *Tetrahedron Lett.* **2000**, *41*, 3833–3835.
- (335) Kantam, M. L.; Aziz, K.; Jeyalakshmi, K.; Likhar, P. R. *Catal. Lett.* **2003**, *89*, 95–97.
- (336) Weil, T.; Kotke, M.; Kleiner, C. M.; Schreiner, P. R. *Org. Lett.* **2008**, *10*, 1513–1516.
- (337) Kahandal, S. S.; Kale, S. R.; Disale, S. T.; Jayaram, R. V. *Catal. Sci. Technol.* **2012**, *2*, 1493–1499.
- (338) Zhou, Y. X.; Chen, Y. Z.; Hu, Y.; Huang, G.; Yu, S. H.; Jiang, H. L. *Chem. Eur. J.* **2014**, *20*, 14976–14980.
- (339) Liu, Y. H.; Liu, Q. S.; Zhang, Z. H. *J. Mol. Catal. A Chem.* **2008**, *296*, 42–46.
- (340) Dhakshinamoorthy, A.; Concepción, P.; Fornés, V.; Garcia, H. *Chem. Commun.* **2012**, *48*, 5443–5445.
- (341) Matos, I.; Neves, P. D.; Castanheiro, J. E.; Perez-Mayoral, E.; Martin-Aranda, R.; Duran-Valle, C.; Vital, J.; Botelho Do Rego, A. M.; Fonseca, I. M. *Appl. Catal. A Gen.* **2012**, *439–440*, 24–30.

Chapter 1

CHAPTER 2

Molybdenum(0) tricarbonyl and tetracarbonyl complexes with a cationic pyrazolylpyridine ligand: synthesis, crystal structures and catalytic performance in olefin epoxidation



cis-[Mo(CO)₄(2-(1-propyltrimethylammonium-3-pyrazolyl)pyridine)]⁺

Chapter 2

Index

2.1. Introduction	75
2.2. Results and discussion	77
2.2.1. Synthesis and characterisation of [ptapzpy]Br, (pre)catalysts [Mo(CO) ₃ (ptapzpy)Br] (1) and <i>cis</i> -[Mo(CO) ₄ (ptapzpy)]Br (2)	77
2.2.2. Single-crystal X-ray structure analyses of [ptapzpy]Br, 1 and 2	80
2.2.3. Oxidative decarbonylation of 1	83
2.2.4. Reactions between Mo complexes and cucurbit[7]uril	85
2.3. Catalytic studies	86
2.3.1. Catalytic epoxidation of <i>cis</i> -cyclooctene with TBHP	86
2.3.2. Catalytic epoxidation of others (bio)olefins (styrene and DL-limonene)	88
2.3.3. Characterization of solids after catalytic epoxidation of Cy with TBHP	88
2.3.4. Ionic liquid-supported metal species for olefin epoxidation	89
2.3.5. Characterization of solids after catalytic epoxidation in the presence of ionic liquid	90
2.3.6. Catalytic epoxidation with H ₂ O ₂	94
2.3.7. Characterization of solids after catalytic epoxidation with H ₂ O ₂	95
2.4. Conclusions	96
2.5. References	97

Chapter 2

2.1. Introduction

The organometallic chemistry of molybdenum dates back to the mid 1930s when Hieber and co-workers described the thermal substitution of CO ligands in $\text{Mo}(\text{CO})_6$ to give octahedral $\text{Mo}(0)$ derivatives of the type $\text{Mo}(\text{CO})_x(\text{L})_y$.^{1,2} The physical properties of one of these compounds, *cis*- $[\text{Mo}(\text{CO})_4(2,2'\text{-bipy})]$ ($2,2'\text{-bipy} = 2,2'\text{-bipyridine}$), were investigated much later by Stiddard³, and the molecular structure of this complex was determined only recently.² Since the report by Stiddard, much attention has been given to molybdenum(0)-diimine-tetracarbonyl complexes containing bidentate ligands (N–N) such as bipyridines^{2,4}, phenanthrolines^{5,6}, 1,4-diazabutadienes^{7,8}, iminopyridines^{9,10}, and pyrazolylpyridines^{11,12}. Further substitution of the carbonyl ligands is possible (without alteration of the formal charge on the central Mo atom), *e.g.* of one carbonyl ligand by a neutral (L) or anionic coligand (X^-) to give tricarbonyl complexes $[\text{Mo}(\text{CO})_3(\text{N–N})(\text{L}/\text{X})]^{0/-}$ ^{8,13,14}, or of two carbonyl ligands by a second diimine ligand to give dicarbonyl complexes $[\text{Mo}(\text{CO})_2(\text{N–N})_2]^{15,16}$. Although anionic complexes $[\text{Mo}(\text{CO})_3(\text{N–N})(\text{X})]^-$ were described by Behrens *et al.* in 1970¹³, molecular structures for this family of compounds were only described six years ago⁸.

Complexes of the type $[\text{Mo}(\text{CO})_3(\text{N–N})(\text{X})]^-$ can be prepared from *cis*- $[\text{Mo}(\text{CO})_4(\text{N–N})]$ ¹⁴ but not in the reverse sense from the pentacarbonyl complexes $[\text{Mo}(\text{CO})_5(\text{X})]^-$, since reaction of the latter with the ligand N–N gives instead the tetracarbonyl derivatives *cis*- $[\text{Mo}(\text{CO})_4(\text{N–N})]$ ¹⁷. This was attributed to preferential halogen displacement (rather than CO substitution) in the intermediate $[\text{Mo}(\text{CO})_4(\text{N–N})(\text{X})]^-$ owing to the fact that bidentate diimines such as 2,2'-bipy are relatively poor π -acceptors, thereby strengthening the remaining Mo–C bonds in the intermediate.¹⁷ Until the present, the direct synthesis of anionic complexes $[\text{Mo}(\text{CO})_3(\text{N–N})(\text{X})]^-$ from molybdenum hexacarbonyl has never been reported.

Carbonyl–diimine complexes of $\text{Mo}(0)$, especially the tetracarbonyl derivatives, have been intensively studied due to their rich electronic absorption spectra, photophysics, and photochemistry.^{18–25} Tetracarbonyl derivatives are strongly colored due to an intense $\text{Mo} \rightarrow$ diimine metal-to-ligand charge-transfer (MLCT) absorption band in the visible spectral region. The low-lying MLCT excited state is associated with several interesting phenomena such as negative solvatochromism^{8,18,24,26}, second-order nonlinear optical responses^{20,25}, luminescence^{18,19,23}, and photochemically induced CO substitution.^{21,23} side from their photo-properties, Mo carbonyl diimine complexes possess other interesting features and have been studied as CO-releasing molecules for therapeutic applications²⁷, catalysts for the electrochemical reduction of CO_2 ^{28–30}, initiators for the polymerisation of methyl methacrylate³¹, alkylation of allylic acetates⁵,

Chapter 2

and precatalysts for the epoxidation of olefins.^{11,12,32} In the latter case, the catalyst precursors undergo oxidative decarbonylation (OD) by reaction with an oxidant to give oxomolybdenum(VI)-diimine compounds, the structures of which vary according to the nature of the organic ligand. With tetracarbonyl precursors, structurally characterised OD products include tetranuclear $[\text{Mo}_4\text{O}_{12}(\text{pzpy})_4]$ ($\text{pzpy} = 2\text{-}[3(5)\text{-pyrazolyl}]\text{pyridine}$)¹¹, octanuclear $[\text{Mo}_8\text{O}_{24}(\text{di-}t\text{Bu-bipy})_4]$ ($\text{di-}t\text{Bu-bipy} = 4,4'\text{-di-}t\text{ert-butyl-}2,20\text{-bipyridine}$)³², and the one-dimensional (1D) molybdenum oxide/ $2,2'$ -bipyridine polymer $[\text{MoO}_3(2,2'\text{-bipy})]$ ³².

In this chapter, the cationic derivative 2-(1-propyltrimethylammonium-3-pyrazolyl)pyridine bromide ($[\text{ptapzpy}]\text{Br}$) was prepared. The introduction of cation-bearing ligands into transition metal complexes can help improve solubility in polar solvents or target the complexes for immobilisation in solid supports with charged frameworks and/or functional groups. The reaction of $[\text{ptapzpy}]\text{Br}$ with $\text{Mo}(\text{CO})_6$ unexpectedly yielded the charge-neutral zwitterionic complex $[\text{Mo}(\text{CO})_3(\text{ptapzpy})\text{Br}]$ rather than the tetracarbonyl derivative $\text{cis-}[\text{Mo}(\text{CO})_4(\text{ptapzpy})]\text{Br}$. For comparison, the latter complex was prepared by a different route and the molecular structures of both complexes have been determined. OD of the complexes with *tert*-butylhydroperoxide (TBHP) is shown to give a hybrid molybdenum oxide/organic material. The catalytic behavior and chemical transformations of all compounds in the epoxidation of *cis*-cyclooctene have been studied using TBHP or H_2O_2 as oxidant.

The necessity to form new supramolecular systems based on metal complexes, which allow the isolation of these compounds from the reaction media, as well as enhanced stability and performance, has led to the development of new supports and consequently new methods of preparation. Cucurbit[n]urils, $\text{CB}[n]$ s: $n = 5\text{-}8, 10, 14$ are built of glycoluril units linked by methylene bridges with highly symmetric structure.^{33,34} The glycoluril unit provides a hydrophobic nanocavity in which the portals are composed of polar carbonyl groups, allowing the $\text{CB}[n]$ s to bind to organic molecules and encapsulate small molecules by noncovalent interactions (*e.g.*, hydrogen-bonding, Van der Waals, coulombic and $\pi\text{-}\pi$ interactions).^{35,36} They are able to form stable complexes with various guests, such as organometallic complex³⁷, inorganic cations³⁸⁻⁴⁰, complexes⁴¹⁻⁴⁵ and other⁴⁶. Due to their rigid structure, ease of synthesis and variety of size and functionality, $\text{CB}[n]$ s can be used for a variety of applications including catalysis.⁴⁷⁻⁴⁹

The emerging research on cucurbit[n]uril $\text{CB}[n]$ has not yet reached the extent of the research on cyclodextrins. Until the present, the publications referring chemical reactions mediated by $\text{CB}[n]$ s, highlight recent progress in cycloadditions, photochemical, hydrolysis/alcoholysis, oxidation, desilylation, Retro-Diels-Alder and

Chapter 2

carbon-carbon/carbon-nitrogen bond forming reactions, and catalysis assisted by metal cations and heterogeneous catalysis.³⁴ However, the role of cucurbit[*n*]urils is hardly explored, mostly due to the poor solubility of CB[*n*]s in organic solvents, limiting the reaction versatility to reactions in aqueous solutions.^{49–53} Some hybrid material based on supramolecular adducts of di- or trinuclear molybdenum oxoclusters with macrocyclic cavitand cucurbit[*n*]urils have already been prepared and characterized, such as {CB[6][Mo₃O₄(H₂O)₆Cl₃]₂}Cl₂·14H₂O⁵⁴, [Mo₂O₄Cl₄(H₂O)₂]·CB[6]·10.5H₂O⁵⁵, {[Mo₃O₄(H₂O)₆Cl₃]₂[(Na₂Cl)CB[5]]}Cl₃·14H₂O⁵⁶, {[Ca(H₂O)₅]₂CB[6]}[Mo₃O₂S₂Cl₆(H₂O)₃]₂·13H₂O⁵⁷ and {[Mo₃(μ₃-S)(μ₂-O)₃(H₂O)₆Cl₃]₂CB[6]}Cl₂·10.88H₂O⁵⁸.

Encouraged by these studies, and by the permanent interest in the preparation of new catalysts based on oxomolybdenum complexes, it was also decided to explore the preparation of supramolecular compounds based on the tetracarbonyl complex [Mo(CO)₄(ptapzpy)]Br and CB[7].

2.2. Results and discussion

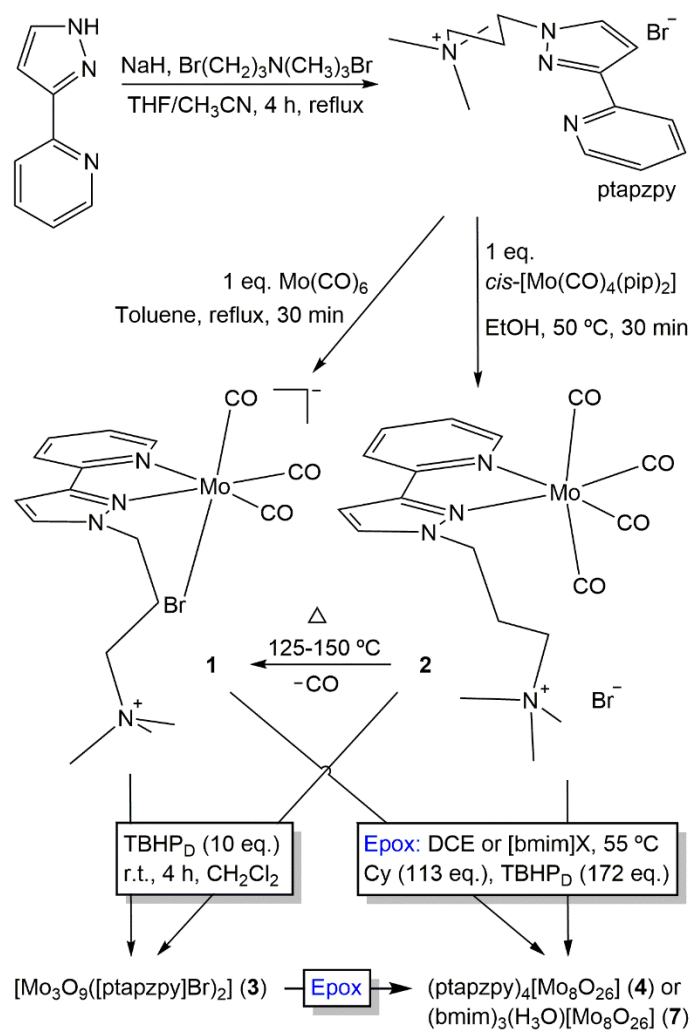
2.2.1. Synthesis and characterisation of [ptapzpy]Br, (pre)catalysts [Mo(CO)₃(ptapzpy)]Br (1) and *cis*-[Mo(CO)₄(ptapzpy)]Br (2)

The ligand [ptapzpy]Br was prepared by deprotonation of 2-(3-pyrazolyl)pyridine followed by addition of (3-bromopropyl)trimethylammonium bromide and reflux for 4 h (Scheme 2.1). Characterisation data (FT-IR, ¹H and ¹³C solution NMR) were in line with those reported previously for related 2-(1-alkyl-3-pyrazolyl)pyridine derivatives.^{59,60} [ptapzpy]Br is highly hygroscopic, soluble in water, ethanol, acetonitrile, dichloromethane and chloroform, and insoluble in acetone, toluene, 1,2-dichloroethane and diethyl ether.

Reaction of pyrazolylpyridine ligands with 1 equivalent of Mo(CO)₆ in refluxing toluene usually gives tetracarbonyl complexes of the type *cis*-[Mo(CO)₄(N–N)].^{11,12} However, in the case of [ptapzpy]Br, this reaction led to the tricarbonyl derivative [Mo(CO)₃(ptapzpy)]Br (1) (Scheme 2.1). The unusual direct synthesis of the tricarbonyl complex from the hexacarbonyl and the ligand results from the presence of the terminal trimethylammonium group in the ligand together with the bromide counterion, which favour the formation of the charge-neutral zwitterionic complex. The tetracarbonyl derivative *cis*-[Mo(CO)₄(ptapzpy)]Br (2) could be prepared by treatment of the precursor *cis*-[Mo(CO)₄(pip)₂] (prepared by the literature method;¹⁵ pip = piperidine) with 1 equivalent of [ptapzpy]Br in ethanol at 50 °C. Complexes 1 and 2 are at best only sparingly soluble in nonpolar solvents such as chloroform. Dissolution of the compounds

Chapter 2

in polar, coordinating solvents such as water, acetonitrile and dimethyl sulfoxide is accompanied by solvolysis (especially for **1**, as reported previously¹⁴ for other tricarbonyl anions $[\text{Mo}(\text{CO})_3(\text{N}-\text{N})(\text{X})]^-$) and fast degradation involving decarbonylation. While complex **2** displays extended stability in the solid-state if stored cold in the dark and under inert atmosphere, complex **1** is unstable and undergoes decarbonylation over a period of a few days.



Scheme 2.1. Preparation of [ptapzpy]Br, complexes **1** and **2**, and the oxidised compounds formed by OD of the carbonyl complexes by reaction with 10 eq. of TBHP_D (in decane solution) or a large excess of TBHP_D under the catalytic epoxidation reaction conditions (denoted Epoxy).

Chapter 2

The FT-IR spectra of freshly prepared **1** and **2** confirmed the formation of tricarbonyl and tetracarbonyl complexes, respectively (Figure 2.1). In the carbonyl stretching region (1700–2020 cm^{-1}), complex **1** displays two overlapping strong bands at 1742 and 1764 cm^{-1} , and one very strong band at 1895 cm^{-1} , in a pattern that is typical of *fac*-[Mo(CO)₃(N–N)(L/X)]^{0/+} complexes.^{8,14} The two lower energy bands arise from splitting of the E mode, while the high-energy band is associated with the A₁ mode. Four carbonyl stretching bands are observed for complex **2** as expected for *cis*-substituted tetracarbonyl complexes. These are assigned as A₁² (medium, 2012 cm^{-1}), B₁ (shoulder, 1888 cm^{-1}), A₁¹ (very strong, 1869 cm^{-1}) and B₂ (very strong, 1815 cm^{-1}).⁶¹ From 300 to 1700 cm^{-1} the vibrational spectra of **1** and **2** exhibit numerous ligand (ptapzpy) modes. Upon complexation the ligand undergoes structural changes which affect the 1550–1650 cm^{-1} region.^{12,60,62} In particular, the pyridyl C–N stretching mode shifts from 1590 cm^{-1} for the free ligand to 1604–1608 cm^{-1} for **1** and **2**.

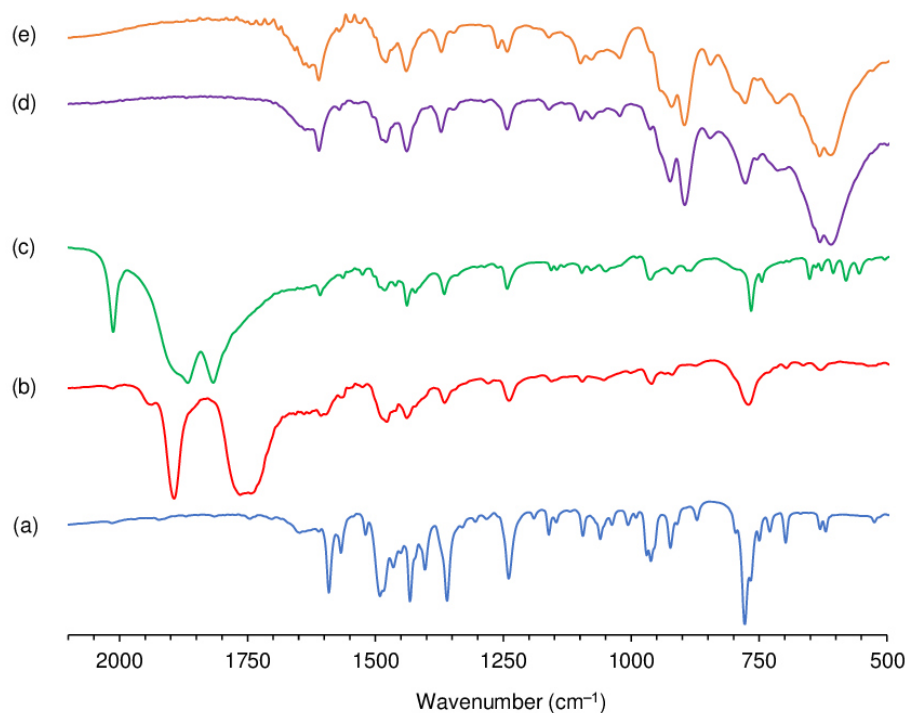


Figure 2.1. FT-IR spectra in the range of 500–2100 cm^{-1} of (a) [ptapzpy]Br, (b) **1**, (c) **2**, (d) the hybrid material **3** prepared from **1** and (e) **2**.

Thermogravimetric analysis (TGA) of **2** revealed a weight loss step of 4.2 % between 90 and 125 °C (Figure 2.2). This is close to the calculated value of 5.0 % for the removal of one CO ligand. Accordingly, ATR FT-IR spectra (not shown) of **2** heated at different temperatures (15 min at each temperature) showed that the compound is stable at 75 °C but is converted at 125–150 °C to the tricarbonyl complex **1** (Scheme 2.1).

Chapter 2

Notably, complex **1** differs from **2** in not displaying a resolved weight loss step around 100 °C. Above 150 °C the TGA curves for **1** and **2** are similar, showing two major decomposition steps in the 200–300 °C and 475–575 °C intervals.

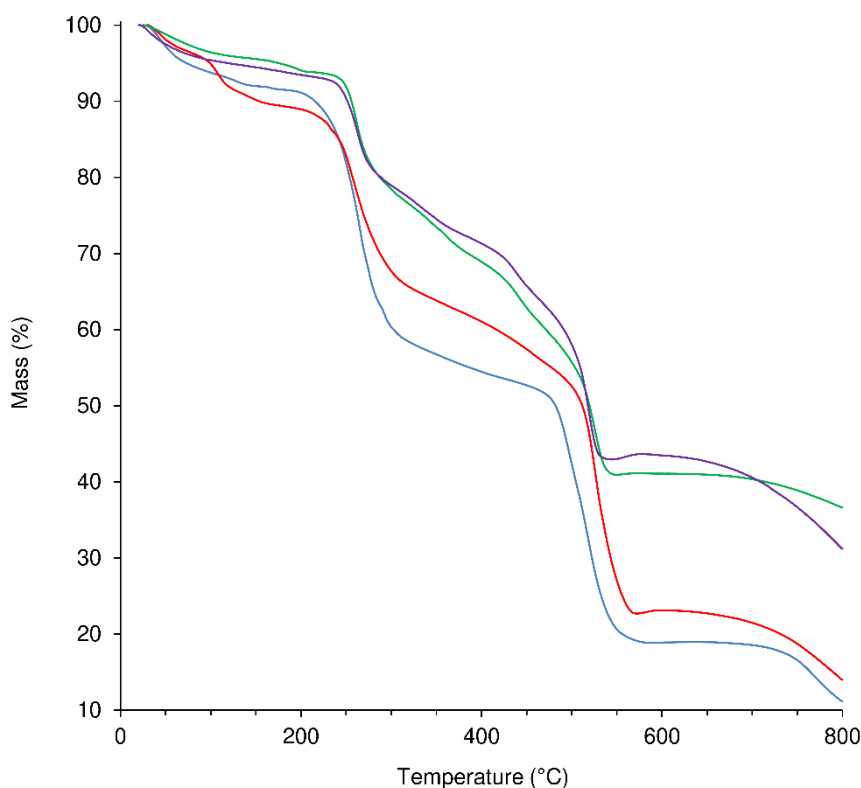


Figure 2.2. TGA curves of the tricarbonyl complex **1** (—), tetracarbonyl complex **2** (—), and the hybrid material **3** prepared from **1** (—) and **2** (—).

2.2.2. Single-crystal X-ray structure analyses of [ptapzpy]Br, **1** and **2**

Single-crystals of [ptapzpy]Br, [Mo(CO)₃(ptapzpy)Br]·CH₃CN (**1**·CH₃CN) and [Mo(CO)₄(ptapzpy)]Br·CH₃CN (**2**·CH₃CN) suitable for X-ray diffraction (XRD) were obtained (Table 10.2 in the Chapter 10). The cationic organic ligand in [ptapzpy]Br crystallised with the counterion Br⁻ in the monoclinic space group *P*2₁/*c* (Figure 2.3, a). In **1**, the neutral tricarbonyl complex crystallised with one CH₃CN molecule of crystallisation in the monoclinic space group *P*2₁ (Figure 2.3, b), while in **2** the cationic tetracarbonyl complex crystallised jointly with one Br⁻ counterion and one uncoordinated CH₃CN molecule in the triclinic space group *P* $\bar{1}$ (Figure 2.3, c).

A striking feature of the crystal structure of [ptapzpy]Br is that the pyrazolylpyridine group adopts a *cisoid* conformation with respect to the pyridine and pyrazole nitrogen atoms. In analogy with the situation usually encountered with uncoordinated 2,2'-bipyridine derivatives in the solid-state, uncoordinated

Chapter 2

pyrazolypyridine ligands typically adopt a *transoid* conformation, *i.e.* the two rings are rotated along the central C5–C6 bond, thereby minimising repulsion between the lone pairs of the nitrogen atoms and between the protons H-4 and H-8. Crystal packing effects together with a complex network of weak intermolecular interactions (involving the bromide anion) may be responsible for this rare conformation of ptapzpy in the solid-state.

In complex **1**, the Mo(0) centre coordinates to three carbonyl groups, one *N,N*-chelating pyrazolypyridine ligand and one bromide anion, leading to a distorted octahedral coordination geometry with wide ranges for the bond lengths and internal bond angles (Figure 2.3, d). The bond lengths range from 1.894(7) °A (Mo–C) to 2.7476(10) °A (Mo–Br). Furthermore, the *cis* angles range between 72.13(19) and 101.9(3), while the *trans* angles are found in the range of 172.9(3)–174.63(19).

The main crystallographic features of the {MoC₄N₂} core of complex **2** are consistent with those observed in the handful of structures reported containing molybdenum tetracarbonyl complexes with chelating 2-(3-pyrazolyl)pyridine residues.^{63–65} The Mo(0) centre is coordinated by four carbonyl groups and one *N,N*-chelating pyrazolypyridine ligand, originating a distorted pseudo-octahedral geometry as confirmed by the distinct Mo–C and Mo–N bond lengths (Figure 2.3, e). The Mo–C bond lengths of the axial carbonyl groups (2.026(3), 2.042(3) °A) are longer than those for the equatorial groups (1.946(2), 1.954(2) °A), most probably as a consequence of distinct π back-bonding, Mo(d) \rightarrow C \equiv O(π^*). The equatorial CO groups are competing with the less π -acidic N-donor atoms from the pyrazolypyridine ligand, while the axial groups compete with each other.⁶⁴ The geometric deformation of the octahedral coordination of the metal centre is further verified by an inspection of the internal bond angles: the *cis* angles are found between 71.71(6) and 101.82(8) °, while the *trans* angles are found in the range of 165.75(9)–173.41(8) °.

A full account of the supramolecular interactions (hydrogen bonding, $\pi \cdots \pi$ contacts, C–H \cdots acceptor) and crystal packing arrangements in the crystal structures of [ptapzpy]Br, **1**·CH₃CN and **2**·CH₃CN is given in the Table 10.3 in the Chapter 10.

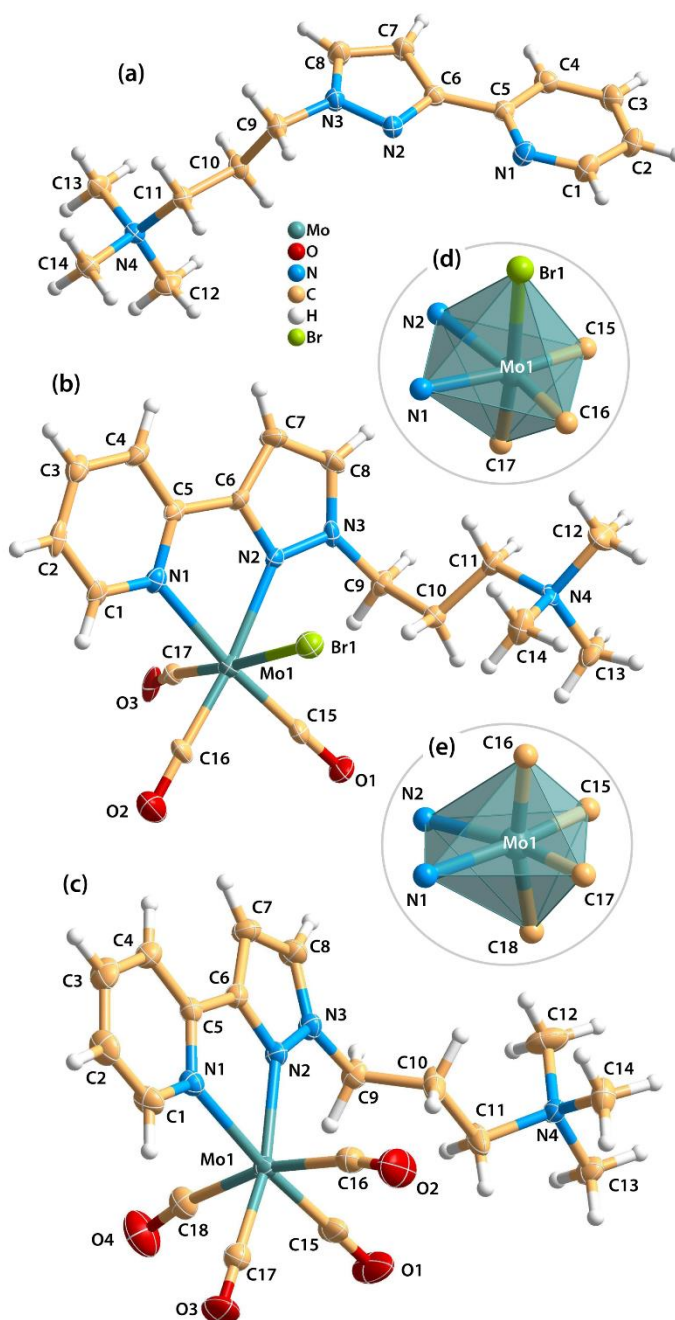


Figure 2.3. Representations of (a) the molecular structure of the cationic ligand in [ptapzpy]Br, (b) the molecular structure of [Mo(CO)₃(ptapzpy)Br] in **1**·CH₃CN, (c) the molecular structure of [Mo(CO)₄(ptapzpy)]⁺ in **2**·CH₃CN, (d) and (e) the Mo(0) coordination centres found in complexes **1** and **2**, respectively.

Thermal ellipsoids are drawn at the 50 % probability level and the labelling scheme is provided for all non H-atoms. **1**·CH₃CN: Selected bond lengths [Å]: Mo1–C15 1.935(6), Mo1–C16 1.894(7), Mo1–C17 2.072(9), Mo1–N1 2.293(5), Mo1–N2 2.259(6), Mo1–Br1 2.7476(10). Selected bond angles [°]: C16–Mo1–C15 85.2(3), N2–Mo1–N1 72.13(19), C17–Mo1–Br1 174.63(19), C15–Mo1–Br1 93.0(2), N1–Mo1–Br1 84.49(13), C17–Mo1–N1 94.6(2). **2**·CH₃CN: Selected bond lengths [Å]: Mo1–C15 1.946(2), Mo1–C16 2.042(3), Mo1–C17 1.954(2), Mo1–C18 2.026(3), Mo1–N1 2.2689(17), Mo1–N2 2.2576(17). Selected bond angles [°]: C15–Mo1–C17 89.13(10), N1–Mo1–N2 71.71(6), C18–Mo1–C16 165.75(9), C15–Mo1–C16 86.81(10), C16–Mo1–N1 93.09(8), C18–Mo1–N1 95.96(8).

2.2.3. Oxidative decarbonylation of **1**

Oxidative decarbonylation of **1** was carried out by the dropwise addition of TBHP (10 equiv.) to a suspension of the complex in CH_2Cl_2 . After stirring at room temperature for 4 h, an off-white solid (**3**) was recovered by filtration. Treatment of complex **2** with TBHP under the same conditions as used for **1** gave rise to the same molybdenum oxide hybrid material **3** (in a comparable yield) on the basis of the similar TGA, PXRD and spectral data (Figures 2.1, 2.2, 2.4-2.5).

TGA (Figure 2.2) and CHN microanalyses for **3** were consistent with the composition $[\text{Mo}_3\text{O}_9([\text{ptapzpy}]\text{Br})_2] \cdot 3\text{H}_2\text{O}$. Powder XRD (PXRD) showed that the solid was amorphous, with only a few very broad overlapping diffraction peaks being observed in the 2θ range of $5\text{--}30^\circ$.

The FT-IR and Raman spectra for **3** confirmed that complete decarbonylation had occurred during the reaction of **1** with the oxidant since no bands were observed in the carbonyl stretching region ($1700\text{--}2020\text{ cm}^{-1}$; Figures 2.1 and 2.4). On the other hand, the spectra retained the characteristic ligand modes of ptapzpy in the range of $1000\text{--}1650\text{ cm}^{-1}$, matching closely the bands observed for **1** and therefore indicating that the ligand is coordinated in a bidentate fashion to Mo centres.

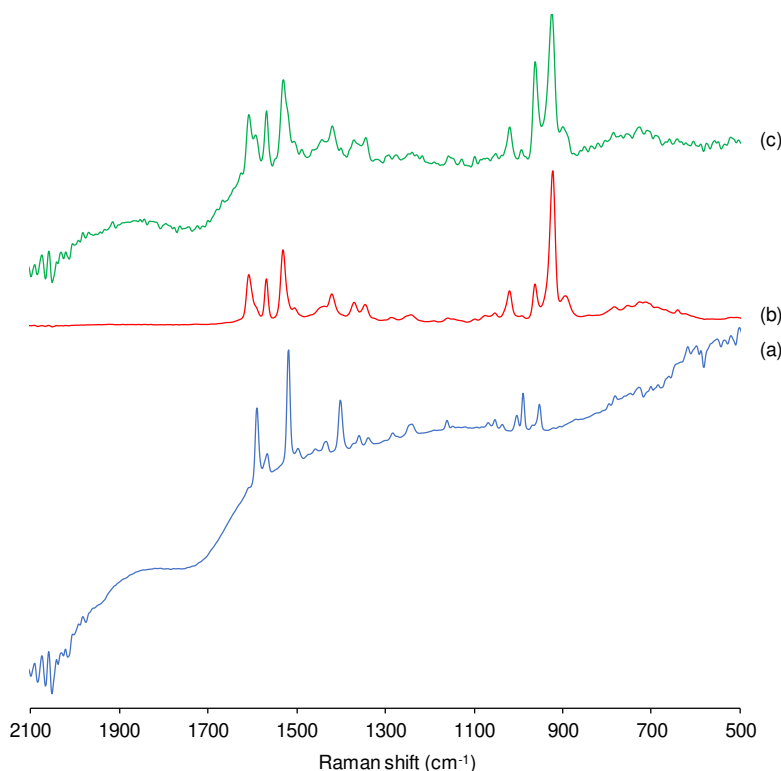


Figure 2.4. FT-Raman spectra in the range of $500\text{--}2100\text{ cm}^{-1}$ of (a) $[\text{ptapzpy}]\text{Br}$, and the hybrid material **3** prepared from **1** (b) and **2** (c).

Chapter 2

New vibrational bands for **3** that arise in the 850–1000 cm^{-1} interval are assigned to Mo–O vibrations. A very broad absorption band centred at 609 cm^{-1} in the IR spectrum is assigned to $\nu(\text{Mo–O–Mo})$ and points towards a polynuclear or polymeric structure. Molybdenum oxide-organonitrogen hybrid materials having the general composition $[\text{Mo}_3\text{O}_9(\text{N–N})_2]$ have been reported previously, namely the 1D materials with N–N = 2,2'-bipy⁶⁶ and 1,1'-phenanthroline.⁶⁷ The Raman spectrum of $[\text{Mo}_3\text{O}_9(2,2'\text{-bipy})_2]$ was reported by Twu *et al.* and found to exhibit three Mo–O bands at 893, 923 and 946 cm^{-1} which coincide quite closely with the three bands observed for **3** at 895, 924 and 962 cm^{-1} , suggesting that the two materials may possess the same type of molybdenum oxide substructure.⁶⁸ The structure of the 2,2'-bipy hybrid consists of 1D chains built up from alternating $\{\text{MoO}_4\}$ tetrahedra and pairs of corner-linked $\{\text{MoO}_4\text{N}_2\}$ octahedra.⁶⁶ The structural integrity of the organic ligand in **3** was verified by comparing its $^{13}\text{C}\{^1\text{H}\}$ CP MAS NMR spectrum with that of the free ligand [ptapzpy]Br (Figure 2.5).

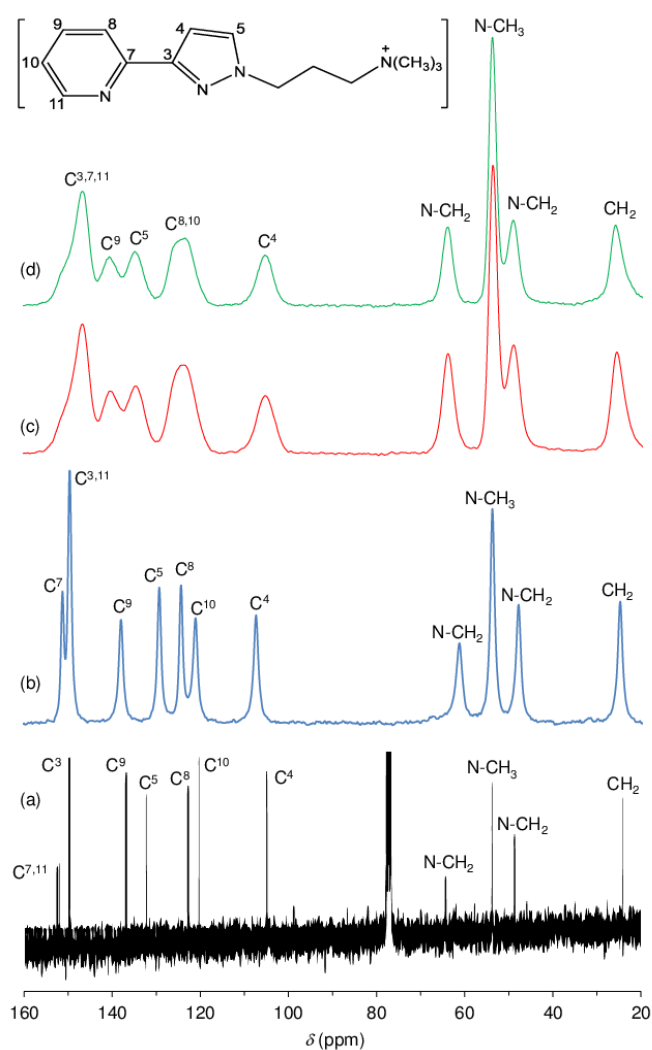
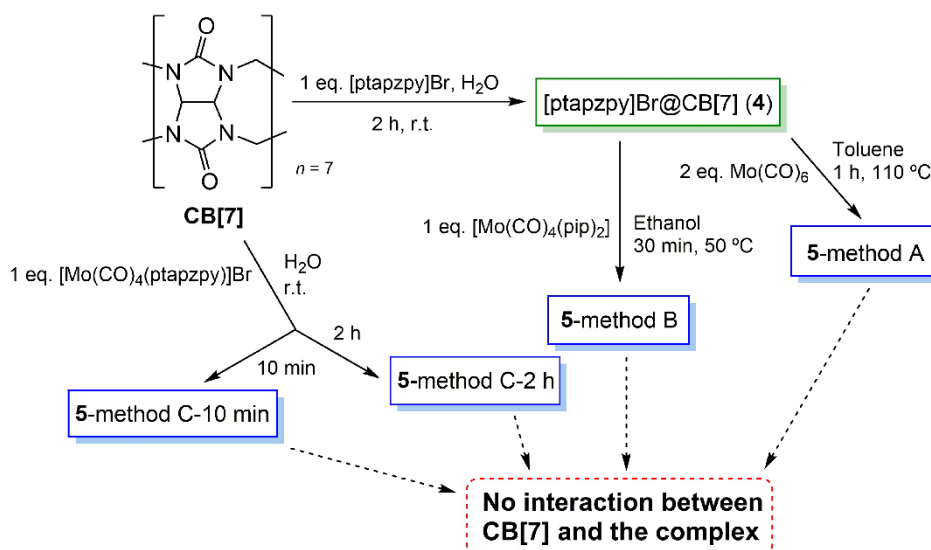


Figure 2.5. ^{13}C solution (a) and $^{13}\text{C}\{^1\text{H}\}$ CP MAS NMR (b-d) spectra with assignments of (a, b) [ptapzpy]Br and the hybrid material **3** prepared from **1** (c) and **2** (d).

2.2.4. Reactions between Mo complexes and cucurbit[7]uril

For the preparation of a supramolecular compound bearing $[\text{Mo}(\text{CO})_4(\text{ptapzpy})]\text{Br}$ (**2**) and CB[7], three different methods were tested starting with a CB[7] source and a molybdenum complex with the Mo complex:CB[7] molar ratio = 1:1 (Scheme 2.2). The CB[7] source was provided directly from free CB[7] or $[\text{ptapzpy}]\text{Br}@CB[7]$. The $[\text{ptapzpy}]\text{Br}@CB[7]$ compound (**4**) was prepared from the reaction between CB[7] and $[\text{ptapzpy}]\text{Br}$ in water, stirred for 2h at room temperature, obtaining a white solid. In methods A and B, the CB[7] source was provided from $[\text{ptapzpy}]\text{Br}@CB[7]$. Method A consists of a reaction between **4** and an excess of $\text{Mo}(\text{CO})_6$ in toluene, stirred for 1 h at 110 °C. The resulting product was a pale orange solid which turned white after some hours. $[\text{Mo}(\text{CO})_4(\text{pip})_2]$ was also used as molybdenum source in method B, reacting with **4** in ethanol under stirring for 30 min at 50 °C. The final colour of the solid remained pale orange. Finally, instead of the CB[7] derivative, free CB[7] was dissolved in water and stirred with complex **2** during 10 min (**5**-method C-10min) or 2 h (**5**-method C-2 h) at room temperature.

The FT-IR spectra of the prepared compounds **5** only reveal the characteristic bands of the cucurbiturils^{49,69}, with no sign of the $[\text{Mo}(\text{CO})_4(\text{ptapzpy})]\text{Br}$ (**2**). A band of medium relative intensity would be expected, assigned to the carbonyl stretching vibration between 1700–2020 cm^{-1} if the complex $[\text{Mo}(\text{CO})_4(\text{ptapzpy})]\text{Br}$ (**2**) remained stable after the reaction, or to $\nu_{\text{as}}(\text{Mo}=\text{O})$ in the region of 800-1000 cm^{-1} if an oxidative compound was interreacting with CB[7]. One possible explanation for the failed methods is the instability of the complex in solution.



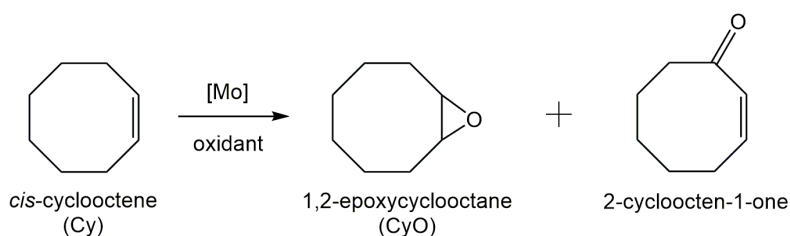
Scheme 2.2. Preparation of the solids **5** obtained from method A, B and C, starting from CB[7].

2.3. Catalytic studies

2.3.1. Catalytic epoxidation of *cis*-cyclooctene with TBHP

Compounds **1–3** were tested for catalytic epoxidation with TBHP [decane solution (TBHP_D) or aqueous solution (TBHP_A)], at 55 °C, using *cis*-cyclooctene (Cy) as a benchmark substrate for olefins (Scheme 2.3). The three compounds led to 1,2-epoxycyclooctane (CyO) as the main product (Table 2.1). With 1,2-dichloroethane (CH₃CHCl₂) as cosolvent and TBHP_D as oxidant, complex **1** led to a higher conversion at 24 h than **2** or **3** (39 % compared with 22 and 17 %, respectively). On the other hand, **1** led to lower CyO selectivity (71 %) than **2** or **3** (86–88 %), at 17–22 % conversion (Figure 2.6); byproducts included 2-cycloocten-1-one and others that were not clearly identified. Without catalyst, the conversion was less than 10 % at 24 h. The system TBHP_D/CH₃CHCl₂ led to better results than TBHP_A/CH₃CN, in the presence of **1**: 27 % and 17 % CyO yield, respectively, at 24 h. These contrasting performances may be partly due to differences in dissolution rate and solubility of the molybdenum compounds.

The catalytic results were improved when no organic cosolvent was added: 87–95 % CyO selectivity at 40–54 % conversion, 24 h. Under these conditions, **1** and **2** display similar performance, leading to about 48 % CyO yield at 24 h. For comparison, the complex *cis*-[Mo(CO)₄(pzpy)] containing the unsubstituted organic ligand led to 78 % epoxide yield under equivalent reaction conditions.¹¹ The catalytic results for **1** and **2** are intermediate between those reported in the literature (for similar reaction conditions: no cosolvent, 55 °C) for complexes of the type [Mo(CO)_n(L)] containing chelating N-heterocyclic carbene (L) ligands (entries 6 and 7 of Table 2.2), which led to 9–16 % conversion at 24 h⁷⁰, and those for [Mo(CO)₄(pyim)] (pyim = N-(*n*-propyl)-2-pyridylmethanimine), which led to 100 % conversion at 5 h (entry 5 of Table 2.2).³



Scheme 2.3. Reaction of *cis*-cyclooctene with TBHP in the presence of **1–3** at 55 °C.

Chapter 2

Table 2.1. *cis*-Cyclooctene epoxidation in the presence of **1–3**.^a

Compound	Oxidant	Cosolvent	Conv. (%) ^b	Yield (%) ^b
-	TBHP _D	-	-/-/4	4/-/-
1	TBHP _D	CH ₃ CHCl ₂	3/18/39	3/13/27
1	TBHP _D	-	9/35/54	9/31/47
1	TBHP _D	[bmim]NTf ₂	6/25/46	6/22/40
1	TBHP _D	[bmim]PF ₆	7/18/29	7/15/24
2	TBHP _D	CH ₃ CHCl ₂	2/10/22	2/9/19
2	TBHP _D	-	5/31/52	5/30/48
2^c	TBHP _D	-	-/31/48	-/28/45
2	TBHP _D	[bmim]NTf ₂	4/16/37	4/16/35
3	TBHP _D	CH ₃ CHCl ₂	3/9/17	3/8/15
3	TBHP _D	-	5/23/40	5/22/38
3	TBHP _D	[bmim]NTf ₂	3/13/34	3/13/31
3	TBHP _D	[bmim]PF ₆	3/29/47	3/26/41
3^d	TBHP _D	[bmim]PF ₆	13/49/62	13/46/58
1	TBHP _A	CH ₃ CN	-/-/21	-/-/17
1	H ₂ O ₂	CH ₃ CN	11	9
1^d	H ₂ O ₂	CH ₃ CN	20	16
2	H ₂ O ₂	CH ₃ CN	67	66
3	H ₂ O ₂	CH ₃ CN	56	56
3^d	H ₂ O ₂	CH ₃ CN	51	51

^a Reaction temperature = 55 °C and initial Mo:olefin:oxidant molar ratio = 1:113:172 (unless otherwise indicated), initial Cy concentration = 1.0 M (organic cosolvent and TBHP_{A/D}), 1.7 M (ionic liquid and TBHP_D), 1.2 M (CH₃CN and H₂O₂) or 2.4 M (no cosolvent). ^b Cy conversion and CyO yield at 1 h/6 h/24 h. Values for H₂O₂ as oxidant are for 24 h. ^c Mo:olefin:oxidant molar ratio = 1:75:114. ^d Reaction carried out at 70 °C.

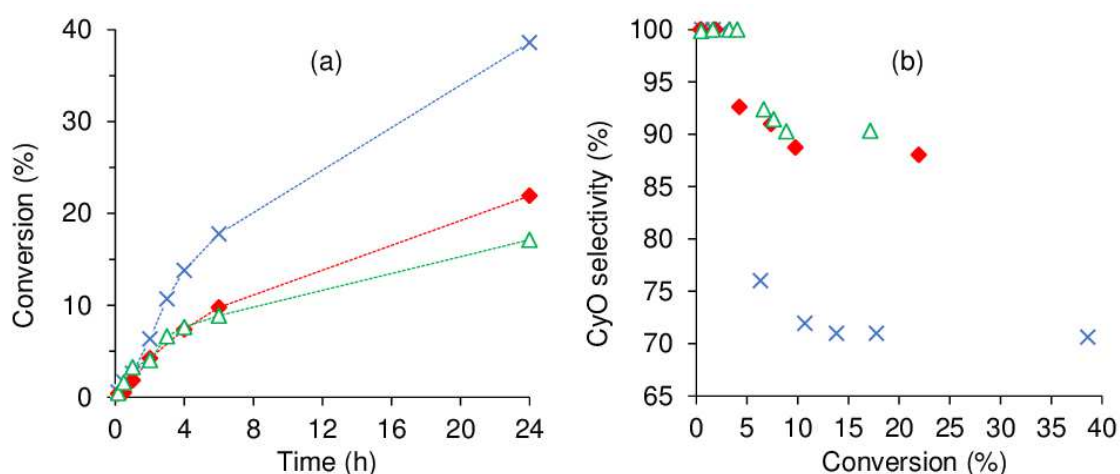


Figure 2.6. *cis*-Cyclooctene epoxidation with TBHP_D at 55 °C (CH₃CHCl₂ as cosolvent) using compounds **1** (x), **2** (♦) and **3** (Δ): (a) Conversion of Cy as a function of time and (b) Selectivity of CyO as a function of Cy conversion. The dashed lines are visual guides.

Chapter 2

2.3.2. Catalytic epoxidation of others (bio)olefins (styrene and DL-limonene)

The catalytic system **2**/TBHP was further investigated for the epoxidation of styrene (which possesses a terminal C=C bond) and DL-limonene (which possesses endocyclic and exocyclic C=C bonds), at 55 °C, without additional solvent (Figure 2.7). Compound **2** led to 20 % / 39 % styrene conversion at 6 h/24 h, and the main reaction products were styrene oxide and benzaldehyde formed with 52 % / 64 % and 42 % / 31 % selectivity, respectively. These results demonstrate the ability of **2**/TBHP for the epoxidation of terminal C=C bonds, which are electron-rich.

The reaction of DL-limonene gave mainly limonene-1,2-oxide formed with 70 % / 71% selectivity at 23 % / 43 % conversion, after 6 h / 24 h, respectively. These results suggest regioselectivity effects in favour of the epoxidation of the endocyclic C=C bond over the exocyclic one. Other reaction products were formed via allylic oxidation, leading to alcohol and carbonyl derivatives of *p*-mentha-1,8-diene.

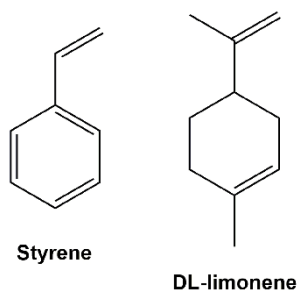


Figure 2.7. (Bio)olefins used in this work: styrene and DL-limonene structure.

2.3.3. Characterization of solids after catalytic epoxidation of Cy with TBHP

The use of the complex *cis*-[Mo(CO)₄(pzpy)] in Cy epoxidation with TBHP_D led to a biphasic solid–liquid mixture and the solid phase was identified as the tetranuclear species [Mo₄O₁₂(pzpy)₄].¹¹ Biphasic solid–liquid mixtures were also obtained for the systems (**1**, **2** or **3**)/TBHP_D. Attempts to isolate metal species from the colourless liquid phases were unsuccessful, suggesting that the concentration of dissolved species after a 24 h batch run was either negligible or very low. The low solubility of the metal species is probably one reason for the poor catalytic results obtained with these systems. Accordingly, for the system **2**/TBHP_D (no cosolvent), a 1.5-fold increase in the catalyst amount (*i.e.* from ca. 0.9 mol % to 1.3 mol %) did not improve the epoxide yield (Table 2.1). This is because the catalytic reaction is homogeneous in nature and, for both catalyst amounts (which lead to biphasic solid–liquid reaction mixtures), the reaction mixtures are saturated with metal species.

Chapter 2

Characterisation of the off-white solid phases **i**-S-TBHP_D (**i** = **1–3**; cosolvent = DCE) by ATR FT-IR spectroscopy indicated that **1–3** were converted to different types of metal species (Figure 2.8). Comparison of these spectra with literature data for polyoxomolybdates of the type (L)_x[Mo₈O₂₆] (where L is an organic cation such as pyridinium and imidazolium) indicates that a similar type of poorly soluble β-octamolybdate salt is formed in the catalytic reaction systems of **1–3** with TBHP_D. In the region of the Mo–O vibrations (< 1000 cm⁻¹), the solids exhibited bands at ca. 942, 910, 840, 705 and 659 cm⁻¹, which match closely with literature values for several (L)_x[Mo₈O₂₆] salts (Table 2.3).⁷⁶⁻⁷⁸ The recovered solids also exhibited a band at 767 cm⁻¹ and several bands between 950 and 1650 cm⁻¹ attributed to the charge-balancing organic cation ptpzpy. CHN microanalyses (Table 2.4) for the solid **2**-S-TBHP_D were consistent with the formulation (ptpzpy)₄[Mo₈O₂₆]. PXRD data for this solid, designated as compound **4** in Scheme 2.1, showed that the material is microcrystalline (Figure 2.9).

Whereas an octamolybdate salt was formed from **1–3** under the catalytic reaction conditions with TBHP_D, the oxidative decarbonylation of **1** and **2** with TBHP_D in the absence of substrate gave **3**. These contrasting outcomes may be attributed to the different reaction conditions used (10 eq. TBHP_D, room temperature/4 h and no substrate for the preparation of **3**; 172 eq. TBHP_D, 55 °C/24 h and presence of Cy for the catalytic reaction). It is still possible that in the catalytic reaction the hybrid material **3** may be an intermediate in the conversion of **1** and **2** to species of the type (L)_x[Mo₈O₂₆].

2.3.4. Ionic liquid-supported metal species for olefin epoxidation

Compounds **1–3** were further tested for Cy epoxidation with TBHP using the ionic liquid (IL) [bmim]NTf₂ (bmim = 1-butyl-3-methylimidazolium; NTf₂ = bis(trifluoromethylsulfonyl)imide) as cosolvent at 55 °C (Table 2.1, Figure 2.10). The use of an IL may enhance the solubility of the metal species, and thus the overall reaction kinetics. In comparison to the volatile organic solvent CH₂ClCHCl₂, the reaction using [bmim]NTf₂ as cosolvent led to superior catalytic results for all three compounds (Table 2.1, Figure 2.10). CyO selectivity of at least 87 % was reached at 34–46 % conversion (31–40 % CyO yield). Complex **1** with [bmim]NTf₂ led to superior catalytic results than those with [bmim]PF₆ (PF₆ = hexafluorofosfato), whereas the opposite was observed for **3**. These results may be due to differences in solubility and rate of formation of the molybdenum species in the different ILs, although this is not trivial to demonstrate since it would require tracking the molybdenum species formed over time, and assessing their intrinsic activities. For the best performing system **3**/[bmim]PF₆, increasing the reaction

Chapter 2

temperature from 55 to 70 °C led to an increase in the CyO yield at 24 h from 41 % to 58 %.

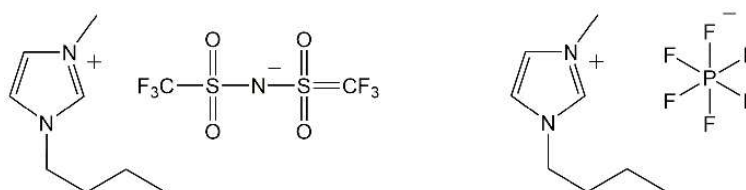


Figure 2.10. Ionic liquids used: [bmim]NTf₂ and [bmim]PF₆.

2.3.5. Characterization of solids after catalytic epoxidation in the presence of ionic liquid

After 24 h-batch runs at 55 °C, the reaction mixtures were liquid (IL)-liquid (organic phase)-solid(S). The ATR FT-IR spectra of the recovered solids *i*-S-TBHP-[bmim]NTf₂ were similar to the spectra of *i*-S-TBHP (*i* = **1–3**) with respect to Mo–O vibrations (700–1000 cm⁻¹), but different in the region of the ligand modes (>1000 cm⁻¹) (Figure 2.8). Similar results were obtained for *i*-S-TBHP-[bmim]PF₆ (not shown). The spectra very closely match that reported previously for the solid obtained upon OD of the tetracarbonyl complex *cis*-[Mo(CO)₄(ppp)] (ppp = 2-(1-pentyl-3-pyrazolyl)pyridine) during Cy epoxidation with TBHP in the presence of [bmim]NTf₂.¹² CHN microanalyses (Table 2.4) for the solid **2**-S-TBHP-[bmim]NTf₂ were consistent with the formulation (bmim)₃(H₃O)[Mo₈O₂₆]. PXRD data for this solid (Scheme 2.1), showed that the material is microcrystalline (Figure 2.9). A comparison of the PXRD pattern of (bmim)₃(NH₃)[Mo₈O₂₆] (**7**) with a simulated pattern calculated using crystal structure data reported for (bmim)₃NH₄[Mo₈O₂₆] (**8**) suggests that the two salts may have similar structures.⁸⁵ Accordingly, FT-IR spectra for the two compounds display a striking correspondence in the region 350–1000 cm⁻¹. For **1–3** (Scheme 2.1), the precipitation of the β-octamolybdate salt with [bmim]⁺ counterions (rather than a cation derived from the ligand ptpzpy) is due to the large excess of IL present in the reaction mixture.

Chapter 2

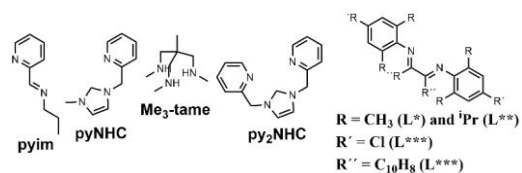
Table 2.2. *cis*-Cyclooctene epoxidation with TBHP_D in the presence of compounds **1** and **2**, and comparison to literature data for molybdenum carbonyl complexes bearing N-donor ligands, tested as pre-catalysts, at 55 °C without additional solvent.

Entry	Complex	Mo:Cy:TBHP _D ^a	<i>t</i> (h)	Conv. (%) ^b	Select. (%) ^c	Ref.
1	1	1:113:172	6/24	35/54	89/85	
2	2	1:113:172	6/24	31/52	97/92	
3	[Mo(CO) ₄ (pzpyH)]	1:100:152	6/24	51/78	100/100	11
4	[Mo(CO) ₄ (pzpyEA)]	1:100:152	6/24	70/92	100/100	11
5	[Mo(CO) ₄ (pyim)]	1:100:153	5	100	100	71
6	[Mo(CO) ₄ (PyNHC)]	1:100:200	4/24	~3/~9	~100/~100	70
7	[Mo(CO) ₃ (Py ₂ NHC)]	1:100:200	4/24	~3/~16	~100/~100	70
8	[Mo(CO) ₃ (Me ₃ -tame)]	1:100:154	24	64	100	72
9	[Mo(η^3 -C ₃ H ₅)Cl(CO) ₂ (CH ₃ CN) ₂]	1:100:159	6/24	99/100	100/100	73
10	[Mo(η^3 -C ₃ H ₅)Br(CO) ₂ (CH ₃ CN) ₂]	1:100:159	6/24	99/100	100/100	73
11	[Mo(η^3 -C ₅ H ₅ O)Br(CO) ₂ (CH ₃ CN) ₂]	1:100:159	6/24	97/100	100/100	73
12	[Mo(η^3 -C ₃ H ₅)Cl(CO) ₂ (L [*])]	1:100:159	6/24	88/95	100/100	73
13	[Mo(η^3 -C ₃ H ₅)Cl(CO) ₂ (L ^{**})]	1:100:159	6/24	68/88	100/100	73
14	[Mo(η^3 -C ₃ H ₅)Cl(CO) ₂ (L ^{***})]	1:100:159	6/24	99/100	100/100	73
15	[Mo(η^3 -C ₃ H ₅)Br(CO) ₂ (L ^{***})]	1:100:159	6/24	99/100	100/100	73
16	[Mo(η^3 -C ₅ H ₅ O)Br(CO) ₂ (L ^{***})]	1:100:159	6/24	97/100	100/100	73
17	[CpMo(CO) ₂ (IMes)(CH ₃ CN)]BF ₄	1:100:200	4/24	~90/~100	~100/~100	74

^a Initial Mo:Cy:TBHP_D molar ratio.

^b *cis*-Cyclooctene conversion.

^c Selectivity to the epoxide (CyO).



Chapter 2

Table 2.3. Comparison of FT-IR bands observed for solids recovered after catalytic reactions (entries 1-7 of table 2.2) with corresponding bands for compounds containing the β -[Mo₈O₂₆]⁴⁻ anion.

Compound ^a	IR bands (cm ⁻¹)					Ref.
1-S-TBHP _D ^b	941 ^c	910 ^c	840 ^d	705 ^d	660 ^d	
1-S-TBHP _D -[bmim]NTf ₂ ^b	937	911/903	838	706/693	659	
1-S-H ₂ O ₂ ^b	940	910	841	705	658	
2-S-TBHP _D ^b	942	910	842	706	660	
2-S-TBHP _D -[bmim]NTf ₂ ^b	937	910/900	837	707/693	658	
3-S-TBHP _D ^b	941	909	841	705	659	
3-S-TBHP _D -[bmim]NTf ₂ ^b	938	911/902	839	705/691	658	
(bmim) ₃ NH ₄ [Mo ₈ O ₂₆] ^b	933	909/898	837	704/692	657	
(H ₃ biim) ₄ [Mo ₈ O ₂₆]	944	919	838	686	670	79
(C ₅ H ₅ NH) ₄ [Mo ₈ O ₂₆]	946	912	839	709	675	76
((CH ₃) ₃ CC ₅ H ₄ NH) ₄ [Mo ₈ O ₂₆]	949	914	837	708	659	76
(HDBU) ₃ (NH ₄)[Mo ₈ O ₂₆] ^b ·H ₂ O	939	910	842	720	669	80
(Hmim) ₄ [Mo ₈ O ₂₆]	946	910	841	710	665	78
(Dhmim) ₄ [Mo ₈ O ₂₆]	956	911	837	714	650	78
(Hpy) ₄ [Mo ₈ O ₂₆] ^b ·H ₂ O	947	911	836	717	632	78
(bmim) ₄ [Mo ₈ O ₂₆]	939	913	842	714	661	81
(BDMLPX) ₃ [Mo ₈ O ₂₆] ₂ (H ₃ O) ₂ ·H ₂ O	944	902	841	711	651	82
(L) _x [β -Mo ₈ O ₂₆] ^b	935	910/898	836	699	657	83

^a H₂biim = 2,2'-biimidazole; DBU = 1,8-diazabicyclo[5.4.0]undec-7-ene; Hmim = 1-hexyl-3-methylimidazolium; Dhmim = 1,2-dimethyl-3-hexylimidazolium; Hpy = 1-hexylpyridinium; BDMLPX = di(1,2-dimethylimidazolium) β -xylenedichloride; L = monoprotonated [4,4'-Hbipy]⁺ cations or, alternatively, a mixture of neutral 4,4'-bipy and diprotonated [4,4'-H₂bipy]²⁺ cations. ^b ATR FT-IR bands. ^c Bands attributed to ν (Mo=O_t) vibrations. ^d Bands attributed to ν (Mo-O-Mo) vibrations.

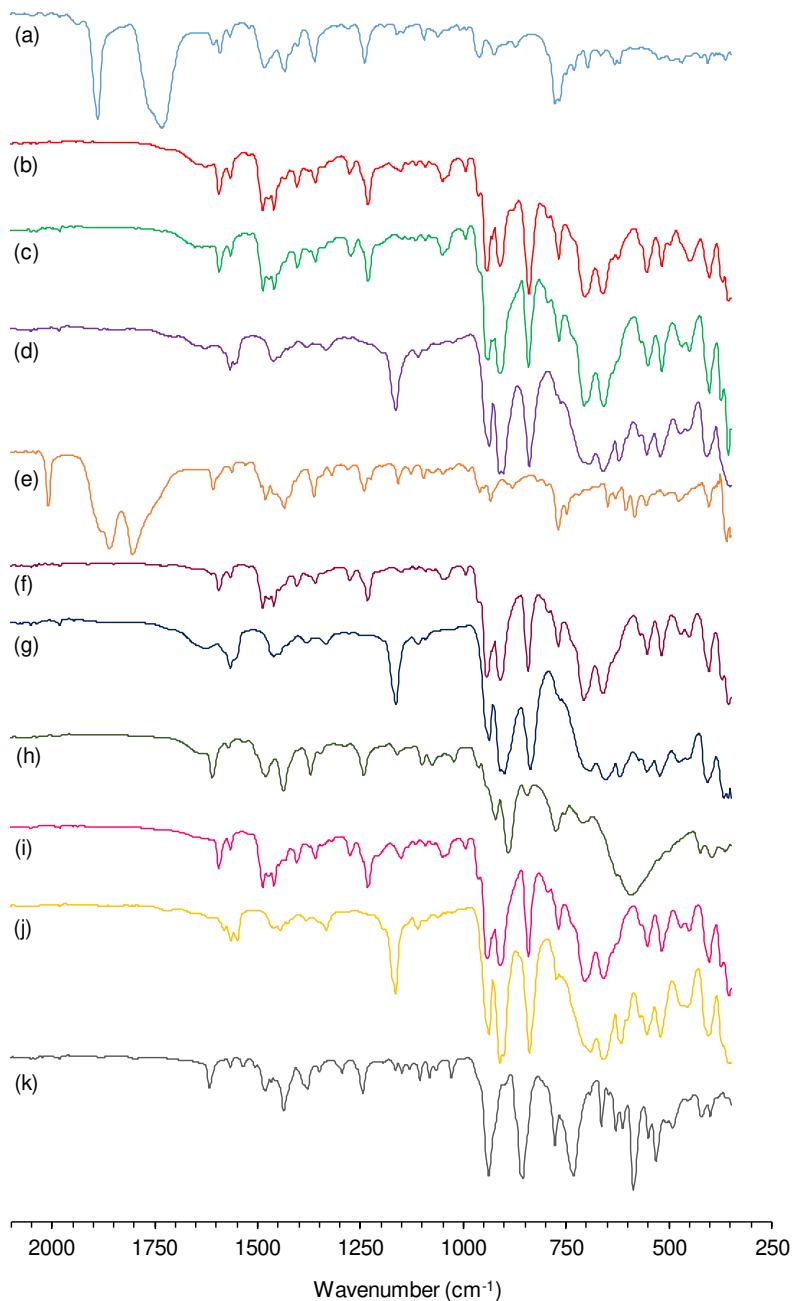


Figure 2.8. ATR FT-IR spectra of (a) **1**, (e) **2** and (h) **3**, and the recovered solids (b) **1-S-TBHP_D**, (c) **1-S-H₂O₂**, (d) **1-S-TBHP_D-[bmim]NTf₂**, (f) **2-S-TBHP_D**, (g) **2-S-TBHP_D-[bmim]NTf₂**, (i) **3-S-TBHP_D**, (j) **3-S-TBHP_D-[bmim]NTf₂**, and (k) **3-L-H₂O**.

Table 2.4. Elemental analysis results.

Compound		C (%)	H (%)	N (%)
(bmim) ₃ NH ₄ [Mo ₈ O ₂₆] (8)	Found	17.89	2.98	6.10
C ₂₄ H ₄₉ N ₇ Mo ₈ O ₂₆	Calcd	17.80	3.05	6.06
Recovered solid 2-S-TBHP _D	Found	30.47	4.10	9.76
(ptapzpy) ₄ [Mo ₈ O ₂₆] (C ₅₆ H ₈₄ N ₁₆ Mo ₈ O ₂₆) (6)	Calcd	31.07	3.91	10.35
Recovered solid 2-S-TBHP _D -[bmim]NTf ₂	Found	17.50	3.31	5.24
(bmim) ₃ (H ₃ O)[Mo ₈ O ₂₆] (C ₂₄ H ₄₈ N ₆ Mo ₈ O ₂₇) (7)	Calcd	17.79	2.99	5.19

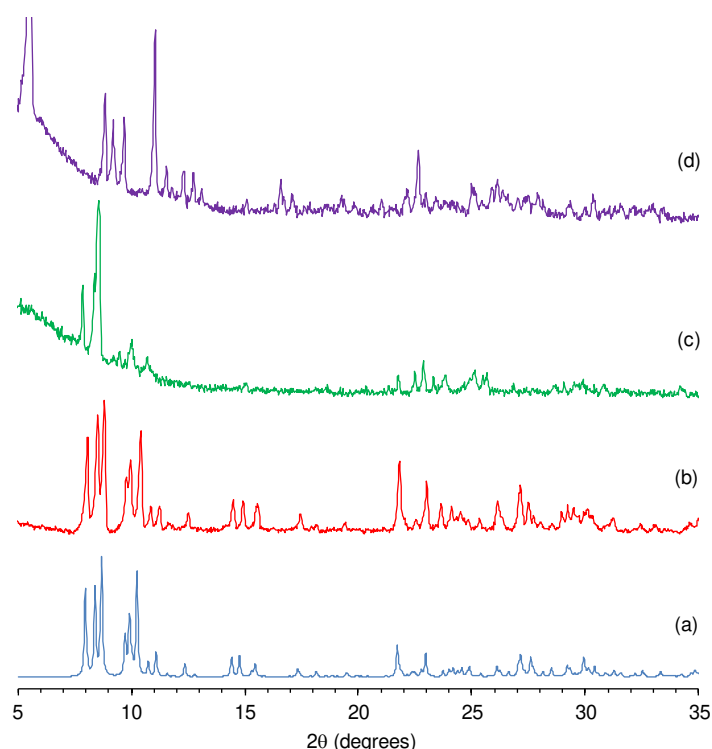


Figure 2.9. Simulated (a) and experimental (b-d) powder XRD patterns of (a) (bmim)₃NH₄[Mo₈O₂₆], (b) (bmim)₃NH₄[Mo₈O₂₆] (**6**), (c) the recovered solid 2-S-TBHP_D-[bmim]NTf₂, and (d) the recovered solid 2-S-TBHP_D. The program Mercury (copyright CCDC, ver. 3.9)⁸⁴ was used to calculate the simulated pattern from the single-crystal X-ray data published for (bmim)₃NH₄[Mo₈O₂₆].⁸⁵

2.3.6. Catalytic epoxidation with H₂O₂

Compounds **1–3** were further studied for Cy reaction with H₂O₂ at 55 °C. Results with **2** and **3** (56–66 % CyO yield at 24 h) were superior to those with **1** (9 %) (Table 2.1). With the exception of complex **1**, the catalytic results are generally better with H₂O₂ as oxidant than with TBHP. Notably, the CyO yield of 66 % obtained with **2** surpasses the 41 % yield obtained with *cis*-[Mo(CO)₄(ppp)] under identical reaction conditions.¹²

Chapter 2

Iodometric titrations performed for **3**/TBHP_D/55 °C and **3**/H₂O₂/55 °C (without substrate) showed that the decomposition of TBHP was not considerable (31 % TBHP conversion at 24 h), whereas that of H₂O₂ was very significant (ca. 98 % decomposition). Hence, the epoxidation process with TBHP does not seem to be compromised by side-reactions of the oxidant (*i.e.* unproductive decomposition into molecular oxygen and *tert*-butanol). On the other hand, the unproductive decomposition of H₂O₂ (into molecular oxygen and H₂O) may compete with use of the oxidant for the catalytic reaction. Increasing the reaction temperature from 55 to 70 °C for the systems (**1** or **3**)/H₂O₂ was only slightly beneficial for **1** and actually led to poorer results with **3** (Table 2.1), presumably due to enhanced decomposition of the oxidant.

2.3.7. Characterization of solids after catalytic epoxidation with H₂O₂

The differences in catalytic results for TBHP or H₂O₂ as oxidant may also be partly due to differences in catalyst stability. The system **1**/H₂O₂ consisted initially of a yellow solution which changed with time into a biphasic solid–liquid mixture, where the liquid phase was colourless (attempts to isolate metal species from this phase were unsuccessful) and the solid was off-white. The FT-IR spectrum of the recovered solid **1**-S-H₂O₂ (at 24 h) indicated that it was a salt of the type (L)_x[Mo₈O₂₆] (similar to that verified for the systems (**1**–**3**)/TBHP) (Figure 2.8, c). For **2**/H₂O₂ and **3**/H₂O₂ the reaction mixture consisted of yellow liquid phases and no undissolved solid. The conversion of **2** and **3** to a different, highly soluble Mo-containing species may explain the superior catalytic results obtained for these systems. For **3**/H₂O₂, a yellow solid was isolated from the liquid phase (**3**-L-H₂O₂), which exhibited a different ATR FT-IR spectrum from those of **3** and the recovered solids discussed above (Figure 2.8, k). The yellow colour is typically indicative of oxoperoxomolybdenum(VI) species. Accordingly, bands in the IR spectrum of the recovered solid may be assigned as $\nu(\text{Mo}=\text{O})$ at 938 cm⁻¹, $\nu(\text{O}-\text{O})$ at 855 cm⁻¹, and $\nu(\text{Mo}(\text{O}_2)_2)$ at 663, 585 and 530 cm⁻¹. An additional strong and broad band at 732 cm⁻¹ may be due to a Mo–O–Mo stretching vibration, suggesting the presence of a polynuclear species. From the characterisation studies, it seems that **1** possesses a different reactivity with H₂O₂ than **3**, being converted to different types of metal species.

2.4. Conclusions

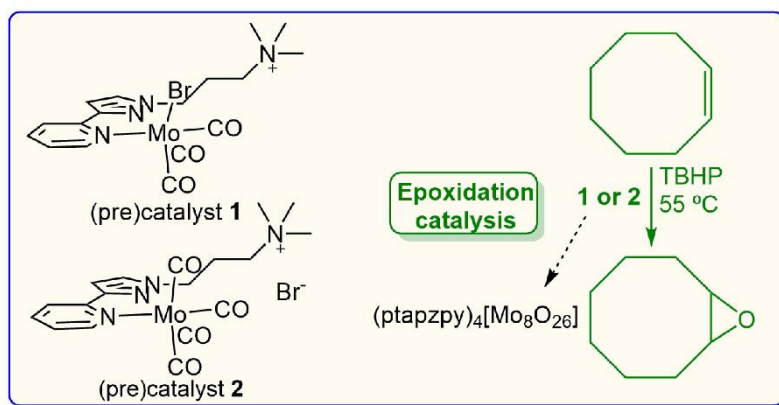
Two distinct synthetic pathways (both starting with $\text{Mo}(\text{CO})_6$) have been established for the synthesis of molybdenum(0) tricarbonyl and tetracarbonyl complexes containing a bidentatecoordinated pyrazolylpyridine ligand (Scheme 2.4). Complex **1** containing the propyltrimethylammonium-functionalised ligand is unstable both in solution and in the solid-state. These characteristics are consistent with the poor stability previously reported for tetracarbonylmolybdenum(0) pyridylpyrazole and associated with the coordination of hard bases such as pyridyl or pyrazole to a soft acid, in this case molybdenum(0).⁶⁵ The tetracarbonyl complex readily undergo OD to give molybdenum oxide/pyrazolylpyridine hybrid compounds.

The attempt to obtain supramolecular complexes was unsuccessful, since no interaction was observed between the complexes and CB[7], possibly due to the instability of the ionic ligand and the carbonyl ligands in solution and in contact with water.

While OD of **1** with a small excess of TBHP leads to a hybrid material formulated as $[\text{Mo}_3\text{O}_9([\text{ptapzpy}]\text{Br})_2]$ (**3**), the complexes **1** and **2** display moderate activity when applied as (pre)catalysts for the epoxidation of *cis*-cyclooctene with TBHP, which can be attributed to the *in situ* formation of poorly soluble β -octamolybdate salts. Better results were obtained with H_2O_2 as oxidant and the tetracarbonyl precatalyst, despite significant non-productive decomposition of the oxidant. The active species are yellow oxoperoxo-molybdenum(VI) species formed by the oxidative decarbonylation of the precursor. When ionic liquids of the type $[\text{bmim}]\text{X}$ are used as cosolvents in the epoxidation reaction with TBHP, the prepared compounds are converted to $[\text{bmim}]_4[\beta\text{-Mo}_8\text{O}_{26}]$ (**7**). Treatment of the carbonyl precursors with TBHP in the absence of olefin gave the compound **3**. Work to isolate a more crystalline form of this hybrid and determine its structure was unsuccessful.

In conclusion, in this work considerable insight has been gained into the chemistry and catalytic performance of tri- and tetracarbonylmolybdenum(0) pyrazolylpyridine complexes, which should help guide future studies on the use of such complexes as (pre)catalysts and/or precursors to molybdenum oxide derivatives.

Chapter 2



Scheme 2.4. Summary of the main syntheses and catalytic studies carried out in this work.

2.5. References

- (1) Hieber, V. W.; Muhlbauer, F. **1935**, *221*, 337–348.
- (2) Braga, S. S.; Coelho, A. C.; Gonçalves, I. S.; Almeida Paz, F. A. *Acta Crystallogr., Sect. E Struct. Rep.* **2007**, *63*, 780–782.
- (3) Stiddard, B. M. H. B. *J. Chem. Soc.* **1962**, 4712, 4712–4715.
- (4) Gomes, A. C.; Bruno, M.; Valente, A. A.; Gonçalves, I. S.; Pillinger, M. *J. Organomet. Chem.* **2013**, *744*, 53–59.
- (5) Frisell, H.; Eriksson, L.; Vitagliano, A. *Organometallics* **1997**, *16*, 942–950.
- (6) Ardizzoia, G. A.; Bea, M.; Therrien, B. *Eur. J. Inorg. Chem.* **2016**, 3829–3837.
- (7) Herrick, R. S.; Ziegler, C. J.; Bohan, H.; Corey, M.; Eskander, M.; Giguere, J.; McMicken, N.; Wrona, I. E. *J. Organomet. Chem.* **2003**, *687*, 178–184.
- (8) Oelkers, B.; Venker, A.; Sundermeyer, J. *Inorg. Chem.* **2012**, *51*, 4636–4643.
- (9) García-Rodríguez, R.; Miguel, D. *Dalton Trans.* **2006**, *6*, 1218–1225.
- (10) Karakus, M.; Davulga, G.; Gómez-Ruiz, S.; Tschirschwitz, S.; Hey-Hawkins, E. *Polyhedron* **2009**, *28*, 91–94.
- (11) Neves, P.; Amarante, T. R.; Gomes, A. C.; Coelho, A. C.; Gago, S.; Pillinger, M.; Gonçalves, I. S.; Silva, C. M.; Valente, A. A. *Appl. Catal., A* **2011**, *395*, 71–77.
- (12) Nogueira, L. S.; Neves, P.; Gomes, A. C.; Valente, A. A.; Pillinger, M.; Gonçalves, I. S. *J. Organomet. Chem.* **2017**, *846*, 185–192.
- (13) Behrens, H.; Lindner E.; Lehnert, G. *J. Organomet. Chem.* **1970**, *22*, 665–676.
- (14) Brisdon, B. J.; Edwards, D. A.; White, J. W. *J. Organomet. Chem.* **1978**, *156*, 427–437.
- (15) Huffman, J. C.; Kober, I. E. M.; Overtonlb, C. *Inorg. Chem.* **1984**, *23*, 2298–2303.
- (16) Han, Y. J.; Lees, A. J. *Inorg. Chim. Acta* **1988**, *147*, 45–49.
- (17) Murdoch, H. D.; Henzi, R.; Calderazzo, F. *J. Organomet. Chem.* **1967**, *7*, 441–448.
- (18) Manuta, D. M.; Lees, A. J. *Inorg. Chem.* **1986**, *25*, 1354–1359.
- (19) Rawlins, K. A.; Lees, J. *Inorg. Chem.* **1989**, *28*, 2154–2160.

Chapter 2

- (20) Cheng, L. T.; Tam, W.; Eaton, D. F. *Organometallics* **1990**, *9*, 2856–2857.
- (21) Fu, W.-F.; Van Eldik, R. *Inorg. Chem.* **1998**, *37*, 1044–1050.
- (22) Vlcek Jr., A. *Coord. Chem. Rev.* **1998**, *177*, 219–256.
- (23) Vlček Jr., A. *Coord. Chem. Rev.* **2002**, *230*, 225–242.
- (24) Veroni, I.; Mitsopoulou, C. A. *Dalton Trans.* **2003**, 255–260.
- (25) Zidan, M. D.; Al-Ktaifani, M. M.; Allahham, A. *Optik* **2016**, *127*, 2570–2574.
- (26) Baxter, P. N. W.; Connor, J. A. *J. Organomet. Chem.* **1995**, *486*, 115–121.
- (27) Rimmer, R. D.; Pierri, A. E.; Ford, P. C. *Coord. Chem. Rev.* **2012**, *256*, 1509–1519.
- (28) Sieh, D.; Lacy, D. C.; Peters, J. C.; Kubiak, C. P. *Chem. Eur. J.* **2015**, *21*, 8497–8503.
- (29) Tory, J.; Setterfield-Price, B.; Dryfe, R. A. W.; Hartl, F. *ChemElectroChem* **2015**, *2*, 213–217.
- (30) Franco, F.; Cometto, C.; Sordello, F.; Minero, C.; Nencini, L.; Fiedler, J.; Gobetto, R.; Nervi, C. *ChemElectroChem* **2015**, *2*, 1372–1379.
- (31) Mentés, A.; Sarbay, M.; Hazer, B.; Arslan, H. *Appl. Organomet. Chem.* **2005**, *19*, 76–80.
- (32) Amarante, T. R.; Neves, P.; Coelho, A. C.; Gago, S.; Valente, A. A.; Paz, F. A.; Pillinger, M.; Gonçalves, I. S. *Organometallics* **2010**, *29*, 883–892.
- (33) Cheng, X. J.; Liang, L. L.; Chen, K.; Ji, N. N.; Xiao, X.; Zhang, J. X.; Zhang, Y. Q.; Xue, S. F.; Zhu, Q. J.; Ni, X. L.; Tao, Z. *Angew. Chem., Int. Ed.* **2013**, *52*, 7252–7255.
- (34) Assaf, K. I.; Nau, W. M. *Chem. Soc. Rev.* **2015**, *44*, 394–418.
- (35) Kim, K.; Selvapalam, N.; Ko, Y. H.; Park, K. M.; Kim, D.; Kim, J. *Chem. Soc. Rev.* **2007**, *36*, 267–279.
- (36) Kim, J.; Jung, I.; Kim, S.; Lee, E.; Kang, J.; Sakamoto, S.; Yamaguchi, K.; Kim, K.; Hyojadong, S.; Korea, R. *J. Am. Chem. Soc.* **2000**, *122*, 540–541.
- (37) Buck, D. P.; Abeysinghe, P. M.; Cullinane, C.; Day, A. I.; Collins, J. G.; Harding, M. M. *Dalton Trans.* **2008**, 2328–2334.
- (38) Heo, J.; Kim, J.; Whang, D.; Kim, K. *Inorg. Chim. Acta* **2000**, *297*, 307–312.
- (39) Corma, A.; García, H.; Montes-Navajas, P.; Primo, A.; Calvino, J. J.; Trasobares, S. *Chem. Eur. J.* **2007**, *13*, 6359–6364.
- (40) Feng, X.; Lu, X. J.; Xue, S. F.; Zhang, Y. Q.; Tao, Z.; Zhu, Q. J. *Inorg. Chem. Commun.* **2009**, *12*, 849–852.
- (41) Jeon, W. S.; Moon, K.; Park, S. H.; Chun, H.; Ko, Y. H.; Lee, J. Y.; Lee, E. S.; Samal, S.; Selvapalam, N.; Rekharsky, M. V.; Sindelar, V.; Sobransingh, D.; Inoue, Y.; Kaifer, A. E.; Kim, K. *J. Am. Chem. Soc.* **1996**, *118*, 9790–9791.
- (42) Samsonenko, D. G.; Sokolov, M. N.; Virovets, A. V.; Pervukhina, N. V.; Fedin, V. P. *Eur. J. Inorg. Chem.* **2001**, 167–172.
- (43) Hernandez-Molina, R.; Sokolov, M.; Esparza, P.; Vicent, C.; Llusar, R. *Dalton Trans.* **2004**, *6*, 847–851.
- (44) Sokolov, M. N.; Gerasko, O. A.; Dybtsev, D. N.; Chubarova, E. V.; Virovets, A. V.; Vicent, C.; Llusar, R.; Fenske, D.; Fedin, V. P. *Eur. J. Inorg. Chem.* **2004**, 63–68.
- (45) Gerasko, O. A.; Mainicheva, E. A.; Naumova, M. I.; Yurjeva, O. P.; Alberola, A.; Vicent,

Chapter 2

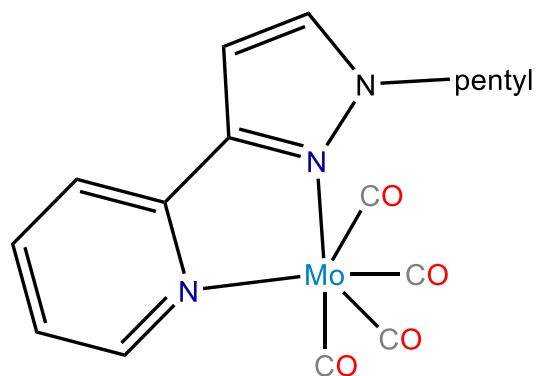
- C.; Llusar, R.; Fedin, V. P. *Chem. Eur. J.* **2008**, *3*, 416–424.
- (46) Ambade, A. V.; Savariar, E. N.; Thayumanavan, S. *Mol. Pharm.* **2005**, *2*, 264–272.
- (47) Kang, J.; Hilmersson, G.; Santamaría, J.; Rebek, J. *J. Am. Chem. Soc.* **1998**, *120*, 3650–3656.
- (48) Castellano, R. K.; Nuckolls, C.; Rebek, J. *J. Am. Chem. Soc.* **1999**, *121*, 11156–11163.
- (49) Bruno, S. M.; Gomes, A. C.; Oliveira, T. S. M.; Antunes, M. M.; Lopes, A. D.; Valente, A. A.; Gonçalves, I. S.; Pillinger, M. *Org. Biomol. Chem.* **2016**, *14*, 3873–3877.
- (50) Dsouza, R. N.; Nau, W. M. *Org. Lett.* **2009**, *11*, 2595–2598.
- (51) De Lima, S.; Gómez, J. A.; Barros, V. P.; Vertuan, G. S.; Assis, M.; Graeff, C. F. O.; Demets, G. J. F. *Polyhedron* **2010**, *29*, 3008–3013.
- (52) Pemberton, B. C.; Singh, R. K.; Johnson, A. C.; Jockusch, S.; Da Silva, J. P.; Ugrinov, A.; Turro, N. J.; Srivastava, D. K.; Sivaguru, J. *Chem. Commun.* **2011**, *47*, 6323–6325.
- (53) Wang, Y. H.; Cong, H.; Zhao, F. F.; Xue, S. F.; Tao, Z.; Zhu, Q. J.; Wei, G. *Catal. Commun.* **2011**, *12*, 1127–1130.
- (54) Samsonenko, D. G.; Virovets, A. V.; Sharonova, A. A.; Fedin, V. P.; Fenske, D. *Russ. Chem. Bull.* **2001**, *50*, 494–496.
- (55) Lin, R. G.; Long, L. S.; Huang, R. Bin; Zheng, L. S.; Ng, S. W. *Acta Cryst.* **2005**, *61*, 885–889.
- (56) Samsonenko, D. G.; Gerasko, O. A.; Virovets, A. V.; Fedin, V. P. *Russ. Chem. Bull.* **2005**, *54*, 1557–1562.
- (57) Adonin, S. A.; Peresyphkina, E. V.; Sokolov, M. N.; Fedin, V. P. *J. Struct. Chem.* **2010**, *51*, 731–736.
- (58) Abramov, P. A.; Yu Laricheva, A.; Peresyphkina, E. V.; Mirzaeva, I. V.; Moroz, N. K.; Sokolov, M. N. *Inorg. Chim. Acta* **2012**, *383*, 7–12.
- (59) Thiel, W. R.; Angstl, M.; Priermeier, T. *Chem. Ber.* **1994**, *127*, 2373–2379.
- (60) Amarante, T. R.; Neves, P.; Paz, F. A. A.; Valente, A. A.; Pillinger, M.; Gonçalves, I. S. *Dalton Trans.* **2014**, *43*, 6059–6069.
- (61) Viček, Jr. A.; Baumann, F.; Kaim, W.; Grevels, F.-W.; Hartl, F. *J. Chem. Soc. Dalton Trans.* **1998**, *4*, 215–220.
- (62) Coelho, A. C.; Nolasco, M.; Balula, S. S.; Antunes, M. M.; Pereira, C. C. L.; Almeida Paz, F. A.; Valente, A. A.; Pillinger, M.; Ribeiro-Claro, P.; Klinowski, J.; Gonçalves, I. S. *Inorg. Chem.* **2011**, *50*, 525–538.
- (63) Thiel, W. R.; Priermeier, T.; Fiedler, D. A. . B. A. M. . M. R. . M. *J. Organomet. Chem.* **1996**, *514*, 137–147.
- (64) Coelho, A. C.; Almeida Paz, F. A.; Klinowski, J.; Pillinger, M.; Gonçalves, I. S. *Molecules* **2006**, *11*, 528–538.
- (65) Arroyo, M.; Miguel, D.; Villafañe, F.; Alegria, E. C. B.; Pombeiro, A. J. L. *Dalton Trans.* **2012**, *41*, 7017–7025.
- (66) Zapf, P. J.; Haushalter, R. C.; Zubieta, J. *Chem. Mater.* **1997**, *4756*, 2019–2024.
- (67) Zhou, Y.; Zhang, L.; Fun, H. K.; You, X.; *Inorg. Chem. Commun.* **2000**, *3*, 114–116.

Chapter 2

- (68) Twu, J.; Yu, Y. Y.; Tang, C. W.; Wang, G. J.; Chen, K. H. *Appl. Spectrosc.* **1999**, *53*, 1083–1086.
- (69) Gomes, A. C.; Magalhães, C. I. R.; Oliveira, T. S. M.; Lopes, A. D.; Gonçalves, I. S.; Pillinger, M. *Dalton Trans.* **2016**, *45*, 17042–17052.
- (70) Wang, Z.; Li, S.; Teo, W. J.; Poh, Y. T.; Zhao, J.; Hor, T. S. A. *J. Org. Chem.* **2015**, *775*, 188–194.
- (71) Gomes, A. C.; Bruno, S. M.; Gago, S.; Lopes, R. P.; Machado, D. A.; Carminatti, A. P.; Valente, A. A.; Pillinger, M.; Gonçalves, I. S. *J. Organomet. Chem.* **2011**, *696*, 3543–3550.
- (72) Petrovski, Ž.; Valente, A. A.; Pillinger, M.; Dias, A. S.; Rodrigues, S. S.; Romão, C. C.; Gonçalves, I. S. *J. Mol. Catal. A Chem.* **2006**, *249*, 166–171.
- (73) Alonso, J. C.; Neves, P.; Da Silva, M. J. P.; Quintal, S.; Vaz, P. D.; Silva, C.; Valente, A. A.; Ferreira, P.; Calhorda, M. J.; Félix, V.; Drew, M. G. B. *Organometallics* **2007**, *26*, 5548–5556.
- (74) Li, S.; Kee, C. W.; Huang, K.; Hor, T. S. A.; Zhao, J. *Organometallics* **2010**, *29*, 1924–1933.
- (75) Holm, R. H. *Chem. Rev.* **1987**, *87*, 1401–1449.
- (76) Gamelas, C. A.; Neves, P.; Gomes, A. C.; Valente, A. A.; Romão, C. C.; Gonçalves, I. S.; Pillinger, M. *Catal. Lett.* **2012**, *142*, 1218–1224.
- (77) Carrasco, C. J.; Montilla, F.; Álvarez, E.; Herbert, M.; Galindo, A. *Polyhedron* **2013**, *54*, 123–130.
- (78) Zhou, M. D.; Liu, M. J.; Huang, L. L.; Zhang, J.; Wang, J. Y.; Li, X. B.; Kühn, F. E.; Zang, S. L. *Green Chem.* **2015**, *17*, 1186–1193.
- (79) Neves, P.; Amarante, T. R.; Valente, A. A.; Pillinger, M.; Gonçalves, I. S. *Catal. Lett.* **2016**, *146*, 841–850.
- (80) Coué, V.; Dessapt, R.; Bujoli-Doeuff, M.; Evain, M.; Jobic, S. *J. Solid State Chem.* **2006**, *179*, 3615–3627.
- (81) Carrasco, C. J.; Montilla, F.; Álvarez, E.; Herbert, M.; Galindo, A. *Polyhedron* **2013**, *54*, 123–130.
- (82) Li, Y.; Hang, X.; Li, N.; Hao, X. *J. Mater. Process. Technol.* **2016**, *230*, 280–287.
- (83) Neves, P.; Gomes, A. C.; Paz, F. A. A.; Valente, A. A.; Gonçalves, I. S.; Pillinger, M. *Mol. Catal.* **2017**, *432*, 104–114.
- (84) Macrae, C. F.; Bruno, I. J.; Chisholm, J. A.; Edgington, P. R.; McCabe, P.; Pidcock, E.; Rodriguez-Monge, L.; Taylor, R.; Van De Streek, J.; Wood, P. A. *J. Appl. Crystallogr.* **2008**, *41*, 466–470.
- (85) Linguito, S. L.; Zhang, X.; Padmanabhan, M.; Biradar, A. V.; Xu, T.; Emge, T. J.; Asefa, T.; Li, J. *New J. Chem.* **2013**, *37*, 2894–2901.

CHAPTER 3

Performance of a tetracarbonylmolybdenum(0) pyrazolylpyridine (pre)catalyst in olefin epoxidation and epoxide alcoholysis



cis-[Mo(CO)₄(2-(1-pentyl-3-pyrazolyl)pyridine)]

Chapter 3

Index

3.1. Introduction	103
3.2. Results and discussion	104
3.2.1. Synthesis and characterisation of ppp and pre-catalysts [Mo(CO) ₄ (ppp)] (1)	104
3.2.2. Oxidative decarbonylation	107
3.3. Catalytic studies	110
3.3.1. Catalytic epoxidation with TBHP	110
3.3.2. Characterization of solids after catalytic epoxidation with TBHP	111
3.3.3. Catalytic epoxidation with H ₂ O ₂	112
3.3.4. Characterization of solids after catalytic epoxidation with H ₂ O ₂	113
3.3.5. [MoO(O ₂) ₂ (ppp)] as active specie for the catalytic epoxidation	114
3.3.6. Ionic liquid-supported metal species for olefin epoxidation	115
3.3.7. Characterization of solids after catalytic epoxidation in ionic liquids	115
3.3.8. Acid catalysis	115
3.3.9. Characterization of solids after acid catalysis	116
3.4. Conclusions	117
3.5. References	118

Chapter 3

3.1. Introduction

The oxidative decarbonylation (OD) of molybdenum carbonyl complexes is a rewarding approach for the preparation of compounds containing Mo centres in high oxidation states.¹⁻³ For example, the oxidation of $[\text{Cp}'\text{Mo}(\text{CO})_3\text{X}]$ [Cp' = unsubstituted or substituted cyclopentadienyl, X = halide, alkyl, alkyl ester, *ansa*-bridged alkyl or cycloalkyl group, etc.] with *tert*-butylhydroperoxide (TBHP) gives molybdenum(VI) complexes of the type $[\text{Cp}'\text{MoO}_2\text{X}]$, $[\text{Cp}'\text{MoO}(\text{O}_2)\text{X}]$, $[(\text{Cp}'\text{MoO}_2)_2(\mu\text{-O})]$ and $[(\text{Cp}'\text{MoO}(\text{O}_2))_2(\mu\text{-O})]$ ²⁻¹⁰, the oxidation of $[\text{Cp}'\text{Mo}(\text{CO})_2(\text{NHC})(\text{CH}_3\text{CN})](\text{BF}_4)$ with TBHP gives $[\text{Cp}'\text{MoO}_2(\text{NHC})]\text{BF}_4$ (NHC = *N*-heterocyclic carbene)¹¹, the oxidation of $[\text{Mo}(\text{CO})_3(\text{HC}(3,5\text{-Me}_2\text{pz})_3)]$ with nitric acid yields $[(\text{HC}(3,5\text{-Me}_2\text{pz})_3)\text{MoO}_3]$ ($\text{HC}(3,5\text{-Me}_2\text{pz})_3$ = tris(3,5-dimethyl-1-pyrazolyl)methane)¹², and the reaction of $\text{Li}[\text{Mo}(\text{CO})_3(\text{tpms})]$ with AgBF_4 in air gives dinuclear $[(\text{MoO}_2(\text{tpms}))_2(\mu\text{-O})]$ (tpms = tris(1-pyrazolyl)methanesulfonate)¹³. These oxomolybdenum complexes have assumed an increasing level of attention in recent years because of their frequently impressive performance as catalysts for organic reactions such as the oxidation of sulfides^{14,15}, alcohols^{9,16} and amines¹⁷, and the epoxidation of olefins.¹⁸⁻²⁰

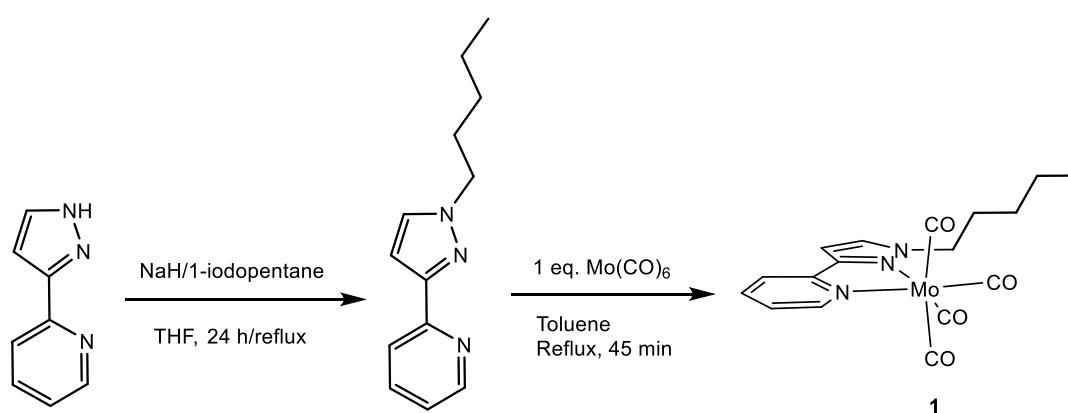
The OD synthetic chemistry is not limited to the formation of mononuclear and dinuclear complexes. Some of the more complex species formed include tetranuclear $[\text{Mo}_4\text{O}_{12}(\text{pypz})_4]$ from *cis*- $[\text{Mo}(\text{CO})_4(\text{pypz})]$ (pypz = 2-[3(5)-pyrazolyl]pyridine)²¹, octanuclear $[\text{Mo}_8\text{O}_{24}(\text{di-}t\text{Bu-bipy})_4]$ from *cis*- $[\text{Mo}(\text{CO})_4(\text{di-}t\text{Bu-bipy})]$ ($\text{di-}t\text{Bu-bipy}$ = 4,4'-di-*tert*-butyl-2,2'-bipyridine)²², and the onedimensional (1D) molybdenum oxide/bipyridine polymer $[\text{MoO}_3(2,2'\text{-bipy})]$ from *cis*- $[\text{Mo}(\text{CO})_4(2,2'\text{-bipy})]$ ($2,2'\text{-bipy}$ = 2,2'-bipyridine)²². The latter reaction is remarkable since it can be performed at ambient temperature with excess of TBHP as oxidant and within a few hours leads to a quantitative yield of the 1D polymer which had only previously been obtained by the hydrothermal treatment of a mixture of MoO_3 , 2,2'-bipy and H_2O at 160 °C for at least 5 days.^{23,24}

This chapter report on the synthesis of the tetracarbonyl complex *cis*- $[\text{Mo}(\text{CO})_4(\text{ppp})]$ (ppp = 2-(1-pentyl-3-pyrazolyl)pyridine) and its oxidative decarbonylation to give oxomolybdenum species. The tetracarbonyl complex and oxidised compounds have been studied as catalysts or catalyst precursors for the epoxidation of *cis*-cyclooctene and the ethanolysis of styrene oxide. Particular attention has been paid to the characterisation of solids recovered after catalytic runs.

3.2. Results and discussion

3.2.1. Synthesis and characterisation of ppp and pre-catalysts
[Mo(CO)₄(ppp)] (1)

The ligand 2-(1-pentyl-3-pyrazolyl)pyridine (ppp) was prepared by deprotonation of 2-(3-pyrazolyl)pyridine followed by addition of 1-iodopentane and reflux for 24 h (Scheme 3.1) with 95 % of yield. Characterisation data (FT-IR, ¹H and ¹³C solution NMR) were in line with those reported previously for ppp and other related 2-(1-alkyl-3-pyrazolyl)pyridine derivatives.^{25,26}



Scheme 3.1. Preparation of the ligand ppp and complex 1.

Proof of ligand ppp formation is provided by the FT-IR spectrum (Figure 3.1). The strong band at 764-796 cm⁻¹ is attributed to the bending mode of the C-H groups out-of-plane. The bending and stretching vibrations of -C-H unities of the pypz are localized between 1037-1095 and 1240 cm⁻¹, respectively. The vibration of ν(C-N) present in pypz is represented by the strong band at 1593 cm⁻¹. The ν(C-C) modes of pyridine and at inter ring are localized at 1649 and 1567 cm⁻¹, respectively. In the region of 2870-3118 cm⁻¹, several bands are observed, which are attributed to ν(=C-H) vibrations in pypz. These observations are in line with the IR spectroscopy of pypz.^{21,25-}

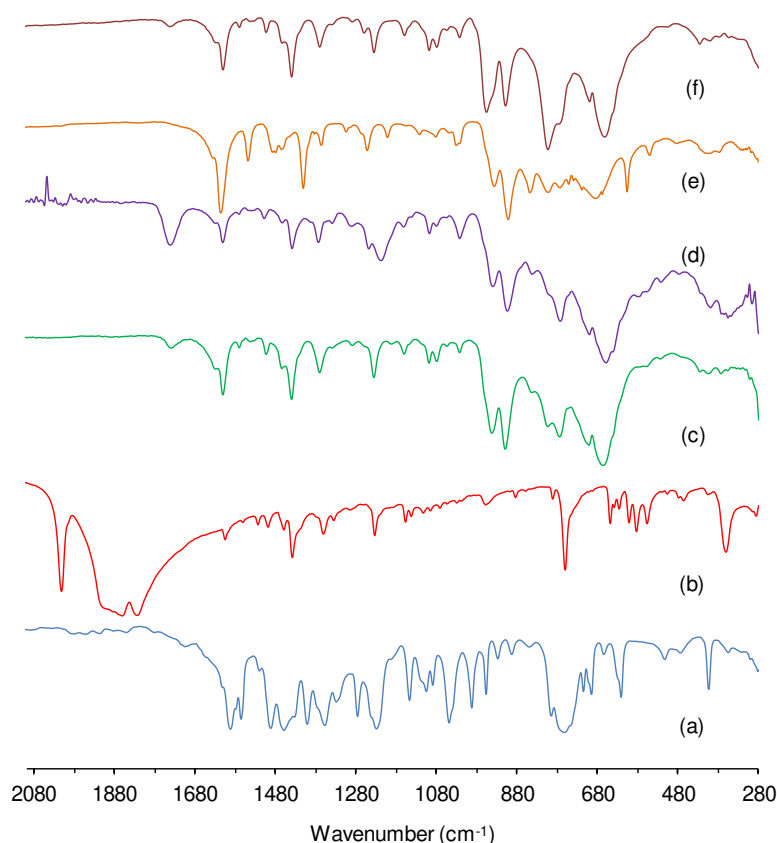


Figure 3.1. FT-IR (KBr) spectra in the 280-2100 cm^{-1} range for (a) ligand ppp, (b) **1**, (c) **2**, (d) $[\text{Mo}_8\text{O}_{24}(\text{eppa})_4]^{21}$, (e) $[\text{Mo}_8\text{O}_{24}(\text{di-}t\text{Bu-bipy})_4]^{22,29}$ and (f) $[\text{Mo}_2\text{O}_6(\text{ppp})]$.

The liquid ^1H NMR spectrum of ppp is in line with the spectra reported by Brunner³⁰ and Thiel²⁵. The proton resonances of heterocyclic pypz are localized between 8.63-6.74. The pentyl fragment is localized between 4.18-0.93 ppm.²⁵ The liquid ^{13}C NMR spectra of ppp display several signals between 104 and 153 ppm that can be readily assigned to the pypz ring carbon atoms. Moreover, signals between 14-53 ppm correspond to the pentyl group, respectively.

The molybdenum tetracarbonyl complex $[\text{Mo}(\text{CO})_4(\text{ppp})]$ (**1**) was obtained directly from $\text{Mo}(\text{CO})_6$ by refluxing a mixture of the hexacarbonyl and the organic ligand ppp in toluene (Scheme 3.1) with 56 % of yield. Complex **1** displays long term stability in the solid-state if stored under inert atmosphere. $[\text{Mo}(\text{CO})_4(\text{ppp})]$ is soluble in various organic solvent, such as acetone, acetonitrile, ethanol, diethyl ether, toluene, chloroform and dichloromethane, and insoluble in water. The complex was characterized by FT-IR, FT-Raman, ^1H and ^{13}C NMR spectroscopy in solution, elemental analysis and thermogravimetry confirming the complexation through these techniques.

Chapter 3

Elemental analyses of **1** (C, H and N) is consistent with the empirical $C_{17}H_{17}MoN_3O_4$. The thermogravimetry of **1** indicates an initial weight loss of 4.8 % and 14.2 % up to 71 and 111 °C, corresponding to the loss of two and four molecules of water by ligand, respectively. The decomposition of the four carbonyl groups is attributed to a weight loss of 22.5 % at 126-219 °C in **1**. The thermal decomposition of the organic ligand occurs in two parts, having a weight loss of 43.3 % between 456 and 524 until 800 °C in **1**.

The FT-IR and FT-Raman spectra of **1** confirm the preparation of the molybdenum tetracarbonyl-based organic–inorganic complex by coordination of the N,N-bidentate donor ligand to the metallic Mo centre. The FT-IR and Raman spectra contain bands for the pyrazolopyridine and carbonyl ligands (Figures 3.1 and 3.2). In the carbonyl stretching region (1800-2020 cm^{-1}) of the IR spectrum, complex **1** displays strong bands at 1824, 1861, ~1885 (sh) and 2013 cm^{-1} (cf. sharp bands at 1819, 1875 and 2011 cm^{-1} in the Raman spectrum). Overall the pattern of bands is consistent with complexes of the type *cis*-[M(CO)₄(L)]. From 300 to 1700 cm^{-1} the vibrational spectra of **1** exhibit numerous ligand (ppp) modes. Upon complexation the ligand undergoes structural changes which affect the 1550-1650 cm^{-1} region.^{26,31} In particular, ligand coordination results in a shift of the pyridyl C-N stretching mode from 1590 cm^{-1} for the free ligand to 1605 cm^{-1} for **1**.

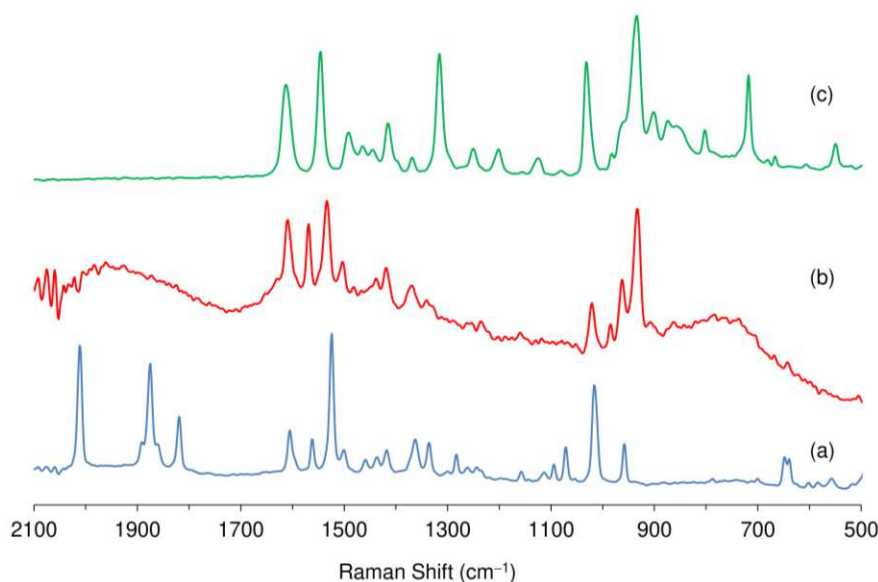


Figure 3.2. FT-Raman spectra in the range of 500-2100 cm^{-1} for (a) **1**, (b) **2** and (c) $[Mo_8O_{24}(di-tBu-bipy)_4]$ ²⁹.

Chapter 3

Solutions of the complex **1** present limited stability and therefore NMR spectra had to be recorded immediately after dissolution in CDCl_3 or CD_3CN . The ^1H NMR spectrum was fully consistent with the presence of the substituted pyrazolylpyridine ligand. In particular, the resonances for the pyrazolylpyridine protons are generally shifted to lower field upon complexation, similar to that reported previously for complexes of the type $[\text{MoO}_2\text{Cl}_2(2-(1\text{-alkyl-3-pyrazolyl})\text{pyridine})]$.^{26,27} Of particular note is the observation that the H-8 and H-9 resonances switch their relative positions on going from ppp ($\delta_{\text{H-8}} > \delta_{\text{H-9}}$) to **1** ($\delta_{\text{H-8}} < \delta_{\text{H-9}}$).

In the ^{13}C NMR in solution spectrum of **1**, two CO resonances were observed signals close to 223 ppm and one resonance is localized at approx. 205 ppm, which are assigned to the two *cis* CO and one *trans* CO ligands. This finding suggests that the molecule possesses a plane of symmetry. The assignment for the carbonyl ligands is quite similar to those previously reported for carbonyls *cis* and *trans* in complexes of the type *cis*- $[\text{Mo}(\text{CO})_4(\text{N}-(n\text{-propyl})\text{-2-pyridylmethanimine})]$ by Gomes *et al.*³², *cis*- $[\text{Mo}(\text{CO})_4\{\text{ethyl}[3-(2\text{-pyridyl})\text{-1-pyrazolyl}]\text{acetate}\}]$ by Coelho *et al.*³³, and $[\text{Mo}(\text{CO})_4(\text{pyridyl-CH=N-CHRCO}_2\text{R}')] (R = \text{H}, \text{CH}_3, \text{CH}(\text{CH}_3)_2, \text{CH}_2\text{CH}(\text{CH}_3)_2)$ by Ederer *et al.*³⁴.

3.2.2. Oxidative decarbonylation

Oxidative decarbonylation of **1** was carried out by the dropwise addition of 5-6 M TBHP (10 equiv.) in *n*-decane to a suspension of the complex in CH_2Cl_2 (45 % of yield). After stirring at room temperature for 4 h, the resultant off-white solid (**2**) was filtered, washed with diethyl ether and vacuum-dried. The resultant solid is stable in air and insoluble in water and organic solvents. Characterisation by elemental analysis, thermogravimetry, FTIR, FT-Raman, $^{13}\text{C}\{^1\text{H}\}$ CP MAS NMR and X-ray powder diffraction were performed for complex **2**.

CHN microanalyses for **2** were consistent with the empirical formula $[\text{Mo}_2\text{O}_6(\text{ppp})]$.

In support, TGA revealed a residual mass of 57.5 % at 600 °C which is in excellent agreement with the calculated value of 57.2 % assuming that the residue at this temperature is MoO_3 (Figure 3.3). Previously reported molybdenum oxide-(bidentate)organonitrogen polynuclear or polymeric compounds that have the same empirical formula include the octanuclear complexes $[\text{Mo}_8\text{O}_{24}(\text{L})_4]$ [$\text{L} = \text{di-}t\text{Bu-bipy}$ and $\text{ethyl}[3-(2\text{-pyridyl})\text{-1-pyrazolyl}]\text{acetate}$ (eppa)]^{21,22}, the 1D hybrid material $[\text{Mo}_2\text{O}_6(2,2'\text{-bipy})]$ ³⁵, and a polymeric hybrid material with the composition $[\text{Mo}_2\text{O}_6(\text{ppp})]$ ²⁶. Whereas the octanuclear complexes were prepared by the oxidative decarbonylation of *cis*-

Chapter 3

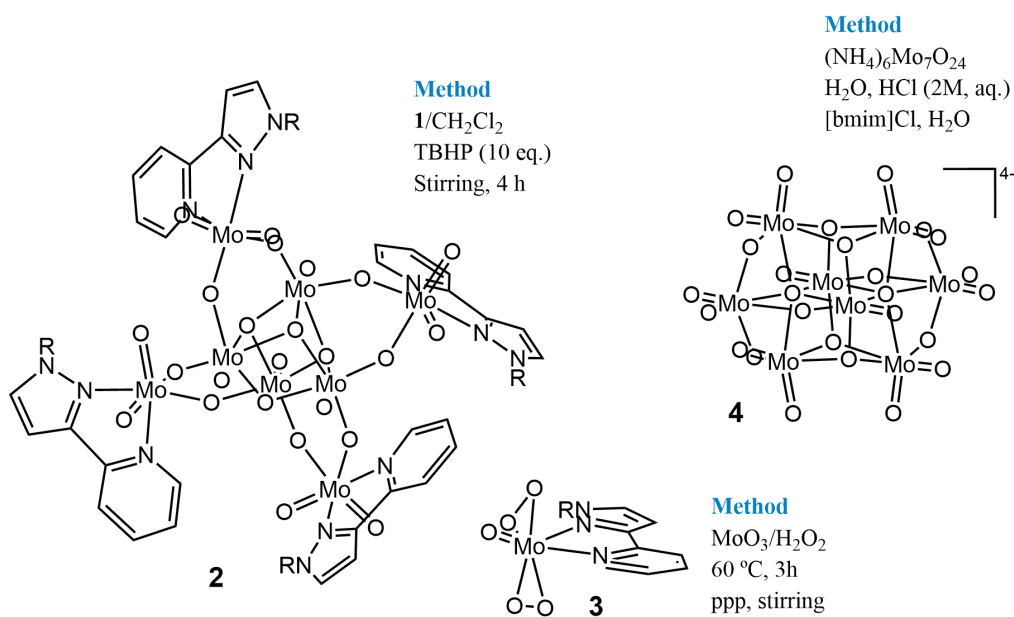
[Mo(CO)₄(L)] in an identical fashion to that performed in the present work, material [Mo₂O₆(ppp)] can be obtained upon the reaction of the complex [MoO₂Cl₂(ppp)] with water.²⁶

To date, the structures of [Mo₈O₂₄(eppa)₄] and **2** have not been unequivocally determined since the compounds precipitate as either amorphous or (poorly) microcrystalline solids. The existence of different structures for **2** and [Mo₂O₆(ppp)] is supported by a comparison of the TGA data (Figure 3.3). While the TGA curves are similar in terms of the weight loss steps and the residual mass at 600 °C, there are significant differences with respect to the onset temperatures for each step. Additional structural information cannot be garnered from the PXRD data for **2** since the material is (like [Mo₂O₆(ppp)] and [Mo₈O₂₄(eppa)₄]) almost amorphous, only giving rise to two extremely broad features centred at 10 and 24° 2θ.

The structural assignment for [Mo₈O₂₄(eppa)₄] was based on the similarity of its FT-IR spectrum in the region of Mo-O stretching vibrations (650-950 cm⁻¹) with that found for [Mo₈O₂₄(di-*t*Bu-bipy)₄]²¹ (Figure 3.1), the structure of which had previously been determined by X-ray crystallography and found to consist of octanuclear windmill-type complexes containing a central cubane-type Mo₄(μ₃-O)₄ core.²² As can be verified in Figure 3.1, the infrared spectral profile for **2** in the region of 500-1000 cm⁻¹ is remarkably similar to that for [Mo₈O₂₄(eppa)₄], suggesting that the two compounds have closely related structures. Both spectra confirm the absence of carboxylate groups between 2015-1745 cm⁻¹. On the other hand, the spectral profile for [Mo₂O₆(ppp)] in this region [Figure 3.1(f)] intensities of some bands. Whereas **2**, [Mo₈O₂₄(eppa)₄] and [Mo₈O₂₄(di-*t*Bu-bipy)₄] display a weak band at 845 ± 2 cm⁻¹, no such band is observed for [Mo₂O₆(ppp)]. Considering the Raman data (Figure 3.2), the group of bands found between 885 and 1000 cm⁻¹ for **2** match well with those observed for [Mo₈O₂₄(di-*t*Bu-bipy)₄]. These informations proof that the organic fragment ppp is intact and coordinated to the metallic Mo(VI) centre as bidentate nitrogen donor ligands.

Hence, we propose that **2** may have a similar octanuclear-type structure based on a central cubane-type core (Scheme 3.2).

Mo(VI) structures



Scheme 3.2. Representations of the proposed structures for Mo(VI) compounds isolated in this work.

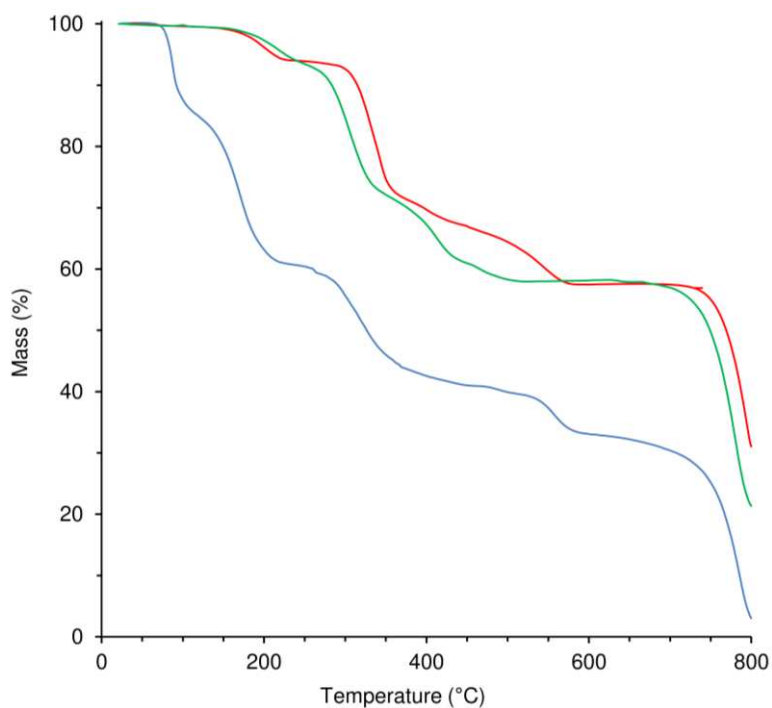


Figure 3.3. TGA curves for compounds **1** (—), **2** (—) and $[\text{Mo}_2\text{O}_6(\text{ppp})]$ (—).

3.3. Catalytic studies

3.3.1. Catalytic epoxidation with TBHP

The reaction of *cis*-cyclooctene (Cy) using TBHP as oxidant in the presence of compounds **1** or **2** led to 1,2-epoxycyclooctane (CyO) with 100 % selectivity. CyO yields reached 93 % for **1** and 99 % for **2** at 6 h/55 °C with TBHP as oxidant (Figure 3.4, Table 3.1). In the absence of oxidant and/or molybdenum species the conversions were negligible. Iodometric titrations performed for **2** in the absence of substrate showed that the undesirable (non-productive) decomposition of TBHP (into molecular oxygen and *tert*-butanol) was not considerable (23 % TBHP conversion at 24 h). Hence, the high epoxidation activity of **2** is accompanied by efficient TBHP consumption for the epoxide product formation.

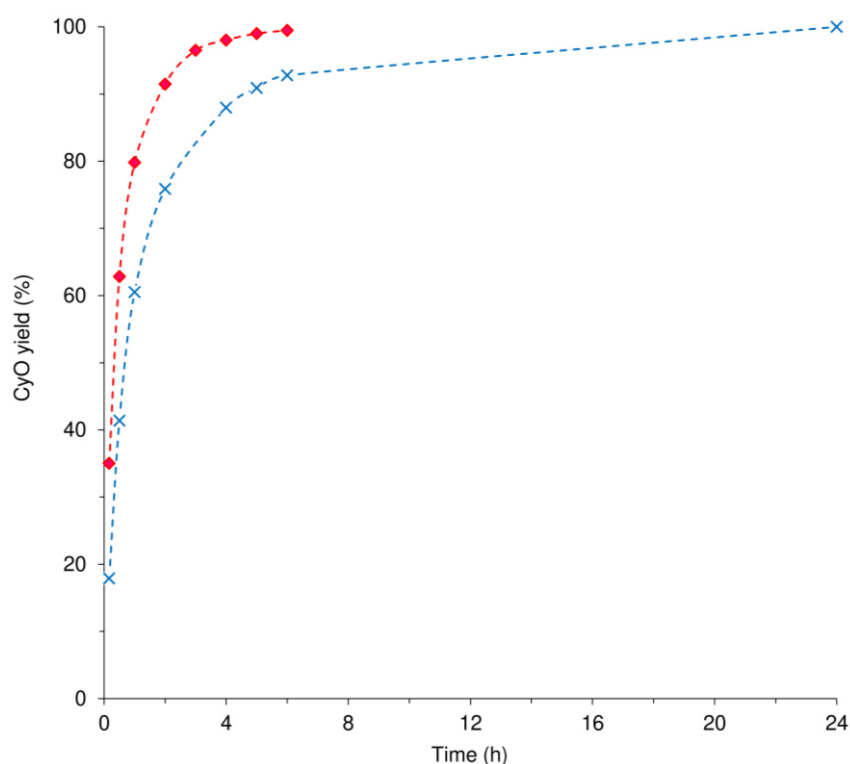


Figure 3.4. *cis*-Cyclooctene epoxidation with TBHP in the presence of **1** (x) and **2** (♦) at 55 °C (CH₃CHCl₂ as cosolvent). The dashed lines are visual guides.

3.3.2. Characterization of solids after catalytic epoxidation with TBHP

The systems (**1** or **2**)/TBHP were biphasic solid-liquid mixtures. The ATR FT-IR spectra of the recovered solids **1**-S-TBHP and **2**-S-TBHP were practically identical and only slightly different from that for **2** (Figure 3.5). The differences essentially concern the relative intensities of bands between 750 and 1000 cm^{-1} . Similarly, the Raman spectrum of **2**-S-TBHP was almost unchanged from that for **2** except for slight changes in the relative intensities of bands between 850 and 1050 cm^{-1} (not shown here). These results suggest that compound **2** may be formed from **1** under the catalytic reaction conditions and that the solid **2** is relatively stable. Nevertheless, the minor spectral differences noted above were found to be reproducible, suggesting that the recovered solids may not be entirely pure (**2**) and/or some structural alteration had occurred. In support, a solid was precipitated from the liquid phase of the **2**/TBHP reaction system (**2**-L-TBHP) and found to display an ATR FT-IR spectrum that was significantly different from that for **2**, especially concerning bands in the 740-1000 cm^{-1} interval (Figure 3.5). While **2** exhibits a strong band centred at 910 cm^{-1} , a slightly weaker one at 942 cm^{-1} , and a weak band at 843 cm^{-1} , in the spectrum of **2**-L-TBHP a band at 910 cm^{-1} is still observed but the strongest band in this region (830-1000 cm^{-1}) is at 952 cm^{-1} and no band is observed at ca. 843 cm^{-1} . Comparison of the spectra for **2** and **2**-L-TBHP with those for **1**-S-TBHP and **2**-S-TBHP suggests that the latter two solids could be mixtures of **2** and **2**-L-TBHP. Furthermore, the IR spectrum of **2**-L-TBHP in the range of 350-1650 cm^{-1} is very close to that for the polymeric hybrid material $[\text{Mo}_2\text{O}_6(\text{ppp})]$ (Figure 3.1). These structural transformations are summarised in Scheme 3.3. The nature of the Mo-containing active species in solution for the **2**/TBHP system cannot be inferred from these results but they may be mono/polynuclear oxo(peroxo)molybdenum(VI) species derived from **2** (see further discussion below) which may precipitate out as $[\text{Mo}_2\text{O}_6(\text{ppp})]$ during the course of the catalytic reaction or upon addition of organic solvents to the liquid phase.

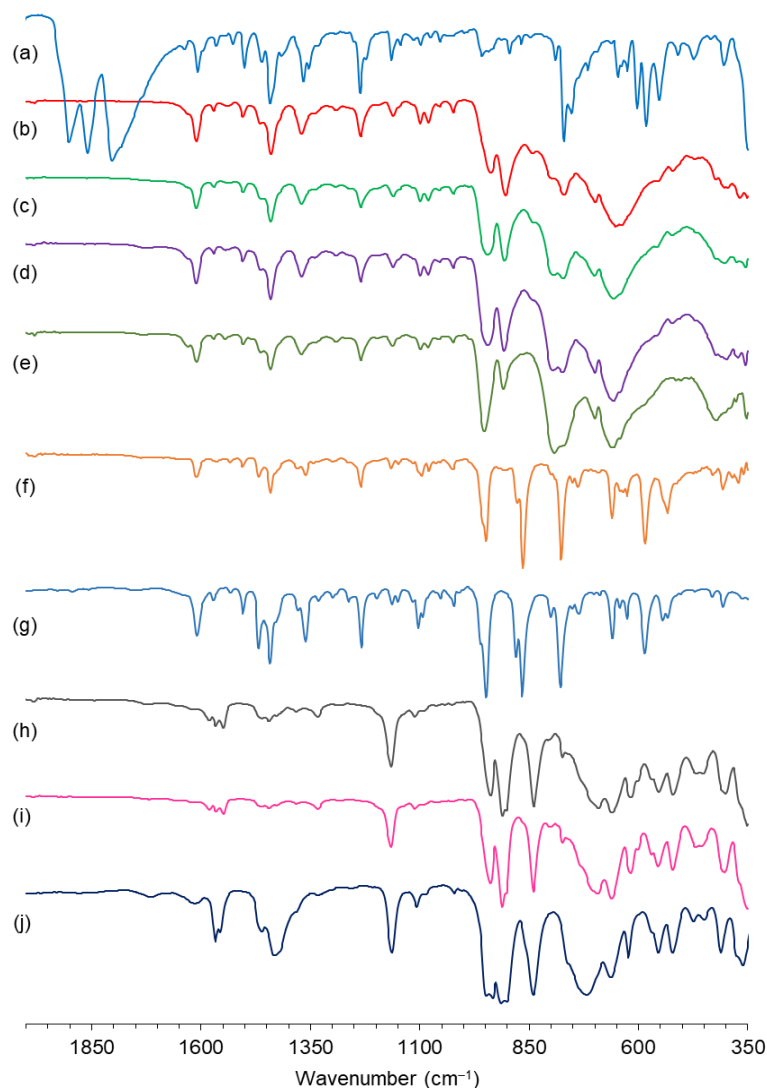


Figure 3.5. ATR FT-IR spectra in the range of 350-2000 cm^{-1} for (a) **1** and (b) **2**, and the recovered solids (c) **1-S-TBHP**, (d) **2-S-TBHP**, (e) **2-L-TBHP**, (f) **2-L-H₂O₂**, (h) **1-S-TBHP-[bmim]NTf₂** and (i) **2-S-TBHP-[bmim]NTf₂**. For comparison, the FT-IR (KBr) spectra of compounds **3** (g) and **4** (j) are shown.

3.3.3. Catalytic epoxidation with H₂O₂

The reaction of Cy using H₂O₂ as oxidant in the presence of compounds **1** or **2** led to 1,2-epoxycyclooctane (CyO) with 100 % selectivity. Like in the presence of TBHP, CyO is stable even in the presence of excess water added together with H₂O₂. This was ascertained by using CyO as substrate instead of Cy, using a very large excess of H₂O₂ (initial molar ratio of ca. 1CyO:15H₂O₂), in the presence of **2**; no reaction of CyO occurred within 24 h reaction, at 55 °C.

Compounds **1** and **2** were less effective when using H₂O₂ as oxidant instead of TBHP, giving 41 % and 55 % conversion, respectively, at 24 h (Table 3.1). The variable

Chapter 3

oxidant-dependent catalytic performance may be partly due to the formation of different types of intermediate oxidising species, leading to differences in activity for olefin epoxidation, since computational studies have indicated distinct reaction mechanisms for the two oxidants.^{36–38} For H₂O₂, a hydroxide-hydroperoxo intermediate possessing the moiety {M(OH)(O_αO_βH)} may be formed via protonation of an oxo ligand (M=O). This step is not possible with TBHP as oxidant, which instead leads to the formation of an intermediate possessing the moiety {M(OH)(O_αO_βtBu)}. On the other hand, the original compounds may be converted to different types of metal species during the catalytic reaction.

Table 3.1 - *cis*-Cyclooctene epoxidation at 55 °C in the presence of compounds **1** and **2**.^a

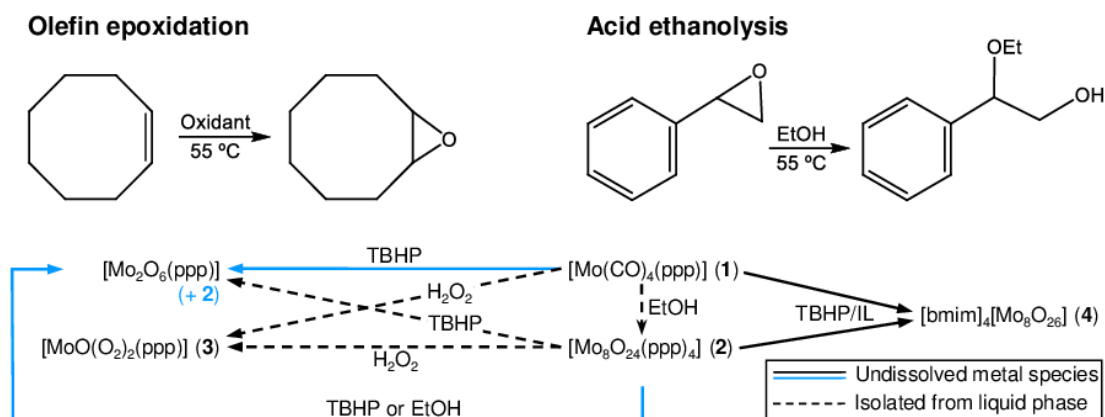
Compound	Oxidant	Cosolvent	Epoxide yield at 1 h/6 h/24 h (%) ^b
1	TBHP	CH ₃ CHCl ₂	18/93/100
1	TBHP	[bmim]NTf ₂	21/55/88
1	TBHP	[bmim]PF ₆	21/64/83
1	H ₂ O ₂	CH ₃ CN	-/-/41
2	TBHP	CH ₃ CHCl ₂	80/99/-
2	TBHP	[bmim]NTf ₂	21/67/95
2	TBHP	[bmim]PF ₆	23/56/93
2	H ₂ O ₂	CH ₃ CN	-/-/55

^a Initial Mo:olefin:oxidant molar ratio = 1:113:172, initial olefin concentration = 1.0 M for TBHP/CH₃CHCl₂, 1.2 M for H₂O₂/CH₃CN and 1.7 M for the system TBHP/IL. ^b Cyclooctene epoxide (CyO) yield (%); selectivity was always 100 %.

3.3.4. Characterization of solids after catalytic epoxidation with H₂O₂

The systems (**1** or **2**)/H₂O₂ consisted of yellow transparent solutions. A yellow solid (**2**-L-H₂O₂) was isolated from the liquid phase of the system **2**/H₂O₂. Compound **2**-L-H₂O₂ was identified by ATR FT-IR spectroscopy as the mononuclear oxodiperoxo complex [MoO(O₂)₂(ppp)] (**3**) (Scheme 3.2), which exhibits bands at 948 cm⁻¹ [ν(Mo=O)], 863 cm⁻¹ [ν(O-O)], 660, 585 and 534 cm⁻¹ (ν[Mo(O₂)₂]) (Figure 3.5).²⁶

Chapter 3



Scheme 3.3. Catalytic reactions studied in this work and summary of the transformations that are proposed to take place during either epoxidation of Cy with TBHP/H₂O₂ or ethanolysis of styrene oxide. The blue reaction arrows indicate that the recovered undissolved solid is likely a mixture of **2** and [Mo₂O₆(ppp)].

3.3.5. [MoO(O₂)₂(ppp)] as active specie for the catalytic epoxidation

In order to check the catalytic contribution of these types of species, complex **3** was synthesised (separately) by the addition of the ligand ppp to a solution obtained by the dissolution of MoO₃ in a large excess of aq. H₂O₂. The Cy reaction with H₂O₂ at 55 °C in the presence of **3** gave 39 % conversion (100 % CyO selectivity). This result is comparable with those obtained for the systems (**1** or **2**)/H₂O₂, suggesting that species of the type [MoO(O₂)₂(ppp)] (**3**) are responsible for the catalytic epoxidation.

A previous report showed that complex **3** possesses epoxidation activity with TBHP as oxidant (76 % / 97 % conversion at 1 h / 6 h, 55 °C), and may be formed *in situ* from the polymeric hybrid material [Mo₂O₆(ppp)].²⁶ The catalytic results with TBHP are superior to those found in this work with H₂O₂, suggesting that the complex is more effective with TBHP. Since the liquid phase for the biphasic system **2**/TBHP was pale yellow and, as discussed above, the solid recovered from this solution (**2**-L-TBHP) appears to be equivalent to [Mo₂O₆(ppp)], one cannot rule out the possibility that complex **3** is formed in solution and contributes to the catalytic reaction (for **2**/TBHP and **3**/TBHP²⁶, conversion at 6 h/55 °C was 99 % and 97 %, respectively). Nevertheless, since it was not possible to isolate this species from the systems (**1** or **2**)/TBHP, its concentration (if formed) may be very low.

Chapter 3

3.3.6. Ionic liquid-supported metal species for olefin epoxidation

Compounds **1** and **2** were tested for Cy epoxidation with TBHP using an ionic liquid (IL) as cosolvent at 55 °C (Table 3.1). The ILs tested were 1-butyl-3-methylimidazolium bis(trifluoromethylsulfonyl)imide ([bmim]NTf₂) and 1-butyl-3-methylimidazolium hexafluorophosphate ([bmim]PF₆), partly due to the successful use of these types of ILs for recycling molybdenum compounds for catalytic epoxidation processes.^{39–44} CyO was always the only reaction product observed and was obtained in yields of 83–88 % for **1** and 93–95 % for **2** (24 h). For each compound, the type of IL had no major influence on the catalytic reaction. The similar catalytic results may be related to the fact that the two ILs possess the same cation. To test for recyclability, the best-performing system **2**/[bmim]NTf₂ was reused in a second 24 h-batch run. Conversion decreased slightly from run **1** (95 %) to run **2** (83 %).

3.3.7. Characterization of solids after catalytic epoxidation in ionic liquids

After 24 h-batch runs, the mixtures were liquid (IL)-liquid (organic phase)-solid for (**1** or **2**)/[bmim]NTf₂ and liquid (IL)-liquid (organic phase) for (**1** or **2**)/[bmim]PF₆. Attempts to isolate soluble metal species from the IL media were unsuccessful. The undissolved solids recovered for the former systems (i-S-TBHP-[bmim]NTf₂) display matching ATR FT-IR spectra (Fig. 6) which, on the basis of literature data⁴⁵, are attributed to the presence of the octamolybdate salt [bmim]₄[Mo₈O₂₆] (**4**) (Scheme 3.2). This was verified by synthesising **4** and comparing its infrared spectrum against those for the recovered solids (Fig. 6). Hence, the conversion of compounds **1** and **2** in the IL medium involves exchange of the pyrazolylpyridine type ligand for the cation of the IL.

3.3.8. Acid catalysis

Compounds **1** and **2** were explored as Lewis acid catalysts for the ethanolysis of styrene oxide (StyOx) at 55 °C (Scheme 3.2). Compound **2** was very effective and led to the formation of the β-alkoxyalcohol product, namely 2-ethoxy-2-phenylethanol (EPE), in 98 % yield at 1 h (100 % selectivity). For **1**, EPE was obtained in 66 % yield at 24 h. Conversion was only 5 % without catalyst.

3.3.9. Characterization of solids after acid catalysis

Biphasic solid-liquid mixtures were formed for the ethanolysis of StyOx in the presence of **1** and **2**. Contact tests indicated that the StyOx reaction essentially occurred in homogeneous phase. Attempts to isolate metal species from the liquid phases of the reaction mixtures were only successful in the case of **1** (**1-L-EtOH**). Compound **1-L-EtOH** exhibited a very similar ATR FT-IR spectrum to **2** (Figure 3.6). A comparison of the ATR FT-IR spectra of **1** and **2** with those for the undissolved metal species (**i-S-EtOH**) reveals that the two compounds were transformed into different types of metal species (Figure 3.6). The spectrum for **1-S-EtOH** is unfamiliar and no structural interpretation can be made. On the other hand, the infrared spectrum for **2-S-EtOH** strongly resembles that for the polymeric hybrid material $[\text{Mo}_2\text{O}_6(\text{ppp})]$ [Figure 3.1(f)]. The apparent conversion of **2** to $[\text{Mo}_2\text{O}_6(\text{ppp})]$ during the ethanolysis reaction somewhat parallels that observed in the epoxidation system **2**/TBHP.

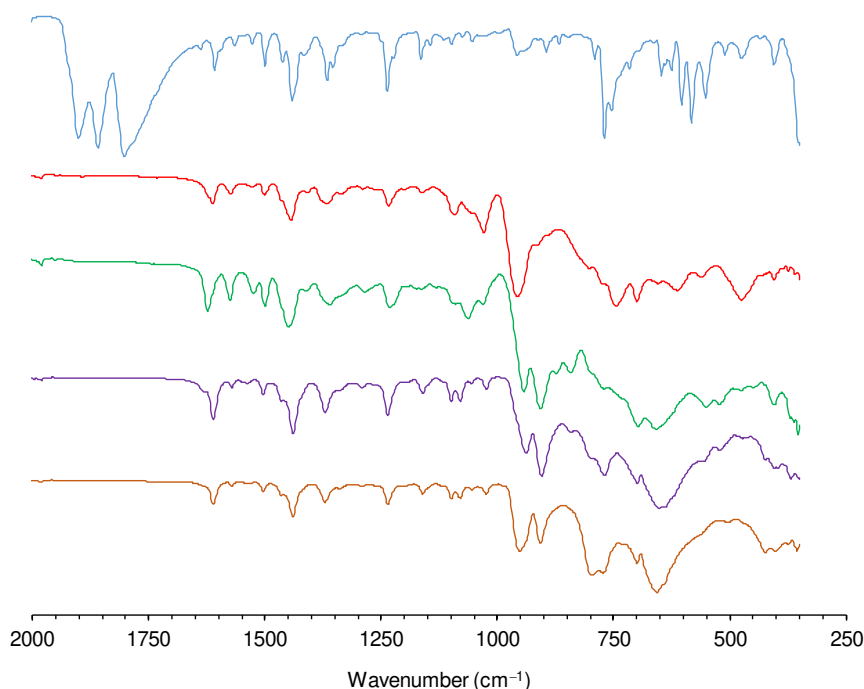


Figure 3.6. ATR FT-IR spectra in the range of 350-2000 cm^{-1} of (a) **1**, (b) **1-S-EtOH**, (c) **1-L-EtOH**, (d) **2** and (e) **2-S-EtOH**.

There are few reports on the use of Mo-containing compounds for homogeneously catalysed styrene oxide alcoholysis. The complexes $[(\eta^5\text{-C}_5\text{H}_4\text{R})\text{Mo}(\text{CO})_2(\eta^3\text{-C}_3\text{H}_5)]$ and $[(\eta^5\text{-C}_5\text{H}_5)\text{Mo}(\text{CO})_3(\text{CH}_2\text{R})]$ ($\text{R} = \text{H}, \text{COOH}$) were previously tested for the same reaction, at 55 °C, using double the molar ratio of Mo:StyOx to that used in the present work.⁴⁶ The dicarbonyl compounds led to a faster

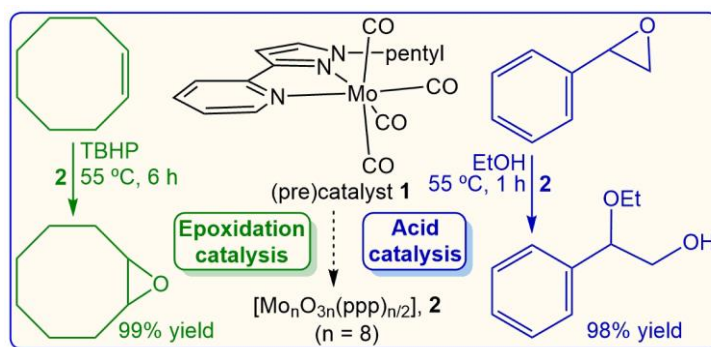
Chapter 3

alcoholysis reaction (100 % conversion at 10 min) than the tricarbonyl complexes (100 % conversion at 2 h for R = H, or at 90 min for R = COOH). In comparison to these compounds, the catalytic results for **2** (98 % conversion at 1 h) are fairly good. In another study, the complexes $[\text{MoO}_2\text{Cl}_2(\text{di-}t\text{Bu-bipy})]$, $[\text{Mo}_2\text{O}_2(\mu_2\text{-O})_2\text{Cl}_2(\text{di-}t\text{Bu-bipy})_2]$ and $[\text{Mo}_8\text{O}_{24}(\text{di-}t\text{Bu-bipy})_4]$ led to 55 %, 23 % and 38 % EPE yields at 1 h, 55 °C (EPE selectivity was always 100 %), which are far inferior catalytic results to those obtained for **2** under similar reaction conditions.⁴⁷ In that work, characterisation data for the recovered metal species suggested that the mononuclear and dinuclear complexes were converted *in situ* to octanuclear $[\text{Mo}_8\text{O}_{24}(\text{di-}t\text{Bu-bipy})_4]$ (structurally comparable to **2**).

3.4. Conclusions

A new tetracarbonylmolybdenum(0) complex containing a pentyl-functionalised pyrazolylpyridine ligand has been prepared and characterised (Scheme 3.4). While complex **1** is stable in the solid-state under inert atmosphere, it is unstable in solution. These characteristics are consistent with the poor stability previously reported for tetracarbonylmolybdenum(0) pyridylpyrazole and associated with the coordination of hard bases such as pyridyl or pyrazole to a soft acid, in this case molybdenum(0). The tetracarbonyl complex readily undergoes oxidative decarbonylation in the presence of the oxidant TBHP to give compounds formulated generally as $[\text{Mo}_n\text{O}_{3n}(\text{ppp})_{n/2}]$, which are proposed to include the octanuclear complex $[\text{Mo}_8\text{O}_{24}(\text{ppp})_4]$ (**2**) and a polymeric hybrid material with the composition $[\text{Mo}_2\text{O}_6(\text{ppp})]$. The formation of **2** from **1** even takes place in the ethanol/styrene oxide system. In this system, compound **2** leads to a nearly quantitative yield of the β -alkoxyalcohol product within 1 h reaction. Good catalytic performance in olefin epoxidation is obtained with **1** and **2**, which are sources of soluble active species such as the oxodiperoxo complex $[\text{MoO}(\text{O}_2)_2(\text{ppp})]$ (**3**). When ionic liquids of the type $[\text{bmim}]\text{X}$ are used as cosolvents in the epoxidation reaction with TBHP, **1** and **2** are converted to the β -octamolybdate salt $[\text{bmim}]_4[\beta\text{-Mo}_8\text{O}_{26}]$ (**4**). In conclusion, in this work considerable insight has been gained into the chemistry and catalytic performance of a tetracarbonylmolybdenum(0) pyrazolylpyridine complex, which should help guide future studies on the use of such complexes as (pre)catalysts and/or precursors to molybdenum oxide derivatives.

Chapter 3



Scheme 3.4. Summary of the main syntheses and catalytic studies carried out in this work.

3.5. References

- (1) Kühn, F. E.; Santos, M.; Abrantes, A. M. *Chem. Rev.* **2006**, *106*, 2455–2475.
- (2) Freund, C.; Abrantes, M.; Kühn, F. E. *J. Organomet. Chem.* **2006**, *691*, 3718–3729.
- (3) Müller, C.; Grover, N.; Cokoja, M.; Kühn, F. E. *Adv. Inorg. Chem.* **2013**, *65*, 33–83.
- (4) Abrantes, M.; Santos, A. M.; Mink, J.; Kühn, F. E.; Romão, C. C. *Organometallics* **2003**, *22*, 2112–2118.
- (5) Martins, A. M.; Romão, C. C.; Abrantes, M.; Azevedo, M. C.; Cui, J.; Dias, A. R.; Duarte, M. T.; Lemos, M. A.; Lourenço, T.; Poli, R. *Organometallics* **2005**, *24*, 2582–2589.
- (6) Ahmad, M. A. A.; Veljanovski, D.; Capapé, A.; Zhao, J.; Herdtweck, E.; Calhorda, M. J.; Kühn, F. E. *Organometallics* **2009**, *28*, 639–645.
- (7) Costa, P. J.; Calhorda, M. J.; Kühn, F. E. *Organometallics* **2010**, *29*, 303–311.
- (8) Grover, N.; Pöthig, A.; Kühn, F. E. *Catal. Sci. Technol.* **2014**, *4*, 4219–4231.
- (9) Grover, N.; Drees, M.; Kühn, F. E. *J. Catal.* **2015**, *329*, 269–285.
- (10) Hauser, S. A.; Reich, R. M.; Mink, J.; Pöthig, A.; Cokoja, M.; Kühn, F. E. *Catal. Sci. Technol.* **2015**, *5*, 2282–2289.
- (11) Li, S.; Kee, C. W.; Huang, K.; Hor, T. S. A.; Zhao, J. *Organometallics* **2010**, *29*, 1924–1933.
- (12) Dhawan, I. K.; Bruck, M. A.; Schillings, B.; Grittini, C.; Enemark, J. H. *Inorg. Chem.* **1995**, *34*, 3801–3808.
- (13) Dinoi, C.; Guedes da Silva, M. F. C.; Alegria, E. C. B. A.; Smoleński, P.; Martins, L. M. D. R. S.; Poli, R.; Pombeiro, A. J. L. *Eur. J. Inorg. Chem.* **2010**, 2415–2424.
- (14) Gamelas, C. A.; Lourenço, T.; da Costa, A. P.; Simplicio, A. L.; Royo, B.; Romão, C. C. *Tetrahedron Lett.* **2008**, *49*, 4708–4712.
- (15) Chandgude, M. G.; Biradar, A. V.; Kotbagi, T. V.; Puranik, V. G.; Dongare, M. K.; Umbarkar, S. B. *Catal. Lett.* **2012**, *142*, 1352–1360.
- (16) Biradar, A. V.; Dongare, M. K.; Umbarkar, S. B. *Tetrahedron Lett.* **2009**, *50*, 2885–2888.
- (17) Biradar, A. V.; Dongare, M. K.; Umbarkar, S. B. *Tetrahedron Lett.* **2009**, *49*, 3616–3619.

Chapter 3

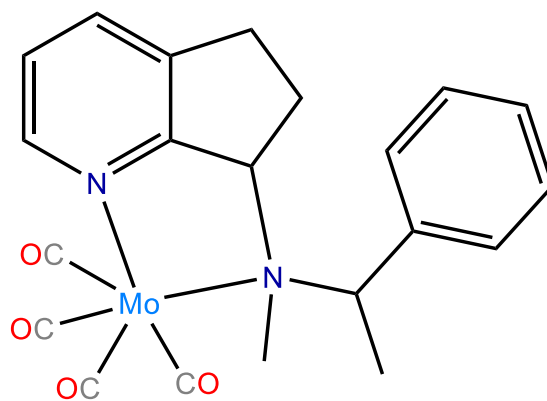
- (18) Grover, N.; Kühn, F. E. *Curr. Org. Synth.* **2012**, *16*, 16–32.
- (19) Amini, M.; Haghdoost, M. M.; Bagherzadeh, M. *Coord. Chem. Rev.* **2013**, *257*, 1093–1121.
- (20) Hauser, S. A.; Cokoja, M.; Kühn, F. E. *Catal. Sci. Technol.* **2013**, *3*, 552–561.
- (21) Neves, P.; Amarante, T. R.; Gomes, A. C.; Coelho, A. C.; Gago, S.; Pillinger, M.; Gonçalves, I. S.; Silva, C. M.; Valente, A. A. *Appl. Catal., A* **2011**, *395*, 71–77.
- (22) Amarante, T. R.; Neves, P.; Coelho, A. C.; Gago, S.; Valente, A. A.; Almeida Paz, F. A.; Pillinger, M.; Gonçalves, I. S. *Organometallics* **2010**, *29*, 883–892.
- (23) Zapf, P. J.; Haushalter, R. C.; Zubieta, J. *Chem. Mater.* **1997**, *4756*, 2019–2024.
- (24) Twu, J. E. N.; Yu, Y.; Tang, C. E. I.; Ang, G. W. A. W.; Chen, K. *Appl. Spectrosc.* **1999**, *53*, 1083–1086.
- (25) Thiel, W. R.; Angstl, M.; Priermeier, T. *Chem. Ber.* **1994**, *127*, 2373–2379.
- (26) Amarante, T. R.; Neves, P.; Paz, F. A. A.; Valente, A. A.; Pillinger, M.; Gonçalves, I. S. *Dalton Trans.* **2014**, *43*, 6059–6069.
- (27) Bruno, S. M.; Pereira, C. C. L.; Balula, M. S.; Nolasco, M.; Valente, A. A.; Hazell, A.; Pillinger, M.; Ribeiro-Claro, P.; Gonçalves, I. S. *J. Mol. Catal. A Chem.* **2007**, *261*, 79–87.
- (28) Amarante, T. R.; Neves, P.; Gomes, A. C.; Nolasco, M. M.; Ribeiro-Claro, P.; Coelho, A. C.; Valente, A. A.; Almeida Paz, F. A.; Smeets, S.; McCusker, L. B.; Pillinger, M.; Gonçalves, I. S. *Inorg. Chem.* **2014**, *53*, 2652–2665.
- (29) Gamelas, C. A.; Gomes, A. C.; Bruno, S. M.; Paz, F. A. A.; Valente, A. A.; Pillinger, M.; Romão, C. C.; Gonçalves, I. S. *Dalton Trans.* **2012**, *41*, 3474–3484.
- (30) Brunner, H.; Scheck, T. *Chem. Ber.* **1992**, *125*, 701–709.
- (31) Coelho, A. C.; Nolasco, M.; Balula, S. S.; Antunes, M. M.; Pereira, C. C. L.; Almeida Paz, F. A.; Valente, A. A.; Pillinger, M.; Ribeiro-Claro, P.; Klinowski, J.; Gonçalves, I. S. *Inorg. Chem.* **2011**, *50*, 525–538.
- (32) Gomes, A. C.; Bruno, S. M.; Gago, S.; Lopes, R. P.; Machado, D. A.; Carminatti, A. P.; Valente, A. A.; Pillinger, M.; Gonçalves, I. S. *J. Organomet. Chem.* **2011**, *696*, 3543–3550.
- (33) Coelho, A. C.; Paz, F. A. A.; Klinowski, J.; Pillinger, M.; Gonçalves, I. S. *Molecules* **2006**, *11*, 940–952.
- (34) Ederer, T.; Herrick, R. S.; Beck, W. *Z. Anorg. Allg. Chem.* **2007**, *633*, 235–238.
- (35) Zapf, P. J.; Haushalter, R. C.; Zubieta, J. *Chem. Mater.* **1997**, *9*, 2019–2024.
- (36) Comas-Vives, A.; Lledos, A.; Poli, R. *Chem. Eur. J.* **2010**, *16*, 2147–2158.
- (37) Dino, C.; Ciclosi, M.; Manoury, E.; Maron, L.; Perrin, L.; Poli, R. *Chem. Eur. J.* **2010**, *16*, 9572–9584.
- (38) Dinoi, C.; Poli, R.; Perrin, L.; Maron, L. *Dalton Trans.* **2012**, *41*, 1131–1133.
- (39) Monteiro, B.; Gago, S.; Neves, P.; Valente, A. A.; Gonçalves, I. S.; Pereira, C. C. L.; Silva, C. M.; Pillinger, M. *Catal. Lett.* **2009**, *129*, 350–357.
- (40) Neves, P.; Pereira, C. C. L.; Almeida, F. A.; Gago, S.; Pillinger, M.; Silva, C. M.; Valente,

Chapter 3

- A. A.; Romão, C. C.; Gonçalves, I. S. *J. Organomet. Chem.* **2010**, *695*, 2311–2319.
- (41) Abrantes, M.; Neves, P.; Antunes, M. M.; Gago, S.; Almeida Paz, F. A.; Rodrigues, A. E.; Pillinger, M.; Gonçalves, I. S.; Silva, C. M.; Valente, A. A. *J. Mol. Catal. A Chem.* **2010**, *320*, 19–26.
- (42) Neves, P.; Gago, S.; Balula, S. S.; Lopes, D.; Valente, A. A.; Cunha-silva, L.; Paz, F. A. A.; Pillinger, M.; Silva, C. M.; Gonçalves, I. S. *Inorg. Chem.* **2011**, *50*, 3490–3500.
- (43) Oliveira, T. S. M.; Gomes, A. C.; Lopes, A. D.; Lourenço, J. P.; Almeida Paz, F. A.; Pillinger, M.; Gonçalves, I. S. *Dalton Trans.* **2015**, *44*, 14139–14148.
- (44) Graser, L.; Reich, R. M.; Cokoja, M.; Pöthig, A.; Kühn, F. E. *Catal. Sci. Technol.* **2015**, *5*, 4772–4777.
- (45) Carrasco, C. J.; Montilla, F.; Álvarez, E.; Herbert, M.; Galindo, A. *Polyhedron* **2013**, *54*, 123–130.
- (46) Bruno, S. M.; Gomes, A. C.; Abrantes, M.; Valente, A. A.; Pillinger, M.; Gonçalves, I. S. *J. Organomet. Chem.* **2015**, *799–800*, 179–183.
- (47) Gomes, A. C.; Neves, P.; Cunha-Silva, L.; Valente, A. A.; Gonçalves, I. S.; Pillinger, M. *Catal. Sci. Technol.* **2016**, *6*, 5207–5218.

CHAPTER 4

Performance of chiral tetracarbonylmolybdenum pyridanyl amine complexes in catalytic olefin epoxidation



cis-[Mo(CO)₄(N-methyl-N-(1-phenylethyl)-6,7-dihydro-5H-cyclopenta[b]pyridin-7-amine)]

Chapter 4

Index

4.1. Introduction	123
4.2. Results and discussion	124
4.2.1. Synthesis and characterisation of [(<i>R,R</i>)-pyC ₅ H ₅ N(CH ₃)CH(CH ₃)Ph] and [(<i>S,S</i>)-pyC ₅ H ₅ N(CH ₃)CH(CH ₃)Ph], (pre)catalysts <i>cis</i> -[Mo(CO) ₄ {(<i>R,R</i>)-pyC ₅ H ₅ N(CH ₃)CH(CH ₃)Ph}] (1) and <i>cis</i> -[Mo(CO) ₄ {(<i>S,S</i>)-pyC ₅ H ₅ N(CH ₃)CH(CH ₃)Ph}] (2)	124
4.3. Catalytic studies	127
4.3.1. Catalytic epoxidation of <i>cis</i> -cyclooctene with TBHP	127
4.3.2. Epoxidation of prochiral olefins	128
4.3.3. Types of active species	134
4.4. Conclusions	135
4.5. References	136

Chapter 4

4.1. Introduction

The family of group 6 metal carbonyl complexes is versatile and effective for several catalytic reactions such as hydrogenation, hydrosilylation, hydrogermylation, hydroxylation, isomerization, olefin metathesis and metathesis polymerization, radical reactions, and (ep)oxidation (e.g. of alkenes, amines, alcohols and sulfides).¹⁻⁴ The application of these carbonyl complexes in catalysis first arose in the late 1960's^{5,6} with the use of Mo(CO)₆ as a precatalyst for the epoxidation of olefins (monoolefins⁵, diolefins⁶ and functionalized olefins⁶), using an organic hydroperoxide as oxidant, namely *tert*-butylhydroperoxide (TBHP) or cumene hydroperoxide. Halcon (later Oxirane, Arco Chemical, and Lyondell Petrochemical⁶) claimed the application of Mo(CO)₆ for the industrial catalytic production of the bulk chemical propylene oxide, which is used in a variety of plastics, foams and paints.^{4,7-9} More recently, in 2007, Dow Global Technologies Inc. claimed the application of various families of molybdenum compounds as homogeneous catalysts to produce epoxides via liquid-phase reaction of olefins with organic hydroperoxides.¹⁰

Since the turn of the century, there has been growing interest in the use of molybdenum carbonyl complexes as precursors to Mo(VI) catalysts for oxidation reactions, with most of the research being focused on dicarbonyl and tricarbonyl complexes.^{2-4,11-13} From 2010 onwards the group have been investigating tetracarbonyl complexes of the type *cis*-[Mo(CO)₄L] (L = N,N-ligand) for the epoxidation of aliphatic and cyclic olefins (e.g. terpenes), using TBHP as oxidant.¹⁴⁻¹⁸ The Mo(0) complexes can be used directly as catalyst precursors since they undergo oxidative decarbonylation *in situ* (by reaction with the oxidant) to give oxomolybdenum compounds in higher (usually +6) oxidation states. A variety of oxidized compounds have been isolated and include the one-dimensional molybdenum oxide/bipyridine polymer [MoO₃(2,2'-bipy)] from *cis*-[Mo(CO)₄(2,2'-bipy)] (2,2'-bipy = 2,2'-bipyridine)¹⁴, the octanuclear cluster [Mo₈O₂₄(di-*t*Bu-bipy)₄] from *cis*-[Mo(CO)₄(di-*t*Bu-bipy)] (di-*t*Bu-bipy = 4,4'-di-*tert*-butyl-2,20-bipyridine)¹⁴, and the tetranuclear species [Mo₄O₁₂(pypzH)₄] from *cis*-[Mo(CO)₄(pypz)] (pypzH = 2-[3(5)-pyrazolyl]pyridine)¹⁵.

Tetracarbonylmolybdenum complexes containing chiral organic ligands have not yet been studied in catalytic olefin epoxidation. Herein it is a report on the synthesis of two chiral tetracarbonylmolybdenum pyridanyl amine complexes and their use as precatalysts for the epoxidation of *cis*-cyclooctene (used as a benchmark substrate), DL-limonene and *trans*- β -methylstyrene. The catalytic performances of the complexes are compared with results reported previously for related complexes. Characterization of recovered catalysts established that the tetracarbonyl complexes are oxidized to

Chapter 4

octamolybdate salts of the type $(LH)_4[Mo_8O_{26}]$ (rather than to hybrid complexes or materials where the organic ligand remains coordinated to the metal center, which has been reported in the literature for different tetracarbonylmolybdenum organo complexes).

4.2. Results and discussion

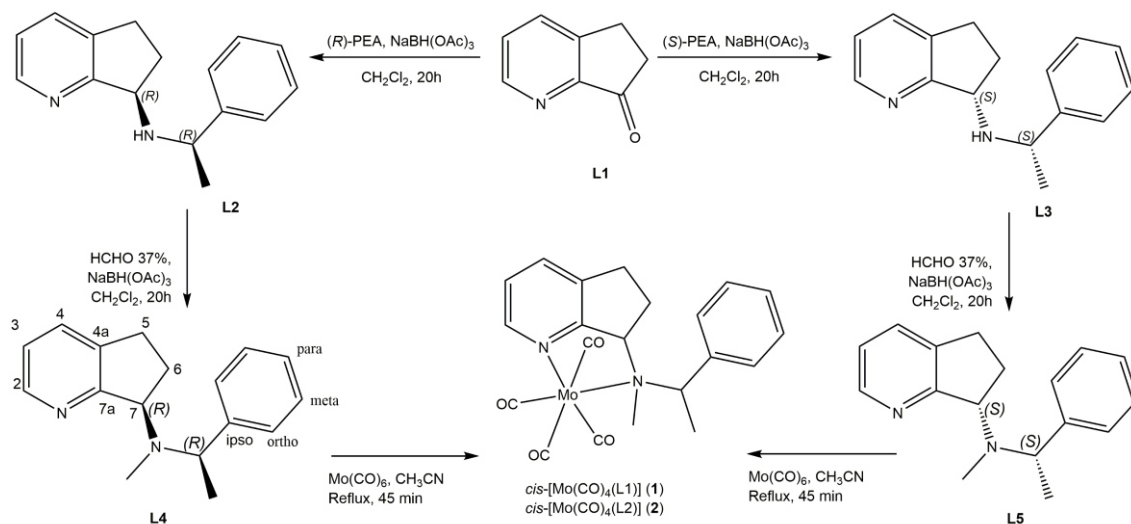
4.2.1. Synthesis and characterisation of $[(R,R)\text{-pyC}_5\text{H}_5\text{N}(\text{CH}_3)\text{CH}(\text{CH}_3)\text{Ph}]$ and $[(S,S)\text{-pyC}_5\text{H}_5\text{N}(\text{CH}_3)\text{CH}(\text{CH}_3)\text{Ph}]$, (pre)catalysts $\text{cis-[Mo(CO)}_4\text{(L4)]}$ (**1**) and $\text{cis-[Mo(CO)}_4\text{(L5)]}$ (**2**)

The ligands used in this work were prepared from ketone L1 (Scheme 4.1), which was obtained from 2,3-cyclopentenopyridine using an optimized protocol previously developed by José Rodríguez-Borges and co-workers.^{19,20} The reductive amination of ketone L1 with (*R*)-(+)- α -methylbenzylamine [*R*]-PEA and (*S*)-(-)- α -methylbenzylamine [*S*]-PEA using $\text{NaBH}(\text{OAc})_3$ (STAB) as reducing agent proceeded diastereoselectively, affording L2-(*R,R*) and L3-(*S,S*), respectively, as major diastereopure amines in good yields (80-84 %). The subsequent N-methylation of the secondary amines L2 and L3 under the same protocol was accomplished using an aqueous solution of formaldehyde, yielding the title tertiary amines, L4 and L5 (74-78 %).

The tetracarbonyl complexes $\text{cis-[Mo(CO)}_4\text{(L4)]}$ (**1**) and $\text{cis-[Mo(CO)}_4\text{(L5)]}$ (**2**) were obtained as brown solids in fair yields (54 % and 64 %, respectively) by reacting Mo(CO)_6 directly with the respective organic ligand L4 or L5 in refluxing acetonitrile during 30 min. Complexes **1** and **2** display long-term stability in the solid-state if stored under inert atmosphere. However, in solution (the complexes are soluble in ethanol, acetone, diethyl ether, acetonitrile, toluene, ethyl acetate, chloroform and dichloromethane), the complexes present limited stability, being susceptible to decarbonylation reactions. Both complexes are insoluble in hexane, pentane and water.

The complexes were characterized by FT-IR, ^1H NMR spectroscopy and elemental analysis, indicating no significant differences between the isomers and leading to consider that the chirality of the ligands remains after complexation. Proofs of ligands coordination in **1** and **2** are provided through these techniques. The elemental analysis (C, H and N) for **1** and **2** are in complete agreement with the analytical results for the $\text{C}_{21}\text{H}_{20}\text{N}_2\text{MoO}_4$ structure.

Chapter 4



Scheme 4.1. Preparation of the ligands (L4 and L5) and corresponding tetracarbonyl complexes (**1** and **2**).

IR spectra of **1** and **2** in the solid-state (KBr pellets) display four CO stretching bands in the region 1810-2020 cm^{-1} in a pattern consistent with a *cis*-tetracarbonyl geometry and in agreement with other complexes of this type containing pyridine ligands (Figure 4.1).^{15,16} The analysis of the vibrational spectra demonstrates some structural changes in the organic ligands upon complexation, such as the vibrational bands of the free ligands in the region of 1100-1000 cm^{-1} are localized to lower wavenumber after complexation (between 1000 and 900 cm^{-1}), in agreement with previous studies for tetracarbonyls of Mo with pyridine derivatives as ligands.¹⁶ Also, these results are also supported by elemental analysis (C, H and N) for **1** and **2**, wherein the results are in complete agreement with the analytical results for the $\text{C}_{21}\text{H}_{20}\text{N}_2\text{MoO}_4$ structure.

The solution ¹H NMR spectra confirm the presence of the organic ligands L4 and L5 and furthermore display peak shifts that can be attributed to coordination of the ligands to the metal center, accordingly with previous studies of 1-pyridane derivatives (Figure 4.2).^{19,21} For example, the resonances for the pyridyl ring protons H-2 and H-3 shift downfield from 8.5 and 7.05 ppm, respectively, for the free ligands to 8.58 and 7.14 ppm for complexes **1** and **2** (CDCl_3 solvent). Similarly, the resonances for the methyne protons at 4.58 (H-7) and 4.16 ppm ($\text{N}(\text{CH}_3)\text{CH}(\text{CH}_3)\text{Ph}$) for the free ligands shift to 4.71 and 4.48 ppm for the complexes.

Chapter 4

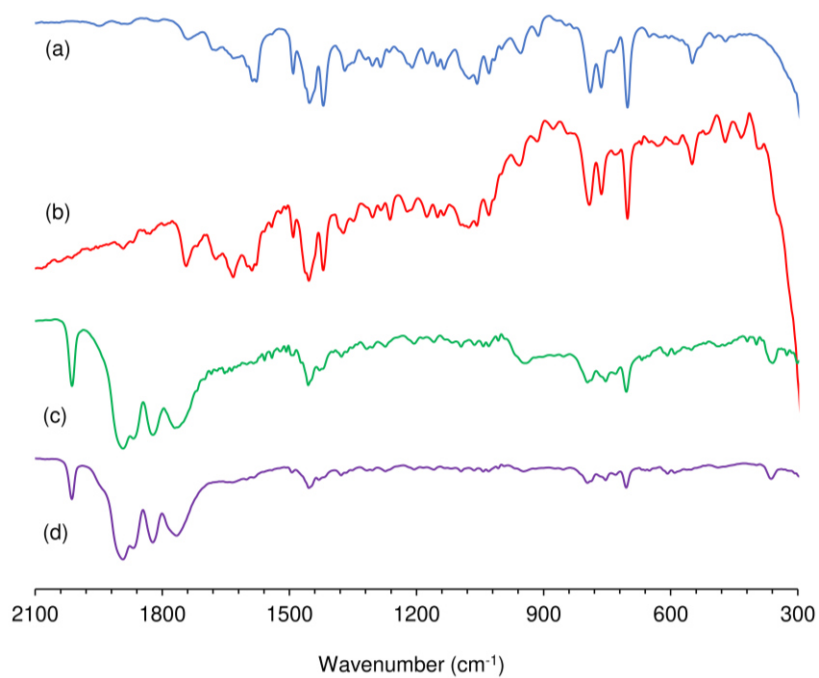


Figure 4.1. FT-IR spectra in the range 300–2100 cm^{-1} for (a) free ligand L4, (b) free ligand L5, (c) complex **1** and (d) complex **2**.

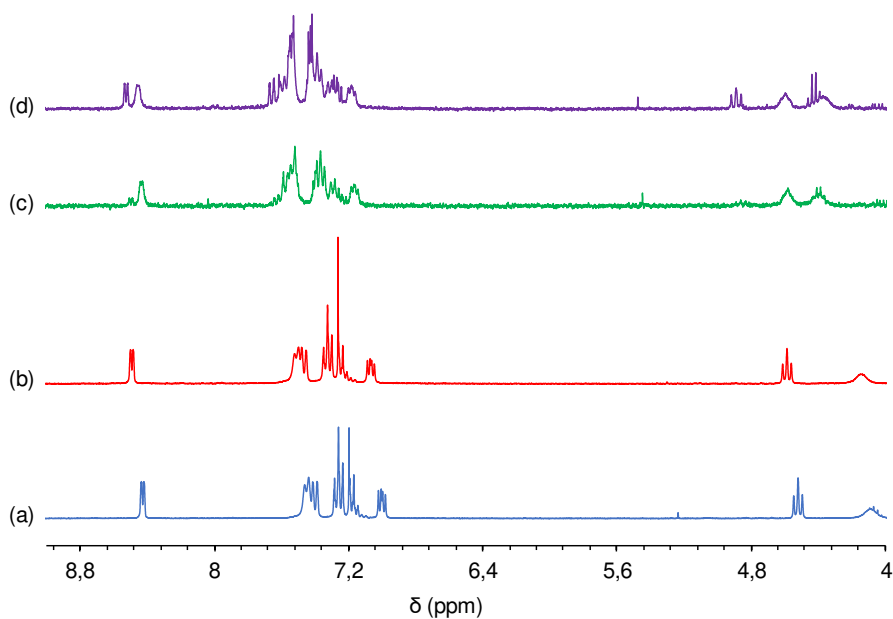


Figure 4.2. ^1H MAS NMR spectra of (a) free ligand L4, (b) free ligand L5, (c) complex **1** and (d) complex **2**.

4.3. Catalytic studies

4.3.1. Catalytic epoxidation of *cis*-cyclooctene with TBHP

Complexes **1** and **2** promoted the epoxidation of *cis*-cyclooctene (Cy) with TBHP at 55 °C (DCE as cosolvent), and 1,2-epoxycyclooctane (CyO) was the only product formed (100 % selectivity) (Figure 4.3). Without molybdenum species and/or TBHP, olefin conversion was negligible, and thus metal species and the oxidant are required for the formation of active species. There is consensus across previously reported mechanistic studies that the active oxidizing species involves the coordination of the oxidant to the metal center.^{22–28} The kinetic curves for **1** and **2** are roughly coincident, suggesting that the two compounds possess similar catalytic activity and stability, despite the chiral differences. High conversions were reached at 6 h (92–94 %), and the reaction was complete within 24 h.

A comparison of the catalytic results for **1** and **2** with literature data (based on epoxide yields at 6 h, where CyO selectivity was always 100 %) for neutral or ionic molybdenum tetracarbonyl compounds bearing pyridine-containing ligands (L), under somewhat comparable reaction conditions, indicates that the performances of **1** and **2** are far superior to the complexes with L = 2,2'-bipy (71 % CyO yield)¹⁴, di-*t*Bu-bipy (84 %)¹⁴, pypzH (51 %)¹⁵, or ethyl[3-(2-pyridyl)-1-pyrazolyl]acetate (70 %)¹⁵ (Table 2.1). N-heterocyclic carbene (NHC) complexes of the type [Mo(CO)₄(NHC)_{*n*}] (NHC = 1,3-dibenzylimidazol-2-ylidene or 1,3-dipropylimidazol-2-ylidene (*n* = 2), or 3-methyl-1-picolylimidazol-2-ylidene (*n* = 1)) led to poorer catalytic results (ca. 9–35 % CyO yield at 24 h, 55 °C; Table 2.1).²⁹ At the higher reaction temperature of 70 °C, the complex [Mo(CO)₄L] with L = N-[3-(trimethoxysilyl)propyl]ethylenediamine led to 47 % CyO yield at 50 % conversion, at 24 h (catalyst:olefin:oxidant = 1:159:317, mesitylene as cosolvent), which is much poorer than that for **1** and **2**.³⁰

The catalytic results for **1** and **2** are on a par with some of the best results reported in the literature for complexes of the type [Mo(CO)₄L] tested as precatalysts for Cy reaction, at 55 °C, specifically with L = 2-(1-pentyl-3-pyrazolyl)pyridine (93 % CyO yield at 6h)¹⁸ and N-(*n*-propyl)-2-pyridylmethanimine (100 % CyO yield at 5 h)¹⁶.

4.3.2. Epoxidation of prochiral olefins

Compounds **1** and **2** were further explored for the epoxidation of prochiral olefins, namely *trans*- β -methylstyrene (*tbms*) and DL-limonene (DL-Lim) with TBHP at 55 °C (TFT as cosolvent) (Figures 4.3). With *tbms* as substrate, complexes **1** and **2** led to similar catalytic results (62 % / 85 % and 59 % / 82 % conversion at 6 h/24 h, for **1** and **2**, respectively), which parallels that observed with Cy as substrate. The catalytic reaction of *tbms* was 100 % selective towards the epoxide isomers (2*S*,3*S*)-2-methyl-3-phenyloxirane and (2*R*,3*R*)-2-methyl-3-phenyloxirane, which were formed in approximately equimolar amounts (enantiomeric excess (*ee*) was always ≤ 1 %). Hence, asymmetric induction was negligible.

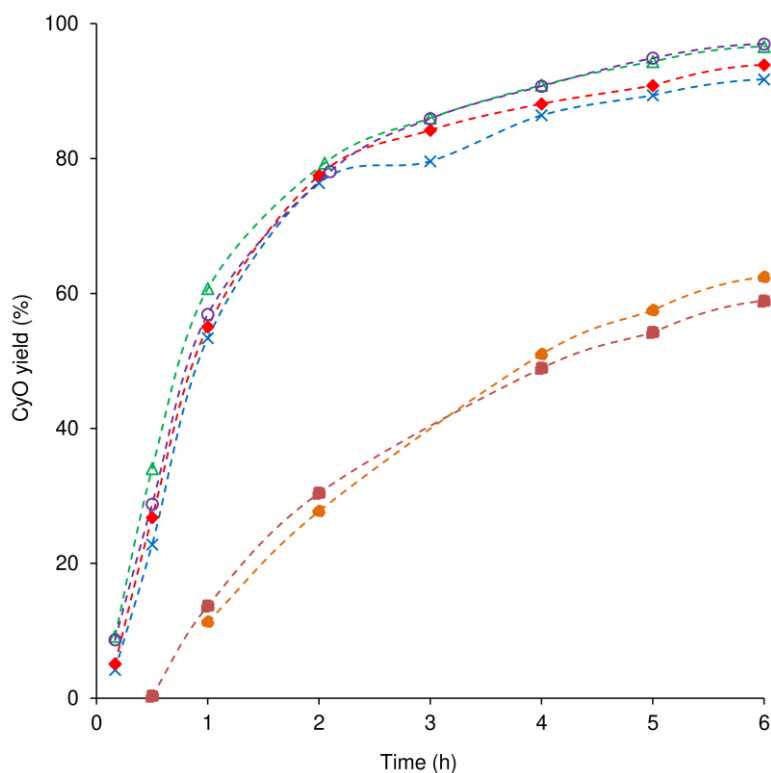


Figure 4.3. Kinetic profiles for the catalytic reactions **1**/Cy (x), **2**/Cy (♦), **1**-Cy-run1/Cy (Δ), **2**-Cy-run1/Cy (○), **1**/*tbms* (●) and **2**/*tbms* (■), using TBHP as oxidant at 55 °C. The dashed lines are visual guides.

Poor asymmetric induction ability was reported for several molybdenum carbonyl complexes (with *tbms* as substrate), excluding chiral molybdenum tetracarbonyl complexes, which, to the best of our knowledge, have not been previously explored in catalytic olefin epoxidation.^{31–35} This feature may be partly due to partial ligand dissociation and/or the pronounced distance between the olefin molecule

Chapter 4

and the chiral centers of the active oxidizing species (negligible stereochemical constraints for chiral induction ability), and/or involvement of radicals in the epoxidation reactions.³²⁻³⁵

The catalytic results for **1** and **2** with *tbms* as substrate are comparable with results published for the chiral complex [(–)-menthylCp]Mo(CO)₃Cl (84 % epoxide yield; 24 h, 55 °C, CHCl₃)³¹, molybdenum carbonyl complexes with *ansa*-bridged η⁵-cyclopentadienyl ligands where the stereogenic centers are located in side chains (50-66% yield; 4 h, 55 °C, toluene)³², and the complex [(N-benzyloxycarbonylpropyl)cyclopentadienyl] Mo(CO)₃Me (84 % yield; 24 h, 57 °C, CHCl₃)³³ (in all these studies, total epoxide selectivity = 100 % and Mo:olefin:oxidant = 1:100:200). Among these studies the maximum *ee* reported was 19-20 % for the *ansa*-bridged complexes (the enantiomer in excess was not specified)³² and the menthyl-derived complex, which favored formation of the (2*R*,3*R*)-2-methyl-3-phenyloxirane enantiomer³¹. Further comparisons of the *tbms* epoxidation results for **1** and **2** with literature data for other molybdenum carbonyl complexes are difficult due to the broad range of reaction conditions used. The best result reported for the complexes (*R*)-Cp^{ox}M(η³-C₃H₅)(CO)₂ (M = Mo, W) and [(*R*)-Cp^{ox}Mo(CO)₂(CH₃CN)]BF₄ (Cp^{ox} = chiral oxazoline pendant group) was 58 % conversion (100 % epoxide selectivity) after 16 h reaction at ambient temperature (Mo:olefin:oxidant = 1:100:200, CHCl₃).³⁴ The complexes CpMo(CO)₃X with X = CHR²CO(OR¹) (R¹ = ethyl, menthyl or bornyl, R² = H; R¹ = ethyl, R² = methyl or phenyl) led to 62-70 % epoxide yield (100 % selectivity) after 8.3 h reaction at ambient temperature (Mo:olefin:oxidant = 1:100:200, CH₂Cl₂).³⁵ The two latter works reported negligible *ee*'s.

Complexes **1** and **2** were further tested for the epoxidation of the bio-derived olefin DL-limonene (DL-Lim). Limonene is produced via distillation of crude turpentine, and is a valuable by-product of pine oil and camphor processes. Limonene epoxidation leads to valuable products, such as 1,2-epoxy-*p*-menth-8-ene (limonene oxide, abbreviated as LimOx) and 1,2:8,9-diepoxy-β-menthane (limonene dioxide, abbreviated as LimDiOx). The relative abundance, low cost, and structural similarity to cyclohexene oxide, make LimOx an attractive choice as a biorenewable epoxide monomer for copolymerization with CO₂, giving a biodegradable polycarbonate (LimDiOx may also be used) and, consequently, providing an attractive green route to non-isocyanate polyurethanes without requiring the use of either toxic isocyanate monomers or phosgene.³⁷⁻³⁹ In the same way, LimOx can give polyesters by reaction with succinic anhydride.⁴⁰ LimOx/LimDiOx can be used as intermediates for the manufacture of perfumes, flavors and fragrances, as green solvents, and as reactive diluents in cationic and UV cure applications.^{39,41,42} Geoghegan and Evans employed LimOx as a

Chapter 4

starting material for the synthesis of (+)-perillyl alcohol⁴³, which may be useful as a “chiral pool” starting material and as an anti-cancer agent.⁴⁴

The reaction of (racemic) DL-Lim with TBHP, in the presence of **1** or **2** at 55 °C, led to similar catalytic results, in parallel to that observed for the two complexes with Cy or *tbms* as substrates. The DL-Lim conversions were 85 % and 96-97 % at 6 h and 24 h, respectively (Figure 4.4). The main reaction products were LimOx isomers, namely (1*S*,4*S*)-(-)-*cis*-limonene-1,2-epoxide and (1*R*,4*S*)-(-)-*trans*-limonene-1,2-epoxide (diastereomers formed from (*S*)-(-)-limonene (*S*-Lim)), and (1*S*,4*R*)-(+)-*cis*-limonene-1,2-epoxide and (1*R*,4*R*)-(+)-*trans*-limonene-1,2-epoxide (diastereomers formed from (*R*)-(+)-limonene (Lim)), which were formed with total (LimOx) selectivity of 80-82 % and 69-70 %, at 6 h and 24 h, respectively (Scheme 2). Slight enantiomeric excesses (*ee*'s) of the (+) LimOx isomers were obtained at 24 h (ca. 4 % of isomer II relative to III and 14-16 % of isomer I relative to IV). On the other hand, slight diastereomeric excess (*de*) of *trans* limonene-1,2-epoxide isomers was obtained at 24 h (3-4 % of isomer I relative to II and 6-9 % of isomer III relative to IV).

Other products of the DL-Lim reaction included LimDiOx (selectivities of 12-13 % at 6 h and 19-20 % at 24 h) and 1-methyl-4-(1-methylethenyl)-cyclohexane-1,2-diol (limonen-1,2-diol, abbreviated as LDOH; selectivities of 0-2 % at 6 h and 8-9 % at 24 h). The ratio LimOx/(LimOx + LimDiOx) was in the range 0.8-1, indicating high chemoselectivity in favor of the epoxidation of the endocyclic double bond. LimOx selectivity decreased with time, and LimDiOx selectivity increased (Figure 4.4). On the other hand, 8,9-epoxy- β -menth-1-ene was not formed, suggesting that LimDiOx is formed via consecutive epoxidation of LimOx.

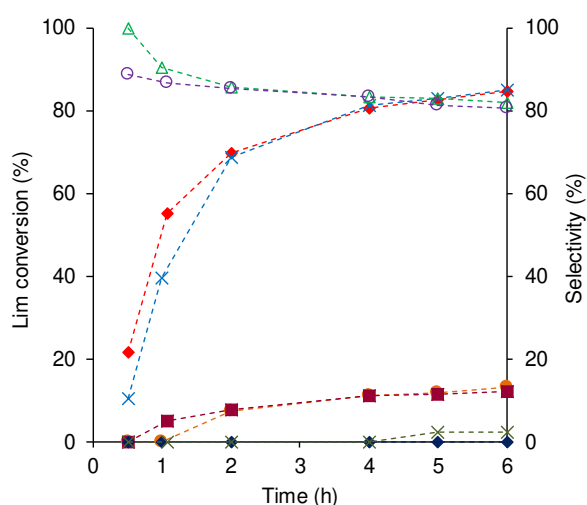


Figure 4.4. Kinetic profile of the reaction of DL-Lim with TBHP, in the presence of **1** (x) or **2** (♦), at 55 °C, and selectivity to the products LimOx (Δ with **1**, ○ with **2**), LimDiOx (● with **1**, ■ with **2**) and LDOH (x with **1**, ♦ with **2**).

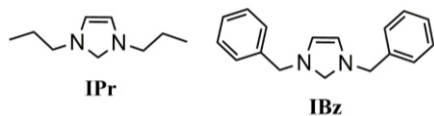
Chapter 4

Table 4.1. *cis*-Cyclooctene epoxidation at 55 °C in the presence of compounds **1** and **2**, and comparison with literature data for molybdenum tetracarbonyl complexes.

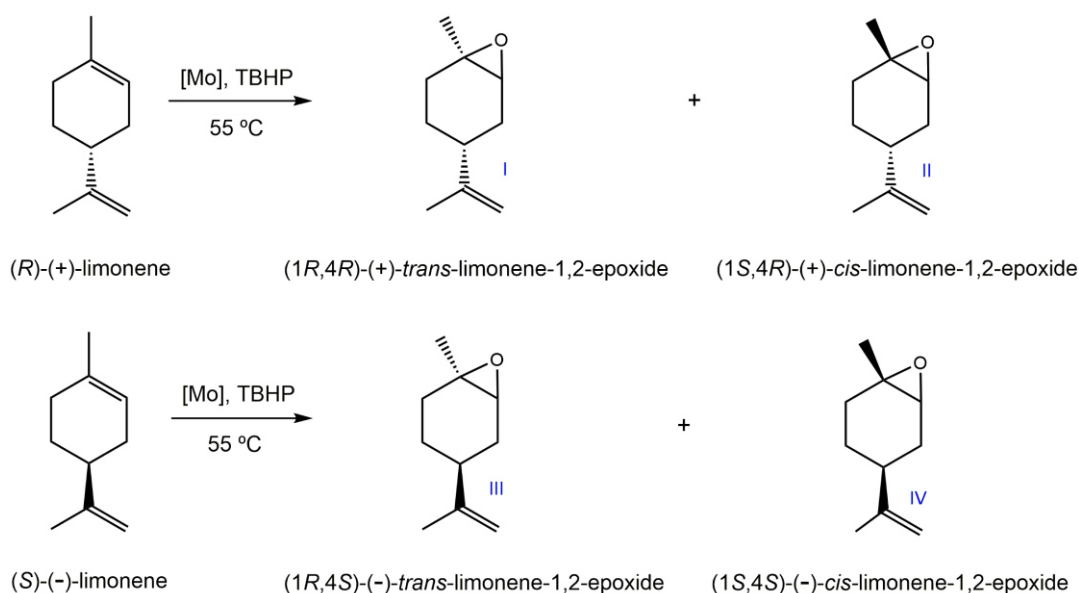
Complex	Mo:Cy:TBHP	Cosolvent	t (h)	Conv. (%) ^a	Select. (%) ^b	Ref.
1	1:100:153	DCE	6/24	92/100	100/100	
2	1:100:153	DCE	6/24	94/100	100/100	
[Mo(CO) ₄ (2,2'-bipy)]	1:100:153	DCE	6	71	100	36
[Mo(CO) ₄ (di- <i>t</i> Bu-bipy)]	1:100:153	DCE	6	84	100	36
[Mo(CO) ₄ (pzpyH)]	1:100:152	None	6/24	51/78	100/100	15
[Mo(CO) ₄ (pzpyEA)]	1:100:152	None	6/24	70/92	100/100	15
[Mo(CO) ₄ (pzpyP)]	1:113:172	DCE	6/24	93/100	100/100	18
[Mo(CO) ₄ (pyim)]	1:100:153	None	5	100	100	16
[Mo(CO) ₄ (IBz) ₂]	1:100:200	None	4/24 h	~7/~35	100/100	29
[Mo(CO) ₄ (IPr) ₂]	1:100:200	None	4/24 h	~10/~32	100/100	29
[Mo(CO) ₄ (PyNHC)]	1:100:200	None	4/24 h	~2/~9	100/100	29

^a *cis*-Cyclooctene conversion.

^b Selectivity to the epoxide (CyO).



Chapter 4



Scheme 4.2. Products formed from DL-limonene epoxidation.

There are no reports on the use of chiral molybdenum carbonyl complexes as precatalysts for the reaction of racemic DL-Lim, although it was reported that they may promote the reaction of the pure isomers of limonene with TBHP. Specifically, the complex $[\text{Mo}(\text{CO})_3]_2(4,4'\text{-dimethyl-2,2'}\text{-bipyridine})$ led to 56% conversion of *R*-(+)-Lim and 91% selectivity to the monoepoxides (1*S*,4*R*)-(+)-*cis*-**II** and (1*R*,4*R*)-(+)-*trans*-limonene-1,2-epoxide (**I**), and *de* was less than 5 % (24 h, 55 °C, Mo:olefin:oxidant = 1:100:200, CH_2Cl_2).⁴⁵ The complexes (*R*)- $\text{Cp}^{\text{ox}}\text{M}(\eta^3\text{-C}_3\text{H}_5)(\text{CO})_2$ (M = Mo, W) and $[(R)\text{-Cp}^{\text{ox}}\text{Mo}(\text{CO})_2(\text{CH}_3\text{CN})]\text{BF}_4$ led to quantitative conversion of *R*-(+)-Lim to LimOx after 1 h reaction at 55 °C;³⁴ an approximately equimolar mixture of LimOx isomers was obtained for the neutral complex, while 20 % *de* of the (+)-*cis* isomer was obtained for the cationic complex (Mo:olefin:oxidant = 1:100:200, CHCl_3). The few published studies that report the Mo-catalyzed reaction of DL-Lim with TBHP use chiral oxomolybdenum compounds as (pre)catalysts (Table 4.2).

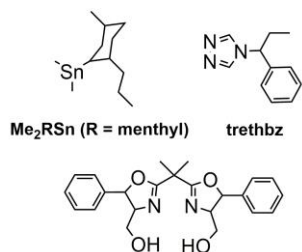
In general, compounds **1** and **2** studied in this work led to comparable results (in terms of LimOx yields at 24 h) to those obtained with the polymeric compound $[\text{((Me)}_2\text{(menthyl)Sn)}_2\text{MoO}_4(\text{H}_2\text{O})_{3.5}]$ ⁴⁶, and slightly better results than those for the complex $[\text{MoO}_2\{(-)\text{-2,2-bis}[(4*S*,5*S*)\text{-4-hydroxymethyl-5-phenyl-1,3-oxazolin-2-yl]propane}\}]$ ⁴⁷. The hybrid polymer $[\text{Mo}_2\text{O}_6(\text{trethbz})_2]\cdot\text{H}_2\text{O}$ (*trethbz* = (*S*)-4-(1-phenylpropyl)-1,2,4-triazole) led to higher yields (74 %).⁴⁸ The (+)-*cis* and (+)-*trans* LimOx isomers were predominantly formed relative to (-)-*cis* and (-)-*trans*, respectively, using all Mo compounds, with the best *ee*'s observed for **1** and **2** and also $[\text{Mo}_2\text{O}_6(\text{trethbz})_2]\cdot\text{H}_2\text{O}$ as (pre)catalysts. The dioxomolybdenum(VI) complex containing the chiral oxazoline ligand led to the highest *de* (18-20 % of *trans* isomers).⁴⁷

Chapter 4

Table 4.2. Limonene epoxidation with TBHP and chiral Mo compounds at 55 °C.

Compound	Sub. ^a	Mo:Sub:TBHP	Solv. ^b	Conv. (%) ^c	Yield (%) ^d	ee (%) ^e	de (%) ^f	Ref.
1	DL-Lim	1:100:153	TFT	96	67	4 (II)	6 (III)	
						14 (I)	3 (I)	
2	DL-Lim	1:100:153	TFT	97	68	4 (II)	9 (III)	
						16 (I)	4 (I)	
[(Me ₂ RSn) ₂ MoO ₄ (H ₂ O) _{3.5}]	DL-Lim	1:100:150	CH ₂ Cl ₂	90	65-67	-	-	46
	R-Lim			85		-	5 ^g	
	S-Lim			97		-	5 ^g	
[Mo ₂ O ₆ (trethbz) ₂] ₂ H ₂ O	DL-Lim	1:100:153	TFT	90	74	12 (II)	3 (IV)	48
						8 (I)	8 (II)	
[MoO ₂ (oxazol)]	DL-Lim	1:138:211	DCE	90	59	13 (III)	18 (I)	47
						25 (I)	20 (III)	
						R-Lim		
	S-Lim			88	59	-	19(III)	

^a Substrates: DL-Lim = DL-limonene; Lim = R-(+)-limonene; S-Lim = S-(—)-limonene. ^b Solv. = cosolvent added. ^c Conversion of the substrate after 24 h. ^d Total yield of 1,2-epoxides after 24 h. ^e Enantiomeric excess at 24 h; the isomer in excess is indicated within brackets (pairs of enantiomers I/IV and II/III). ^f Diastereomeric excess at 24 h; the isomer in excess is indicated within brackets (pairs of diastereomers I/II and III/IV). ^g The isomer in excess was not specified.



Oxazol = (-)-2,2-bis[(4S,5S)-4-hydroxymethyl-5-phenyl-1,3-oxazolin-2-yl]

4.3.3. Types of active species

Complexes **1** and **2** are converted into active oxidizing species (discussed above) *in situ* during the catalytic process. Structural modification of the starting complexes is somewhat supported by the fact that the colour of the Cy reaction mixtures containing (**1** or **2**)/olefin/TBHP changed from greenish to light brown upon addition of the oxidant to the reactor. The metal species were isolated after a 24 h batch run, giving the solids **1**-Cy-run1 and **2**-Cy-run1, and characterized by ATR FT-IR spectroscopy (Figure 4.5). Indicators for oxidative decarbonylation of the precatalysts are the disappearance of the CO stretching bands in the region 1810-2020 cm^{-1} and the appearance of several new bands in the Mo–O stretching region of 650-950 cm^{-1} . Similar spectra were obtained for the solids isolated after catalytic reactions with the other substrates (Figure 4.5). The pattern of bands in the Mo–O stretching region is highly characteristic of the β -octamolybdate anion, $\beta\text{-}[\text{Mo}_8\text{O}_{26}]^{4-}$, as supported by the literature data given in Table 4.3 for comparison.

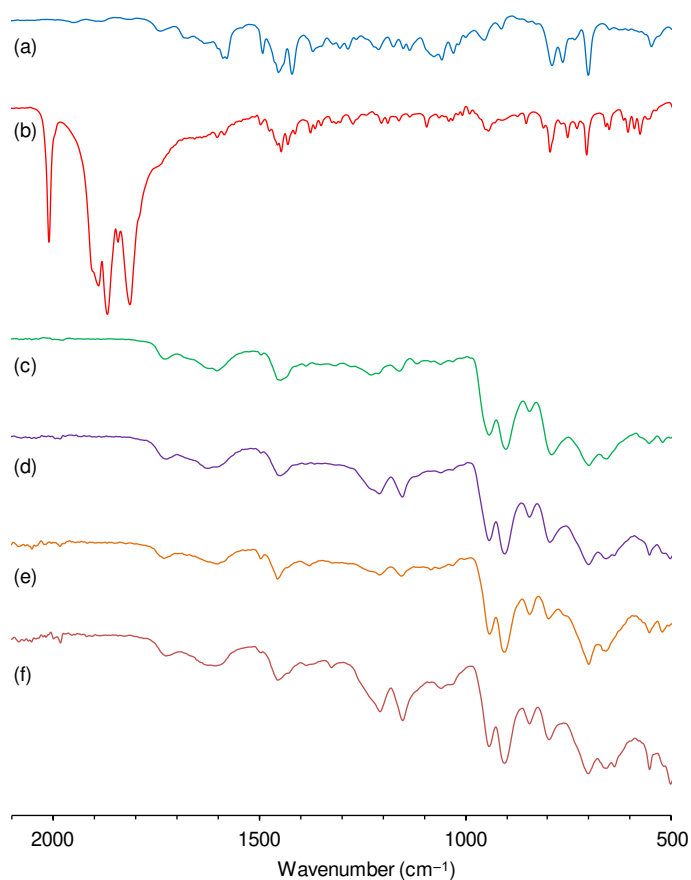


Figure 4.5. FT-IR spectra in the range 500-2100 cm^{-1} of (a) L1, and (b) **1**, and ATR FT-IR spectra of solids recovered after catalytic reactions (c) **1**-Cy-run1, (d) **1**-Cy-run2, (e) **1**-*tbms*-run1 and (f) **1**-DL-Lim-run1.

Chapter 4

This polyoxomolybdate had previously been identified as the product of oxidative decarbonylation of the complexes $[\text{Mo}(\text{CO})_3\text{I}_2\text{L}_2]$ ($\text{L} = \text{pyridine}$ or $4\text{-tert-butylpyridine}$), which gave the salts $(\text{LH})_4[\text{Mo}_8\text{O}_{26}]$.⁴⁹ The Cy/TBHP reaction in the presence of **1-Cy-run1** or **2-Cy-run1** led to similar catalytic results to the respective parent compounds **1** and **2** (Figure 4.3). Compounds **1-Cy-run2** and **2-Cy-run2** exhibited similar ATR FT-IR spectra to **1-Cy-run1** and **2-Cy-run1**, suggesting that the polynuclear species formed is chemically stable during the catalytic reaction (Figure 4). On the other hand, these results suggest that the active species formed from the precursors **1** and **2** are responsible for the catalytic epoxidation process in the first and second batch runs.

Table 4.3. Comparison of infrared bands observed for the recovered compounds **1-Cy-run1** and **2-Cy-run1** in the range $650\text{-}950\text{ cm}^{-1}$ with bands exhibited by β -octamolybdate salts.

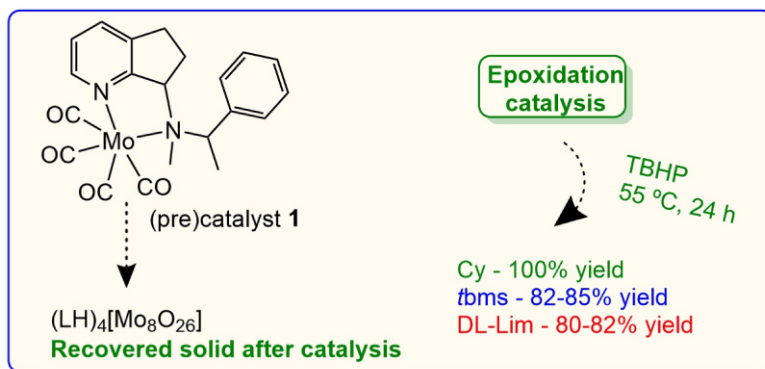
Compound ^a	IR bands (cm^{-1})					Ref.
1-Cy-run1, 2-Cy-run1^b	942	903	844	701	659	
(pyH)₄[Mo₈O₂₆]	946	912	839	709	675	49
(tBupyH)₄[Mo₈O₂₆]	949	914	837	708	659	49
(H₃biim)₄[Mo₈O₂₆]	944	919	838	686	670	50
(HDBU)₃(NH₄)[Mo₈O₂₆]\cdotH₂O	939	910	842	720	669	51
(Hmim)₄[Mo₈O₂₆]	946	910	841	710	665	52
(Dhmim)₄[Mo₈O₂₆]	956	911	837	714	650	52
(Hpy)₄[Mo₈O₂₆]\cdotH₂O	947	911	836	717	632	53
(Bmim)₄[Mo₈O₂₆]	939	913	842	714	661	54
(dmimX)₃[Mo₈O₂₆]₂(H₃O)₂\cdotH₂O	944	902	841	711	651	55
(4,4'-Hybipy)_{4/y}[Mo₈O₂₆]^b	935	910	836	699	657	56

4.4. Conclusions

The efficacy of molybdenum carbonyl complexes as precatalysts for olefin epoxidation reactions has motivated some efforts to prepare chiral catalyst precursors in the hope that these may promote asymmetric induction. In the present work we have described the first report of the application of chiral molybdenum tetracarbonyl complexes in catalytic olefin epoxidation (Scheme 4.3). Although epoxides were either the main or only products formed from *cis*-cyclooctene, *trans*- β -methylstyrene and DL-limonene, stereoselectivities were low with the prochiral olefins. The lack of success in asymmetric epoxidation may be partly due to the labile behaviour of the 7-(1-pyridanyl)amine ligands, which decoordinate upon oxidative decarbonylation of the

Chapter 4

precursors to give β -octamolybdate salts in which the protonated organic ligand is present as charge-balancing cation. The previous work Chapters 2 and 3 with *cis*-[Mo(CO)₄(L)] catalyst precursors has indicated that chelating ligands such as bipyridines and pyrazolylpyridines tend to remain coordinated to the metal center upon oxidative decarbonylation to give either discrete polynuclear oxo-complexes or hybrid molybdenum oxide/organic polymers, and therefore better success in asymmetric epoxidation may be achieved by employing chiral derivatives of these types of ligands.



Scheme 4.3. Summary of the main syntheses and catalytic studies carried out in this work.

4.5. References

- (1) Szymańska-Buzar, T. *Coord. Chem. Rev.* **2006**, *250*, 976–990.
- (2) Szymańska-Buzar, T. *Curr. Org. Chem.* **2012**, *16*, 3–15.
- (3) Wang, Z.; Jiang, L.; Mohamed, D. K. B.; Zhao, J.; Hor, T. S. A. *Coord. Chem. Rev.* **2015**, *293–294*, 292–326.
- (4) Kück, J. W.; Reich, R. M.; Kühn, F. E. *Chem. Rec.* **2016**, *16*, 349–364.
- (5) Sheng, M. N.; Zajacek, J. G. *ACS Adv. Chem. Ser.* **1968**, *76*, 418–432.
- (6) Sheng, M. N.; Zajacek, J. G. *J. Org. Chem.* **1970**, *35*, 1839–1843.
- (7) Kollar, J.; Epoxidation process. 3 351 635, 1970.
- (8) Rameswaran, M. Epoxidation process. 5 081 267, 1992.
- (9) Brégeault, J. M. *J. Chem. Soc. Dalton Trans.* **2003**, *3*, 3289–3302.
- (10) Strickler, G. R.; Quarderer, J. G. J., Lindner, J. P. Process of preparing an olefin oxide from olefin and organic hydroperoxide. 7 273 941, 2007.
- (11) Abrantes, M.; Santos, A. M.; Mink, J.; Kühn, F. E.; Romão, C. C. *Organometallics* **2003**, *22*, 2112–2118.
- (12) Valente, A. A.; Seixas, J. D.; Gonçalves, I. S.; Abrantes, M.; Pillinger, M.; Romão, C. C. *Catal. Lett.* **2005**, *101*, 127–130.
- (13) Calhorda, M. J.; Costa, P. *Curr. Org. Chem.* **2012**, *16*, 65–72.

Chapter 4

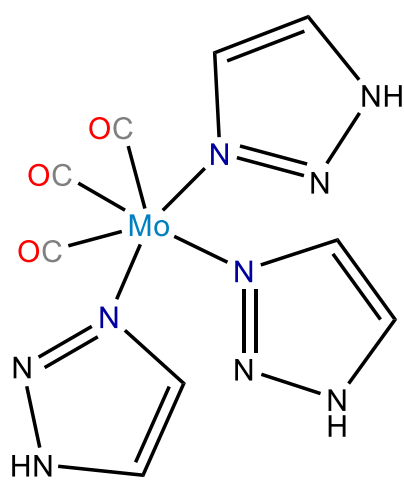
- (14) Amarante, T. R.; Neves, P.; Coelho, A. C.; Gago, S.; Valente, A. A.; Almeida Paz, F. A.; Pillinger, M.; Gonçalves, I. S. *Organometallics* **2010**, *29*, 883–892.
- (15) Neves, P.; Amarante, T. R.; Gomes, A. C.; Coelho, A. C.; Gago, S.; Pillinger, M.; Gonçalves, I. S.; Silva, C. M.; Valente, A. A. *Appl. Catal., A* **2011**, *395*, 71–77.
- (16) Gomes, A. C.; Bruno, S. M.; Gago, S.; Lopes, R. P.; Machado, D. A.; Carminatti, A. P.; Valente, A. A.; Pillinger, M.; Gonçalves, I. S. *J. Organomet. Chem.* **2011**, *696*, 3543–3550.
- (17) Figueiredo, S.; Gomes, A. C.; Fernandes, J. A.; Paz, F. A.; Lopes, A. D.; Lourenço, J. P.; Pillinger, M.; Gonçalves, I. S. *J. Org. Chem.* **2013**, *723*, 56–64.
- (18) Nogueira, L. S.; Neves, P.; Gomes, A. C.; Valente, A. A.; Pillinger, M.; Gonçalves, I. S. *J. Organomet. Chem.* **2017**, *846*, 185–192.
- (19) Pereira, C.; Salgado, S.; Rizzo-Aguiar, F.; Garcia-Mera, X.; Rodríguez-Borges, J. *Synlett* **2013**, *24*, 837–838.
- (20) Sousa, C. A. D.; Sampaio-Dias, I. E.; Rizzo-Aguiar, F.; Garcia-Mera, X.; Rodríguez-Borges, J. E. *RSC Adv.* **2015**, *5*, 104509–104515.
- (21) Rizzo-Aguiar, F.; Sousa, C. A. D.; Garcia-Mera, X.; Rodríguez-Borges, J. E. *Chem. Data Collect.* **2016**, *5–6*, 21–27.
- (22) Thiel, W. R.; Priermeier, T. *Angew. Chem., Int. Ed.* **1995**, *34*, 1737–1738.
- (23) Thiel, W. R.; Eppinger, J. *Chem. Eur. J.* **1997**, *3*, 696–705.
- (24) Kühn, F. E.; Groarke, M.; Bencze, É.; Herdtweck, E.; Prazeres, A.; Santos, A. M.; Calhorda, M. J.; Romão, C. C.; Gonçalves, I. S.; Lopes, A. D.; Pillinger, M. *Chem. Eur. J.* **2002**, *8*, 2370–2383.
- (25) Veiros, L. F.; Prazeres, Â.; Costa, P. J.; Romão, C. C.; Kühn, F. E.; Calhorda, M. J. *J. Chem. Soc.* **2006**, *60*, 1383–1389.
- (26) Comas-Vives, A.; Lledos, A.; Poli, R. *Chem. Eur. J.* **2010**, *16*, 2147–2158.
- (27) Costa, P. J.; Calhorda, M. J.; Kühn, F. E. *Organometallics* **2010**, *29*, 303–311.
- (28) Morlot, J.; Uyttebroeck, N.; Agustin, D.; Poli, R. *ChemCatChem* **2013**, *5*, 601–611.
- (29) Wang, Z.; Li, S.; Teo, W. J.; Poh, Y. T.; Zhao, J.; Hor, T. S. A. *J. Org. Chem.* **2015**, *775*, 188–194.
- (30) Baskaran, T.; Kumaravel, R.; Christopher, J.; Ajithkumar, T.G.; Sakthivel, A. *New J. Chem.* **2015**, *39*, 3758–3764.
- (31) Abrantes, M.; Sakthivel, A.; Romão, C. C.; Kühn, F. E. *J. Organomet. Chem.* **2006**, *691*, 3137–3145.
- (32) Zhao, J.; Herdtweck, E.; Kuehn, F. E. *J. Org. Chem.* **2006**, *691*, 2199–2206.
- (33) Abrantes, M.; Paz, F. A. A.; Valente, A. A.; Pereira, C. C. L.; Gago, S.; Rodrigues, A. E.; Klinowski, J.; Pillinger, M.; Gonçalves, I. S. *J. Organomet. Chem.* **2009**, *694*, 1826–1833.
- (34) Reis, P. M.; Gamelas, C. A.; Brito, J. A.; Saffon, N.; Gómez, M.; Royo, B. *Eur. J. Inorg. Chem.* **2011**, 666–673.
- (35) Grover, N.; Pöthig, A.; Kühn, F. E. *Catal. Sci. Technol.* **2014**, *4*, 4219–4231.
- (36) Amarante, T. R.; Neves, P.; Coelho, A. C.; Gago, S.; Valente, A. A.; Almeida Paz, F. A.;

Chapter 4

- Pillinger, M.; Gonçalves, I. S. *Organometallics* **2010**, *29*, 883–892.
- (37) Bähr, M.; Bitto, A.; Mülhaupt, R. *Green Chem.* **2012**, *14*, 1447–1454.
- (38) Wilbon, P. A.; Chu, F.; Tang, C. *Macromol. Rapid Commun.* **2013**, *34*, 8–37.
- (39) Li, C.; Sablong, R. J.; Koning, C. E. *Angew. Chem., Int. Ed.* **2016**, *55*, 11572–11576.
- (40) Jeske, R. C.; DiCiccio, A. M.; Coates, G. W. *J. Am. Chem. Soc.* **2007**, *129*, 11330–11331.
- (41) Costa, V. V.; Da Silva Rocha, K. A.; Kozhevnikov, I. V.; Kozhevnikova, E. F.; Gusevskaya, E. V. *Catal. Sci. Technol.* **2013**, *3*, 244–250.
- (42) Wróblewska, A. *Molecules* **2014**, *19*, 19907–19922.
- (43) Geoghegan, K.; Evans, P. *Tetrahedron Lett.* **2014**, *55*, 1431–1433.
- (44) Cho, H.-Y.; Wang, W.; Jhaveri, N.; Torres, S.; Tseng, J.; Leong, M. N.; Lee, D. J.; Goldkorn, A.; Xu, T.; Petasis, N. A.; Louie, S. G.; Schonthal, A. H.; Hofman, F. M.; Chen, T. C. *Mol. Canc. Ther.* **2012**, *11*, 2462–2472.
- (45) Fernandes, C. I.; Saraiva, M. S.; Nunes, T. G.; Vaz, P. D.; Nunes, C. D. *J. Catal.* **2014**, *309*, 21–32.
- (46) Abrantes, M.; Valente, A. A.; Pillinger, M.; Romão, C. C.; Gonçalves, I. S. *Catal. Lett.* **2007**, *114*, 103–109.
- (47) Neves, P.; Gago, S.; Pereira, C. C. L.; Figueiredo, S.; Lemos, A.; Lopes, A. D.; Gonçalves, I. S.; Pillinger, M.; Silva, C. M.; Valente, A. A. *Catal. Lett.* **2009**, *132*, 94–103.
- (48) Lysenko, A. B.; Senchyk, G. A.; Domasevitch, K. V.; Kobalz, M.; Krautscheid, H.; Cichos, J.; Karbowski, M.; Neves, P.; Valente, A. A.; Gonçalves, I. S. *Inorg. Chem.* **2017**, *56*, 4380–4394.
- (49) Gamelas, C. A.; Neves, P.; Gomes, A. C.; Valente, A. A.; Romão, C. C.; Gonçalves, I. S.; Pillinger, M. *Catal. Lett.* **2012**, *142*, 1218–1224.
- (50) Neves, P.; Amarante, T. R.; Valente, A. A.; Pillinger, M.; Gonçalves, I. S. *Catal. Lett.* **2016**, *146*, 841–850.
- (51) Coué, V.; Dessapt, R.; Bujoli-Doeuff, M.; Evain, M.; Jobic, S. *J. Solid State Chem.* **2006**, *179*, 3615–3627.
- (52) Zhou, M. D.; Liu, M. J.; Huang, L. L.; Zhang, J.; Wang, J. Y.; Li, X. B.; Kühn, F. E.; Zang, S. L. *Green Chem.* **2015**, *17*, 1186–1193.
- (53) Hill, C. L. *Chem. Rev.* **1998**, *98*, 1–2.
- (54) Carrasco, C. J.; Montilla, F.; Álvarez, E.; Herbert, M.; Galindo, A. *Polyhedron* **2013**, *54*, 123–130.
- (55) Li, Y.; Hang, X.; Li, N.; Hao, X. *J. Mater. Process. Technol.* **2016**, *230*, 280–287.
- (56) Neves, P.; Gomes, A. C.; Paz, F. A. A.; Valente, A. A.; Gonçalves, I. S.; Pillinger, M. *Mol. Catal.* **2017**, *432*, 104–114.

CHAPTER 5

A comparative study of molybdenum carbonyl and oxomolybdenum derivatives bearing 1,2,3-triazole or 1,2,4-triazole in catalytic olefin epoxidation



$[Mo(CO)_3(1,2,3\text{-triazole})_3]$

Chapter 5

Index

5.1. Introduction	141
5.2. Results and discussion	142
5.2.1. Synthesis and characterization of complexes $\text{Mo}(\text{CO})_3(1,2,3\text{-trz})_3$ (1) and $[\text{Mo}(\text{CO})_3(1,2,4\text{-trz})_3]$ (2)	142
5.2.2. Oxidative decarbonylation compounds from $[\text{Mo}(\text{CO})_3(1,2,3\text{-trz})_3]$ (1^{OD}) and $[\text{Mo}(\text{CO})_3(1,2,4\text{-trz})_3]$ (2^{OD})	145
5.2.3. Dinuclear complex $(\text{NH}_4)_{1.8}(\text{H}_3\text{O})_{0.2}[\text{Mo}_2\text{O}_2(\mu_2\text{-O})(\text{O}_2)_4(1,2,4\text{-trz})]\cdot\text{H}_2\text{O}$ (5)	149
5.2.4. Single-crystal X-ray structure analyses of 5	149
5.3. Catalytic studies	150
5.3.1. Catalytic epoxidation of <i>cis</i> -cyclooctene with TBHP	150
5.3.2. Characterization of solids after catalytic epoxidation of Cy with TBHP	152
5.3.3. Catalytic epoxidation with H_2O_2	153
5.4. Conclusions	155
5.5. References	155

Chapter 5

5.1. Introduction

Molecular and polymeric molybdenum oxides that incorporate organic moieties as either charge-balancing counter-ions or ligands have proven to be excellent catalysts for several oxidation reactions in organic synthesis [1-5].¹⁻⁴ Some illustrative and significant examples of molybdenum(VI)-catalyzed reactions described in the last fifteen years include complexes of the type $[\text{Cp}'\text{MoO}_2\text{X}]$ (Cp' = unsubstituted or substituted cyclopentadienyl, X = halide, alkyl, alkyl ester, *ansa*-bridged alkyl or cycloalkyl group, etc.) for the epoxidation of olefins with *tert*-butyl hydroperoxide (TBHP)^{1,2}, with activities that surpass that of the $\text{CH}_3\text{ReO}_3/\text{H}_2\text{O}_2$ system, enantioselective oxidation of olefins catalyzed by a chiral bishydroxamic acid complex⁵, enantioselective sulfoxidation using a chiral bisguanidinium dinuclear oxodiperoxomolybdate catalyst⁶, amino triphenolate complexes as catalysts for sulfoxidation, epoxidation and haloperoxidation⁷, a polyoxomolybdate-calix[4]arene hybrid as a heterogeneous catalyst for sulfoxidation⁸, selective olefin epoxidation using nanoparticle-supported, magnetically recoverable complexes⁹, and reaction-induced self-separating catalysts for the oxidation of olefins, sulfides and alcohols, based on octamolybdate salts¹⁰ or a MoO_3 -triazole hybrid material¹¹.

A common feature of molybdenum(VI)-catalyzed reactions is that the starting complex acts as a precatalyst, being transformed under the reaction conditions to oxoperoxo-molybdenum(VI) complexes, which may be the actual catalysts responsible for activating the oxidant toward the oxidation reaction. Experimental and computational studies showed this to be the case with the cyclopentadienyl complexes $[\text{Cp}'\text{MoO}_2\text{X}]$, which react with the oxidant ROOH to give species of the type $[\text{Cp}'\text{MoO}(\text{O}_2)\text{X}]$.^{12,13} An important discovery was that the tricarbonyl complexes $[\text{Cp}'\text{Mo}(\text{CO})_3\text{X}]$ could be used as precatalysts rather than the dioxomolybdenum(VI) complexes.² In analogy with the Arco-Lyondell process for the epoxidation of propene, where the precursor $\text{Mo}(\text{CO})_6$ is oxidized *in situ* by TBHP to a dioxomolybdenum(VI) complex¹⁴, the tricarbonyl complexes undergo rapid oxidative decarbonylation in the presence of excess TBHP to form complexes of the type $[\text{Cp}'\text{MoO}_2\text{X}]$, $[\text{Cp}'\text{MoO}(\text{O}_2)\text{X}]$, $[(\text{Cp}'\text{MoO}_2)_2(\mu\text{-O})]$ and $[(\text{Cp}'\text{MoO}(\text{O}_2))_2(\mu\text{-O})]$.^{1,2,15} This work inspired studies with other types of molybdenum carbonyl complexes and led to the isolation of a variety of mononuclear, dinuclear, polynuclear and polymeric molybdenum(VI) oxides. Examples include $[\text{CpMoO}_2(\text{NHC})]\text{BF}_4$ from $[\text{CpMo}(\text{CO})_2(\text{NHC})(\text{CH}_3\text{CN})](\text{BF}_4)$ (NHC = N-heterocyclic carbene)¹⁶, tetranuclear $[\text{Mo}_4\text{O}_{12}(\text{pypz})_4]$ from *cis*- $[\text{Mo}(\text{CO})_4(\text{pypz})]$ (pypz = 2-[3(5)-pyrazolyl]pyridine)¹⁷, octanuclear $[\text{Mo}_8\text{O}_{24}(\text{di-}t\text{Bu-bipy})_4]$ from *cis*- $[\text{Mo}(\text{CO})_4(\text{di-}t\text{Bu-bipy})]$ ($\text{di-}t\text{Bu-bipy}$ = 4,4'-di-*tert*-butyl-2,2'-bipyridine)¹⁸, polyoxomolybdate salts

Chapter 5

containing the anion $[\beta\text{-Mo}_8\text{O}_{26}]^{4-}$ from *cis*- $[\text{Mo}(\text{CO})_4(\text{L})]$ (L = chiral 7-(1-pyrindanyl)amine ligand)¹⁹, and the one-dimensional (1D) molybdenum oxide/bipyridine polymer $[\text{MoO}_3(2,2'\text{-bipy})]$ from *cis*- $[\text{Mo}(\text{CO})_4(2,2'\text{-bipy})]$ (2,2'-bipy = 2,2'-bipyridine)¹⁸.

In the present chapter, the molybdenum(0)-carbonyl-triazole complexes $[\text{Mo}(\text{CO})_3(\text{L})_3]$ [L = 1*H*-1,2,3-triazole (1,2,3-trz) or 1*H*-1,2,4-triazole (1,2,4-trz)] have been prepared and examined as precursors to molybdenum(VI) oxide catalysts for olefin epoxidation using TBHP or H_2O_2 as oxidant. One motivation for this research was the finding mentioned above that the MoO_3 -triazole hybrid material $[\text{MoO}_3(1,2,4\text{-trz})_{0.5}]$ could be used as a self-separating catalyst for oxidation reactions with aq. H_2O_2 as oxidant.²⁰ In a later study, the reaction of MoO_3 with H_2O_2 in the presence of 1,2,4-trz led to the isolation of the trinuclear oxoperoxo complex $(1,2,4\text{-Htrz})_2[\text{Mo}_3\text{O}_6(\text{O}_2)_4(1,2,4\text{-trz})_2]$, which constituted the first case of a discrete Mo(VI) complex bearing triazole ligands.²¹ These studies point to the untapped potential of oxomolybdenum(VI)-triazole compounds in oxidation catalysis. A particular focus of the present work was to compare in parallel the chemistry and catalytic behavior of the two tricarbonyl complexes containing the isomeric ligands, and also the hybrid materials $[\text{MoO}_3(1,2,3\text{-trz})_{0.5}]$ and $[\text{MoO}_3(1,2,4\text{-trz})_{0.5}]$, which have isomorphous layered perovskite-like structures.^{20,22,23} Transition-metal 1,2,3-triazole-based catalysts have attracted major interest^{24,25} and the examination of isostructural catalysts bearing 1,2,3-trz or 1,2,4-trz ligands should be of great value in improving our understanding of ligand influences on catalytic performance.

5.2. Results and discussion

5.2.1. Synthesis and characterization of complexes $\text{Mo}(\text{CO})_3(1,2,3\text{-trz})_3$ (**1**) and $[\text{Mo}(\text{CO})_3(1,2,4\text{-trz})_3]$ (**2**)

The triazole tricarbonyl complexes $[\text{Mo}(\text{CO})_3(1,2,3\text{-trz})_3]$ (**1**) and $[\text{Mo}(\text{CO})_3(1,2,4\text{-trz})_3]$ (**2**) were obtained in very good to excellent yields by the direct reaction of $\text{Mo}(\text{CO})_6$ with three equivalents of the organic ligand in refluxing toluene. Both complexes **1** and **2** display long-term stability in the solid-state if stored cold in the dark and under inert atmosphere. Complex **2** decomposes within seconds upon exposure to air to give a black solid. Complex **1** is partially soluble in diethyl ether, and insoluble in pentane. Complex **2** is highly insoluble in polar and nonpolar solvents. The poor solubility of **2** is in line with the known characteristic of the unsubstituted 1,2,4-triazole ligand to produce microcrystalline/insoluble precipitates immediately with transition metal ions in solution.²⁶

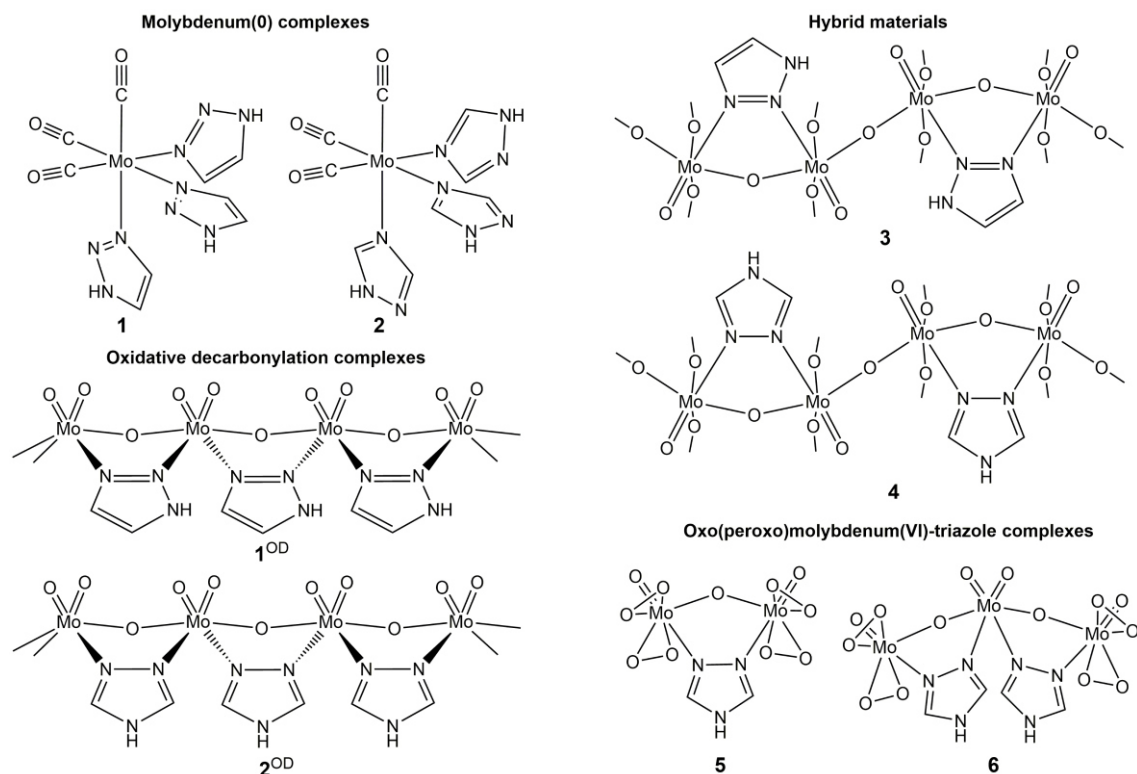


Figure 5.1. Schematic representations of the proposed structures for **1**, **2**, **1^{OD}** and **2^{OD}**, and the known structures for **3**, **5** and **6**.

For **1** and **2** the carbonyl stretching region of the IR spectra contains two bands near 1905 cm^{-1} (A_1 mode) and 1760 cm^{-1} (E mode), as expected for facial tricarbonyl complexes with approximate C_{3v} symmetry (Figure 5.2 b, f).²⁷ The lower-energy band is broadened and split, presumably due to low site symmetry in the solid-state.²⁷ These observations are in line with the general rule that octahedral $[M(\text{CO})_3\text{L}_3]$ complexes (L = planar N-donor heterocycle such as pyridine or azole) occur exclusively as the *fac* isomer.^{28,29} The spectra for **1** and **2** are in agreement with that reported for *fac*- $[\text{Mo}(\text{CO})_3(\text{Hpz})_3]$ (Hpz = pyrazole), which showed three strong absorptions at 1897, 1777 and 1730 cm^{-1} due to carbonyl stretching.²⁸ In Figure 5.2 the spectra of solid 1,2,3-trz and 1,2,4-trz are included for comparison. In the region containing the triazole ligand modes ($500\text{--}1600\text{ cm}^{-1}$), the spectra of **1** and **2** resemble those of the free ligand; this is especially noticeable for **1** and 1,2,3-trz. According to Haasnoot *et al.*, this is indicative of a monodentate triazole coordination mode rather than a bridging one.³⁰ For 1,2,3-trz, N3 is a better donor than N2²⁴, and therefore we may predict that in **1** the ligands are coordinated through N3. For structurally characterized complexes containing only monodentate 1,2,4-trz, the coordination is always through N4.³¹ These coordination modes are represented in Figure 5.1.

Chapter 5

The ^1H NMR spectrum of **1** reveal three signals corresponding to the triazole ring protons between 7.7-8.4 ppm (Figure 5.3). In the regions of 14-16 ppm, this spectrum containing signals due to 1,2,3-trz NH protons. The assignment of the ^1H -NMR spectrum is based on the coexistence of Mo-coordinated $1H$ (T- $1H$) and $2H$ (T- $2H$) annular tautomers of 1,2,3-trz, in correspondence with that known to exist for free 1,2,3-trz in the solid, liquid and gas phases^{32,33}.

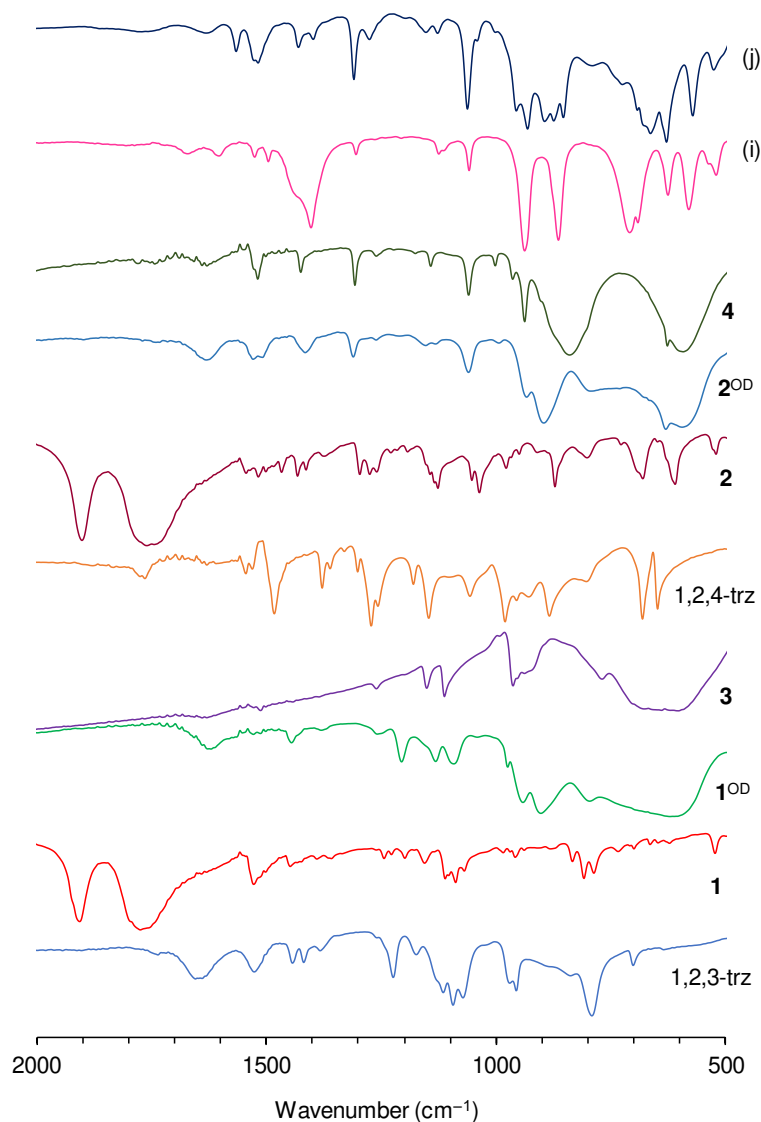


Figure 5.2. FT-IR spectra in the range of 500-2000 cm^{-1} of (a) 1,2,3-trz, (b) tricarbonyl complex **1**, (c) oxidized derivative **1^{OD}**, (d) hybrid **3**, (e) 1,2,4-trz, (f) tricarbonyl complex **2**, (g) oxidized derivative **2^{OD}**, (h) hybrid **4**, (i) dinuclear complex **5**, and (j) trinuclear complex **6²¹**.

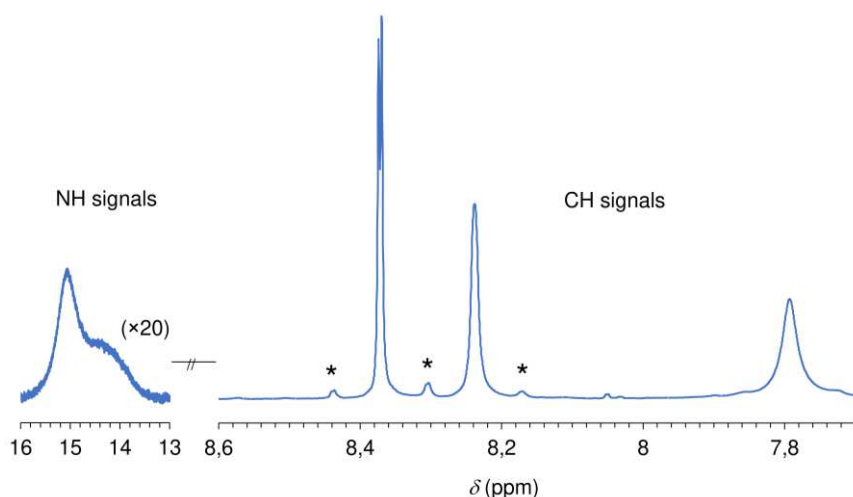


Figure 5.3. Regions of the ^1H NMR spectrum of **1** in $(\text{CD}_3)_2\text{CO}$ containing signals due to 1,2,3-trz NH and CH protons. The asterisks denote spinning sidebands.

5.2.2. Oxidative decarbonylation compounds from $[\text{Mo}(\text{CO})_3(1,2,3\text{-trz})_3]$ (1^{OD}) and $[\text{Mo}(\text{CO})_3(1,2,4\text{-trz})_3]$ (2^{OD})

Oxidative decarbonylation (OD) of **1** and **2** was carried out by the dropwise addition of 5–6 M TBHP (10 equiv.) in *n*-decane to a suspension of the tricarbonyl complex in CH_2Cl_2 . The resultant suspensions were filtered to isolate the solids referred to as 1^{OD} and 2^{OD} . For **1**, performing the reaction at ambient temperature for 4 h was sufficient to achieve complete decarbonylation (verified by the absence of CO stretching absorption bands in the FT-IR spectrum of the solid product). For the much less soluble complex **2**, a longer reaction time and higher temperature (70 °C, 48 h) were required to achieve complete decarbonylation. Microanalyses (CHN) and TGA data (Figure 5.4) for 1^{OD} were consistent with the composition $[\text{MoO}_3(\text{C}_2\text{H}_3\text{N}_3)] \cdot \text{H}_2\text{O}$.

The presence of a polymeric molybdenum oxide microstructure in 1^{OD} and 2^{OD} is supported by the FT-IR spectra which present several common features in the Mo–O stretching region (500–1000 cm^{-1}). The very broad band centered around 610 cm^{-1} for both compounds may be assigned to a $\nu_{\text{as}}(\text{Mo}–\text{O}–\text{Mo})$ vibration, while the strong bands near 900 and 940 cm^{-1} may be assigned to terminal $\nu(\text{Mo}=\text{O})$ stretching modes (Figure 5.2 c, g). The presence of a pair of $\nu(\text{Mo}=\text{O})$ bands is indicative of *cis*- $[\text{MoO}_2]^{2+}$ structural units, with the lower-energy band being the asymmetric vibration and the higher-energy band being the symmetric vibration.³⁴ For both 1^{OD} and 2^{OD} the pattern of bands in the Mo–O stretching region closely resembles that observed for the 1D hybrid molybdenum oxide/bipyridine materials $[\text{MoO}_3(2,2'\text{-bipy})]$ and $[\text{MoO}_3(\text{Hbpd})]$ (H_2bpd = 2,2'-bipyridine-5,5'-dicarboxylic acid), which display bands at 622/882/914 cm^{-1} and 576/901/922 cm^{-1} , respectively.^{18,35} An additional sharp band at 630 cm^{-1} for 2^{OD} (not

Chapter 5

observed for **1^{OD}**) is attributed to a 1,2,4-trz ring torsion vibration.³⁰ In a study of the infrared spectra of several transition metal 1,2,4-trz complexes, Haasnoot *et al.* determined that the presence of one ring torsion band in the 600-700 cm⁻¹ range, typically around 630 cm⁻¹, is indicative of 4-*H*,1,2-coordinating triazole rather than 1-*H*,2,4-coordinating triazole.³⁰ A similar band is observed for the layered hybrid [MoO₃(1,2,4-trz)_{0.5}] (**4**) (Figure 5.2 h). Accordingly, in the region containing triazole ligand modes (980-1600 cm⁻¹), the spectrum of **2^{OD}** closely resembles that of **4** (Figure 5.2 g, h), suggesting that the ligand adopts a similar coordination mode. The structure of **4**^{20,22} (and the isomorphous [MoO₃(1,2,3-trz)_{0.5}]²³ (**3**) consists of layers of corner-sharing {MoO₅N} octahedra composed of one terminal Mo=O group, four bridging Mo-O_b groups, and one N atom from a 1,2-bicoordinating triazole ligand that forms single [Mo(VI)–(N–N)–Mo(VI)] bridges (Figure 5.1). The layered perovskite-like structure in **4** gives rise to two very broad ν(Mo–O–Mo) absorption bands near 600 and 840 cm⁻¹, whereas **2^{OD}** (and **1^{OD}**) only displays one band around 610 cm⁻¹. Both **2^{OD}** and **4** exhibit a medium-intensity band near 1310 cm⁻¹ that is assigned to a CH-bending vibration.³⁰ The shift of this band towards higher-energy (vs. 1272 cm⁻¹ for solid 1,2,4-trz (Figure 5.2 e) and 1275 cm⁻¹ for **2** (Figure 5.2 f) is another marker for bidentate triazole.³⁰ From these observations we may tentatively propose chain-like structures for **1^{OD}** and **2^{OD}** consisting of corner-sharing {MoO₄N₂} octahedra composed of two terminal Mo=O groups, two bridging Mo-O_b groups, and two N atoms from two 1,2-bicoordinating triazole ligands that form single bridges between adjacent Mo(VI) centers (Figure 5.1). This type of structural element has recently been identified in the trinuclear complex (1,2,4-Htrz)₂[Mo₃O₆(O₂)₄(1,2,4-trz)₂]·H₂O (**6**) (Figure 5.1).²¹ The 1D chain-like structural motif is analogous to that found for [MoO₃(2,2'-bipy)]³⁶ and [MoO₃(HbpdC)]³⁵, which contain {MoO₂(μ₂-O)₂(bipy)} repeat units.

A satisfactory match was obtained between the PXRD pattern of the microcrystalline hybrid **3** and a simulated pattern calculated using the crystallographic data published for the structure of [MoO₃(1,2,3-trz)_{0.5}] (Figure 5.5).²³

Chapter 5

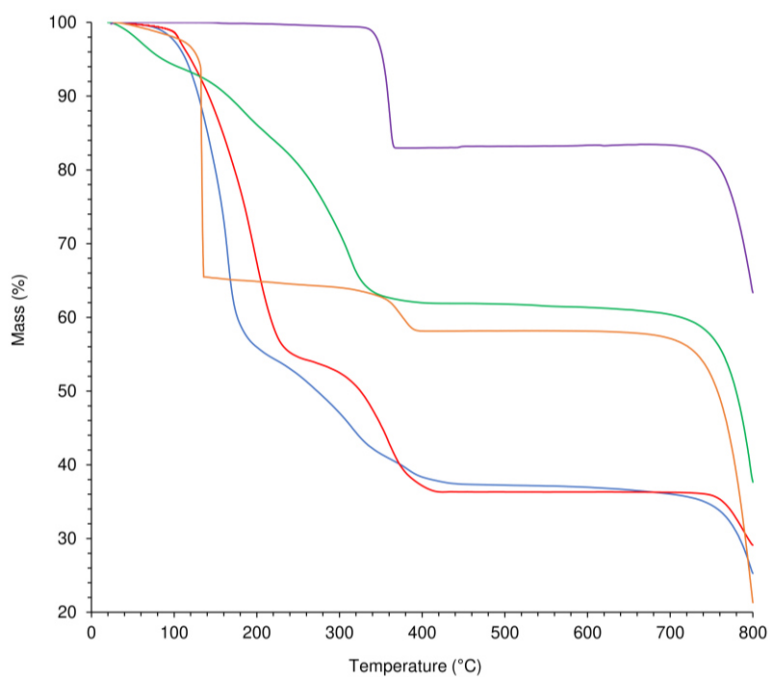


Figure 5.4. TGA curves for **1** (—), **2** (—), **1^{OD}** (—), **3** (—), and **5** (—).

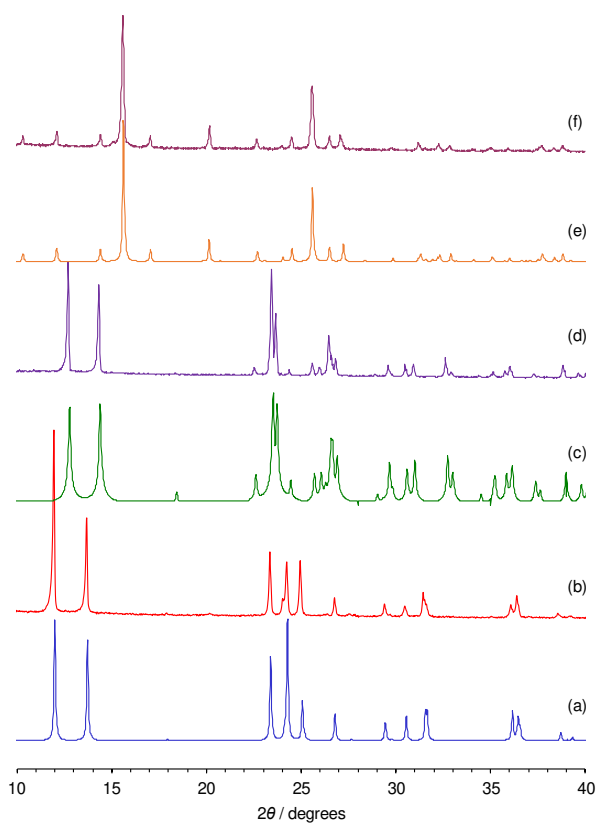


Figure 5.5. Computed (a, c, e) and experimental (b, d, f) PXRD patterns of (a, b) $[\text{MoO}_3(1,2,3\text{-trz})_{0.5}]$ (**3**), (c, d) $[\text{MoO}_3(1,2,4\text{-trz})_{0.5}]$ (**4**), and (e, f) $(\text{NH}_4)_{1.8}(\text{H}_3\text{O})_{0.2}[\text{Mo}_2\text{O}_2(\mu_2\text{-O})(\text{O}_2)_4(1,2,4\text{-trz})]\cdot\text{H}_2\text{O}$ (**5**). The program Mercury was used to generate the computed patterns from the crystal structure data published for **3** and **4**, and the data reported in this work for **5**.

Chapter 5

The $^{13}\text{C}\{^1\text{H}\}$ CP MAS NMR spectra of $\mathbf{1}^{\text{OD}}$ and $\mathbf{2}^{\text{OD}}$ provided further support for a bidentate bridging coordination of triazole molecules through the 1,2-nitrogen sites, analogous to that present in the hybrids $\mathbf{3}$ and $\mathbf{4}$ (Figure 5.6). As expected, the 1,2,3-trz layered hybrid $\mathbf{3}$ displays two peaks for the non-equivalent carbon atoms C4 (128.1 ppm) and C5 (133.3 ppm), while the 1,2,4-trz hybrid $\mathbf{4}$ displays a single peak at 145.5 ppm attributed to C3 and C5, which are chemically equivalent due to the N1,N2 bridging mode (Figure 5.6 b, e). The spectra of $\mathbf{1}^{\text{OD}}$ and $\mathbf{2}^{\text{OD}}$ (Figure 5.6 a, d) resemble those for $\mathbf{3}$ and $\mathbf{4}$, respectively, since $\mathbf{1}^{\text{OD}}$ displays two peaks at 127.0 (C4) and 134.8 ppm (C5), while $\mathbf{2}^{\text{OD}}$ displays one main peak centered at 143.9 ppm (C3, C5). The observation of broader resonances for $\mathbf{1}^{\text{OD}}$ and $\mathbf{2}^{\text{OD}}$ when compared with $\mathbf{3}$ and $\mathbf{4}$ may be partly due to a higher degree of structural disorder for the former, since these solids were found by PXRD to be X-ray amorphous (not shown), while the layered hybrids are obtained as microcrystalline solids.

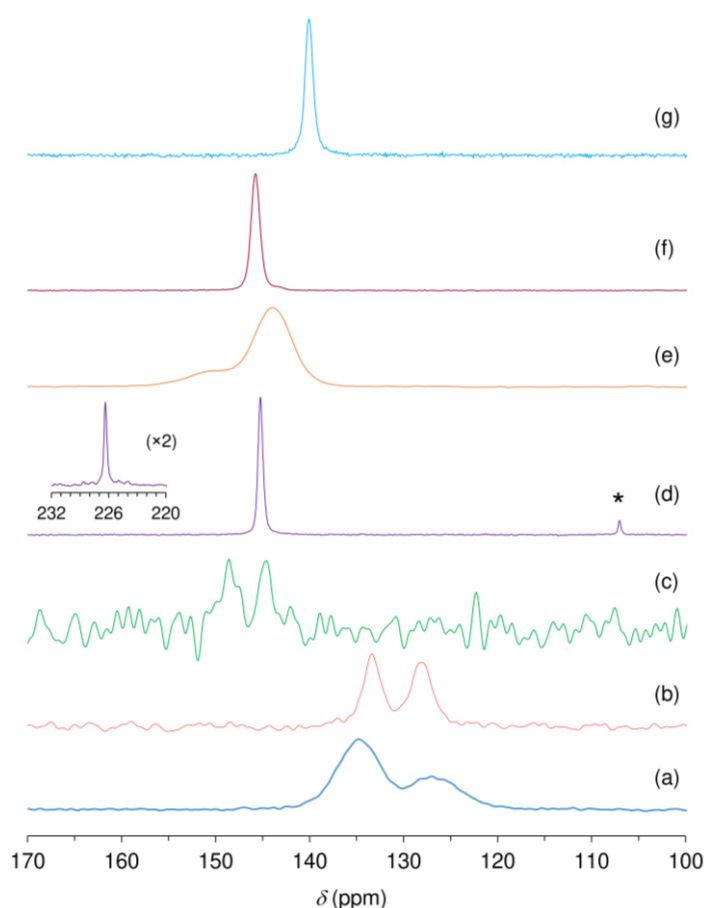


Figure 5.6. $^{13}\text{C}\{^1\text{H}\}$ CP MAS NMR spectra of (a) $\mathbf{1}^{\text{OD}}$, (b) $\mathbf{3}$, (c) 1,2,4-trz, (d) $\mathbf{2}$, (e) oxidized derivative $\mathbf{2}^{\text{OD}}$, (f) $\mathbf{4}$, and (g) $\mathbf{5}$. The inset shows the single ^{13}C resonance observed for the CO groups of $\mathbf{2}$ (d). The asterisk denotes a spinning sideband.

Chapter 5

5.2.3. Dinuclear complex $(\text{NH}_4)_{1.8}(\text{H}_3\text{O})_{0.2}[\text{Mo}_2\text{O}_2(\mu_2\text{-O})(\text{O}_2)_4(1,2,4\text{-trz})]\cdot\text{H}_2\text{O}$ (**5**)

The discovery that the layered hybrid $[\text{MoO}_3(1,2,4\text{-trz})_{0.5}]$ (**4**) could be used as a reaction-induced self-separating catalyst²⁰ emphasized the need to study the solution chemistry and to characterize oxo(peroxo)molybdenum(VI)-triazole complexes, which had not been previously reported. The first species to be isolated and structurally characterized was the yellow trinuclear complex $(1,2,4\text{-Htrz})_2[\text{Mo}_3\text{O}_6(\text{O}_2)_4(1,2,4\text{-trz})_2]$ (**6**), which precipitated upon addition of 1,2,4-trz to the solution obtained by reaction of MoO_3 with excess aq. H_2O_2 (in the absence of organic solvents).²¹ In the present work, further reactivity studies were performed in which **4** or **6** were treated with excess H_2O_2 in the presence of acetonitrile. Both reactions led to yellow solutions from which the dinuclear complex $(\text{NH}_4)_{1.8}(\text{H}_3\text{O})_{0.2}[\text{Mo}_2\text{O}_2(\mu_2\text{-O})(\text{O}_2)_4(1,2,4\text{-trz})]\cdot\text{H}_2\text{O}$ (**5**) crystallized. The FT-IR spectrum of **5** pointed to the unexpected formulation with the appearance of a strong band near 1400 cm^{-1} assigned to an NH bending vibration of NH_4^+ ions (Figure 5.2). Two possible explanations for the presence of ammonium ions are the hydrolysis of CH_3CN and the oxidative degradation of 1,2,4-trz.

The IR spectrum of **5** displays additional diagnostic bands at 520 , 579 and 625 cm^{-1} ($\nu(\text{Mo}(\text{O}_2)_2)$) and/or trz ring-torsion), 709 cm^{-1} [$\nu_{\text{as}}(\text{Mo}-\text{O}-\text{Mo})$], 864 cm^{-1} [$\nu(\text{O}-\text{O})$], and 937 cm^{-1} [$\nu(\text{Mo}=\text{O})$]. The solid-state $^{13}\text{C}\{^1\text{H}\}$ CP MAS NMR spectrum of **5** displays one single sharp resonance at 140.0 ppm assigned to C3 and C5 carbon atoms (Figure 5.6 f). The spectrum resembles that for the hybrid **4** (Figure 5.6 e) except that in the former the resonance is shifted by 5.7 ppm towards higher field. These data point to the presence of a triazole N1,N2 bridging mode in **5**, analogous to that present in **4**, and this was subsequently confirmed by X-ray crystallographic studies.

A satisfactory match was obtained between the PXRD pattern of the microcrystalline complex **5** and the simulated pattern calculated using the crystal structure data (Figure 5.5).

5.2.4. Single-crystal X-ray structure analyses of **5**

The crystal structure of **5** reveals the presence of a centrosymmetric dinuclear anionic complex in which the mirror plane of the $Pn\text{nm}$ orthorhombic space group bisects the entire molecular unit. Within this mirror plane the crystal structure contains both the charge-balancing ammonium and hydronium cations as well as the water molecule of crystallization (not shown).

Chapter 5

The anionic $[\text{Mo}_2\text{O}_2(\mu_2\text{-O})(\text{O}_2)_4(1,2,4\text{-trz})]^{2-}$ complex is built up from a single Mo(VI) metal center which is coordinated to a μ_2 -bridging oxo group (also located on the mirror plane), a terminal oxo moiety, two peroxy ligands, and one nitrogen atom from a N,N-bridging triazole molecule as depicted in Figure 5.7. Taking the centers of gravity of the peroxy ligands as the coordinative positions, the overall coordination geometry resembles a slightly distorted bipyramid. Considering the equatorial plane of the polyhedron as being formed by the peroxy ligands and the μ_2 -bridging oxo group, the metal center appears raised towards the apical oxo moiety by ca. 0.35 Å. This latter group clearly exerts the well-known *trans* effect on the opposite coordinative bond to the N,N-bridging triazole molecule, with the refined Mo–N distance being 2.398(9) Å. This organic linker imposes a “kink” angle in the anionic dinuclear complex of 141.7(5)° and a Mo···Mo distance of 3.6731(5) Å.

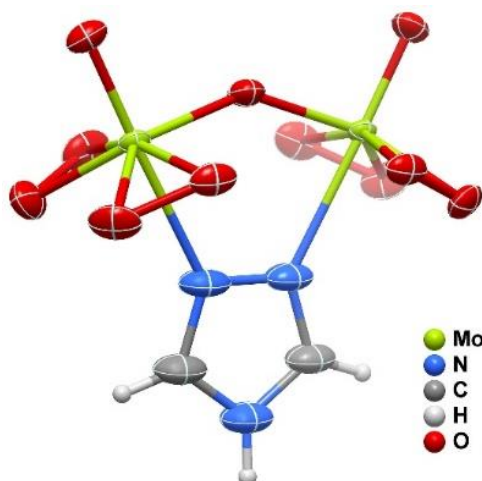


Figure 5.7. Schematic representation of the anionic dinuclear $[\text{Mo}_2\text{O}_2(\mu_2\text{-O})(\text{O}_2)_4(1,2,4\text{-trz})]^{2-}$ complex present in the crystal structure of **5**. Non-hydrogen atoms are depicted as thermal ellipsoids drawn at the 50 % probability level and hydrogen atoms as small spheres with arbitrary radii.

5.3. Catalytic studies

5.3.1. Catalytic epoxidation of *cis*-cyclooctene with TBHP

The tricarbonyl complexes **1** and **2** were tested as catalyst precursors for the epoxidation of *cis*-cyclooctene (Cy) with TBHP at 70 °C, using α,α,α -trifluorotoluene (TFT) as a co-solvent (Table 5.1, Figure 5.8). Complex **1** bearing 1,2,3-trz led to a faster epoxidation reaction than complex **2** bearing 1,2,4-trz, with cyclooctene oxide

Chapter 5

(CyO) always being the only product formed (100 % selectivity): **1** led to 99 % conversion at 2 h, while **2** led to 60 % conversion. The very favorable catalytic performance obtained using **1** is on a par with that reported previously for the complex $[\text{Mo}(\text{CO})_3(\text{HC}(\text{pz})_3)]$ ($\text{HC}(\text{pz})_3$ = tris(1-pyrazolyl)methane), which led to 99 % CyO yield after 2 h reaction at 55 °C (1,2-dichloroethane as co-solvent).³⁷ The latter tricarbonyl complex was shown to undergo oxidative decarbonylation *in situ*, possibly leading to hexamolybdate species ($\text{Mo}_6\text{O}_{19}^{2-}$) and/or an oxo-bridged dinuclear complex of the type $[\{\text{MoO}_2(\text{HC}(\text{pz})_3)\}_2(\mu\text{-O})]^{2+}$.

The compounds **1**^{OD} and **2**^{OD} were tested as catalysts for Cy epoxidation and were found to be more active than the corresponding tricarbonyl precursors: **1**^{OD} led to 97 % Cy conversion at 30 min, while **2**^{OD} led to 96 % conversion at 6 h (Table 5.1, Figure 5.8). These results may be partly due to the involvement of an additional OD step when starting from the pre-catalysts, which is required for the formation of the active oxidizing species. This may retard the initial epoxidation reaction in relation to the direct use of the oxidized metal species (which avoids the *in situ* OD step).

The catalytic performance of the oxidized compounds **1**^{OD} and **2**^{OD} was found to be greatly superior to that for the layered hybrids **3** and **4**: compound **3** led to 83 % / 100 % Cy conversion at 6 h/24 h, while **4** led to 54 % / 91 % conversion (Table 5.1, Figure 5.8).

Table 5.1. Catalytic results for the epoxidation of *cis*-cyclooctene.^a

Compound	Oxidant	Conv. or epoxide yield at 1 h/6 h/24 h (%) ^b
1	TBHP	91/100/-
2	TBHP	34/76/96
1 ^{OD}	TBHP	100/-/-
2 ^{OD}	TBHP	43/96/98
3	TBHP	24/83/100
4	TBHP	3/54/91
1	H ₂ O ₂	-/77/93
2	H ₂ O ₂	-/75/100
1 ^{OD}	H ₂ O ₂	-/53/92
2 ^{OD}	H ₂ O ₂	-/64/94
3	H ₂ O ₂	-/62/73
4	H ₂ O ₂	-/90/98 ¹¹

^a Reaction conditions: Initial molar ratio Mo: Cy: oxidant = 1:100:153, $[\text{Cy}]_0 = 1.0$ M, 2 mL co-solvent (TFT for TBHP and CH₃CN for H₂O₂), 70 °C. ^b Cyclooctene oxide (CyO) yield (selectivity was 100 %). Blank reactions (no catalyst): Less than 7 % CyO yield at 24 h with TBHP; negligible Cy reaction with H₂O₂.

5.3.2. Characterization of solids after catalytic epoxidation of Cy with TBHP

For complexes **1** and **2**, the ATR FT-IR spectra of undissolved solids recovered after batch catalytic runs of 24 h (denoted **1^r** and **2^r**) very strongly resembled those of **1^{OD}** and **2^{OD}**, suggesting that oxomolybdenum(VI)-triazole compounds were formed under the catalytic conditions and that these were structurally very similar to those obtained upon treatment of **1** and **2** with excess TBHP (Figure 5.9). After batch catalytic runs of 24 h with **1^{OD}** and **2^{OD}**, the resultant undissolved solids (**1^{ODr}** and **2^{ODr}**) were recovered and characterized by ATR FT-IR spectroscopy (Figure 5.9). The spectra were unchanged from those for the starting materials **1^{OD}** and **2^{OD}**, showing that these underwent no further conversion to a structurally different solid phase. In parallel with that observed for **1^{OD}** and **2^{OD}**, ATR FT-IR spectra for the undissolved solids recovered after batch catalytic runs of 24 h (**3^r** and **4^r**) did not differ significantly from those for the starting materials **3** and **4** (Figure 5.9). The better catalytic activity of the 1,2,3-trz hybrid in relation to the 1,2,4-trz hybrid is in line with the results obtained with **1** and **2**, and **1^{OD}** and **2^{OD}**. This apparent ligand influence on the epoxidation activity with TBHP may be partly due to solubility effects, with 1,2,3-trz leading to metal species with enhanced solubility.

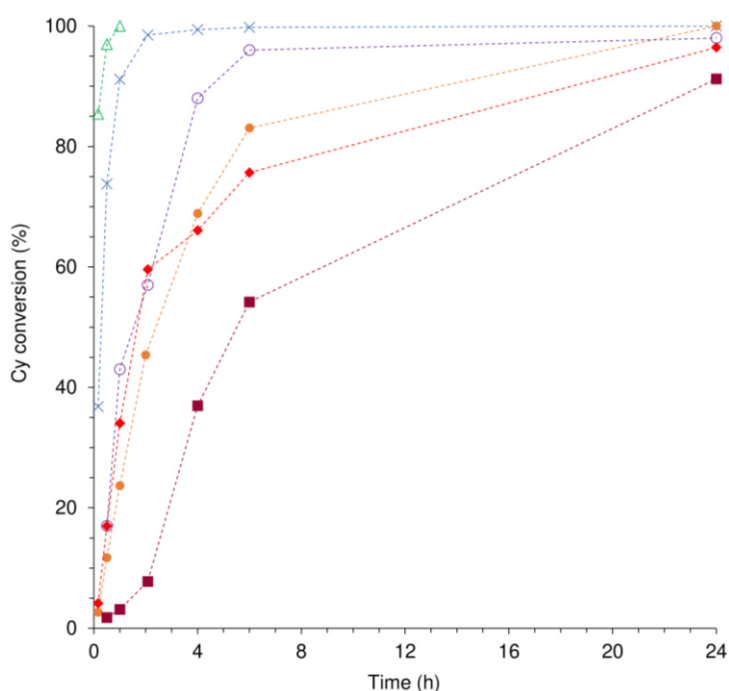


Figure 5.8. Kinetic profiles for the reaction of Cy with TBHP, in the presence of **1** (x), **2** (♦), **1^{OD}** (Δ), **2^{OD}** (○), **3** (●) and **4** (■), at 70 °C. The CyO selectivity was always 100 %. The dashed lines are visual guides.

5.3.3. Catalytic epoxidation with H₂O₂

The catalytic performance of all compounds for Cy epoxidation was subsequently studied using H₂O₂ as the oxidant instead of TBHP, with acetonitrile as the co-solvent instead of TFT (Table 5.1). With the notable exception of the layered hybrid **4**, the reaction kinetics was generally slower using H₂O₂ than TBHP, suggesting that the former oxidizing medium led to the formation of less active (and different) metal species. In contrast to that seen with TBHP as oxidant (comparing **1** vs. **2**, and **1**^{OD} vs. **2**^{OD}), changing the ligand had no considerable influence on catalytic performance with H₂O₂, since **1** and **2** led to (75-77 %)/(93-100 %) conversion at 6 h/24 h, while **1**^{OD} and **2**^{OD} led to (53-64 %)/(92-94 %) conversion. For all four compounds the liquid phases of the H₂O₂-based reactions mixtures were yellow, while the TBHP-based ones were colorless. Attempts to isolate compounds from the yellow solutions were unsuccessful, possibly because the dissolved species were very strongly solvated. With the layered hybrids, **4** led to much better performance than **3** with H₂O₂ as oxidant, while the opposite was the case with TBHP. As described previously, the hybrid **4** displays unique behavior with H₂O₂ as a reaction-induced self-separating (RISS) catalyst.¹¹ Under the catalytic conditions, the RISS catalyst transforms into soluble metal species, giving a homogeneous mixture. Upon consumption of the oxidant, the soluble species convert reversibly into the original form of the catalyst, which precipitates and can be easily separated from the reaction mixture. Both **3** and **4** lead to yellow homogeneous solutions under the reaction conditions used for Cy epoxidation with H₂O₂. However, although **3** and **4** possess isomorphous solid-state structures, the hybrid **3** did not display RISS behavior, *i.e.* no precipitate formed upon completion of the reaction and consumption of the oxidant.

The yellow solutions formed by reaction of **3** and **4** with H₂O₂ under the Cy epoxidation conditions are assumed to contain discrete molecular oxoperoxomolybdenum(VI) complexes. In the case of 1,2,4-trz, these may only be stable in the presence of excess oxidant, *i.e.* the consumption of the oxidant promotes a reverse reaction in which the molecular species recombine to form the layered hybrid **4**. For 1,2,3-trz, this reverse reaction does not take place, which may be partly due to differences in the structure and solubility of the soluble active species, pointing to a significant ligand effect despite the subtle structural differences between the two isomeric triazoles. Attempts to isolate species from the solution obtained from **3** were not successful, suggesting that they may be strongly solvated. As mentioned above, Antunes *et al.* were previously successful in isolating the trinuclear complex **6** from a MoO₃/1,2,4-trz/H₂O₂ mixture.²¹ The catalytic performance of **6** for Cy epoxidation with

Chapter 5

H₂O₂ at 70 °C in the presence of CH₃CN (92 % / 99 % CyO yield at 6 h/24 h) was comparable with that for **4**, and accordingly it was found that the undissolved solid present at the end of the catalytic reaction was microcrystalline **4**, *i.e.* **6** converted *in situ* to **4**.²¹ These observations prompted our studies in the present work on the treatment of **4** and **6** with excess aq. H₂O₂ in the presence of CH₃CN, which led to the isolation of the dinuclear complex **5** from yellow solutions. The catalytic performance of complex **5** for Cy epoxidation with aq. H₂O₂ at 70 °C (39 % CyO yield at 24 h) was inferior to that for **4** and **6** (90-92 % yield). Nevertheless, these studies suggest that dinuclear or trinuclear oxoperoxomolybdenum(VI) complexes bearing bridging triazole ligands are likely to be the homogeneous catalysts responsible for activating the oxidant for olefin epoxidation when using the hybrids **3** and **4** as pre-catalysts.

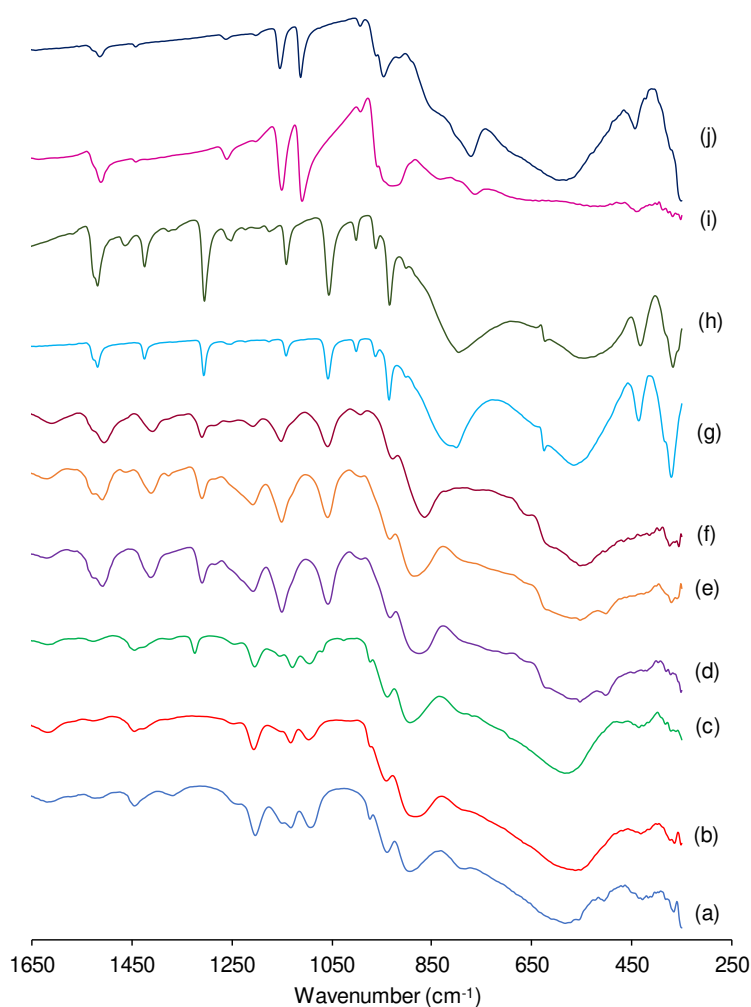
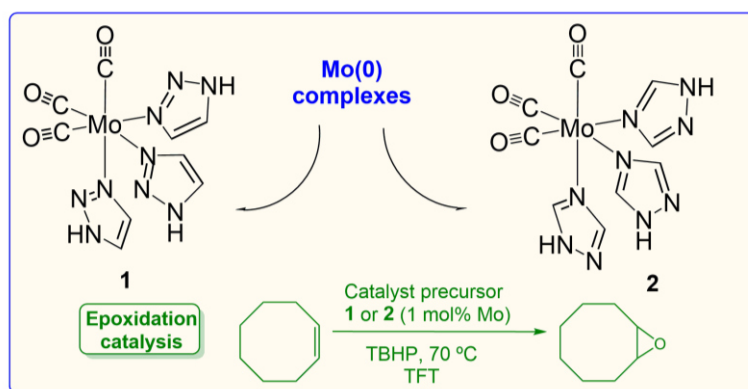


Figure 5.9. ATR FT-IR spectra in the range of 350-1600 cm⁻¹ of (a) **1**^{OD}, (b) recovered solid **1**^{ODr}, (c) recovered solid **1**^r, (d) **2**^{OD}, (e) recovered solid **2**^{ODr}, (f) recovered solid **2**^r, (g) hybrid **3**, (h) recovered solid **3**^r, (i) hybrid **4**, and (j) recovered solid **4**^r.

5.4. Conclusions

The main advances made in the present work can be summarized as follows: (i) synthesis of molybdenum tricarbonyl complexes with the two isomeric unsubstituted triazoles; (ii) use of the tricarbonyl complexes as precursors to molybdenum oxide-triazole hybrids; (iii) demonstration of ligand effects in Mo-catalyzed olefin epoxidation using either the tricarbonyl precursors directly or the oxidized derivatives (Scheme 5.1); (iv) synthesis and X-ray structure determination of a new oxoperoxomolybdenum(VI) complex bearing 1,2,4-triazole ligands, which provides a valuable insight into the type of solution species that may be involved in the H₂O₂-based processes with Mo-triazole catalysts. Based on the results obtained, molybdenum compounds with 1,2,3-triazole are promising and warrant further investigation for a broader range of oxidation reactions such as sulfoxidation and the oxidation of amines.



Scheme 5.1. Summary of the main syntheses and catalytic studies carried out in this work.

5.5. References

- (1) Abrantes, M.; Santos, A. M.; Mink, J.; Kühn, F. E.; Romão, C. C. *Organometallics* **2003**, *22*, 2112–2118.
- (2) Kühn, F. E.; Santos, M.; Abrantes, A. M. *Chem. Rev.* **2006**, *106*, 2455–2475.
- (3) Sanz, R.; Pedrosa, M. R. *Curr. Org. Synth.* **2009**, *6*, 239–263.
- (4) Amini, M.; Haghdoost, M. M.; Bagherzadeh, M. *Coord. Chem. Rev.* **2013**, *257*, 1093–1121.
- (5) Barlan, A. U.; Basak, A.; Yamamoto, H. *Angew. Chem., Int. Ed.* **2006**, *45*, 5849–5852.
- (6) Zong, L.; Wang, C.; Moeljadi, A. M. P.; Ye, X.; Ganguly, R.; Li, Y.; Hirao, H.; Tan, C. H. *Nat. Commun.* **2016**, *7*, 1–7.
- (7) Romano, F.; Linden, A.; Mba, M.; Zonta, C.; Licini, G. *Adv. Synth. Catal.* **2010**, *352*,

Chapter 5

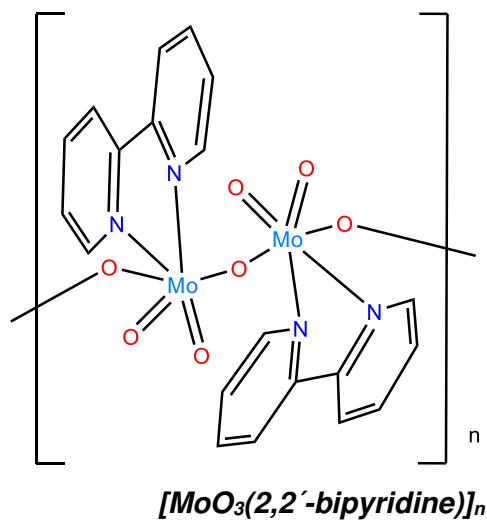
- 2937–2942.
- (8) Meninno, S.; Parrella, A.; Brancatelli, G.; Geremia, S.; Gaeta, C.; Talotta, C.; Neri, P.; Lattanzi, A. *Org. Lett.* **2015**, *17*, 5100–5103.
 - (9) Shylesh, S.; Schweizer, J.; Demeshko, S.; Schünemann, V.; Ernst, S.; Thiel, W. R. *Adv. Synth. Catal.* **2009**, *351*, 1789–1795.
 - (10) Zhou, M. D.; Liu, M. J.; Huang, L. L.; Zhang, J.; Wang, J. Y.; Li, X. B.; Kühn, F. E.; Zang, S. L. *Green Chem.* **2015**, *17*, 1186–1193.
 - (11) Amarante, T. R.; Neves, P.; Valente, A. A.; Paz, F. A. A.; Pillinger, M.; Gonçalves, I. S. *J. Catal.* **2016**, *340*, 354–367.
 - (12) Ahmad, M. A. A.; Veljanovski, D.; Capapé, A.; Zhao, J.; Herdtweck, E.; Calhorda, M. J.; Kühn, F. E. *Organometallics* **2009**, *28*, 639–645.
 - (13) Veiros, L. F.; Gamelas, C. A.; Calhorda, M. J.; Romão, C. C. *Organometallics* **2011**, *30*, 1454–1465.
 - (14) Brégeault, J. M. *J. Chem. Soc. Dalt. Trans.* **2003**, *3*, 3289–3302.
 - (15) Martins, A. M.; Romão, C. C.; Abrantes, M.; Azevedo, M. C.; Cui, J.; Dias, A. R.; Duarte, M. T.; Lemos, M. A.; Lourenço, T.; Poli, R. *Organometallics* **2005**, *24*, 2582–2589.
 - (16) Li, S.; Kee, C. W.; Huang, K.; Hor, T. S. A.; Zhao, J. *Organometallics* **2010**, *29*, 1924–1933.
 - (17) Neves, P.; Amarante, T. R.; Gomes, A. C.; Coelho, A. C.; Gago, S.; Pillinger, M.; Gonçalves, I. S.; Silva, C. M.; Valente, A. A. *Appl. Catal., A* **2011**, *395*, 71–77.
 - (18) Amarante, T. R.; Neves, P.; Coelho, A. C.; Gago, S.; Valente, A. A.; Paz, F. A.; Pillinger, M.; Gonçalves, I. S. *Organometallics* **2010**, *29*, 883–892.
 - (19) Neves, P.; Nogueira, L. S.; Valente, A. A.; Pillinger, M.; Gonçalves, I. S.; Sampaio-Dias, I. E.; Sousa, C. A. D.; Rizzo-Aguiar, F.; Rodríguez-Borges, J. E. *J. Organomet. Chem.* **2018**, *858*, 29–36.
 - (20) Amarante, T. R.; Neves, P.; Valente, A. A.; Paz, F. A. A.; Pillinger, M.; Gonçalves, I. S. *J. Catal.* **2016**, *340*, 354–367.
 - (21) Antunes, M. M.; Amarante, T. R.; Valente, A. A.; Almeida Paz, F. A.; Gonçalves, I. S.; Pillinger, M. *ChemCatChem* **2018**, *10*, 2782–2791.
 - (22) Hagrman, P. J.; LaDuca, R. L.; Koo, H. J.; Rarig, R.; Haushalter, R. C.; Whangbo, M. H.; Zubieta, J. *Inorg. Chem.* **2000**, *39*, 4311–4317.
 - (23) Chuang, J.; Ouellette, W.; Zubieta, J. *Inorg. Chim. Acta* **2008**, *361*, 2357–2364.
 - (24) Huang, D.; Zhao, P.; Astruc, D. *Coord. Chem. Rev.* **2014**, *272*, 145–165.
 - (25) Zurro, M.; Mancheño, O. G. *Chem. Rec.* **2017**, *17*, 485–498.
 - (26) Liu, K.; Shi, W.; Cheng, P. *Dalt. Trans.* **2011**, *40*, 8475–8490.
 - (27) Allis, D. G.; Burkholder, E.; Zubieta, J. *Polyhedron* **2004**, *23*, 1145–1152.
 - (28) Ardizzioia, G. A.; Brenna, S.; LaMonica, G.; Maspero, A.; Masciocchi, N. *J. Organomet. Chem.* **2002**, *649*, 173–180.
 - (29) Pérez, J.; Riera, L. *Chem. Commun.* **2008**, *8*, 533–543.
 - (30) Haasnoot, J. G.; Vos, G.; Groeneveld, W. L. *Z. Naturforsch.* **1977**, *32b*, 1421–1430.

Chapter 5

- (31) Haasnoot, J. G. *Coord. Chem. Rev.* **2000**, 200–202, 131–185.
- (32) Lunazzi, L.; Parisi, F.; Macciantelli, D. *J. Chem. Soc.* **1984**, 1025.
- (33) Bellagamba, M.; Bencivenni, L.; Gontrani, L.; Guidoni, L.; Sadun, C. *Struct. Chem.* **2013**, 24, 933–943.
- (34) Coelho, A. C.; Nolasco, M.; Balula, S. S.; Antunes, M. M.; Pereira, C. C. L.; Almeida Paz, F. A.; Valente, A. A.; Pillinger, M.; Ribeiro-Claro, P.; Klinowski, J.; Gonçalves, I. S. *Inorg. Chem.* **2011**, 50, 525–538.
- (35) Amarante, T. R.; Neves, P.; Valente, A. A.; Almeida Paz, F. A.; Fitch, A. N.; Pillinger, M.; Gonçalves, I. S. *Inorg. Chem.* **2013**, 52, 4618–4628.
- (36) Zapf, P. J.; Haushalter, R. C.; Zubieta, J. *Chem. Mater.* **1997**, 4756, 2019–2024.
- (37) Gomes, A. C.; Neves, P.; Figueiredo, S.; Fernandes, J. A.; Valente, A. A.; Almeida, F. A.; Pillinger, M.; Lopes, A. D.; Gonçalves, I. S. **2013**, 370, 64–74.

CHAPTER 6

High-yield synthesis and catalytic response of chainlike hybrid materials of the $[(\text{MoO}_3)_m(2,2'\text{-bipyridine})_n]$ family



Chapter 6

Index

6.1. Introduction	161
6.2. Results and discussion	162
6.2.1. Synthesis and characterization of complexes $[\text{MoO}_3(2,2'\text{-bipy})]_n$, $[\text{Mo}_2\text{O}_6(2,2'\text{-bipy})]_n$ and $[\text{Mo}_3\text{O}_9(2,2'\text{-bipy})_2]_n$	162
6.3. Catalytic studies	171
6.3.1. Catalytic epoxidation of <i>cis</i> -cyclooctene with TBHP	171
6.3.2. Catalytic epoxidation of <i>cis</i> -cyclooctene with H_2O_2	175
6.3.3. Characterization of solids after catalytic epoxidation	175
6.3.4. Catalytic epoxidation of other cyclic and linear non-functionalized olefins	179
6.3.5. Catalytic epoxidation of the biomass-derived olefins	180
6.3.6. Acid catalysis	181
6.4. Conclusions	184
6.5. References	185

Chapter 6

6.1. Introduction

The oxides and oxide-hydrates of molybdenum display a rich variety of structural types and have been extensively studied for applications in catalysis, solar energy conversion, batteries, semiconductors and electronics, amongst others.^{1,2} The thermodynamically stable form of molybdenum trioxide, α -MoO₃, has an orthorhombic structure consisting of distorted {MoO₆} octahedra that share edges and corners to form two dimensional (2D) MoO₃ sheets separated in the lattice by van der Waals gaps.^{1,3} The unique layered structure of α -MoO₃ permits topotactic redox chemistry involving the intercalation of small ions (*e.g.* alkali metal cations and H⁺) and a partial reduction of the Mo oxidation state.^{4,5} Protons intercalate to give hydrogen molybdenum bronzes (HMB) H_xMoO₃ (0 < x ≤ 2) with metallic features and molybdenum/oxygen frameworks that are almost unchanged as compared to the host lattice MoO₃.^{6–8} HMB can react further in a topotactic fashion with Lewis bases (L) such as pyridine (py) to give the layered intercalation compound py_{0.3}H_{0.5}MoO₃.⁹ On the other hand, when excess pyridine is heated with α -MoO₃ under anhydrous conditions, the structure of the MoO₃ layers completely changes and a different phase is obtained ([MoO₃(py)]) in which {MoO₅N} octahedra share corners with four other octahedra to form infinite molybdenum oxide sheets with alternate apical arrangements of Mo–N(py) and Mo=O.¹⁰ Performing the intercalation reaction with 4,4'-bipyridine led to the compound formulated as [MoO₃(4,4'-bipy)_{0.5}] which was proposed to possess an analogous structure with the difference that the organic ligand acts as a pillar cross-linking adjacent layers.¹⁰

The compounds [MoO₃(py)] and [MoO₃(4,4'-bipy)_{0.5}] were the first members of a class of hybrid materials that have been termed metal oxide–organic frameworks or coordination polymers.^{11–13} These compounds are distinguished by having an extended metal oxide component decorated by organic ligands (frequently an organoamine or organocarboxylate). The organic ligands play a critical role in dictating the inorganic oxide substructure. The original syntheses of [MoO₃(py)] and [MoO₃(4,4'-bipy)_{0.5}] were tedious, involving long reaction times of two to four weeks, elevated temperatures (160–250 °C), and intermediate regrinding of the solid phase.¹⁰ In later years the techniques of hydrothermal synthesis were found to be much more effective for the isolation of novel hybrid materials based on metal oxides. Zubieta and coworkers confirmed the structure of [MoO₃(4,4'-bipy)_{0.5}] by isolating single-crystals of the compound through the hydrothermal reaction of MoO₃ with 4,4'-bipy at 150 °C.¹⁴ The layered perovskite-like motif found in this compound and in [MoO₃(py)] has also been identified in the tungsten isostructures¹⁵ and in the hybrid materials [MO₃(pyrazine)_{0.5}]

Chapter 6

(M = Mo, W)^{15–17}, [WO₃(1,2-bipyridylethane)]¹⁷, [MO₃(trz)_{0.5}] (M = Mo, W; trz = 1,2,3-triazole or 1,2,4-triazole)^{14,18,19}, and [MoO₃(3,8-phenanthroline)_{0.5}]²⁰. Chelating ligands such as 2,2'-bipy tend to restrict the oxide dimensionality to chains or ribbons since their coordination blocks at least two condensation sites on the same metal center.^{21–24} In the case of 2,2'-bipy, a hydrothermal synthesis led to the compound [MoO₃(2,2'-bipy)], which has a structure consisting of 1D chains of corner-sharing distorted {MoO₄N₂} octahedra.²¹ By variation of the synthesis conditions, derivatives of this 1D polymer have been obtained in which the repeat unit consists of one {MoO₄} tetrahedron and either one, two or three {MoO₄N₂} octahedra.^{21,22}

Hydrothermal methods for the preparation of molybdenum oxide–organoamine hybrid materials suffer from common problems such as low yields and the formation of mixtures that must be mechanically separated. In this group, it has been explored alternative approaches involving the use of metallo-organic complexes as synthesis precursors.^{25–27} The oxidative decarbonylation of molybdenum carbonyl complexes under mild conditions has proved to be a particularly useful technique and, in the case of the tetracarbonyl complex *cis*-[Mo(CO)₄(2,2'-bipy)], allowed the isolation of [MoO₃(2,2'-bipy)]_n (**1**) in near quantitative yield.²⁵ Polymeric **1** has given interesting results as a catalyst for the epoxidation of olefins²⁵, the oxidation of secondary amines to nitrones²⁸, and the oxidation of sulfides to sulfoxides or sulfones²⁸. The existence of the bipy-deficient derivatives of **1** provides a potential avenue for systematically studying structure–performance relationships with respect to the use of the compounds in catalysis. With this in mind, in this chapter it was sought to improve syntheses of these hybrid materials to make them readily available for catalytic investigations. The synthetic advances reported herein comprise the use of polymeric **1** as a starting material to prepare [Mo₂O₆(2,2'-bipy)]_n (**2**) (by a solid state thermal transformation) and [Mo₃O₉(2,2'-bipy)₂]_n (**3**) (by a hydrothermal reaction). A comparative study has been performed on the catalytic performances of **1–3** in the epoxidation of *cis*-cyclooctene.

6.2. Results and discussion

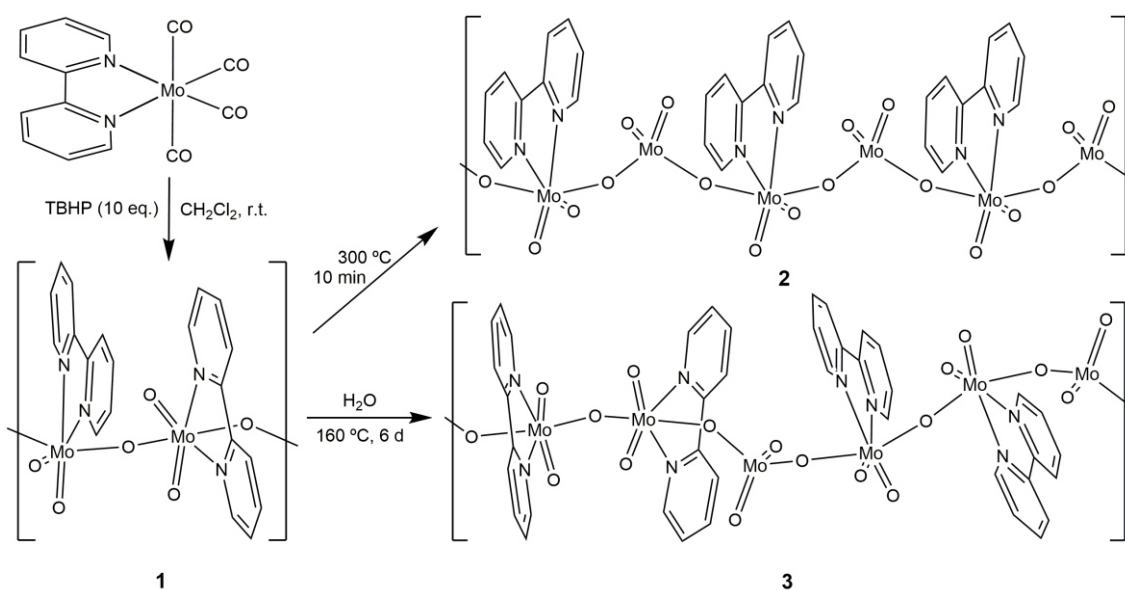
6.2.1. Synthesis and characterization of complexes [MoO₃(2,2'-bipy)]_n (**1**), [Mo₂O₆(2,2'-bipy)]_n (**2**) and [Mo₃O₉(2,2'-bipy)₂]_n (**3**)

Compound [MoO₃(2,2'-bipy)]_n (**1**) was prepared in very good yield (97 %) through oxidative decarbonylation of [Mo(CO)₄(2,2'-bipy)], carried out by the dropwise addition of 5–6 M TBHP (10 equiv.) in *n*-decane to a suspension of the tetracarbonyl

Chapter 6

complex in CH_2Cl_2 (Scheme 6.1). The compound **1** was characterized by FT-IR and Raman spectroscopy, powder X-ray diffraction and thermogravimetry, proving to be the organic-inorganic hybrid compound $[\text{MoO}_3(2,2'\text{-bipy})]_n$, which was first reported by Zubieta and coworkers⁴.

Thermogravimetric analysis of $[\text{MoO}_3(2,2'\text{-bipy})]_n$ (**1**) under air shows a mass loss of 48.8 % in the interval 200–425 °C, divided into three sequential steps, corresponding to the decomposition of 2,2'-bipy moieties (Figure 6.1). No further weight loss takes place until 625 °C.



Scheme 6.1. Synthesis of compounds **1–3**.

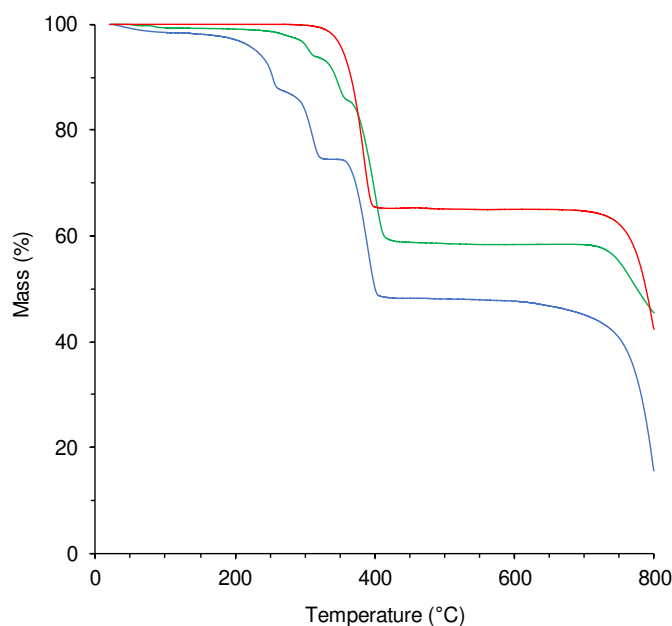


Figure 6.1. TGA curves for the complexes **1** (—), **2** (—), and **3** (—).

Chapter 6

The residual mass of 48.3 % at 425 °C is in very good agreement with the calculated value of 48.0 % assuming that full decomposition of the organic ligands leads to MoO₃. This was confirmed by performing a variable temperature PXRD experiment (Figure 6.2). The results show that reflections characteristic of microcrystalline **1** are present up to 320 °C, although a slight loss of crystallinity is apparent when comparing the pattern obtained at this temperature (Figure 6.2b) with that obtained for **1** at ambient temperature (Figure 6.2a).

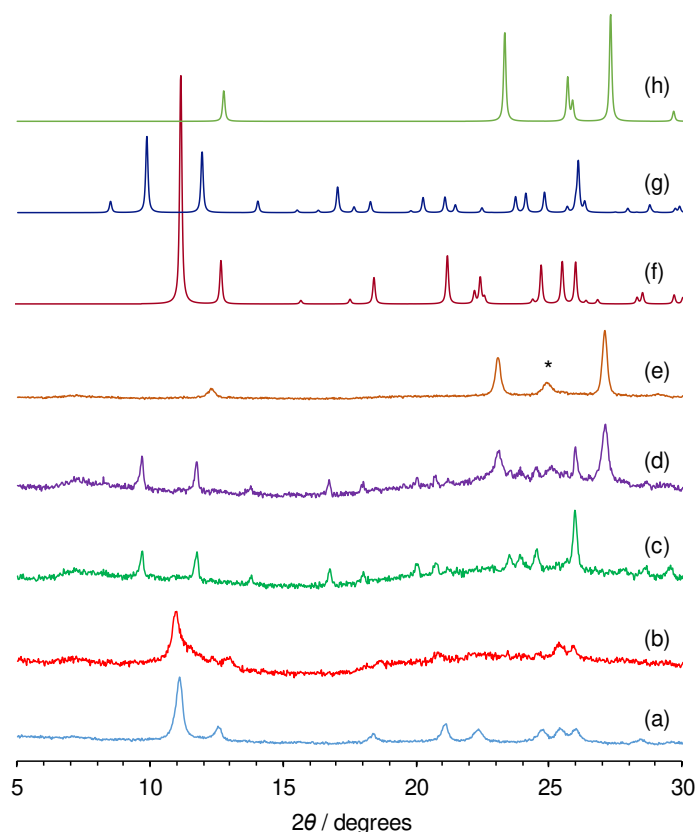


Figure 6.2. Variable temperature PXRD study of **1**: (a) ambient temperature, (b) 320 °C, (c) 350 °C, (d) 420 °C, (e) 570 °C. The computed patterns for **1** (f), **2** (g) and α -MoO₃ (h) were generated using the program Mercury (copyright CCDC, ver. 3.9)²⁹ with crystallographic data published for **1/2**²¹ and α -MoO₃³⁰. The asterisk in pattern (e) identifies an unassigned reflection; all other reflections are due to α -MoO₃.

Further heating to 350 °C (Figure 6.2c) leads to complete loss of reflections due to **1** and the appearance of a new phase with reflections that match those present in the simulated PXRD pattern for the 1D polymeric material [Mo₂O₆(2,2'-bipy)]_n (**2**) (Figure 6.2g). Accordingly, the residual mass of 74.4 % at 350 °C in the TGA profile of **1** (*i.e.*, the mass registered at the well-defined plateau observed after the second of three sequential weight loss steps) is in excellent agreement with the calculated value

Chapter 6

of 74.0 % assuming complete conversion of **1** to **2** with the loss of 0.5 equiv. of 2,2'-bipy. In line with the TGA profile, the *in situ* PXRD study shows that the intermediate phase **2** only persists over a narrow temperature range since the pattern recorded at 420 °C (Figure 6.2d) contains peaks characteristic of orthorhombic α -MoO₃ (Figure 6.2h). The PXRD pattern recorded at 570 °C (Figure 6.2e) shows loss of all reflections due to **2**. Sublimation of molybdenum oxide occurs above 625 °C (Figure 6.1). These results for the thermal behaviour of **1** are in agreement with the *in situ* Raman study reported by Twu *et al.*³¹

The thermal behaviour of **1** suggests that it could be used as a starting material for the synthesis of **2** via a carefully controlled thermal treatment in the solid-state. A new high-yield synthesis of **2** is desirable since the hydrothermal method reported by Zubietta and coworkers, consisting of heating a mixture of Na₂MoO₄, MoO₃, 2,2'-bipy, MnCl₂ and H₂O for 4 days at 200 °C, only led to a 10 % yield of **2** (based on molybdenum) as single-crystals (colourless plates).³² In their *in situ* Raman study, Twu *et al.* found that heating **1** to 330 °C gave **2**, but that cooling of this sample to ambient temperature led to the appearance of additional phases identified as MoO₃ and [Mo₃O₉(2,2'-bipy)₂]_n (**3**).³¹ The thermal treatment of **1** was optimised and it was found that pure **2** could be prepared in quantitative yield by heating **1** at 300 °C for 10 min in a muffle furnace, which constitutes a clean and efficient protocol (Scheme 6.1). The PXRD pattern of the resultant solid cooled to ambient temperature matched the simulated pattern calculated using the crystal structure data published for **2**³², and did not display reflections due to MoO₃ and/or **3** (Figure 6.3).

TGA of the polymer **2** shows that decompositions start above 350 °C (DTG_{max} = 385 °C; DTG = derivative thermogravimetric) (Figure 6.1). An *in situ* PXRD study confirmed that the compound is stable at 285 °C, while the pattern recorded at 420 °C corresponds to MoO₃ (Figure 6.4). These data are consistent with the thermal behaviour of **1** above 300 °C, *i.e.* after partial loss of 2,2'-bipy moieties to give the intermediate phase **2**.

The Raman spectrum of **2** displays bands at 895 [$\nu_{as}(\text{Mo}=\text{O})$] and 936 cm⁻¹ [$\nu_s(\text{Mo}=\text{O})$], which concord with the bands reported by Twu *et al.* (Figure 6.5).³¹ Four $\nu(\text{Mo}=\text{O})$ bands are observed in the FT-IR spectrum at 883, 903, 919 and 941 cm⁻¹ (Figure 6.6). A very strong, broad band at 704 cm⁻¹ is assigned as a Mo–O–Mo asymmetric stretching vibration. The corresponding band for **1** is centred around 640 cm⁻¹.



Figure 6.3. Experimental (a, c, e, g, i) and computed (b, d, f^{44,5} h^{7,8}, j⁹) PXRD patterns of (a, b) **1**, (c, d) **2**, (e, f) **3**, (g, h) **4**, (i, j) **5**.

Chapter 6

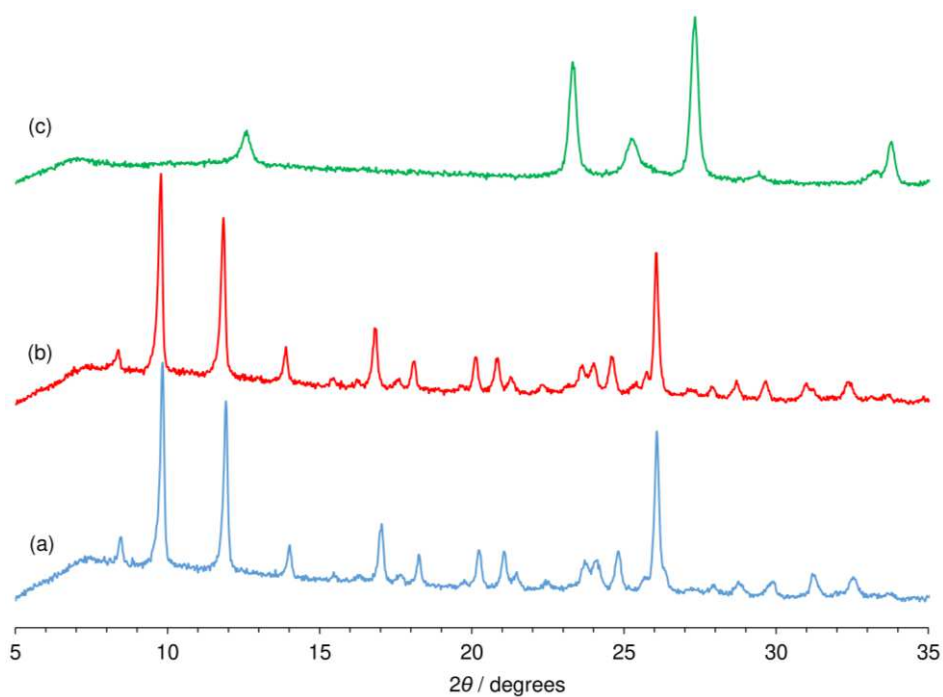


Figure 6.4. Variable temperature PXRD study of **2**: (a) ambient temperature, (b) 285 °C and (c) 420 °C.

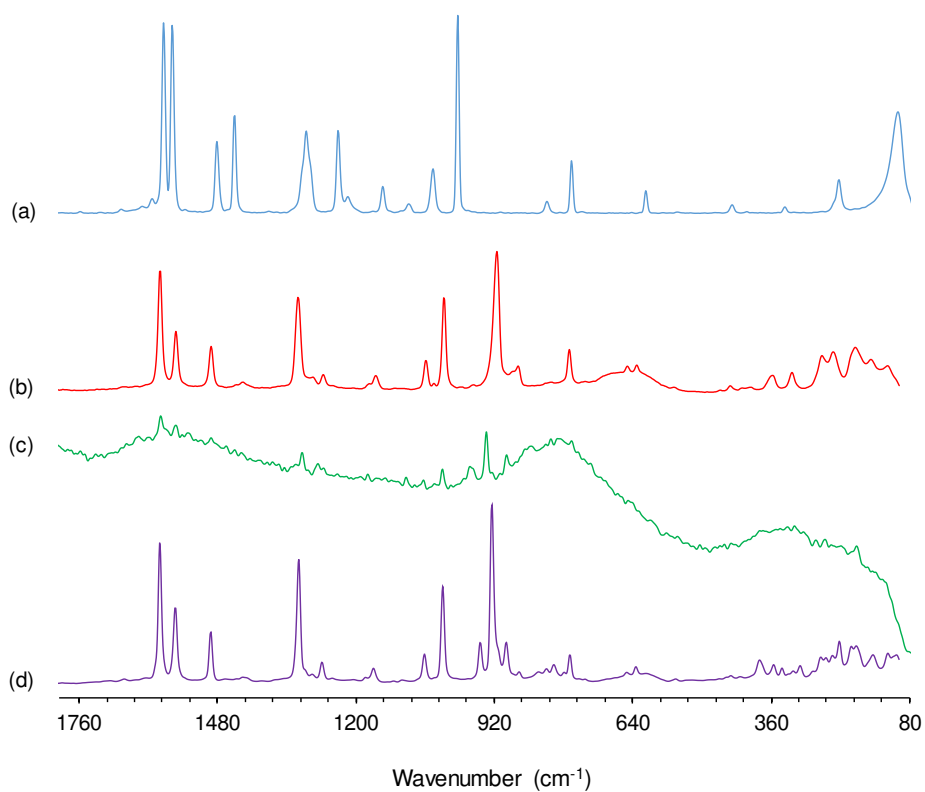


Figure 6.5. FT-Raman spectra in the range of 80-1800 cm^{-1} for (a) free ligand 2,2'-bipy, (b) **1**, (c) **2** and (d) **3**.

Chapter 6

Regarding the internal 2,2'-bipy vibrational modes, the strong band at 771 cm^{-1} is due to a CH out-of-plane bending vibration (cf. 756 cm^{-1} for free 2,2'-bipy in the solid-state). The shift of the ring stretching bands from ca. 1556 and 1572 cm^{-1} for the free ligand to 1574 and $1598/1606\text{ cm}^{-1}$ for **2** is a direct consequence of bidentate coordination of 2,2'-bipy to the Mo(VI) centers. It is noteworthy that the spectra of **1** (Figure 6.6, b) and **2** (Figure 6.6, c) are very similar in the $1000\text{--}1620\text{ cm}^{-1}$ region containing ligand-centred modes.

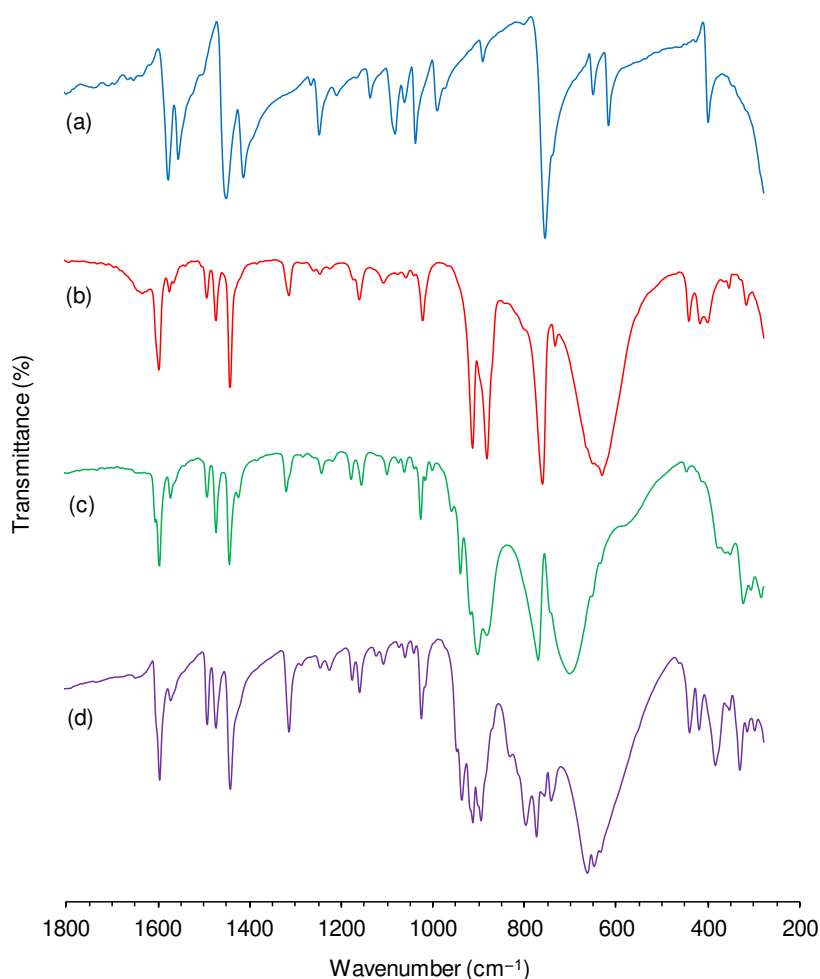


Figure 6.6. FTIR spectra in the range $200\text{--}1800\text{ cm}^{-1}$ for (a) free ligand 2,2'-bipy, (b) **1**, (c) **2** and (d) **3**.

The $^{13}\text{C}\{^1\text{H}\}$ CP MAS NMR spectra of **1** and **2** display between seven and eight resolved peaks, some of which clearly comprise overlapping resonances (Figure 6.7). These spectra are therefore consistent with the reported crystal structures which show that each polymer contains one crystallographically distinct 2,2'-bipy moiety, with the carbon atoms of each C_n/C_n' pair being crystallographically inequivalent.

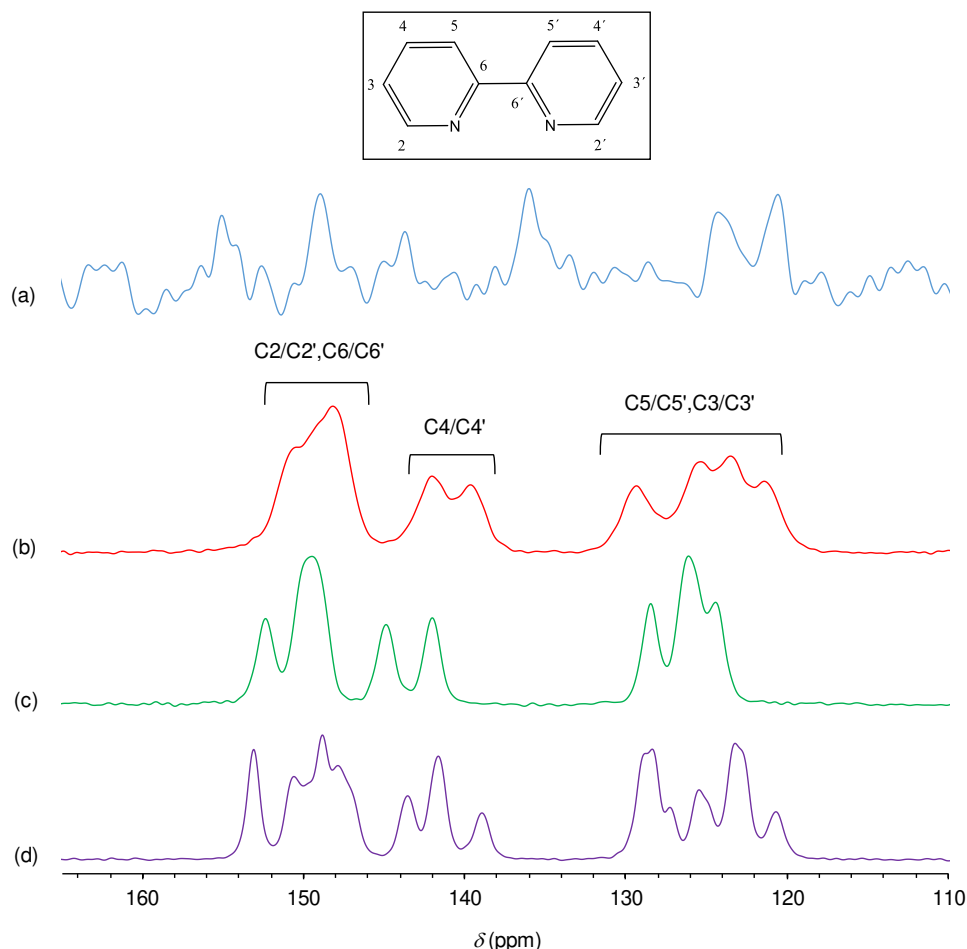


Figure 6.7. $^{13}\text{C}\{^1\text{H}\}$ CP MAS NMR spectra of (a) free ligand 2,2'-bipy, (b) **1**, (c) **2** and (d) **3**.

The polymer formulated as $[\text{Mo}_3\text{O}_9(2,2'\text{-bipy})_2]_n$ (**3**) was the third member of the series $[(\text{MoO}_3)_m(2,2'\text{-bipy})_n]$ described by Zubieta and coworkers.³² The repeat unit of the 1D polymer chain in **3** consists of one $\{\text{MoO}_4\}$ tetrahedron and two $\{\text{MoO}_4\text{N}_2\}$ octahedra (Scheme 6.1), as opposed to one $\{\text{MoO}_4\}$ tetrahedron and one $\{\text{MoO}_4\text{N}_2\}$ octahedron in **2**. Our attempts to prepare **3** by the literature method³², consisting of the hydrothermal treatment of a mixture of MoO_3 , 2,2'-bipy and H_2O at 160 °C for 6 days (under both static and dynamic conditions), were unsuccessful, leading to mixtures of **3** and other unidentified phases. A successful synthesis of **3** in 85 % yield was subsequently achieved by the hydrothermal treatment of $[\text{MoO}_3(2,2'\text{-bipy})]_n$ (**1**) in H_2O at 160 °C for 6 days.

The vibrational spectra of **3** display several Mo=O stretching bands in the region 880–950 cm^{-1} . According to Twu *et al.*, the Raman bands at 896, 925, and 948 (Figure 6.5) can be ascribed to $\nu_{\text{as}}(\text{Mo}=\text{O})$ of MoO_4N_2 octahedra, $\nu_{\text{s}}(\text{Mo}=\text{O})$ of MoO_4N_2 octahedra, and $\nu_{\text{s}}(\text{Mo}=\text{O})$ of MoO_4 tetrahedra, respectively.³¹ Three $\nu(\text{Mo}=\text{O})$ bands (with additional shoulders) are observed in the FT-IR spectrum at 897, 914 and 938

Chapter 6

cm^{-1} (Figure 6.6). Strong, overlapping bands for $\nu_{\text{as}}(\text{Mo}-\text{O}-\text{Mo})$ are observed at 649 and 665 cm^{-1} , *i.e.* at intermediate frequencies when compared with the corresponding bands for **1** and **2**. The spectrum in the region containing ligand-centred modes ($1000\text{--}1620 \text{ cm}^{-1}$) is very similar to those for **1** and **2**. According to the crystal structure reported for **3**³², the asymmetric unit contains two non-equivalent 2,2'-bipy moieties, with the carbon atoms of each C_n/C_n' pair being crystallographically inequivalent. The $^{13}\text{C}\{^1\text{H}\}$ CP MAS NMR spectrum of **3** is consistent with this structure since at least sixteen peaks/shoulders can be observed in the aromatic region ($114\text{--}155 \text{ ppm}$) (Figure 6.7).

The thermal decomposition behaviour of **3** was examined by TGA (Figure 6.1) and *in situ* PXRD (Figure 6.8). The compound is stable up to $250 \text{ }^\circ\text{C}$. Phase purity was confirmed by PXRD (Figure 6.8). The PXRD pattern recorded at this temperature is similar to that for **3** at ambient temperature, although a general shift of reflections towards lower angles took place upon heating. A further shift of the high angle peaks towards lower angles is evident upon increasing the temperature to $280 \text{ }^\circ\text{C}$, while the relative intensity of low angle peaks around $11^\circ 2\theta$ decreases significantly, which can be associated with the onset of thermal removal of the organic ligands. Loss of 2,2'-bipy moieties takes place in three sequential steps up to $425 \text{ }^\circ\text{C}$ with DTG_{max} at 305, 348 and $402 \text{ }^\circ\text{C}$. The PXRD recorded at $315 \text{ }^\circ\text{C}$, *i.e.* after the first weight loss step (3.7 % mass loss between 280 and $315 \text{ }^\circ\text{C}$), shows complete loss of reflections below $15^\circ 2\theta$, while higher-angle reflections are retained, albeit with a further shift towards lower angles. These results suggest that the 1D polymeric chain structure may be retained up to $315 \text{ }^\circ\text{C}$ despite partial loss of organic ligands. Some of the high-angle reflections persist even after the second weight loss step up to $360 \text{ }^\circ\text{C}$. A residual mass of 58.8 % is obtained at $450 \text{ }^\circ\text{C}$ after complete 2,2'-bipy decomposition, which is close to the calculated value of 58.0 % for MoO_3 . However, unlike **1** and **2**, PXRD did not show the formation of a crystalline $\alpha\text{-MoO}_3$ phase between 450 and $700 \text{ }^\circ\text{C}$.

Chapter 6

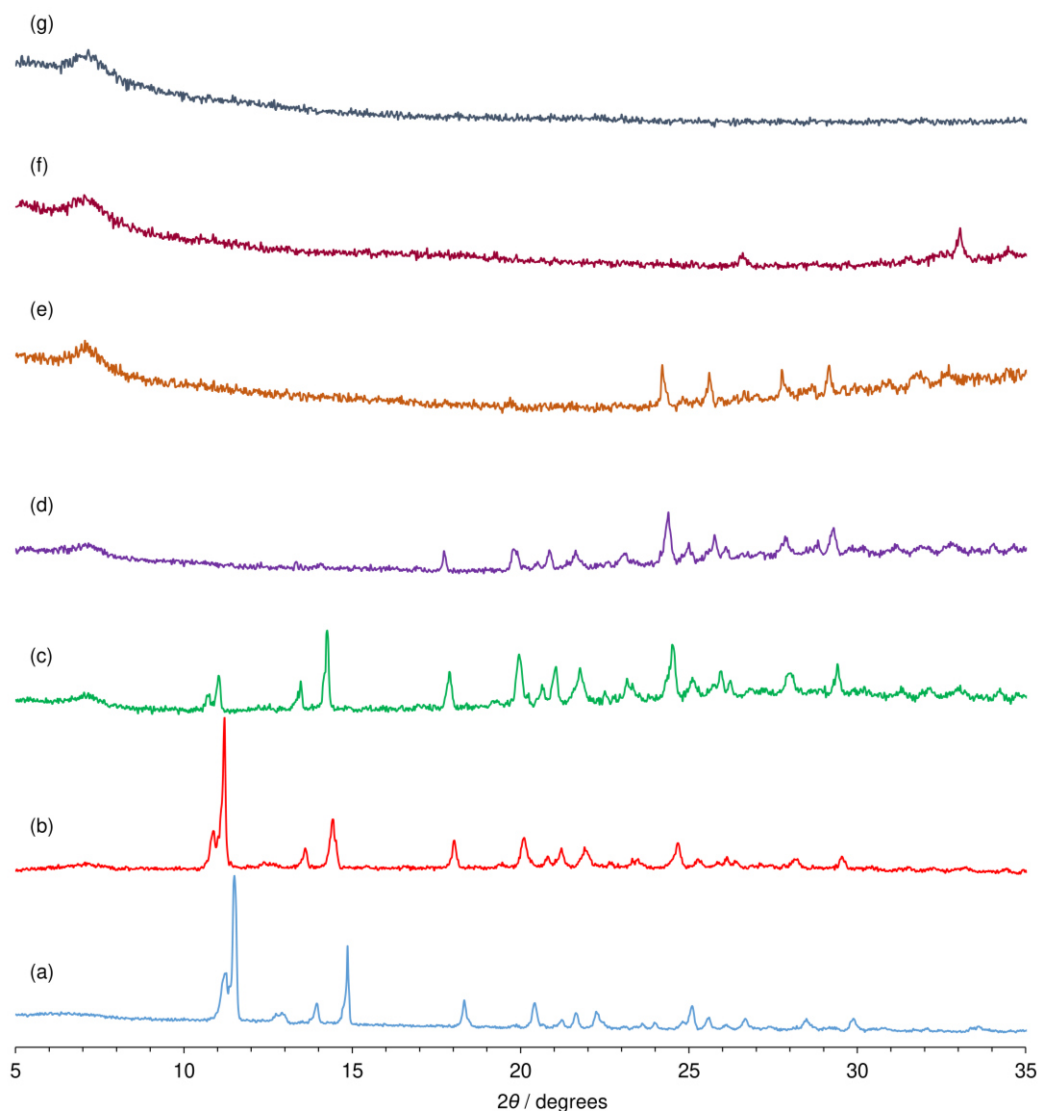


Figure 6.8. Variable temperature PXRD study of **3**: (a) ambient temperature, (b) 250 °C, (c) 280 °C, (d) 315 °C, (e) 360 °C, (f) 450 °C and (g) 700 °C.

6.3. Catalytic studies

6.3.1. Catalytic epoxidation of *cis*-cyclooctene with TBHP

The polymeric compounds **2** and **3** were investigated for the liquid-phase epoxidation of *cis*-cyclooctene (Cy) using TBHP as oxidant, α, α, α -trifluorotoluene (TFT) as cosolvent, and a reaction temperature of 55 °C (Figure 6.9). For comparison, the MoO₃/bipyridine hybrid compounds **1** and {[MoO₃(2,2'-bipy)][MoO₃(H₂O)]}_n (**4**) were tested under identical Cy reaction conditions. Commercial MoO₃ and the mononuclear complex [MoO(O₂)₂(2,2'-bipy)] (**5**) were chosen for catalyst benchmarking. In all cases Cy was converted to cyclooctene oxide (CyO) with 100 % selectivity (Figure 6.9). The reaction without catalyst gave 6 % conversion at 24 h. Based on mechanistic studies

Chapter 6

reported in the literature for Mo-catalysed olefin epoxidation with hydroperoxide oxidants, a Lewis acid–base reaction (heterolytic mechanism) is generally involved in the formation of an active oxidising species. Specifically, the coordination reaction between the metal center (Lewis acid) and the oxidant TBHP (Lewis base) leads to an active oxidising species responsible for O-atom transfer to the olefin, giving the respective epoxide product.^{33–35}

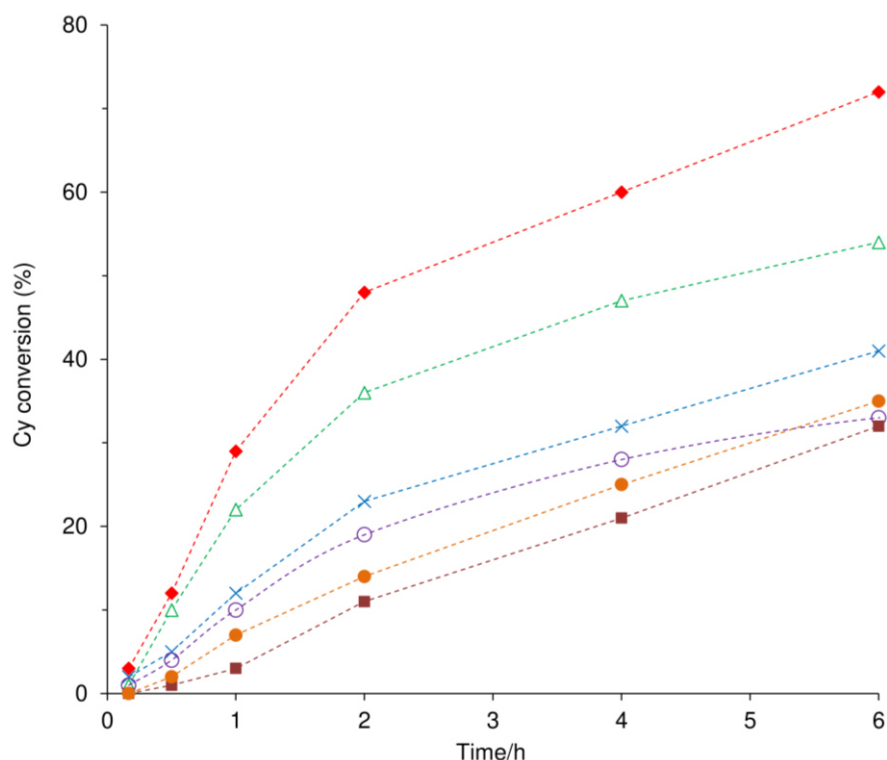


Figure 6.9. Kinetic profiles of the catalytic epoxidation of Cy with TBHP, in the presence of 1 (x), 2 (♦), 3 (Δ), 4 (○), 5 (●), and MoO₃ (■), at 55 °C.

The Cy reaction mixtures in the presence of 1–5 and MoO₃ were biphasic solid–liquid (S–L). To check for a possible homogeneous phase catalytic contribution, contact tests (CTs) were performed in which each compound was treated with oxidant and cosolvent (but no Cy) for 24 h at 55 °C. The resultant liquid phases, denoted i-CT-TBHP-L (i = 1–5 or MoO₃), were tested for Cy reaction, and led to significant conversions (Figure 6.10). Hence, the catalytic reactions in the presence of the studied molybdenum compounds occurred in homogeneous phase. The kinetic differences between the homogenous catalytic reaction using i-CT-TBHP-L and the original catalyst i may be partly due to differences in the amount of active species (in contrast to the CTs, in the normal catalytic tests the olefin is present from the initial instant, which may influence the polarity of the medium and catalyst solubility). The solids i-CT-

Chapter 6

TBHP-S ($i = 1-4$) recovered from the CTs were effective for Cy epoxidation, and the kinetic profiles were roughly coincident with those for the respective as-synthesised catalysts (Figure 6.10a-d). For MoO_3 and **5**, differences in reaction kinetics were verified in relation to the respective solids MoO_3 -CT-TBHP-S and **5**-CT-TBHP-S (Figure 6.10e and f).

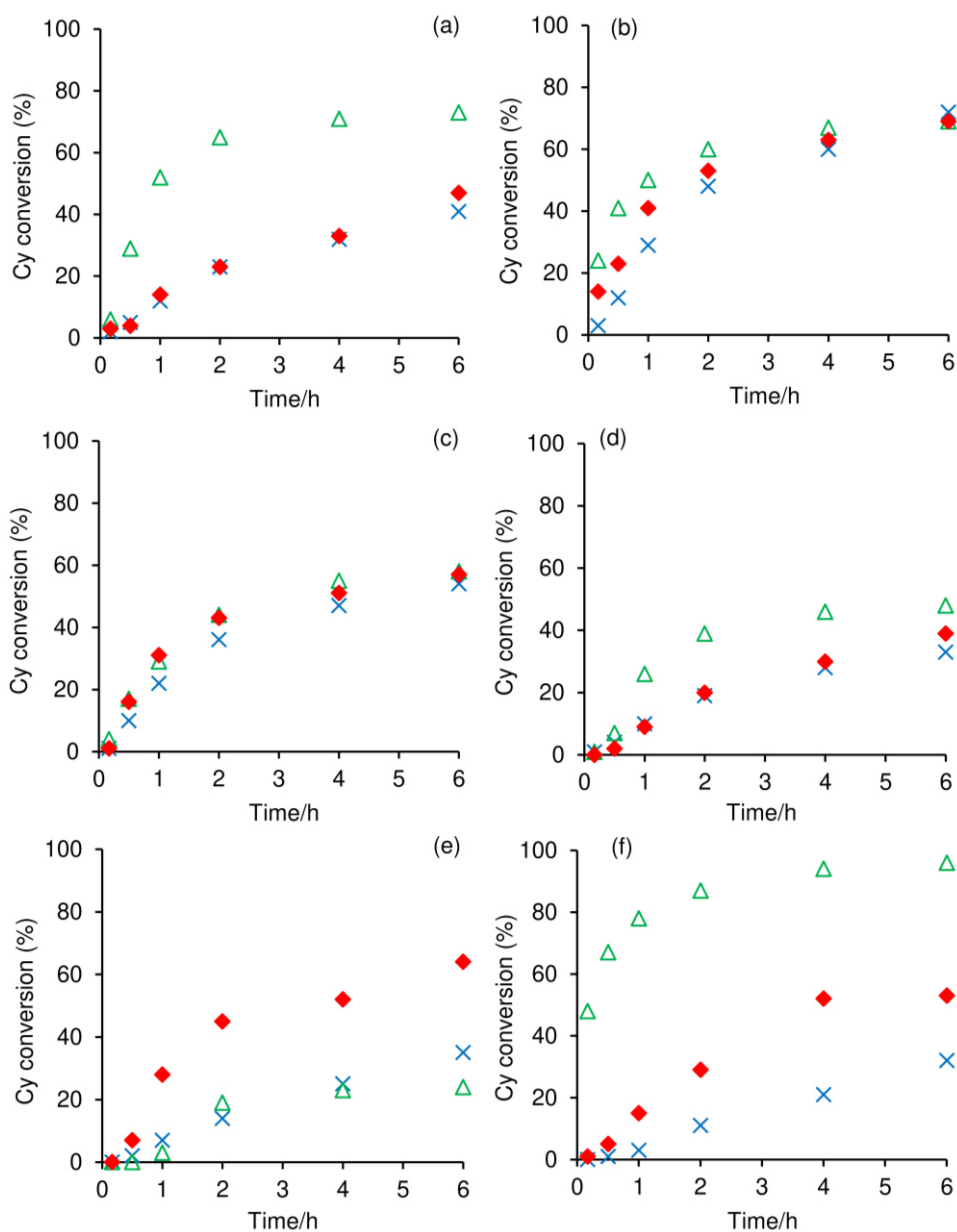


Figure 6.10. Contact tests (CTs) carried out for (a) **1**, (b) **2**, (c) **3**, (d) **4**, (e) **5**, and (f) MoO_3 , at 55 °C. In each case kinetic profiles for Cy epoxidation are compared for reactions performed using the original catalyst (x), the respective recovered solid i -CT-TBHP-S ($i = 1-5$ or MoO_3) (♦), or the solutions (i -CT-TBHP-L) of the CTs (Δ).

Chapter 6

Based on the amount of dissolved compound, the initial turnover frequencies for Cy epoxidation (TOF, mol mol_{Mo}⁻¹ h⁻¹) were calculated, and increased in the order **5** (42) < MoO₃ (75) < **3** (147) < **1** (200) < **4** (248) < **2** (288). On the other hand, Cy conversion (%) at 24 h increased in the order **4** (62) < **1** (71) < MoO₃ (77) ≈ **3** (78) ≈ **5** (90) < **2** (96). Hence, **2** possessed the highest initial activity, and led to the highest Cy conversion at 24 h. Based on these results and literature data for **1** and **4** tested for Cy/TBHP (with CH₃CHCl₂ as cosolvent)²⁵, the two compounds performed worse than **2**. Several other polynuclear or polymeric oxomolybdenum compounds have been tested for this specific reaction using comparable catalytic conditions (Table 6.1). Higher Cy conversions were reported for [Mo₂O₆(di-*t*Bu-bipy)₂]³⁶, [Mo₈O₂₄(pzpyEA)₄]³⁷, and [Mo₂O₆(ppp)]³⁸.

Table 6.1. Comparison of the catalytic results for **2** for Cy epoxidation with TBHP with literature data for organo-oxomolybdenum compounds containing a bidentate N,N-ligand coordinated Mo centers.^a

Compound	Solvent/T (°C)	Time (h)	Conv. ^b [%]	Ref.
2	TFT/55	6/24	72/96	
1	CH ₃ CHCl ₂ /55	6/24	48/81	25
4	CH ₃ CHCl ₂ /55	24	45	39
5	[bmim]PF ₆ /60	12	10	40
[Mo ₂ O ₆ (di- <i>t</i> Bu-bipy) ₂]	ws/55	6/24	93/100	36
[Mo ₈ O ₂₄ (di- <i>t</i> Bu-bipy) ₄]	CH ₃ CHCl ₂ /55	6/24	65/90	25
[Mo ₃ O ₉ (pzpy)] ^c	ws/55	6/24	29/51	27
[Mo ₄ O ₁₂ (pzpy) ₄]	ws/55	6/24	55/92	37
[Mo ₂ O ₆ (ppp)] ^c	CH ₃ CHCl ₂ /55 ^d	6	99	38
[MoO(O ₂) ₂ (pzpyEA)]	TFT/55 ^e	6/24	~10/~20	41
[Mo ₈ O ₂₄ (pzpyEA) ₄]	ws/55	6/24	89/100	37
[MoO ₃ (pbim)]	TFT/55	6/24	30/56	42
[MoO(O ₂) ₂ (pbim)]	TFT/70	6/24	81/98	42

^a Reaction conditions (unless otherwise specified): Mo: Cy: TBHP = 1:100:150. ^b Cy conversion. ^c Homogeneous catalyst formed *in situ* identified as [MoO(O₂)₂(L)]. ^d Mo: Cy: TBHP = 1:113:172. ^e Mo: Cy: TBHP = 0.1:100:152.

The oxidant efficiency for the molybdenum catalysts is an important factor for sustainable catalytic epoxidation processes. Iodometric titrations indicated very high or excellent TBHP efficiencies of 92–100 % for the molybdenum catalysts tested (Figure 6.11).

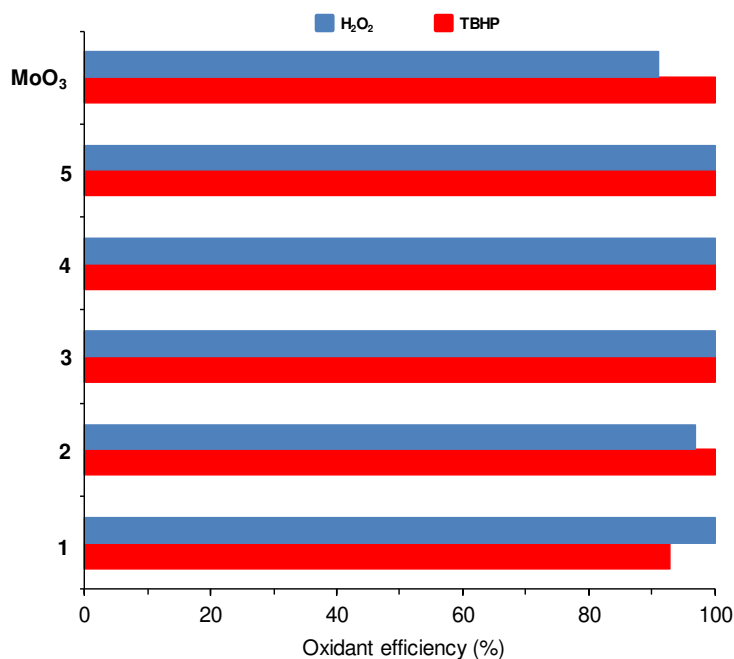


Figure 6.11. Oxidant efficiency (determined for 24 h reaction) for the different catalysts, at 55 °C.

6.3.2. Catalytic epoxidation of *cis*-cyclooctene with H₂O₂

The catalytic performances of **1–4** were further studied using H₂O₂ as oxidant instead of TBHP, and keeping the remaining reaction conditions constant. The Cy/H₂O₂ reaction in the presence of **1–4** led to poor results (< 5 % conversion at 24 h), which may be partly due to mass transfer limitations since these systems consisted of triphasic solid–liquid(aqueous)–liquid(organic) mixtures. Changing the cosolvent from TFT to CH₃CN led to biphasic solid–liquid mixtures, and the catalytic results improved (Figure 6.12): conversion (%) at 24 h increased in the order **1** (16) < **3** (31) < **4** (53) = **2** (53). The kinetic profiles for (**1–4**)/H₂O₂/CH₃CN were intermediate between those for **5** (21 % conversion at 24 h) and MoO₃ (74 % conversion at 24 h). In general, the H₂O₂ efficiencies were high (97–100 %), with MoO₃ leading to the lowest efficiency (91 %) (Figure 6.11).

6.3.3. Characterization of solids after catalytic epoxidation

After the catalytic reactions with TBHP or H₂O₂, work-up was performed to separate the solid and liquid phases, and the solids (**i**-Cat-oxidant) were characterised by ATR FT-IR spectroscopy and PXRD. The data indicated that the chemical and microstructural features of the undissolved solids **i**-Cat-TBHP (**i** = **1–5** or MoO₃) were unchanged relative to those for the original catalysts (Figure 6.13).

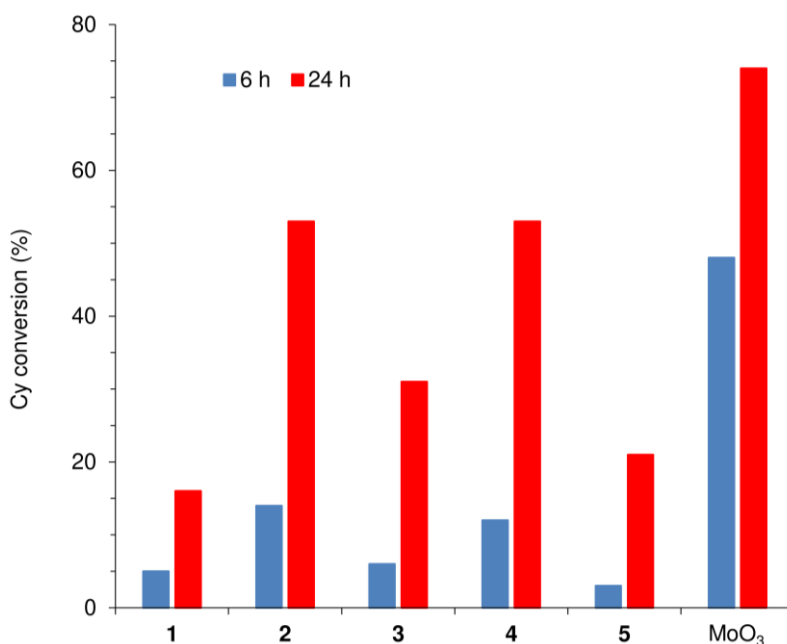


Figure 6.12. Cy conversion using H₂O₂ as oxidant, in the presence of **1-5** or MoO₃, at 55 °C.

On the other hand, for the undissolved solids *i*-Cat-H₂O₂ (*i* = **1-4**), the data were consistent with the exclusive presence of the oxodiperoxo complex **5** (Figure 6.14). Accordingly, the solid and liquid phases for (**1-4**)/Cy/H₂O₂ changed colour from white/colourless to yellow (complex **5** is yellow), while no comparable colour change was observed for (**1-4**)/Cy/TBHP. The catalytic activity of **5** for the Cy/H₂O₂ reaction (Figure 6.12) indicates that this species contributes at least partially to the reaction kinetics of the systems (**1-4**)/Cy/H₂O₂. The catalytic performance of **5** resembles more closely that of the (pre)catalyst **1** than **2** and **3** (Figure 6.12), which may be partly associated with the fact that the 2,2'-bipy/Mo ratio (*R*) in **5** and **1** is the same (equal to **1**). There seems to be a relationship between catalytic activity and the ratio *R* in the (pre)catalyst, *i.e.* conversions at 6/24 h approximately follow the sequence $R = 1$ (**1**, **5**) < $R = 0.67$ (**3**) < $R = 0.5$ (**2**, **4**) < $R = 0$ (MoO₃). One cannot exclude the possibility that inorganic MoO₃-derived oxoperoxo species may be formed (together with **5**) from the precatalyst, and the amount of such species (which could be more active than **5**) may increase as the ratio *R* decreases. It is known that the reaction of MoO₃ with excess H₂O₂ can lead to oxodiperoxo species of the type [MoO(O₂)₂(L)₂] and [O{MoO(O₂)₂(L)}₂]²⁻ (L = H₂O, CH₃CN), which may contribute to the catalytic process.⁴³

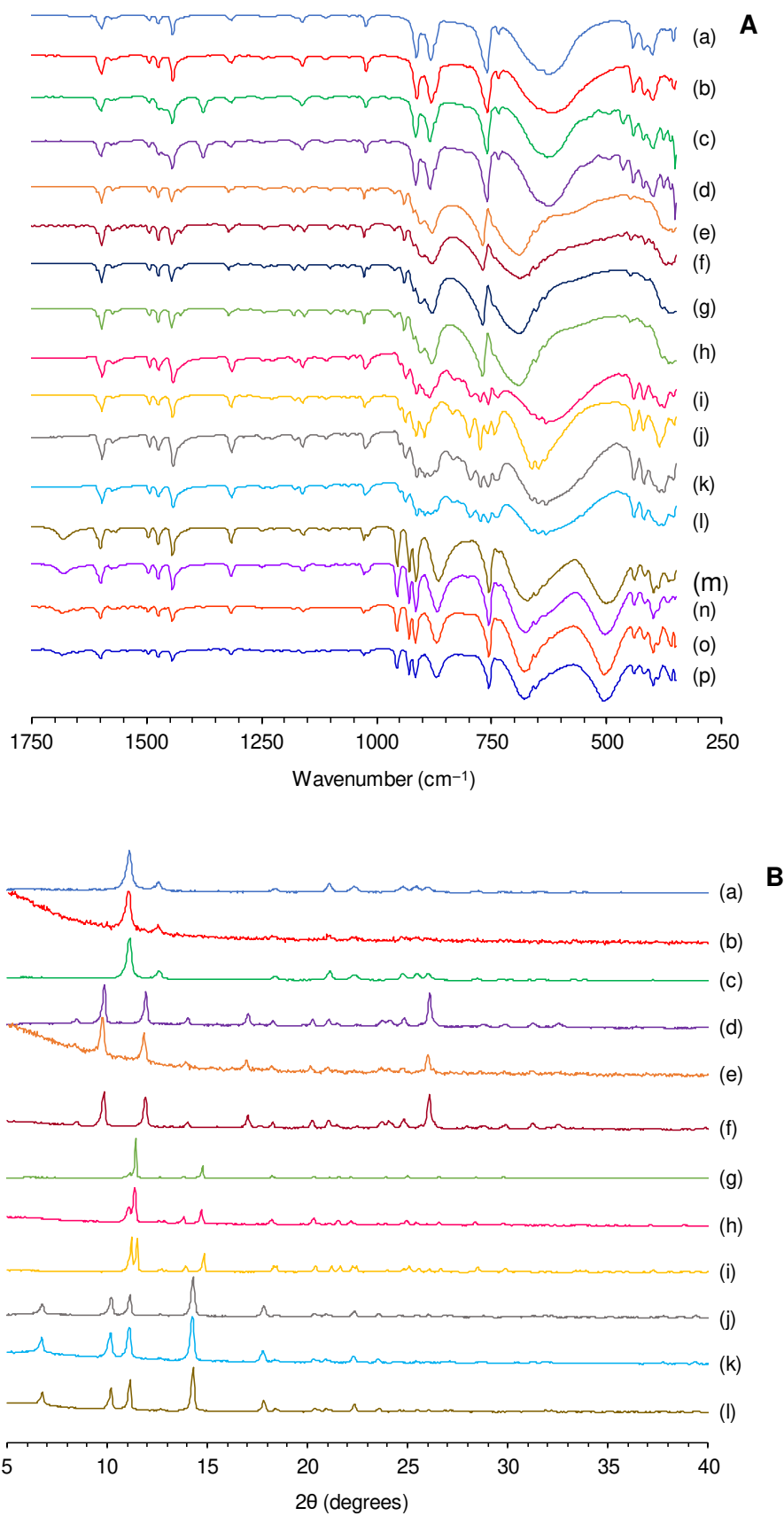


Figure 6.13. ATR FTIR spectra (A) in the range of 250-1750 cm⁻¹ and PXRD patterns (B) for (a) **1**, (b) **1**-Cat-TBHP, (c) **2**, (d) **2**-Cat-TBHP, (e) **3**, (f) **3**-Cat-TBHP, (g) **4**, (h) **4**-Cat-TBHP, (i) **5**, (j) **5**-Cat-TBHP, (k) MoO₃, and (l) MoO₃-Cat-TBHP.

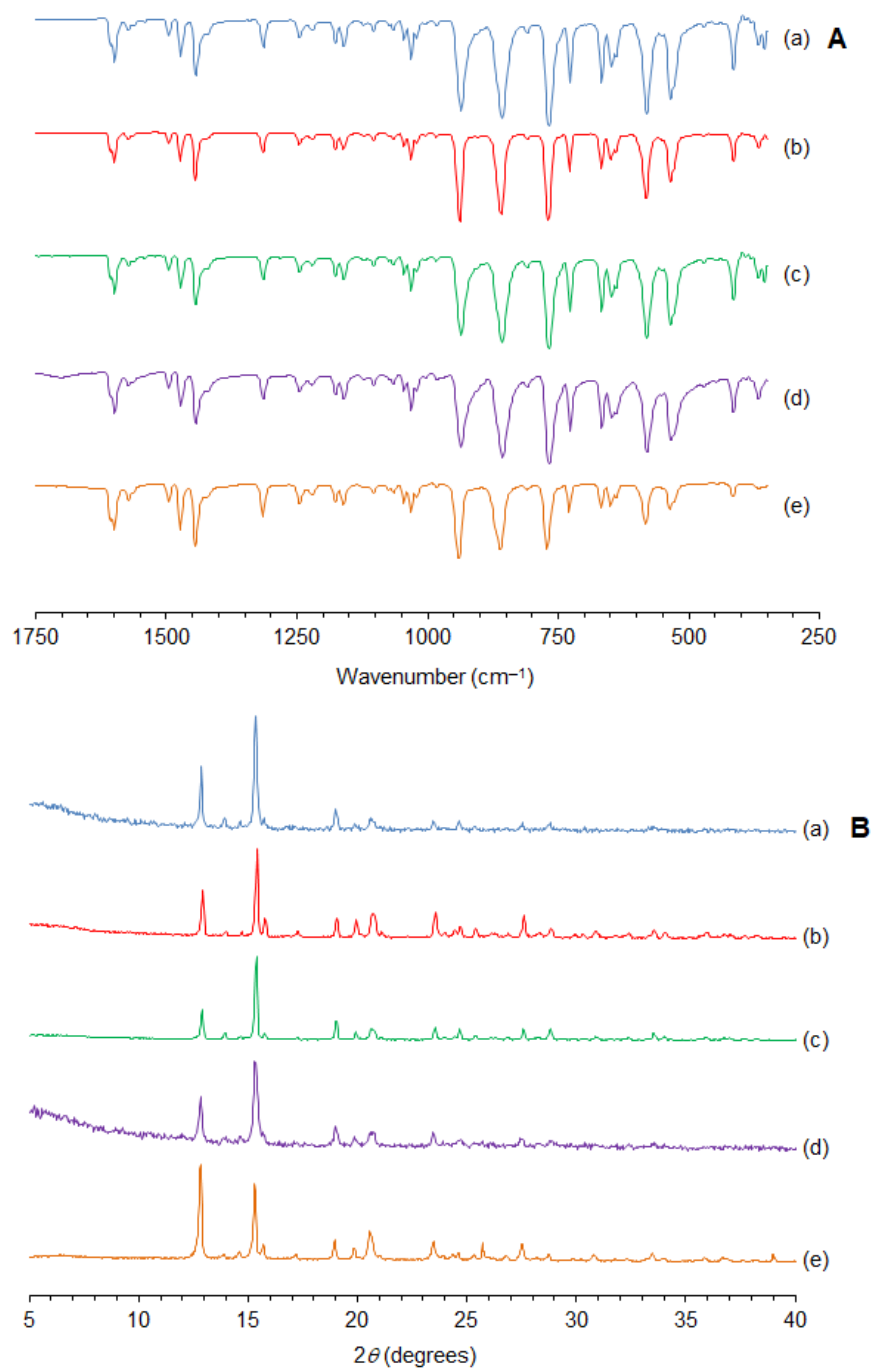
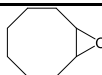
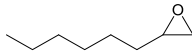
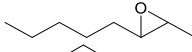
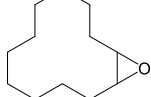
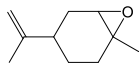
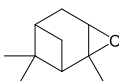
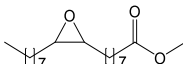


Figure 6.14. ATR FTIR spectra (A) in the range of 250-1750 cm⁻¹ and PXRD patterns (B) for (a) 1-Cat-H₂O₂, (b) 2-Cat-H₂O₂, (c) 3-Cat-H₂O₂, (d) 4-Cat-H₂O₂, and (e) 5.

6.3.4. Catalytic epoxidation of other cyclic and linear non-functionalized olefins

The catalytic performance of **2** was further investigated for the epoxidation of other cyclic and linear non-functionalised olefins, namely cyclododecene (Cy12), 1-octene (1C8) and *trans*-2-octene (2C8), under similar reaction conditions (Table 6.2). For these substrates the respective epoxides were always the only reaction products. The epoxidation of Cy12 gave 87 % yield of 1,2-epoxycyclododecane at 24 h. A comparison of the cyclic monoenes Cy12 and Cy indicates that the former is less reactive, which may be partly due to steric effects associated with the larger Cy12 molecules. On the other hand, a comparison of the linear monoenes 1C8 and 2C8 indicates that the latter is more reactive, which may be partly due to electronic effects favouring the epoxidation of internal C=C bonds in relation to that of terminal ones. These results are consistent with the literature in that the reaction mechanism of olefin epoxidation in the presence of molybdenum compounds may involve an O-atom transfer step where an electrophilic oxidising species (formed via reaction of the oxidant with the molybdenum catalyst) attacks the olefin.^{35,44–46} Overall, these results suggest that **2** is active for the epoxidation of cyclic and linear olefins, and may lead to high regioselectivity towards more substituted C=C bonds.

Table 6.2. Epoxidation of olefins with TBHP in the presence of **2**.^a

Substrate	Conv. ^b [%]	Epoxide	Sel. ^b [%]	TOF ^c
Cy	72/96		100/100	288
1C8	9/32		100/100	0
2C8	30/71		100/100	30
Cy12	41/ 87		100/100	70
DL-Lim	63/88		96/90	130
Pin	29/37		54/50	80
Ole	25/57		100/100	50

^a Reaction conditions: Mo:TBHP:olefin = 1:100:150, 55 °C. ^b Olefin conversion and epoxide selectivity at 6 h/24 h. ^c Turnover frequency (mol mol_{Mo}⁻¹ h⁻¹).

6.3.5. Catalytic epoxidation of the biomass-derived olefins

The hybrid **2** was further explored for the epoxidation of the biomass-derived olefins DL-limonene (DL-Lim), α -pinene (Pin) and methyl oleate (Ole). The major sources of these compounds are citrus peel for DL-Lim, turpentine (a byproduct of the wood pulp industry) for Pin, and vegetable oils for Ole. The corresponding epoxides, 1,2-epoxy-*p*-menth-8-ene (LimOx), α -pinene oxide (PinO) and methyl 9,10-epoxyoctadecanoate (OleO), have a broad range of potential uses, *e.g.* as intermediates for the synthesis of perfumes, flavours, pharmaceuticals and biopolymers.^{47–52}

The catalytic epoxidation of DL-Lim gave LimOx as the main product in 79 % yield at 24 h (Table 6.2), revealing a high regioselectivity towards epoxidation at the internal and more electron-rich endocyclic double bond. These results are comparable or superior to those reported for other polymeric oxomolybdenum compounds bearing pyridine-containing ligands (71–86 % yield).^{36,38,42,53,54} Besides LimOx, 1,2:8,9-diepoxy-*p*-menthane and limonene diol were formed in 7 and 2 % yield, respectively. Increasing the TBHP:DL-Lim molar ratio from 1.5 to 2 still led to LimOx as the main product (79% yield at 24 h), further demonstrating the pronounced regioselectivity in favour of internal C=C bonds.

The reaction of Pin gave PinO as the main product in 19 % yield at 24 h (Table 6.2). Other products included campholenic aldehyde (CPA), *trans*-pinocarveol (PCV) and iso-pinocamphone (IPC), formed in up to 9 % total yield. The formation of PinO rearrangement products like CPA and IPC is favoured in the presence of Lewis acid catalysts.⁵⁵ CPA is the most industrially important, being useful as an aroma chemical or as an intermediate in the synthesis other aromas (*e.g.* sandalwood-like fragrances) and some drugs.⁵⁶ IPC is one of the main components of Hyssop essential oil, which stimulates digestion, has expectorate properties, and antibacterial/fungal activity.⁵⁷

The epoxidation of Ole gave mainly OleO, formed in 57% yield at 24 h (Table 6.2). This performance compares favourably with that reported in the literature for the polymeric compound [MoO₃(pbim)], which led to 42 % OleO yield at 69 % conversion (70 °C, 24 h).⁴² Under comparable reaction conditions, [(CH₃)₂NH₂][MoO₃(HbpdC)] (H₂bpdC = 2,2'-bipyridine-5,5'-dicarboxylic acid), [Mo₂O₆(ppp)] and [Mo₈O₂₂(OH)₄(di-*t*Bu-bipy)₄] led to 77–92 % OleO yield at 77–94 % conversion (6–24 h).^{38,53,54}

Chapter 6

6.3.6. Acid catalysis

The Lewis acidity of **1–4** was assessed via the model reaction of the acid-catalysed ethanolysis of styrene oxide. The four compounds led to 2-ethoxy-2-phenylethanol as the only product, at 70–100 % conversion, at 24 h, 55 °C (Table 6.3); catalysts **2** and **4** led to the highest EPE yields. Compounds **5** and MoO₃ were also effective for the acid-catalysed reaction (Table 6.3). The reaction without catalyst gave 6 % conversion at 24 h.

Based on the literature, the reaction mechanism of the Lewis acid-catalysed reaction of the epoxide in alcohol media may involve the interaction of the Mo center and the oxygen atom of epoxide, followed by nucleophilic attack of the alcohol reagent at the more substituted carbon atom of the oxirane, leading to the formation of the corresponding β -alkoxy alcohol product.^{58,59}

Table 6.3 Acid-catalysed reaction of StyO with ethanol in the presence of **1-5** and MoO₃.^a

Catalyst	StyO conversion at 6 h / 24 h (%)
[MoO ₃ (2,2'-bipy)] _n	86/99
[Mo ₂ O ₆ (2,2'-bipy)] _n	91/100
[Mo ₃ O ₉ (2,2'-bipy) ₂] _n	36/70
{[MoO ₃ (2,2'-bipy)][MoO ₃ (H ₂ O)]} _n	97/100
[MoO(O ₂) ₂ (2,2'-bipy)]	64/66
MoO ₃	42/99

^a Reaction conditions: Mo:StyO = 1:10, 55 °C, 0.38 M StyO in ethanol (2 mL).

The solid phases recovered from the biphasic solid-liquid reaction mixtures after 24 h batch runs (denoted *i*-AcidCat, *i* = **1-4**) were characterised by ATR FT-IR spectroscopy (Figure 6.15) and powder XRD (Figure 6.15), which indicated that the structural features were preserved and the compounds were stable.

For the contact tests, the catalyst and solvent (without substrate) were stirred for 24 h at 55 °C, after which the solid (*i*-CT-Acid-S, *i* = **1-4**) and liquid (*i*-CT-Acid-L) phases were separated by centrifugation and membrane filtration. The liquid and solid phases obtained from the CTs were tested separately for StyO reaction at 55 °C. The reaction of StyO using *i*-CT-Acid-L led to significant conversion, indicating that the catalytic reactions occurred in homogeneous phase; StyO conversion at 24 h of StyO reaction was 74, 100, 69 and 83 % for **1**, **2**, **3**, and **4**, respectively (Figure 6.16). The solids *i*-CT-Acid-S recovered from the CTs exhibited similar ATR FT-IR spectra (Figure

Chapter 6

6.15) and powder XRD patterns (Figure 6.15) to those for the respective original catalysts, and no drop in conversion at 24 h was verified in relation to the respective original catalysts (Figure 6.16). Moreover, the catalysts (*i*-CT-Acid-S-Cat) which were recovered from a 24 h batch run of StyO reaction in the presence of *i*-CT-Acid-S exhibited similar ATR FT-IR spectra (Figure 6.15) to the respective original catalysts. These results further confirm the fairly good stability of the studied catalysts, under the alcoholysis reaction conditions.

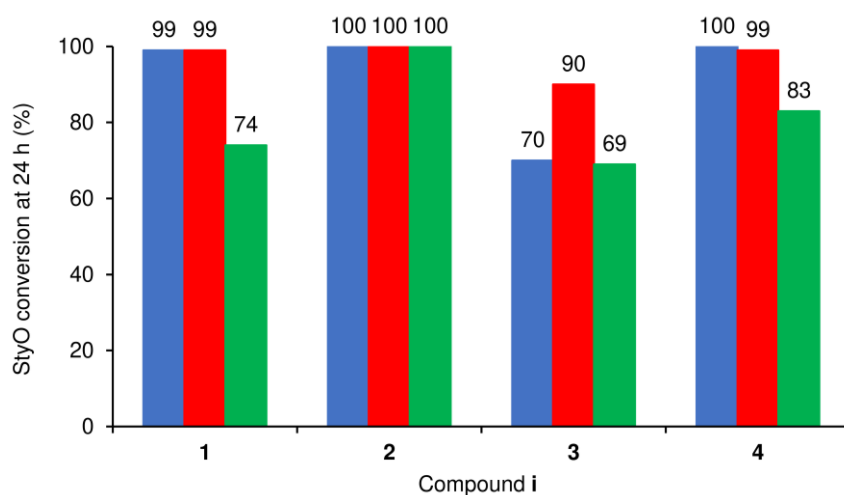


Figure 6.16 Conversion of StyO with ethanol, at 24 h, 55 °C, in the presence of compounds **1-4** (red), the respective solids *i*-CT-Acid-S (green), or using the solutions *i*-CT-Acid-L (blue) obtained from the contact tests for **1-4**.

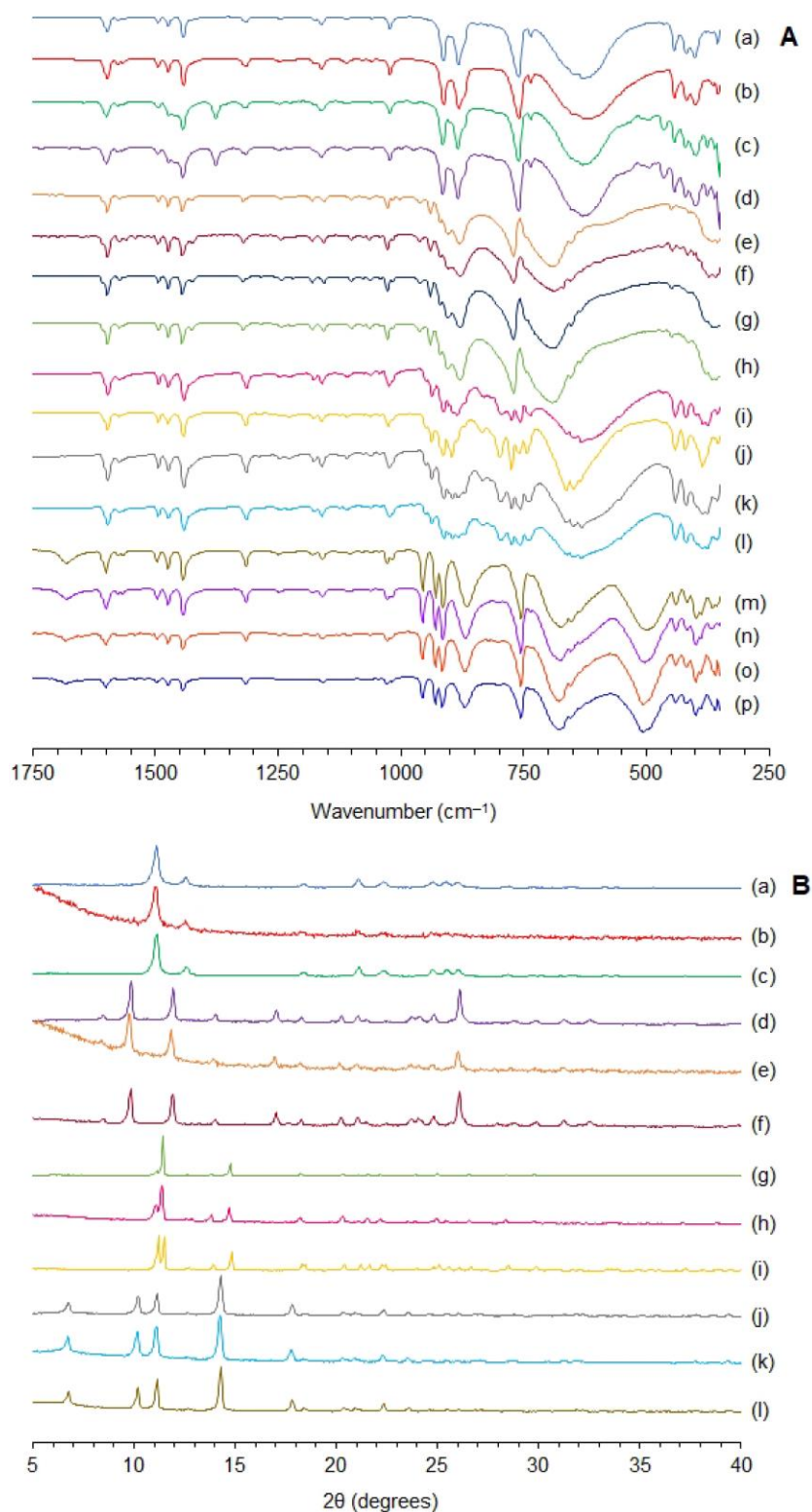
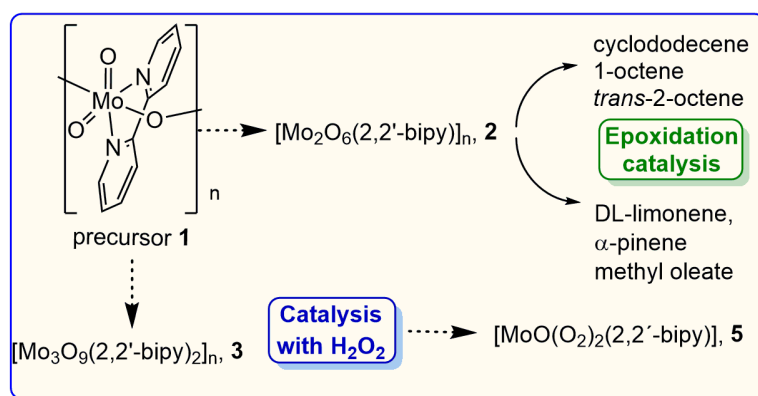


Figure 6.15. ATR FT-IR spectra (A) in the range of 250-1750 cm^{-1} of (a) **1**, (b) **1-AcidCat**, (c) **1-CT-Acid-S**, (d) **1-CT-Acid-S-Cat**, (e) **2**, (f) **2-AcidCat**, (g) **2-CT-Acid-S**, (h) **2-CT-Acid-S-Cat**, (i) **3**, (j) **3-AcidCat**, (k) **3-CT-Acid-S**, (l) **3-CT-Acid-S-Cat**, (m) **4**, (n) **4-AcidCat**, (o) **4-CT-Acid-S**, and (p) **4-CT-Acid-S-Cat**. PXRD patterns (B) of (a) **1**, (b) **1-AcidCat**, (c) **1-CT-Acid-S**, (d) **2**, (e) **2-AcidCat**, (f) **2-CT-Acid-S**, (g) **3**, (h) **3-AcidCat**, (i) **3-CT-Acid-S**, (j) **4**, (k) **4-AcidCat**, and (l) **4-CT-Acid-S**.

6.4. Conclusions

The study of the (hydro)thermal stability of the chainlike hybrid material $[\text{MoO}_3(2,2'\text{-bipy})]_n$ (**1**) has provided new syntheses of the related compounds $[\text{Mo}_2\text{O}_6(2,2'\text{-bipy})]_n$ (**2**) and $[\text{Mo}_3\text{O}_9(2,2'\text{-bipy})_2]_n$ (**3**) (Scheme 6.2) with yields that are superior to those obtained by hydrothermal methods using the free ligand 2,2'-bipy and simple molybdate salts as starting materials. It is remarkable that the thermal removal of 2,2'-bipy from **1**, in the presence or absence of water, can be achieved selectively and in a stoichiometric fashion, with retention of the 1D molybdenum oxide chain structure, to give **2** and **3**. Compounds **1-3** belong to the $[(\text{MoO}_3)_m(2,2'\text{-bipyridine})_n]$ family of hybrid materials and provide an interesting opportunity to study the effect of the organic ligand ordering and distribution on the materials' properties. In the present work it has been shown that the ratio m/n influences catalytic performance for the epoxidation of olefins using hydroperoxide oxidants, with compound **2** leading to the best results. Under the reaction conditions used, the hybrid acts as a precatalyst for active species formed *in situ*, which promote high selectivities in the epoxidation of a variety of olefins. The hybrid phase **2** may therefore be a better oxidation (pre)catalyst than **1**, which has already demonstrated interesting behaviour when applied for the oxidation of other substrates such as sulfides and amines.



Scheme 6.2. Summary of the main syntheses and catalytic studies carried out in this work.

6.5. References

- (1) Balendhran, S.; Walia, S.; Nili, H.; Ou, J. Z.; Zhuiykov, S.; Kaner, R. B.; Sriram, S.; Bhaskaran, M.; Kalantar-Zadeh, K. *Adv. Funct. Mater.* **2013**, *23*, 3952–3970.
- (2) Castro, I. A.; Datta, R. S.; Ou, J. Z.; Castellanos-Gomez, A.; Sriram, S.; Daeneke, T.; Kalantar-zadeh, K. *Adv. Mater.* **2017**, *29*, 1–31.
- (3) Behrend, R.; Meyer, E.; Rusche, F. *Justus Liebigs Ann. Chem.* **1905**, *339*, 1–37.
- (4) Greenblatt, M. *Chem. Rev.* **1988**, *88*, 31–53.
- (5) Huang, Q.; Hu, S.; Zhuang, J.; Wang, X. *Chem. - A Eur. J.* **2012**, *18*, 15283–15287.
- (6) Braïda, B.; Adams, S.; Canadell, E. *Chem. Mater.* **2005**, *17*, 5957–5969.
- (7) Hu, X. K.; Qian, Y. T.; Song, Z. T.; Huang, J. R.; Cao, R.; Xiao, J. Q. *Chem. Mater.* **2008**, *20*, 1527–1533.
- (8) Borgschulte, A.; Sambalova, O.; Delmelle, R.; Jenatsch, S.; Hany, R.; Nüesch, F. *Sci. Rep.* **2017**, *7*, 1–9.
- (9) Schöllhorn, R.; Schulte-Nölle, T.; Steinhoff, G. *J. Less-Common Met.* **1980**, *71*, 71–78.
- (10) Johnson, J. W.; Jacobson, A. J.; Rich, S. M.; Brody, J. F. *J. Am. Chem. Soc.* **1981**, *103*, 5246–5247.
- (11) Hagrman, P. J.; Hagrman, D.; Zubieta, J. *J. Angew. Chem.* **1999**, *38*, 2638–2684.
- (12) Vougo-Zanda, M.; Wang X.; Jacobson, A. J. *Inorg. Chem.* **2007**, *46*, 8819–8824.
- (13) Lysenko, A. B.; Senchyk, G. A.; Lincke, J.; Lässig, D.; Fokin, A. A.; Butova, E. D.; Schreiner, P. R.; Krautscheid, H.; Domasevitch, K. V. *Dalton Trans.* **2010**, *39*, 4223–4231.
- (14) Hagrman, P. J.; LaDuca, R. L.; Koo, H. J.; Rarig, R.; Haushalter, R. C.; Whangbo, M. H.; Zubieta, J. *Inorg. Chem.* **2000**, *39*, 4311–4317.
- (15) Yan, B.; Xu, Y.; Goh, N. K.; Chia, L. S. *Chem. Commun.* **2000**, *21*, 2169–2170.
- (16) Xu, Y.; Lu, J.; Goh, N. K. *J. Mater. Chem.* **1999**, *9*, 1599–1602.
- (17) Zhang, X.; Hejazi, M.; Thiagarajan, S. J.; Woerner, W. R.; Banerjee, D.; Emge, T. J.; Xu, W.; Teat, S. J.; Gong, Q.; Safari, A.; Yang, R.; Parise, J. B.; Li, J. *J. Am. Chem. Soc.* **2013**, *135*, 17401–17407.
- (18) Chuang, J.; Ouellette, W.; Zubieta, J. *Inorg. Chim. Acta* **2008**, *361*, 2357–2364.
- (19) Amarante, T. R.; Neves, P.; Valente, A. A.; Paz, F. A. A.; Pillinger, M.; Gonçalves, I. S. *J. Catal.* **2016**, *340*, 354–367.
- (20) Anyik, J. L.; Oluwafemi, O. S. *Mater. Lett.* **2017**, *196*, 141–144.
- (21) Zapf, P. J.; Haushalter, R. C.; Zubieta, J. *Chem. Mater.* **1997**, *4756*, 2019–2024.
- (22) Kim, J.; Lim, W. T.; Koo, B. K. *Inorg. Chim. Acta* **2007**, *360*, 2187–2191.
- (23) Amarante, T. R.; Antunes, M. M.; Valente, A. A.; Paz, F. A. A.; Pillinger, M.; Gonçalves, I. S. *Inorg. Chem.* **2015**, *54*, 9690–9703.
- (24) Lysenko, A. B.; Senchyk, G. A.; Domasevitch, K. V.; Hauser, J.; Fuhrmann, D.; Kobalz, M.; Krautscheid, H.; Neves, P.; Valente, A. A.; Gonçalves, I. S. *Inorg. Chem.* **2015**, *54*, 8327–8338.

Chapter 6

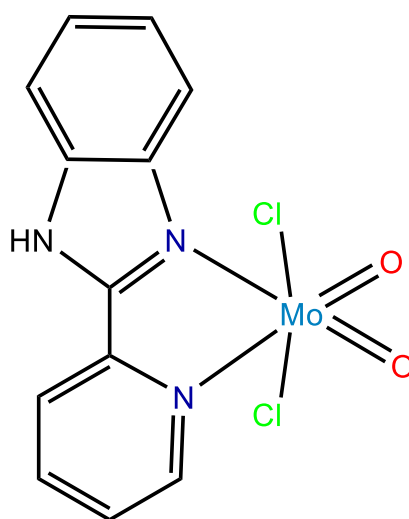
- (25) Amarante, T. R.; Neves, P.; Coelho, A. C.; Gago, S.; Valente, A. A.; Paz, F. A.; Pillinger, M.; Gonçalves, I. S. *Organometallics* **2010**, *29*, 883–892.
- (26) Abrantes, M.; Amarante, T. R.; Antunes, M. M.; Gago, S.; Almeida Paz, F. A.; Margiolaki, I.; Rodrigues, A. E.; Pillinger, M.; Valente, A. A.; Gonçalves, I. S. *Inorg. Chem.* **2010**, *49*, 6865–6873.
- (27) Amarante, T. R.; Neves, P.; Gomes, A. C.; Nolasco, M. M.; Ribeiro-Claro, P.; Coelho, A. C.; Valente, A. A.; Almeida Paz, F. A.; Smeets, S.; McCusker, L. B.; Pillinger, M.; Gonçalves, I. S. *Inorg. Chem.* **2014**, *53*, 2652–2665.
- (28) Tosi, I.; Vurchio, C.; Abrantes, M.; Gonçalves, I. S.; Pillinger, M.; Cavani, F.; Cordero, F. M.; Brandi, A. *Catal. Commun.* **2018**, *103*, 60–64.
- (29) Macrae, C. F.; Bruno, I. J.; Chisholm, J. A.; Edgington, P. R.; McCabe, P.; Pidcock, E.; Rodriguez-Monge, L.; Taylor, R.; Van De Streek, J.; Wood, P. A. *J. Appl. Crystallogr.* **2008**, *41*, 466–470.
- (30) Sitepu, H.; O'Connor, B. H.; Li, D. *J. Appl. Crystallogr.* **2005**, *38*, 158–167.
- (31) Twu, J.; Yu, Y. Y.; Tang, C. W.; Wang, G. J.; Chen, K. H. *Appl. Spectrosc.* **1999**, *53*, 1083–1086.
- (32) Zapf, P. J.; Haushalter, R. C.; Zubieta, J. *Chem. Mater.* **1997**, *9*, 2019–2024.
- (33) Kühn, F. E.; Groarke, M. .; Bencze, É.; Herdtweck, E.; Prazeres, A.; Santos, A. M. .; Calhorda, M. J.; Romão, C. C.; Gonçalves, I. S. .; Lopes, A. D. .; Pillinger, M. *Chem. Eur. J.* **2002**, *8*, 2370–2383.
- (34) Veiros, L. F.; Prazeres, Â.; Costa, P. J.; Romão, C. C.; Kühn, F. E.; Calhorda, M. J. *J. Chem. Soc.* **2006**, *60*, 1383–1389.
- (35) Comas-Vives, A.; Lledos, A.; Poli, R. *Chem. Eur. J.* **2010**, *16*, 2147–2158.
- (36) Amarante, T. R.; Neves, P.; Paz, F. A. A.; Pillinger, M.; Valente, A. A.; Gonçalves, I. S. *Inorg. Chem. Commun.* **2012**, *20*, 147–152.
- (37) Neves, P.; Amarante, T. R.; Gomes, A. C.; Coelho, A. C.; Gago, S.; Pillinger, M.; Gonçalves, I. S.; Silva, C. M.; Valente, A. A. *Appl. Catal., A* **2011**, *395*, 71–77.
- (38) Amarante, T. R.; Neves, P.; Paz, F. A. A.; Valente, A. A.; Pillinger, M.; Gonçalves, I. S. *Dalton Trans.* **2014**, *43*, 6059–6069.
- (39) Abrantes, M.; Amarante, T. R.; Antunes, M. M.; Gago, S.; Almeida Paz, F. A. A.; Margiolaki, I.; Rodrigues, A. E.; Pillinger, M.; Valente, A. A.; Gonçalves, I. S. *Inorg. Chem.* **2010**, *49*, 6865–6873.
- (40) Herbert, M.; Montilla, F.; Álvarez, E.; Galindo, A. *Dalton Trans.* **2012**, *41*, 6942–6956.
- (41) Amarante, T. R.; Gomes, A. C.; Neves, P.; Almeida Paz, F. A.; Valente, A. A.; Pillinger, M.; Gonçalves, I. S. *Inorg. Chem. Commun.* **2013**, *32*, 59–63.
- (42) Neves, P.; Nogueira, L. S.; Gomes, A. C.; Oliveira, T. S. M.; Lopes, A. D.; Valente, A. A.; Gonçalves, I. S.; Pillinger, M. *Eur. J. Inorg. Chem.* **2017**, 2617–2627.
- (43) Piquemal, J. Y.; Briot, E.; Brégeault, J. M. *Dalton Trans.* **2013**, *42*, 29–45.
- (44) Costa, P. J.; Calhorda, M. J.; Kühn, F. E. *Organometallics* **2010**, *29*, 303–311.
- (45) Calhorda, M. J.; Costa, P. J. *Curr. Org. Chem.* **2012**, *16*, 65–72.

Chapter 6

- (46) Grover, N.; Drees, M.; Kühn, F. E. *J. Catal.* **2015**, *329*, 269–285.
- (47) Canos, A. C.; Iborra, S.; Velty, A. *Chem. Rev.* **2007**, *107*, 2411–2502.
- (48) Mäki-Arvela, P.; Holmbom, B.; Salmi, T.; Murzin, D. Y. *Catal. Rev.* **2007**, *49*, 197–340.
- (49) Köckritz, A.; Martin, A. *Eur. J. Lipid Sci. Technol.* **2008**, *110*, 812–824.
- (50) Lee, A. F.; Bennett, J. A.; Manayil, J. C.; Wilson, K. *Chem. Soc. Rev.* **2014**, *43*, 7887–7916.
- (51) Golets, M.; Ajaikumar S.; Mikkola, J.-P. *Chem. Rev.* **2015**, *115*, 3147–3169.
- (52) Danov, S. M.; Kazantsev, O. A.; Esipovich, A. L.; Belousov, A. S.; Rogozhin, A. E.; Kanakov, E. A. *Catal. Sci. Technol.* **2017**, *7*, 3659–3675.
- (53) Amarante, T. R.; Neves, P.; Tomé, C.; Abrantes, M.; Valente, A.; A.; Paz, F. A. A.; Pillinger, M.; Gonçalves, I. S. *Inorg. Chem.* **2012**, *51*, 3666–3676.
- (54) Amarante, T. R.; Neves, P.; Valente, A. A.; Almeida Paz, F. A.; Fitch, A. N.; Pillinger, M.; Gonçalves, I. S. *Inorg. Chem.* **2013**, *52*, 4618–4628.
- (55) Neri, G.; Rizzo, G.; Pistone, A.; De Luca, L.; Donato, A.; Musolino, M. G.; Pietropaolo, R. *Appl. Catal., A* **2007**, *325*, 25–33.
- (56) Brocke, C.; Eh, M.; Finke, A. *Chem. Biodivers.* **2008**, *5*, 1000–1010.
- (57) Zawislak, G. *J. Essent. Oil-Bear. Plants* **2016**, *19*, 699–705.
- (58) Zhang, L.; Hu, C.; Mei, W.; Zhang, J.; Cheng, L.; Xue, N.; Ding, W.; Chen, J.; Hou, W. *Appl. Surf. Sci.* **2015**, *457*, 1951–1957.
- (59) Anbu, N.; Dhakshinamoorthy, A. *J. Ind. Eng. Chem.*, **2018**, *58*, 9–17.

CHAPTER 7

Chemistry and catalytic performance of pyridyl-benzimidazole oxidomolybdenum(VI) compounds in (bio)olefin epoxidation



[MoO₂Cl₂(2-(2-pyridyl)-benzimidazole)]

Chapter 7

Index

7.1. Introduction	191
7.2. Results and discussion	192
7.2.1. Synthesis and characterisation of (pre)catalysts [MoO ₂ Cl ₂ (pbim)] (1) and [MoO(O ₂) ₂ (pbim)] (2)	192
7.2.1. Hydrolytic stability of 1	198
7.3. Catalytic studies	200
7.3.1. Catalytic epoxidation with TBHP	200
7.3.2. Influence of cosolvent on the catalytic epoxidation with TBHP	202
7.3.3. Characterization of solids after catalytic epoxidation with TBHP	205
7.3.4. Reuse of recovered solids	206
7.3.5. Characterization of reused solids	206
7.3.6. Identification of the catalytic active specie in catalytic epoxidation with TBHP	207
7.3.7. <i>cis</i> -Cyclooctene epoxidation with H ₂ O ₂ (including cosolvent influence and characterization of recovered solids)	210
7.3.8. Bio-olefins epoxidation with H ₂ O ₂ (including characterization of recovered solids)	212
7.4. Conclusions	214
7.5. References	215

Chapter 7

7.1. Introduction

High-valent oxidomolybdenum(VI) complexes have proven to be excellent molecular catalysts for a plethora of organic transformations, including oxidations, C–X bond-forming reactions, reductions, and deoxygenations.^{1–5} Complexes that have attracted particular attention include $[\text{MoO}_2(\text{acac})_2]$ (acac = acetylacetonate), Schiff base complexes $[\text{MoO}_2(\text{L})_2]$, MoO_2Cl_2 and its Lewis base adducts $[\text{MoO}_2\text{Cl}_2(\text{L})_n]$, organometallic derivatives $[\text{MoO}_2\text{R}_2(\text{L})_n]$ and $[(\eta^5\text{-C}_5\text{R}_5)\text{MoO}_2\text{X}]$, and oxidodiperoxido complexes $[\text{MoO}(\text{O}_2)_2(\text{L})_n]$. The systematic investigation of ligand effects has allowed the rational design of ligands to prepare more efficient homogeneous catalysts.^{6–9} Aromatic bidentate nitrogen ligands (N–N), such as 2,2'-bipyridine derivatives and pyrazolylpyridines, are excellent options, since they are resistant to oxidative degradation and afford complexes of the type $[\text{MoO}_2\text{X}_2(\text{N-N})]$ and $[\text{MoO}(\text{O}_2)_2(\text{N-N})]$ with high coordinative stability.^{6–8} Going beyond mononuclear complexes, the $\{\text{MoO}_2\text{X}_2(\text{N-N})\}$ and $\{\text{MoO}(\text{O}_2)_2(\text{N-N})\}$ (X = Cl or bridging $\mu\text{-O}$) coordination environments can be found in oligonuclear complexes, such as $[\{\text{MoO}_2\text{X}(\text{N-N})\}_2(\mu_2\text{-O})]^{10,11}$, $[\{\text{MoO}_2(\mu_2\text{-O})(\text{N-N})\}_2]^{12}$, and $[\text{Mo}_4\text{O}_{12}(\text{N-N})_4]^{13}$; polymeric hybrid structures, such as $[\text{MoO}_3(\text{N-N})]$, consisting of infinite one-dimensional (1D) chains^{14,15}; and complexes supported on ligand-modified silicas¹⁶, organic polymers¹⁷, and metal–organic frameworks^{18,19}.

Among ligands containing nitrogen donor atoms, the coordination chemistry of imidazolyl (and benzimidazolyl) ligands has been of great interest, due to the critical role played by these groups as metal-binding sites in a variety of biologically important molecules.^{20–22} Several molybdenum(VI) complexes containing imidazole (im) as a monodentate ligand have been reported and include Schiff base complexes of the type $[\text{MoO}_2\text{L}(\text{im})]^{23–26}$, peroxido complexes $[\text{MoO}(\text{O}_2)_2(\text{im})(\text{H}_2\text{O})]^{27}$, and dinuclear complexes $[\text{Mo}_2\text{O}_4(\text{ox})_2(\text{im})_2]^{2-}$ (H_2ox = oxalic acid) and $[\text{Mo}_2\text{O}_6(\text{im})_4]^{28–30}$. To the best of our knowledge, mono- or dinuclear oxidomolybdenum(VI) complexes bearing unsubstituted benzimidazole (bim) have not been reported. On the other hand, several complexes bearing bidentate 2-substituted benzimidazole derivatives have been described; for example, $[\text{MoO}_2(\text{L})_2]$, where $\text{LH} = 2\text{-(}\alpha\text{-hydroxyalkyl)benzimidazole}^{31}$, and $[\text{MoO}(\text{O}_2)_2\text{L}]$, where $\text{L} = 2\text{-(2-pyridyl)benzimidazole (pbim)}^{32}$. The *N,N*-diimine chelating ligand pbim has a rich history in coordination chemistry, and metal complexes containing this ligand have been used to catalyze various organic reactions^{33–36}. An appealing feature of pbim is that facile alkylation of the bim NH group allows a wide variety of substituents to be attached, which is of interest in the context of catalyst optimization. With respect to the epoxidation of olefins, the published studies include the use of $[\text{CH}_3\text{ReO}_3(\text{pbim})]$ as a catalyst, with aq. H_2O_2 as the oxidant³⁷, and the use of $[\text{Mo-(}\eta^3\text{-}$

Chapter 7

$\text{C}_3\text{H}_5\text{Br}(\text{CO})_2(\text{pbim})$] as a catalyst precursor, with TBHP as the oxidant.³⁴ As far as it is aware, the complexes $[\text{MoO}(\text{O}_2)_2(\text{pbim})]$ ³² and $[\text{MoO}_2\text{Cl}_2(\text{pbim})]$ (not previously reported) have not been studied as catalysts in olefin epoxidation.

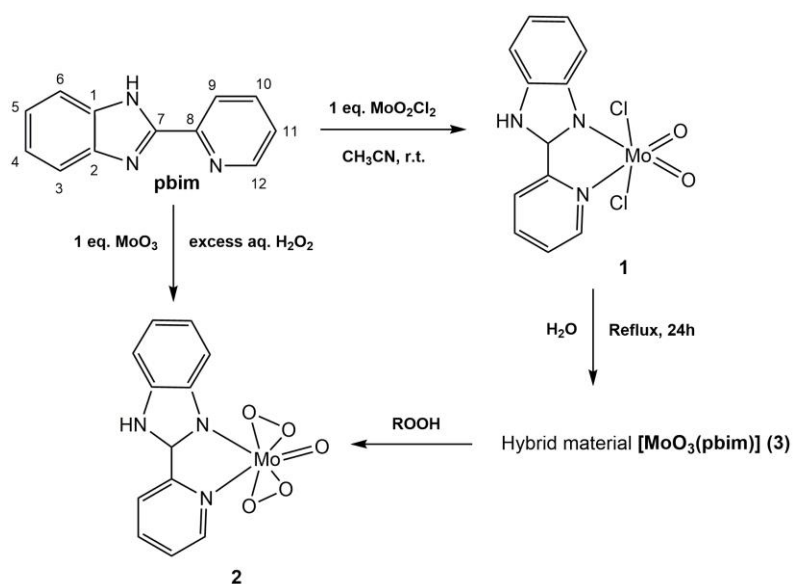
In the field of Mo-catalyzed olefin epoxidation, complexes of the type $[\text{MoO}_2\text{Cl}_2(\text{N-N})]$ have been quite extensively studied, especially in relation to ligand effects, and this has resulted in the development of effective catalytic systems. However, questions about the stability of the (pre)catalyst, the homogeneous/heterogeneous nature of the reaction and the form of the true catalytic species have often been overlooked. In this chapter, these issues are especially discussed for the dichlorido complex $[\text{MoO}_2\text{Cl}_2(\text{pbim})]$ (**1**). Post-use catalyst characterization shows that, depending on the oxidant used, **1** is transformed *in situ* to the oxidodiperoxido complex $[\text{MoO}(\text{O}_2)_2(\text{pbim})]$ (**2**), or a hybrid molybdenum(VI) oxide solid, formulated as $[\text{MoO}_3(\text{pbim})]$ (**3**). Compounds **2** and **3** were prepared separately to allow a more complete characterization and, for **3**, a study of its performance in the catalytic epoxidation of bio-olefins. In addition to elucidating the homogeneous/heterogeneous nature of each system, chemical transformations of **1–3** under the reaction conditions have been studied by characterizing recovered catalysts, leading to a good understanding of the chemistry and catalytic behavior.

7.2. Results and discussion

7.2.1. Synthesis and characterisation of (pre)catalysts $[\text{MoO}_2\text{Cl}_2(\text{pbim})]$ (**1**) and $[\text{MoO}(\text{O}_2)_2(\text{pbim})]$ (**2**)

MoO_2Cl_2 was dissolved in acetonitrile to give a solution of the complex $[\text{MoO}_2\text{Cl}_2(\text{NCCH}_3)_2]$. Addition of the ligand pbim (1 equiv.) to this solution and stirring at room temperature for 1 h led to the precipitation of the dichlorido complex $[\text{MoO}_2\text{Cl}_2(\text{pbim})]$ (**1**) as a yellow solid, which was isolated in excellent yield (88 %) (Scheme 7.1). This procedure has proved to be a good alternative to the traditional method of synthesis for complexes $[\text{MoO}_2\text{Cl}_2\text{L}]$ (L = ligand), since it is not necessary to obtain the precursor complex $[\text{MoO}_2\text{Cl}_2(\text{THF})_2]$ as first step.^{10,38–41} Complex **1** was characterised by elemental analysis, PXRD, TGA, FT-IR, FT-Raman, ¹H NMR and ¹³C{¹H} MAS NMR spectroscopies.

Chapter 7



Scheme 7.1. Preparative routes used to obtain **1-3**.

Elemental analyses of **1** (C, H and N) is satisfactory with the empirical $\text{C}_{12}\text{H}_9\text{Cl}_2\text{MoN}_3\text{O}_2$. The thermal decomposition behaviour of the complex was studied by thermogravimetry (Figure 7.1). The onset of decomposition for complex **1** is at ca. 260 °C. An abrupt weight loss above 340 °C (DTGmax = 365 °C) leads to a residual mass of 31.8 % at 600 °C.

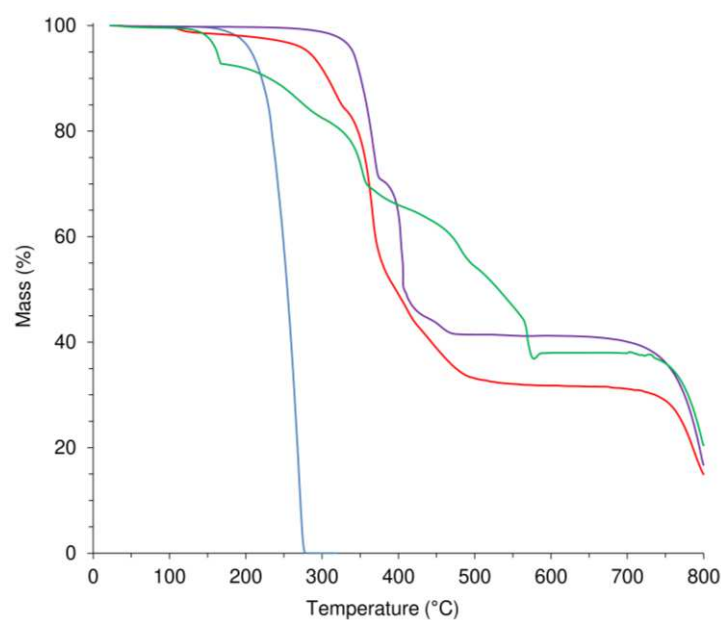


Figure 7.1. TGA curves for the free ligand pbim (—), complex **1** (—), complex **2** (—), and hybrid material **3** (—).

Chapter 7

Solid **1** was characterized by PXRD, which showed a reasonable microcrystalline phase (Figure 7.2). Some diffracted peaks were shifted in the PXRD pattern comparing with the free ligand, suggesting that Hpbim undergoes structural changes during the reaction with MoO_2Cl_2 as it was expected.

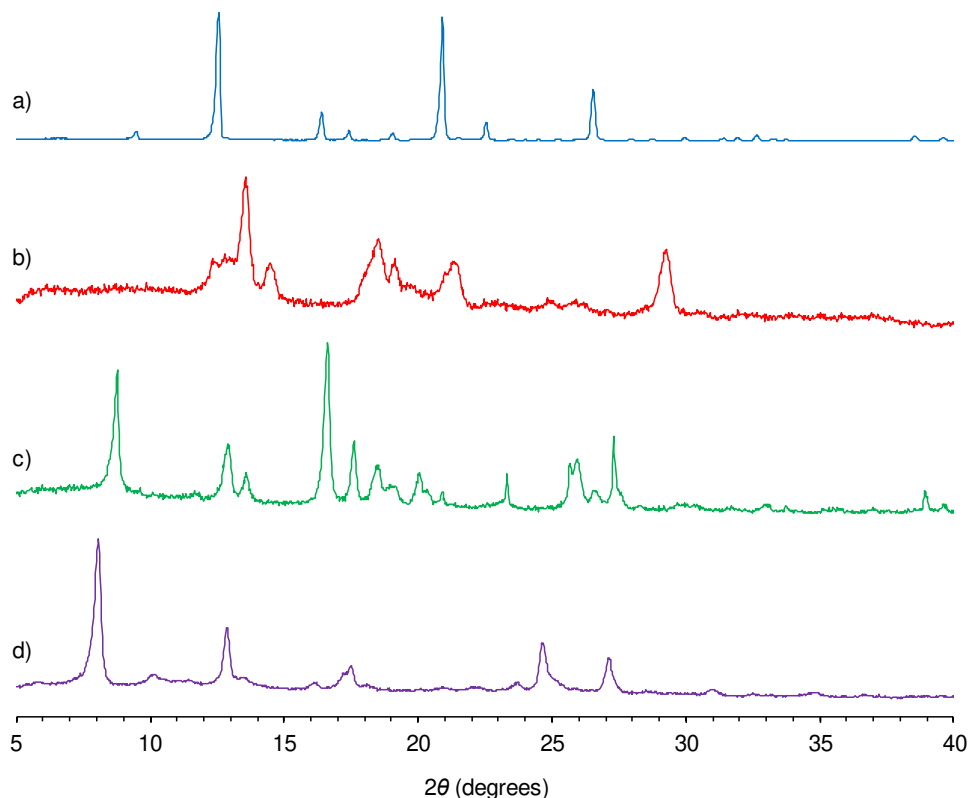


Figure 7.2. PXRD patterns of a) free ligand pbim, b) $[\text{MoO}_2\text{Cl}_2(\text{pbim})]$ (**1**), c) $[\text{MoO}(\text{O}_2)_2(\text{pbim})]$ (**2**) and d) $[\text{MoO}_3(\text{pbim})]$ (**3**).

Proof of ligand coordination in **1** is provided by the FT-IR and FT-Raman spectra. The FT-IR and FT-Raman spectra of **1** contain bands that are typical of complexes of the type $[\text{MoO}_2\text{Cl}_2(\text{L})]$, where L is a N,N'-chelating biheteroaromatic ligand. Bands at $942 \pm 1 \text{ cm}^{-1}$ (strong in IR and Raman) and 886 cm^{-1} (very strong in IR and weak in Raman) are assigned to symmetric and asymmetric Mo=O stretching modes, respectively (Figures 7.3 and 7.4).¹⁰ A weak band at 385 cm^{-1} is attributed to the out-of-plane deformation mode, $\gamma(\text{MoO}_2)$, in agreement with calculated and experimentally observed values previously reported for similar complexes containing the *cis*- $[\text{MoO}_2]^{2+}$ core.^{10,42} A strong IR band at 341 cm^{-1} is assigned to $\nu_{\text{as}}(\text{Mo}-\text{Cl})$. Several weak bands in the range $150\text{--}250 \text{ cm}^{-1}$ in the Raman spectrum are difficult to assign, but have previously been associated with $\beta(\text{MoO}_2)$, $\nu_{\text{s}}(\text{Mo}-\text{Cl})$, and $\nu(\text{Mo}-\text{N})$ vibrations.^{10,42}

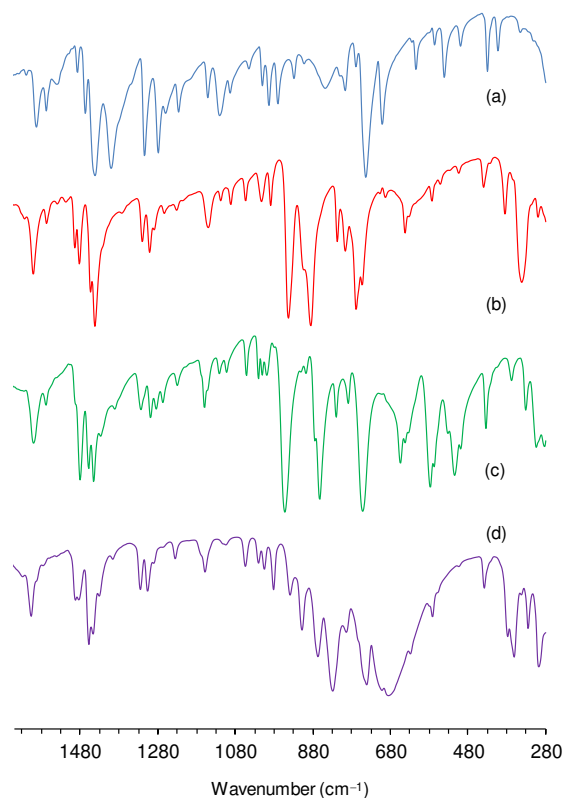


Figure 7.3. FT-IR spectra in the range 280–1650 cm^{-1} for (a) free ligand pbim; (b) complex **1**; (c) complex **2**; and (d) hybrid material **3**.

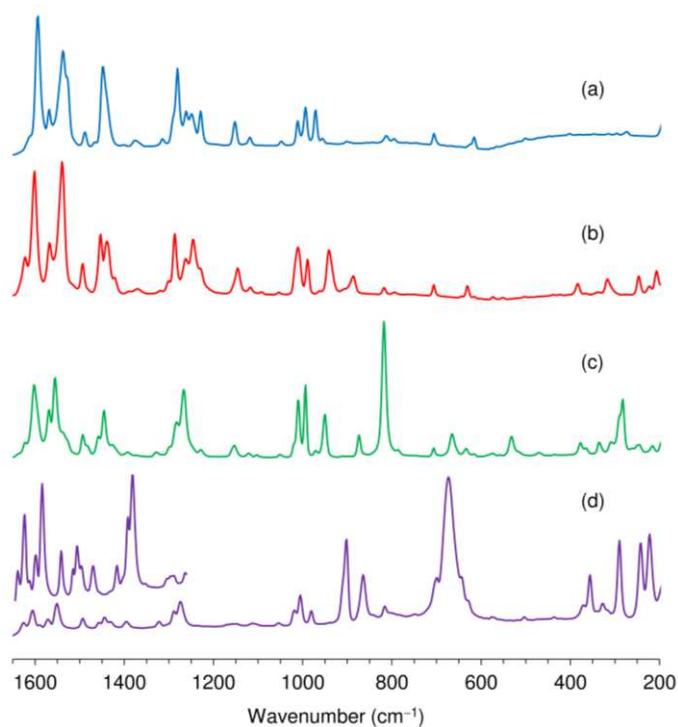


Figure 7.4. FT-Raman spectra in the range 300–1650 cm^{-1} for (a) free ligand pbim; (b) complex **1**; (c) complex **2**; and (d) hybrid material **3**. The inset shows an expansion of the 1110–1650 cm^{-1} region for (d).

Chapter 7

Further evidence of the N,N-chelation mode of pbim in **1** comes from an analysis of ligand-centered vibrational modes. In the spectral region containing inter-ring C–C and C=C/C=N (ring) stretching vibrations, complex **1** displays three bands at 1539, 1568, and 1601 cm^{-1} in both the FT-IR and FT-Raman spectra. The latter band is shifted from 1593 cm^{-1} for the free ligand pbim, which is consistent with coordination of the imine nitrogen atom of the imidazole group to the Mo(VI) center.^{37,43} Support for the coordination of the pyridyl nitrogen atom comes from the observation of a shift of the in-plane ring deformation band (FT-IR) from 614 cm^{-1} for the free ligand to 642 cm^{-1} for **1**.⁴³

The ^1H NMR spectrum of **1** in DMSO- d_6 exhibit several resonances in the 7.40-8.90 ppm region and presents six signals for the eight aryl and pyridyl protons. In general, these are shifted downfield significantly with respect to the corresponding signals for the free ligand. For example, the signal at $\delta = 8.73$ ppm for H-12 (the sp^2 hydrogen alpha to the nitrogen of the pyridine ring) of the free ligand in DMSO- d_6 shifts to 8.87 ppm in complex **1**. These downfield shifts show that the ligand remains coordinated to the metal center, despite recording the spectrum in a strongly coordinating solvent, has already reported in other studies.^{10,41,44} However, the signal referring the NH proton of the benzimidazole moiety could not be located at 12-13 ppm. This may be explained if the proton resonates along with aromatic protons or appears beyond 15 ppm. Other previous studies have also observed the absence of this signal, for example, Maurya *et al.* work³² with $[\text{MO}(\text{O}_2)_2\text{L}]$ (M = Mo or W, L = 2-(2-pyridyl)-benzimidazole, 2-(3-pyridyl)benzimidazole) and Mohanty *et al.* work²³ with mononuclear $[\text{MoO}_2\text{L}(\text{im})]$ (LH_2 = Schiff base ligands, im = imidazole) complexes.

The $^{13}\text{C}\{^1\text{H}\}$ CP MAS NMR spectrum of complex **1** displays signals between 154 and 116 ppm for the benzimidazole and pyridine aromatic carbon atoms (Figure 7.5).⁴⁵ Carbons at the position 7, 12, 8, 1, and 10 can be localized at 153.58, 145.64, 142.73, 138.49 and 133.12 ppm for **1**, respectively. The others signals between 130-115 ppm comprise overlapping resonances. The signals of the carbon atoms of the benzimidazole and pyridine rings of **1** were shifted to higher or lower chemical values relative to the corresponding signals of the free ligand.

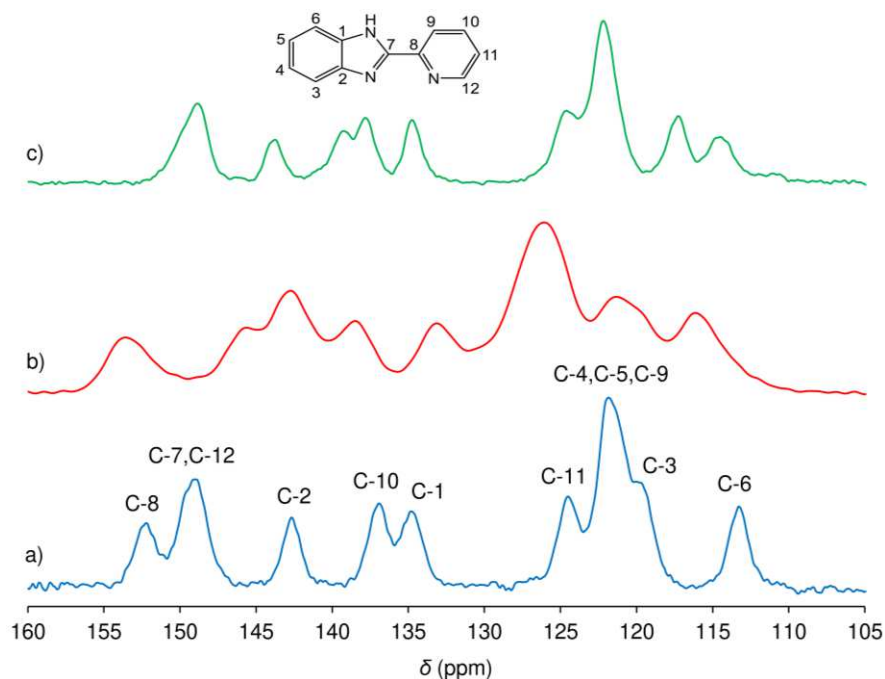


Figure 7.5. $^{13}\text{C}\{^1\text{H}\}$ CP MAS NMR spectra of a) free ligand pbim, b) $[\text{MoO}_2\text{Cl}_2(\text{pbim})]$ (**1**) and c) $[\text{MoO}_3(\text{pbim})]$ (**3**).

The oxidodiperoxido complex $[\text{MoO}(\text{O}_2)_2(\text{pbim})]$ (**2**) was prepared by the standard method³² for complexes of the type $[\text{MoO}(\text{O}_2)_2(\text{L})]$, involving addition of the organic ligand to an aqueous solution containing the species $[\text{MoO}(\text{O}_2)_2(\text{H}_2\text{O})_2]$ [prepared by dissolving $\alpha\text{-MoO}_3$ in a large excess of H_2O_2 (30 %)] with 84 % of yield.

The elemental analysis data for C, H and N led to the empirical formula $\text{C}_{12}\text{H}_9\text{MoN}_3\text{O}_5$. The oxidodiperoxido complex **2** displays a small step at ca. 160 °C (7.3 % mass loss), due to the loss of a peroxido group, followed by a gradual loss of 10.5 %, up to 305 °C, and a more abrupt loss of 16.1 %, up to 400 °C (DTG: $T_{\text{max}} = 350$ °C), associated to the pbim decomposition. Further decomposition leads to a residual mass of 38.0 % at 600 °C, in good agreement with the calculated value of 38.8 % for MoO_3 .

Compound **2** is micro-crystalline and displays several angles (5–30° 2 θ) reflections in the powder XRD pattern.

FT-IR spectroscopic data for **2** were in agreement with those reported by Maurya and Jayaswal for the same complex prepared by a similar route.³² In the range 500–1000 cm^{-1} , the FT-IR spectrum contains two strong bands at 953 [$\nu(\text{Mo}=\text{O})$] and 863 cm^{-1} [$\nu(\text{O}-\text{O})$], a weak shoulder at 875 cm^{-1} [$\nu(\text{O}-\text{O})$], and medium-intensity bands at 577 and 515 cm^{-1} due to $\nu(\text{Mo}-\text{O})_{\text{peroxido}}$ (Figure 7.3). Corresponding bands in the FT-Raman spectrum are found at 950, 874, 574, and 532 cm^{-1} . As found for complex **1**, the ligand-centered bands at 614 cm^{-1} (IR spectroscopy) and 1593 cm^{-1} (IR/Raman spectroscopy) for free pbim are shifted to 642 and 1601 ± 1 cm^{-1} , respectively, in the

Chapter 7

spectra of **2**. These structural modifications proof that the ligand pbim is coordinated to the metal center.

7.2.2. Hydrolytic stability of **1**

With the aim of studying the hydrolytic stability of **1**, the complex was treated with water under reflux for 24 h. The reaction of hydrolysis and condensation of **1** gave an insoluble white solid (**3**) suspended in an acidic (pH 1) mother liquor with 71 % of yield. The low pH of the solution is due to the presence of HCl, resulting from the hydrolysis of the Mo–Cl bonds in **1**. Compound **3** was characterised by elemental analysis, PXRD, TGA, FT-IR, FT-Raman and $^{13}\text{C}\{^1\text{H}\}$ MAS NMR spectroscopies.

Elemental analysis for **3** was consistent with the composition $[\text{MoO}_3(\text{pbim})]$. This was supported by the TGA data (Figure 7.1). No mass loss is observed until 300 °C. A 58.6 % mass loss is then registered between 300 and 500 °C, consisting of two overlapping mass-loss steps (DTG: $T_{\text{max}} = 370, 405$ °C). Assuming that decomposition leads to MoO_3 at 500 °C, the residual mass of 41.4 % is in good agreement with the calculated value of 42.4 % for an initial composition of $[\text{MoO}_3(\text{pbim})]$ (**3**). A further mass-loss step above 700 °C is due to sublimation of MoO_3 . From these data, it is evident that material **3** exhibits good thermal stability with respect to decomposition of the organic ligand. The powder X-ray diffraction pattern for **3** contains several fairly broad Bragg peaks between 5 and 30° 2θ , indicating that the material is microcrystalline, albeit with low crystallinity (Figure 7.2). No crystal structure solution is possible using this data, and to date, we have not been successful in obtaining single crystals of **3** suitable for XRD. Hence, the structure of **3** has not yet been determined unambiguously. Nevertheless, some additional indications about the structure of **3** can be obtained from an analysis of the FTIR spectra, the Raman spectra, and the ^{13}C CP-MAS NMR spectra.

In the spectral region 1200–1650 cm^{-1} , containing bands for the internal ligand modes, the vibrational spectra of **3** display a strong resemblance to those for complex **1**, confirming the presence of the ligand pbim in **3** with a bidentate coordination mode (Figures 7.3 and 7.4). For instance, the band at 1593 cm^{-1} for free pbim is shifted to 1606 cm^{-1} for **3**. Two bands at 902 and 864 cm^{-1} in the Raman spectrum, with medium and weak intensities, respectively, can be assigned as $\nu_s(\text{Mo}=\text{O})$ and $\nu_{\text{as}}(\text{Mo}=\text{O})$, indicating the presence of a *cis*- $[\text{MoO}_2]^{2+}$ core. The corresponding bands in the IR spectrum appear at 908 and 868 cm^{-1} , with medium and strong intensities, respectively. The main features observed in the IR spectrum below 850 cm^{-1} are an intense band at 829 cm^{-1} and an intense/broad band centered at 685 cm^{-1} ; the Raman

Chapter 7

spectrum contains a very weak band at 816 cm^{-1} and a very strong band at 674 cm^{-1} . The bands around 820 cm^{-1} can be assigned as $\nu_{\text{as}}(\text{Mo-O-Mo})$, while those around 680 cm^{-1} may be due to $\delta(\text{Mo-O-Mo})$, or more likely, $\nu_{\text{s}}(\text{Mo-O-Mo})$.⁴² Towards lower wavenumbers, the most important observation concerns the absence of a band around 340 cm^{-1} for $\nu_{\text{as}}(\text{Mo-Cl})$. The spectra therefore suggest a polymeric structure for **3** consisting of repeating $\{\text{MoO}_2(\mu_2\text{-O})(\text{pbim})\}$ units. This is in agreement with the microanalytical and TGA data, which indicate a 1:1 MoO_3/pbim stoichiometry.

The $^{13}\text{C}\{^1\text{H}\}$ CP MAS NMR spectrum of material **3** shows some differences concerning the chemical values of the resonances comparing with complex **1**, however the ligand is still intact after the reaction of **1** with water (Figure 7.5). Benzimidazole and pyridine carbon atoms in **3** are localized between 149 and 114 ppm. The $^{13}\text{C}\{^1\text{H}\}$ CP-MAS NMR spectrum for the free ligand pbim contains about nine resolved peaks between $\delta = 110$ and 155 ppm that can be assigned to the pyridyl and benzimidazolyl carbon atoms (some of which give rise to overlapping resonances) (Figure 7.5) in consonance with the solution spectrum. Approximately nine peaks are also evident in this chemical shift range for complex **1** and material **3**, supporting the presence of one chemically (and, possibly, crystallographically) distinct pbim molecule in each compound. Comparing these two spectra, there are some differences concerning the positions and relative intensities of some peaks, which reflect the different chemical environments of the coordinated ligands.

The apparent composition of $[\text{MoO}_3(\text{pbim})]$ for **3** is significant, since, until now, reactions of complexes of the type $[\text{MoO}_2\text{Cl}_2(\text{L})]$ with water have given hybrid materials with lower overall ligand contents; for example, $\text{Mo/L} = 2:1$ in the octanuclear complex $[\text{Mo}_8\text{O}_{22}(\text{OH})_4(4,4'\text{-di-tert-butyl-2,2'-bipyridine})_4]$ ⁴⁶ and the polymeric materials $\{[\text{MoO}_3(2,2'\text{-bipy})][\text{MoO}_3(\text{H}_2\text{O})]\}_n$ ($2,2'\text{-bipy} = 2,2'\text{-bipyridine}$)⁴⁷ and $[\text{Mo}_2\text{O}_6(\text{L})]$ ($\text{L} = [3\text{-pyridinium-2-yl-1H-pyrazol-1-yl}]$ acetate or $2\text{-}(1\text{-pentyl-3-pyrazolyl})$ pyridine (ppp))^{48,49}, and $\text{Mo/L} = 3:1$ in the polymeric material $[\text{Mo}_3\text{O}_9(\text{pzpy})]$ $\{\text{pzpy} = 2\text{-}[3(5)\text{-pyrazolyl}]$ -pyridine⁴². The structures for three of these polymeric materials share a common feature, consisting of a ladder-type inorganic core built from interconnected $\{\text{MoO}_6\}$ octahedra.^{42,47,48} As indicated in the introduction, oligomeric or polymeric molybdenum oxide/organonitrogen hybrid structures that contain only $\{\text{MoO}_2(\mu_2\text{-O})(\text{L})\}$ repeat units are actually quite rare, being limited to the tetranuclear species $[\text{Mo}_4\text{O}_{12}(\text{pzpy})_4]$ ¹³ and the polymeric materials $[\text{MoO}_3(2,2'\text{-bipy})]$ ¹⁴ and $[(\text{CH}_3)_2\text{NH}_2][\text{MoO}_3(\text{H}_2\text{bpdc})]$ ($\text{H}_2\text{bpdc} = 2,2'\text{-bipyridine-5,5-dicarboxylic acid}$)¹⁵, both of which are composed of 1D chains formed by corner-sharing $\{\text{MoO}_4\text{N}_2\}$ octahedra. The FTIR spectrum of $[\text{MoO}_3(2,2'\text{-bipy})]$ exhibits bands at 882 and 914 cm^{-1} , assigned to $\nu(\text{Mo=O})$ from *cis*- $[\text{MoO}_2]^{2+}$ units, and a broad, intense band at 622 cm^{-1} , attributed to $\nu(\text{Mo-O-Mo})$; a similar set of bands is

Chapter 7

found for $[(\text{CH}_3)_2\text{NH}_2][\text{MoO}_3(\text{Hbpd})]$.¹⁵ Hence, on the basis of the spectroscopic data for **3**, the material seems to possess a similar 1D hybrid polymeric structure, $[\text{MoO}_3(\text{pbim})]$.

7.3 Catalytic studies

7.3.1. Catalytic epoxidation with TBHP

Compounds **1–3** promoted the epoxidation of *cis*-cyclooctene (Cy), used as a model olefin, with TBHP as the oxygen donor, a reaction temperature in the range 55–70 °C, and (optionally) a cosolvent (Table 7.1, Figure 7.6). With TFT as the cosolvent, increasing the reaction temperature had a positive effect on the kinetics, without affecting product selectivity, which was always 100 % to CyO. For instance, at 55 °C, conversions at 24 h were 49 % and 56 % for **1** and **3**, rising to 97–98 % for a reaction temperature of 70 °C. All three compounds performed similarly at the higher reaction temperature, giving 72–82 % conversion at 6 h and 97–98 % conversion at 24 h. Without a catalyst, conversion was 7 % at 70 °C. Iodometric titration was carried out after stirring a mixture of **3**, TBHP, and TFT for 24 h at 70 °C. The results showed no measurable TBHP decomposition, indicating that oxidant consumption for olefin epoxidation using the catalytic system **3**/TBHP is efficient.

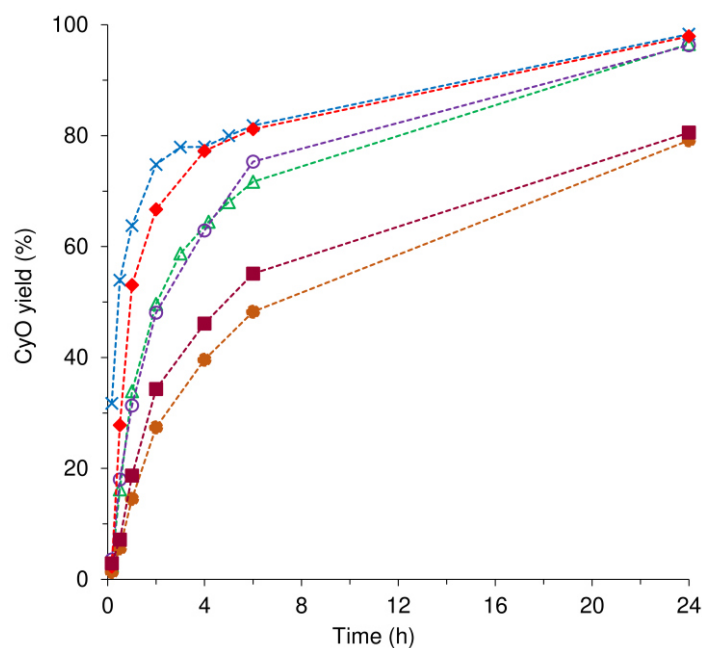


Figure 7.6. *cis*-Cyclooctene epoxidation with TBHP at 70 °C for the systems **1**/TFT (x), **2**/TFT (♦), **3**/TFT (Δ), **3**/toluene (○), **3**/CH₃CHCl₂ (●), and **3**/ws (■). The dashed lines are visual guides.

Chapter 7

Table 7.1. *cis*-Cyclooctene epoxidation with TBHP or H₂O₂ using compounds **1**, **2**, and **3**.^a

Oxidant	Compound	Cosolvent	T [°C]	Epoxide conversion at 6 h/24 h (%) ^b
TBHP	1	TFT	55	39/49
	1	TFT	70	82/98
	2	TFT	70	81/98
				(93/98; 96/99) ^c
	2^d	TFT	70	53/99
	3	TFT	55	30/56
	3	TFT	70	72/97
				(88/99) ^d
	3^f	TFT	70	61/90
	3-CT-TBHP-S^g	TFT	70	92/100
	3	CH ₃ CHCl ₂	70	70 48/79
	3	Toluene	70	75/96
	3	wt	70	55/81
3	EtOH	70	-/73	
H ₂ O ₂	1	CH ₃ CN	70	17
	2	CH ₃ CN	70	35
	3	CH ₃ CN	70	16
	3	EtOH	70	35
	3	EtOAc	70	5
	3	ws	70	20
	3	PrOH	70	36

^a Initial Mo/Cy/oxidant molar ratio = 1:100:153; [Cy] = 1.0 M. ^b Cy conversion at either 6 h/24 h (for TBHP) or 24 h (for H₂O₂) reaction (CyO selectivity was 100 %). ^c Values in brackets are for second and third 24 h batch runs, using the same initial solid/oxidant/olefin mass ratio. ^d Initial Mo/Cy/TBHP molar ratio = 1:6680:10206. ^e Values in brackets are for a second run carried out with **3**-TBHP-TFT-70-S1, using the same initial solid/oxidant/olefin mass ratio. ^f In the presence of the radical scavenger 2,6-di-*tert*-butyl-4-methyl-phenol, used in an equimolar amount relative to Cy. ^g Using the same initial solid/oxidant/olefin mass ratio.

The catalytic result for **1** at 55 °C (Cy conversion at 24 h) is similar to that reported previously for the complex [Mo(η^3 -C₃H₅)Br(CO)₂(pbim)] (45 % Cy conversion, using an initial Mo/Cy/TBHP molar ratio of 1:100:200).³⁴ Various hybrid molybdenum(VI) oxide/organic compounds have been described in the literature as catalysts for the Cy/TBHP reaction, although it is not always possible to clearly compare catalytic performances, due to considerable differences in the reaction conditions used.

7.3.2. Influence of cosolvent on the catalytic epoxidation with TBHP

For the hybrid material **3** and a reaction temperature of 70 °C, the type of cosolvent influenced the reaction kinetics, but not the epoxide selectivity, which was always 100 %. The CyO yield at 24 h followed the order: TFT = toluene > no cosolvent (ws) = CH₃CHCl₂ > EtOH (Table 7.1, Figure 7.6). The polarity of the cosolvent could partly influence the solubility of metal species and thereby have an effect on catalytic performance. However, there is no direct relationship between the catalytic results and the dipole moments of the solvents which follow the order: TFT (2.86) > CH₃CHCl₂ (1.8) > EtOH (1.7) > toluene (0.4).⁵⁰ Possibly, the catalytic results are due to a complex interplay between various factors, which may include solubility of metal species and coordination ability and/or stabilizing effects of the cosolvent on transition states.

Focusing on results obtained with TFT as the cosolvent and a reaction temperature of 70–75 °C, the catalytic results for **3** at 70 °C may be compared with those obtained with molybdenum(VI) oxide hybrid solids with the general compositions [Mo_nO_{3n}(L)_m] (*n* = 1-3; *m* = 0.5 or 1) and [Mo₂O₆(L)(H₂O)₂], where L = triazole-based ligand^{51,52} or pzpy⁴². For example, the material [Mo₃O₉(pzpy)] led to 60 % Cy conversion after 6 h at 75 °C⁴², and [MoO₃(1,2,4-triazole)_{0.5}] led to 35 % conversion at 24 h/70 °C⁵³, which is lower than that obtained with **3** at 70 °C (72 %). On the other hand, [Mo₃O₉(pzpy)] gave 85 % Cy conversion with CH₃CHCl₂ as the cosolvent (6 h, 75 °C), while **3** gave 48 % conversion (6 h, 70 °C). The hybrid material with the composition [MoO₃(2,2'-bipy)]_n which, as discussed above, seems to be structurally related with **3**, gave 100 % Cy conversion with CH₃CHCl₂ as the cosolvent (6 h, 75 °C).⁵⁴ The different catalytic performances for these materials may be due to various factors, such as Lewis acidity, steric effects, structural dimensionality of the hybrid polymers, and/or solubility and stability of the molybdenum compounds.

Although the system **3**/TBHP was biphasic solid–liquid (TFT as the cosolvent), filtration and contact tests indicated that the catalytic reaction occurred in the homogeneous phase. Specifically, the filtration test showed increasing Cy conversion after separating the undissolved solid from the reaction mixture at 1 h (from 34 % conversion at 1 h to 77 % conversion at 24 h/70 °C). Accordingly, for the liquid phase obtained after contacting **3** with TBHP in TFT at 70 °C for 24 h (**3**-CT-TBHP-L), Cy conversion increased from 17 % at 1 h to 91 % at 24 h/70 °C. Hence, dissolved metal species promoted the homogeneous catalytic reaction.

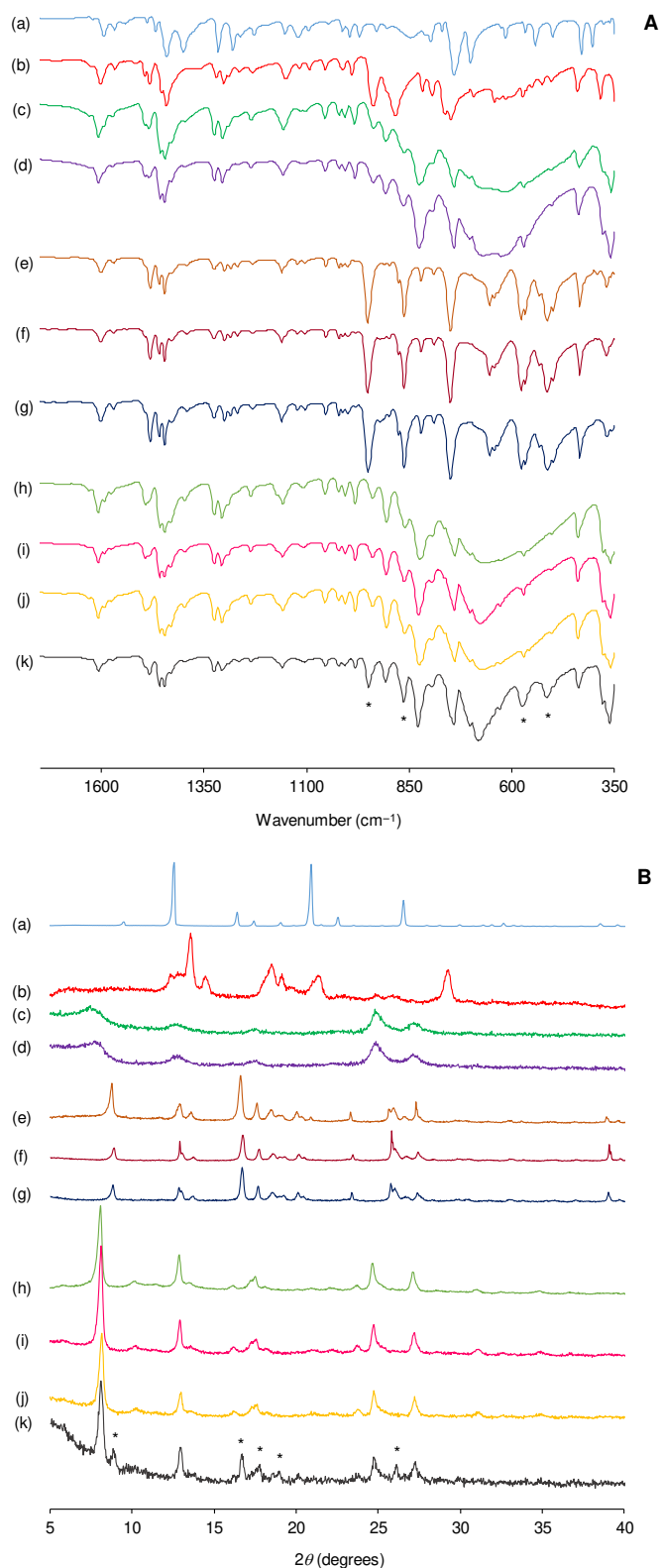


Figure 7.7. ATR FTIR spectra (**A**) in the range of 350-2000 cm⁻¹ and PXRD patterns (**B**) for (a) the ligand pbim; (b) complex **1**; (c) **1**-TBHP-TFT-55 °C-S1; (d) **1**-TBHP-TFT-70 °C-S1; (e) complex **2**; (f) **2**-TBHP-TFT-70 °C-S1; (g) **2**-TBHP-TFT-70 °C-S2; (h) material **3**; (i) **3**-TBHP-TFT-55 °C-S1; (j) **3**-TBHP-TFT-70 °C-S1; and (k) **3**-TBHP-TFT-70 °C-S2.

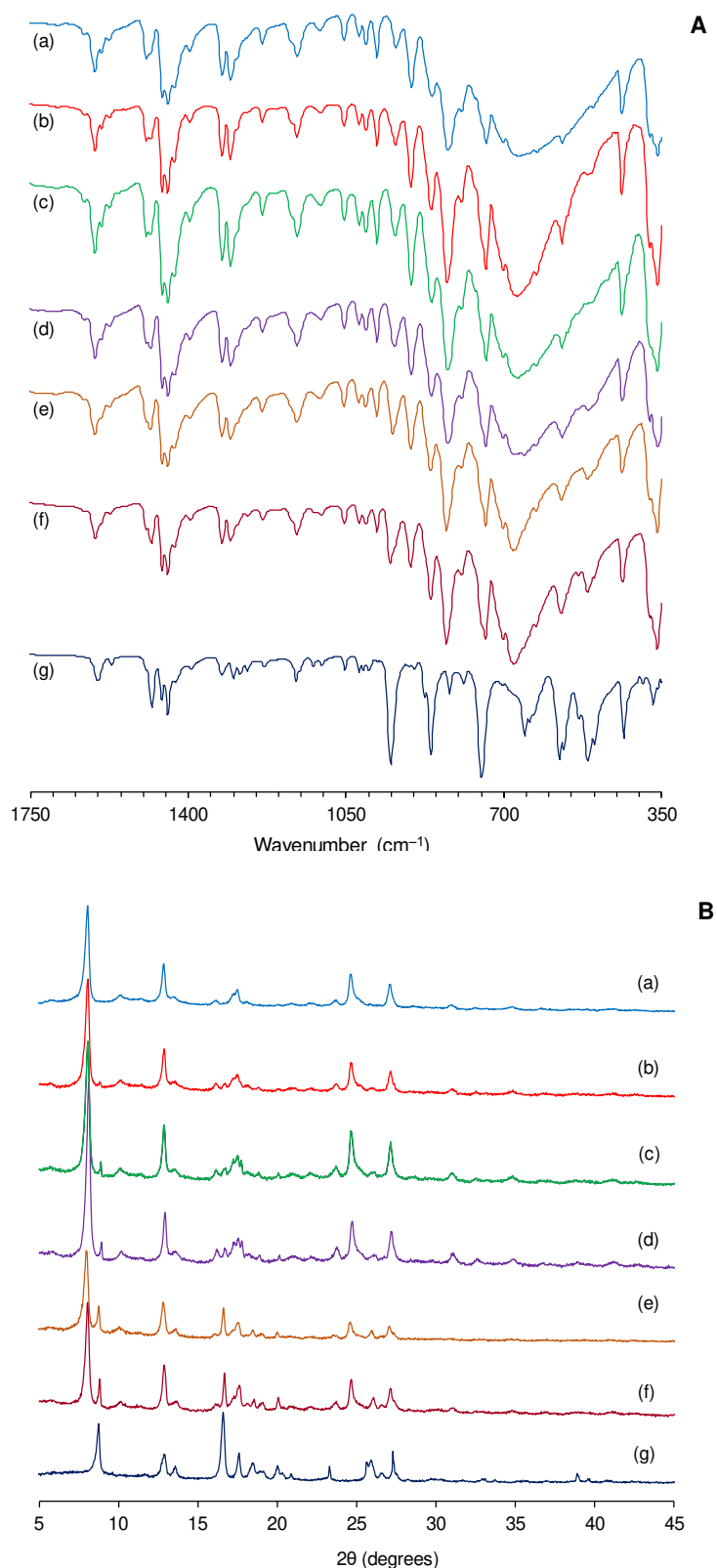


Figure 7.8. ATR FTIR spectra (**A**) in the range of 350-1750 cm⁻¹ and PXRD patterns (**B**) of (a) material **3**, (b) **3**-TBHP-EtOH-70 °C-S1, (c) **3**-TBHP-TFT-70 °C-S1, (d) **3**-TBHP-CH₃CHCl₂-70 °C-S1 and (e) **3**-TBHP-ws-70 °C-S1, and of the compounds recovered from the reaction systems (f) **3**/TBHP/70 °C/Ole, (g) **3**/TBHP/70°C/LinOle and (h) **3**/TBHP/70 °C/Lim.

7.3.3. Characterization of solids after catalytic epoxidation with TBHP

To further understand the catalytic behavior of **1–3** in Cy epoxidation with TBHP, undissolved solids (referred to as i-TBHP-solv- T -S1, where T = reaction temperature and S1 indicates the solid was recovered after run 1) were recovered at the end of catalytic batch runs and characterized by ATR FTIR spectroscopy, PXRD, and SEM. FTIR spectroscopic and PXRD data for the solids recovered from the catalytic system **1**-TBHP-TFT (55 or 70 °C) indicate that **1** is converted *in situ* to a similar, albeit less crystalline, compound of the type **3** (Figure 7.7).

Conversely, data for the solids recovered from the reactions using **2** or **3** (i-TBHP-TFT-70 °C-S1) do not unveil any obvious chemical or structural changes. Similar results were obtained using **3** and either no cosolvent or a solvent other than TFT (Figure 7.8).

SEM images for the recovered metal species **1**-TBHP-TFT-70 °C-S1 and **3**-TBHP-TFT-70 °C-S1 show morphologies that are similar to that for **3** (and very different from that for **1**; Figure 7.9).

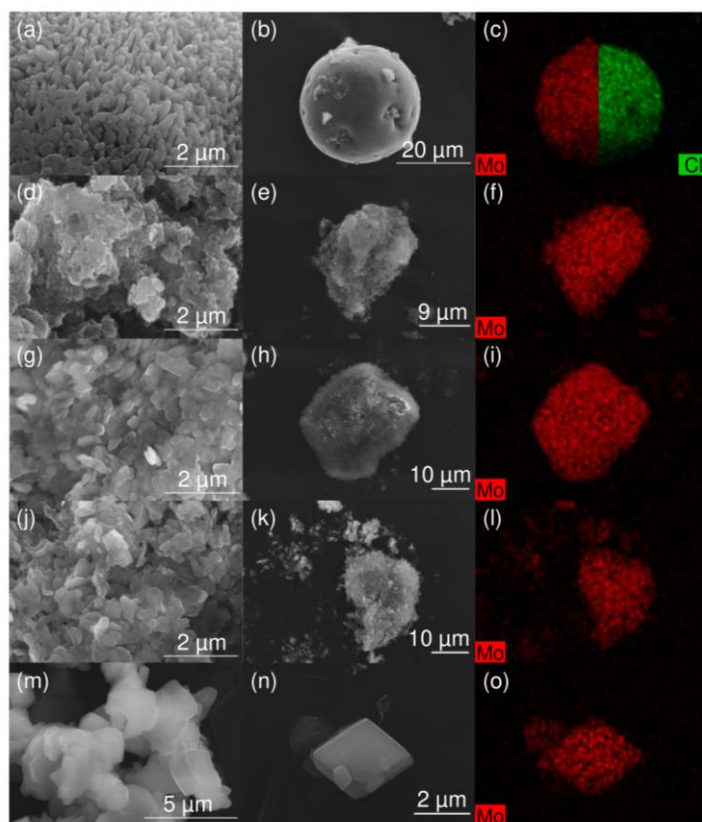


Figure 7.9. SEM images and Mo/Cl distribution maps for (a–c) complex **1**; (d–f) **1**-TBHP-TFT-70 °C-S1; (g–i) material **3**; (j–l) **3**-TBHP-TFT-70 °C-S1; and (m–o) **3**-H₂O₂-CH₃CN-70 °C-S1.

7.3.4. Reuse of recovered solids

The solids **i**-TBHP-TFT-70 °C-S1 (**i** = **2**, **3**) obtained from the normal catalytic tests were tested for Cy epoxidation at 70 °C using the same initial solid/Cy/TBHP mass ratios as used for **2** and **3**. These two reactions led to similar results (98–99 % conversion at 24 h) and the conversions at 6 h were slightly higher than those for **2** and **3** (Table 7.1, Figure 7.10). CyO selectivity was always 100 %. A slightly higher conversion of 96 % at 6 h was obtained in a third run, performed using the solid **2**-TBHP-TFT-70 °C-S2, recovered from the reaction using **2**-TBHP-TFT-70 °C-S1.

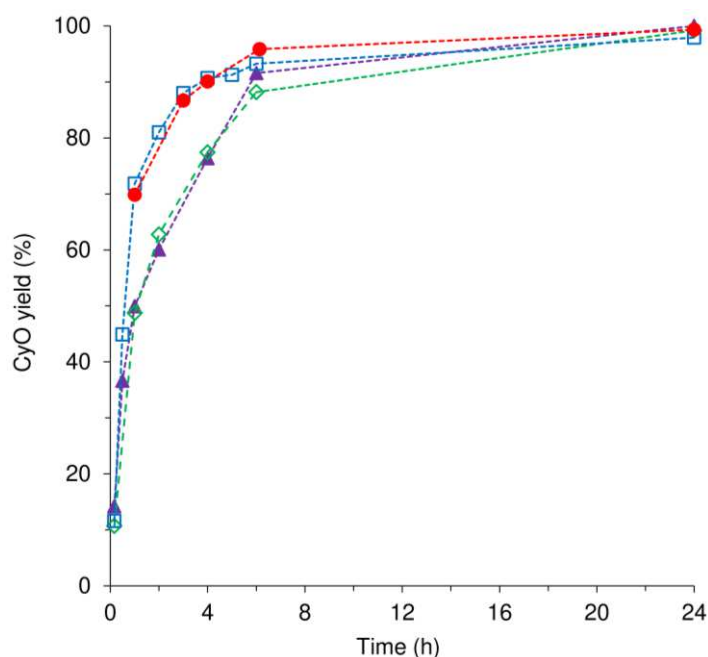


Figure 7.10. *cis*-Cyclooctene epoxidation with TBHP at 70 °C for the systems (**2**-TBHP-TFT-70 °C-S1)/TFT (□), (**2**-TBHP-TFT-70 °C-S2)/TFT (●), (**3**-TBHP-TFT-70 °C-S1)/TFT (◇), and (**3**-CT-TBHP-S1)/TFT (▲). The dashed lines are visual guides.

7.3.5. Characterization of reused solids

Whereas FTIR spectroscopic and PXRD data for **2**-TBHP-TFT-70 °C-S2 match those for **2**-TBHP-TFT-70 °C-S1 (and **2**), the corresponding data for **3**-TBHP-TFT-70 °C-S2 show some significant alterations when compared with the data for **3** and **3**-TBHP-TFT-70 °C-S1 (Figure 7.7). Some additional peaks and changes in relative intensities (highlighted with asterisks in Figure 7.7) can be ascribed to the presence of a small amount of the oxidodiperoxo complex **2** in the solid recovered after the second catalytic run.

Chapter 7

The tendency of **3** to partially convert to **2** in the presence of TBHP was confirmed by performing the contact test of **3** with TBHP in TFT at 70 °C and isolating the undissolved solid after 4, 5, 6, and 24 h. FTIR spectroscopic and PXRD data showed a progressive increase in the relative amount of **2**, upon going from the 4 h sample to the 24 h one (Figure 7.11). The kinetic curves for the Cy/TBHP reactions performed using the recovered solids **i**-TBHP-TFT-70 °C-S1 (**i** = **2**, **3**) and **3**-CT-TBHP-S1 are similar (Figure 7.10), suggesting that the same type of active species may be involved; that is, complexes of the type **2**.

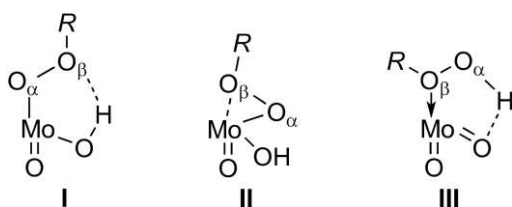
7.3.6. Identification of the catalytic active specie in catalytic epoxidation with TBHP

A contact test carried out for **2**/TBHP indicated that catalytic reactions performed with **2** occur in the homogeneous phase, since the liquid phase isolated in the test (**2**-CT-TBHP-L) led to 74 % Cy conversion at 24 h. To further gauge the possible catalytic contribution of **2** in the reactions performed using **1** or **3** (or the recovered solids), the Cy/TBHP reaction was performed in the presence of **2**, using an initial Mo/Cy/TBHP molar ratio of 1:6680:10206; that is, 0.015 mol-% Mo instead of the usual 1 mol-%. Despite the much lower molar amount of molybdenum, the reaction led to 98 % CyO yield at 24 h [TON = 6550 mol_{Cy} mol_{Mo}⁻¹]. Hence, the catalytic contribution of **2** may be considerable, even if present at a very low concentration. This may explain why catalytic activity was higher for the recovered solids **3**-TBHP-TFT-70 °C-S1 and **3**-CT-TBHP-S1 than for as-synthesized **3**; that is, the recovered solids contain a small amount of **2** in addition to **3**. The formation of catalytically active oxidodiperoxido complexes of the type [MoO(O₂)₂(L)] during Cy/TBHP epoxidation reactions using molybdenum(VI) hybrid solids has been verified previously for the materials [Mo_nO_{3n}(L)] [*n* = 2, L = ppp;⁴⁹ *n* = 3, L = pzpy].⁴² In these two examples, the solubilities of the oxidodiperoxido complexes, under the reaction conditions used, were sufficiently high to permit subsequent isolation from the liquid phases.

The inclusion of the radical scavenger 2,6-di-*tert*-butyl-4-methyl-phenol (in an equimolar amount relative to Cy) in the system **3**/TBHP/Cy led to catalytic results roughly comparable with those obtained without a scavenger (Table 7.1), which suggests that the reaction mechanism does not involve free radicals and is likely heterolytic. The mechanism of olefin epoxidation with alkyl hydroperoxides may involve the primary formation of an active oxidizing species through hydrogen-atom transfer from the hydroperoxide oxidant (ROOH) to an oxidomolybdenum group (Mo=O converts to Mo–OH), with the concomitant formation of a peroxido ligand involving the

Chapter 7

anion ROO^- , thus resulting in a moiety of the type $\{\text{Mo}(\text{OH})(\text{O}_\alpha\text{O}_\beta)\}$.^{55,56} The oxidizing species may be stabilized by hydrogen bonding between the proton of the group $\text{Mo}-\text{OH}$ and the O_β atom of the peroxido ligand (species I in Scheme 7.2), or by a weak interaction between the O_β atom and the metal center (η^2 -asymmetric coordination mode; species II). Alternatively, species of the type $\{\text{MoO}_2(\text{L})(\text{ROOH})\}$ (III in Scheme 7.2), involving a very weak $\text{Mo}\cdots\text{O}_\beta$ interaction and a hydrogen bond between the alkylhydroperoxide and an oxido ligand, have been proposed for five-coordinate compounds of the type $[\text{MoO}_2(\text{L})]$ or for pseudo-six-coordinate complexes after partial dissociation of the chelating ligand L.⁵⁷ Subsequently, the O_α atom of the oxidizing species may be transferred to the olefin to give the epoxide, and the type of transition state involved in this step will depend partly on the structure of the active oxidizing species formed in the first step.^{56,58,59}



Scheme 7.2. Structures of active oxidizing intermediate species that have been proposed in the literature for the epoxidation of olefins with hydroperoxide oxidants in the presence of (per)oxidomolybdenum complexes (R = alkyl or H).

In an attempt to recycle the catalytic system **2**/TBHP, the Cy reaction was carried out using an ionic liquid at 70 °C. The IL 1-butyl-3-methylimidazolium tetrafluoroborate ($[\text{bmim}]\text{BF}_4$) was chosen, since it is readily available, relatively cheap, and has been successfully employed for recovering and reusing molybdenum complexes in olefin epoxidation.^{60–62} The catalytic activity was steady for three consecutive batch runs with conversions of 61–65 % at 6 h and 82–87 % at 24 h; selectivity for CyO was always 100 % (Figure 7.12). The epoxidation reaction for the IL system may be slower than with TFT, due to mass transfer limitations. Until the present, this is the first report demonstrating the recyclability of oxidodiperoxido-molybdenum(VI) complexes for Cy epoxidation, with TBHP using an IL.

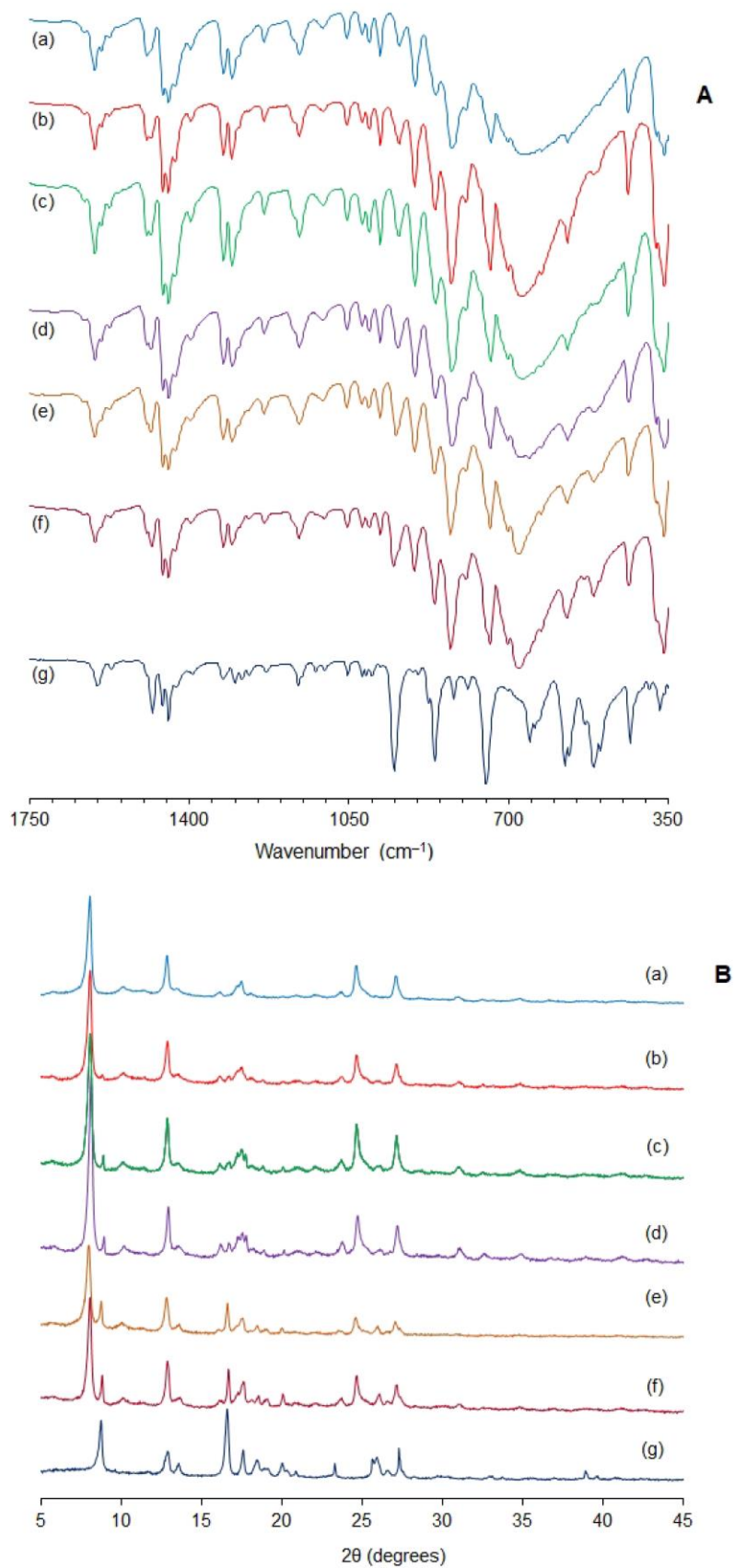


Figure 7.11. ATR FTIR spectra (**A**) and PXRD patterns (**B**) of (a) material **3**, (b) **3-CT-TBHP-S1** (4 h), (c) **3-CT-TBHP-S1** (5 h), (d) **3-CT-TBHP-S1** (6 h), (e) **3-CT-TBHP-S1** (24 h), (f) **3-CT-TBHP-S2** (24 h), and (g) complex **2**.

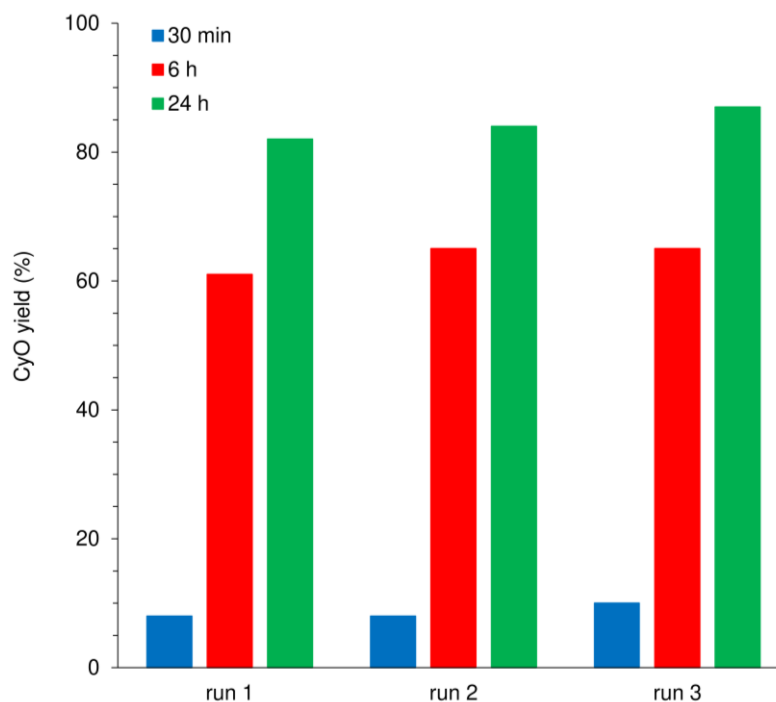


Figure 7.12. Three consecutive catalytic runs of Cy epoxidation with TBHP at 70 °C for the system **2**/[bmim]BF₄.

7.3.7. *cis*-Cyclooctene epoxidation with H₂O₂ (including cosolvent influence and characterization of recovered solids)

The catalytic performance of **1–3** for the epoxidation of Cy was subsequently studied using aq. H₂O₂ as the oxidant, instead of TBHP, with acetonitrile as the cosolvent (Table 7.1). Cy conversions at 24 h (70 °C) were only 16–17 % for **1** and **3**, and 35 % for **2**; CyO selectivity was always 100 %. Iodometric titrations for **2**/H₂O₂/CH₃CN and **3**/H₂O₂/CH₃CN (after 24 h reaction at 70 °C in the absence of substrate) indicated negligible oxidant decomposition. For the hybrid material **3** and different cosolvents, conversion at 24 h increased in the order: ethyl acetate < CH₃CN < no cosolvent < EtOH = 1-propanol. The reactions were biphasic solid–liquid. Characterization of the undissolved solids recovered after the catalytic runs showed the exclusive presence of the oxidodiperoxido complex **2**; that is, **1** and **3** react with aq. H₂O₂ under the conditions used for catalysis to give partially soluble **2** (Figure 7.13). The poor catalytic results obtained with aq. H₂O₂ (especially in relation to those obtained with TBHP) may be due to poor catalyst solubility, differences in reaction mechanisms,^{55,59,63} and unfavorable formation of active oxidizing species with H₂O₂.

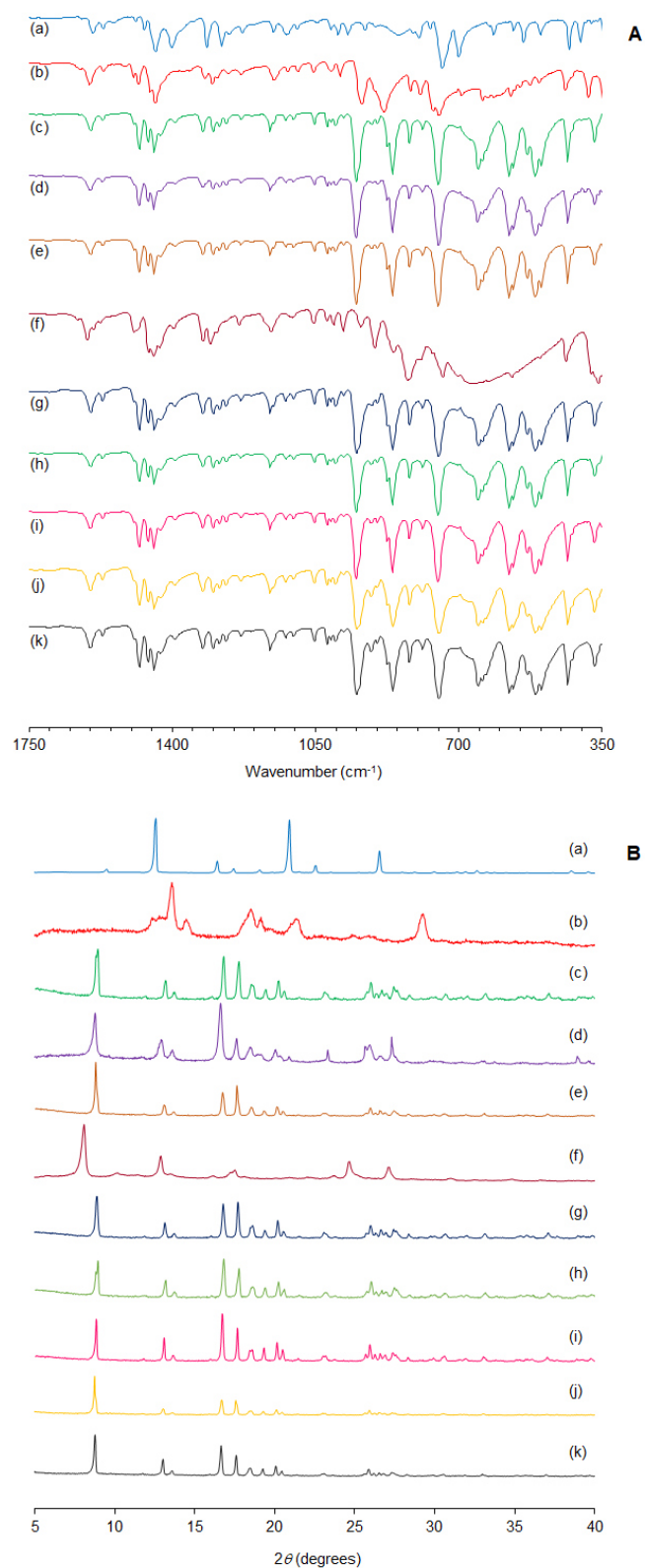


Figure 7.13. ATR FTIR spectra (**A**) and PXRD patterns (**B**) of (a) the ligand pbim, (b) complex **1**, (c) **1**-H₂O₂-CH₃CN-70 °C-S1, (d) complex **2**, (e) **2**-H₂O₂-CH₃CN-70 °C-S1, (f) material **3**, (g) **3**-H₂O₂-CH₃CN-70 °C-S1, (h) **3**-H₂O₂-PrOH-70 °C-S1, (i) **3**-H₂O₂-EtOAc-70 °C-S1, (j) **3**-H₂O₂-EtOH-70 °C-S1 and (k) **3**-H₂O₂-ws-70 °C-S1 (PrOH = 1-propanol, EtOAc = ethyl acetate).

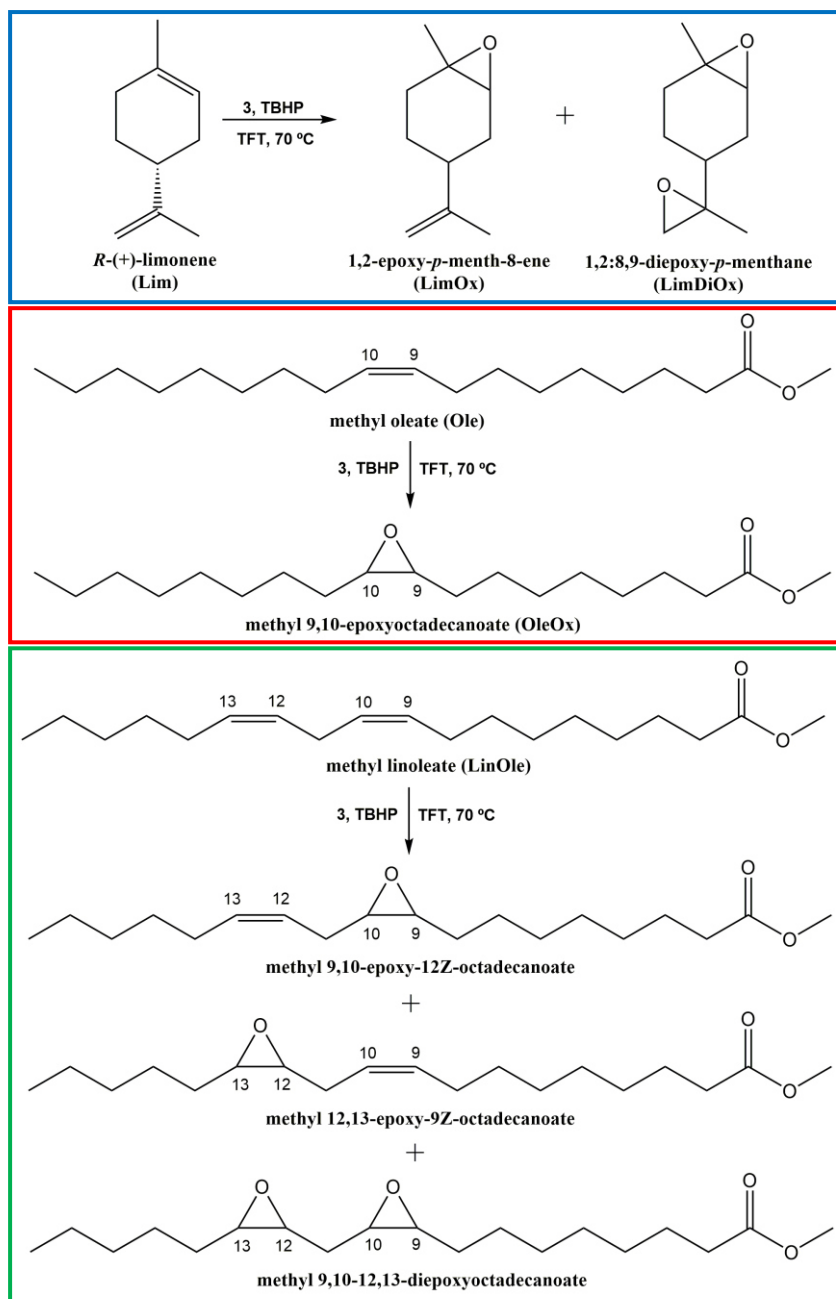
Chapter 7

7.3.8. Bio-olefins epoxidation with H₂O₂ (including characterization of recovered solids)

The catalytic system **3**/TBHP was further explored for the epoxidation of the biorenewable olefins methyl oleate (Ole), methyl linoleate (LinOle), and (*R*)-(+)-limonene (Lim) at 70 °C (Scheme 7.3, Table 7.2). Lim is a terpenic olefin obtained from citrus oils.⁶⁴ Its epoxide products, 1,2-epoxy-*p*-menth-8-ene (LimOx) and 1,2:8,9-diepoxy-*p*-menthane (LimDiOx), have commercial importance for the production of paints, protective coatings, and resins, for example, and can be used as intermediates in the synthesis of flavors, fragrances, agrochemicals, biodegradable polymers, and therapeutically active compounds, amongst others.^{65,66} The olefins Ole and LinOle are model substrates for fatty-acid methyl esters (FAMEs), which are produced from vegetable oils by transesterification.⁶⁷ Epoxidized FAMEs have widespread use, for example, as solvents, lubricants, PVC stabilizers and plasticizers, and as intermediates in the production of polyurethane polyols, cosmetics, and pharmaceuticals.⁶⁸ Traditionally, at the industrial level, plant oils and their derivatives are epoxidized under homogeneous conditions by using the Prilezhaev reaction, involving peracids generated *in situ* by the reaction of organic acids with hydrogen peroxide in the presence of a mineral-acid catalyst.^{65,68,69} Environmental and safety concerns associated with this stoichiometric process have motivated the search for alternative catalytic methods that employ more convenient oxidants.

The system **3**/TBHP/Ole gave methyl 9,10-epoxyoctadecanoate (OleOx) as the main product in 42 % yield at 69 % conversion (24 h). Methyl 9,10-dihydroxyoctadecanoate and methyl 9-oxooctadecanoate were formed in yields of 25 % and 4 %, respectively. The formation of the diol was possibly due to the presence of water (ca. 4 %) in the as-received oxidant solution. Relatively good catalytic results were obtained previously for the epoxidation of Ole using hybrid molybdenum(VI) oxide solids as (pre)catalysts. For example, with TFT as the cosolvent at 75 °C, the compound [(CH₃)₂NH₂][MoO₃(HbpdC)] led to 98 % OleOx yield (24 h).¹⁵ With CH₃CHCl₂ as the cosolvent, [MoO₃(2,2'-bipy)]_n led to 99 % OleOx yield (24 h/75 °C)⁷⁰, and [Mo₂O₆(ppp)]_n led to 78 % OleOx yield (6 h/55 °C).⁴⁹ The differences in the catalytic results, in comparison with **3**, may be partly due to differences in the stability of the hybrid solids, and the nature and solubility of the active species; for example, [(CH₃)₂NH₂][MoO₃(HbpdC)] suffered structural modifications¹⁵, and [Mo₂O₆(ppp)] acted as a source of soluble active species of the type [MoO(O₂)₂(ppp)]_n.⁴⁹

Chapter 7



Scheme 7.3. Bio-olefin epoxidation reactions studied in this work.

With LinOle as the substrate, a conversion of 92 % was reached at 24 h. The main products were the monoepoxide isomers methyl 9,10-epoxy-12 Z -octadecenoate and methyl 12,13-epoxy-9 Z -octadecenoate, which were formed in equimolar amounts and a total yield of 46 %. Methyl 9,10-12,13-diepoxyoctadecanoate isomers were formed with 25 % yield. By-products included cyclization products (8 % yield at 24 h), such as methyl 10,13-epoxy-9,12-dihydroxyoctadecanoate, which are typically formed by intramolecular interactions between epoxide and diol groups of epoxydiol intermediates formed from the acid hydrolysis of an oxirane group.^{71,72}

Chapter 7

Table 7.2. Oxidation of bio-olefins with TBHP using compound **3**.^a

Olefin	Conv. [%] ^b	Product	Yield [%] ^b
Ole	46/69	methyl 9,10-epoxyoctadecenoate	27/42
		methyl 9,10-dihydroxyoctadecenoate	17/25
		methyl 9-oxooctadecenoate	3/4
LinOle	59/92	methyl 9,10-epoxy-12Z-octadecenoate	20/23
		methyl 12,13-epoxy-9Z-octadecenoate	20/23
		methyl 9,10-12,13-diepoxyoctadecenoate	14/25
Lim	69/91	1,2-epoxy- <i>p</i> -menth-8-ene	60/73
		1,2:8,9-diepoxy- <i>p</i> -menth-8-ene	4/14
		Limonene diol	2/2
		<i>p</i> -mentha-dienols	5/4

^a Reaction conditions: initial Mo/Cy/TBHP molar ratio = 1:100:153; [olefin] = 1.0 M, cosolvent = TFT, reaction temperature = 70 °C. ^b Conversion and yield at 6 h/24 h.

Compound **3** promoted Lim epoxidation, leading to 91 % conversion at 24 h and a LimOx yield of 73 %, indicating high regioselectivity towards the epoxidation of the endocyclic double bond (C1=C2). The mono- and diepoxide products were formed in a LimOx/LimDiOx molar ratio of 14 at 6 h and 5.4 at 24 h. Limonene diol and *p*-mentha-dienols were minor products, formed in yields of 5 % or less. There are few studies reported in the literature for Lim epoxidation with TBHP in the presence of hybrid molybdenum(VI) oxide solids. The catalytic results for Lim epoxidation in the presence of **3** compare unfavourably with data for [Mo₂O₆(ppp)], which led to 79 % LimOx yield at 6 h/55 °C (Mo/Lim/TBHP molar ratio = 1:113:172; CH₃CHCl₂ as the cosolvent)⁴⁹, and [(CH₃)₂NH₂][MoO₃(HbpdC)], which led to 84 % LimOx yield at 24 h/55 °C or 76 % LimOx yield at 24 h/ 75 °C (Mo/Lim/TBHP molar ratio = 1:103:160; TFT as the cosolvent)¹⁵.

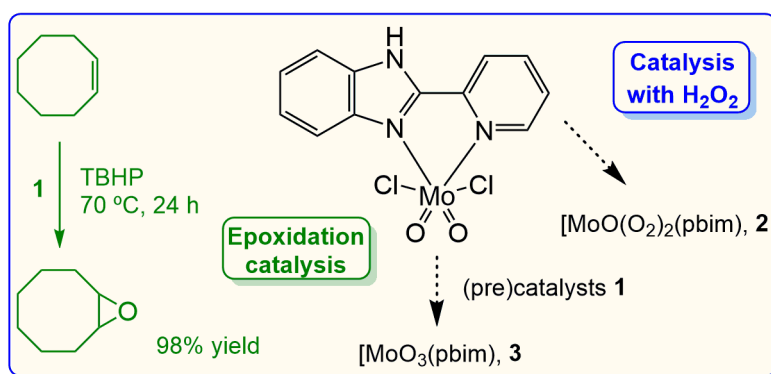
The solids recovered from the reactions of the different olefin substrates with TBHP, in the presence of **3**, were characterized by ATR FTIR spectroscopy and PXRD, and were found to exhibit data unchanged from those for the as-synthesized **3** (Figure 7.8).

7.4. Conclusions

In this chapter, it was found that oxidomolybdenum(VI) compounds bearing the chelating bidentate ligand 2-(2-pyridyl)-benzimidazole can be effectively used in olefin epoxidation reactions using TBHP as the oxidant (Scheme 7.4). The dichlorido complex [MoO₂Cl₂(pbim)] (**1**) presents limited stability, and even in the presence of

Chapter 7

residual amounts of water (present, for example, in the TBHP/decane solution used as the oxidant), undergoes hydrolysis and condensation reactions to give a hybrid molybdenum(VI) oxide solid formulated as $[\text{MoO}_3(\text{pbim})]$ (**3**). Both **1** and **3** react with aq. H_2O_2 to give the oxidodiperoxido complex $[\text{MoO}(\text{O}_2)_2(\text{pbim})]$ (**2**). Studies show that **3** partially transforms to **2** in the presence of TBHP. The homogeneous catalyst **2** exhibits high activity for the epoxidation of *cis*-cyclooctene, giving the epoxide as the only product, although catalytic performance may be limited by the poor solubility of the complex. Accordingly, high activity (quantitative yield of the epoxide within 24 h at 70 °C) is maintained, even with a 67-fold reduction in the relative molar amount of the complex (0.015 mol-%). Preliminary results have shown that ionic liquids can be used as solvents for these complexes to give recyclable catalytic systems.



Scheme 7.4. Summary of the main syntheses and catalytic studies carried out in this work.

7.5. References

- (1) Kühn, F. E.; Santos, M.; Abrantes, A. M. *Chem. Rev.* **2006**, *106*, 2455–2475.
- (2) Sanz, R.; Pedrosa, M. R. *Curr. Org. Synth.* **2009**, *6*, 239–263.
- (3) Sousa, S. C. A.; Cabrita, I.; Fernandes, A. C. *Chem. Soc. Rev.* **2012**, *41*, 5641–5653.
- (4) Amini, M.; Haghdoost, M. M.; Bagherzadeh, M. *Coord. Chem. Rev.* **2013**, *257*, 1093–1121.
- (5) Sousa, S. C. A.; Fernandes, A. C. *Coord. Chem. Rev.* **2015**, *284*, 67–92.
- (6) Thiel, W. R.; Eppinger, J. *Chem. Eur. J.* **1997**, *3*, 696–705.
- (7) Kühn, F. E.; Zhao, J.; Herrmann, W. A. *Tetrahedron Asymmetry* **2005**, *16*, 3469–3479.
- (8) Günyar, A.; Zhou, M. D.; Drees, M.; Baxter, P. N. W.; Bassioni, G.; Herdtweck, E.; Kühn, F. E. *Dalton Trans.* **2009**, *40*, 8746–8754.
- (9) Günyar, A.; Betz, D.; Drees, M.; Herdtweck, E.; Kühn, F. E. *J. Mol. Catal. A Chem.* **2010**, *331*, 117–124.
- (10) Coelho, A. C.; Nolasco, M.; Balula, S. S.; Antunes, M. M.; Pereira, C. C. L.; Almeida Paz,

Chapter 7

- F. A.; Valente, A. A.; Pillinger, M.; Ribeiro-Claro, P.; Klinowski, J.; Gonçalves, I. S. *Inorg. Chem.* **2011**, *50*, 525–538.
- (11) Amarante, T. R.; Gomes, A. C.; Neves, P.; Almeida Paz, F. A.; Valente, A. A.; Pillinger, M.; Gonçalves, I. S. *Inorg. Chem. Commun.* **2013**, *32*, 59–63.
- (12) Amarante, T. R.; Neves, P.; Paz, F. A. A.; Pillinger, M.; Valente, A. A.; Gonçalves, I. S. *Inorg. Chem. Commun.* **2012**, *20*, 147–152.
- (13) Li, D.; Liu, Y.; Wei, P.; Hu, B.; Zhang, X. *Acta Cryst.* **2009**, *65*, 1074–1081.
- (14) Zapf, P. J.; Haushalter, R. C.; Zubieta, J. *Chem. Mater.* **1997**, *4756*, 2019–2024.
- (15) Amarante, T. R.; Neves, P.; Valente, A. A.; Almeida Paz, F. A.; Fitch, A. N.; Pillinger, M.; Gonçalves, I. S. *Inorg. Chem.* **2013**, *52*, 4618–4628.
- (16) Yang, J.; Ma, J. F.; Liu, Y. Y.; Li, S. L.; Zheng, G. L. *Eur. J. Inorg. Chem.* **2005**, 2174–2180.
- (17) Hinner, M. J.; Grosche, M.; Herdtweck, E.; Thiel, W. R. *Z. Anorg. Allg. Chem.* **2003**, *629*, 2251–2257.
- (18) Leus, K.; Liu, Y. Y.; Meledina, M.; Turner, S.; Van Tendeloo, G.; Van Der Voort, P. *J. Catal.* **2014**, *316*, 201–209.
- (19) Neves, P.; Gomes, A. C.; Amarante, T. R.; Paz, F. A. A.; Pillinger, M.; Gonçalves, I. S.; Valente, A. A. *Microporous Mesoporous Mater.* **2015**, *202*, 106–114.
- (20) Sundberg, R. J. *Chem. Rev.* **1974**, *74*, 471–517.
- (21) Téllez, F.; López-Sandoval, H.; Castillo-Blum, S. E.; Barba-Behrens, N. *Arkivoc* **2008**, *5*, 245–275.
- (22) Molina, P.; Tárraga, A.; Otón, F. *Org. Biomol. Chem.* **2012**, *10*, 1711–1724.
- (23) Chakravorty, V.; Vihar, V. *Polyhedron* **1991**, *10*, 33–35.
- (24) Dinda, R.; Sengupta, P.; Ghosh, S.; Mayer-Figge, H.; Sheldrick, W. S. *J. Chem. Soc. Dalton Trans.* **2002**, *23*, 4434–4439.
- (25) Dinda, R.; Sengupta, P.; Ghosh, S.; Sheldrick, W. S. *Eur. J. Inorg. Chem.* **2003**, 363–369.
- (26) Vrdoljak, V.; Dilović, I.; Cindrić, M.; Matković-Čalogović, D.; Strukan, N.; Gojmerac-Ivšić, A.; Novak, P. *Polyhedron* **2009**, *28*, 959–965.
- (27) Martín-Zarza, P.; Gili, P.; Rodríguez-Romero, F. V.; Ruiz-Pérez, C.; Solans, X. *Inorg. Chim. Acta* **1994**, *223*, 173–175.
- (28) Lin, Y. W.; Tong, Y. P.; Yang, C.; Lin, Y. R. *Inorg. Chem. Commun.* **2009**, *12*, 252–254.
- (29) Tong, Y. P.; Lin, Y. W. *J. Mol. Struct.* **2010**, *952*, 61–66.
- (30) Chen, Q. L.; Chen, H. B.; Cao, Z. X.; Zhou, Z. H. *Dalton Trans.* **2013**, *42*, 1627–1636.
- (31) Maurya, M. R.; Bharti, N. *Trans. Met. Chem.* **1999**, *24*, 389–393.
- (32) Maurya, M. R.; Jayaswal, M. N. *J. Chem. Res.* **1998**, *8*, 446–447.
- (33) Haneda, S.; Gan, Z.; Eda, K.; Hayashi, M. *Organometallics* **2007**, *26*, 6551–6555.
- (34) Saraiva, M. S.; Quintal, S.; Portugal, F. C. M.; Lopes, T. A.; Félix, V.; Nogueira, J. M. F.; Meireles, M.; Drew, M. G. B.; Calhorda, M. J. *J. Organomet. Chem.* **2008**, *693*, 3411–3418.

Chapter 7

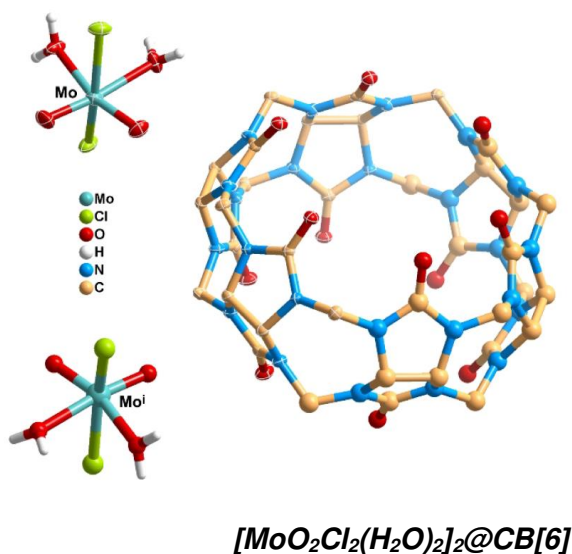
- (35) Haneda, S.; Adachi, Y.; Hayashi, M. *Tetrahedron* **2009**, *65*, 10459–10462.
- (36) Dayan, O.; Demirmen, S.; Özdemir, N. *Polyhedron* **2015**, *85*, 926–932.
- (37) Li, S.; Zhang, B.; Kühn, F. E. *J. Org. Chem.* **2013**, *730*, 132–136.
- (38) Kühn, F. E.; Groarke, M. .; Bencze, É.; Herdtweck, E.; Prazeres, A.; Santos, A. M. .; Calhorda, M. J.; Romão, C. C.; Gonçalves, I. S. .; Lopes, A. D. .; Pillinger, M. *Chem. Eur. J.* **2002**, *8*, 2370–2383.
- (39) Petrovski, Ž.; Pillinger, M.; Valente, A. A.; Gonçalves, I. S.; Hazell, A.; Romão, C. C. *J. Mol. Catal. A Chem.* **2005**, *227*, 67–73.
- (40) Bruno, S. M.; Pereira, C. C. L.; Balula, M. S.; Nolasco, M.; Valente, A. A.; Hazell, A.; Pillinger, M.; Ribeiro-Claro, P.; Gonçalves, I. S. *J. Mol. Catal. A Chem.* **2007**, *261*, 79–87.
- (41) Brito, J. A.; Ladeira, S.; Teuma, E.; Royo, B.; Gómez, M. *Appl. Catal., A* **2011**, *398*, 88–95.
- (42) Amarante, T. R.; Neves, P.; Gomes, A. C.; Nolasco, M. M.; Ribeiro-Claro, P.; Coelho, A. C.; Valente, A. A.; Almeida Paz, F. A.; Smeets, S.; McCusker, L. B.; Pillinger, M.; Gonçalves, I. S. *Inorg. Chem.* **2014**, *53*, 2652–2665.
- (43) Khalil, M. M. H.; Mohamed, H. A.; El-Medani, S. M.; Ramadan, R. M. *Spectrochim. Acta Part A* **2003**, *59*, 1341–1347.
- (44) Bruno, S. M.; Fernandes, J. A.; Martins, L. S.; Gonçalves, I. S.; Pillinger, M.; Ribeiro-Claro, P.; Rocha, J.; Valente, A. A. *Catal. Today* **2006**, *114*, 263–271.
- (45) Wang, M.; Sun, H.; Wang, Y.; Wang, X.; Li, F.; Sun, L. *Appl. Organomet. Chem.* **2004**, *18*, 277–281.
- (46) Amarante, T. R.; Neves, P.; Tomé, C.; Abrantes, M.; Valente, A.; A.; Paz, F. A. A.; Pillinger, M.; Gonçalves, I. S. *Inorg. Chem.* **2012**, *51*, 3666–3676.
- (47) Abrantes, M.; Amarante, T. R.; Antunes, M. M.; Gago, S.; Almeida Paz, F. A. A.; Margiolaki, I.; Rodrigues, A. E.; Pillinger, M.; Valente, A. A.; Gonçalves, I. S. *Inorg. Chem.* **2010**, *49*, 6865–6873.
- (48) Figueiredo, S.; Gomes, A. C.; Neves, P.; Amarante, T. R.; Paz, F. A.; Soares, R.; Lopes, A. D.; Valente, A. A.; Pillinger, M.; Gonçalves, I. S. *Inorg. Chem.* **2012**, *51*, 8629–8635.
- (49) Amarante, T. R.; Neves, P.; Paz, F. A. A.; Valente, A. A.; Pillinger, M.; Gonçalves, I. S. *Dalton Trans.* **2014**, *43*, 6059–6069.
- (50) Ogawa, A.; Curran, D. P. *J. Org. Chem.* **1997**, *62*, 450–451.
- (51) Lysenko, A. B.; Senchyk, G. A.; Domasevitch, K. V.; Hauser, J.; Fuhrmann, D.; Kobalz, M.; Krautscheid, H.; Neves, P.; Valente, A. A.; Gonçalves, I. S. *Inorg. Chem.* **2015**, *54*, 8327–8338.
- (52) Amarante, T. R.; Neves, P.; Valente, A. A.; Paz, F. A. A.; Pillinger, M.; Gonçalves, I. S. *J. Catal.* **2016**, *340*, 354–367.
- (53) Amarante, T. R.; Neves, P.; Valente, A. A.; Paz, F. A. A.; Pillinger, M.; Gonçalves, I. S. *J. Catal.* **2016**, *340*, 354–367.
- (54) Amarante, T. R.; Neves, P.; Coelho, A. C.; Gago, S.; Valente, A. A.; Almeida Paz, F. A.;

Chapter 7

- Pillinger, M.; Gonçalves, I. S. *Organometallics* **2010**, *29*, 883–892.
- (55) Comas-Vives, A.; Lledos, A.; Poli, R. *Chem. Eur. J.* **2010**, *16*, 2147–2158.
- (56) Dinoi, C.; Ciclosi, M.; Manoury, E.; Maron, L.; Perrin, L.; Poli, R. *Chem. Eur. J.* **2010**, *16*, 9572–9584.
- (57) Morlot, J.; Uyttebroeck, N.; Agustin, D.; Poli, R. *ChemCatChem* **2013**, *5*, 601–611.
- (58) Veiros, L. F.; Prazeres, Â.; Costa, P. J.; Romão, C. C.; Kühn, F. E.; Calhorda, M. J. *J. Chem. Soc.* **2006**, *60*, 1383–1389.
- (59) Dreisch, K.; Andersson C.; StHlhandske, C. *Polyhedron* **1993**, *12*, 303–311.
- (60) Neves, P.; Gago, S.; Balula, S. S.; Lopes, D.; Valente, A. A.; Cunha-silva, L.; Paz, F. A. A.; Pillinger, M.; Silva, C. M.; Gonçalves, I. S. *Inorg. Chem.* **2011**, *50*, 3490–3500.
- (61) Balula, S. S.; Bruno, S. M.; Gomes, A. C.; Valente, A. A.; Pillinger, M.; Gonçalves, I. S.; MacQuarrie, D. J.; Clark, J. H. *Inorg. Chim. Acta* **2012**, *387*, 234–239.
- (62) Oliveira, T. S. M.; Gomes, A. C.; Lopes, A. D.; Lourenço, J. P.; Paz, F. A.; Pillinger, M.; Gonçalves, I. S. *Dalton Trans.* **2015**, *44*, 14139–14148.
- (63) Sözen-Aktaş, P.; Manoury, E.; Demirhan, F.; Poli, R. *Eur. J. Inorg. Chem.* **2013**, 2728–2735.
- (64) Negro, V.; Mancini, G.; Ruggeri, B.; Fino, D. *Bioresour. Technol.* **2016**, *214*, 806–815.
- (65) Michel, T.; Cokoja, M.; Sieber, V.; Kühn, F. E. *J. Mol. Catal. A Chem.* **2012**, *358*, 159–165.
- (66) Wróblewska, A.; Makuch, E.; Miadlicki, P. *Catal. Today* **2016**, *268*, 121–129.
- (67) Lee, A. F.; Bennett, J. A.; Manayil, J. C.; Wilson, K. *Chem. Soc. Rev.* **2014**, *43*, 7887–7916.
- (68) Milchert, E.; Malarczyk, K.; Kłos, M.; Novak, L. *Molecules* **2015**, *20*, 21481–21493.
- (69) Köckritz, A.; Martin, A. *Eur. J. Lipid Sci. Technol.* **2008**, *110*, 812–824.
- (70) Gamelas, C. A.; Neves, P.; Gomes, A. C.; Valente, A. A.; Romão, C. C.; Gonçalves, I. S.; Pillinger, M. *Catal. Lett.* **2012**, *142*, 1218–1224.
- (71) Piazza, G. J.; Nuñez, A.; Foglia, T. A. *J. Am. Oil Chem. Soc.* **2003**, *80*, 901–904.
- (72) Neves, P.; Gomes, A. C.; Paz, F. A. A.; Valente, A. A.; Gonçalves, I. S.; Pillinger, M. *Mol. Catal.* **2017**, *432*, 104–114.

CHAPTER 8

A hydrogen-bonded assembly of cucurbit[6]uril and $[\text{MoO}_2\text{Cl}_2(\text{H}_2\text{O})_2]$ with catalytic efficacy for the one-pot conversion of olefins to alkoxy products



Chapter 8

Index

8.1. Introduction	221
8.2. Results and discussion	222
8.2.1. Synthesis and single-crystal X-ray structure analyses of supramolecular adduct $2[\text{MoO}_2\text{Cl}_2(\text{H}_2\text{O})_2] \cdot (\text{C}_{36}\text{H}_{36}\text{N}_{24}\text{O}_{12}) \cdot x\text{H}_2\text{O} \cdot y\text{HCl} \cdot z(\text{CH}_3\text{COCH}_3)$ (1)	222
8.2.2. Complementary characterization of 1	226
8.3. Catalytic studies	230
8.3.1. Olefin epoxidation	230
8.3.2. One-pot conversion of olefins to alkoxy products	232
8.3.3. Catalyst reuse	236
8.4. Conclusions	240
8.5. References	242

Chapter 8

8.1. Introduction

Molybdenum(VI) dichloride dioxide, MoO_2Cl_2 , was first reported by Berzelius in 1826, and is generally believed to be the first molybdenum oxo compound.¹ MoO_2Cl_2 is a very useful starting material for synthesizing a variety of molybdenum compounds and in recent years has gained importance as a catalyst in organic transformations.²⁻⁴ Anhydrous MoO_2Cl_2 has a layered structure in the solid-state consisting of infinite chains ($\cdots\text{O}=\text{Mo}\cdots\text{O}=\text{Mo}\cdots$) in two directions, with the Cl atoms occupying the apical positions of distorted $\{\text{MoO}_4\text{Cl}_2\}$ octahedra.⁵ Although MoO_2Cl_2 is moisture sensitive, monohydrate and dihydrate derivatives are known. In $\text{MoO}_2\text{Cl}_2\cdot\text{H}_2\text{O}$, the introduction of a water molecule into the coordination sphere of Mo atoms breaks down the layers into chains in which one of the oxygen atoms is terminal and the other is bridging.⁶ When two H_2O molecules are coordinated to the Mo atom, the structure consists of isolated $[\text{MoO}_2\text{Cl}_2(\text{H}_2\text{O})_2]$ molecules.

The neutral species $[\text{MoO}_2\text{Cl}_2(\text{H}_2\text{O})_2]$ exists in solutions of alkali molybdates in concentrated hydrochloric acid and can be extracted with oxygenated organic solvents such as diethyl ether.⁷ Two main avenues have been pursued to isolate air-stable crystalline solids containing the diaqua complex: 1) adduct formation with polyethers such as diglyme⁸ or crown ethers such as 18-crown-6^{9,10}; 2) co-crystallization with ammonium ions such as pyridinium¹¹, triethylammonium¹², 1,3-bis(4-pyridinium)propane ($\text{H}_2\text{dipy-pra}$)¹³ and 2,2'-dipyridylammonium (Hdpa)¹⁴ (all with chloride as the counterion). These compounds display intricate hydrogen-bonding networks that give rise to supramolecular frameworks. The two-dimensional (2D) network material $[\text{MoO}_2\text{Cl}_2(\text{H}_2\text{O})_2]\cdot(\text{H}_2\text{dipy-pra})\text{Cl}_2$ was found to be an efficient catalyst, with H_2O_2 as the oxidant and NaHCO_3 as the cocatalyst, in the epoxidation of olefins.¹³ Later, Costa *et al.* reported that the 3D framework material $[\text{MoO}_2\text{Cl}_2(\text{H}_2\text{O})_2]\cdot\text{Hdpa}\cdot\text{Cl}\cdot\text{H}_2\text{O}$ was an effective catalyst (without any cocatalyst added such as NaHCO_3) for the H_2O_2 -mediated epoxidation of cyclooctene.¹⁴

The present chapter reports a new supramolecular approach to the solid-state isolation of $[\text{MoO}_2\text{Cl}_2(\text{H}_2\text{O})_2]$ with the use of the macrocyclic cavitand cucurbit[6]uril (CB[6]). Cucurbit[n]urils (CB[$n = 5-8, 10$]) are composed of n glycoluril units lined by $2n$ methylene bridges to form a hydrophobic cavity accessible through two carbonyl-lined portals.¹⁵⁻¹⁷ CB[n]s can interact with metal complexes to form either host-guest inclusion compounds, in which the CB[n] acts as a molecular container,¹⁵⁻¹⁷ or outer-sphere exclusion complexes, in which the CO groups coordinate either directly or indirectly with metal ions, complexes or clusters.^{18,19} Fedin and co-workers have made the largest contribution to CB[n]-based coordination chemistry with metal cations.²⁰⁻²³

Chapter 8

In aqueous solution, transition-metal aqua complexes generally interact with CB[*n*]s indirectly via hydrogen bonds between the coordinated water molecules and the portal oxygen atoms of the CB[*n*]. This gives rise to supramolecular adducts which crystallize with complex network structures, such as that found with CB[6] and the trinuclear molybdenum oxo cluster $[\text{Mo}_3\text{O}_4(\text{H}_2\text{O})_6\text{Cl}_3]^+$.²²

Although CB[6] is virtually insoluble in water, it is soluble in acidic aqueous solution. Fedin and co-workers were successful in isolating poorly soluble CB[6] coordination complexes by pairing the cavitand with metal complexes that were stable in HCl solution, such as the trinuclear molybdenum complex mentioned above. In this work, it was used an analogous strategy to isolate a supramolecular adduct from a HCl solution containing CB[6] and $[\text{MoO}_2\text{Cl}_2(\text{H}_2\text{O})_2]$. The crystal structure of the adduct determined by X-ray diffraction consists of a 3D hydrogen-bonding framework built from assemblies of CB[6] and the diaqua complex in a net ratio of 1:2. Encouraged by the catalytic results reported previously for adducts containing the diaqua complex, the utility of the CB[6] adduct in catalyzed organic reactions, namely oxidation catalysis (the epoxidation of olefins) and oxidation/acid catalysis (the one-pot conversion of olefins with aqueous H_2O_2 to alkoxy ketone and alcohol products) has been investigated. The catalyst stability was studied and mechanistic insights were obtained by using different types of intermediates as substrates.

8.2. Results and discussion

8.2.1. Synthesis and single-crystal X-ray structure analyses of supramolecular adduct $2[\text{MoO}_2\text{Cl}_2(\text{H}_2\text{O})_2] \cdot (\text{C}_{36}\text{H}_{36}\text{N}_{24}\text{O}_{12}) \cdot x\text{H}_2\text{O} \cdot y\text{HCl} \cdot z(\text{CH}_3\text{COCH}_3)$ (1)

The supramolecular adduct **1** precipitated after mixing an aqueous solution of $[\text{MoO}_2\text{Cl}_2(\text{H}_2\text{O})_2]$ (prepared by dissolving MoO_3 in 6 M HCl) with a hydrochloric acid solution of CB[6]. Prolonged standing of the mother liquor at ambient temperature led to the formation of pale yellow single-crystals suitable for structure determination by X-ray diffraction (XRD).

According to the XRD study, compound **1** is a supramolecular adduct of a CB[6] molecule and two $[\text{MoO}_2\text{Cl}_2(\text{H}_2\text{O})_2]$ complexes (Figure 8.1), with a high number of water molecules of crystallization and HCl, ultimately formulated as $2[\text{MoO}_2\text{Cl}_2(\text{H}_2\text{O})_2] \cdot (\text{C}_{36}\text{H}_{36}\text{N}_{24}\text{O}_{12}) \cdot 17\text{H}_2\text{O} \cdot 2\text{HCl}$.

Chapter 8

The crystal structure was solved in the centrosymmetric triclinic space group $P\bar{1}$ with the asymmetric unit containing one neutral complex $[\text{MoO}_2\text{Cl}_2(\text{H}_2\text{O})_2]$, one half of a CB[6] molecule, and several solvent molecules (8.5 H_2O molecules of crystallization and one HCl molecule; the CB[6] cavity is occupied by H_2O molecules, with the crystal refined model pointing to 2.5 molecules occupying six potential sites). The most important structural features of the $\{\text{MoO}_4\text{Cl}_2\}$ center of the inorganic complex in **1** are consistent with those observed in the previous crystal structures containing this complex, reported in the Cambridge Structural Database (version 5.39 – 2018)^{24,25}: CSD codes YEYWO,⁸ FEKCED,⁹ FEKCED01,⁹ KEQBUE,⁹ XMOPYC10,¹¹ LAPPOH,¹² KICNIU,¹³ MUPGIO,¹⁴ and VONXUS.²⁶ The Mo(VI) coordination center displays a distorted octahedral geometry, with the four O-atoms (two oxido groups, $\text{Mo}=\text{O}$, and two water molecules, $\text{Mo}-\text{O}_w$) in the basal plane, and two chlorine atoms, $\text{Mo}-\text{Cl}$, occupying the axial positions (Figure 8.1; Table 8.1 gives details about the coordination bond lengths and internal angles).

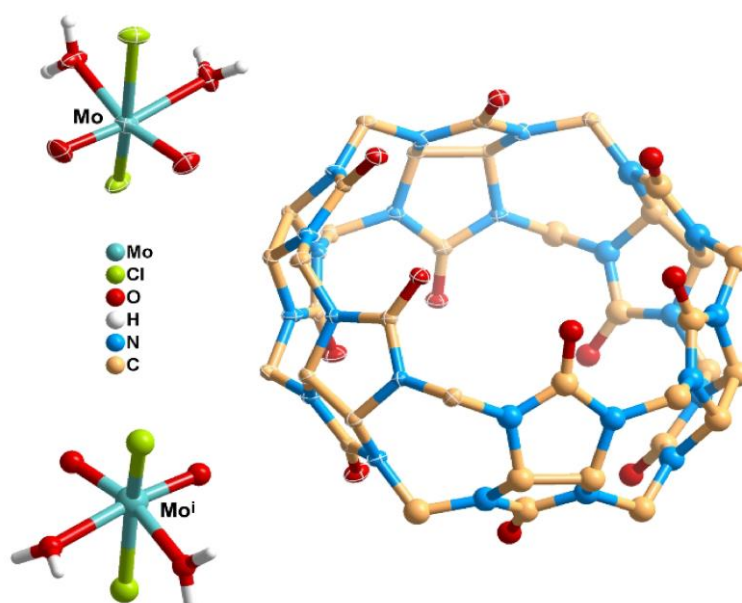


Figure 8.1. Crystal structure of the supramolecular adduct of $[\text{MoO}_2\text{Cl}_2(\text{H}_2\text{O})_2]$ and CB[6] (**1**). Non-H atoms are represented as ellipsoids with thermal displacement at the 50 % probability level, while those generated by symmetry are drawn in ball-and-stick mode, and most of the H-atoms are omitted for clarity (symmetry transformation used to generate equivalent atoms: (i) $-x, 2-y, 1-z$).

Chapter 8

The extended crystal structure of the adduct **1** reveals a supramolecular assembly of metal complexes with CB[6]. Since the Mo complex is not incorporated into the hydrophobic cavity of CB[6], it can be envisaged as an exclusion complex or, alternatively, a lattice exclusion compound (Figure 8.2).²⁷

The structural cohesion of this novel adduct is guaranteed by an extensive network of intermolecular interactions, mainly strong O–H···O and C–H···Cl hydrogen bonds, intermediated by numerous water molecules of crystallization and HCl molecules. Interestingly, five carbonyl groups of each CB[6] rim interact with five water molecules by O–H···O hydrogen bonds, leading to the formation of barrel-shape supramolecular entities, {CB[6]·10(H₂O)} (Figure 8.2a; geometric information concerning all the strong hydrogen bonds are detailed in Table 8.2). These barrel-shape supramolecular entities are involved in further contacts with the remaining water molecules of crystallization and HCl molecules, as well as with the complex [MoO₂Cl₂(H₂O)₂], leading to the formation of a 3D hydrogen-bonded framework (Figure 8.2b and 8.2c). The occurrence of a high number of water molecules of crystallization and, consequently, the extensive network of strong intermolecular interactions is crucial in reinforcing the cohesion of the crystalline structure.

Table 8.1. Selected bond lengths and angles for the Mo(VI) coordination centre of the neutral complex [MoO₂Cl₂(H₂O)₂] in the crystal structure of [MoO₂Cl₂(H₂O)₂]₂@CB[6].

Bond lengths / Å		Angles / °			
Mo1-O1	1.6779(15)	O1-Mo1-O2	103.55(8)	O2-Mo1-Cl1	97.11(5)
Mo1-O2	1.6859(14)	O1-Mo1-O1W	95.01(7)	OW1-Mo1-OW2	77.22(6)
Mo1-O1W	2.2231(14)	O1-Mo1-O2W	172.23(7)	OW1-Mo1-Cl2	79.56(4)
Mo1-O2W	2.2750(14)	O1-Mo1-Cl2	96.12(6)	OW1-Mo1-Cl1	81.52(4)
Mo1-Cl2	2.3672(5)	O1-Mo1-Cl1	95.48(6)	OW2-Mo1-Cl2	82.95(4)
Mo1-Cl1	2.3804(5)	O2-Mo1-O1W	161.42(7)	OW1-Mo1-Cl1	83.12(4)
		O2-Mo1-O2W	84.21(6)	Cl2-Mo1-Cl1	158.563(19)
		O2-Mo1-Cl2	97.61(5)		

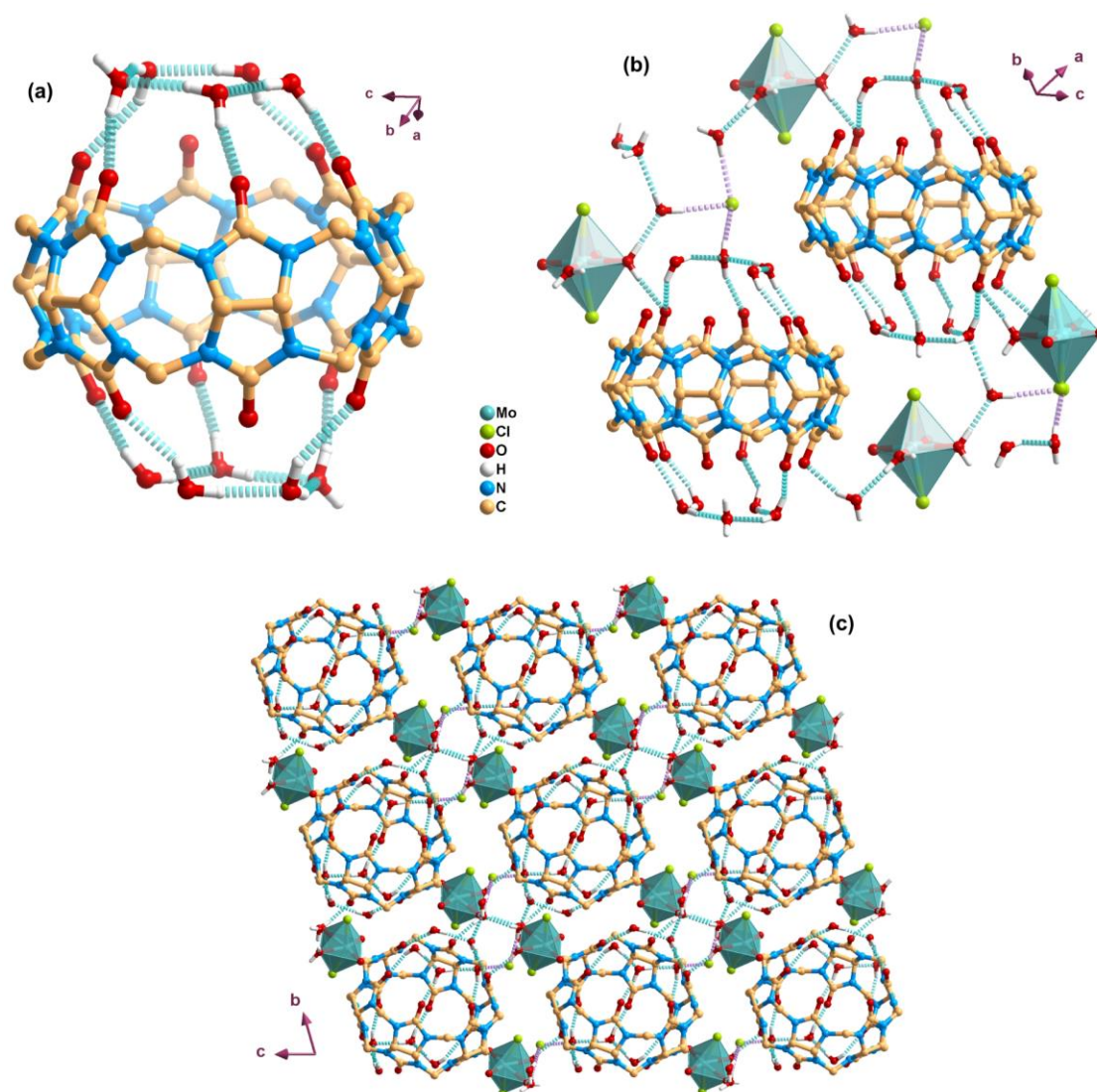


Figure 8.2. Selected features in the crystal structure of the supramolecular adduct of $[\text{MoO}_2\text{Cl}_2(\text{H}_2\text{O})_2]$ and CB[6] (**1**): (a) barrel-shape supramolecular entity $\{\text{CB}[6] \cdot 10(\text{H}_2\text{O})\}$; (b) $\text{O}-\text{H} \cdots \text{O}$ and $\text{O}-\text{H} \cdots \text{Cl}$ interactions between adjacent neutral Mo complexes and CB[6] molecules, intermediated by water and HCl molecules; (c) overall crystalline arrangement viewed along the $[1\ 0\ 0]$ direction of the unit cell. $\text{O}-\text{H} \cdots \text{O}$ and $\text{O}-\text{H} \cdots \text{Cl}$ interactions are represented as blue and pink dashed lines, respectively.

Chapter 8

Table 8.2. Geometric information (distances in Å and angles in degrees) for the O–H...A hydrogen bond interactions of the compound $2[\text{MoO}_2\text{Cl}_2(\text{H}_2\text{O})_2] \cdot (\text{C}_{36}\text{H}_{36}\text{N}_{24}\text{O}_{12}) \cdot 17\text{H}_2\text{O} \cdot 2\text{HCl}$ (**1**).^a

C–H...A	<i>d</i> (H...A)	<i>d</i> (O...A)	∠(OHA)
O1W–H1W...O5 ⁱⁱ	1.966(11)	2.8088(18)	170(2)
O1W–H2W...O3W	1.781(10)	2.624(2)	173(3)
O2W–H3W...O4W ⁱⁱ	2.017(16)	2.7898(19)	151(2)
O2W–H4W...O4W	1.905(11)	2.743(2)	171(3)
O3W–H5W...Cl3 ⁱⁱⁱ	2.327(12)	3.1625(16)	166(3)
O3W–H6W...O7W ^{iv}	2.080(18)	2.857(2)	152(3)
O4W–H7W...Cl3	2.244(10)	3.0815(14)	172(2)
O4W–H8W...O4	1.995(12)	2.7990(18)	159(2)
O5W–H9W...O7	1.800(11)	2.6316(19)	168(3)
O5W–H10W...O6W	1.880(11)	2.716(2)	172(3)
O6W–H11W...O6	1.879(14)	2.6972(19)	160(3)
O6W–H12W...Cl3 ^v	2.290(10)	3.1349(16)	174(3)
O7W–H13W...O4 ⁱ	2.42(2)	2.9891(19)	125(2)
O7W–H13W...O5 ⁱ	2.251(19)	2.9034(18)	134(2)
O7W–H14W...O6W	1.908(13)	2.730(2)	160(3)
O8W–H15W...O3 ⁱ	2.007(18)	2.7019(19)	140(2)
O8W–H15W...O4 ⁱ	2.54(2)	3.000(2)	115(2)
O8W–H16W...O7W	1.838(10)	2.678(2)	175(3)
O9W–H17W...O8	1.844(16)	2.6139(19)	155(3)
O9W–H18W...O5W	1.654(11)	2.483(3)	175(3)

^[a] Symmetry transformations used to generate equivalent atoms: (i) $-x+1, -y+1, z+1$; (ii) $-x+1, -y+2, -z$; (iii) $x-1, y, z$; (iv) $-x, -y+1, -z+1$; (v) $x-1, y-1, z+1$.

8.2.2. Complementary characterization of **1**

The bulk powder obtained in the reaction for **1** was further characterized by elemental analysis, powder XRD (PXRD), TGA, and the spectroscopic techniques FT-IR, FT-Raman and $^{13}\{\text{H}\}$ CP MAS NMR. Figure 8.3 compares the observed PXRD pattern of the bulk microcrystalline sample of **1** with a simulated pattern based on the single crystal structure data. The good match between the two patterns proves that the powder had the same crystalline structure with a high degree of phase purity.

Chapter 8

Elemental analysis of the powder indicated the composition $2[\text{MoO}_2\text{Cl}_2(\text{H}_2\text{O})_2] \cdot (\text{C}_{36}\text{H}_{36}\text{N}_{24}\text{O}_{12}) \cdot 15\text{H}_2\text{O} \cdot 1.5\text{HCl} \cdot 0.6(\text{CH}_3\text{COCH}_3)$, which is similar to that determined by X-ray crystallography except for minor differences in the water and HCl contents, and the presence of acetone.

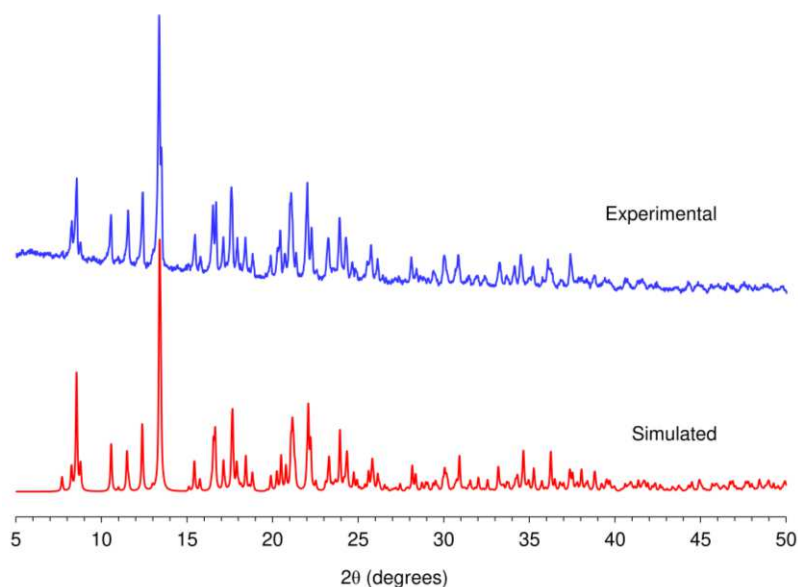


Figure 8.3. Experimental powder X-ray diffraction pattern of **1** compared with the simulated pattern calculated from the crystal structure data reported in this paper for $2[\text{MoO}_2\text{Cl}_2(\text{H}_2\text{O})_2] \cdot (\text{C}_{36}\text{H}_{36}\text{N}_{24}\text{O}_{12}) \cdot 17\text{H}_2\text{O} \cdot 2\text{HCl}$.

The presence of acetone (originating from the CB[6] starting material) was confirmed by $^{13}\text{C}\{^1\text{H}\}$ CP MAS NMR, while the water content was supported by TGA measurements which revealed a mass loss step of 20.6 % up to 150 °C attributed to the removal of water and acetone (Figure 8.4). Acetone was not detected by X-ray crystallography, possibly because of disorder. The TGA profiles of the starting material CB[6] and compound **1** show that the organic cavitaⁿd starts to decompose around 290 °C. Two overlapping steps are clearly visible for **1**, a slightly prolonged one with a derivative thermogravimetric (DTG) maximum at 330 °C, followed by a more abrupt loss with $\text{DTG}_{\text{max}} = 390$ °C. For comparison, the DTG_{max} value for CB[6] is 400 °C. Decomposition of the organic matter in **1** is complete at 500 °C, leaving residual MoO_3 (12.0 %), which starts to sublime above 700 °C.

Chapter 8

The FT-IR and FT-Raman spectra of **1** are dominated by the characteristic bands of CB[6] (Figure 8.5). Nevertheless, a few additional bands are present that can be assigned to the incorporated molybdenum complex: (IR, cm^{-1}) 334 ($\nu_{\text{as}}(\text{Mo}-\text{Cl})$), 915 ($\nu_{\text{as}}(\text{Mo}=\text{O})$); (Raman, cm^{-1}) 252 ($\rho(\text{MoO}_2)$), 310 ($\nu_{\text{s}}(\text{Mo}-\text{Cl})$), 920 ($\nu_{\text{as}}(\text{Mo}=\text{O})$), 960 ($\nu_{\text{s}}(\text{Mo}=\text{O})$).⁹ The reference complex $[\text{MoO}_2\text{Cl}_2(\text{H}_2\text{O})_2]\cdot(\text{diglyme})_2$ (**2**)⁸ displays bands at near-identical frequencies: (IR) 334, 914 and 953 cm^{-1} ; (Raman) 252, 315, 920 and 951 cm^{-1} .

$^{13}\text{C}\{^1\text{H}\}$ CP MAS NMR spectra for CB[6] and **1** are shown in Figure 8.6. The spectrum for CB[6] shows three somewhat broad and featureless signals at 155.5, 70.5 and 52.0 ppm for the three chemically distinct carbon types (C=O, C-H and bridging CH_2 , respectively). The spectrum for **1** is slightly different in that each of the three resonances is split, showing between two and three resolved lines. This can be attributed to the fact that the crystallographically inequivalent carbons for each type of carbon functionality (*i.e.*, six CO groups, six C-H and six CH_2) may have slightly different environments and therefore small differences in chemical shift, which can result in the observation of multiple sharp resonances for one chemically distinct carbon type.

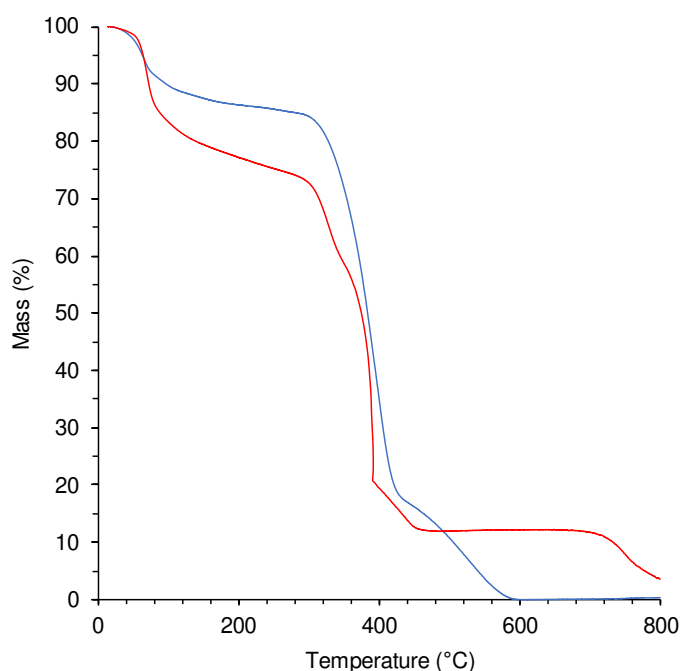


Figure 8.4. TGA curves of the starting material CB[6] (—) and the supramolecular adduct **1** (—).

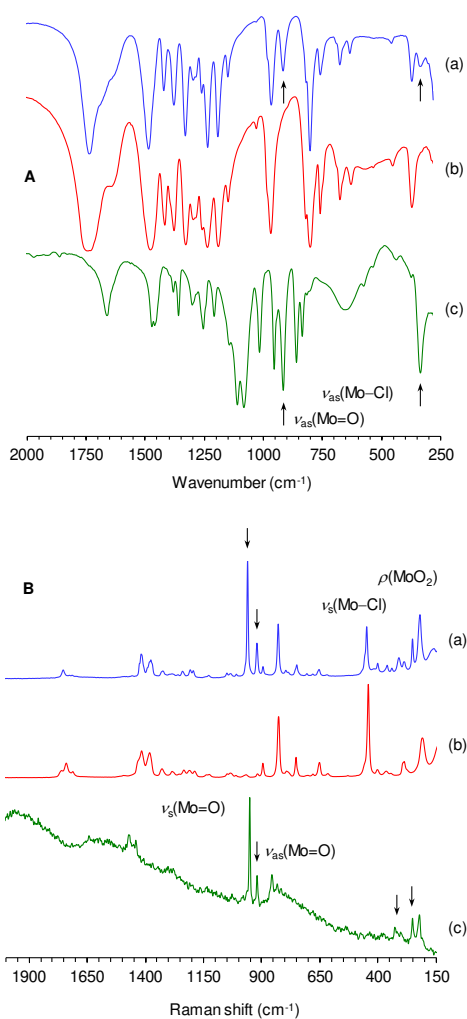


Figure 8.5 FT-IR (A) and Raman (B) spectra of compound (a) **1**, (b) CB[6] and (c) complex **2**.

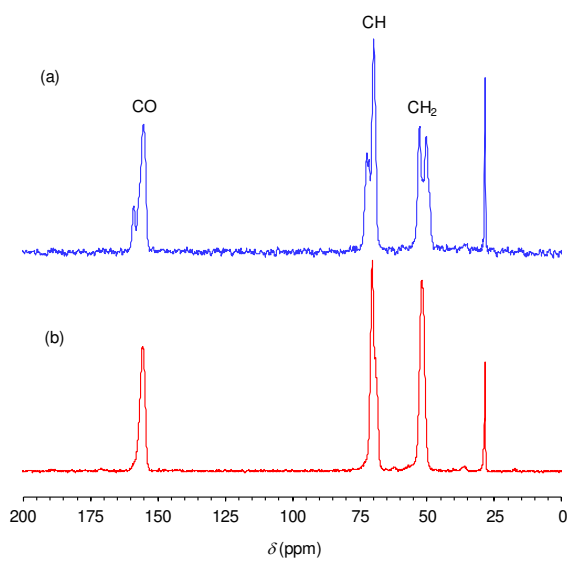


Figure 8.6. $^{13}\text{C}\{^1\text{H}\}$ CP MAS NMR spectra for CB[6] and the supramolecular adduct (a) **1** and (b) CB[6].

8.3. Catalytic studies

Olefins, which may derive from fossil or renewable sources, can be converted to many useful products such as epoxides, 1,2-alkoxy alcohols and 1,2-alkoxy ketones.²⁸ Hydrogen peroxide is an attractive oxidant for catalytic olefin epoxidation due to its relatively low cost and eco-friendliness, giving water as the coproduct from its consumption.²⁹ Epoxides are versatile intermediates for various organic reactions with, for example, nucleophiles, acids, bases, reducing and oxidizing agents.²⁸ In particular, epoxides may be converted in alcohol media to 1,2-disubstituted products (which usually have a *trans* configuration), such as 1,2-alkoxy alcohols and 1,2-alkoxy ketones, which have important applications as intermediates in the pharmaceutical sector.^{30–32} For example, *trans*-2-methoxycyclohexanol is a key intermediate for the synthesis of tricyclic beta-lactam antibiotics.³³ On the other hand, the conversion of olefins in alcohol medium to alkoxy products is a useful tool in organic synthesis for improving product selectivity by enabling protective group formation.³⁴ With these considerations in mind, it was studied the catalytic ability of **1** in two stages, firstly to assess its performance for the epoxidation of olefins with H₂O₂, and secondly to apply this catalytic efficacy in the one-pot conversion of olefins to alkoxy ketone and alcohol products.

8.3.1. Olefin epoxidation

The catalytic properties of **1** were explored starting with *cis*-cyclooctene (Cy) as a model substrate (Table 8.3). The reaction of Cy with H₂O₂ at 70 °C in the presence of **1**, using acetonitrile as a cosolvent, led to 100 % epoxide (CyO) selectivity at 85 % conversion (24 h). Pristine CB[6] led to a sluggish reaction of Cy (7–10 % conversion), suggesting that the epoxidation reaction with **1** involved molybdenum-containing active species. The results for the model complex **2** (100 % CyO selectivity at 93 % conversion) are comparable with those for **1**. An important difference between compounds **2** and **1** is that the former was completely soluble in the reaction medium and therefore difficult to separate, whereas **1** could be recovered and reused in consecutive batch runs (discussed below). Decreasing the reaction temperature from 70 to 55 °C led to slower kinetics in the presence of **1** (100 % CyO selectivity at 73 % conversion), as did the use of *N,N'*-dimethylformamide (DMF) as cosolvent instead of CH₃CN (100 % CyO selectivity at 28 % conversion). Without a cosolvent or using water, the reaction was very sluggish (\leq 2 % Cy conversion at 24 h). Hence, the reaction kinetics seemed to be favoured by non-protic polar solvents.

Chapter 8

Table 8.3. Oxidation of different olefins with H₂O₂ in the presence of compounds **1**, **2** and CB[6].^a

Catalyst	Substrate	Product	T (°C)	Cosolvent	Conv. (%)	Select. (%)
CB[6]	Cy	CyO	70	CH ₃ CN	10	100
1			55	CH ₃ CN	73	100
1			70	CH ₃ CN	85	100
1			70	DMF	28	100
1			70	none	2	100
1			70	H ₂ O	1	100
1	Cy ₆	Cy ₆ (OH) ₂	70	CH ₃ CN	42	100
1	Sty	BA	70	CH ₃ CN	47	100
2	Cy	CyO	70	CH ₃ CN	93	100

^a Reaction conditions: Molar ratios Mo:Substrate:H₂O₂ = 1:100:152, 24 h reaction.

There are relatively few reports on catalytic olefin epoxidation with H₂O₂ as the oxygen source and complexes of the type [MoO₂Cl₂(L)_n] as the catalyst source. With the 2D network material [MoO₂Cl₂(H₂O)₂](H₂dipy-pra)Cl₂ as the catalyst (1 mol %), NaHCO₃ as cocatalyst (25 mol %) and CH₃CN as cosolvent, Wang and co-workers obtained a high CyO yield of 99 % after 1 h at 25 °C.¹³ Under conditions more similar to those used in the present work (no NaHCO₃ cocatalyst), the 3D framework material [MoO₂Cl₂(H₂O)₂].Hdpa·Cl·H₂O led to a CyO yield of 80 % after 24 h at 50 °C,¹⁴ which is comparable with the catalytic performance measured for **1**.

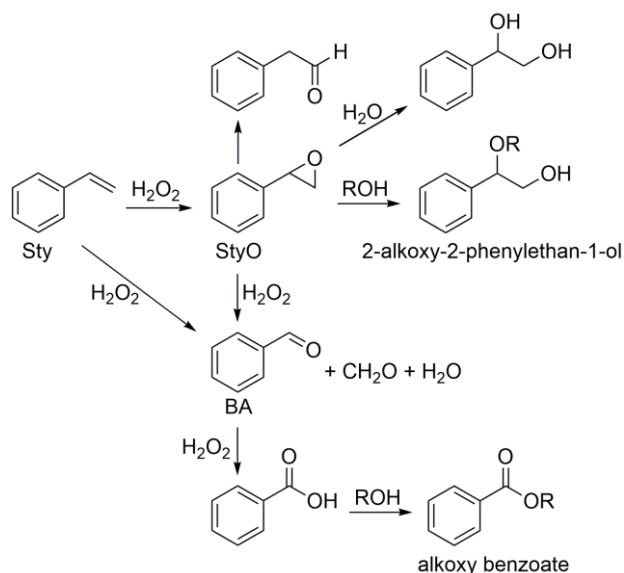
Compound **1** was effective for the catalytic conversion of other alkenes, namely styrene (Sty) and cyclohexene (Cy₆) (Table 8.3). There are several reports of the oxidation of styrene or cyclohexene catalyzed by dioxomolybdenum(VI) complexes, where H₂O₂ has been used as an oxidant.^{35,36} In many cases, especially for styrene, aqueous 30 % H₂O₂ as the sole oxidant gives poor catalytic efficiency, with low styrene oxide (StyO) selectivity, whereas the addition of the cocatalyst NaHCO₃ activates the catalytic oxidation process and leads to much higher StyO selectivity. The results obtained in the present work without a cocatalyst are consistent with these observations. Thus, the oxidation of Sty at 70 °C gave benzaldehyde (BA) with 100 % selectivity at 47 % conversion (24 h). According to literature studies on the mechanism of Sty oxidation, styrene oxide (StyO) is an intermediate to BA, and the latter may be formed via nucleophilic attack of H₂O₂ on StyO giving a hydroxyl-hydroperoxy intermediate followed by oxidative cleavage,^{37–39} or BA may be formed via the direct oxidative cleavage of the side chain C=C double bond of Sty via a radical mechanism (Scheme 8.1).^{37,38,40} The reaction of Cy₆ with H₂O₂ in the presence of **1** gave

Chapter 8

cyclohexanediol (Cy₆(OH)₂) in 100 % selectivity at 42 % conversion. The diol may be formed via the intermediate formation of cyclohexene oxide (Cy₆O),⁴¹ as suggested in Scheme 8.1 for StyO.

8.3.2. One-pot conversion of olefins to alkoxy products

Compound **1** was tested as a multifunctional catalyst for the integrated conversion of olefins to alkoxy products in alcohol media. These reaction systems involve oxidation and acid chemistry. The one-pot conversion was carried out in two stages (24 h reaction at 70 °C, followed by 24 h reaction at 90 °C) with the objective of enhancing selectivity to the intermediates in the first stage (involving oxidation catalysis), followed by conversion of the intermediates to the alkoxy products in the second stage (involving acid catalysis).



Scheme 8.1. Possible products of the oxidation reaction of styrene with H₂O₂.^{37,38,40}

The one-pot first-stage process of **1**/Cy/H₂O₂/ethanol led to high epoxide selectivity of 90 % at 89 % conversion, and the products 2-ethoxycyclooctanol [Cy(OH)(OEt)] and 2-ethoxycyclooctanone [Cy(=O)(OEt)] were formed in low yields of 3 % and 5 %, respectively (Table 8.4). Using methanol (MeOH) or 1-butanol (BuOH) as reacting solvent led to high epoxide selectivity (93-99 %) at high conversion (80-90 %), and the alkoxy products were formed (for BuOH), albeit in low yields, or were not formed (for MeOH). BuOH and EtOH led to higher Cy conversions than MeOH.

Chapter 8

Table 8.4. Catalytic results for the oxidation of cyclooctyl substrates with H₂O₂ in the presence of **1** using an alcohol as reacting solvent.^a

Catalyst	Substrate	Product	T (°C)	t (h)	Solvent	Conv. (%)	Select. (%)
1	Cy	CyO	70	24	MeOH	80	> 99
		Cy(OH)(OMe)					<1
		CyO	90 ^[b]	48	MeOH	82	51
		Cy(OH)(OMe)					46
		Cy(OMe) ₂					3
		CyO	70	24	EtOH	89	90
		Cy(OH)(OEt)					3
		Cy(=O)(OEt)					6
		CyO	90 ^[b]	48	EtOH	90	57
		Cy(OH)(OEt)					18
		Cy(=O)(OEt)					26
		CyO	70	24	BuOH	90	93
		Cy(OH)(OBu)					2
		Cy(=O)(OBu)					5
		CyO	90 ^[b]	48	BuOH	90	64
		Cy(OH)(OBu)					10
		Cy(=O)(OBu)					27
		1	CyO	Cy(OH)(OEt)	70	24	EtOH
Cy(=O)(OEt)							52
none		Cy(OH)(OEt)	70	24	EtOH	0	0
		Cy(=O)(OEt)					
1	Cy(OH)	Cy(=O)	70	24	EtOH	50	100
		Cy(=O)	70	24	EtOH	14	100
1	Cy(OH) ₂	Cy(OH)(OEt)	70	24	EtOH	100	5
		Cy(=O)(OEt)					52
		Cy(=O)OH					28
		Cy(=O) ₂					15
none		Cy(OH)(OEt)	70	24	EtOH	99	8
		Cy(=O)(OEt)					91
		Cy(=O)OH					0
		Cy(=O) ₂					0

^[a] Reaction conditions: Molar ratio Mo:substrate:H₂O₂ = 1:100:152. ^[b] First 24 h at 70 °C.

Chapter 8

In the one-pot two-stage process with ethanol as reacting solvent, pristine CB[6] gave a sluggish reaction (ca. 25 % conversion at 48 h). The model complex **2** led to 92 % conversion and a total yield of 59 % for Cy(OH)(OEt) and Cy(=O)(OEt), which represents similar performance to that obtained with **1** (90 % conversion, 40 % yield of alkoxy products). However, as mentioned above, complex **2** has different solubility characteristics compared to **1**, which has a major impact on catalyst recovery processes.

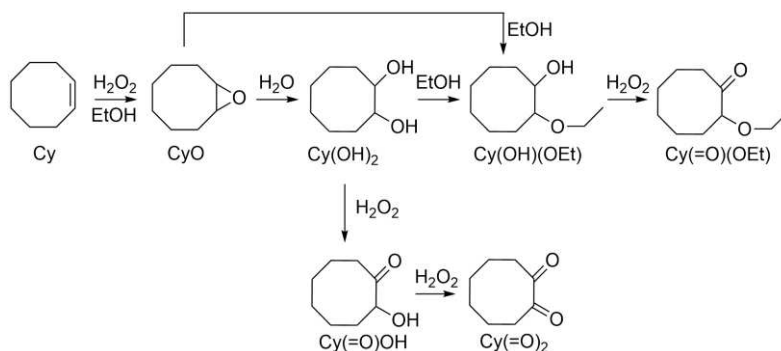
In the one-pot two-stage process in the different alcohol media, **1** led to epoxide yields of 42-58 % and relatively high yields of alkoxy products (33-40 % total yield at 48 h) (Table 8.4). The reaction in MeOH was slowest. The epoxide yield decreased and the total yield of alkoxy products increased in the order: BuOH → EtOH → MeOH. The differences in kinetics may be partly due to differences in nucleophilicity of the alcohols. For example, since EtOH is a stronger nucleophile than MeOH, the formation of the respective hydroxy alkoxy product (via alcoholysis) may be faster, driving the epoxidation step forward and thus increasing Cy conversion (compared to the reaction using MeOH).

To gain mechanistic insights into these reaction systems, **1** was tested with cyclooctyl substrates at 70 °C using H₂O₂/EtOH. The epoxide CyO gave Cy(OH)(OEt) and Cy(=O)(OEt) in ca. 6 % yield each at 12 % conversion (24 h) (Table 8.4). These results, taken together with those for the one-pot two-stage process, indicate that the alkoxy products are formed via the intermediate formation of the epoxide, with this consecutive step being favored at higher temperature (in the second stage at 90 °C). The alkoxy alcohol may be converted to the corresponding alkoxy ketone via oxidative dehydrogenation with H₂O₂. The oxidative dehydrogenation activity of **1** for converting alcohols to carbonyls was confirmed by the finding that the reaction of cyclooctanol [Cy(OH)] led to cyclooctanone [Cy(=O)] as the sole product in 50 % yield at 24 h.

An overall mechanistic proposal is presented in Scheme 8.2. *cis*-1,2-Cyclooctanediol [Cy(OH)₂] was not present in measurable amounts, although its formation via acid-catalyzed hydrolysis of the epoxide cannot be completely excluded since water was added together with H₂O₂. With Cy(OH)₂ as substrate, the catalytic reaction was very fast (100 % conversion at 24 h), indicating that the diol is a very reactive intermediate when compared to CyO. The diol was converted to Cy(OH)(OEt) and Cy(=O)(OEt) in 5 % and 52 % yield, respectively, together with a 28 % yield of 2-hydroxycyclooctanone [Cy(=O)OH] and a 15 % yield of 1,2-cyclooctanedione [Cy(=O)₂]. Hence, the diol, once formed, may undergo etherification with EtOH to give the alkoxy products. The ketones Cy(=O)₂ and Cy(=O)OH may be formed via oxidative dehydrogenation of the diol with H₂O₂. From these results one cannot fully exclude the

Chapter 8

possibility of the diol being an intermediate in the reaction of the olefin to the alkoxy products in $\text{H}_2\text{O}_2/\text{EtOH}$. Nevertheless, since $\text{Cy}(=\text{O})_2$ and $\text{Cy}(=\text{O})\text{OH}$ were not present in measurable amounts in the catalytic system **1**/ $\text{Cy}/\text{H}_2\text{O}_2/\text{EtOH}$, the epoxide alcoholysis route seems to be more important.



Scheme 8.2. One-pot conversion of cyclooctene in $\text{H}_2\text{O}_2/\text{EtOH}$ to alkoxy alcohol and alkoxy ketone products; a mechanistic proposal involving hydrolysis and alcoholysis.

Compound **1** was further explored for the one-pot conversion of Cy_6 and Sty to alkoxy products using $\text{H}_2\text{O}_2/\text{EtOH}$ at 70 °C. The reaction of Cy_6 gave 2-ethoxycyclohexanol [$\text{Cy}_6(\text{OH})(\text{OEt})$] as the main product in 60 % yield at 64 % conversion (24 h), while the diol $\text{Cy}_6(\text{OH})_2$ was formed in 5 % yield (Table 8.5). These results are interesting in that the alkoxy product was the main product in a one-pot strategy at the lower temperature of 70 °C. The absence of the alkoxy ketone product suggests that the oxidative dehydrogenation of $\text{Cy}_6(\text{OH})(\text{OEt})$ is demanding. In support of this supposition, the catalytic reaction of cyclohexanol [$\text{Cy}_6(\text{OH})$] with $\text{H}_2\text{O}_2/\text{EtOH}$ in the presence of **1** only resulted in 12 % conversion after 24 h. Although the epoxide Cy_6O was not present in measurable amounts with Cy as substrate, it may be an intermediate in the formation of the diol and alkoxy products, as proposed in Scheme 8.2 for Cy. Accordingly, Cy_6O was found to be a very reactive substrate with **1**/ $\text{H}_2\text{O}_2/\text{EtOH}$, giving the diol and alkoxy alcohol in 8 % and 92 % yield, respectively, after 24 h (Table 8.5).

There are very few reports describing the reaction $\text{Cy}_6/\text{H}_2\text{O}_2$ in alcohol medium in the presence of molybdenum(VI) catalysts without a cocatalyst, where alkoxy products were formed. For the reaction $\text{Cy}_6/\text{H}_2\text{O}_2/\text{MeOH}$ at 60 °C in the presence of the homogeneous catalyst [$\text{Mo}(\text{O})(\text{O}_2)_2(\text{H}_2\text{O})_n$], Carrasco *et al.* found that the epoxide Cy_6O was formed in trace amounts, while the main products were the diol and alkoxy alcohol (12 and 87 % selectivity at 65 % conversion, 18 h), somewhat in parallel with that observed for **1**.⁴²

Chapter 8

With Sty as substrate, **1** led mainly to styrene glycol [Sty(OH)₂] (58 % selectivity at 57 % conversion); other products included StyO, BA and ethyl benzoate (Ph(COOEt)) formed in 5, 15 and 3 % yield, respectively (Table 8.5). The corresponding alkoxy alcohol product was not present in measurable amounts. The results somewhat parallel those reported by Biradar *et al.* for Sty/H₂O₂/BuOH in the presence of the complex [CpMo(CO)₃(C≡CPh)] (0.2 mol %) in that the main product was the diol (82 % selectivity at 95 % conversion, 65 °C/10 h), and other reaction products included BA and (1,2-diethoxyethyl)benzene.⁴³ The diol may be formed via acid-catalyzed hydrolysis of the epoxide in a manner similar to that represented in Scheme 8.2.

Table 8.5. Catalytic results for the oxidation of cyclohexyl substrates and styrene with H₂O₂ in the presence of **1** using ethanol as reacting solvent.^a

Substrate	Product	T (°C)	t (h)	Conv. (%)	Select. (%)
Cy₆	Cy ₆ (OH) ₂	70	24	64	7
	Cy ₆ (OH)(OEt)				93
Cy₆O	Cy ₆ (OH) ₂	70	24	100	8
	Cy ₆ (OH)(OEt)				92
Cy₆(OH)	Cy ₆ (=O)	70	24	12	100
Sty	BA	70	24	57	26
	StyO				9
	Ph(COOEt)				5
	Sty(OH) ₂				58

^[a] Reaction conditions: Molar ratio Mo:Substrate:H₂O₂ = 1:100:152.

8.3.3. Catalyst reuse

With CH₃CN as cosolvent or EtOH as reacting solvent, the reactions of Cy with H₂O₂ in the presence of **1** always led to biphasic solid-liquid mixtures after 24 h batch runs. Solids were recovered for reuse by centrifugation, washing with acetone, and drying. Compound **1** was reused for three consecutive batch runs of the reaction Cy/H₂O₂/CH₃CN and two consecutive batch runs of the reaction Cy/H₂O₂/EtOH at 70 °C for 24 h. For CH₃CN, Cy conversion decreased from run 1 to run 2, and then remained similar (Figure 8.7). In the EtOH medium, partial loss activity was observed from the first to the second run (Figure 8.7).

Chapter 8

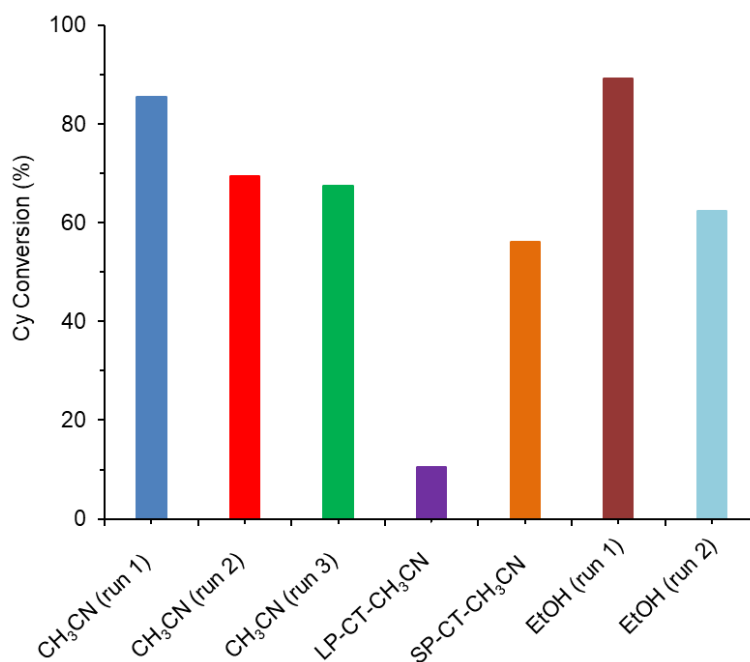


Figure 8.7. Reaction of Cy at 70 °C for 24 h using 1/H₂O₂/CH₃CN (catalyst reuse for three runs), the liquid (LP) or solid (SP) phases from the CT for 1, and 1/H₂O₂/EtOH (catalyst reuse for two runs).

A contact test (CT) was carried out for 1 by mixing it with H₂O₂/CH₃CN (without substrate) at 70 °C for 24 h. The resultant liquid and solid phases (denoted LP-CT-CH₃CN and SP-CT-CH₃CN, respectively) were separated and tested for the reaction Cy/H₂O₂/ACN at 70 °C for 24 h. The liquid phase LP-CT-CH₃CN did not lead to significant olefin conversion (10 % at 24 h), while the solid phase SP-CT-CH₃CN led to similar catalytic results to those for run 2 (Figure 8.5). These results suggest that the catalytic reaction occurred essentially in heterogeneous phase.

The solids recovered after each batch run were characterized by FT-IR spectroscopy, PXRD and SEM (with EDS elemental mapping). Representative results are shown below for the reactions 1/Cy/H₂O₂/CH₃CN, 1/Sty/H₂O₂/CH₃CN and 1/Sty/H₂O₂/EtOH performed at 70 °C, and 1/Cy/H₂O₂/EtOH performed at 90 °C. The FT-IR spectra, PXRD patterns and SEM images of the solids recovered after the first run of each reaction system were similar but displayed differences when compared with those for 1. No further significant alterations were observed for the solids recovered after the runs 2 and 3. Hence, structural features of 1 changed during the first contact with the reaction medium and then remained similar, which correlates with the catalytic activity in consecutive batch runs for the reaction 1/Cy/H₂O₂/CH₃CN.

Chapter 8

Regarding the FT-IR spectra, the major change between **1** and the recovered solids was the weakening (or complete loss) of the $\nu_{\text{as}}(\text{Mo}=\text{O})$ absorption band at 915 cm^{-1} (Figure 8.8). This was accompanied by the appearance of some very weak bands between 850 and 900 cm^{-1} , especially one at 888 cm^{-1} , which may be due to peroxide ligands $[\nu(\text{O}-\text{O})]$ formed via the coordination of H_2O_2 to molybdenum centers.

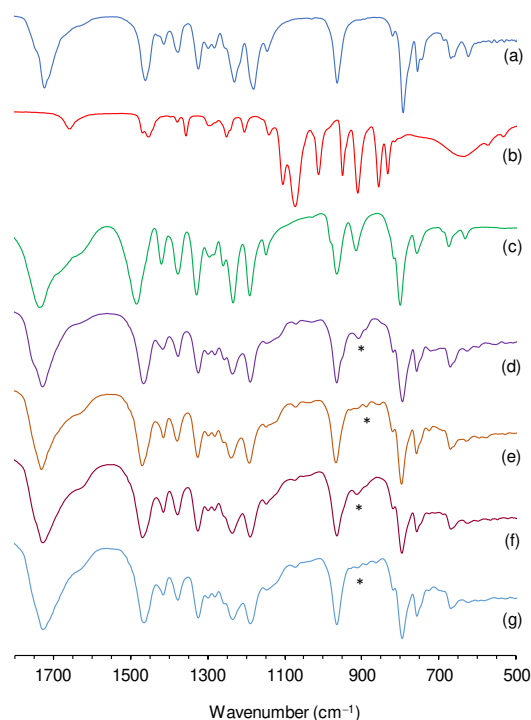


Figure 8.8. ATR FT-IR spectra of (a) CB[6], (b) complex **2**, (c) compound **1**, and the solids recovered from the reactions (d) **1**/Cy/ H_2O_2 /MeCN/ $70\text{ }^\circ\text{C}$, (e) **1**/Sty/ H_2O_2 /MeCN/ $70\text{ }^\circ\text{C}$, (f) **1**/Cy/ H_2O_2 /EtOH/ $90\text{ }^\circ\text{C}$, and (g) **1**/Sty/ H_2O_2 /EtOH/ $70\text{ }^\circ\text{C}$. The asterisk denotes a new band not observed for **1**.

The PXRD patterns of all the recovered solids indicated that the crystalline structure of **1** underwent a reorganization under the different reaction conditions to give a CB[6] crystal packing arrangement equivalent to that present in as-synthesized CB[6] (Figure 8.9).

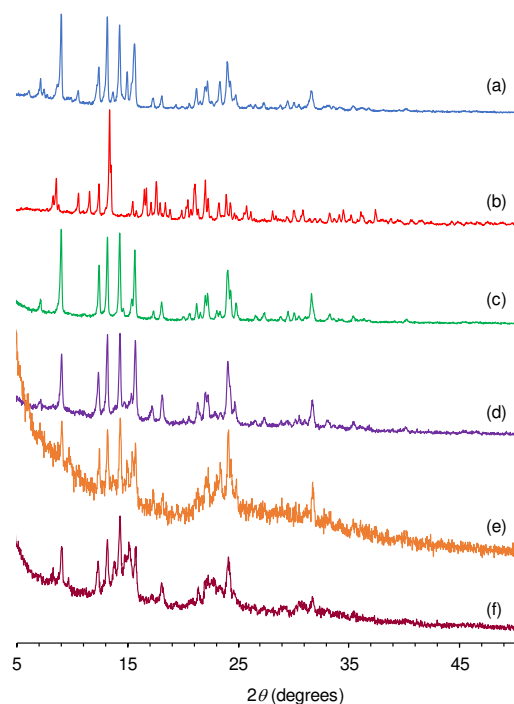


Figure 8.9. PXRD patterns of (a) CB[6], (b) compound **1**, and the solids recovered from the reactions (c) **1**/Cy/H₂O₂/CH₃CN/70 °C, (d) **1**/Sty/H₂O₂/CH₃CN/70 °C, (e) **1**/Cy/H₂O₂/EtOH/90 °C and (f) **1**/Sty/H₂O₂/EtOH/70 °C.

No marked change in morphology occurred according to SEM (Figure 8.10). EDS elemental mappings of **1** and all the recovered solids revealed uniform distributions of Mo, N and O (Figure 8.10). The EDS-determined N/Mo atomic ratio was 9.4 for **1**, and 12.7 for the solid recovered after run 1 of the reaction **1**/Cy/H₂O₂/CH₃CN performed at 70 °C. This may point to slight metal leaching during the first catalytic run. However, after run 1, the N/Mo ratio remained roughly constant (less than 5 % variance), which correlates with the steady catalytic activity after run 1. With ethanol as the reacting solvent (**1**/Cy/H₂O₂/EtOH), the N/Mo ratio for the used catalyst was 9.2, suggesting fairly good stability towards metal leaching in alcohol media. These results, together with those for the contact test, suggest that any metal species leached into solution had negligible catalytic contribution. Further studies examining the stability and active species of these systems are currently the subject of investigation in the laboratories of the group.

Chapter 8

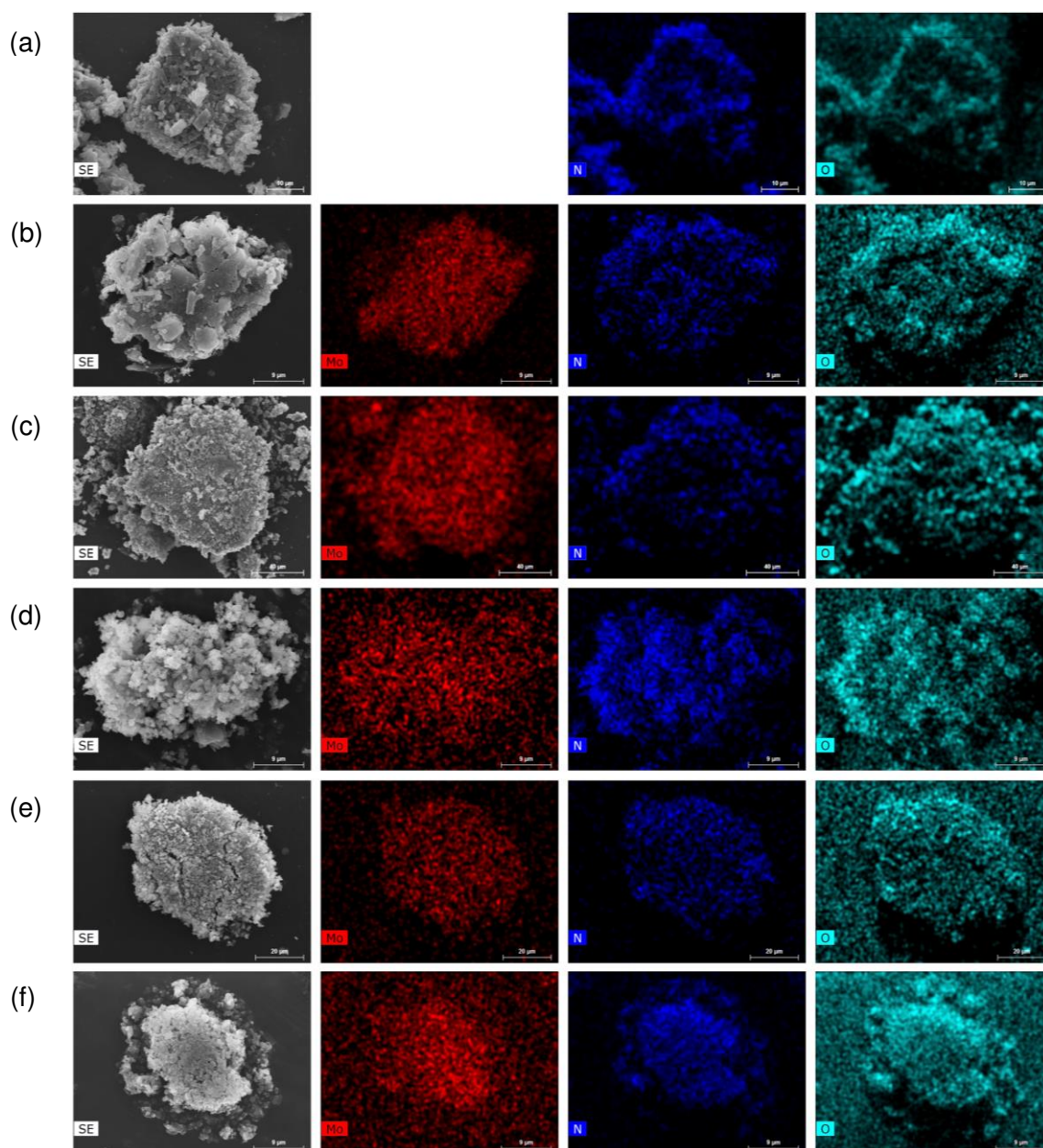


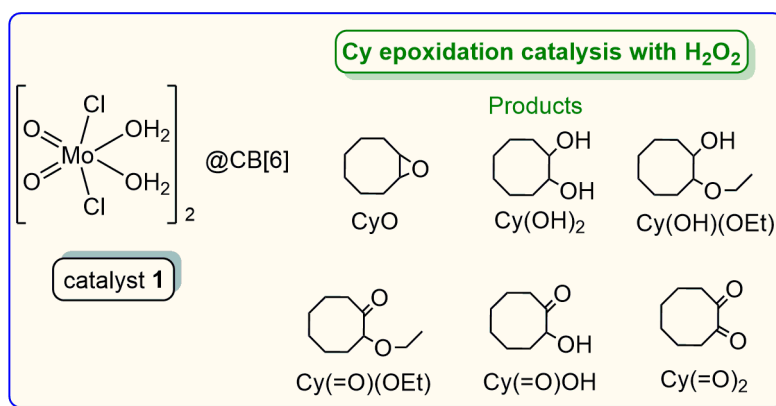
Figure 8.10. SEM images and corresponding EDS Mo/N/O mapping images of (a) CB[6], (b) compound **1**, and the solids recovered from the reactions (c) **1**/Cy/H₂O₂/CH₃CN/70 °C, (d) **1**/Sty/H₂O₂/CH₃CN/70 °C, (e) **1**/Cy/H₂O₂/EtOH/90 °C, and (f) **1**/Sty/H₂O₂/EtOH/70 °C.

8.4. Conclusions

In conclusion, it was demonstrated that the macrocyclic cavitand cucurbit[6]uril can be used for the solid-state isolation of the complex [MoO₂Cl₂(H₂O)₂] from hydrochloric acid solution. In the resultant crystalline supramolecular compound (**1**), the diaqua complexes are embedded between barrel-shaped hydrogen-bonded entities, {CB[6]·10(H₂O)}, which are arranged in layers. Although the activity of compound **1** for

Chapter 8

the catalytic oxidation of *cis*-cyclooctene is moderate, it has the advantage of using H_2O_2 as oxidant, and the selectivity towards the epoxide is very high (90-100 %) for reaction temperatures up to 70 °C and different cosolvents (Scheme 8.3). Another advantage is that the reaction outcome with an alcohol as solvent can be shifted towards the formation of alkoxy ketone and alkoxy alcohol products by adopting a one-pot strategy comprising an oxidation stage at 70 °C (with H_2O_2) followed by an acid-catalyzed stage at 90 °C. This is the first report of the one-pot Mo-catalyzed oxidation of an alkene with H_2O_2 in alcohol medium to give alkoxy ketone products. While the reaction of cyclohexene in CH_3CN gave the diol with 100 % selectivity, the reaction in ethanol gave 2-ethoxycyclohexanol as the main product (93 % selectivity) even at the lower temperature of 70 °C. Mechanistic studies using the probable cyclooctyl and cyclohexyl intermediates as substrates indicate that epoxide alcoholysis is the most important pathway for the formation of the alkoxy products. The $\text{CB}[6]/\text{Mo(VI)}$ catalyst presented steady performance after run 2, which correlated with the similar characterization results of the catalyst recovered from run 2 onwards. Considering the known effectiveness of molybdenum(VI) catalysts for olefin epoxidation, the data presented here encourage a more comprehensive study Mo(VI)-containing supramolecular compounds as multifunctional catalysts for the target integrated catalytic reaction systems.



Scheme 8.3. Summary of the main syntheses and catalytic studies carried out in this work.

Chapter 8

8.5. References

- (1) Colton, R.; Tomkins, I. B. *Aust. J. Chem* **1965**, *18*, 447–452.
- (2) Jeyakumar, K.; Chand, D. K. *J. Chem. Sci.* **2009**, *121*, 111–123.
- (3) Sousa, S. C. A.; Cabrita, I.; Fernandes, A. C. *Chem. Soc. Rev.* **2012**, *41*, 5641–5653.
- (4) Noronha, R. G.; Fernandes, A. C. *Curr. Org. Chem.* **2012**, *16*, 33–64.
- (5) Atovmyan, L. O.; Aliev, Z. G.; Tarakanov, B. M. *J. Struct. Chem.* **1969**, *9*, 985–986.
- (6) Atovmyan, L. O.; Aliev, Z. G. *J. Struct. Chem.* **1971**, *12*, 668–669.
- (7) Coddington, J. M.; Taylor, M. J. *J. Chem. Soc. Dalt. Trans.* **1990**, 41–47.
- (8) Arnaiz, F. J.; Aguado, R.; Sanz-Aparicio, J.; Martinez-Ripoll, M. *Polyhedron* **1994**, *13*, 2745–2749.
- (9) Taylor, M. J.; Rickard, C. E. F.; Kloo, L. A. *J. Chem. Soc. Dalt. Trans.* **1998**, *461*, 3195–3198.
- (10) Levason, W.; Ratnani, R.; Reid, G.; Webster, M. *Inorg. Chim. Acta* **2006**, *359*, 4627–4630.
- (11) Kamenar, B.; Penavic, M. *Acta Cryst. B* **1976**, *785*, 3323–3324.
- (12) Taylor, M. J.; Jirong, W.; Rickard, C. E. F. *Polyhedron* **1993**, *12*, 1433–1435.
- (13) Luan, Y.; Wang, G.; Luck, R. L.; Yang, M. *Eur. J. Inorg. Chem.* **2007**, 1215–1218.
- (14) Costa, J. S.; Markus, C. M.; Mutikainen, I.; Gamez, P.; Reedijk, J. *Inorg. Chim. Acta* **2010**, *363*, 2046–2050.
- (15) Masson, E.; Ling, X.; Joseph, R.; Kyeremeh-Mensah, L.; Lu, X. *RSC Adv.* **2012**, *2*, 1213–1247.
- (16) Assaf, K. I.; Nau, W. M. *Chem. Soc. Rev.* **2015**, *44*, 394–418.
- (17) Barrow, S. J.; Kasera, S.; Rowland, M. J.; Barrio, J. del; Scherman, O. A. *Chem. Rev.* **2015**, *115*, 12320–12406.
- (18) Lü, J.; Lin, J.-X.; Cao, M.-N.; Cao, R. *Coord. Chem. Rev.* **2013**, *257*, 1334–1356.
- (19) Ni, X.-L.; Xiao, X.; Cong, H.; Zhu, Q.-J.; Xue, S.-F.; Tao, Z. *Acc. Chem. Res.* **2014**, *47*, 1386–1395.
- (20) Sitepu, H.; O'Connor, B. H.; Li, D. *J. Appl. Crystallogr.* **2005**, *38*, 158–167.
- (21) Gerasko, O. A.; Mainicheva, E. A.; Naumova, M. I.; Yurjeva, O. P.; Alberola, A.; Vicent, C.; Llusar, R.; Fedin, V. P. *Chem. Eur. J.* **2008**, *3*, 416–424.
- (22) Samsonenko, D. G.; Virovets, A. V.; Sharonova, A. A.; Fedin, V. P.; Fenske, D. *Russ. Chem. Bull.* **2001**, *50*, 494–496.
- (23) Gerasko, O. A.; Mainicheva, E. A.; Naumov, D. Y.; Fedin, V. P. *Russ. Chem. Bull. Int. Ed.* **2007**, *56*, 1972–1977.
- (24) Allen, F. H. *Acta Cryst. B* **2002**, 407–422.
- (25) Allen, F. H. *Acta Cryst. B* **2002**, 380–388.
- (26) Luan, Y.; Wang, G.; Luck, R. L.; Wang, Y.; Ding, H.; Beijing, T. *Chem. Lett.* **2008**, *37*, 1144–1145.
- (27) Wagner, B. D.; Macrae, A. I. *J. Phys. Chem. B* **1999**, *103*, 10114–10119.

Chapter 8

- (28) Smith, J. G. *Synthesis*. **1984**, 629–656.
- (29) Biswal, D.; Pramanik, N. R.; Chakrabarti, S.; Drew, M. G. B.; Sarkar, B.; Maurya, M. R.; Mukherjee, S. K.; Chowdhury, P. *New J. Chem.* **2017**, *41*, 4116–4137.
- (30) Conolly, M. E.; Kersting, F.; Dollery, C. T. *Prog. Cardiovasc. Dis.* **1976**, *19*, 203–234.
- (31) Joossens, J.; Van Der Veken, P.; Lambeir, A. M.; Augustyns, K.; Haemers, A. *J. Med. Chem.* **2004**, *47*, 2411–2413.
- (32) Stead, P.; Madey, H.; Mahmoudian, M.; Webb, G.; Noble, D.; Ip, Y. T.; Piga, E.; Rossi, T.; Roberts, S.; Dawson, M. J. *Tetrahedron: Asymmetry* **1996**, *7*, 2247–2250.
- (33) Liang, M.; Zou, D.-H. *Inorg. Nano-Metal Chem.* **2017**, *47*, 110–115.
- (34) Greene, T. W.; Wuts, P. G. M. *Protective Groups in Organic Synthesis*, Third.; John Wiley & Sons: New Jersey, 2006.
- (35) Roy, S.; Saswati; Lima, S.; Dhaka, S.; Maurya, M. R.; Acharyya, R.; Eagle, C.; Dinda, R. *Inorg. Chim. Acta* **2018**, *474*, 134–143.
- (36) Maurya, M. R.; Kumar, N. *J. Mol. Catal. A Chem.* **2015**, *406*, 204–212.
- (37) Hulea, V.; Dumitriu, E. *Appl. Catal., A* **2004**, *277*, 99–106.
- (38) Patel, A.; Pathan, S. *Ind. Eng. Chem. Res.* **2012**, *51*, 732–740.
- (39) Maurya, M. R.; Arya, A.; Adão, P.; Pessoa, J. C. *Appl. Catal., A* **2008**, *351*, 239–252.
- (40) Huang, X.; Guo, W.; Wang, G.; Yang, M.; Wang, Q.; Zhang, X.; Feng, Y.; Shi, Z.; Li, C. *Mater. Chem. Phys.* **2012**, *135*, 985–990.
- (41) Zhao, J.; Santos, A. M.; Herdtweck, E.; Kühn, F. E. *J. Mol. Catal. A Chem.* **2004**, *222*, 265–271.
- (42) Carrasco, C. J.; Montilla, F.; Álvarez, E.; Herbert, M.; Galindo, A. *Polyhedron* **2013**, *54*, 123–130.
- (43) Biradar, A. V.; Sathe, B. R.; Umbarkar, S. B.; Dongare, M. K. *J. Mol. Catal. A Chem.* **2008**, *285*, 111–119.

CHAPTER 9

Final considerations



Chapter 9

Index

9.1. Conclusions and future considerations	247
9.2. References	250

9.1. Conclusions and future considerations

The present thesis describes the design, synthesis, detailed characterization and application in catalysis of new oxomolybdenum organic-inorganic hybrid materials. Six distinct N,N'-chelate ligands were investigated, which include 2-(1-propyltrimethylammonium-3-pyrazolyl)pyridine bromide, 2-(1-pentyl-3-pyrazolyl)pyridine (ppp), N-methyl-N-(1-phenylethyl)-6,7-dihydro-5H-cyclopenta[b]pyridin-7-amine, 1,2,3-triazole, 2,2'-bipyridine (2,2'-bipy) and 2-(2-pyridyl)-benzimidazole (pbim). The selection of these ligands was based on structural diversity, which includes neutral and ionic molecules, symmetrical and unsymmetrical, some with substituent groups and more and less sterically hindered, and possible chirality. The diversity of these N,N'-chelating ligands led to the formation of new materials, which reflect their strong structure-directing roles and influence on their applications. Different molybdenum(VI) complexes can be easily prepared with high purity and yields by oxidation of the respective precursors, specifically via the oxidative decarbonylation of tri- and tetracarbonyls complexes with excess TBHP in decane, or the hydrolysis and condensation of complexes $[\text{MoO}_2\text{Cl}_2\text{L}]$ in water. The simplicity and moderate reactions conditions of these preparation methods make them particularly attractive to prepare molybdenum-based organic-inorganic hybrid materials, which may act as effective homogeneous catalysts.

The prepared high-valent oxomolybdenum compounds possessed catalytic activity for the epoxidation of several olefins and bio-olefins, as well as the ethanolysis of styrene oxide. Although it was possible to recover the catalysts in some cases, there was a decrease in activity.

Tri- and tetracarbonylmolybdenum(0) complexes of the type *cis*- $[\text{Mo}(\text{CO})_4(\text{L})]$ are attractive synthetic precursors of high oxidation state oxomolybdenum catalysts, since the by-products (CO/CO₂) readily separate from the reaction mixture, facilitating separation/purification procedures (e.g. avoiding contamination/acidification of the medium). These observations were confirmed with the studies reported in Chapters 2-5. The synthesis of molybdenum(0) tricarbonyl and tetracarbonyl complexes of the form $[\text{Mo}(\text{CO})_3(\text{ptapzpy})\text{Br}]$ and *cis*- $[\text{Mo}(\text{CO})_4(\text{ptapzpy})]\text{Br}$ was reported, where ptapzpy = 2-(1-propyltrimethylammonium-3-pyrazolyl)pyridine. Preparation of these derivatives was accomplished either through thermal substitution of CO in $\text{Mo}(\text{CO})_6$ or substitution under milder conditions of piperidine ligands in the precursor *cis*- $[\text{Mo}(\text{CO})_4(\text{pip})_2]$. On the other hand, oxidative decarbonylation of both complexes by reaction with excess of TBHP (in decane) gives a molybdenum oxide hybrid material formulated as $[\text{Mo}_3\text{O}_9([\text{ptapzpy}]\text{Br})_2] \cdot n\text{H}_2\text{O}$. The characterisation of the Mo-containing solids isolated

Chapter 9

after the catalytic reaction showed that poorly soluble β -octamolybdate salts, $(L)_x[Mo_8O_{26}]$, were formed from the prepared carbonyl complexes with TBHP, and from the tricarbonyl complex with H_2O_2 . On the other hand, soluble oxoperoxo species were formed from $[Mo_3O_9(L)_2]$ with H_2O_2 . These findings helped to explain the differences in catalytic performances, since better results were obtained with H_2O_2 as oxidant and the tetracarbonyl precatalyst $cis-[Mo(CO)_4(ptapzpy)]Br$.

The tetracarbonyl complex $cis-[Mo(CO)_4(ppp)]$ ($ppp = 2-(1\text{-pentyl-3-pyrazolyl})pyridine$) was explored for liquid phase oxidation and acid catalysis, specifically the epoxidation of *cis*-cyclooctene with hydroperoxide oxidants, and the alcoholysis of styrene oxide. The prepared compounds revealed to be sources of soluble active species such as the oxodiperoxo complex $[MoO(O_2)_2(ppp)]$. When ionic liquids of the type $[bmim]X$ were used as cosolvents in the epoxidation reaction with TBHP, the compounds were converted to $[bmim]_4[\beta-Mo_8O_{26}]$. In this thesis considerable insight has been gained into the chemistry and catalytic performance of tetracarbonylmolybdenum(0) pyrazolylpyridine derived complexes, which should help guide future studies on the use of such complexes as (pre)catalysts and/or precursors to molybdenum oxide derivatives.

Tetracarbonylmolybdenum(0) complexes of the type $cis-[Mo(CO)_4(L)]$ containing chiral 7-(1-pyrindanyl) amine ligands were prepared and found to be effective precatalysts for the epoxidation of achiral (*cis*-cyclooctene) and prochiral (DL-limonene and *trans*- β -methylstyrene) olefins. Epoxides were the only products formed from *trans*- β -methylstyrene (100% selectivity) and the main products formed from DL-limonene (80-82% 1,2-epoxide selectivity). However stereoselectivities were low, possibly due to the formation of the salt $[\beta-Mo_8O_{26}]^{4-}$, after dissociation of the labile 7-(1-pyrindanyl) amine ligands. In the future, it will be interesting to explore more $cis-[Mo(CO)_4(L)]$ catalyst precursors bearing chelating ligands such as bipyridines and pyrazolylpyridines, since these types of ligands tend to remain coordinated to the metal center upon oxidative decarbonylation, and possibly better success in asymmetric epoxidation may be achieved by employing chiral derivatives of these types of ligands.

Reaction of the molybdenum(0)-carbonyl-triazole complexes $[Mo(CO)_3(L)_3]$ [$L = 1H\text{-}1,2,3\text{-triazole}$ (1,2,3-trz) or $1H\text{-}1,2,4\text{-triazole}$ (1,2,4-trz)] carbonyl complexes with TBHP (either separately or *in situ*) gives oxomolybdenum(VI) hybrid materials that are proposed to possess one-dimensional polymeric structures in which adjacent oxo-bridged dioxomolybdenum(VI) moieties are further linked by bidentate bridging triazole (trz) ligands. A pronounced ligand influence on catalytic performance for the epoxidation of *cis*-cyclooctene was found and the best result was obtained with the 1,2,3-triazole oxomolybdenum(VI) hybrid. Both molybdenum oxide-triazole compounds

Chapter 9

displayed superior catalytic performance in comparison with the hybrid materials $[\text{MoO}_3(\text{trz})_{0.5}]$ in the presence of TBHP. However, with aqueous H_2O_2 , all compounds dissolve to give active species in solution. A pronounced ligand influence on catalytic performance was only found for the hybrids $[\text{MoO}_3(\text{trz})_{0.5}]$. In these systems, the 1,2,4-trz based hybrid was the only catalyst that displayed reaction-induced self-precipitation behavior.

The one-dimensional organic-inorganic hybrid material $[\text{MoO}_3(2,2'\text{-bipy})]_n$ (2,2'-bipy = 2,2'-bipyridine) was used as a starting material to prepare the 2,2'-bipy-deficient phases $[\text{Mo}_2\text{O}_6(2,2'\text{-bipy})]_n$ and $[\text{Mo}_3\text{O}_9(2,2'\text{-bipy})_2]_n$ in excellent yields. The hybrid $[\text{Mo}_2\text{O}_6(2,2'\text{-bipy})]_n$ was obtained by a solid-state thermal treatment of $[\text{MoO}_3(2,2'\text{-bipy})]_n$ while $[\text{Mo}_3\text{O}_9(2,2'\text{-bipy})_2]_n$ was obtained by a hydrothermal treatment of $[\text{MoO}_3(2,2'\text{-bipy})]_n$. From this study it was shown that the increase in the Mo/ligand molar ratio of the hybrid ($1 < 1.5 < 2$) can be responsible for the catalytic performances obtained in the epoxidation of *cis*-cyclooctene with TBHP or aqueous H_2O_2 , as following the order $[\text{MoO}_3(2,2'\text{-bipy})]_n < [\text{Mo}_3\text{O}_9(2,2'\text{-bipy})_2]_n < [\text{Mo}_2\text{O}_6(2,2'\text{-bipy})]_n$. All three hybrids react with aqueous H_2O_2 to give the catalytically active oxodiperoxo complex $[\text{MoO}(\text{O}_2)_2(2,2'\text{-bipy})]$ (in different concentrations).

The chemistry and catalytic performance of a dichlorodioxomolybdenum complex was also investigated. $[\text{MoO}_2\text{Cl}_2(\text{pbim})]$ [pbim = 2-(2-pyridyl)-benzimidazole] showed to be more effective with TBHP as the oxidant than with hydrogen peroxide in the epoxidation of olefins. The dichloro complex is transformed *in situ* to the oxodiperoxo complex $[\text{MoO}(\text{O}_2)_2(\text{pbim})]$ with H_2O_2 , or a hybrid molybdenum(VI) oxide solid formulated as $[\text{MoO}_3(\text{pbim})]$ with TBHP. The latter compound revealed to be a good catalyst for the epoxidation of the biorenewable olefins methyl oleate, methyl linoleate and (*R*)-(+)-limonene. However, $[\text{MoO}_3(\text{pbim})]$ can be converted to the oxodiperoxo complex in the presence of TBHP, which can also be recycled by using an ionic liquid as solvent.

The necessity to development new hybrid materials based on metallic complexes with new supports, has led to the immobilization of a pre-made aqua molybdenum complex ($[\text{MoO}_2\text{Cl}_2(\text{H}_2\text{O})_2]$) in CB[6], giving the compound $2[\text{MoO}_2\text{Cl}_2(\text{H}_2\text{O})_2]\cdot\text{CB}[6]\cdot 2(\text{HCl})\cdot 14\text{H}_2\text{O}$. The immobilized aqua molybdenum complex ($[\text{MoO}_2\text{Cl}_2(\text{H}_2\text{O})_2]$) in CB[6] revealed to be efficient in a one-pot single-stage strategy, converting olefins to alkoxy products, involving oxidation (using H_2O_2) and acid chemistry. The results demonstrated the ability of molybdenum-cucurbit[*n*]uril compounds to function as acid-oxidation multifunctional catalysts, and their recovery and reuse via relatively simple procedures. This study was the first report of the one-

Chapter 9

pot oxidation of alkenes with H₂O₂ in alcohol medium to give alkoxy ketone products, in the presence of molybdenum-based catalysts.

In the future, it will be interesting to explore other type of Mo-based cucurbiturils catalysts containing preferably polar ligands for the epoxidation of other olefins, like bio-olefins, and other organic reactions, such as sulfoxidation in desulfurization systems for treating model and real diesel under sustainable conditions^{4,5} and the oxidation of amines⁶. Since this work had several difficulties concerning the stability of the prepared Mo(VI) precursors in solution, it will be recommended to prepare stable organometallic compounds, beyond molybdenum as transition metal, in solution taking into account their solubility. New metallic compounds could be posteriorly incorporated into other macrocyclic receptors, such as cucurbiturils congeners via covalent bonds, *e.g.* functionalized CB[*n*]s, inverted-CB[*n*]s and *nor-sec*-CB[*n*]s⁷, or organic polymers obtained from biomass, *e.g.* chitosan, cellulose and amide. In the last 15 years, researchers have looked to biopolymers as supports for transition metal catalysts due to their appealing abundance in nature, renewability, biodegradability and non-toxicity.^{8–13}, and thus of great economic and environmental importance¹⁴.

In parallel, molybdenum carbonyl complexes can be tested as CO-releasing molecules (CORM) for therapeutic treatment, since the carbon monoxide can actually, in appropriate doses, exert a therapeutic effect.^{15,16} The immobilization of CORMs in cucurbiturils can promote effective and controlled delivery of these molecules to specific sites of the organism and mitigate side effects of the currently used implementations.

9.2. References

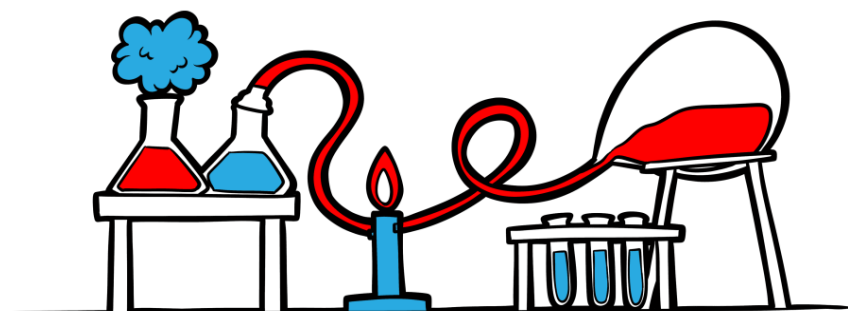
- (1) Amarante, T. R.; Neves, P.; Valente, A. A.; Paz, F. A. A.; Pillinger, M.; Gonçalves, I. S. *J. Catal.* **2016**, *340*, 354–367.
- (2) Hagrman, P. J.; LaDuca, R. L.; Koo, H. J.; Rarig, R.; Haushalter, R. C.; Whangbo, M. H.; Zubieta, J. *Inorg. Chem.* **2000**, *39*, 4311–4317.
- (3) Chuang, J.; Ouellette, W.; Zubieta, J. *Inorg. Chim. Acta* **2008**, *361*, 2357–2364.
- (4) Julião, D.; Gomes, A. C.; Pillinger, M.; Valença, R.; Ribeiro, J. C.; Gonçalves, I. S.; Balula, S. S. *Dalton Trans.* **2016**, *45*, 15242–15248.
- (5) Julião, D.; Gomes, A. C.; Pillinger, M.; Valença, R.; Ribeiro, J. C.; Gonçalves, I. S.; Balula, S. S. *Appl. Catal., B* **2018**, *230*, 177–183.
- (6) Tosi, I.; Vurchio, C.; Abrantes, M.; Gonçalves, I. S.; Pillinger, M.; Cavani, F.; Cordero, F. M.; Brandi, A. *Catal. Commun.* **2018**, *103*, 60–64.
- (7) Assaf, K. I.; Nau, W. M. *Chem. Soc. Rev.* **2015**, *44*, 394–418.
- (8) Macquarrie, D. J.; Hardy, J. J. E. *Ind. Eng. Chem. Res.* **2005**, *44*, 8499–8520.

Chapter 9

- (9) Gronnow, M. J.; Luque, R.; Macquarrie, D. J.; Clark, J. H. *Green Chem.* **2005**, *7*, 552–557.
- (10) Reddy, K. R.; Kumar, N. S.; Reddy, P. S.; Sreedhar, B.; Kantam, M. L. *J. Mol. Catal. A Chem.* **2006**, *252*, 12–16.
- (11) Makhubela, B. C. E.; Jardine, A.; Smith, G. S. *Green Chem.* **2012**, *14*, 338–347.
- (12) Honarkar, H.; Barikani, M. *Monatsh Chem* **2009**, *140*, 1403–1420.
- (13) Lee, M.; Chen, B.-Y.; Den, W. *Appl. Sci.* **2015**, *5*, 1272–1283.
- (14) Zhang, L.; Li, B.; Meng, X.; Huang, L.; Wang, D. *Environ. Sci. Pollut. Res.* **2015**, *22*, 15104–15112.
- (15) Kromer, L.; Coelho, A. C.; Bento, I.; Marques, A. R.; Romão, C. C. *J. Organomet. Chem.* **2014**, *760*, 89–100.
- (16) Jeremias, H. F.; Lousa, D.; Hollmann, A.; Coelho, A. C.; Baltazar, C. S.; Seixas, J. D.; Marques, A. R.; Santos, N. C.; Romão, C. C.; Soares, C. M. *PLoS One* **2018**, *13*, 1–15.

CHAPTER 10

Experimental techniques and characterization methods



Chapter 10

Index

10.1. List of chemical compounds	255
10.2. Experimental techniques	257
10.3. Characterization and analytical techniques	257
10.3.1. Elemental analysis	258
10.3.2. Inductively coupled plasma optical emission spectrometry (ICP-OES)	258
10.3.3. Thermogravimetric analysis (TGA)	258
10.3.4. Vibrational spectroscopy (FT-IR and FT-Raman)	258
10.3.5. Nuclear magnetic resonance spectroscopy (NMR)	259
10.3.6. X-ray powder diffraction (PXRD)	259
10.3.7. Mass spectrometry (MS)	260
10.3.8. Polarimetry	260
10.3.9. Scanning electron microscopy (SEM) / Energy-dispersive X-ray spectroscopy (EDS)	260
10.4. Synthesis	260
10.4.1. Chapter 2	260
10.4.2. Chapter 3	265
10.4.3. Chapter 4	267
10.4.4. Chapter 5	270
10.4.5. Chapter 6	273
10.4.6. Chapter 7	276
10.4.7. Chapter 8	277
10.5. Single-crystal X-ray diffraction studies	278
10.5.1. Chapter 2	278
10.5.2. Chapter 5	283
10.5.3. Chapter 8	285
10.6. Catalytic tests	286
10.6.1. Gas chromatography	286
10.6.2. Formulae - catalytic studies	287
10.6.3. Chapter 2	288
10.6.4. Chapter 3	288
10.6.5. Chapter 4	290
10.6.6. Chapter 5	291
10.6.7. Chapter 6	291
10.6.8. Chapter 7	293
10.6.9. Chapter 8	294
10.7. References	297

Chapter 10

10.1. List of chemical compounds

Table 10.1 – List of chemical reagents used in this work.

Compound	Chemical trademark	Purity
Acetone	Sigma-Aldrich	99.5 %
Ammonium heptamolybdate tetrahydrate	Merck	-
Acetonitrile (anhydrous)	Sigma-Aldrich	99.8 %
α,α,α -Trifluorotoluene (TFT, anhydrous)	Sigma-Aldrich	99.8 %
2,2'-Bipyridine (2,2'-bipy)	Sigma-Aldrich	≥ 99 %
1-Butanol (BuOH)	Alfa Aesar	99.4 %
1-Butyl-3-methylimidazolium bis(trifluoromethylsulfonyl)imide ([bmim]NTf ₂)	Iolitec	99 %
1-Butyl-3-methylimidazolium chloride ([bmim]Cl)	Solchemar	98 %
1-Butyl-3-methylimidazolium hexafluorophosphate ([bmim]PF ₆)	Iolitec	99 %
1-Butyl-3-methylimidazolium tetrafluoroborate ([bmim]BF ₄)	Iolitec	99 %
<i>tert</i> -Butyl hydroperoxide (TBHP) (aqueous)	Sigma-Aldrich	70 wt. %
<i>tert</i> -Butyl hydroperoxide (in decane)	Sigma-Aldrich	5-6 M
Chloroform (CHCl ₃)	Sigma-Aldrich	99.8 %
Cyclododecene (Cy12, mixture of <i>cis</i> and <i>trans</i> isomers)	Sigma-Aldrich	96 %
Cyclohexanol (Cy6OH)	Merck	>99 %
Cyclohexene (Cy6)	Riedel-de Haën	99 %
<i>cis</i> -1,2-cyclooctanediol (Cy(OH) ₂)	Sigma-Aldrich	99 %
Cyclooctanol (CyOH)	Alfa Aesar	97 %
<i>cis</i> -Cyclooctene (Cy)	Alfa Aesar	95 %
Cyclooctene oxide (CyO)	Sigma-Aldrich	99 %
1,2-Dichloroethane (CH ₃ CHCl ₂)	Sigma-Aldrich	≥ 99 %
Dichloromethane (CH ₂ Cl ₂)	Sigma-Aldrich	Puriss.
2,6-Di- <i>tert</i> -butyl-4-methyl-phenol	Sigma-Aldrich	≥ 99.9 %
Diethylene glycol dimethyl ether (diglyme)	Fluka	99 %
Diethyl ether	Sigma-Aldrich	99.8 %
3-(Dimethylamino)-1-(2-pyridyl)-2-propen-1-one	Sigma-Aldrich	95 %
N,N-Dimethylformamide	Sigma-Aldrich	≥ 99 %
Dimethyl sulfoxide-d ₆ (DMSO-d ₆)	Sigma-Aldrich	99.5 %
Ethanol (EtOH)	Scharlau	≥ 99.9 %
Ethanol (anhydrous absolute)	Carlo-Erba	≥ 99.9 %
Ethyl acetate (AcOEt)	Sigma-Aldrich	99.9 %
Formaldehyde solution	Sigma-Aldrich	37 %
Glycoluril	Sigma-Aldrich	-

Chapter 10

Table 10.1. continuation

Hexane	Sigma-Aldrich	>99 %
Hydrazine (hydrate solution)	Sigma-Aldrich	80 %
Hydrochloric acid (HCl)	Sigma-Aldrich	37 %
Hydrogen peroxide (H ₂ O ₂)	Sigma-Aldrich	30 wt. %
1-Iodopentane	Sigma-Aldrich	98 %
DL-limonene (DL-Lim)	Merck	≥95 %
(<i>R</i>)-(+)-Limonene (Lim)	Sigma-Aldrich	97 %
Magnesium sulfate heptahydrate	Panreac	98 %
(<i>R</i>)-(+)- α -Methylbenzylamine ((<i>R</i>)-PEA)	Sigma-Aldrich	98 %
(<i>S</i>)-(-)- α -Methylbenzylamine ((<i>S</i>)-PEA)	Sigma-Aldrich	98 %
Methanol (MeOH)	Sigma-Aldrich	≥99.9
Methyl decanoate	Sigma-Aldrich	99 %
Methyl linoleate (LinOle)	Alfa Aesar	95 %
Methyl oleate (Ole)	Sigma-Aldrich	99 %
<i>trans</i> - β -Methylstyrene (<i>tbms</i>)	Sigma-Aldrich	99 %
Molybdenum(VI) dichloride dioxide (MoO ₂ Cl ₂)	Sigma-Aldrich	-
Molybdenum hexacarbonyl (Mo(CO) ₆)	Sigma-Aldrich	98 %
Molybdenum trioxide (MoO ₃)	Analar	99.5 %
1-Octene	Sigma-Aldrich	98 %
<i>trans</i> -2-Octene	Sigma-Aldrich	97 %
Paraformaldehyde	Sigma-Aldrich	95 %
η -Pentane	Carlo Erba	≥95 %
α -Pinene (Pin)	Sigma-Aldrich	98 %
Piperidine (pip)	Carlo-Erba	99.5 %
1-Propanol	Sigma-Aldrich	99.9 %
2-(2-Pyridyl)benzimidazole (pbim)	Sigma-Aldrich	97 %
Sodium bicarbonate (NaHCO ₃)	Sigma-Aldrich	≥99.7 %
Sodium hydride (dispersion in mineral oil) (NaH)	Sigma-Aldrich	60 %
Sodium molybdate dihydrate ([Na ₂ MoO ₄]·2H ₂ O)	Riedel-de Haën	99.5 %
Sodium sulfate (anhydrous) (Na ₂ SO ₄)	Sigma-Aldrich	≥95 %
Sodium triacetoxyborohydride (NaBH(OAc) ₃)	Sigma-Aldrich	97 %
Styrene (Sty)	Fluka	≥97
Styrene oxide (StyOx)	Sigma-Aldrich	98 %
Tetrahydrofuran (THF)	Sigma-Aldrich	99.9 %
1 <i>H</i> -1,2,3-triazole (1,2,3-trz)	Manchester Organics	97 %
1 <i>H</i> -1,2,4-triazole (1,2,4-trz)	Sigma-Aldrich	98 %
α,α,α -Trifluorotoluene (anhydrous) (TFT)	Sigma-Aldrich	≥99.9 %
Toluene	Sigma-Aldrich	99.9 %
Undecane	Sigma-Aldrich	>99 %

Chapter 10

10.2. Experimental techniques

Generally, the reagents and compounds prepared in this work are sensitive to air and, therefore, the proper techniques to avoid their decomposition were to dry and handle them in an inert gas atmosphere (industrial nitrogen supplied by Air Liquide), using vacuum / nitrogen line techniques and Schlenk type systems.

The vacuum / nitrogen line consists of a glass column with dual manifold and several ports, connected to the nitrogen bottle and the vacuum pump. One manifold is connected to nitrogen, while the other is connected to the vacuum pump. The nitrogen is vented through an oil bubbler, while the connection to the vacuum pump has a trap which is immersed in a liquid nitrogen bath to promote condensation of gases and avoid the presence of solvent vapours and gaseous reaction products inside the vacuum pump.

The vacuum is also used to evaporate and remove traces of solvent from a sample. Since, the vacuum and gas line have several ports and lines, with care, it is possible to run simultaneously several reactions or operations.

In order to avoid solvent contamination with water, the practical method for safer handling and drying of solvents is provided by using drying agents. Drying agents are hygroscopic substances that induces or sustains a state of dryness in its vicinity, which generally are chemically stable and chemically inert. In this work, the deuterated solvents (acetone-d₆, acetonitrile-d₃ and chloroform-d) were stored with molecular sieves (alumino silicates) under a nitrogen atmosphere. The size pore of the molecular sieves used to dry acetonitrile-d₃ was 3Å, while the pore size used for acetone-d₆ and chloroform-d was 4Å. The molecular sieves were activated with pre-dry for 12 hours at 300 °C with a heating ramp of 2 °C/min under vacuum.

10.3. Characterization and analytical techniques

Characterization and analytical techniques are methods used to identify, isolate or quantify chemicals or materials, or to characterize their physical properties. The most part of characterization techniques were realized in the University of Aveiro, except the inductively coupled plasma optical emission spectroscopy (ICP-OES), mass spectrometry (MS) and polarimetry. Elemental analysis, thermogravimetric analysis, vibrational spectroscopy, nuclear magnetic resonance spectroscopy, X-ray diffraction and UV-Vis spectroscopy are localized in the Department of Chemistry, while the scanning electron microscopy was made in the Department of Materials and Ceramics Engineering, in University of Aveiro. ICP-OES was performed at CACTI, University of

Chapter 10

Vigo, Spain. The mass spectroscopy was realized in the CEMUP, University of Porto. The polarimetry results were measured in the Department of Chemistry, University of Porto.

10.3.1. Elemental analysis

Microanalysis of carbon, hydrogen and nitrogen in solid samples were carried out with a Leco Truspec Micro CHNS 630-200-200 elemental analyser. The accepted deviation of elemental analysis results from the calculated applied was 5 % for organometallic and inorganic compounds, and 3 % for organic compounds.

10.3.2. Inductively coupled plasma optical emission spectrometry (ICP-OES)

In this work, molybdenum was determined by ICP-OES and the analysis was carried out with a spectrophotometer Perkin Elmer Optima 4300 DV. The samples were treated with acid attack with aqua regia (HCl + HNO₃) in open and hot beaker (approx. 140 °C).

10.3.3. Thermogravimetric analysis (TGA)

TGA was performed using a Shimadzu TGA-50 thermobalance system at a heating rate of 5 °C min⁻¹ to 800 °C under air. The equipment is composed of a tubular electric heating furnace, with a range of accessible temperatures from room temperature to 1000 °C, allowing rates of variation of temperature from 0.1 °C/h to 99.9 °C/min, a high resolution scale, an atmosphere conditioning unit and a computerized data collection and processing system.

10.3.4. Vibrational spectroscopy (FT-IR and FT-Raman)

FT-IR spectra were recorded on a Mattson 7000 FT-IR spectrometer with 128 scans and a resolution of 4.0 cm⁻¹, in the frequency range of 4000 to 280 cm⁻¹, using KBr pellets. Attenuated total reflectance (ATR) FT-IR spectra were measured using a Specac Golden Gate Mk II ATR accessory having a diamond top plate and KRS-5 focusing lenses. The vibrational bands are indicated in wavenumber (ν , cm⁻¹) with the following intensities: vs - very strong, s - strong, m - medium, w – weak and sh – as shoulder. FT-Raman spectra were recorded on an RFS-100 Bruker FT-Spectrometer

Chapter 10

equipped with a Nd:YAG laser, an excitation wavelength of 1064 nm and a resolution of 4.0 cm^{-1} , in the frequency range of 4000 to 0 cm^{-1} , at room temperature.

10.3.5. Nuclear magnetic resonance spectroscopy (NMR)

Liquid state NMR (^1H and ^{13}C)

^1H and ^{13}C solution NMR spectra were recorded on Bruker Avance 300 and 400 spectrometers. Chemical shifts (δ) are quoted in parts per million (ppm) using tetramethylsilane (TMS) as reference ($\delta = 0,0$ ppm). The number of protons in the neighbourhood of a determinate hydrogen nucleus are represented by the multiplicity of the signal: s - singlet, d - doublet, t - triplet, q - quartet and m - multiplet.

Solid state NMR (^1H and ^{13}C)

Solid-state ^1H MAS and $^{13}\text{C}\{^1\text{H}\}$ CP MAS NMR spectra were recorded using a Bruker Avance 400 (narrow bore) spectrometer with an ultrashielded static magnetic field of 100.6 MHz. The spectra were recorded with $2.75 \mu\text{s}$ ^1H 90° pulses, 2.0 ms contact time, spinning rate of 12 kHz and 14 kHz, and 5 s recycle delays, respectively. Chemical shifts are quoted in ppm from TMS.

10.3.6. X-ray powder diffraction (PXRD)

PXRD data were collected at ambient temperature using a PANalytical Empyrean instrument equipped with a PIXcel 1D detector set at 240 mm from the sample. $\text{Cu-K}_{\alpha 1,2}$ X-radiation ($\lambda_1 = 1.540598 \text{ \AA}$; $\lambda_2 = 1.544426 \text{ \AA}$) filtered with a nickel foil was used along with a standard transmission sample holder. Working operating conditions for the X-ray tube: 45 kV and 40 mA. Intensity data were collected in continuous mode in the ca. $3.5 \leq 2\theta \leq 70^\circ$ range.

Variable temperature PXRD was carried out using a PANalytical X'Pert PRO3 HTK 16N high temperature chamber containing a Pt heating filament and a Pt–Pt/Rh (10 %) thermocouple. The powdered sample was deposited on a Pt sheet which was then placed over the heating element. Heating rates of $5 \text{ }^\circ\text{C min}^{-1}$ were used. At a given temperature, samples were step-scanned in 0.02° 2θ steps with a counting time of 200 s per step.

Chapter 10

The program Mercury (copyright CCDC, ver. 3.9) was used to generate the computed patterns from the crystal structure data published for the prepared compounds.

10.3.7. Mass spectrometry

Mass spectra were recorded on a LTQ Orbitrap XL mass spectrometer (Thermo Fisher Scientific) controlled by LTQ Tune Plus 2.5.5 and Xcalibur 2.1.0.

10.3.8. Polarimetry

Optical rotations were measured on a thermostated Jasco P-2000 digital polarimeter using a sodium lamp.

10.3.9. Scanning electron microscopy (SEM) / Energy-dispersive X-ray spectroscopy (EDS)

Scanning electron microscopy (SEM) images, energy dispersive X-ray spectroscopy analysis and elemental (Mo, Cl, N and O) mappings were obtained on a Hitachi SU-70 microscope equipped with a Bruker Quantax 400 detector at 15 kV. Samples were prepared by deposition on aluminium sample holders followed by carbon coating using an Emitech K 950 carbon evaporator.

10.4. Synthesis

10.4.1. Chapter 2

Synthesis of 2-[3(5)-pyrazolyl]pyridine

The preparation of the ligand 2-[3(5)-pyrazolyl]pyridine was adapted from the literature.¹ Hydrazine was added dropwise to a mixture of 3-(dimethylamino)-1-(2-pyridyl)-2-propen-1-one (6.00 g, 34.0 mmol) and ethanol (80 mL) heated to 95 °C under stirring. The mixture was refluxed during 1 h, and then the solvent was removed through the rotary evaporator. Finally, the brown solid obtained was dried under vacuum.

Yield: 1.89 g, 38 %. Selected FT-IR (KBr, cm⁻¹): 116 (s), 284 (m), 356 (w), 455 (w), 627 (w), 706 (w), 796 (w), 921 (w), 949 (m), 992 (m), 999 (m), 1046 (w), 1059 (w),

Chapter 10

1078 (w), 1128 (w), 1147 (w), 1191 (w), 1244 (w), 1275 (w), 1302 (m), 1355 (m), 1453 (m), 1498 (s), 1533 (m), 1567 (m), 1590 (s), 3056 (w), 3077 (w), 3117 (w), 3139 (w), 3150 (w). Selected FT-Raman (cm^{-1}): 288 (m), 359 (w), 403 (m), 454 (w), 503 (m), 615 (m), 627 (l), 695 (sh), 704 (w), 760 (s), 796 (w), 838 (m), 876 (mm), 923 (w), 949 (m), 952 (m), 992 (sh), 999 (m), 1036 (sh), 1048 (m), 1052 (sh), 1087 (m), 1129 (m), 1134 (m), 1191 (w), 1271 (m), 1302 (m), 1356 (m), 1416 (m), 1452 (m), 1501 (m), 1565 (m), 1590 (m), 1658 (m), 1698 (m), 2895 (w), 2933 (w), 3021 (w), 3092 (w), 3142 (s).

2-(1-Propyltrimethylammonium-3-pyrazolyl)pyridine bromide ([ptapzpy]Br)

2-[3(5)-Pyrazolyl]pyridine (2 g, 13.78 mmol) was added slowly to a suspension of NaH (0.50 g, 20.80 mmol) in THF (40 mL), resulting in a yellow mixture. A solution of (3-bromopropyl) trimethylammonium bromide (3.6 g, 13.79 mmol) in acetonitrile (90 mL) was added dropwise and the mixture stirred under reflux for 4 h, resulting in a yellow solution and a white precipitate. The mixture was evaporated to dryness under reduced pressure. The residue was extracted with CHCl_3 (4 x 50 mL) and the combined extracts were evaporated to dryness under reduced pressure, giving a brown oil. The oil was washed with diethyl ether (50 mL) and then dissolved in acetone (50 mL). Diethyl ether (50 mL) was added to precipitate the product, which was filtered, washed with diethyl ether/acetone, and finally vacuum-dried to give the ligand [ptapzpy] Br as a cream solid.

Yield: 2 g, 45 %. Anal. calcd for $\text{C}_{14}\text{H}_{21}\text{BrN}_4 \cdot 1.6\text{H}_2\text{O}$ (354.07): C, 47.49; H, 6.89; N, 15.82. Found: C, 47.60; H, 6.45; N, 15.74 %. FT-IR (KBr, cm^{-1}): 404 (m), 470 (w), 524 (w), 619 (m), 630 (m), 698 (m), 728 (m), 750 (w), 777 (vs), 871 (m), 923 (m), 962 (s), 970 (s), 991 (w), 1037 (w), 1060 (m), 1095 (m), 1147 (w), 1160 (m), 1189 (w), 1240 (s), 1282 (w), 1303 (w), 1330 (w), 1359 (s), 1403 (m), 1432 (s), 1450 (w), 1465 (w), 1490 (s), 1519 (m), 1567 (m), 1590 (s, $\nu(\text{C}=\text{N})$), 1649 (w), 2954 (m), 3002 (m), 3024 (m), 3083 (m), 3118 (w). ^1H NMR (300.1 MHz, 295 K, CDCl_3): δ = 8.63 (d, H-11), 7.83 (td, H-8), 7.73 (dt, H-9), 7.64 (d, H-5), 7.24 (ddd, H-10), 6.84 (d, H-4), 4.41 (t, N- CH_2), 3.80 (m, N- CH_2), 3.39 (s, N- CH_3), 2.55 (m, CH_2) ppm. ^{13}C NMR (75.4 MHz, 295 K, CDCl_3): δ = 152.51 (C-7), 152.07 (C-11), 149.76 (C-3), 136.92 (C-9), 132.32 (C-5), 122.82 (C-8), 120.37 (C-10), 104.91 (C-4), 64.48 (N- CH_2), 53.88 (N- CH_3), 48.73 (N- CH_2), 24.26 (CH_2) ppm. $^{13}\text{C}\{^1\text{H}\}$ CP MAS NMR: δ = 151.3 (C-7), 149.6 (C-11 and C-3), 138.0 (C-9), 129.3 (C-5), 124.4 (C-8), 121.1 (C-10), 107.4 (C-4), 61.2 (N- CH_2), 53.7 (N- CH_3), 47.8 (N- CH_2), 24.7 (CH_2) ppm.

Chapter 10

[Mo(CO)₄(pip)₂]

Mo(CO)₆ (0.5 mg, 1.89 mmol) and piperidine (1.25 mL, 12.65 mmol) were refluxed in heptane (10 mL) for 4 h. In the end of the reaction, a yellow product precipitated from the solution. The reaction mixture was filtered hot to remove any heptane-soluble Mo(CO)₅(pip). The product was washed with cold heptane (2 x 10 mL) and finally vacuum-dried.

Yield: 0.6 g, 84 %. Selected FT-IR (KBr, cm⁻¹): 309 (w), 320 (w), 359 (s), 397 (w), 451 (w), 469 (w), 561 (m), 580 (m), 613 (m), 658 (m), 808 (m), 850 (w), 872 (m), 935 (m), 954 (w), 987 (m), 1030 (m), 1059 (w), 1082 (m), 1107 (w), 1155 (w), 1180 (m), 1265 (m), 1313 (w), 1340 (w), 1414 (s), 1446 (m), 1776 (vs, ν(CO)), 1838 (vs, ν(CO)), 1888 (vs, ν(CO)), 2011 (s, ν(CO)), 2864 (m), 2941 (s), 2968 (m), 3267 (m), 3427 (w), 3606 (w), 3676 (w), 3870 (w).

[Mo(CO)₃(ptapzpy)Br] (1)

In a Schlenk tube, Mo(CO)₆ (0.2 g, 0.76 mmol) and [ptapzpy]Br (0.25 g, 0.77 mmol) were added to toluene (20 mL) and the mixture was refluxed under N₂ for 30 min, resulting in an orange solid and solution. Hexane (20 mL) was added to promote product precipitation. The solution was filtered off and the solid washed with hexane (2 x 20 mL), diethyl ether (2 x 20 mL), and finally vacuum-dried.

Yield: 0.34 g, 83 %. Anal. calcd for C₁₇H₂₁BrMoN₄O₃·2H₂O (541.25): C, 37.72; H, 4.66; N, 10.35. Found: C, 37.58; H, 4.81; N, 10.1 %. TGA showed a mass loss of 6.2 % at 100 °C (calcd for loss of 2H₂O: 6.6 %). Selected FT-IR (KBr, cm⁻¹): 494 (w), 629 (w), 771 (m), 873 (w), 960 (m), 1095 (w), 1157 (w), 1239 (m), 1365 (m), 1439 (m), 1477 (m), 1604 (w, ν(C=N)), 1742 (vs, ν(CO)), 1764 (vs, ν(CO)), 1895 (vs, ν(CO)).

[Mo(CO)₄(ptapzpy)]Br (2)

[Mo(CO)₄(pip)₂] (0.11 g, 0.3 mmol) was added to a solution of [ptapzpy]Br (0.1 g, 0.3 mmol) in ethanol (10 mL) and the mixture was heated at 50 °C, with stirring, for 30 min. The solvents were evaporated under reduced pressure, and the resultant red solid was washed with hexane (2 x 7 mL) and ethanol (2 x 7 mL).

Yield: 0.13 g, 79 %. Anal. calcd for C₁₈H₂₁BrMoN₄O₄·1.5H₂O (560.25): C, 38.59; H, 4.32; N, 10.00. Found: C, 38.90; H, 4.58; N, 10.14 %. TGA showed a mass loss of 4.2 % at 90 °C (calcd for loss of 1.5H₂O: 4.8 %). Selected FT-IR (KBr, cm⁻¹): 364 (s), 471 (w), 580 (m), 650 (m), 765 (s), 962 (m), 1097 (w), 1241 (m), 1365 (m), 1438 (m), 1482

Chapter 10

(w), 1608 (w, $\nu(\text{C}=\text{N})$), 1815 (vs, $\nu(\text{CO})$), 1869 (vs, $\nu(\text{CO})$), 1888 (sh, $\nu(\text{CO})$), 2012 (s, $\nu(\text{CO})$).

[Mo₃O₉([ptapzpy]Br)₂] (3)

In a Schlenk tube, 5–6 M TBHP in decane (0.35 mL, ca. 2 mmol) was added to a mixture comprising complex **1** (0.1 g, 0.2 mmol) and CH₂Cl₂ (10 mL), and stirring was continued for 4 h under N₂ at room temperature. The resultant off-white solid was recovered by filtration, washed with diethyl ether (2 x 10 mL), and finally vacuum dried.

Yield: 0.04 g, 53 %. Anal. calcd for C₂₈H₄₂Br₂Mo₃N₈O₉·3H₂O (1136.36): C, 29.59; H, 4.26; N, 9.86. Found: C, 29.51; H, 4.47; N, 9.99 %. TGA showed a mass loss of 5.5 % at 150 °C (calcd for loss of 3H₂O: 4.8 %). Selected FT-IR (KBr, cm⁻¹): 326 (w), 399 (w), 426 (w), 609 (s), 631 (s), 777 (m), 846 (w), 895 (s), 924 (s), 962 (w), 1022 (w), 1076 (w), 1099 (w), 1161 (w), 1242 (m), 1371 (m), 1439 (m), 1479 (m), 1610 (m, $\nu(\text{C}=\text{N})$), 2850 (w), 3026 (w). Selected FT-Raman (cm⁻¹): 641 (w), 727 (w), 752 (w), 783 (m), 893 (w), 923 (vs), 963 (m), 1020 (m), 1053 (w), 1159 (w), 1242 (w), 1287 (w), 1346 (m), 1372 (m), 1422 (m), 1532 (m), 1568 (m), 1609 (m, $\nu(\text{C}=\text{N})$), 2826 (w), 2966 (m), 3022 (m), 3065 (m). ¹³C{¹H} CP MAS NMR: δ = 146.8 (C-7, C-11 and C-3), 140.5 (C-9), 134.7 (C-5), 124.8 (C-8 and C-10), 105.2 (C-4), 63.8 (N-CH₂), 53.6 (N-CH₃), 48.9 (N-CH₂), 25.2 (CH₂) ppm.

[ptapzpy]Br@CB[7] (4)

CB[7] (0.1 g, 0.08 mmol) was dissolved in H₂O (10 mL). The ligand [ptapzpy]Br (0.02 g, 0.08 mmol) was added directly to the solution under nitrogen. The mixture was stirred for 2 h at room temperature. The resulting solution was concentrated (under vacuum). In order to promote the precipitation of the product, acetone was added to the solution, obtaining a white solid. The mixture was evaporated to dryness and finally the product was washed with acetone (2 x 10 mL), dried and stored under N₂.

Yield: 0.05 g, 45 %. Selected FT-IR (KBr, cm⁻¹): 368 (m), 447 (w), 627 (w), 673 (m), 758 (m), 804 (s), 825 (m), 966 (s), 1028 (w), 1151 (w), 1190 (s), 1232 (s), 1294 (w), 1323 (m), 1375 (m), 1421 (m), 1471 (s), 1597 (w), 1732 (s), 2856 (w), 2927 (m), 2997 (w), 3463 (s).

Chapter 10

[Mo(CO)₄(ptapzpy)]Br@CB[7] (5)

Method A. Compound **4** (0.02 g, 0.02 mmol,) and toluene (7 mL) were mixed – solution A. Mo(CO)₆ (0.01 g, 0.03 mmol, in excess) was dissolved in toluene (3 mL) under nitrogen – solution B. Solution B was added to solution A. The mixture was stirred for 1 h at 110 °C. The resulting solution was concentrated (under vacuum) almost entirely and rest of the solution was filtered (pale yellow liquid phase). The resulting pale orange solid was washed with pentane (2 x 10 mL), dried and stored under N₂.

Selected FT-IR (KBr, cm⁻¹): 366 (m), 631 (w), 675 (m), 758 (m), 806 (s), 825 (sh), 968 (m), 1028 (w), 1153 (w), 1192 (s), 1234 (s), 1294 (w), 1323 (m), 1377 (m), 1421 (m), 1475 (s), 1641 (w), 1730 (s), 1898 (m), 2015 (w), 2929 (w), 3001 (w), 3436 (s).

Method B. Compound **4** (0.03 g, 0.02 mmol,) and ethanol (3 mL) were mixed – solution A. [Mo(CO)₄(pip)₂] (0.01 g, 0.02 mmol,) was dissolved in ethanol (2 mL) under nitrogen – solution B. Solution B was added to solution A forming immediately an orange mixture. The mixture was stirred for 30 min at 50 °C (no evolution was observed). The resulting solution was concentrated (under vacuum) almost entirely and rest of the solution was filtered (pale yellow liquid phase). The resulting pale orange solid was washed with pentane (2 x 5 mL), dried and stored under N₂.

Selected FT-IR (KBr, cm⁻¹): 366 (w), 629 (w), 673 (w), 758 (w), 804 (s), 968 (m), 1153 (w), 1190 (m), 1232 (s), 1292 (w), 1323 (m), 1377 (m), 1423 (m), 1471 (s), 1631, (w) 1641 (w), 1729 (s), 1898 (w), 2923 (w), 3429 (m).

Method C. CB[7] (0.05 g, 0.04 mmol,) was dissolved in H₂O (5 mL) – solution A. [Mo(CO)₄(ptapzpy)]Br (0.02 g, 0.04 mmol,) was dissolved in H₂O (2 mL) under nitrogen – solution B. Solution B was added to solution A. The mixture was stirred for 10 min (**5-method C-10 min**) or 2 h (**5-method C-2 h**) at room temperature. The resulting solutions were concentrated (under vacuum) to half and rest of the solutions were filtered (liquid phase orange). The resulting pale orange solids were washed with pentane (2 x 7 mL), dried and stored under N₂.

Selected FT-IR (KBr, cm⁻¹) for **5-method C-10 min**: 310 (w), 318 (w), 345 (w), 366 (m), 391 (w), 629 (w), 673 (w), 758 (w), 804 (s), 816 (sh), 966 (m), 1026 (w), 1151 (w), 1190 (m), 1232 (s), 1284 (w), 1321 (m), 1375 (m), 1421 (m), 1471 (s), 1630 (w), 1641 (w), 1732 (s), 2920 (s), 3427 (m).

Selected FT-IR (KBr, cm⁻¹) for **5-method C-2 h**: 345 (w), 364 (m), 411 (w), 476 (m), 553 (w), 582 (w), 606 (w), 627 (w), 650 (w), 675 (w), 777 (m), 806 (m), 877 (w), 960 (m), 1047 (w), 1097 (w), 1157 (w), 1192 (m), 1236 (m), 1288 (m), 1323 (m), 1383 (m), 1442 (s) 1477 (m), 1527 (w), 1552 (w), 1610 (m), 1630 (m), 1641 (m), 1658 (w), 1730 (m), 1797 (m), 1865 (s), 1898 (s), 1919 (s), 2015 (m), 2968 (w), 3402 (s).

Chapter 10

10.4.2. Chapter 3

Synthesis of 2-(1-pentyl-3-pyrazolyl)pyridine (ppp)

The preparation of the ligand ppp was adapted from the literature.² In a Schlenk tube, NaH (0.05 g, 20.42 mmol) was washed in THF (2 x 10 mL) under N₂ at room temperature, removing the solvent through filtration. NaH was dissolved in THF (15 mL), forming a grey solution. The precursor 2-[3(5)-pyrazolyl]pyridine (1.49 g, 10.26 mmol, prepared in chapter 2, please see the preparation method in section 10.3.1.1) was dissolved in THF (20 mL) and the solution was added slowly to the solution prepared previously. 1-Iodopentane (1.6 mL, 12.4 mmol) was added to the mixture and the mixture was refluxed for 24 h. The solution was evaporated to dryness, resulting in a yellow solid. The product was extracted with diethyl ether (5 x 25 mL). The several fractions were evaporated to dryness, obtained a yellow oil which was vacuum-dried.

Yield: 2.5 g, 95 %. Selected FT-IR (KBr, cm⁻¹): 403 (m), 621 (m), 667 (m), 694 (m), 715 (w), 764 (s, $\gamma(\text{C-H})_{\text{out-of-plane}}$), 796 (s, $\gamma(\text{C-H})_{\text{out-of-plane}}$), 895 (w), 928 (w), 956 (m), 993 (m), 1049 (s, $\gamma(\text{-C-H})_{\text{pypz}}$), 1090 (m, $\gamma(\text{-C-H})_{\text{pypz}}$), 1105 (m), 1147 (m), 1228 (s), 1277 (m), 1329 (w), 1358 (m), 1402 (m), 1458 (s), 1493 (s), 1566 (m, $\nu(\text{C-C})_{\text{inter ring}}$), 1593 (s, $\nu(\text{C-N})_{\text{pypz}}$), 2870 (s), 2931 (s), 2956 (s), 3016 (w, $\nu(\text{=C-H})_{\text{pypz}}$), 3053 (w, $\nu(\text{=C-H})_{\text{pypz}}$). ¹H NMR (300.13 MHz, 295 K, CDCl₃): δ = 8.57 (dq, H-11), 7.95 (dt, H-8), 7.78 (td, H-9), 7.60 (d, H-5), 7.26 (m, H-10), 6.84 (d, H-4), 4.18 (t, N-CH₂), 1.88 (m, CH₂), 1.34 (m, 2 x CH₂), 0.93 (t, CH₃) ppm. ¹³C NMR (300.13 MHz, 295 K, CDCl₃): δ = 153.43 (C-7), 152.11 (C-11), 150.16 (C-3), 137.50 (C-9), 131.93 (C-5), 123.17 (C-8), 120.20 (C-10), 104.55 (C-4), 52.92 (N-CH₂), 30.75 (CH₂), 29.36 (CH₂), 22.82 (CH₂), 14.16 (CH₃) ppm.

[Mo(CO)₄(2-(1-pentyl-3-pyrazolyl)pyridine)] (1)

In a Schlenk tube, Mo(CO)₆ (0.5 g, 1.89 mmol) and ppp (0.41 g, 1.9 mmol) were added to toluene (30 mL) and the mixture was refluxed under N₂ for 45 min. After concentrating the resultant solution, hexane (15 mL) and pentane (5 mL) were added, and the mixture was left undisturbed overnight. The resultant yellowish green precipitate was washed with pentane (2 x 15 mL) and finally vacuum-dried.

Yield: 0.45 g, 56 %. Anal. Calcd for C₁₇H₁₇MoN₃O₄ (423.27): C, 48.24; H, 4.05; N, 9.93. Found: C, 48.18; H, 4.20; N, 9.79 %. Selected FT-IR (KBr, cm⁻¹): 361 (s), 405 (w), 467 (w), 478 (w), 557 (m), 584 (m), 602 (m), 627 (w), 648 (m), 760 (vs), 791 (w), 883 (w), 958 (w), 1030 (w), 1157 (w), 1234 (m), 1336 (w), 1361 (m), 1439 (s), 1460 (w), 1498 (w), 1523 (w), 1606 (m, $\nu(\text{C-N})_{\text{py}}$), 1824 (vs, $\nu(\text{CO})$), 1861 (vs, $\nu(\text{CO})$), 2013 (vs,

Chapter 10

$\nu(\text{CO})$, 2864 (m), 2933 (m), 2960 (w). ^1H NMR (300.1 MHz, 295 K, CDCl_3): δ = 9.04 (qd, H-11), 7.83 (dt, H-9), 7.73 (td, H-8), 7.60 (d, H-5), 7.26 (H-10, overlap with solvent peak), 6.81 (d, H-4), 4.44 (t, N- CH_2), 2.02 (m, CH_2), 1.40 (m, CH_2), 0.93 (t, CH_3) ppm. ^{13}C NMR (75.4 MHz, 295 K, CD_3CN): δ = 223.13 (CO_{cis}), 222.62 (CO_{cis}), 204.74 (CO_{trans}), 153.62 (C-7), 152.38 (C-11), 151.77 (C-3), 139.37 (C-9), 135.58 (C-5), 124.91 (C-8), 122.50 (C-10), 105.53 (C-4), 54.21 (N- CH_2), 31.12 (CH_2), 29.15 (CH_2), 22.88 (CH_2), 14.08 (CH_3) ppm.

[Mo₈O₂₄(2-(1-pentyl-3-pyrazolyl)pyridine)₄] (2)

In a Schlenk tube, 5-6 M TBHP in decane (1.3 mL, ca. 7.1 mmol) was added to a mixture comprising complex **1** (0.3 g, 0.71 mmol) and CH_2Cl_2 (30 mL), and stirring was continued for 4 h under N_2 at room temperature. The resultant off-white solid was recovered by filtration, washed with diethyl ether (2 x 30 mL), and finally vacuum-dried.

Yield: 0.08 g, 45 %. Anal. Calcd for $\text{C}_{52}\text{H}_{68}\text{Mo}_8\text{N}_{12}\text{O}_{24}$ (2012.68): C, 31.03; H, 3.41; N, 8.35. Found: C, 30.91; H, 3.57; N, 8.48 %. TGA revealed a residual mass of 57.5 % at 600 °C (calcd, for MoO_3 : 57.2 %). Selected FT-IR (KBr, cm^{-1}): 357 (w), 374 (w), 405 (w), 426 (w), 524 (w), 559 (w), 667 (vs), 702 (s), 775 (s), 804 (s), 843 (w), 910 (s), 942 (s), 1024 (w), 1055 (w), 1080 (w), 1099 (m), 1161 (w), 1192 (w), 1236 (m), 1371 (m), 1442 (s), 1466 (m), 1504 (m), 1543 (w), 1570 (w), 1612 (s), 1630 (m), 1741 (w), 2865 (m), 2927 (m), 2956 (m), 3116 (m). Selected FT-Raman (cm^{-1}): 203 (m), 220 (sh), 933 (vs), 962 (m), 985 (w), 1021 (m), 1235 (w), 1369 (m), 1419 (m), 1438 (w), 1502 (m), 1534 (s), 1569 (s), 1609 (s).

[MoO(O₂)₂(2-(1-pentyl-3-pyrazolyl)pyridine)] (3)

A mixture of MoO_3 (0.25 g, 1.73 mmol) and 30 % H_2O_2 (2.50 mL, 24.5 mmol) was stirred for 3 h at 60 °C under N_2 . The resultant yellow solution was cooled in an ice-bath and then added slowly to a Schlenk tube containing ppp (0.37 g, 1.73 mmol). A yellow solution and paste were obtained at this stage. After the addition of H_2O (4 mL), the mixture was stirred until a yellow solid was obtained, which was recovered by filtration, washed with H_2O (2 x 5 mL) and pentane (2 x 4 mL), and finally vacuum-dried.

Yield: 0.41 g, 60 %. Anal. Calcd for $\text{C}_{13}\text{H}_{17}\text{MoN}_3\text{O}_5$ (391.23): C, 39.91; H, 4.38; N, 10.74. Found: C, 40.15; H, 4.45; N, 10.65 %. Selected FT-IR (KBr, cm^{-1}): 320 (w), 407 (w), 432 (w), 534 (m), 546 (m), 585 (m), 627 (w), 642 (w), 660 (m), 737 (w), 779 (s), 800 (w), 863 (s), 881 (m), 948 (s), 1022 (w), 1053 (w), 1093 (m), 1103 (m), 1151 (w), 1163 (w), 1198 (w), 1234 (m), 1263 (w), 1300 (w), 1332 (w), 1361 (m), 1442 (m), 1468 (m),

Chapter 10

1504 (m), 1531 (w), 1574 (w), 1610 (m), 2866 (m), 2935 (m), 2951 (m), 3142 (w), 3136 (w). Selected FT-Raman (cm^{-1}): 221 (w), 252 (m), 281 (m), 301 (m), 318 (w), 406 (w), 471 (w), 502 (w), 532 (m), 550 (w), 584 (w), 642 (w), 661 (w), 702 (w), 798 (w), 866 (w), 882 (m), 953 (s), 1022 (m), 1053 (w), 1093 (w), 1102 (w), 1119 (w), 1163 (w), 1331 (m), 1362 (m), 1421 (m), 1441 (m), 1504 (m), 1535 (s), 1572 (m), 1608 (m), 2730 (w), 2861 (m), 2906 (m), 2997 (w), 3065 (m), 3088 (w), 3134 (m).

Synthesis of [bmim]₄[β -Mo₈O₂₆] (4)

The preparation of the octamolybdate salt was adapted from the literature.³ Ammonium heptamolybdate (1.99, 1.61 mmol) was dissolved in water (25 mL) and acidified to pH = 4 with HCl (2 M). The ionic liquid [bmim]Cl (1.00 g, 5.65 mmol) was dissolved in the minimum amount of water and then added to the previous mixture, obtaining a white solid. The product was washed with ethanol and ethylic ether, and finally vacuum-dried.

Yield: 1.56 g, 58 % Anal. Calcd for C₃₂H₆₀Mo₈N₈O₂₆ (1755.60): C, 21.87; H, 3.44; N, 6.38. Found: C, 18.33; H, 2.98; N, 6.24 %. Selected FT-IR (KBr, cm^{-1}): 361 (m), 413 (m), 451 (w), 474 (w), 623 (m), 665 (s), 719 (s), 841 (s), 902 (s), 914 (s), 933 (s), 949 (s), 1022 (w), 1088 (w), 1107 (w), 1163 (m), 1255 (w), 1335 (w), 1433 (m), 1462 (m), 1556 (m), 1568 (m), 1614 (w), 1714 (w), 2360 (w), 2341 (w), 2839 (w), 2871 (w), 2931 (w), 2958 (w), 3064 (m), 3140 (m), 3159 (m), 3224 (w), 3440 (m).

10.4.3. Chapter 4

General protocol for reductive amination

In a round bottomed flask, the appropriate amine was dissolved in anhydrous CH₂Cl₂ (20 mL) followed by addition of anhydrous Na₂SO₄ and the carbonyl compound (ketone L1 or formaldehyde) (Scheme 4.1 in Chapter 4). The reaction was left under magnetic stirring for 4 h at room temperature. After that period, the reducing agent, NaBH(OAc)₃, was carefully added and the reaction allowed to proceed for a further 20 h. The reaction mixture was filtered under reduced pressure and saturated NaHCO₃ (20 mL) was added to the filtrate. The phases were transferred to a separating funnel and the aqueous phase was washed with CH₂Cl₂ (3 x 20 mL). The organic extracts were combined and dried over anhydrous Na₂SO₄, filtered, and the solvent removed in vacuo. The crude oil was chromatographed using AcOEt as eluent, affording the desired amine.

Chapter 10

(R,R)-N-(1-phenylethyl)-6,7-dihydro-5H-cyclopenta[b]pyridin-7-amine (L2)

Following the general protocol for reductive amination, (*R*)-(+)- α -methylbenzylamine (0.73 mL, 5.6 mmol) was reacted with ketone L1 (0.50 g, 3.75 mmol) and NaBH(OAc)₃ (1.19 g, 5.63 mmol). After the work-up procedure and purification, amine L2 was obtained as a brown oil.

Yield: 0.72 g, 80 %. ¹H NMR (CDCl₃, 400 MHz): δ = 8.40 (d, H-2), 7.50-7.39 (m, ArH), 7.35-7.28 (m, ArH), 7.27-7.20 (m, ArH), 7.05 (dd, H-3), 4.24 (q, NHCH(CH₃)Ph), 4.12 (t, H-7), 2.79 (ddd, H-5_{syn}), 2.68-2.57 (m, H-5_{anti}), 2.53 (br s, NH), 1.97 (dtd, H-6_{syn}), 1.58 (ddd, H-6_{anti}), 1.47 (d, NHCH(CH₃)Ph). ¹³C NMR (CDCl₃, 101 MHz): δ = 165.5 (C-7a), 147.8 (C-2), 146.5 (C, C_{ipso}), 136.5 (C-4a), 132.6 (C-4), 128.4 (2 x C_{meta}), 127.4 (2 x C_{ortho}), 127.1 (C_{para}), 122.2 (C-3), 62.5 (C-7), 58.7 (NHCH(CH₃)Ph), 33.8 (C-6), 28.3 (C-5), 24.4 (NHCH(CH₃)Ph). ESI-MS: calculated for [C₁₆H₁₉N₂]⁺, 239.15; obtained, 239.19. $\alpha_D^{20\text{ }^\circ\text{C}}$ = + 28.6 (c1, CHCl₃).

(S,S)-N-(1-phenylethyl)-6,7-dihydro-5H-cyclopenta[b]pyridin-7-amine (L3)

Following the general protocol for reductive amination, (*S*)-(–)- α -methylbenzylamine (0.73 mL, 5.6 mmol) was reacted with ketone L1 (0.5 g, 3.75 mmol) and NaBH(OAc)₃ (1.19 g, 5.63 mmol). After the work-up procedure and purification, amine L3 was obtained as a brown oil.

Yield: 0.75 g, 84 %. ¹H NMR (CDCl₃, 400 MHz): δ = 8.40 (d, H-2), 7.50-7.41 (m, ArH), 7.36-7.28 (m, ArH), 7.27-7.20 (m, ArH), 7.05 (ddd, H-3), 4.25 (q, NHCH(CH₃)Ph), 4.12 (t, H-7), 2.80 (ddd, H-5_{syn}), 2.73-2.45 (m, H-5_{anti}, NH), 1.97 (dtd, H-6_{syn}), 1.60 (ddd, 1H, H-6_{anti}), 1.48 (d, NHCH(CH₃)Ph). ¹³C NMR (CDCl₃, 101 MHz): δ = 165.2 (C-7a), 147.8 (C-2), 146.0 (C, C_{ipso}), 136.7 (C-4a), 132.7 (C-4), 128.8 (ArC), 127.5 (ArC), 127.2 (ArC), 122.3 (C-3), 62.3 (C-7), 58.6 (NHCH(CH₃)Ph), 33.6 (C-6), 28.2 (C-5), 24.5 (NHCH(CH₃)Ph). ESI-MS: calculated for [C₁₆H₁₉N₂]⁺, 239.15; obtained, 239.39. $\alpha_D^{20\text{ }^\circ\text{C}}$ = - 27.9 (c1, CHCl₃).

(R,R)-N-methyl-N-(1-phenylethyl)-6,7-dihydro-5H-cyclopenta[b]pyridin-7-amine [(R,R)-pyC₅H₅N(CH₃)CH(CH₃)Ph = L4]

Following the general protocol for reductive amination, amine L2 (0.70 g, 2.94 mmol) was reacted with an aqueous 37 % solution of formaldehyde (0.33 mL, 4.4 mmol) and NaBH(OAc)₃ (1.87 g, 8.82 mmol). After the work-up procedure and purification, amine L4 was obtained as a brown oil.

Chapter 10

Yield: 0.58 g, 78 %. ^1H NMR (CDCl_3 , 400 MHz): δ = 8.60-8.38 (m, H-2), 7.55-7.48 (m, ArH), 7.45 (dd, ArH), 7.35-7.28 (m, ArH), 7.26-7.20 (m, ArH), 7.05 (dd, H-3), 4.57 (t, H-7), 4.16 (d, $\text{N}(\text{CH}_3)\text{CH}(\text{CH}_3)\text{Ph}$), 2.88 (ddd, H-5_{syn}), 2.74 (ddd, H-5_{anti}), 2.14-1.93 (m, H-6_{syn}, H-6_{anti} and $\text{N}(\text{CH}_3)\text{CH}(\text{CH}_3)\text{Ph}$), 1.49 (d, $\text{NHCH}(\text{CH}_3)\text{Ph}$). ^{13}C NMR (CDCl_3 , 101 MHz): δ = 164.6 (C-7a), 148.2 (C-2), 145.8 (C_{ipso}), 137.1 (C-4a), 133.0 (C-4), 128.4 (2 x C_{meta}), 127.8 (2 x C_{ortho}), 126.9 (C_{para}), 121.8 (C-3), 65.2 (C-7), 63.0 ($\text{N}(\text{CH}_3)\text{CH}(\text{CH}_3)\text{Ph}$), 33.3 ($\text{N}(\text{CH}_3)\text{CH}(\text{CH}_3)\text{Ph}$) 28.3 (C-6), 24.3 (C-5), 21.3 ($\text{N}(\text{CH}_3)\text{CH}(\text{CH}_3)\text{Ph}$). ESI-MS: calculated for $[\text{C}_{17}\text{H}_{21}\text{N}_2]^+$, 253.17; obtained, 253.15. $\alpha_D^{20\text{ }^\circ\text{C}}$ = + 26.2 (c1, CHCl_3).

(S,S)-N-methyl-N-(1-phenylethyl)-6,7-dihydro-5H-cyclopenta[b]pyridin-7-amine
[(S,S)-pyC₅H₅N(CH₃)CH(CH₃)Ph = L5]

Following the general protocol for reductive amination, amine L3 (0.7 g, 2.94 mmol) was reacted with an aqueous 37 % solution of formaldehyde (0.33 g, 4.4 mmol) and $\text{NaBH}(\text{OAc})_3$ (1.87 g, 8.82 mmol). After the work-up procedure and purification, amine L5 was obtained as a brown oil.

Yield: 0.55 g, 74 %. ^1H NMR (CDCl_3 , 400 MHz): δ = 8.52-8.46 (m, H-2), 7.55-7.48 (m, ArH), 7.45 (dd, 1H, ArH), 7.35-7.28 (m, ArH), 7.26-7.20 (m, ArH), 7.05 (dd, H-3), 4.57 (t, H-7), 4.16 (br s, $\text{N}(\text{CH}_3)\text{CH}(\text{CH}_3)\text{Ph}$), 2.88 (ddd, H-5_{syn}), 2.74 (ddd, H-5_{anti}), 2.15-1.97 (m, H-6_{syn}, H-6_{anti} and $\text{N}(\text{CH}_3)\text{CH}(\text{CH}_3)\text{Ph}$), 1.49 (d, $\text{NHCH}(\text{CH}_3)\text{Ph}$). ^{13}C NMR (CDCl_3 , 101 MHz): δ = 164.2 (C-7a), 148.2 (C-2), 145.9 (C_{ipso}), 137.1 (C-4a), 132.5 (C-4), 128.4 (2 x C_{meta}), 127.9 (2 x C_{ortho}), 126.9 (C_{para}), 121.9 (C-3), 65.2 (C-7), 63.0 ($\text{N}(\text{CH}_3)\text{CH}(\text{CH}_3)\text{Ph}$), 33.4 ($\text{N}(\text{CH}_3)\text{CH}(\text{CH}_3)\text{Ph}$), 28.3 (C-6), 24.3 (C-5), 21.3 ($\text{N}(\text{CH}_3)\text{CH}(\text{CH}_3)\text{Ph}$). ESI-MS: calculated for $[\text{C}_{17}\text{H}_{21}\text{N}_2]^+$, 253.17; obtained, 253.19. $\alpha_D^{20\text{ }^\circ\text{C}}$ = - 27.3 (c1, CHCl_3).

General procedure for synthesis of tetracarbonyl complexes

In a Schlenk tube, $\text{Mo}(\text{CO})_6$ and organic ligand L4 or L5 were reacted in refluxing anhydrous CH_3CN (40 mL) for 30 min under N_2 . Solvent was removed from the resultant brown mixture by evaporation under reduced pressure, giving a brown solid that was washed with hexane (2 x 40 mL) and pentane (20 mL), and finally vacuum-dried.

Chapter 10

cis-[Mo(CO)₄(L1)] (1)

Mo(CO)₆ (0.31 g, 1.17 mmol) was reacted with L4 (0.3 g, 1.19 mmol) giving **1**.

Yield: 0.29 g, 54 %. Anal. Calcd for C₂₁H₂₀N₂MoO₄ (460.33): C, 54.79; H, 4.38; N, 6.08. Found: C, 54.40; H, 4.45; N, 6.10 %. Selected FT-IR (KBr, cm⁻¹): 359 (m), 705 (m), 796 (m), 944 (m), 1455 (m), 1822 (vs, ν(CO)), 1868 (vs, ν(CO)), 1892 (s, ν(CO)), 2013 (s, ν(CO)), 2854 (w), 2927 (m). ¹H NMR (CDCl₃, 300 MHz): δ = 8.58 (d, H-2), 7.6-7.2 (overlapping signals and multiplets, aryl-H and H-4), 7.14 (dd, H-3), 4.71 (t, H-7), 4.48 (q, 1H, N(CH₃)CH(CH₃)Ph), 2.93-2.63 (overlapping multiplets, H-5_{syn}, H-5_{anti}), 2.6-2.0 (m, H-6_{syn}, H-6_{anti} and N(CH₃)CH(CH₃)Ph), 1.95 (d, N(CH₃)CH(CH₃)Ph).

cis-[Mo(CO)₄(L2)] (2)

Mo(CO)₆ (0.27 g, 1.02 mmol) was reacted with L5 (0.26 g, 1.03 mmol) giving **2**.

Yield: 0.29 g, 64 %. Anal. Calcd for C₂₁H₂₀N₂MoO₄ (460.33): C, 54.79; H, 4.38; N, 6.08. Found: C, 54.57; H, 4.79; N, 6.13 %. Selected FT-IR (KBr, cm⁻¹): 363 (m), 705 (m), 795 (m), 944 (m), 1454 (m), 1822 (vs, ν(CO)), 1868 (vs, ν(CO)), 1893 (s, ν(CO)), 2013 (s, ν(CO)), 2857 (w), 2927 (m). ¹H NMR (CDCl₃, 300 MHz): δ = 8.58 (d, H-2), 7.6-7.2 (overlapping signals and multiplets, aryl-H and H-4), 7.14 (dd, H-3), 4.71 (t, H-7), 4.48 (q, N(CH₃)CH(CH₃)Ph), 2.93-2.63 (overlapping multiplets, H-5_{syn} and H-5_{anti}), 2.6-2.0 (m, H-6_{syn}, H-6_{anti} and N(CH₃)CH(CH₃)Ph), 1.95 (d, N(CH₃)CH(CH₃)Ph).

10.4.4. Chapter 5

[Mo(CO)₃(1,2,3-trz)₃] (1)

Mo(CO)₆ (0.5 g, 1.90 mmol) and 1*H*-1,2,3-trz (0.34 mL, 5.7 mmol) were added to toluene (20 mL) in a Schlenk tube and the mixture was refluxed under N₂ for 90 min, resulting in a dark green precipitate and a yellow solution. The solid was filtered, washed with pentane (2 x 20 mL), and vacuum-dried.

Yield: 0.60 g, 82 %. Anal. Calcd for C₉H₉MoN₃O₃ (387.17): C, 27.92; H, 2.34; N, 32.56. Found: C, 27.35; H, 2.15; N, 32.64 %. Selected FT-IR (KBr, cm⁻¹): 476 (w), 523 (m), 700 (w), 735 (w), 787 (m), 808 (m), 833 (w), 958 (w), 1070 (w), 1088 (m), 1155 (w), 1198 (w), 1448 (w), 1527 (m), 1774 (vs, bd, ν(CO)), 1907 (s, ν(CO)), 3140 (m), 3165 (m), 3311 (m). ¹H-NMR ((CD₃)₂CO): δ = 7.79 (br, s), 8.24 (s), 8.37 (d), 14.45 (vbr, sh), 15.06 (vbr, s). A tentative assignment of the ¹H-NMR spectrum is based on the coexistence of Mo-coordinated 1*H* (T-1*H*) and 2*H* (T-2*H*) annular tautomers of 1,2,3-trz, in

Chapter 10

correspondence with that known to exist for free 1,2,3-trz in the solid, liquid and gas phases^{4,5}: δ (T-2H) 7.79 (2H, H-4 and H-5), 14.45 (1H, NH); δ (T-1H) 8.24 (1H, H-4 or H-5), 8.37 (1H, H-4 or H-5), 15.06 (1H, NH); approximate T-2H:T-1H ratio = 1:1.8. TGA showed a residual mass of 37.4 % at 450 °C (Calcd for MoO₃: 37.2 %).

[Mo(CO)₃(1,2,4-trz)₃] (2)

Mo(CO)₆ (0.25 g, 0.95 mmol) and 1H-1,2,4-trz (0.2 g, 2.85 mmol) were added to toluene (10 mL) in a Schlenk tube and the mixture was refluxed under N₂ for 2 h. The resultant cream-colored precipitate was filtered, washed with acetone (2 x 20 mL) and diethyl ether (2 x 20 mL), and vacuum-dried.

Yield: 0.34 g, 95 %. Anal. Calcd for C₉H₉MoN₃O₃ (387.17): C, 27.92; H, 2.34; N, 32.56. Found: C, 27.99; H, 2.45; N, 32.88 %. Selected FT-IR (KBr, cm⁻¹): 482 (w), 517 (w), 527 (w), 605 (m), 699 (w), 859 (w), 879 (w), 947 (w), 1031 (m), 1125 (m), 1296 (m), 1410 (m), 1425 (m), 1512 (m), 1760 (vs, bd, ν (CO)), 1905 (s, ν (CO)), 3138 (w), 3159 (m), 3170 (m), 3382 (m). ¹³C{¹H} CP MAS NMR: δ = 145.2 (C-3, C-5), 226.3 (CO). TGA showed a residual mass of 36.3 % at 450 °C (Calcd for MoO₃: 37.2 %).

Oxidative decarbonylation reactions

Oxidative decarbonylation of **1** or **2** was performed in a Schlenk tube under nitrogen by addition of 5-6 M TBHP in decane to a suspension of the tricarbonyl complex in CH₂Cl₂. Reaction conditions for **1**: TBHP (2 mL, ca. 10.9 mmol), **1** (0.35 g, 1.11 mmol), CH₂Cl₂ (45 mL), 4 h, r.t. The resultant light violet solid (**1**^{OD}) was recovered by filtration, washed with diethyl ether (2 x 45 mL), and vacuum-dried. Reaction conditions for **2**: TBHP (2.10 mL, ca. 11.4 mmol), **2** (0.12 g, 0.38 mmol), CH₂Cl₂ (20 mL), 70 °C, 48 h. The resultant light brown solid (**2**^{OD}) was filtered, washed with CH₂Cl₂ (2 x 20 mL) and acetone (2 x 20 mL), and vacuum-dried.

Data for **1**^{OD}: Yield: 0.19 g (74 %). Anal. Calcd for C₂H₃MoN₃O₃·H₂O (231.02): C, 10.40; H, 2.18; N, 18.19. Found: C, 9.86; H, 1.82; N, 17.53 %. Residual masses recorded by TGA were 6.3 % at 110 °C (Calcd for H₂O: 7.8 %) and 62.0 % at 400 °C (Calcd for MoO₃: 62.3 %). FT-IR (KBr, cm⁻¹): 615 (vbd, $\nu_{\text{as}}(\text{Mo}-\text{O}-\text{Mo})$), 796 (m), 902 (vs, $\nu(\text{Mo}=\text{O})$), 941 (s, $\nu(\text{Mo}=\text{O})$), 974 (m), 1092 (m), 1132 (m), 1205 (m), 1260 (w), 1446 (m), 2870 (w), 3140 (m). ¹³C{¹H} CP MAS NMR: δ = 127.0 (C-4), 134.8 (C-5). ¹³C{¹H} CP MAS NMR: δ = 127.0 (C-4), 134.8 (C-5).

Data for **2**^{OD}: Yield: 0.07 g. C, 10.88; H, 2.09; N, 17.03 %. FT-IR (KBr, cm⁻¹): 610 (vbd, $\nu_{\text{as}}(\text{Mo}-\text{O}-\text{Mo})$), 630 (m), 899 (vs, $\nu(\text{Mo}=\text{O})$), 936 (s, $\nu(\text{Mo}=\text{O})$), 1059 (m), 1153 (m),

Chapter 10

1212 (w), 1310 (m), 1385 (w), 1413 (m), 1510 (m), 1528 (sh), 1628 (w), 2814 (w), 2895 (w), 2977 (w), 3128 (m), 3440 (vbd). $^{13}\text{C}\{^1\text{H}\}$ CP MAS NMR: $\delta = 143.9$ (C-3, C-5). $^{13}\text{C}\{^1\text{H}\}$ CP MAS NMR: $\delta = 143.9$ (C-3, C-5).

[MoO₃(1,2,3-trz)_{0.5}] (3)

A mixture of MoO₃ (0.43 g, 3 mmol), 1,2,3-trz (0.18 mL, 3 mmol) and water (20 mL) was heated in a static Teflon-lined stainless steel digestion bomb at 180 °C for 48 h. After cooling down to ambient temperature, the resultant black precipitate was filtered and washed with water (2 x 10 mL), acetone (2 x 10 mL) and diethyl ether (2 x 10 mL), and vacuum-dried.

Yield: 0.29 g, 55 %. TGA showed a residual mass of 83.0 % at 400 °C (Calcd for MoO₃: 80.6 %). FT-IR (KBr, cm⁻¹): 580 (vbd), 675 (vbd), 769 (m), 920 (sh), 938 (sh), 953 (sh), 962 (s), 1112 (s), 1150 (s), 1260 (w). $^{13}\text{C}\{^1\text{H}\}$ CP MAS NMR: $\delta = 128.1$ (C-4), 133.3 (C-5).

[MoO₃(1,2,4-trz)_{0.5}] (4)

The hybrid metal oxide-triazole material [MoO₃(1,2,4-trz)_{0.5}] was prepared by the hydrothermal reaction of MoO₃, 1,2,4-trz and water at 180 °C for 1 h.⁶ The phase purity of the microcrystalline product was verified by a comparison of its powder X-ray diffraction (PXRD) pattern with a simulated pattern calculated using the crystal structure data published for **4** (please see the XRD pattern in Chapter 5, Figure 5.4)⁶.

(NH₄)_{1.8}(H₃O)_{0.2}[Mo₂O₂(μ₂-O)(O₂)₄(1,2,4-trz)]·H₂O (5)

Trinuclear (1,2,4-Htrz)₂[Mo₃O₆(O₂)₄(1,2,4-trz)₂]·H₂O (**6**) (0.2 g, 0.24 mmol) in CH₃CN (45 mL) was treated with 30 % H₂O₂ (12.75 mL, 125 mmol) and the resultant yellow solution was stirred at 70 °C for 24 h. After concentrating the solution under reduced pressure, hexane (10 mL) and diethyl ether (20 mL) were added, followed by dropwise addition of acetone to precipitate **5** as a dark yellow microcrystalline solid, which was recovered by filtration and vacuum-dried.

The trinuclear complex (**6**) was prepared as described previously by the addition of 1,2,4-trz to the solution obtained upon reaction of MoO₃ with a large excess of H₂O₂.⁶

Yield: 0.13 g, 71 %. Anal. Calcd for C₂H_{12.8}Mo₂N_{4.8}O_{12.2} (491.23): C, 4.89; H, 2.63; N, 13.69. Found: C, 4.67; H, 2.99; N, 13.76. TGA showed a residual mass of 58.1 % at 400 °C (Calcd for MoO₃: 58.6 %). FT-IR (KBr, cm⁻¹): 520 (m, ν_s(Mo(O₂)₂)), 579 (s,

Chapter 10

$\nu_{\text{as}}(\text{Mo}(\text{O}_2)_2)$, 625 (s, $\nu(\text{Mo}(\text{O}_2)_2)$ and/or trz ring-torsion), 691 (m), 709 (vs, $\nu_{\text{as}}(\text{Mo}-\text{O}-\text{Mo})$), 864 (vs, $\nu(\text{O}-\text{O})$), 937 (vs, $\nu(\text{Mo}=\text{O})$), 1059 (m), 1125 (w), 1305 (w), 1403 (vs, $\delta(\text{NH}_4^+)$), 1496 (w), 1526 (w), 1604 (w), 1672 (w), 3125 (m, $\nu(\text{C}-\text{H})$), 3220 (bd), 3621 (m). Raman (cm^{-1}): 314 (m), 419 (w), 542 (s, $\nu_{\text{s}}(\text{Mo}(\text{O}_2)_2)$), 573 (m, $\nu_{\text{as}}(\text{Mo}(\text{O}_2)_2)$), 636 (w), 875 (m, $\nu(\text{O}-\text{O})$), 940 (vs, $\nu(\text{Mo}=\text{O})$), 1056 (w), 1125 (w), 1305 (m), 1401 (vw). $^{13}\text{C}\{^1\text{H}\}$ CP MAS NMR: $\delta = 140.0$ (C-3, C-5).

Alternative synthesis of **5**: 30 % H_2O_2 (4.4 mL, 43 mmol) was added to $[\text{MoO}_3(1,2,4\text{-trz})_{0.5}]$ (**4**) (0.050 g, 0.28 mmol) and CH_3CN (15 mL) in a Schlenk tube. The suspension was stirred for 24 h at 70 °C. After cooling to room temperature, the resultant yellow solution was concentrated under reduced pressure and stored under nitrogen. After 2 weeks, the mother liquor was filtered off and allowed to evaporate slowly at ambient temperature under air, leading to yellow crystals of **5** (confirmed by PXRD). Yield: 0.03 g, 37 %.

10.4.5. Chapter 6

$[\text{MoO}_3(2,2'\text{-bipy})]_n$ (**1**)

$[\text{MoO}_3(2,2'\text{-bipy})]_n$ was prepared according with the literature.⁷ A solution of 5-6 M TBHP in *n*-decane (29.8 mmol) was added dropwise to a magnetically stirred suspension of $[\text{Mo}(\text{CO})_4(2,2'\text{-bipy})]$ (1.08 g, 2.97 mmol) in dichloromethane (60 mL). A white solid precipitated, and the solution turned to cream. After stirring the mixture for 4 h at room temperature, a white solid was filtered, washed with hexane (1 x 30 mL), CH_2Cl_2 (1 x 30 mL) and diethyl ether (2 x 30 mL), and finally vacuum-dried.

Yield: 0.86 g, 97 %. Satisfactory elemental analysis was obtained for compound **1** and FT-IR and Raman spectra were in agreement with published data.¹ Selected FT-IR (KBr, cm^{-1}): $\nu = 316$ (m), 355 (w), 401 (m), 418 (m), 444 (m), 632 (vs, $\nu(\text{Mo}-\text{O}-\text{Mo})$), 652 (s), 735 (w), 762 (vs), 845 (w), 883 (vs, $\nu(\text{Mo}=\text{O})$), 914 (vs, $\nu(\text{Mo}=\text{O})$), 1024 (m), 1041 (w), 1059 (w), 1078 (w), 1109 (w), 1161 (m), 1226 (w), 1248 (w), 1261 (w), 1315 (m), 1442 (vs), 1473 (s), 1494 (m), 1576 (w), 1599 (s), 1637 (w), 3078 (w). Selected FT-Raman (cm^{-1}): 190 (m), 234 (m), 257 (m), 318 (w), 357 (w), 419 (w), 442 (w), 632 (w), 651 (w), 768 (m), 872 (w), 915 (vs), 1022 (s), 1058 (m), 1160 (w), 1266 (w), 1317 (s), 1429 (w), 1493 (m), 1564 (m), 1596 (vs), 3032 (w), 3078 (m). $^{13}\text{C}\{^1\text{H}\}$ CP MAS: $\delta = 148.15$ (C-2/C-2'), 142.02 (C-6/C-6'), 139.65 (C-4/C-4'), 129.34 (C-5/C-5'), 125.34-121.39 (C-3/C-3').

Chapter 10

[Mo₂O₆(2,2'-bipy)]_n (2)

[MoO₃(2,2'-bipy)]_n (1) (21 mg, 0.07 mmol) was heated under air for 10 min in a muffle furnace preheated to 300 °C.

Yield: 15 mg, 96 %. Anal. Calcd for C₁₀H₈Mo₂N₂O₆ (444.06): C, 27.05; H, 1.82; N, 6.30. Found: C, 26.80; H, 1.87; N, 6.00 %. FT-IR (KBr, cm⁻¹): 308 (m), 324 (m), 355 (m), 380 (m), 704 (vs), 771 (vs), 883 (vs, ν(Mo=O)), 903 (vs, ν(Mo=O)), 919 (sh), 941 (s, ν(Mo=O)), 960 (m), 1003 (w), 1028 (m), 1062 (w), 1101 (w), 1157 (w), 1180 (w), 1221 (w), 1243 (w), 1284 (w), 1320 (m), 1425 (m), 1444 (s), 1473 (m), 1493 (m), 1574 (m), 1598 (s), 1606 (sh), 3058 (w), 3105 (w), 3420 (br). Selected FT-Raman (cm⁻¹): 895 (w), 936 (m, ν(Mo=O)), 969 (w), 1025 (w), 1308 (w), 1564 (w), 1595 (m), 3073 (w). ¹³C{¹H} CP MAS NMR: δ = 152.3 (C-2/C-2'), 149.5 (C-2/C-2', C-6/C-6'), 144.9, 142.0 (C-4/C-4'), 128.4 (C-5/C-5'), 126.1 (C-5/C-5', C-3/C-3'), 124.4 (C-3/C-3').

[Mo₃O₉(2,2'-bipy)₂]_n (3)

A mixture of [MoO₃(2,2'-bipy)]_n (1) (0.2 g, 0.67 mmol) and H₂O (25 mL) was heated under autogenous pressure and dynamic conditions (25 rpm) for 6 days at 160 °C in a Teflon-lined stainless-steel digestion bomb. The resultant solid was filtered, washed with water (3 x 5 mL), acetone (3 x 5 mL) and diethyl ether (2 x 5 mL), and finally vacuum-dried.

Yield: 0.14 g, 85 %. Anal. Calcd for C₂₀H₁₆Mo₃N₄O₉ (744.18): C, 32.28; H, 2.17; N, 7.53. Found: C, 32.10; H, 2.17; N, 7.30 %. FT-IR (KBr, cm⁻¹): 301 (w), 316 (w), 332 (m), 386 (m), 420 (w), 442 (w), 635 (sh), 649 (vs, ν(Mo-O-Mo)), 665 (vs, ν(Mo-O-Mo)), 742 (s), 758 (s), 775 (vs), 798 (vs), 897 (vs, ν(Mo=O)), 914 (vs, ν(Mo=O)), 938 (s, ν(Mo=O)), 1026 (m), 1161 (w), 1176 (w), 1227 (w), 1248 (w), 1315 (m), 1442 (s), 1473 (m), 1493 (m), 1574 (w), 1597 (s), 3035 (w), 3076 (w), 3105 (w), 3438 (br). FT-Raman (cm⁻¹): 106 (w), 124 (w), 154 (w), 188 (w), 198 (w), 222 (w), 236 (w), 249 (w), 259 (w), 301 (w), 315 (w), 338 (w), 355 (w), 383 (w), 634 (w), 652 (w), 767 (w), 779 (w), 800 (w), 814 (w), 830 (w), 870 (w), 896 (m, ν(Mo=O)), 925 (vs, ν(Mo=O)), 948 (m, ν(Mo=O)), 1024 (s), 1061 (w), 1164 (w), 1269 (w), 1288 (vw), 1316 (vs), 1494 (m), 1565 (s), 1597 (vs), 2984 (w), 3078 (m), 3131 (w). ¹³C{¹H} CP MAS NMR: δ = 153.1, 150.5 (C-2/C-2'), 148.8, 147.8 (C-6/C-6'), 143.5, 141.6, 138.9 (C-4/C-4'), 128.8 (sh), 128.4, 127.3, 125.5 (C-5/C-5'), 125.0 (sh), 123.2, 122.8 (sh), 120.7 (C-3/C-3').

Chapter 10

$[[\text{MoO}_3(2,2'\text{-bipy})][\text{MoO}_3(\text{H}_2\text{O})]]_n$ (4)

$[[\text{MoO}_3(2,2'\text{-bipy})][\text{MoO}_3(\text{H}_2\text{O})]]_n$ was prepared according with the literature.⁸ A mixture of $[\text{MoO}_2\text{Cl}_2(2,2'\text{-bipy})]$ (0.22 g, 0.62 mmol) and water (30 mL) was refluxed in the air (atmospheric pressure) for 12 h. At the end of the reaction, a white solid suspended in a pale pink solution (pH = 2) was obtained. After cooling to room temperature, the solid was recovered filtered, washed with water (2 x 10 mL), acetone (2 x 10 mL), and diethyl ether (2 x 10 mL) and dried at 80 °C under vacuum.

Yield: 0.14 g, 100 %. Elemental analysis and FT-IR data are in excellent agreement with literature data.⁸ Anal. Calcd for $\text{C}_{10}\text{H}_{10}\text{Mo}_2\text{N}_2\text{O}_7$ (462.08): C, 25.99; H, 2.18; N, 6.06. Found: C, 28.22; H, 2.41; N, 6.62 %. Selected FT-IR (KBr, cm^{-1}): 316 (w), 355 (w), 366 (w), 400 (m), 418 (w), 440 (w), 511 (s,br, $\nu(\text{OMo}_3)$), 654 (sh), 681 (s, br, $\nu(\text{Mo-O-Mo})$), 758 (s), 802 (w), 872 (vs, $\nu(\text{Mo=O})$), 916 (s, $\nu(\text{Mo=O})$), 931 (s, $\nu(\text{Mo=O})$), 956 (m, $\nu(\text{Mo=O})$), 1028 (m), 1101 (w), 1161 (w), 1178 (w), 1248 (w), 1315 (m), 1444 (m), 1475 (m), 1496 (w), 1541 (w), 1575 (w), 1575 (w), 1599 (m), 1680 (m, $\delta(\text{OH}_2)$), 3079 (w), 3122 (w), 3224 (m).

The complex $[\text{MoO}_2\text{Cl}_2(2,2'\text{-bipy})]$ was prepared as described previously⁸ by a reaction of ligand substitution between the adduct complex $[\text{MoO}_2\text{Cl}_2(\text{NCCH}_3)_2]$ and 2,2'-bipy in CH_3CN under stirring during 40 min.

$[\text{MoO}(\text{O}_2)_2(2,2'\text{-bipy})]$ (5)

A mixture of MoO_3 (0.25 g, 1.73 mmol) and 30 % H_2O_2 (2.5 mL, 24.5 mmol) was stirred for 3 h at 60 °C under N_2 . The resultant yellow solution was cooled in an ice-bath and then 2,2'-bipy (0.27 g, 1.73 mmol) was added slowly. A yellow paste was obtained at this stage. After decanting off the supernatant, the residue was washed with H_2O (3 x 10 mL), pentane (4 x 10 mL) and diethyl ether (2 x 10 mL), obtaining a yellow solid, which was finally vacuum-dried.

Yield: 0.43 g, 75 %. Selected FT-IR (KBr, cm^{-1}): 318 (w), 364 (w), 415 (w), 536 (m, $\nu(\text{Mo-O})_{\text{peroxo}}$), 582 (m, $\nu(\text{Mo-O})_{\text{peroxo}}$), 650 (m, $\nu(\text{Mo-O})_{\text{peroxo}}$), 667 (m), 729 (m), 771 (s), 862 (s, $\nu(\text{O-O})$), 941 (vs, $\nu(\text{Mo=O})$), 1032 (m), 1045 (m), 1074 (w), 1103 (w), 1161 (m), 1176 (m), 1221 (w), 1246 (m), 1315 (m), 1444 (s), 1473 (m), 1494 (m), 1572 (w), 1599 (m), 1630 (w), 1741 (m), 2856 (m), 2925 (m), 2954 (sh), 3035 (w), 3084 (m), 3112 (m), 3442 (m). Selected FT-Raman (cm^{-1}): 128 (m), 158 (w), 254 (w), 282 (w), 308 (w), 528 (w), 818 (w), 869 (w), 940 (m, $\nu(\text{Mo=O})$), 1032 (m), 1272 (w), 1314 (s), 1494 (m), 1563 (m), 1598 (s), 3083 (w). FT-IR and Raman spectral data for **5** were in agreement with those reported previously.^{9,10}

Chapter 10

10.4.6. Chapter 7

[MoO₂Cl₂(pbim)] (1)

A precipitate formed immediately upon addition of pbim (0.54 g, 2.77 mmol) to a solution of MoO₂Cl₂ (0.55 g, 2.77 mmol) in anhydrous CH₃CN (20 mL) at room temperature. After stirring the mixture at room temperature for 1 h, the yellow solid was filtered, washed with diethyl ether (3 × 20 mL), and vacuum dried.

Yield: 0.95 g, 88 %. Anal. Calcd for C₁₂H₉Cl₂MoN₃O₂ (394.06): C 36.57, H 2.30, N 10.66. Found C 36.54, H 2.05, N 11.10. Selected FT-IR (KBr, cm⁻¹): 282 (w), 341 (m, ν_{as}(Mo-Cl)), 385 (m, γ(MoO₂)), 440 (w), 573 (w), 642 (m), 752 (sh), 759 (s), 796 (w), 818 (w), 886 (s, ν_{as}(Mo=O)), 942 (s, ν_s(Mo=O)), 989 (w), 1012 (w), 1053 (w), 1092 (w), 1149 (m), 1302 (m), 1319 (m), 1442 (s), 1437 (sh), 1458 (m), 1479 (m), 1568 (w), 1601 (m), 3097 (w). Selected FT-Raman (cm⁻¹): 116 (w), 205 (w), 884 (w, ν_{as}(Mo=O)), 940 (m, ν_s(Mo=O)), 992 (m), 1009 (m), 1144 (w), 1244 (m), 1285 (m), 1435 (m), 1454 (m), 1491 (w), 1537 (s), 1566 (m), 1603 (s), 1620 (w). ¹H NMR (300 MHz, 25 °C, DMSO-d₆): δ = 8.87 (ddd, H-12), 8.48 (td, H-9), 8.17 (dt, H-10), 7.78 (dd, H-3 and H-6), 7.70 (ddd, H-11), 7.48 (dd, H-4 and H-5) ppm. ¹³C{¹H} CP MAS NMR: δ = 153.6, 145.6, 142.7, 138.5, 133.1, 126.1, 121.3, 116.1 ppm.

[MoO(O₂)₂(pbim)] (2)

A mixture of MoO₃ (0.25 g, 1.74 mmol) and 30 % H₂O₂ (5 mL, 49 mmol) was stirred for 3 h at 60 °C. The resultant yellow solution was cooled in an ice bath and then added slowly to a Schlenk tube containing the ligand pbim (0.34 g, 1.74 mmol). A yellow solution and paste were obtained at this stage. After addition of H₂O (4 mL), the mixture was stirred until a yellow solid was obtained. The product was washed with H₂O (2 × 5 mL) and pentane (2 × 4 mL), and vacuum-dried.

Yield: 0.41 g, 64 %. Anal. Calcd for C₁₂H₉MoN₃O₅ (371.16): C 38.83, H 2.44, N 11.32. Found C 39.00, H 1.70, N 11.30. Selected FT-IR (KBr, cm⁻¹): 285 (m), 305 (m), 332 (m), 368 (w), 434 (m), 525 (s), 577 (s, ν(Mo-O)_{peroxido}), 654 (m), 752 (vs), 788 (w), 826 (m), 863 (vs, ν(Mo=O)), 875 (sh, ν(O-O)), 953 (vs, ν(Mo=O)), 999 (w), 1020 (w), 1051 (m), 1103 (w), 1122 (w), 1159 (m), 1230 (w), 1267 (w), 1284 (w), 1299 (m), 1323 (m), 1446 (s), 1458 (m), 1481 (s), 1565 (w), 1601 (m). Selected FT-Raman (cm⁻¹): 115 (m), 127 (sh), 156 (m), 282 (m), 532 (w), 574 (w, ν(Mo-O)_{peroxido}), 665 (w), 818 (vs), 874 (w, ν(O-O)), 950 (m, ν(Mo=O)), 994 (s), 1010 (m), 1267 (s), 1283 (sh), 1445 (m), 1493 (w), 1555 (s), 1569 (m), 1602 (s), 3077 (w). ¹H NMR spectroscopic data could not be

Chapter 10

recorded for **2** (in DMSO- d_6), due to its limited solubility and the propensity for degradation of the complex by stoichiometric oxidation of the sulfoxide solvent.¹¹

[MoO₃(pbim)] (3)

A mixture of complex **1** (1.61 g, 4.08 mmol) and distilled water (40 mL) was refluxed for 24 h. The resultant solid was separated from the mother liquor (pH = 1) by filtration, washed with water (2 × 25 mL), acetone (20 mL), and diethyl ether (20 mL), and vacuum-dried to give **3** as a white solid.

Yield: 0.99 g, 71 %. Anal. Calcd for C₁₂H₉MoN₃O₃ (339.16): C 42.50, H 2.67, N 12.39. Found C 42.40, H 2.75, N 12.30. Selected FT-IR (KBr, cm⁻¹): 297 (m), 326 (m), 361 (m), 438 (w), 573 (w), 685 (s), 740 (s), 829 (s, $\nu_{\text{as}}(\text{Mo-O-Mo})$), 868 (m, $\nu_{\text{as}}(\text{Mo=O})$), 908 (m, $\nu_{\text{s}}(\text{Mo=O})$), 939 (w), 982 (m), 1005 (w), 1020 (w), 1055 (w), 1159 (w), 1236 (w), 1306 (m), 1325 (m), 1446 (m), 1458 (m), 1483 (m), 1606 (m), 2546 (w), 2646 (w), 2709 (w), 2752 (w), 2810 (w), 2860 (w), 2914 (w), 2966 (w), 3058 (w). Selected FT-Raman (cm⁻¹): 118 (w), 159 (w), 191 (w), 222 (m), 243 (m), 290 (m), 292 (m), 357 (w), 672 (s), 864 (m, $\nu_{\text{as}}(\text{Mo=O})$), 902 (m, $\nu_{\text{s}}(\text{Mo=O})$), 978 (w), 1005 (w), 1272 (w), 1549 (w), 1603 (w). ¹³C{¹H} CP MAS NMR: δ = 148.9, 143.8, 139.2, 137.8, 134.8, 124.6, 122.2, 117.2, 114.5 ppm.

10.4.7. Chapter 8

[MoO₂Cl₂(H₂O)₂]₂@CB[6] (1)

A suspension of MoO₃ (1.20 g, 8.30 mmol) and 6 M HCl (10 mL) was heated near the boiling point for 2 h until most of the MoO₃ was dissolved, and then cooled to room temperature and filtered. A portion (2 mL) of the solution containing the complex [MoO₂Cl₂(H₂O)₂] was slowly added to a solution of CB[6] (0.4 g, 0.32 mmol) in 3.8 M HCl (17.2 mL). The mixture was stirred for 2 h at room temperature during which time a colorless or very pale yellow solid precipitated. After allowing the mixture to stand for one day, the precipitate was filtered and vacuum-dried.

Yield: 0.17 g, 29 %. Anal. Calcd for 2[MoO₂Cl₂(H₂O)₂]·(C₃₆H₃₆N₂₄O₁₂)·15H₂O·1.5HCl·0.6(CH₃COCH₃) (1826.3): C, 24.86; H, 4.37; N, 18.41. Found: C, 25.07; H, 4.11; N 18.52. Selected FT-IR (KBr, cm⁻¹): 334 (w, $\nu_{\text{as}}(\text{Mo-Cl})$), 370 (m), 632 (w), 675 (w), 756 (w), 800 (s), 812 (sh), 915 (m, $\nu_{\text{as}}(\text{Mo=O})$), 964 (m), 1147 (w), 1190 (s), 1234 (s), 1246 (sh), 1294 (w), 1329 (s), 1377 (m), 1419 (m), 1483 (s), 1732 (s). Selected FT-Raman (cm⁻¹): 216 (m), 252 (m, $\rho(\text{MoO}_2)$), 281 (w), 310

Chapter 10

(w, $\nu_s(\text{Mo}-\text{Cl})$), 447 (m), 746 (w), 827 (m), 891 (w), 920 (m, $\nu_{\text{as}}(\text{Mo}=\text{O})$), 960 (s, $\nu_s(\text{Mo}=\text{O})$), 1372 (w), 1411 (w). $^{13}\text{C}\{^1\text{H}\}$ CP MAS NMR: $\delta = 155.92$ (C=O), 70.74 (CH), 51.58 (CH₂), 29.39 (acetone residue).

[MoO₂Cl₂(H₂O)₂](diglyme)₂ (2)

The complex [MoO₂Cl₂(H₂O)₂](diglyme)₂ (2) was prepared as described previously and gave concordant elemental analysis, FT-IR and ¹H NMR data.[6]

10.5. Single-crystal X-ray diffraction studies

10.5.1. Chapter 2

Experimental

Single crystals of [ptapzpy]Br suitable for X-ray diffraction were obtained by slow diffusion of diethyl ether into a concentrated solution of [ptapzpy]Br in dichloromethane. To obtain single crystals of **1** and **2**, a mixture of Mo(CO)₆ (0.08 g, 0.30 mmol), [ptapzpy]Br (0.10 g, 0.30 mmol) and CH₃CN (10 mL) was refluxed under N₂ for 30 min, and the resultant solution was filtered off. Yellow (**1**·CH₃CN) and orange (**2**·CH₃CN) single crystals were obtained after vapor diffusion of diethyl ether into the solution at ambient temperature.

Crystalline material of the compounds [ptapzpy]Br, [Mo(CO)₃(ptapzpy)Br]·CH₃CN (**1**·CH₃CN) and [Mo(CO)₄(ptapzpy)Br]·CH₃CN (**2**·CH₃CN) was harvested from the crystallization vials, immersed in Fomblin® Y oil, and a single-crystal of each sample was mounted on the respective CryoLoops with the support of a stereomicroscope.¹² Full diffraction data sets were obtained at 150(2) K on a Bruker X8 APEX II CCD area-detector diffractometer (Mo K_α graphite-monochromated radiation, $\lambda = 0.71073$ Å), with the acquisition controlled by APEX2 software.^{13,14} Collected images were processed using SAINT+^{15,16}, and absorption effects were corrected through the multi-scan semi-empirical method implemented in SADABS.^{17,18} The crystal structures were solved using the algorithms implemented in SHELXT-2014^{19–22}, and all non-H atoms were located from difference Fourier maps calculated from successive full matrix least squares refinement cycles on F^2 using SHELXL-v.2014 (Mo, C, Br, N and O atoms were successfully refined with anisotropic displacement parameters).^{19,20,23}

Chapter 10

The relatively long bond length of 2.072(9) Å for Mo-C17 (axial CO) in the structure of **1**·CH₃CN is due to a slight crystalline disorder between Br1 and C17-O3, which was not possible to modulate in the crystal refinement. The positional disorder of these two groups originates an increase in the Mo-C17 bond length. H-atoms connected to the distinct carbons were fixed at geometrical positions using the following *HFIX* instructions in SHELXL-v.2014: 137 for the terminal –CH₃, 23 for the –CH₂– and 43 for the aromatic groups and included in refinement cycles in riding motion approximation with isotropic thermal displacement parameters (U_{iso}) fixed at 1.2 × or 1.5 × U_{eq} of the parent C-atom. Table 10.2 shows selected information about the single-crystal X-ray data collection and the structure refinements.

Supramolecular interactions and crystal packing

The absence of hydrogen atoms attached to either oxygen or nitrogen in the ligand ptapzpy and the complexes **1** and **2** prevents the occurrence of strong hydrogen bonds in the three structures. Consequently, the packing arrangement of the organic ligand (in the structure of [ptapzpy]Br) and complexes (in the structures of **1**·CH₃CN and **2**·CH₃CN) is basically driven by effective space filling closely mediated by an extensive network weak of C–H···Acceptor and π ··· π intermolecular interactions (Figure 10.1; geometric details about weak hydrogen bonds are summarized in Table 10.3).

The bromide anion in the three crystal structures, acting as either a counterion or metal-coordinated ligand, plays a decisive role in the establishment of a large number of such interactions. In the extended structure of [ptapzpy]Br the adjacent ligands interact by weak C–H···N hydrogen bonds (light blue dashed lines in Figure 10.1, a). These intermolecular interactions lead to the formation of one-dimensional (1D) supramolecular networks (infinite chains) along the [0 1 0] direction of the unit cell (not shown). Furthermore, the bromide anions interconnect these organic chains by numerous and distinct C–H···Br interactions (drawn as light green dashed lines) ultimately leading to a 3D supramolecular network.

Chapter 10

Table 10.2. Crystal and structure refinement data for the compounds [ptapzpy]Br, [Mo(CO)₃(ptapzpy)Br]·CH₃CN (**1**·CH₃CN) and [Mo(CO)₄(ptapzpy)]Br·CH₃CN (**2**·CH₃CN).

	[ptapzpy]Br	1 ·CH ₃ CN	2 ·CH ₃ CN
Chemical formula	C ₁₄ H ₂₁ BrN ₄	C ₁₉ H ₂₄ BrMoN ₅ O ₃	C ₂₀ H ₂₄ BrMoN ₅ O ₄
<i>M_r</i>	325.26	546.28	574.23
Crystal description	Colorless prism	Yellow prism	Orange prism
Crystal size/mm	0.19 x 0.07 x 0.05	0.08 x 0.02 x 0.02	0.08 x 0.05 x 0.03
Crystal system, space group	Monoclinic, <i>P</i> 2 ₁ / <i>c</i>	Monoclinic, <i>P</i> 2 ₁	Triclinic, <i>P</i> -1
<i>a</i>/Å	9.0727(4)	7.4060(6)	7.5420(12)
<i>b</i>/Å	7.6409(3)	9.7868(7)	8.9322(12)
<i>c</i>/Å	22.0574(10)	15.3808(8)	17.705(3)
<i>α</i>/°	90	90	87.812(7)
<i>β</i>/°	94.711(2)	97.385(4)	88.701(8)
<i>γ</i>/°	90	90	87.216(7)
Volume/Å³	1523.93(11)	1105.6(2)	1190.2(3)
<i>Z</i>	4	2	2
<i>ρ</i>_{calculated}/g cm⁻³	1.418	1.641	1.602
<i>F</i>(000)	672	548	576
<i>μ</i>/mm⁻¹	2.691	2.429	2.264
<i>θ</i> range/°	3.659 to 30.033	3.843 to 28.278	3.688 to 26.370
Index ranges	-12 ≤ <i>h</i> ≤ 12	-9 ≤ <i>h</i> ≤ 8	-9 ≤ <i>h</i> ≤ 9
	10 ≤ <i>k</i> ≤ 10	-13 ≤ <i>k</i> ≤ 11	-11 ≤ <i>k</i> ≤ 11
	-30 ≤ <i>l</i> ≤ 31	-20 ≤ <i>l</i> ≤ 20	-22 ≤ <i>l</i> ≤ 22
Reflections collected	55072	18898	40010
Independent reflections	4440	5075	4843
	(<i>R</i> _{int} = 0.0311)	(<i>R</i> _{int} = 0.0477)	(<i>R</i> _{int} = 0.0364)
Final <i>R</i> indices	<i>R</i> ₁ = 0.0232	<i>R</i> ₁ = 0.0412	<i>R</i> ₁ = 0.0241
[<i>I</i> > 2σ(<i>I</i>)]	<i>wR</i> ₂ = 0.0511	<i>wR</i> ₂ = 0.0825	<i>wR</i> ₂ = 0.0529
Final <i>R</i> indices (all data)	<i>R</i> ₁ = 0.0386	<i>R</i> ₁ = 0.0578	<i>R</i> ₁ = 0.0313
	<i>wR</i> ₂ = 0.0564	<i>wR</i> ₂ = 0.0889	<i>wR</i> ₂ = 0.0555
Δ<i>ρ</i>_{max} and Δ<i>ρ</i>_{min}/e Å⁻³	0.363 and -0.212	1.313 and -0.701	0.776 and -0.550

The packing arrangement of neighbouring cationic complexes [Mo(CO)₄(2-(1-propyltrimethylammonium-3-pyrazolyl)pyridine)]⁺ in **2**·CH₃CN is driven by C–H···O intermolecular interactions (light pink dashed lines in Figure 10.1, b) involving the carbonyl groups, as well as by π···π stacking between the pyridine rings of adjacent complexes [Cg···Cg distances of 3.7901(6) and 3.8623(6) Å; grey shadow in Figure 10.1, c]. Furthermore, the CH₃CN molecule of crystallisation establishes C–H···N interactions with the complexes (light blue dashed lines in Figure 10.1, b). In a mode analogous to

Chapter 10

that described for [ptapzpy]Br, the bromide anions are involved in an extensive network of weak C–H···Br hydrogen bonds (light green dashed lines in Figure 10.1, b), strengthening the cohesion of the 3D supramolecular structure of the compound **2**·CH₃CN. Similarly, the packing arrangement of adjacent neutral complexes [Mo(CO)₃(ptapzpy)Br] (**1**) is also driven by diverse C–H···O, C–H···N and C–H···Br weak hydrogen bonds, involving adjacent complexes and also the CH₃CN molecules (not shown; for geometric details about these interactions see Table 10.3).

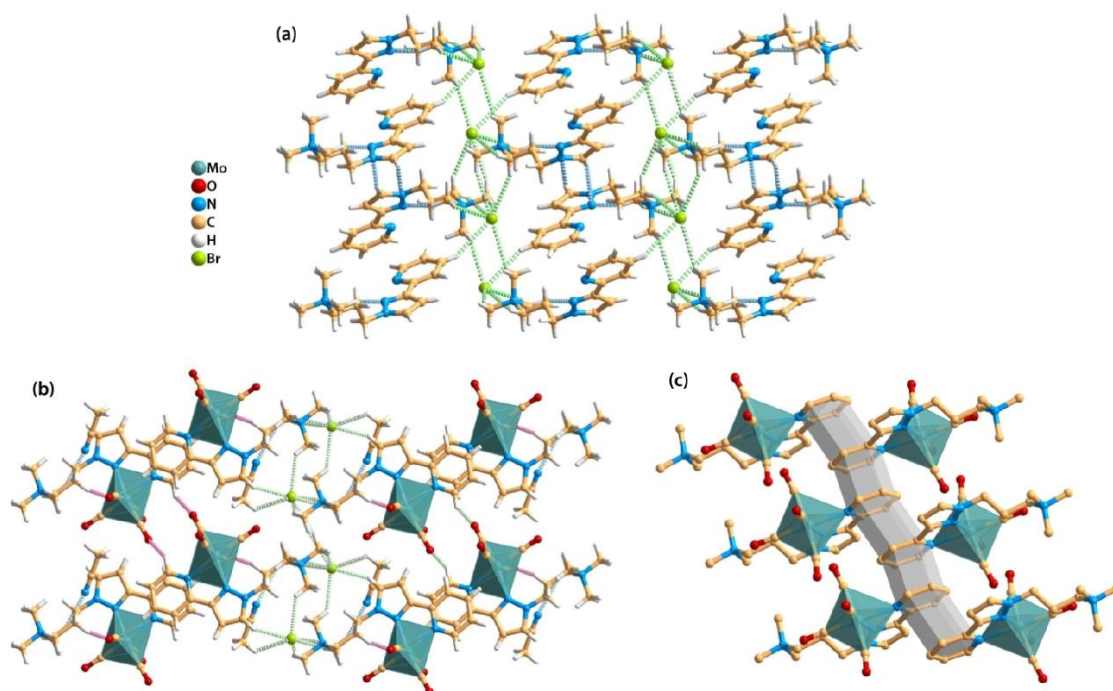


Figure 10.1. Representation of selected features of the extended crystal structures: (a) C–H···N and C–H···Br hydrogen bonds in [ptapzpy]Br; (b) C–H···O, C–H···N and C–H···Br interactions in **2**·CH₃CN; (c) π ··· π stacking between the pyridine rings of adjacent complexes **2** (grey shadow). Weak C–H···O, C–H···N and C–H···Br hydrogen bonds are shown as pink, blue and green dashed lines, respectively. The geometric details of these interactions are listed in Table 10.3.

Table 10.3. Geometric information for the C–H...A hydrogen bonding interactions of the compounds [ptapzpy]Br, **1**·CH₃CN and **2**·CH₃CN.^a

Compound	C–H...A	<i>d</i> (H...A) / Å	<i>d</i> (C...A) / Å	∠(CHA) / °
[ptapzpy]Br	C4–H4...Br1 ⁱ	2.97	3.9123(14)	172.0
	C7–H7...Br1 ⁱ	2.87	3.8173(14)	172.9
	C8–H8...N2 ⁱⁱ	2.68	3.4852(19)	143.2
	C11–H11A...Br1	2.73	3.6717(13)	159.5
	C11–H11B...Br1 ⁱⁱⁱ	3.00	3.9100(13)	153.0
	C12–H12A...Br1 ^{iv}	3.08	3.5585(15)	111.8
	C13–H13A...Br1 ^v	2.93	3.8404(15)	154.6
	C13–H13B...N2 ^v	2.58	3.2034(18)	121.3
	C14–H14A...Br1 ⁱⁱⁱ	2.95	3.8783(16)	159.3
	C14–H14C...Br1 ^v	2.88	3.8003(14)	156.9
1·CH₃CN	C8–H8...N5 ^{vi}	2.53	3.434(10)	158.4
	C9–H9A...Br1 ^{vii}	3.09	3.573(6)	111.5
	C10–H10A...Br1	2.97	3.940(6)	165.1
	C10–H10B...Br1 ^{vii}	3.03	3.650(6)	121.9
	C12–H12B...O2 ^{ix}	2.57	3.509(11)	160.7
	C12–H12B...Br1 ^{viii}	3.11	3.987(9)	149.4
	C13–H13A...Br1 ^{viii}	2.98	3.849(8)	148.7
	C13–H13C...O2 ^{viii}	2.62	3.443(10)	141.8
	C14–H14C...Br1 ^{viii}	2.98	3.881(7)	154.0
	C14–H14C...Br1 ^{viii}	2.98	3.881(7)	154.0
2·CH₃CN	C19–H19B...O2 ^{xi}	2.47	3.441(10)	169.4
	C19–H19C...O3 ^{xi}	2.59	3.348(10)	134.5
	C1–H1...O3 ^{xii}	2.54	3.272(3)	134.1
	C8–H8...Br1 ^{xiii}	2.88	3.736(2)	150.5
	C10–H10A...O4 ^{xiv}	2.53	3.266(3)	130.8
	C11–H11B...Br1 ^{xv}	2.83	3.773(3)	159.6
	C12–H12A...Br1 ^{xiii}	2.90	3.589(3)	128.0
	C13–H13A...Br1 ^{xv}	2.94	3.842(3)	154.2
	C13–H13B...Br1	2.79	3.751(2)	166.2
	C14–H14A...Br1 ^{xvi}	2.87	3.826(3)	165.7
C14–H14C...N5 ^{xiii}	2.65	3.582(4)	158.6	
C19–H19A...Br1	2.97	3.592(3)	122.3	

^a Symmetry transformations used to generate equivalent atoms: (i) $x, -y+3/2, z-1/2$; (ii) $-x+1, y+1/2, -z+1/2$; (iii) $-x+1, -y+2, -z+1$; (iv) $-x, -y+2, -z+1$; (v) $x, y+1, z$; (vi) $-x+1, y-1/2, -z+1$; (vii) $x-1, y, z$; (viii) $-x+1, y-1/2, -z+2$; (ix) $x-1, y-1, z$; (x) $-x+2, y+1/2, -z+1$; (xi) $-x+2, y-1/2, -z+1$; (xii) $-x+2, -y+1, -z$; (xiii) $x, y+1, z$; (xiv) $x-1, y, z$; (xv) $-x+1, -y+1, -z+1$; (xvi) $-x, -y+1, -z+1$.

Chapter 10

10.5.2. Chapter 5

Experimental

Single-crystals of $(\text{NH}_4)_{1.8}(\text{H}_3\text{O})_{0.2}[\text{Mo}_2\text{O}_2(\mu_2\text{-O})(\text{O}_2)_4(1,2,4\text{-trz})]\cdot\text{H}_2\text{O}$ (**5**) suitable for XRD were obtained by addition of a small quantity (ca. 1 mL) of acetone to the $\text{CH}_3\text{CN}/\text{H}_2\text{O}$ mother liquor (2 mL) obtained from the synthesis, followed by slow evaporation at ambient temperature. Single crystals of **5** were manually harvested from the crystallization vial and immersed in highly viscous FOMBLIN Y perfluoropolyether vacuum oil (LVAC 140/13, Sigma-Aldrich) to avoid degradation caused by the evaporation of the solvent.²⁴ Crystals were mounted on Hampton Research CryoLoops with the help of a Stemi 2000 stereomicroscope equipped with Carl Zeiss lenses. X-ray diffraction data for **5** were collected on a Bruker D8 QUEST at 150(2) K equipped with a Mo- $\text{K}\alpha$ sealed tube ($\lambda = 0.71073 \text{ \AA}$), a multilayer TRIUMPH X-ray mirror, a PHOTON 100 CMOS detector, and an Oxford Instruments Cryostream 700+ Series low temperature device.

Diffraction images were processed using the software package SAINT²⁵, and data were corrected for absorption by the multiscan semi-empirical method implemented in SADABS.²⁶ The structure was solved using the algorithm implemented in SHELXT-2014/5²⁷, which allowed the immediate location of almost all of the heaviest atoms composing the molecular unit. The remaining missing and misplaced non-hydrogen atoms were located from difference Fourier maps calculated from successive full-matrix least-squares refinement cycles on F2 using the latest SHELXL from the 2018/3 release.^{27–29} All structural refinements were performed using the graphical interface ShelXle.³⁰

Hydrogen atoms belonging to the organic linker were placed at their idealized positions using the HFIX 43 instructions in SHELXL. These hydrogen atoms were included in subsequent refinement cycles with isotropic thermal displacement parameters U_{iso} fixed at $1.2 \times U_{eq}$ of the parent atoms.

Hydrogen atoms associated with the NH_4^+ , H_3O^+ and H_2O moieties were directly located from difference Fourier maps. These hydrogen atoms were included in the final structural model with the N–H and O–H distances restrained to $0.95(1) \text{ \AA}$, and with U_{iso} fixed at $1.5 \times U_{eq}$ of the parent atoms. The intra-unit H...H distances were further restrained to $1.55(1) \text{ \AA}$ in order to ensure chemically reasonable geometries for these moieties. Table 10.4 gives selected bond lengths and angles for the crystallographically independent Mo center.

Chapter 10

The last difference Fourier map synthesis showed the highest peak ($1.592 \text{ e}\text{\AA}^{-3}$) and the deepest hole ($-2.048 \text{ e}\text{\AA}^{-3}$) located at 0.06 and 0.08 Å from N1 and N2, respectively. Structural drawings have been created using the software package Crystal Impact Diamond.³¹

Crystal data: $\text{C}_2\text{H}_{12.8}\text{Mo}_2\text{N}_{4.8}\text{O}_{12.2}$, $M = 491.23$, orthorhombic, space group $Pn\bar{m}$, $Z = 4$, $a = 11.3410(15) \text{ \AA}$, $b = 13.0981(17) \text{ \AA}$, $c = 8.8302(12) \text{ \AA}$, $V = 1311.7(3) \text{ \AA}^3$, $\mu(\text{Mo-K}\alpha) = 1.989 \text{ mm}^{-1}$, $D_c = 2.488 \text{ mg cm}^{-3}$, yellow block, crystal size of $0.22 \times 0.10 \times 0.10 \text{ mm}^3$. Of a total of 25388 reflections collected, 1261 were independent ($R_{\text{int}} = 0.0713$). Final $R1 = 0.0614 [I > 2\sigma(I)]$ and $\omega R2 = 0.1338$ (all data). Data completeness to theta = 25.24° , 98.0 %.

Table 10.4. Bond distances (in Å) and angles (in degrees) for the crystallographically independent Mo(VI) metal center present in **5**.

Mo...L (L = O, N)	$d(\text{Mo}\cdots\text{L})/\text{\AA}$	L...Mo...L (L = O, N)	$\angle (\text{LMoL})/^\circ$
Mo1–O1	1.944(3)	O1–Mo1–O3	86.9(4)
Mo1–O2	1.700(6)	O1–Mo1–O6	88.3(3)
Mo1–O3	1.951(6)	O1–Mo1–N1	80.0(3)
Mo1–O4	1.933(7)	O2–Mo1–O1	98.1(3)
Mo1–O5	1.941(6)	O2–Mo1–O3	101.5(3)
Mo1–O6	1.958(6)	O2–Mo1–O4	101.1(3)
Mo1–N1	2.398(9)	O2–Mo1–O5	100.5(3)
		O2–Mo1–O6	101.2(3)
		O2–Mo1–N1	178.0(3)
		O3–Mo1–O6	157.3(3)
		O3–Mo1–N1	78.8(3)
		O4–Mo1–O1	130.2(4)
		O4–Mo1–O3	44.4(3)
		O4–Mo1–O5	89.2(3)
		O4–Mo1–O6	131.1(3)
		O4–Mo1–N1	80.4(3)
		O5–Mo1–O1	131.4(4)
		O5–Mo1–O3	131.6(3)
		O5–Mo1–O6	44.1(3)
		O5–Mo1–N1	80.7(3)
		O6–Mo1–N1	78.6(3)

Chapter 10

10.5.3. Chapter 8

Experimental

During the synthesis of the compound $[\text{MoO}_2\text{Cl}_2(\text{H}_2\text{O})_2]_2@\text{CB}[6]$ described above, after isolating the precipitate, the mother liquor was left to stand, which led to the formation of yellow single-crystals suitable for X-ray diffraction. Single crystals of $[\text{MoO}_2\text{Cl}_2(\text{H}_2\text{O})_2]_2@\text{CB}[6]$ were harvested from the crystallization vial, immersed in highly viscous oil (Fomblin Y, Aldrich), and a selected crystal was mounted on a CryoLoop.²⁴ Full diffraction data were collected on a Bruker X8 APEX II CCD area-detector diffractometer controlled by the APEX2 software package (Mo K_α graphite-monochromated radiation, $\lambda = 0.71073 \text{ \AA}$; the crystal was distanced at 40 mm from the detector; the exposure time per frame was 15 s).³² The temperature of acquisition, 150(2) K, was set up with a cryosystem by the Oxford Cryosystems Series 700 monitored by the interface Cryopad.³³ Collected images were processed using the software package SAINT+,²⁵ and the absorption effects were corrected by the multi-scan semi-empirical method implemented in SADABS.³⁴ The structure was solved using SHELXT-2014,^{27,28} the non-H atoms were located from difference Fourier maps calculated and refined by using anisotropic displacement from successive full-matrix least squares refinement cycles on F^2 using SHELXL-v.2014.^{28,29}

H-atoms bound to carbon of CB[6] were placed at geometrical positions using *HFIX* instructions in SHELXL (23 for the CH_2 and 13 for the CH groups) and included in subsequent refinement cycles in riding-motion approximation with isotropic thermal displacements parameters (U_{iso}) fixed at $1.2 \times U_{\text{eq}}$. Furthermore, the H-atoms associated with the coordinated and fully occupied uncoordinated water molecules were markedly visible in the difference Fourier maps, and included in subsequent refinement stages with the O–H and H \cdots H distances restrained to 0.87(1) and 1.43(2) \AA , respectively, and using a riding-motion approximation with an isotropic thermal displacement parameter fixed at $1.5 \times U_{\text{eq}}$ of the parent oxygen atom. Despite the H-atoms of the partially occupied crystallization water molecules were not located from difference Fourier maps or positioned in calculated positions, they were considered to the final molecular formula.

Table 10.5 summarize main information about the crystal data, the single-crystal X-ray data collection and the structure refinement.

Table 10.5. Crystal and structure refinement data for $[\text{MoO}_2\text{Cl}_2(\text{H}_2\text{O})_2]_2@[\text{CB}][6]$ structure.

$[\text{MoO}_2\text{Cl}_2(\text{H}_2\text{O})_2]_2@[\text{CB}][6]$	
Chemical formula	$\text{C}_{36}\text{H}_{80}\text{Cl}_6\text{Mo}_2\text{N}_{24}\text{O}_{37}$
M_r	1845.82
Crystal description	Yellow prism
Crystal size/mm	0.30 x 0.21 x 0.12
Crystal system, space group	Triclinic, <i>P</i> -1
$a/\text{\AA}$	11.5039(11)
$b/\text{\AA}$	11.9145(10)
$c/\text{\AA}$	14.6279(13)
$\alpha/^\circ$	74.687(4)
$\beta/^\circ$	68.753(4)
$\gamma/^\circ$	87.232(4)
Volume/\AA^3	1799.8(3)
Z	1
$P_{\text{calculated}}/\text{g cm}^{-3}$	1.703
$F(000)$	946
μ/mm^{-1}	0.678
Θ range/$^\circ$	3.78 to 28.28
Index ranges	$-15 \leq h \leq 13$ $-15 \leq k \leq 15$ $-19 \leq l \leq 19$
Reflections collected	60089
Independent reflections	8909
Final R indices [$I > 2\sigma(I)$]	$R_{\text{int}} = 0.0311$ $R_1 = 0.0283$ $wR_2 = 0.0732$
Final R indices (all data)	$R_1 = 0.0326$ $wR_2 = 0.0755$
$\Delta\rho_{\text{max}}$ and $\Delta\rho_{\text{min}}/\text{e \AA}^{-3}$	0.877 and -0.624

10.6. Catalytic tests

10.6.1. Gas chromatography

Gas chromatography (GC) is an analytical separation technique used to analyse volatile substances in the gas phase. In gas chromatography, the components of a sample are dissolved in a solvent and vaporized in order to separate the analytes, distributing the components between two phases: a stationary phase of the GC column and a mobile phase. The mobile phase is a chemically inert gas that serves as carrier to

Chapter 10

the analyte, flowing inside the heated column. The stationary phase is a chemical substance which allows different chemical affinities with the compounds in the sample mixture.

The reaction mixtures were analyzed with a Varian 3900 GC equipped with a DB-5 capillary column (30 m x 0.25 mm x 0.25 μm), while the reaction mixtures from chapter 6 and 8 were analyzed with a Varian 3800 GC equipped with a BR-5 (Bruker) capillary column (30 m x 0.25 mm x 0.25 μm), accompanied with a FID detector, with H_2 as the carrier gas. The concentrations of reactants/products were determined using the internal calibration method, *i.e.* based on calibration curves with an inert and stable internal standard. The FID response was linear in the ranges of concentrations used for the calibration curves and sample analysis. Using the internal calibration method, the determined concentrations of reactants/products are reliable (experimental range of error of ca. 5-6 %), *i.e.* the conversion values account for substrate consumption irrespective of the types of products formed being detected or not by GC. The reactant/products were quantified by GC calibrations. The products were identified using GC-MS (Trace GC 2000 Series Thermo Quest CE Instruments GC; Thermo Scientific DSQ II), or GC-MS (GC-qMS Agilent Technologies, 6890 N Network GC system, 5973 Network mass selective detector) with using He as the carrier gas. The product identifications were based on commercial mass spectrometry databases (Wiley6, NIST2.0, NIST Chemistry WebBook, MAINLIB) and mass spectral matching to available literature data.

10.6.2 Formulae - catalytic studies

The formulas used for the determination of substrate (Sub) conversion ($\text{Conv.}_{\text{Sub}}$), product (Prod) selectivity ($\text{Select.}_{\text{Prod}}$), product yield ($\text{Yield}_{\text{Prod}}$) and turnover frequency (TOF) for the reaction time t , are as follows:

$$\text{Conv.}_{\text{Sub},t} (\%) = \frac{(n_{\text{Sub},i} - n_{\text{Sub},t})}{n_{\text{Sub},i}} \times 100$$

$$\text{Select.}_{\text{Prod}} (\%) = \frac{n_{\text{Prod},t}}{n_{\text{Total of formed products},t}} \times 100$$

$$\text{Yield}_{\text{Prod}} (\%) = \frac{\text{Conv.}_{\text{Sub},t} (\%) \times \text{Select.}_{\text{Prod},t} (\%)}{100}$$

$$\text{TOF} (\text{mol mol}_{\text{Mo}}^{-1} \text{h}^{-1}) = \frac{\text{Conv.}_{\text{Sub},t} \times 0.01 \times n_{\text{Sub},i}}{t \times n_{\text{Mo},i}}$$

$$\text{TON} (\text{mol mol}_{\text{Mo}}^{-1}) \text{ for a period of time, } t = \frac{\text{Conv.}_{\text{Sub},t} \times 0.01 \times n_{\text{Sub},i}}{n_{\text{Mo},i}}$$

Chapter 10

The enantiomeric (*ee*) or diastereomeric (*de*) excess of the isomer *i* to the isomer *ii* are given by:

$$\text{Excess (\%)} = \frac{n_{i,t} - n_{ii,t}}{n_{\text{Total of isomers } i \text{ and } ii}} \times 100$$

10.6.3. Chapter 2

The typical epoxidation experiments with TBHP (in decane or aqueous solution) were carried out in 10 mL borosilicate batch reactors possessing a valve for sampling. Reaction mixtures were stirred magnetically (1000 rpm, PTFE-coated stirring bar) and heated to 55 °C with a thermostatically controlled oil bath. The reactors were charged with the (pre)catalyst (amount equivalent to 16 μmol Mo), *cis*-cyclooctene (1.8 mmol), and a cosolvent [1 mL of 1,2-dichloroethane or CH₃CN, or 0.3 mL of an ionic liquid (IL)]. The reactor containing the catalyst, olefin and cosolvent was preheated for 10 min at the reaction temperature. In a separate flask, the oxidant was preheated in a similar fashion, and subsequently added to the reactor to give a Mo:Cy:oxidant molar ratio of 1:113:172; this was marked as the initial instant of the catalytic reaction.

Catalytic tests using 30 wt % aq. H₂O₂ as oxidant were carried out using tubular borosilicate batch reactors with pear-shaped bottoms (ca. 12 mL capacity), equipped with a PTFE-coated magnetic stirring bar (1000 rpm) and a valve for (un)charging of the reactor. Catalyst (16 mmol Mo), Cy (1.8 mmol), CH₃CN (1 mL) and H₂O₂ (Mo:Cy:oxidant molar ratio of 1:113:172) were added to the reactor, which was subsequently immersed in an oil bath heated to 55 or 70 °C. Separate catalytic experiments were carried out for each reaction time.

10.6.4. Chapter 3

Epoxidation tests

The typical epoxidation experiments were carried out in 10 mL borosilicate batch reactors, equipped with an appropriate PTFE-coated magnetic stirring bar (1000 rpm) and a valve for sampling. The heating source was a thermostatically controlled oil bath (55 °C). The reactors were charged with the (pre)catalyst (amount equivalent to 16 μmol Mo), 1.8 mmol of *cis*-cyclooctene (Cy), and a cosolvent [1 mL of 1,2-dichloroethane (CH₃CHCl₂) or 0.3 mL of an ionic liquid]. The reactor containing the catalyst, olefin and cosolvent was preheated for 10 min at the reaction temperature. In a separate flask, the

Chapter 10

oxidant TBHP (5-6 M in decane) was preheated in a similar fashion, and subsequently added to the reactor to give a Mo: Cy: oxidant molar ratio of 1:113:172; this instant was taken as time zero.

Catalytic tests using 30 wt % aq. H_2O_2 as oxidant were carried out using tubular borosilicate batch reactors with pear-shaped bottoms (ca. 12 mL capacity), equipped with an appropriate PTFE-coated magnetic stirring bar (1000 rpm) and a valve for (un)charging of the reactor. Catalyst (16 mmol Mo), Cy (1.8 mmol), CH_3CN (1 mL) and H_2O_2 (Mo: Cy: oxidant molar ratio of 1:113:172) were added to the reactor, which was subsequently immersed in a thermostatically controlled oil bath (55 °C). Separate catalytic experiments were carried out for each reaction time.

Iodometric titrations were carried out in order to quantify the non-productive decomposition of the oxidant (TBHP or H_2O_2). The reactors containing the (pre)catalyst, solvent and oxidant, without substrate, were heated at 55 °C for 24 h (stirring rate of 1000 rpm). After cooling the reactors to ambient temperature, liquid samples were withdrawn for titration.

Catalyst reuse was investigated for Cy/TBHP/2 using an ionic liquid, namely [bmim]PF₆. After a catalytic batch run, the reactant/products were separated from the IL phase by adding *n*-hexane (immiscible with the IL) to the reaction mixture, followed by centrifugation, decantation and removal of the upper liquid phase from the (denser) IL phase; this procedure was repeated five times, allowing the complete removal of reactant/products from the IL phase, as confirmed by gas chromatography (GC) analysis. Prior to reuse, the IL mixture was heated at 40 °C under vacuum for 1 h. A second batch run was initiated by adding Cy (preheated at 55 °C) and TBHP to the reactor containing the IL mixture (preheated at 55 °C); the reactants were added in equal amounts to those used for the first batch.

Alcoholysis tests

The catalytic alcoholysis of styrene oxide (StyOx) was carried out at 55 °C in a similar fashion to that described above for the system Cy/TBHP. The reactor was charged with the catalyst (amount equivalent to 20 μmol Mo), 1 mL of ethanol (EtOH) and styrene oxide (0.4 mmol). The analytical equipment and methods used were similar to those for the system Cy/TBHP. For these systems, the catalytic contribution of the solubilised species was checked by carrying out contact tests (CT) as follows. After heating the mixture of (pre)catalyst and solvent (no substrate) at 55 °C for 24 h, the reactor was cooled to ambient temperature. The solid-liquid phases were separated by filtration using a 200 nm membrane. The liquid phase was transferred to a separate

Chapter 10

reactor for a subsequent homogeneous catalytic test at 55 °C. The substrate StyOx was added to the recovered liquid phase in an amount calculated to give an initial substrate concentration equal to that used for a normal catalytic test. The homogeneous catalytic reaction of StyOx was monitored for 24 h at 55 °C, as described above for Cy epoxidation.

Isolation of metal species after catalytic reactions

For reaction mixtures which were biphasic solid-liquid, the solid phase was separated from the catalytic reaction mixture (TBHP/CH₂Cl₂ or H₂O₂/CH₃CN) by centrifugation (3500 rpm), washed with organic solvents (pentane, hexane, ethanol and/or acetone), dried overnight under atmospheric conditions, and subsequently under vacuum (ca. 4 mbar) for 1 h at 60 °C. These undissolved solids are denoted **i-S-oxid** where oxid is the oxidant (TBHP or H₂O₂) and **i** is compound **1** or **2**. For epoxidation systems using ionic liquids, the recovered solids (when present) are denoted **i-S-TBHP-IL** {IL = [bmim]NTf₂}, and for StyOx reactions the recovered solids are denoted as **i-S-EtOH**.

In some cases, metal species could be isolated from the liquid phases of the catalytic reactions by precipitation of solids after addition of an appropriate organic solvent. The precipitated solids were washed and dried as described above for the recovery of the undissolved solids. The precipitated solids are denoted as **i-L-oxid** for catalytic epoxidation of Cy and **i-L-EtOH** for alcoholysis of StyOx. The isolated solids were characterised by ATR FT-IR.

10.6.5. Chapter 4

Epoxidation tests

The catalytic reactions were carried out at 55 °C under autogenous pressure in 10mL borosilicate reactors possessing a Teflon valve for sampling, under magnetic stirring (1000 rpm). The reactor containing the catalyst (18 μmol), substrate (1.8 mmol) and 2 mL of cosolvent was immersed in a thermostated oil bath (under stirring) and, after 10 min, 2.75 mmol of oxidant TBHP (also preheated) was added (corresponding to the initial instant of the reaction). *cis*-Cyclooctene DL-limonene (DL-Lim), *trans*-β-methylstyrene (*tbms*) were the substrates; CH₂Cl₂ and α,α,α-trifluorotoluene (TFT) were used as cosolvents (other than the decane present in the oxidant solution) for reactions of Cy and DL-Lim/*tbms*, respectively.

Chapter 10

A biphasic solid/liquid reaction mixture was obtained for all systems after 24 h and, with the objective of identifying the active species, the liquid phase was separated from the solid phase by centrifugation (3000 rpm). The solids were thoroughly washed with diethyl ether (3 x 10 mL) and pentane (2 x 10 mL), dried at ambient temperature overnight, and finally vacuum-dried (ca. 0.1 bar) at 60 °C for 1 h. These recovered solids are denoted as *i*-sub-run1, where *i* = 1 or 2, and sub = Cy, DL-Lim or *t*bms.

The recovered solids **1-Cy-run1** and **2-Cy-run1** were tested for Cy reaction using the same mass ratio of molybdenum compound:olefin:oxidant as that used for the typical reaction conditions; after a 24 h batch run, the corresponding solids were recovered (denoted **1-Cy-run2** and **2-Cy-run2**) using the same procedure described above for the original compounds.

10.6.6. Chapter 5

The epoxidation reaction of the model olefin substrate Cy was carried at 70 °C using a temperature-controlled oil bath. Typically, an initial molybdenum catalyst/substrate molar ratio of 0.01, an oxidant/substrate molar ratio of 0.65 (1.8 mmol substrate), and 2 mL of cosolvent were used. Reactions with TBHP were performed with TFT as the cosolvent in 10 mL borosilicate reactors equipped with a valve for sampling. The reaction mixture (catalyst, olefin and solvent) was preheated to 70 °C under magnetic stirring (PTFE-coated stirring bar) for 10 min, and then the oxidant (also preheated under similar conditions in a separate vessel) was added. Samples were taken at different instants from the same reactor. After the catalytic tests, solid phases were isolated by centrifugation (3500 rpm), thoroughly washed with diethyl ether, pentane or acetone, and vacuum-dried at 60 °C for 1 h. With H₂O₂ as the oxidant, CH₃CN was used as the cosolvent and the catalytic tests were carried with magnetic stirring in tubular borosilicate reactors with pear-shaped bottoms (ca. 12 mL of capacity), equipped with a valve for sampling. Separate catalytic experiments were carried out for each reaction time, and the reactors were cooled to ambient temperature prior to sampling.

10.6.7. Chapter 6

The catalytic reactions were carried out in magnetically stirred, closed borosilicate reaction vessels (10 mL capacity) which were immersed in an oil bath set to 55 °C. For the epoxidation reaction, the reactor was loaded with molybdenum complex (18 μmol), *cis*-cyclooctene (1.8 mmol), oxidant (TBHP or H₂O₂, 2.75 mmol) and solvent (1 mL *α,α,α*-trifluorotoluene or CH₃CN). The solvent and catalyst were pre-heated at the reaction

Chapter 10

temperature for 10 min prior to addition of the reactants (instant taken as zero time). The course of the reaction was monitored using a Varian 3800 GC equipped with a Bruker BR-5 capillary column (30 m x 0.25 mm; 0.25 mm) and a flame ionisation detector, using H₂ as the carrier gas. Undecane was used as an internal standard added after the reaction. The products were identified by GC-MS (Trace GC 2000 Series (Thermo Quest CE Instruments) – DSQ II (Thermo Scientific)), equipped with an Agilent J&W capillary DB-5 column (30 m x 0.25 mm; 0.25 mm) and using He as carrier gas.

After the catalytic reaction, the catalysts were separated from the reaction mixtures by centrifugation, thoroughly washed with pentane and dried under reduced pressure (ca. 1 mbar) for 1 h at 60 °C. The recovered catalysts (*i*-Cat-ox, where *i* is the compound number and ox is the oxidant) were characterised by ATR FT-IR spectroscopy and PXRD.

Contact tests (CTs) were carried out by mixing the original catalyst with oxidant and solvent (without substrate) and stirring for 24 h at 55 °C. Subsequently the solid phase was separated by centrifugation, and the supernant (L) was filtered through a 0.22 mm PTFE membrane, giving the solution denoted *i*-CT-ox-L. The solid (S) was washed with pentane and dried under reduced pressure for 1 h at 60 °C, giving *i*-CT-ox-S. These solids were characterised by ATR FT-IR spectroscopy and PXRD, and tested for the Cy reaction under similar conditions to those used for the original catalysts. The liquid phase *i*-CT-ox-L was transferred to a new reactor, and pre-heated to 55 °C for 10 min. Subsequently, the pre-heated substrate was added to the reactor in an amount to give the same initial molar concentration of Cy as that used for a normal catalytic run.

The oxidant efficiency was determined by iodometric titration of the reaction mixtures, after a 24 h batch run at 55 °C. The values indicated in the discussion are the average of three replicates (range of experimental error was ca. 10 %).

The Lewis acidity of compounds **1-4** was assessed through the model acid reaction of StyO with ethanol at 55 °C (the same temperature as that used for catalytic epoxidation, and without oxidant). The catalytic tests with StyO and absolute ethanol were carried out in a similar fashion to that described for catalytic epoxidation. Contact tests were carried out for **1-4** in a similar fashion to that described for this chapter for the catalysts tested in the epoxidation reaction systems.

Chapter 10

10.6.8. Chapter 7

Epoxidation tests

Catalytic oxidation reactions were performed at 55 or 70 °C using **1**, **2** or **3** (18 μmol), a substrate (1.8 mmol), an oxidant (2.75 mmol), and (optionally) a cosolvent (1 mL). Reactions with TBHP were performed in borosilicate reactors (10 mL), equipped with a PTFE magnetic stirring bar and valves for sampling. The reactor was charged with the catalyst, the substrate, and the cosolvent, and immersed in a temperature-controlled oil bath. After stirring (1000 rpm) for 10 min, the oxidant was added, and the reaction time was counted from this instant. Catalytic tests using H₂O₂ as the oxidant were carried out using tubular borosilicate batch reactors with pear-shaped bottoms (ca. 12 mL capacity), equipped with an appropriate PTFE-coated magnetic stirring bar (1000 rpm) and a valve. The catalyst, the substrate, the cosolvent, and H₂O₂ were added to the reactor, which was then immersed in a thermostatically controlled oil bath (70 °C). With H₂O₂ as the oxidant, separate catalytic experiments were carried out for each reaction time.

Iodometric titrations were carried out to quantify the non-productive decomposition of the oxidants. The reactors containing the (pre)catalyst, cosolvent, and oxidant, but no substrate, were heated for 24 h at 70 °C (stirring rate of 1000 rpm). After cooling the reactors to ambient temperature, liquid samples were withdrawn, filtered, and titrated.

The contribution of dissolved metal species to the catalytic reaction was checked by performing two experiments at 70 °C: a filtration test and a contact test. For the former, the reaction of Cy with TBHP in the presence of catalyst was interrupted after 1 h, and the mixture was immediately filtered (while still at the reaction temperature) through a PTFE membrane (0.2 μm) to remove any undissolved solid. The reaction solution was then transferred to an empty and clean reactor (preheated at 70 °C) and stirred for a further 23 h at 70 °C. For the CT experiment, the (pre)catalyst (i) was treated with TBHP and solvent under similar conditions to those used for a typical batch run, but without substrate, for 24 h. Subsequently, the mixture was cooled to ambient temperature and centrifuged (3500 rpm). The liquid phase (L) was passed through a filter equipped with a 0.2 μm PTFE membrane, giving i-CT-TBHP-L. These solutions were tested for the homogeneous catalytic epoxidation reaction by adding Cy (preheated at 70 °C) to give an initial substrate concentration similar to that used for a normal catalytic run, and then stirring the mixture for 24 h at 70 °C.

Chapter 10

Catalyst reuse was investigated for **3**/TBHP/Cy using the ionic liquid [bmim]BF₄. After a catalytic batch run, the reactants/products were separated from the IL phase by adding *n*-hexane (immiscible with the IL) to the reaction mixture, followed by centrifugation, decantation, and removal of the upper liquid phase from the denser IL phase; this procedure was repeated five times, allowing the complete removal of reactant/products from the IL phase, as confirmed by GC analysis. Prior to reuse, the IL mixture was treated at 40 °C under reduced pressure for 1 h. Second and third batch runs were initiated by adding Cy (preheated at 70 °C) and TBHP to the reactor containing the IL mixture (preheated to 70 °C); the reactants were added in equal amounts to those used for the first batch.

Undissolved solids remaining in the reaction mixtures after 24 h catalytic batch runs or CTs were isolated by centrifugation (3500 rpm), thoroughly washed with either diethyl ether/pentane (for reactions performed with organic solvents) or acetone (for reactions with IL), dried overnight under atmospheric conditions, and finally vacuum-dried (ca. 4 bar) at 60 °C for 1 h. The recovered undissolved solids (S) are denoted as *i*-oxid-solv-*T*-S1 (for catalytic batch runs) and *i*-CT-TBHP-S1 (for CT experiments), where oxid = TBHP or H₂O₂, solv = type of cosolvent used (ws denotes without solvent), *T* = 55 or 70 °C, *i* = **1**, **2**, or **3**. For some reactions, the solids *i*-CT-TBHP-S1 and *i*-oxid-solv-*T*-S1 were reused once or twice for Cy epoxidation with TBHP or H₂O₂ (the initial mass ratios of olefin/oxidant/metal compound were the same for all catalytic runs). After 24 h batch runs using *i*-CT-TBHP-S1 or *i*-oxid-solv-*T*-S1, the undissolved solids were recovered as described above, giving the samples *i*-CT-TBHP-S2 and *i*-oxid-solv-*T*-S2.

10.6.9. Chapter 8

Catalytic oxidation tests

The catalytic experiments were performed in tubular glass pear-shaped reactors, equipped with an appropriate polytetrafluoroethylene (PTFE)-coated magnetic stirring bar and a valve, under batch operation mode. Typically, for the oxidation reactions, the reagents were loaded to the reactor in the molar proportion 1:100:152 (Mo:substrate:oxidant); specifically, 18 μmol Mo, 1.8 mmol substrate, 2.75 mmol hydrogen peroxide and 2 mL of a cosolvent. The substrates were *cis*-cyclooctene (Cy), cyclooctene oxide (CyO), cyclooctanol (CyOH), *cis*-1,2-cyclooctanediol (Cy(OH)₂), cyclohexene (Cy6), cyclohexene oxide (Cy6O), cyclohexanol (Cy6OH) and styrene (Sty). The cosolvents were CH₃CN, DMF or the alcohols MeOH, EtOH or BuOH. The loaded reactor was immersed in a thermostatically controlled oil bath heated at 70 °C

Chapter 10

(stirring rate of 800 rpm to avoid mass transfer limitations) which was taken as the instant that the reaction began (zero time).

Catalyst stability studies involved the reuse of the recovered catalyst, a contact test, and characterisation of the used catalysts. Compound **1** was used for three consecutive catalytic batch runs, under similar reaction conditions (Cy/H₂O₂/CH₃CN, 70 °C, 24 h). Catalyst recovery involved separation of the solid from the reaction mixture by centrifugation (approximately 38000 rpm for 5 min), thoroughly washing with acetone, drying at room temperature overnight and then under vacuum at 50 °C for 1 h.

The CT was carried out to check for the presence of leached active metal species in the liquid phase. First, the original catalyst was contacted with CH₃CN/H₂O₂ at 70 °C/24 h, under similar conditions to those used for a normal catalytic test, but without substrate. Subsequently, the mixture was cooled to ambient temperature, centrifuged (38000 rpm), and passed through a filter containing a 0.2 µm PTFE membrane in order to separate the solid and liquid phases. The liquid phase (LP) obtained from the CT (LP-CT-CH₃CN) was transferred to a separate clean reactor and the substrate Cy was then added to the reactor in order to give the same initial concentration (0.76 M) as that used for a normal catalytic test. Afterwards, the homogeneous reaction mixture was heated at 70 °C for 24 h (800 rpm). The undissolved solid obtained from the CT was washed, dried overnight under atmospheric conditions and then under vacuum for 1 h at 50 °C, giving SP-CT-CH₃CN.

Quantification and identification of the products

The reactors were cooled to ambient temperature in cold water before opening and suitable work-up procedures. The analyses were always carried out for freshly prepared samples. Individual experiments were performed for each reaction of 24 h (experimental error of ca. 5 %). The evolution of the catalytic reactions was monitored by GC, using a Varian 3800 instrument equipped with a capillary column (VF-5 ms, 30 m x 0.25 mm x 0.25 µm), a flame ionisation detector, H₂ as the carrier gas, and undecane as internal standard.

The MS data for the bioproducts are as follows. When using CH₃CN as solvent, the reactions of the alkenes tested were more selective than when using an alcohol medium, giving only one product. Specifically, CyO from Cy, cyclooctanone (Cy=O) from CyOH, 1,2-cyclohexanediol (Cy₆(OH)₂) from Cy₆ and benzaldehyde (BA) from Sty. When using an alcohol medium (MeOH, EtOH or BuOH) a mixture of various products were obtained, specifically: CyO, 2-alkoxycyclooctanone [Cy(=O)(OR)], 2-alkoxycyclooctanol [Cy(OH)(OR)] and 2-dialkoxycyclooctane [Cy(OR)₂] from Cy; Cy₆(OH)₂ and 2-

Chapter 10

alkoxycyclohexanol [$\text{Cy}_6(\text{OH})(\text{OR})$] from Cy6; and BA, acetophenone, styrene oxide, ethyl benzoate and 1,2-ethanediol-1-phenyl from Sty. The mass spectral data are indicated for selected products:

- 2-Ethoxycyclooctanone [$\text{Cy}(=\text{O})(\text{OEt})$], m/z (relative intensity): 170 [M^+] (2), 169 (8), 156 (9), 155 (79), 127 (9), 110 (10), 109 (100), 97 (8), 83 (16), 81 (17), 67 (60), 57 (12), 55 (24), 43 (18), 41 (14), 39 (7), 29 (9).

- 2-Butoxycyclooctanone [$\text{Cy}(=\text{O})(\text{OBu})$], m/z (relative intensity): 198 [M^+] (1), 197 (5), 156 (9), 155 (79), 127 (9), 110 (10), 109 (100), 97 (3), 83 (8), 81 (12), 67 (51), 57 (7), 55 (17), 43 (8), 41 (10), 39 (3), 29 (3).

- 2-Methoxycyclooctanol [$\text{Cy}(\text{OH})(\text{OMe})$], m/z (relative intensity): 158 [M^+] (0.8), 144 (1), 143 (13), 128 (3), 127 (8), 126 (8), 125 (29), 112 (4), 109 (6), 108 (11), 99 (2), 98 (15), 97 (21), 93 (18), 87 (3), 85 (11), 83 (17), 82 (25), 79 (12), 76 (6), 72 (8), 71 (100), 70 (18), 69 (10), 67 (18), 66 (2), 61 (1), 59 (6), 58 (16), 57 (13), 55 (16), 54 (4), 51 (1), 45 (10), 43 (7), 41 (13), 39 (4).

- 2-Ethoxycyclooctanol [$\text{Cy}(\text{OH})(\text{OEt})$], m/z (relative intensity): 172 [M^+] (1), 155 (0.3), 143 (22), 141 (16), 126 (8), 125 (46), 110 (10), 108 (11), 99 (15), 97 (15), 93 (15), 85 (100), 82 (32), 81 (27), 79 (26), 72 (12), 70 (16), 67 (22), 57 (61), 55 (30), 44 (16), 43 (22), 41 (29).

- 2-Butoxycyclooctanol [$\text{Cy}(\text{OH})(\text{OBu})$], m/z (relative intensity): 200 [M^+] (1.6), 170 (4), 169 (18), 159 (7), 143 (30), 126 (15), 125 (74), 113 (38), 109 (26), 97 (34), 93 (26), 85 (20), 83 (44), 82 (56), 79 (40), 70 (36), 67 (42), 57 (100), 55 (56), 43 (22), 41 (52), 39 (10), 29 (12), 18 (14).

- 2-Dimethoxycyclooctane [$\text{Cy}(\text{OCH}_3)_2$], m/z (relative intensity): 172 [M^+] (8), 171 (82), 143 (2), 142 (11), 140 (3), 139 (22), 137 (100), 130 (8), 129 (100), 128 (8), 127 (5), 125 (2), 121 (1), 115 (3), 114 (13), 111 (22), 110 (19), 109 (3), 102 (1), 101 (8), 100 (3), 99 (4), 98 (7), 97 (78), 96 (7), 95 (5), 94 (2), 93 (5), 92 (2), 91 (2), 88 (6), 87 (50), 86 (1), 85 (8), 84 (14), 83 (48), 82 (18), 81 (10), 79 (6), 75 (6), 74 (88), 73 (14), 71 (6), 70 (8), 69 (90), 68 (20), 67 (14), 59 (50), 57 (6), 56 (12), 55 (72), 54 (8), 53 (8), 45 (8), 43 (30), 42 (11), 41 (31), 39 (9), 29 (4), 28 (4), 27 (3), 18 (2), 15 (3).

- 2-Hydroxycyclooctanone [$\text{Cy}(=\text{O})\text{OH}$], m/z (relative intensity): 142 [M^+] (8), 125 (6), 124 (54), 109 (6), 99 (6), 98 (42), 97 (12), 96 (28), 95 (38), 82 (18), 81 (60), 80 (40), 71 (16), 70 (16), 68 (38), 67 (30), 58 (8), 57 (100), 55 (28), 54 (11), 53 (7), 45 (3), 44 (14), 43 (13), 42 (12), 41 (20), 39 (10), 31 (2), 29 (4), 27 (3).

- 1,2-Cyclooctanedione [$\text{Cy}(=\text{O})_2$], m/z (relative intensity): 141 [M^+1] (6), 140 (66), 112 (16), 98 (22), 97 (18), 84 (54), 83 (28), 70 (12), 69 (44), 68 (100), 67 (12), 56 (36), 55 (86), 43 (8), 42 (20), 41 (30), 39 (13), 28 (4).

Chapter 10

- 1,2-Cyclohexanediol [Cy₆(OH)₂], m/z (relative intensity): 116 [M⁺] (10), 99 (4), 98 (43), 97 (17), 83 (44), 80 (10), 70 (100), 69 (26), 67 (8), 57 (38), 55 (13), 44 (12), 41 (12), 39 (6), 29 (2).
- Ethoxycyclohexanol [Cy₆(OH)(OEt)], m/z (relative intensity): 144 [M⁺] (18); 127 (1.2), 126 (2.2), 115 (6), 111 (1.6), 98 (39), 97 (26), 85 (100), 82 (68), 81 (20), 70 (68), 69 (22), 57 (44). 55 (10), 43 (10), 41 (17), 39 (5), 29 (4).
- 2-Ethanediol-1-phenyl [Sty(OH)₂], m/z (relative intensity): 138 [M⁺] (6), 120 (0.6), 108 (9), 107 (100), 91 (8), 79 (61), 77 (48), 65 (3), 51 (6).

10.7. References

- (1) Brunner, H.; Scheck, T. *Chem. Ber.* **1992**, *125*, 701–709.
- (2) Amarante, T. R.; Neves, P.; Paz, F. A. A.; Valente, A. A.; Pillinger, M.; Gonçalves, I. S. *Dalton Trans.* **2014**, *43*, 6059–6069.
- (3) Carrasco, C. J.; Montilla, F.; Álvarez, E.; Herbert, M.; Galindo, A. *Polyhedron* **2013**, *54*, 123–130.
- (4) Lunazzi, L.; Parisi, F.; Macciantelli, D. *J. Chem. Soc.* **1984**, 1025.
- (5) Bellagamba, M.; Bencivenni, L.; Gontrani, L.; Guidoni, L.; Sadun, C. *Struct. Chem.* **2013**, *24*, 933–943.
- (6) Amarante, T. R.; Neves, P.; Valente, A. A.; Paz, F. A. A.; Pillinger, M.; Gonçalves, I. S. *J. Catal.* **2016**, *340*, 354–367.
- (7) Amarante, T. R.; Neves, P.; Coelho, A. C.; Gago, S.; Valente, A. A.; Almeida Paz, F. A.; Pillinger, M.; Gonçalves, I. S. *Organometallics* **2010**, *29*, 883–892.
- (8) Kühn, F. E.; Groarke, M.; Bencze, É.; Herdtweck, E.; Prazeres, A.; Santos, A. M.; Calhorda, M. J.; Romão, C. C.; Gonçalves, I. S.; Lopes, A. D.; Pillinger, M. *Chem. Eur. J.* **2002**, *8*, 2370–2383.
- (9) Chakravorti, M. C.; Ganguly, S.; Bhattacharjee, M. *Polyhedron* **1993**, *12*, 55–58.
- (10) Gamelas, C. A.; Gomes, A. C.; Bruno, S. M.; Paz, F. A.; Valente, A. A.; Pillinger, M.; Romão, C. C.; Gonçalves, I. S. *Dalton Trans.* **2012**, *41*, 3474–3484.
- (11) Carrasco, C. J.; Montilla, F.; Álvarez, E.; Mealli, C.; Manca, G.; Galindo, A. *Dalton Trans.* **2014**, *43*, 13711–13730.
- (12) Frisell, H.; Eriksson, L.; Vitagliano, A. *Organometallics* **1997**, *16*, 942–950.
- (13) Herrick, R. S.; Ziegler, C. J.; Bohan, H.; Corey, M.; Eskander, M.; Giguere, J.; McMicken, N.; Wrona, I. E. *J. Organomet. Chem.* **2003**, *687*, 178–184.
- (14) Oelkers, B.; Venker, A.; Sundermeyer, J. *Inorg. Chem.* **2012**, *51*, 4636–4643.
- (15) García-Rodríguez, R.; Miguel, D. *Dalton Trans.* **2006**, *6*, 1218–1225.
- (16) Karakus, M.; Davulga, G.; Gómez-Ruiz, S.; Tschirschwitz, S.; Hey-Hawkins, E. *Polyhedron* **2009**, *28*, 91–94.
- (17) Neves, P.; Amarante, T. R.; Gomes, A. C.; Coelho, A. C.; Gago, S.; Pillinger, M.;

Chapter 10

- Gonçalves, I. S.; Silva, C. M.; Valente, A. A. *Appl. Catal., A* **2011**, *395*, 71–77.
- (18) Nogueira, L. S.; Neves, P.; Gomes, A. C.; Valente, A. A.; Pillinger, M.; Gonçalves, I. S. *J. Organomet. Chem.* **2017**, *846*, 185–192.
- (19) Behrens, H.; Lindner E.; Lehnert, G. *J. Organomet. Chem.* **1970**, *22*, 665–676.
- (20) Brisdon, B. J.; Edwards, D. A.; White, J. W. *J. Organomet. Chem.* **1978**, *156*, 427–437.
- (21) Huffman, J. C.; Kober, I. E. M.; Overtonlb, C. *Inorg. Chem.* **1984**, *23*, 2298–2303.
- (22) Han, Y. J.; Lees, A. J. *Inorg. Chim. Acta* **1988**, *147*, 45–49.
- (23) Murdoch, H. D.; Henzi, R.; Calderazzo, F. *J. Organomet. Chem.* **1967**, *7*, 441–448.
- (24) Kottke, T.; Stalke, D. *J. Appl. Crystallogr.* **1993**, *26*, 615–619.
- (25) SAINT+ Data Integration Engine v. 8.27b© 1997-2012, Bruker AXS, Madison, Wisconsin, USA.
- (26) Krause, L.; Herbst-Irmer, R.; Sheldrick, G. M.; Stalke, D. *J. Appl. Crystallogr.* **2015**, *48*, 3–10.
- (27) Sheldrick, G. M. *Acta Crystallogr. Sect. A Found. Crystallogr.* **2015**, *71*, 3–8.
- (28) Sheldrick, G. M. *Acta Crystallogr. Sect. A Found. Crystallogr.* **2008**, *64*, 112–122.
- (29) Sheldrick, G. M. *Acta Crystallogr. Sect. C Struct. Chem.* **2015**, *71*, 3–8.
- (30) Hübschle, C. B.; Sheldrick, G. M.; Dittrich, B. *J. Appl. Crystallogr.* **2011**, *44*, 1281–1284.
- (31) Brandenburg, K. DIAMOND, Version 3.2f, Crystal Impact GbR, Bonn, Germany, 1997-2010.
- (32) APEX2, Data Collection Software Version 2012.4, Bruker AXS, Delft, The Netherlands, 2012.
- (33) Cryopad, Remote monitoring and control, Version 1.451, Oxford Cryosystems, Oxford, United Kingdom, 2006.
- (34) Sheldrick, G. M.; SADABS 2012/1, Bruker AXS Area Detector Scaling and Absorption Correction Program, 2012, Bruker AXS, Madison, Wisconsin, USA.

